Doctoral Thesis

Structural and functional analysis of the photosynthetic apparatus of Norway spruce

Monika Opatíková

Department of Biophysics

Faculty of Science, Palacký University Olomouc, Czech Republic

Olomouc 2023

Bibliographical identification

Name of the author:	Monika Opatíková
Title of the doctoral thesis:	Structural and functional analysis of the photosynthetic apparatus of Norway spruce
Study field:	Biophysics
Year of defence:	2023
Supervisor:	RNDr. Roman Kouřil, Ph.D.
Keywords:	Norway spruce, photosystem II, light-harvesting antennae, non-photochemical quenching, ultracentrifugation, electrophoretic separation, cryogenic electron microscopy
Number of pages:	80
Language:	English

Annotation: This dissertation thesis is divided into four main sections. The first focuses on a brief and general overview of photosynthesis with the main focus on the Norway spruce. The main aim of this section is to familiarise the reader with the current knowledge of spruce photosynthetic apparatus and its related functional properties. The motivation behind the detailed study is primarily the importance of spruce as a significant contributor to global oxygen production and secondary its uniqueness as an evergreen plant with the ability to withstand harsh environmental conditions, precisely the combination of freezing temperatures with simultaneous high light radiation during winter. The second section builds on the current knowledge and continues with a description of the spruce research conducted by our group with my contribution. The primary justification for our research performed on spruce is followed by a clarification of the achieved progress in this area. It is enclosed with a summary and future perspectives. While my primary focus is on structural analysis of the unique photosystem II of spruce obtained by cryogenic electron microscopy, the related research focuses on (i) determining the origin of spruce's modified PSII shape by analysing specific Arabidopsis knock-out mutants, (ii) formation of PSII supercomplexes and megacomplexes in spruce, and (iii) its acclimation to long-term light intensity changes. The third and fourth sections focus on (i) a general description of the experimental methods performed in our research on the spruce and (ii) their optimisation. Since I have built on previous research carried out in our group, I did not intend to explain in detail the methods used. Instead, I have concentrated on the optimisation of these methods involving two main issues. The first part focuses on the optimisation of solubilisation conditions and separation methods for isolated thylakoid membranes. The second part of the optimisation deals with setting the ideal conditions for the extraction of fragile protein complexes, such as the photosystem I supercomplex binding two LHCII trimers from spruce.

Bibliografická identifikácia

Meno a priezvisko autora:	Monika Opatíková
Názov dizertačnej práce:	Štruktúrna a funkčná analýza fotosyntetického aparátu Smreku obyčajného
Študijný odbor:	Biofyzika
Rok obhajoby:	2023
Vedúci práce:	RNDr. Roman Kouřil, Ph.D.
Kľúčové slová:	Smrek obyčajný, fotosystém II, svetlo-zberné antény, nefotochemické zhášanie, ultracentrifugácia, elektroforetická separácia, kryogénna elektrónová mikroskopia
Počet strán:	80
Jazyk práce:	Angličtina

Anotácia: Táto dizertačná práca je rozdelená do štyroch hlavných sekcií. Prvá sekcia je zameraná na stručný a všeobecný prehľad fotosyntézy so zameraním na Smrek obyčajný. Cieľom tohto prehľadu je oboznámiť čitateľa s aktuálnymi poznatkami o fotosyntetickom aparáte smreku a jeho súvisiacou funkciu. Motiváciou k výskum fotosyntézy u smreku je na jednej strane jeho signifikantný príspevok ku globálnej produkcii kyslíku, na strane druhej jeho unikátnosť ako evergreenu, ktorý je schopný prežiť nepriaznivé environmentálne podmienky, konkrétne kombináciu mrznúcich teplôt a intenzívneho osvetlenia v priebehu zimy. Druhá sekcia nadväzuje na aktuálne poznatky o smreku a pokračuje výskumom prevedeným v rámci našej skupiny súčasne zahŕňajúc môj príspevok. Táto sekcia začína odôvodnením nášho zamerania sa na špecifickú oblasť fotosyntetického výskumu u smreku, pokračuje vysvetlením dosiahnutého pokroku v danej oblasti a je ukončená krátkym zhrnutím a vyhliadkami do budúcna. Popri primárnom výskume unikátnej štruktúry fotosystému II u smreku získanej pomocou kryogénnej elektrónovej mikroskopie, je v tejto sekcii predstavený aj súvisiaci výskum, zameraný na (i) hľadanie pôvodu pozmenenej štruktúry PSII u smreku s využitím "knock-out" mutantov Arabidopsis, (ii) tvorbu superkomplexov a megakomplexov PSII u smreku a (iii) aklimačné štúdie zamerané na efekt pôsobenia dlhodobých zmien vo svetelnej intenzite. Tretia a štvrtá sekcia sa zameriavajú na (a) všeobecný a stručný popis experimentálnych metód, ktoré boli prevedené výlučne mnou a (b) ich optimalizáciu. Z dôvodu nadväznosti na predchádzajúci výskum na našom pracovisku nebolo mojim zámerom dopodrobna vysvetliť použité metódy. Namiesto toho som sa zamerala na detailný popis optimalizácie dvoch konkrétnych metód. Prvá časť sa zameriava na optimalizáciu podmienok solubilizácie a separačných metód pre izolované tylakoidné membrány. Druhá čas optimalizácie sa zaoberá vytvorením ideálnych podmienok pre extrakciou labilných proteínových komplexov, ako je napríklad superkomplex fotosystému I s dvoma naviazanými LHCII trimermi u smreku.

Declaration

I hereby declare that this Ph.D. thesis is my original work written based on my experiments performed during my doctoral study with the guidance of my supervisor RNDr. Roman Kouřil, Ph.D. The detailed list of all other sources of information used to complete the thesis is given in the Section References.

Signature:

Date and Place:

Acknowledgement:

Dear reader, thank You for finding time to read my thesis…

To begin with, my deepest gratitude belongs to the people, who gave me the opportunity to realise this goal for me, specifically my supervisor Dr. Roman Kouřil and the head of the Department of Biophysics, Prof. Peter Ilík. I would also like to include here all the people from our department who supported me throughout the entire journey, whether by helping me with the experiments, making me laugh, giving me free, invaluable, and many times unasked advice or just by saying: "Everything will be OK, just give it time and another try! Now, let's go grab some coffee!" You know, who you are, as you have already heard my thanks in person.

To continue, I would like to thank Prof. Eva-Mari Aro, for accepting me for my internship and letting me "sneak peek" into her working group. The truth is that in addition to the helpful work-related advice I received, there was such a warm welcome and acceptance, for which I will always be grateful. To be precise, Stephen, Vipu, Mika, Tapio and Sana … one big "Thank You" from me. Moreover, Vipu, thank you for introducing me to a different method of gradient preparation, because you practically set my experiments on the right pathway.

And finally, I would like to express my gratitude to all the people outside the work who took their time to listen and comfort me when I was down, stressed and unpleasant, but still, they did not give up on me. To the people, who forced me out of my comfort zone just to show me that there is a world out there, and to those who deliberately decided to stay in my life, because they think I am worth it. I hope I won't let you down. My family, my friends ... Thank You.

This work was supported by the Grant Agency of the Czech Republic (GAČR) project "Role proteinu Lhcb8 v organizaci a funkci světlosběrného komplexu fotosystému II rostlin" (no. 21-05497S) and the European Regional Development Fund (ERDF) project "Plants as a tool for sustainable global development" (no. CZ.02.1.01/0.0/0.0/16_019/0000827).

List of Publications

Opatíková M., Semchonok, D.A., Kopečný D., Ilík P., Pospíšil P., Ilíková I., Roudnický P., Zeljković S.Ć., Tarkowski P., Kyrilis F.L., Hamdi F., Kastritis P.L., Kouřil R. (2023) Cryo-EM structure of plant photosystem II supercomplex with light-harvesting protein LHCB8 and α-tocopherol. *Nat. Plants* (in press) IF(2022): 18.0 (Opatíková M *designed the experiments, prepared samples for all experiments, optimised separation on sucrose gradient to achieve a sufficiently high concentrated sample of photosystem II supercomplex for cryo-EM, partially analysed and interpreted data and prepared the article.*)

Štroch M., Karlický V., Ilík P., Ilíková I., **Opatíková M.**, Nosek L., Pospíšil P., Svrčková M., Rác M., Roudnický P., Zdráhal Z., Špunda V., Kouřil R. (2022) Spruce versus Arabidopsis: different strategies of photosynthetic acclimation to light intensity change. *Photosynth. Res.* **154**, 21–40. IF(2022): 3.7 (Opatíková M *performed a biochemical analysis of Arabidopsis thaliana and Norway spruce seedlings including isolation of thylakoid membranes and its optimisation together with preliminary biochemical experiments, which were not included in this publication.*)

Ilíková I., Ilík P., **Opatíková M.**, Arshad R., Nosek L., Karlický V., Kučerová Z., Roudnický P., Pospíšil P., Lazár D., Bartoš J., Kouřil R. (2021) Towards spruce-type photosystem II supercomplex: consequences of the loss of LHCB3 and LHCB6 in Arabidopsis. *Plant Physiol.* **187**, 2691–2715. IF(2021): 8.005 (Opatíková M *performed a biochemical analysis of Arabidopsis thaliana mutants including isolation of thylakoid membranes, optimisation of conditions for solubilisation and electrophoretic separation of protein complexes, isolation of proteins and subsequent western blot analysis, preparation of samples for transmission electron microscopy, data collection and analysis.*)

Kouřil R., Nosek L., **Opatíková M.**, Arshad R., Semchonok D.A., Chamrád I., Lenobel R., Boekema E.J., Ilík P. (2020) Unique organization of photosystem II supercomplexes and megacomplexes in Norway spruce. *Plant J.* **104**, 215–225. IF(2020): 6.486 (Opatíková M *performed a biochemical analysis of Norway spruce and Scots pine, including isolation of thylakoid membranes, optimisation of conditions for solubilisation and electrophoretic separation, preparation of samples for transmission electron microscopy, data collection and analysis.*)

Abbreviations:

$^1O_2$	singlet oxygen
2D-SDS-PAGE	two-dimensional sodium dodecyl sulphate polyacrylamide gel electrophoresis
ACA	aminocaproic acid
AEF	alternative electron flow
At	*Arabidopsis thaliana*
ATP	adenosine triphosphate
BN-PAGE	blue-native polyacrylamide gel electrophoresis
C_2	dimeric core of photosystem II
cc	core complex
CET	cyclic electron transport
CMC	critical micelle concentration
CN-PAGE	clear-native polyacrylamide gel electrophoresis
Cr	*Chlamydomonas reinhardtii*
EM	electron microscopy
Cyt_{b6f}	cytochrome b6/f complex
ETC	electron transport chain
Fd	ferredoxin
FDP	C-class of flavodiiron protein
FNR	Fd-$NAD(P)^+$-reductase
F_V/F_M	maximum quantum efficiency of the photochemistry of photosystem II for dark-adapted state
HL	high light
Chl	chlorophyll
LET	linear electron transport
LHCI	light-harvesting complex of photosystem I
LHCII	light-harvesting complex of photosystem II
LL	low light
L-LHCII	loosely bound light-harvesting antenna of photosystem II
$NAD(P)^+$/NAD(P)H	oxidised/reduced nicotinamide adenine dinucleotide (phosphate)
NDH-like	NAD(P)H dehydrogenase-like
NPQ	non-photochemical chlorophyll fluorescence quenching parameter
mc/mcs	megacomplex/megacomplexes
M-LHCII	moderately bound light-harvesting antenna of photosystem II
OEC	oxygen evolving complex
P680	summary labelling group of chlorophylls representing primary electron donor in PSII
P700	summary labelling group of chlorophylls representing primary electron donor in PSI
PC	plastocyanin
Pp	*Physcomitrella patens*
PQ	plastoquinone (oxidised)
PQH_2	plastoquinol (reduced and protonated plastoquinone)
PGR5/PGRL1	PROTON GRADIENT REGULATION 5 PROTEIN/PROTON GRADIENT REGULATION-LIKE 1 PROTEIN
PSI	photosystem I
PSII	photosystem II
Q_A	first quinone in photosystem II, quinone A
Q_B	second quinone in photosystem II, quinone B

qE	regulating energy dependent non-photochemical quenching of chlorophyll fluorescence
RC	reaction centre
ROS	reactive oxygen species
sc/scs	supercomplex/supercomplexes
S-LHCII	strongly bound light-harvesting antenna of photosystem II
SMA	styrene maleic acid
S-NPQ	sustained non-photochemical quenching of chlorophyll fluorescence
SPA	single particle analysis
STN7/STT7	serine/threonine-protein STATE TRANSITION 7 kinase/orthologue of serine/threonine-protein STATE TRANSITION 7 kinase in green algae
STN8	serine/threonine-protein STATE TRANSITION 8 kinase
TEM	transmission electron microscopy
X-ray	Röntgen crystallography
Y(II)	effective quantum yield of PSII photochemistry in light-adapted state
Y(NO)	quantum yield of constitutive non-regulatory energy dissipation of photosystem II in light-adapted state
Y_Z	tyrosine Z
Zm	*Zea mays*
α DDM	n-Dodecyl-α-D-Maltopyranoside
β DDM	n-Dodecyl-β-D-Maltopyranoside
α-Toc/α-TQ	α-tocopherol/α-tocopherolquinone
ΔpH	difference of pH across the thylakoid membrane
Δψ	difference of electric potential across thylakoid membrane; the membrane potential

General formatting (excluding subunits of photosystems):

PROTEIN
GENE
gene mutant

1. Norway spruce in the headlights of the photosynthesis research

Norway spruce (*Picea abies* (L.) H. Karst.) (hereafter spruce) is an evergreen conifer with global distribution, but especially a dominant plant of the boreal forests together with the Scots pine (*Pinus sylvestris* L.) (hereafter pine). Boreal forests have an important role as carbon sinks responsible for nearly one-third of the global carbon uptake (Pan *et al.*, 2011; Shorohova *et al.*, 2011; Gauthier *et al.*, 2015). They are significant producers of breathable oxygen and contribute to reducing the harmful effects of greenhouse gases. Somewhat unique among land plants, conifers can simultaneously withstand harsh environmental conditions, explicitly freezing temperatures, in parallel with high irradiance (Nystedt *et al.*, 2013). This combination poses a severe complication for the smooth running of photosynthesis, as the absorbed light energy cannot be adequately utilised. At the same time, the photosynthetic apparatus is concurrently affected by low temperature, which inhibits the activity of essential photosynthetic enzymes. Without any photoprotective mechanisms, this would undoubtedly lead to severe photodamage of the individual components of the photosynthetic apparatus and the uncoupling of the entire electron transport chain (ETC), as the excess energy would lack any safety valve for its release (Öquist and Huner, 2003). In order to minimise the effect of these unfavourable conditions, the evolution of spruce has led to the development of various photoprotective mechanisms. These mechanisms, specifically those observed only in evergreens such as spruce, and their regulations are subject of intensive studies (see, e.g. Grebe *et al.*, 2020; Yang *et al.*, 2020). The specific focus is on the mechanism of evergreens' acclimation to these specific environmental conditions by alternating between periods of active growth during long warm summer days and periods of forced dormancy during short winter days with freezing temperatures (Öquist and Huner, 2003; Ensminger *et al.*, 2006).

From an evolutionary point of view, spruce belongs to the gymnosperm genera *Picea* (family *Pinaceae*) and represents one of the intermediate stages between green algae, representatives of aquatic photosynthetic organisms, and angiosperm, the last stage of evolution of land plants. As water and land represent incomparable environmental niches, the life strategies of these photosynthetic organisms are expected to differ significantly, with implications for the functioning and efficiency of photosynthesis itself.

The main focus of my work was the structural analysis of the photosynthetic apparatus of spruce, specifically its photosystem II (PSII) and optimisation of the sample preparation for this analysis. My work included identifying the detailed composition of PSII in spruce, determining its variability compared to its counterparts in other plant species, and putting all the obtained knowledge into the context of its functional specification. Optimisation of sample preparation focused on getting high yields of homogeneous and concentrated sample for cryogenic electron microscopy (cryo-EM) and extraction of fragile protein supercomplex (sc) from thylakoid membranes. Nevertheless, I consider it appropriate to first provide the reader with a brief introduction to photosynthesis and a comprehensive picture of photosynthesis research performed on spruce, before continuing with the section about my research. Since several important studies on spruce are quite extensive, I have devoted an entire subsection to them so they are not omitted. Those include (i) the evolutionary loss of LHCB3 and LHCB6 proteins (as a subsection of the structural characteristic of the light-harvesting complex of PSII (LHCII)), (ii) sustained non-photochemical quenching of chlorophyll fluorescence (S-NPQ) and reactivation of photosynthesis in overwintering evergreens (as a subsection of ETC regulation) and (iii) chlorophyll (Chl) synthesis in the darkness (as a subsection of functional properties of ETC).

1.1. Brief introduction to photosynthesis

Photosynthesis is undoubtedly one of the most important processes necessary to sustain life on the planet. Across photosynthetic organisms, from the first photosynthesising cyanobacteria up to more complex vascular plants, we can study this process, which may vary in some details from organism to organism because it has evolved in parallel with the evolution of plants. This unique mechanism combines biophysical and biochemical processes, in which light energy is used to fix CO_2 into organic molecules, with oxygen produced as a by-product. It should be noted that in addition to the typical oxygenic photosynthesis mentioned above, there are several organisms, e.g. sulphur bacteria that use anoxygenic photosynthesis instead. These organisms use a broad range of either organic or inorganic electron donors for fixation CO_2 and produce sulphur compounds instead of oxygen (see e. g. Ke, 2001; Raymond and Blankenship, 2004; George *et al.*, 2020).

It is necessary to emphasise that the generally known strict division of photosynthesis into two parts, primary and secondary phases, is inaccurate, since all biophysical and biochemical processes are interconnected and interdependent at a lower or higher level. Thus, we can only speak of hypothetical division, where the function of the first part is (i) light harvesting, (ii) use of this energy to excite Chl molecules leading to primary charge separation in the PSII and photosystem I (PSI) reaction centres (RC), (iii) splitting water molecules into electrons, oxygen and protons leading to acidification of chloroplast lumen and (iv) generating proton motive force across the thylakoid membrane used in the subsequent ATP production, while (v) the transported electrons are used to reduce $NAD(P)^+$ to NAD(P)H. The second phase, the Calvin-Benson-Bassham cycle, uses the products of the first phase, i.e. NAD(P)H and ATP to incorporate atmospheric CO_2 into carbohydrates (Johnson, 2016; Stirbet *et al.*, 2020). To avoid the misinterpretation that often arises from the summary equation of photosynthesis, it must be emphasised that the released oxygen originates in water and that CO_2 is not directly incorporated into the sugar hexose, but is fixed in a stepwise process (see, e.g. Poolman and Fell, 2000; Anderson and Backlund, 2008).

With the detailed functional and structural characterisation of the main components of the electron transfer pathway involved in the first phase of photosynthesis, we can understand in depth their individual significance, specific function and contribution to the overall process. These include the four main protein complexes, namely PSI, PSII, cytochrome b6/f (Cyt_{b6f}) and ATP synthase, all embedded in the thylakoid membrane (Dekker and Van Grondelle, 2000; Nelson and Yocum, 2006).

1.2. Photosystem I and photosystem II in structural detail

In the last decades, the structures of PSI and PSII originally obtained from Röntgen crystallography (X-ray) and 2D single particle analysis (SPA) from lower resolution transmission electron microscopy (TEM) images have been gradually replaced by more detailed cryo-EM data with near-atomic resolution. These high-resolution PSI and PSII structures are currently known for several representatives of angiosperms (see, e.g. Wei *et al.*, 2016; Su *et al.*, 2017; van Bezouwen *et al.*, 2017; Graça *et al.*, 2021; Su *et al.*, 2022), green and red algae (see, e.g. Shen *et al.*, 2019; Sheng *et al.*, 2019; Suga *et al.*, 2019; Huang *et al.*, 2021; Naschberger *et al.*, 2022; You *et al.*, 2023), diatoms (see, e.g. Xu *et al.*, 2020; Nagao *et al.*, 2022) and cyanobacteria (see, e.g. Gisriel *et al.*, 2022; Semchonok *et al.*, 2022).

In addition to improvements in structural analysis methods due to significant advances in technology, this breakthrough would be unreachable without simultaneous detailed biochemical analysis of the genome, transcriptome and proteome of the organisms. This

knowledge serves as a basis for the aforementioned structural analysis, specifically for data processing. Regarding spruce, significant progress in deepening the knowledge of its photosynthetic apparatus has been made by the thorough analysis of its protein composition by mass spectrometry by Grebe *et al.* (2019). Their work builds on the extensive work of Nystedt *et al.* (2013) focused on the analysis of the spruce genome. Revealing the specific composition of thylakoid membrane proteins of spruce has led to a detailed characterisation of its photosynthetic apparatus and allowed a broader understanding of its function.

As one of the main objectives of my PhD study was the structural analysis of the photosynthetic apparatus of spruce using single particle EM, I devoted the following subsections to a detailed description of the structural attributes of both photosystems, with a primary focus on PSII. Further on, the main focus is on eukaryotic organisms. Any mention of cyanobacteria is for comparison purposes only.

1.2.1. Photosystem I core complex (PSI cc)

PSI is a pigment-binding multi-protein sc embedded in the thylakoid membrane of chloroplasts with the ability to process solar energy into energy of chemical bonds with a near-maximum quantum efficiency (Nelson, 2009; Croce and van Amerongen, 2013). In higher plants, the PSI is exclusively localised at the periphery of grana stacks, in grana margins, and stromal lamellae. The reason for this distribution is a spatial restriction of the "bulky" PSI with its stromal subunits (PsaC, D, E), due to which it cannot fit into appressed grana. Functional benefits of this arrangement can be summarised in two main points. Firstly, the localisation of PSI on the periphery allows its reversible interaction with the NAD(P)H dehydrogenase-like (NDH-like) complex or PROTON GRADIENT REGULATION 5 PROTEIN/PROTON GRADIENT REGULATION-LIKE 1 PROTEIN (PGR5/PGRL1) (see, e.g. Yamori and Shikanai, 2016; Ma *et al.*, 2021). Secondly, the lateral heterogeneity of the thylakoid membrane and its flexibility provides a plant with an additional source for the potential regulation of its ETC (Mullineaux, 2008; Kirchhoff *et al.*, 2011).

PSI cc of green algae, mosses and land plants is mostly conserved, consisting of 12 stably bound subunits (PsaA–PsaL) and additional four subunits with (i) either weak binding on the lumenal side (PsaN) (He and Malkin, 1992), (ii) subunit creating a docking site for LHCII after binding to PSI, PsaO (Pan *et al.*, 2018), (iii) predicted PsaP subunit with unknown position, or (iv) subunit with unclear function PsaR (Mazor *et al.*, 2015, 2017). PsaA and PsaB subunits form a heterodimer and represent the RC binding overall ~ 85 Chl *a* molecules, 2 phylloquinones and a Fe_4S_4 cluster (Pan *et al.*, 2018; Huang *et al.*, 2021; Shen *et al.*, 2022; Su *et al.*, 2022), while the function of the remaining subunits is assigned as follows: i) PsaC–PsaE – ferredoxin (Fd) binding, with the primary function of PsaC, as a mediator of F_A and F_B (two Fe_4-S_4 clusters) binding, ii) PsaF – plastocyanin (PC) binding, iii) PsaF, PsaG, PsaJ, PsaK – LHCA proteins binding, iv) PsaH, PsaI, PsaL, PsaO – LHCII binding (Nelson and Ben-Shem, 2004; Gorski *et al.*, 2022). The PsaG, PsaH, PsaO and PsaN subunits are not present in cyanobacteria (Caspy and Nelson, 2018) and are considered to be gained during evolution. However, due to gradual evolution, there are organisms with part of the subunits already evolved while lacking the remaining ones. This phenomenon was observed, e.g. in the green alga *Dunaliella salina*, which poses the PsaG, PsaH and PsaO subunits, while it lacks the PsaN subunit (Caspy *et al.*, 2020). Oppositely, PsaM represents a subunit, which was lost during evolution. This subunit was lost in green algae up to the higher plants (Nelson and Junge, 2015, Qin *et al.*, 2019), with only one known exception of its presence in the moss *Physcomitrella patens* (*Pp*) (Gorski *et al.*, 2022). For the detailed structural composition of the PSI sc, including individual subunits and contained pigments, see Tab. 1.

Table 1: Subunit compositions and identified pigments in the most complete cryo-EM structures of PSI-LHCI supercomplex from different plant species.

	Subunits	*Chlamydomonas reinhardtii* 7D0J			*Zea mays* 5ZJI		
PSI cc	PsaA	✓	45 Chl *a*	6 β-car	✓	45 Chl *a*	6 β-car
	PsaB	✓	40 Chl *a*	7 β-car	✓	40 Chl *a*	7 β-car
	PsaC	✓			✓		
	PsaD	✓			✓		
	PsaE	✓			✓		
	PsaF	✓	3 Chl *a*	1 β-car	✓	3 Chl *a*	1 β-car
	PsaG	✓	**2 Chl *a***	1 β-car	✓	3 Chl *a*	1 β-car
	PsaH	✓	**3 Chl *a***	**1 β-car**	✓	1 Chl *a*	
	PsaI	✓		1 β-car	✓		1 β-car
	PsaJ	✓	1 Chl *a*	1 β-car	✓	1 Chl *a*	1 β-car
	PsaK	✓	4 Chl *a*	2 β-car	✓	4 Chl *a*	2 β-car
	PsaL	✓	**4 Chl a**	3 β-car	✓	3 Chl *a*	3 β-car
	PsaN	-			✓	2 Chl *a*	
	PsaO	✓	**3 Chl *a***	**2 β-car**	✓	2 Chl *a*	
LHCI	LHCA1 (isoform a/b for *Cr*)	✓	12/12 Chl *a* 2/2 Chl *b*	3/3 Lut	✓	12 Chl *a* 2 Chl *b*	2 Lut 1 Vio 1 β-car
	LHCA2	✓	13 Chl *a*	2 Lut 1 β-car	✓	9 Chl *a* 5 Chl *b*	1 Lut 1 β-car 1 Vio
	LHCA3	✓	13 Chl *a* 1 Chl *b*	2 Lut 3 β-car	✓	12 Chl *a* 1 Chl *b*	1 Lut 1 β-car 1 Vio
	LHCA4	✓	11 Chl *a* 4 Chl *b*	2 Lut 1 β-car	✓	11 Chl *a* 4 Chl *b*	1 Lut 1 β-car 1 Vio
	LHCA5	✓	14 Chl *a* 3 Chl *b*	2 Lut 2 β-car	-		
	LHCA6	✓	13 Chl *a* 4 Chl *b*	2 Lut 2 β-car	-		
	LHCA7	✓	14 Chl *a* 1 Chl *b*	2 Lut 2 β-car	-		
	LHCA8	✓	13 Chl *a* 1 Chl *b*	2 Lut 1 β-car	-		
	LHCA9	✓	8 Chl *a* 2 Chl *b*	2 Lut	-		
SUM			248	59		160	35

Structures of PSI scs from *Chlamydomonas reinhardtii* (Huang *et al.*, 2021) and *Zea mays* (Pan *et al.*, 2018), excluding lipids and other ions or molecules. *Abbreviations: LHCI - light-harvesting complex of photosystem I, β-car - β-carotene, Chl (a/b) - chlorophyll a/b, Lut - lutein, Vio - violaxanthin, subunit presence (✓) and absence (-) in the structure. The four-letter code below the name of the organism represents the PDB identifier of the structure. Differences observed between structures in their PSI cc, either in the means of the presence/absence of the specific subunit or the presence/absence of different number of identified cofactors are highlighted. Differences in LHCAs were not highlighted, because their presence/absence in given PSI sc is species dependent.*

1.2.2. Light-harvesting complex of photosystem I (LHCI)

Higher variability within PSI in the plant kingdom originates in the structure and organisation of the LHCI complex, which is responsible for the increase in its light-harvesting capacity due to the bound pigments (for detailed pigment composition of LHCI see Tab. 1).

In vascular plants, LHCI is represented by LHCA1–6 proteins, the latter two of which are sub-stoichiometrically abundant. With some exceptions, the *LHCA1–4* are comparably expressed in land plants and the encoded antennae bind to the PSI cc at specific positions in a "belt-like" nature as heterodimers, specifically (i) the LHCA1/4 dimer interacts with the core via PsaG, PsaB (LHCA1) and PsaF subunits (LHCA4) and (ii) the LHCA2/3 dimer binds to the core via the PsaA, PsaJ (LHCA2) and PsaA, PsaK subunits (LHCA3), respectively (see, e.g. Jansson *et al.*, 1996; Ben-Shem *et al.*, 2003; Mazor *et al.*, 2015; Pan *et al.*, 2018; Shen *et al.*, 2019; Su *et al.*, 2022). Studies on mutants have revealed that LHCA1–3, highly conserved from green algae to vascular plants, are mutually irreplaceable, even by other LHCAs. However, the absence of LHCA4 can be complemented by other LHCAs. In vascular plants, its substitution was confirmed by LHCA5 (Storf *et al.*, 2005; Wientjes *et al.*, 2009). In the moss *Pp*, the absence of LHCA4 is the result of evolutionary loss (Alboresi *et al.*, 2008) and is substituted by the LHCA2 isoform (Gorski *et al.*, 2022). The LHCA5 and LHCA6 are present in almost all angiosperms with a few exceptions, and while LHCA5 is present in most gymnosperms, LHCA6 is specific for angiosperms only (for detailed overview, see Grebe *et al.*, 2019). The importance of these two proteins lies in the mediating of the NDH-like binding to PSI (Peng *et al.*, 2009) and their absence in spruce is thus consistent with its simultaneous loss of plastid genes encoding NDH-like (Nystedt *et al.*, 2013; Grebe *et al.*, 2019). More information about the loss of *NDH-like* in spruce is in the following sections.

In the green algae, characterised by a broader variety of LHCI isoforms (designated either as LHCA1–10 or LHCA a–j), PSI binds two LHCI semi-rings and forms a two-layered belt on the PsaF–G and Psa J–K side of PSI, plus a contingent LHCs dimer bound opposite the main semi-rings on the PsaB-H-I-M side (Qin *et al.*, 2019). See the structure from pea and green algae *Cr* in Fig. 1.

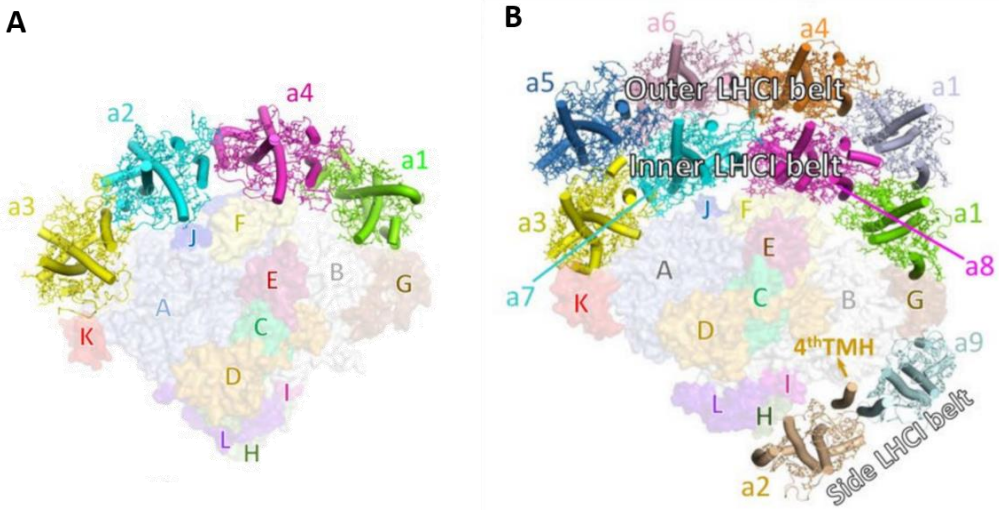

Figure 1: Structure of PSI-LHCI supercomplex from *Pisum sativum* and *Chlamydomonas reinhardtii*. Stromal view of PSI scs from pea (A) and *Cr* (B), the core subunits are represented as surface areas with single-letter designations. LHCA antennae with their assignment are visualised as cartoon with pigments and other cofactors in the form of sticks. Adapted from Shang *et al*. (2023), original structure of pea from Mazor *et al*. (2015) (PDB identifier: 4Y28) and *Cr* from Su *et al*. (2019) (PDB identifier: 6IJO).

1.2.3. Functional PSI assemblies

In addition to the typical monomeric form, PSI scs can form larger assemblies.

(I) PSI-PSI$_{(n)}$ assemblies are characteristic for (i) cyanobacteria, in which they can form oligomers, as dimers, trimers or tetramers (Malavath *et al.*, 2018; Semchonok *et al.*, 2021; Cao *et al.*, 2022) characterised by the predominant formation of trimers with typical symmetry and interaction via PsaL subunit (Jordan *et al.*, 2001), or (ii) for green algae, where their presence in dimeric form was confirmed (Naschberger *et al.*, 2022).

However, the PSI oligomers observed in vascular plants appeared to be only an artificial result of the PSI scs tendency to mutually associate, since they are no longer comprised in an overcrowded membrane (Boekema *et al.*, 1987; Chitnis and Chitnis, 1993; Boekema *et al.*, 2001; Kouřil *et al.*, 2005b). Moreover, the oligomers typical for cyanobacteria cannot be formed in higher plants due to the additional PsaH subunit, which spatially blocks the access to the PsaL subunit (Ben-Shem *et al.*, 2003).

(II) PSI-NDH-like sc (PSI assembly with NAD(P)H dehydrogenase-like) is an essential component involved in one type of cyclic electron transport (CET) around PSI, which transports the electrons from reduced Fd via NDH-like back to plastoquinone (PQ) (Peng *et al.*, 2008, 2009; Kouřil *et al.*, 2014; Yadav *et al.*, 2017; Zhang *et al.*, 2020). Its activation has two main functions: i) it prevents over-reduction of stroma and ii) balances ATP/NAD(P)H production (Shikanai, 2014; Yamori and Shikanai, 2016; Shikanai, 2020). The recently obtained cryo-EM structures from barley (Shen *et al.*, 2022) and *Arabidopsis thaliana (At)* (Su *et al.*, 2022) characterise this complex in detail with one NDH-like protein and two attached PSI scs, confirming the previously proposed function of LHCA5 and LHCA6 as mediators and stabilisers of the NDH-like connection with PSI (Kouřil *et al.*, 2014; Otani *et al.*, 2018).

(III) PSI-Cyt$_{b6f}$ assembly was observed using TEM by Yadav *et al.* (2017), with its binding on the LHCA belt of PSI. Its function has been assigned to electron transport regulation due to the distance adjustment between its individual components (Yadav *et al.*, 2017) and has been hypothesised to undergo reversible phosphorylation during state transitions (Hamel *et al.*, 2000) with the effect on the CET initiation (Iwai *et al.*, 2010).

(IV) PSI-PSII assembly has been observed in higher plants such as spinach, *At* and rice, but not in the green algae. Their interactions, either via core or antennae, function as conductors of energy spillover from PSII to PSI, thus protecting the PSII (Kim *et al.*, 2023).

(V) PSI-LHCI-LHCII assembly is formed during the state transition (state 2) that serves as an equaliser of energy distribution between PSI and PSII in a case of their excitation imbalance caused by the variable quality and quantity of light in the natural environment (Allen, 2003). The different effect of light quality coincides with the different pigment composition of PSI and PSII and their related distinct absorption characteristics, with the absorption of PSI closer to far-red light and the absorption of PSII to red light (Rochaix, 2007; Minagawa, 2011). In general, in a state of light-induced over-reduction of the PQ pool, reduced plastoquinol (PQH_2) preferentially binds to the Qo site of Cyt$_{b6f}$, leading to a relative reduction imbalance between PSII and PSI. This leads to activation of the serine/threonine protein kinase STN7 (STT7: orthologue in green algae *Cr*), which is, besides the LHCB1 phosphorylation, responsible for phosphorylation of LHCB2 in LHCII trimers that subsequently bind to the PSI scs and effectively transfer the harvested energy to its cc (Depege *et al.*, 2003; Bellafiore *et al.*, 2005). Conversely, when the preferential excitation pressure on PSII dissipates, e.g. during high light (HL) or low light (LL) illumination, the STN7 kinase is inactivated due to the change in the redox state of thioredoxins, and the constitutively active serine/threonine protein THYLAKOID-ASSOCIATED PHOSPHATASE OF 38kDa/PROTEIN PHOSPHATASE 1 (TAP38/PPH1) dephosphorylates LHCIIs (LHCB1 and LHCB2), leading to uncoupling of

these LHCII trimers from PSI and their subsequent return to their initial position (state 1) (Rintamäki *et al.*, 2000; Pribil *et al.*, 2010; Shapiguzov *et al.*, 2010; Cariti *et al.*, 2020). It was confirmed that LHCII trimers with phosphorylated LHCB2 protein have a higher affinity to PSI than PSII and are able to bind via PsaO to the PSI (Lunde *et al.*, 2000; Galka *et al.*, 2012, Pan *et al.*, 2018).

The recently revealed high-resolution structures of this sc at 3.42 Å (Huang *et al.*, 2021) and at 2.84 Å (Pan *et al.*, 2021) resolution for *Cr* or at 3.3 Å resolution for *Zea mays* (*Zm*) (Pan *et al.*, 2018), provided necessary information about its structural and functional significance (see the structure of this sc in Fig. 2).

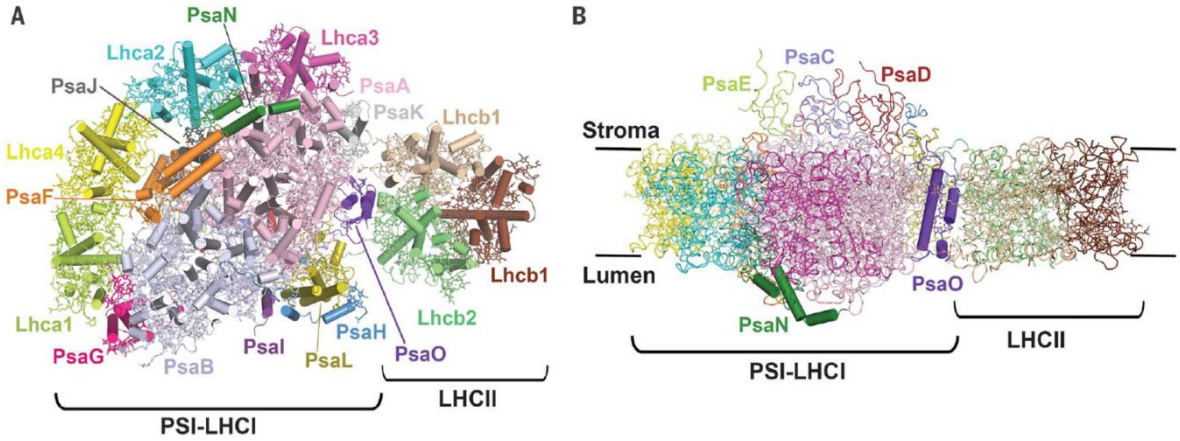

Figure 2: Structure of *Zea mays* PSI-LHCI-LHCII supercomplex obtained by cryo-EM at 3.3 Å resolution. (A) View from the lumenal side with assigned PSI cc and LHCA subunits, (B) Side view along the membrane plane. Adapted from Pan *et al.* (2018) (PDB identifier: 5ZJI).

A long discussion on the origin of phosphorylated LHCII trimers led to the conclusion that they represent either loosely bound LHCII (L-LHCII) (Galka *et al.*, 2012) or, most likely, originate from a pool of free LHCIIs (Wientjes *et al.*, 2013). These free LHCIIs are located near the grana margins, the target destination of phosphorylated LHCII trimers, where they bind to PSI-LHCI. Since these specific LHCII trimers involved in state transitions are more strongly bound to PSI than to PSII, the resulting excitation energy transfer from these additional trimers to PSI is more efficient compared to PSII, as was documented in independent studies (Galka *et al.*, 2012; Wientjes *et al.*, 2013; Le Quiniou *et al.*, 2015; Bos *et al.*, 2017).

However, the existence of a mutually shared L-LHCII system has also been proposed, where the function of state 2 is conditioned by forming a PSII-LHCII-PSI-LHCI sc in grana margins and the LHCII antennae are shared by both photosystems (Svensson and Albertsson, 1989; Benson *et al.*, 2015; Crepin and Caffarri, 2015; Grieco *et al.*, 2015; Suorsa *et al.*, 2015; Rantala *et al.*, 2017).

Recently, based on the results of physiological and biochemical studies (e.g. Akhtar *et al.*, 2016; Bressan *et al.*, 2018; Schiphorst *et al.*, 2022) and observed structures using single particle electron microscopy (EM) (e.g. Yadav *et al.*, 2017), the possibility of binding an additional, not necessarily phosphorylated LHCII trimer in vascular plants has opened up for a discussion. These conclusions were also led by analysis performed by Benson *et al.* (2015) on *At* and its mutants (*lhca1*, *lhca2*, *lhca3*, *lhca4*), which supported the assumption that the size of PSI antenna in the grana margins (*in vivo*) is definitely larger than that observed for isolated PSI-LHCI-LHCII (hereafter PSI-LHCII) and also demonstrated the importance of the LHCA belt for LHCII attachment.

However, confirming the existence of PSI with two bound LHCII trimers (PSI-LHCII$_2$) in vascular plants, as it is in green algae (Drop *et al.*, 2014b; Huang *et al.*, 2021), is challenging since PSI sc with one LHCII trimer is already quite fragile and difficult to obtain in sufficient quantities for structural studies. Logically, the implication of even less specific interaction of the second trimer based on the variety in its observed attachment position toward PSI would complicate its extraction. The situation is further complicated by the fact that the regulatory mechanisms of PSI-LHCII formation appear to be more complex than originally thought, rejecting the necessity of LHCII phosphorylation for its binding to PSI (see, e.g. Benson *et al.*, 2015; Chukhutsina *et al.*, 2020; Schiphorst *et al.*, 2022) or emphasising the presence of additional post-translational modifications, such as acetylation, that would regulate state transitions and influence PSI-LHCII sc formation (see, e.g. Koskela *et al.*, 2020). Combined with the hard-to-refute argument that the variable structures of PSI-LHCII$_2$ observed by EM by Yadav *et al.* (2017) could have been the result of post-elution artificial binding of free LHCIIs to PSI-LHCII, analogous to the formation of the aforementioned PSI oligomers in higher plants, their verification definitely requires more thorough studies. For a detailed discussion, see Section 4.

1.2.4. Photosystem II core complex (PSII cc)

PSII is a multi-subunit pigment-protein complex embedded in the thylakoid membrane. In higher plants characterised by lateral segregation of the membrane, PSII scs are localised in the appressed grana. PSII consists of (i) a dimeric core (C_2), including the RC with 35 molecules of Chl *a* and other redox cofactors (see Tab. 2, for better comparison already including spruce PSII structure, Opatíková *et al.*, 2023), (ii) LHCII, responsible for increasing the area for solar energy harvesting and its delivery to the core, and (iii) Oxygen Evolving Complex (OEC) (Minagawa and Takahashi, 2004; Dekker and Boekema, 2005; Caffarri *et al.*, 2009; Natali and Croce, 2015). In detail, the PSII cc includes a heterodimer composed of PsbA (D1) and PsbD (D2) proteins and, together with α and β subunit of cytochrome b559 (PsbE and PsbF, respectively), represents the RC of PSII, which binds other two Chl-binding inner antennae PsbB (CP47) and PsbC (CP43) (Nanba and Satoh, 1987; Webber *et al.*, 1989; Croce and van Amerongen, 2011). In addition, PSII cc binds the extrinsic subunits of the OEC on the lumenal side composed of PsbO, PsbP, PsbQ and PsbR. PsbO subunit is present in two isoforms, presumably possessing different functions, with the PsbO1 isoform responsible for stabilising PSII activity and the less abundant PsbO2 isoform contributing to the regulation of dephosphorylation and D1 subunit turnover in the PSII repair cycle (Lundin *et al.*, 2007). In addition to PsbO, other subunits encoded by two genes are PsbP and PsbQ (see review by Ifuku *et al.*, 2010). The rest of the PSII cc is represented by at least 11 small subunits with low molecular weight, namely PsbH–M, with assigned functions as follows: (i) PsbH is involved in antenna association, (ii) PsbJ and PsbK in core stabilisation, (iii) PsbL and PsbM in PSII dimerisation. Rest of the subunits is represented by (iv) PsbW, PsbX and PsbZ/Ycf9 functioning in antenna association and core stabilisation, (v) PsbTc involved in PSII dimerisation, (vi) PsbTn contributing to light acclimation, and (vii) PsbS, the structurally elusive subunit involved in thermal dissipation of absorbed light energy (Shi and Schroder, 2004; Müh *et al.*, 2008). In the structure of PSII from green alga *Chlamydomonas reinhardtii* (*Cr*), the presence of additional subunits of PSII cc was confirmed, including Psb30 (Ycf12) and two unidentified subunits designated as USP (unidentified stromal protein) and SLP (small lumenal protein also designated as Psb27) (Kashino *et al.*, 2007; Sheng *et al.*, 2019). The position of the PsbTn subunit, absent in red and green algae and evolutionary older organisms, was in *Cr* occupied by the aforementioned SLP with similar binding (Sheng *et al.*, 2019).

Table 2: Subunit compositions and identified pigments per one monomer in the most complete cryo-EM structures of PSII-LHCII supercomplex from different plant species.

	Subunits	*Pisum sativum* 5XNL $C_2S_2M_2$			*Chlamydomonas reinhardtii* 6KAC/6KAD $C_2S_2/C_2S_2M_2L_2$			*Picea abies* 8C29 C_2S_2		
PSII cc	PsbA (D1)	✓	4 Chl *a* 2 Pheo	1 β-car	✓	4 Chl *a* 2 Pheo	1 β-car	✓	4 Chl *a* 2 Pheo	1 β-car
	PsbB (CP47)	✓	16 Chl *a*	3 β-car	✓	16 Chl *a*	3 β-car	✓	16 Chl *a*	3 β-car
	PsbC (CP43)	✓	13 Chl *a*	4 β-car	✓	13 Chl *a*	4 β-car	✓	13 Chl *a*	4 β-car
	PsbD (D2)	✓	2 Chl *a*	1 β-car	✓	2 Chl *a*	1 β-car	✓	2 Chl *a*	1 β-car
	PsbE (α Cyt b_{559})	✓			✓			✓		
	PsbF (β Cyt b_{559})	✓			✓			✓		
	PsbH	✓		1 β-car	✓		1 β-car	✓		1 β-car
	PsbI	✓			✓			✓		
	PsbJ	✓			✓			-		
	PsbK	✓			✓			✓		
	PsbL	✓			✓			✓		
	PsbM	✓			✓			✓		
	PsbO	✓			✓			✓		
	PsbP	✓			✓/-			-		
	PsbQ	✓			✓/-			-		
	PsbR	-			✓/-			-		
	PsbX	✓			✓			✓		
	PsbZ	✓			✓			✓		
	PsbW	✓			✓			✓		
	Psb30 (Ycf12)	-			✓			✓		
	PsbTc	✓		**1 β-car**	✓			✓		
	PsbTn	-			-			✓		
	SLP (Psb27)	-			✓/-			-		
	USP	-			✓/-			-		
LHCII	**CP24** (LHCB6)	✓	6 Chl *a* 5 Chl *b*	1 β-car 1 Lut 1 Vio	-			-		
	CP26 (LHCB5)	✓	9 Chl *a* 4 Chl *b*	2 Lut 1 Neo	✓	**10 Chl *a*** 4 Chl *b*	2 Lut 1 Neo	✓	9 Chl *a* 4 Chl *b*	2 Lut 1 Neo
	CP29 (LHCB4/8)	✓	10 Chl *a* **4 Chl *b***	1 Lut 1 Neo 1 Vio	✓	**5**/10 Chl *a* 3 Chl *b*	**0**/1 Lut 1 Neo 1 Vio	✓	**9 Chl *a*** 3 Chl *b*	1 Lut 1 Neo 1 Vio
	S-trimer	✓	24 Chl *a* 18 Chl *b*	6 Lut 3 Neo 3 Vio	✓	24 Chl *a* 18 Chl *b*	6 Lut 3 Neo 3 Vio	✓	24 Chl *a* 18 Chl *b*	6 Lut 3 Neo 3 Vio
	M-trimer	✓	24 Chl *a* 18 Chl *b*	6 Lut 3 Neo 3 Vio	-/✓	24 Chl *a* **17 Chl *b***	6 Lut 3 Neo 3 Vio	-		
	L-trimer	-			-/✓	24 Chl *a* 16 Chl *b*	5 Lut 2 Neo 1 Vio	-		
SUM			159	44		101/187	27/48		104	28

Structures of PSII scs from pea (Su *et al.*, 2017), *Cr* (Sheng *et al.*, 2019) and spruce (Opatíková *et al.*, 2023), excluding lipids and other cofactors. *Abbreviations: Cyt b_{559} - cytochrome b559, β-car - β-carotene, Chl (a/b) - chlorophyll a/b, car - carotenoids, Pheo - pheophytin, Lut - lutein, Neo - neoxanthin, Vio - violaxanthin, subunit presence (✓) and absence (-) in the structure. For Cr, the composition of two independent structures was analysed at the same time and when the presence of a subunit or cofactor in them differs, the numbers or ✓ and - symbols are separated by "/". The four-letter code below the name of the organism represents the PDB identifier of the structure. Highlighted are differences observed between structures, either in the means of the presence/absence of the specific subunit or the presence/absence of a different number of identified cofactors.*

1.2.5. Light-harvesting complex of photosystem II (LHCII)

The peripheral LHCII is mostly conserved in gene coding across the land plants and green algae and we currently distinguish between nine LHCB proteins (1–9) based on their homology. In vascular plants, LHCIIs are represented by light-harvesting pigment-binding proteins that either form trimers (sub-classes LHCB1–3) or are present as monomeric antennae (LHCB4–6, also denoted according to their molecular weight CP29, CP26 and CP24, respectively) (For detailed pigment composition of LHCII see Tab. 2). Due to the absence of sequence motives used in vascular plants to distinguish major LHCB proteins, a different designation, namely LHCBMx, is used to distinguish them in the non-vascular plants *Chlorophyta*, *Marchantiophyta*, *Bryophyta* and *Anthocerotophyta* (x represents a progressive number (1–9) defining each isoform based on sequence similarity, M (major) representing the gene orthologues of *LHCB1* and *LHCB2* of land plants in the indicated divisions) (except in bryophyte for *LHCB3*). LHCBMx in *Cr* can be further divided into four types (I–IV) based on their sequence similarity (see, e.g. Crepin and Caffarri, 2018).

In addition to the specific sequence markers used for classification, the amino acid sequences of LHCB proteins often differ at several other sites, potentially affecting the final structure and function of a particular LHCB protein. This leads to a reasonably significant diversity within the LHCB protein family, which consists of different types and isoforms, also referred to as sub-isoforms.

Of the LHCB proteins, the LHCB4 protein is the most variable in its distribution between angiosperms and gymnosperms. The LHCB4 can be present in three isoforms (4.1, 4.2 and 4.3), with the first two sharing high sequence identity and similarity and containing longer C-terminus compared to the third isoform 4.3, also referred to as LHCB8 (Klimmek *et al.*, 2006; Grebe *et al.*, 2019). The occurrence of the first two isoforms, 4.1 and 4.2, is conserved in the angiosperms, whereas LHCB8 was confirmed to be present only in a few selected groups, for example, in family *Brassicaceae*, *Fabaceae*, *Cactaceae*, etc. (Alboresi *et al.*, 2008; Iwai and Yokono, 2017). In gymnosperms, the situation is even more complex, as there are groups with: i) only LHCB4 (*Cycadaceae*, *Zamiaceae*), ii) only LHCB8 (*Pinaceae*, *Gnetaceae*, *Welwitschiaceae*) and iii) both LHCB4 and LHCB8 (e.g. *Araucariaceae*, *Cupressaceae*), all with no apparent relationship to their evolutionary classification (for an overview, see Grebe *et al.*, 2019). While the C-terminus of LHCB4.1 and LHCB4.2, specifically their 15 amino-acid motif, is relatively conserved in length and sequence in the plant kingdom, this is not the case for LHCB8, which varies in both length and sequence (see Tab. 3 for a comparison of the sequences of LHCB4.1–4.3 and LHCB8 isoforms from different organisms). In a more detailed view, signs of conservation are only evident within individual orthologue groups (for specification, see Grebe *et al.*, 2019). The N-terminus of this protein is thought to participate in grana stacking by mediating interactions between

PSII scs from adjacent membranes (Albanese *et al.*, 2020). Since considerable sequence variability was observed at the mentioned N-terminus of LHCB8, this variability could also lead to different regulation and subsequent dynamics of grana stacking (Grebe, 2022).

Moreover, the abundance of specific isoforms of this monomeric antenna strongly depends on light conditions. The *LHCB4.1* and *LHCB4.2* isoforms, which are expressed under standard growing conditions, are substituted by the expressed *LHCB4.3* isoform under HL intensity, whose product is subsequently incorporated into the PSII structure (Klimmek *et al.*, 2006; Sawchuk *et al.*, 2008; Albanese *et al.*, 2016). In spruce, however, this position is known to be occupied exclusively by LHCB8 independently on the light conditions (Grebe *et al.*, 2019).

Table 3: Sequence alignment of different isoforms of Chl *a-b* binding protein LHCB4

```
                        10        20        30        40        50        60        70
                ....|....| ....|....| ....|....| ....|....| ....|....| ....|....| ....|....|
At LHCB4.1      1   ---MAATSAA AAAASSIMGT RVAPGIHPGS GRFTAVFG-- -FGKKKAAPK KSAKKTVTTD ----------  54
At LHCB4.2      1   ---......-T .......... ..VSD.SSN. S....R..-- -..T...S.. .--A...IS. ----------  51
At LHCB4.3      1   ---..T.T-- .....G.F.I .IQ-DPR..T ..VQ.R..FS -.....P..P PKKSRQ.QD. G---------  54
Ps LHCB4.3      1   ---------- ---------- ---------- ---------- ---------- ---------- ----------   1
Cr LHCB4.3      1   ---.VFKFPT PPGTQKKA.. TATKPAPKAT TKKV.TST-- --.TRSGGVG Y---RKYQG. ----------  50
Pa LHCB8        1   MASAT.A.SL .S.S..FFAG GQQLKAEKNV S.IY.R.SFS GLK..TK.VA .PKT.A.AKP KTKAVAKPKP  70

                        80        90       100       110       120       130       140
                ....|....| ....|....| ....|....| ....|....| ....|....| ....|....| ....|....|
At LHCB4.1      54  -------RPL WYPGAISPDW LDGSLVGDYG FDPFGLGKPA EYLQFDIDSL DQNLAKNLAG DVIGTRTEAA 117
At LHCB4.2      51  -------... .F...K..EY .......... .......... ......L... ........Y. E........V 114
At LHCB4.3      54  ------D.LV .F...NP.E. ....MI..R. .......... ....Y.F.G. .......V.. .I..IIQ.SS 118
Ps LHCB4.3      1   -------GLV .F...QP.E. ...TMI..R. ...L.FA... ......L... .......... ......V..G  63
Cr LHCB4.3      50  --------A. .L.NTTR.E. .....P..R. ...L..S..S .FVVIGV.EN ...A...NK. S.EAIVQATP 112
Pa LHCB8        71  KPRAPTG... .L...KA.E. .......... ...L.....S ....Y.V... ....DL..P. .LL.DFVGDP 140

                       150       160       170       180       190       200       210
                ....|....| ....|....| ....|....| ....|....| ....|....| ....|....| ....|....|
At LHCB4.1      118 DAKSTP--FQ PYSEVFGIQR FRECELIHGR WAMLATLGAL SVEWLTGVTW QDAGKVELVD GSSYLGQPLP 185
At LHCB4.2      115 .P....--.. .......L.. .......... ..........I T......... .......... .......... 182
At LHCB4.3      119 EI.P..--.. ..T....... .......... ....G....I A..A...IA. .........E .......... 186
Ps LHCB4.3      64  EV.P..--.. ........E. .......... ....GA.... A..AF...A. .........E .A..F.FS.. 131
Cr LHCB4.3      113 .EV.SENRLA .......LA. .......... .....C.... VA.AT...S. VE......-. .A..A.LS.. 181
Pa LHCB8        141 .I.PS---I. .......L.. .......... ....GV.... A..GF..IY. .........E ....F.FS.. 207

                       220       230       240       250       260       270       280
                ....|....| ....|....| ....|....| ....|....| ....|....| ....|....| ....|....|
At LHCB4.1      186 FSISTLIWIE VLVIGYIEFQ RNAELDSEKR LYPGGKFFDP LGLAA-DPEK TAQLQLAEIK HARLAMVAFL 254
At LHCB4.2      183 .......... .......... .......... .......... ....S-..V. K......... .......G.. 251
At LHCB4.3      187 ..LT...... ...V...... ..S...P... I....-Y... .....-.... LDT.K..... .S........ 254
Ps LHCB4.3      132 ..LTA..... .......... ......P... .......... ....N-...E KER..... .S.....V.. 200
Cr LHCB4.3      182 ...TQ..... .ILV.GA..Y ..S.TNP... C....-V... .K..SE.E.R AFR.KT.... .......S.F 250
Pa LHCB8        208 .NM....L.. ..LL..... ....V.P.T. ......Y... F...V-.EI. KDR.K..... .......... 276

                       290       300       310
                ....|....| ....|....| ....|....| ....|....
At LHCB4.1      255 GFAVQAAATG KGPLNNWATH LSDPLHTTII DTFSSS--- 290
At LHCB4.2      252 .......... .......... .......... .......--- 287
At LHCB4.3      255 I..L...F.. ...VS----- --------FL A..NN---- 276
Ps LHCB4.3      201 V..I...VS. ...IG----- --------F. A..NQ---- 222
Cr LHCB4.3      251 .YG...LS.. E.A.G----- ----SLAKFA .GLNNGKGL 280
Pa LHCB8        277 I..I...V.S ....T----- -------LFV EFLGKK--- 300
```

Multiple sequence alignment by ClustalW algorithm (scoring matrix BLOSUM62) of LHCB4.1–4.3/8 amino acid sequences from *Arabidopsis thaliana*, *Pisum sativum*, *Chlamydomonas reinhardtii* and *Picea abies*. Selected positions in the red rectangle represent a 15-amino-acid motif that is strictly conserved in LHCB4.1 and LHCB4.2 C-terminus (WxTHLxDPLHTTIxD; residues 271–285) and is absent in LHCB8 sequences. Source of sequences: UniProt for *At* (Q07473, Q9XF88, Q9S7W1), RCSB PDB for Pea (5XNL) and *Cr* (6KAC) and for *P. abies* database S254 (Grebe *et al.*, 2019). Amino acids identical to the reference sequence (first row) in specific positions of alignment are plotted as dots in the remaining sequences. *Abbreviations: At - Arabidopsis thaliana, Ps - Pisum sativum, Cr - Chlamydomonas reinhardtii, Pa - Picea abies.*

The LHCB1 and LHCB2 proteins also have different isoforms, when LHCB1 shows a higher variety with five isoforms, LHCB1_A1–A3 and LHCB1_B1–B2, compared to LHCB2 with four isoforms LHCB2_A1–A4, whereas LHCB3 and LHCB5 have only one isoform. However, it seems that isoforms LHCB2.3 and LHCB2.1 share the encoding gene and represent only different alleles (Jansson, 1999). Moreover, it should be emphasised that the molar ratio of these three major isoforms seems to correlate with the copy numbers of the genes encoding each isoform, and the ratio of LHCB1:LHCB2:LHCB3 in *At* was found to be 7:3:1 (Peter and Thornber, 1991; Galka *et al.*, 2012; Crepin and Caffarri, 2018). However, this ratio can fluctuate and is highly dependent on light conditions. These major LHCII proteins differ primarily by the amino acid sequence at the N-terminus, the composition of which has a significant impact on their function because it contains a reversibly phosphorylated threonine that is involved in transitions between states (Alboresi *et al.*, 2008; Goldschmidt-Clermont and Bassi, 2015; Iwai and Yokono, 2017; Crepin and Caffarri, 2018).

Moreover, in different organisms, the number of individual isoforms may vary; for example, the two isoforms of LHCB3 in the moss *Pp* (Alboresi *et al.*, 2008) or the additional isoform of LHCB2 confirmed in spruce (Grebe *et al.*, 2019). In addition, LHCB3, which is able to form only heterotrimers, is more divergent from LHCB1 and LHCB2 and shows different biochemical and spectroscopic attributes characteristic with the red-shift in its fluorescence emission (Caffarri *et al.*, 2004). The importance of the evolution of individual isoforms and their associated specific function is shown, for example, in the regulation of phosphorylation mentioned above. For instance, triple phosphorylation of the N-terminus is not possible in the LHCB1_B isoforms because they differ in the number of their serine and threonine residues, whereas this specific phosphorylation was observed in the LHCB1_A isoform. Thus, phosphorylation of particular isoforms has a specific impact, where in general summary (i) single phosphorylation of LHCB2 is associated with state transitions, (ii) single phosphorylation of LHCB1 leads to grana destacking, and (iii) triple phosphorylation of LHCB1 leads to destacking and concomitant linearisation of thylakoids, loss of lateral heterogeneity and increased PSII-PSI spillover (for a general overview see Grebe *et al.*, 2020).

As for LHCB3, its presence, together with the LHCB6 protein, is not uniform in photosynthetic organisms. It was considered an indisputable fact that land plants share high similarity not only within the PSII cc but even within light-harvesting complexes (Alboresi *et al.*, 2008). Surprisingly, this dogma turned out to be wrong, as the genera *Picea*, together with *Pinus* and *Gnetum*, were proved to lack the two antennae, LHCB3 and LHCB6, the evolutionarily youngest of LHCII (Kouřil *et al.*, 2016, Grebe *et al.*, 2019). These antennae, which are absent in green algae (Alboresi *et al.*, 2008) and present in angiosperms, are surprisingly also present in other gymnosperm species and even evolutionary older non-seed plants. The loss of *LHCB3* and *LHCB6* genes and its impact on the structure of PSII is discussed in detail in the following subsection.

Within the LHCB protein family, LHCB9 and LHCB7 are among the least studied. LHCB9 has only been detected in the moss *Pp* (Alboresi *et al.*, 2008; Grebe *et al.*, 2019), where it is part of the PSI antenna (Iwai *et al.*, 2018; Pinnola *et al.*, 2018; Zhang *et al.*, 2023). The function of LHCB7, along with its rare expression, remains a mystery (Klimmek *et al.*, 2006; Peterson and Schultes, 2014). However, it is hypothesised that this protein could affect RubisCO (ribulose-1,5-bisphosphate carboxylase/oxygenase) turnover, as has been shown in *lhcb7* mutants, along with lowering the plant irradiance threshold required for initiation of non-photochemical quenching of chlorophyll fluorescence (NPQ) (Ballottari *et al.*, 2012).

Moreover, additional variability of LHCIIs lies in their potential to form homo- or heterotrimers. To some extent, these trimers are composed of variable triplets of major LHCB1/2/3 and attach to PSII either directly or via minor monomeric antennae (Jansson, 1999; Jackowski *et al.*, 2001; Caffarri *et al.*, 2004). The association of LHCII trimers to the PSII cc is either (i) strong (S-LHCII) via LHCB4 and LHCB5, (ii) moderate (M-LHCII) via LHCB4/(LHCB6) (Dekker and Boekema, 2005; Caffarri *et al.*, 2009; Kouřil *et al.*, 2012, 2018; Caffarri *et al.*, 2014; Pagliano *et al.*, 2014), and (iii) occasionally loose (L-LHCII) without the participation of any monomeric antenna (Boekema *et al.*, 1999a, b; Dekker and Boekema, 2005). In the majority of studied land plants, S-trimer is formed by LHCB1 and LHCB2 in different ratios, whereas M-trimer is formed by LHCB1, 2 and 3, and L-trimer mainly composed of LHCB1, LHCB2 (Dainese and Bassi, 1991; Caffarri *et al.*, 2004, 2009; Rantala *et al.*, 2017; Su *et al.*, 2017; Crepin and Caffarri, 2018). The one copy of LHCB3 in M-trimer represents the interacting partner for LHCB6 and is thus responsible for its stable binding to C_2S_2 in *At*. This arrangement of antennae provides more flexible regulation of PSII antenna size in response to fluctuating light (Caffarri *et al.*, 2004; Kovács *et al.*, 2006; Caffarri *et al.*, 2009; Kouřil *et al.*, 2013; van Bezouwen *et al.*, 2017).

In greater detail, the size of the LHCII antenna, and thus its absorption cross-section, changes dynamically depending on the actual light conditions to which the photosynthetic organism is exposed. The ability to adjust the antennae size represents a highly efficient way for plants to dynamically adapt to the changes in light irradiance, either short- or long-term in their duration, and thus maintain optimal light energy utilisation while minimising potential photodamage (Bailey *et al.*, 2001; Ballottari *et al.*, 2007; Betterle *et al.*, 2009; Kouřil *et al.*, 2013; Albanese *et al.*, 2016; Bielczynski *et al.*, 2016). The aforementioned increased expression of the *LHCB4.3*, which product LHCB4.3 is characterised by a shorter C-terminus, is observed in land plants in response to HL. The LHCB4 C-terminus is involved in the LHCB6 binding to the PSII cc, thereby influencing the lateral organisation of PSII in the thylakoid membrane (Guardini *et al.*, 2022). Thus, the incorporation of LHCB4.3 to the prevalence of PSII scs leads to its weaker interaction with LHCB6 and its disconnection. In the absence of LHCB6, the M-trimer lacks an interacting partner and thus cannot bind to the PSII cc (de Bianchi *et al.*, 2011). For a structural detail of PSII sc, see Fig. 3.

It was presumed that even with a few differences in PSII structure within the plant kingdom, the fundamental patterns are preserved since they are essential for its function. However, significant differences in PSII composition and its arrangement were described. The aforementioned evolutionary loss of *LHCB3* and *LHCB6* genes did not restrict the M-trimer attachment to PSII cc as was expected based on the original assumption about their essentiality. Moreover, in the absence of LHCB3 and LHCB6, green algae are able to bind additional trimers besides M-trimer, specifically N-trimer (naked-LHCII), and the composition of their LHCII antennae differs from that observed in land plants. In addition, it was confirmed that several land plants are able to bind even multiple antennae's trimers to form large PSII scs with loosely bound LHCII trimers of functional significance (Boekema *et al.*, 1999b; Tokutsu *et al.*, 2012; Drop, 2014a; Nosek *et al.*, 2017).

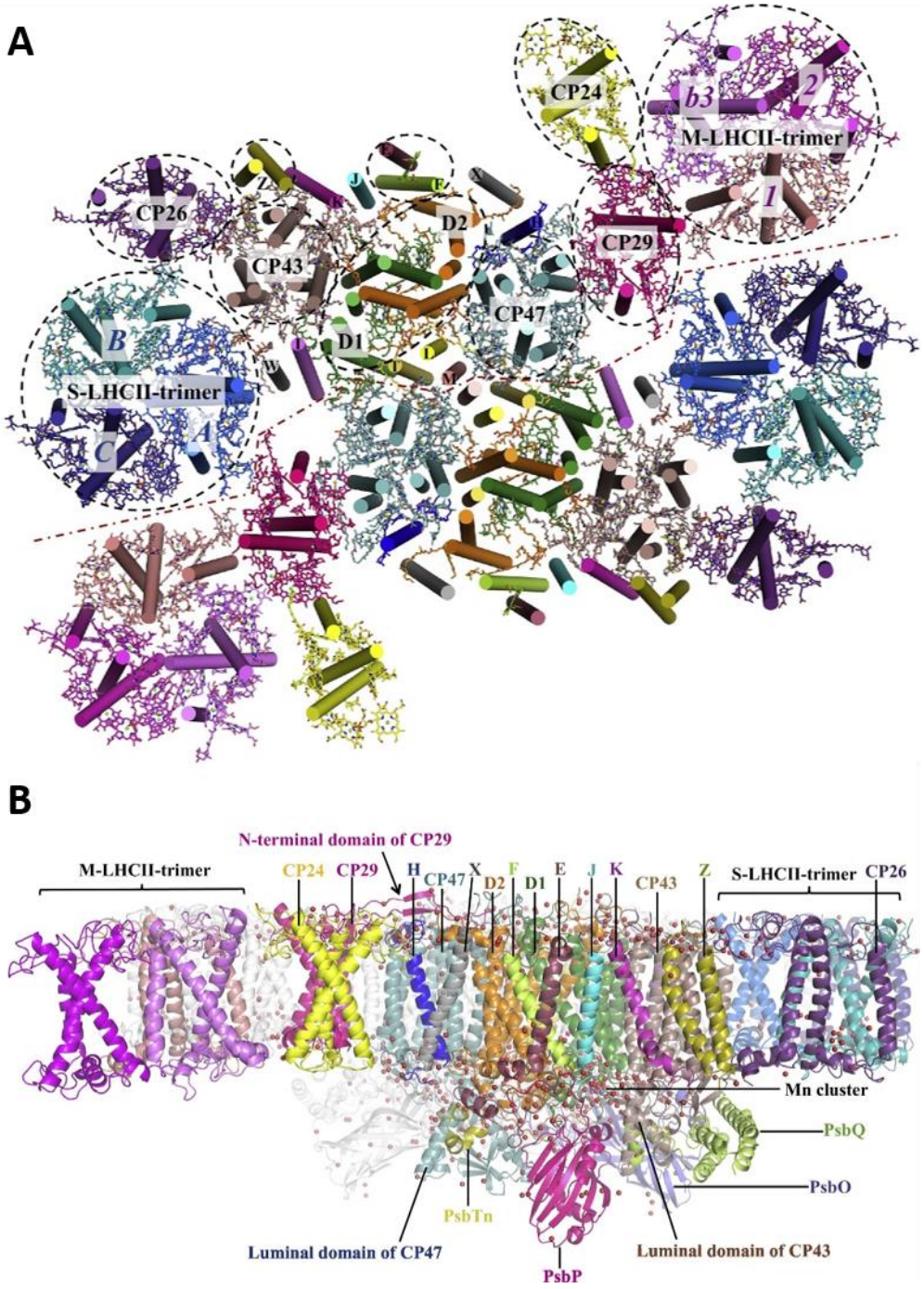

Figure 3: Structure of PSII supercomplex $C_2S_2M_2$ from *Pisum sativum* at 2.7 Å resolution. (A) View from the stromal side with exclusive visualisation of transmembrane helices (stick mode) and cofactors (cartoon). The red dashed line illustrates an imaginary division between two monomers. In one monomer, individual subunits are outlined in circles with their designations, and low-molecular-mass subunits of PSII cc are labelled with a single letter. (B) Side view along the membrane plane with coloured subunits only in one monomer. Adapted from Cao *et al.*, 2018, the original structure of pea PSII sc from Su *et al.* (2017) (5XNM) and supplemented with PsbTn subunit from spinach, Wei *et al.* (2016) (3JCU).

1.2.5.1. Loss of LHCB3 and LHCB6 antennae and its relevance

In angiosperms, the LHCB3 protein is the building stone of the M-trimer, which binds to the PSII cc specifically via its LHCB3 protein through the interaction with LHCB6 and with the contribution of LHCB4 (Kovács *et al.*, 2006; de Bianchi *et al.*, 2008, 2011; Caffarri

et al., 2009; Kouřil *et al.*, 2013). The evolutionary loss of *LHCB3* and *LHCB6* in *Pinaceae*, *Gnetaceae* and *Welwitschiaceae* (Kouřil *et al.*, 2016) understandably has a significant impact on the structure of PSII in spruce. The most likely candidates for replacing the LHCB3 in the spruce M-trimer are LHCB1 and LHCB2, both capable of forming trimers, as was hypothesised also in the *lhcb3* mutant of *At* that was characterised by increased expression of these two proteins. However, only a detailed high-resolution analysis of this trimer structure in spruce can provide a reliable answer.

Oppositely to LHCB3, the impact of LHCB6 absence is more straightforward, as this antenna is not substituted by any protein or other molecule. Compared to *At* PSII sc, spruce has its M-trimers rotated clockwise by 52°, resulting in a tighter association of the M- and S-trimers (closing the distance by 7 Å), thus more resembling PSII structure from *Cr* (Fig. 4, adapted from Kouřil *et al.*, 2016). Regarding the green algae, the observed different spatial organisation of their LHCII trimers within PSII sc and the ability to bind additional N-trimers compared to angiosperms is mainly attributed to the absence of LHCB6. It is also hypothesised that the binding of N-trimers in green algae could stabilise their entire PSII sc, including the attachment of the M-trimer (Tokutsu *et al.*, 2012; Drop *et al.*, 2014a). From the functional point of view, the shifted position of M-trimer towards PSII cc and the absence of LHCB6 in spruce compared to angiosperms affects the regulation of the related macro-organisation of PSII scs in grana membrane and the interactions between the individual PSII scs, which reflects on the whole photochemistry of spruce PSII. Moreover, the change in Chl numbers due to the absence of LHCB6 and rotated M-trimer results in alteration in the main excitation energy transfer pathways, its rates and efficiency in PSII, compared with the land plants (Kovács *et al.*, 2006; Caffarri *et al.*, 2009, Kouřil *et al.*, 2016; Kouřil *et al.*, 2020; Croce and van Amerongen, 2020).

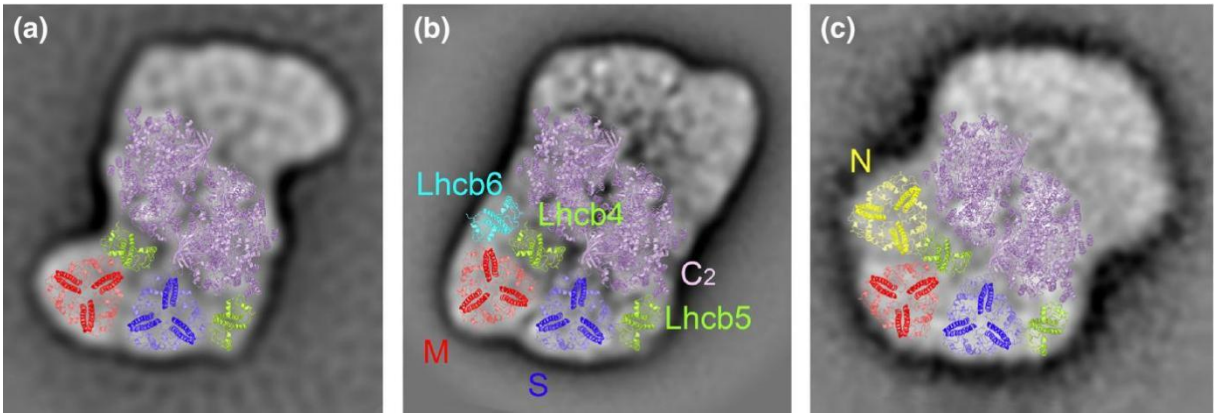

Figure 4: Electron density maps of PSII $C_2S_2M_2$ supercomplex from *spruce* (a), *Arabidopsis thaliana* (b) and $C_2S_2M_2N_2$ supercomplex from *Chlamydomonas reinhardtii* (c) with assigned subunit composition. Subunits determined based on the fitting by high-resolution structures of PSII sc, C_2 dimer (light violet), trimeric antennae S-/M-/N-trimers (blue, red and yellow, respectively) and monomeric antennae LHCB4/LHCB5/LHCB6 (green, green and cyan, respectively). Adapted from Kouřil *et al.* (2016).

A partial functional resemblance between angiosperms and spruce in terms of LHCB3 and LHCB6 function can be seen in the adaptation of *At* to HL intensity. Under prolonged exposure to excessive light, angiosperms deliberately downregulate the expression of *LHCB3* and *LHCB6* (with the concurrent upregulation of *Lhcb4.3* at the expense of *Lhcb4.1* and *Lhcb4.2*, as mentioned above). However, this regulation leads explicitly to the disconnection

of the M-LHCII trimers and thus to an increase in their C_2S_2:$C_2S_2M_2$ ratio, not to the formation of a PSII structure with rotated M-trimer observed in spruce (Kouřil *et al.*, 2013, 2016; Albanese *et al.*, 2016).

It is presumed that LHCB6 could play a role in the NPQ process. Together with the M-trimer, it creates a docking site for PsbS (Kovács *et al.*, 2006), a subunit necessary for full NPQ activation (Li *et al.*, 2000). Although it can be argued that the same scenario should also apply to evolutionary older non-vascular plants (with the exception of red and likely some green algae), these organisms have additional LIGHT-HARVESTING COMPLEXES-STRESS RELATED PROTEINS (LHCSR) involved in NPQ (Koziol *et al.*, 2007; Peers *et al.*, 2009).

It is hypothesised that this evolutionary loss is related to the harsh environment of the Triassic period after the enormous extinction event, also known as the "Great Dying". This period was characterised by HL intensity, which globally affected surviving organisms, including also the common ancestors of *Pinaceae* and *Gnetales* (Miller, 1999; Clarke *et al.*, 2011; He *et al.*, 2012).

1.2.6. Functional PSII assemblies

PSII is capable of mutual lateral interactions in variable arrangements, either in a parallel or non-parallel way, forming PSII megacomplexes (mcs) (Dekker and Boekema, 2005; Kirchhoff, 2008). These interactions were observed at the level of thylakoid grana membranes, confirming their existence *in vivo* (Nosek *et al.*, 2017; Kouřil *et al.*, 2020). Moreover, PSII scs are able to form semi-crystalline arrays within the membrane with a functional impact on photosynthesis itself (see, e.g. Boekema *et al.*, 1999a,b, 2000; Yakushevska *et al.*, 2001; Kirchhoff *et al.*, 2007; Kouřil *et al.*, 2013; Nosek *et al.*, 2017). These two-dimensional crystals are formed by either $C_2S_2M_2$, C_2S_2M or C_2S_2 scs as building blocks. Their abundance and the composition of the individual sc forms depend on conditions such as light intensity, temperature, growing medium, or the conditions used in isolation (Garber and Steponkus, 1976; Semenova, 1995; Kouřil *et al.*, 2013). The function of arrays is still controversial and disputable, attributed to the NPQ via PsbS, grana formation via interaction of adjacent membranes and, most importantly, to have an influence on PQ diffusion with a major impact on ETC (Ilíková *et al.*, 2021). To be more specific, the arrangement of PSII scs into the semi-crystalline arrays may result in a significant limitation of PQ diffusion (de Bianchi *et al.*, 2008). In the original concept, the formation of $C_2S_2M_2$ arrays led to the establishment of so-called "lipid channels", allowing easy diffusion of PQ, whereas the much tighter packing of C_2S_2 arrays strictly limited this diffusion (Tietz *et al.*, 2015). However, the situation is even more complex as it has been confirmed that the same type of PSII C_2S_2 is able to form arrays with different tightness, thus providing further possibilities for the regulation of PQ diffusion rates. In this scenario, the small rearrangement of C_2S_2 arrays has a significant impact on photosynthesis efficiency (Ilíková *et al.*, 2021).

1.3. In action - the principle of the electron transport chain and its regulations

The following subsections are focused on a general explanation of the function of the photosynthetic apparatus and its regulation, again with the main focus on spruce and its specialities as an evergreen conifer. In the final subsection, the most commonly used methods for a study of the photosynthetic apparatus are shortly listed, including physiological, biochemical and structural methods.

1.3.1. Photosynthetic electron transport chain

The basic concept of light-dependent photosynthetic reactions, the first phase of photosynthesis, can be summarised as follows: the energy of photons harvested by the pigments in the PSII antennae is transferred to the PSII RC, specifically to its primary electron donor, commonly referred to as P680, and triggers the primary charge separation. According to common textbooks, the designation P680 refers to a specific Chl *a* pair, but it probably represents four Chl molecules (P_{D1}, P_{D2}, $AccChl_{D1}$, $AccChl_{D2}$), for a review, see, e.g. Kern and Renger (2007). The separated electron gives rise to an oxidised $P680^+$, which is immediately reduced by an electron from tyrosine Z (Y_Z). Oxidised tyrosine Z (Y_Z^+) is reduced by an electron donated from manganese (Mn) in the Mn cluster of OEC located at the lumenal side of PSII. In the four-step Mn cluster reaction, every separated electron from P680 is donated three times in succession via Y_Z from one of the incorporated Mn ions. The fourth electron comes from split water in the OEC, while the rest of the released electrons from the water molecule reduce the Mn ions in the cluster. Besides the electrons, the split water is the source of protons and oxygen released into the lumen of thylakoid membranes. Electrons captured by the primary electron acceptor pheophytin are further transported via the ETC, where they reduce PQ to PQH_2. In detail, the first quinone in PSII, Q_A, as the immobile primary single electron acceptor, transfers electrons to the second, double electron acceptor quinone, Q_B. Q_B is a molecule from the PQ pool that binds to the stromal side of PSII (to the Q_B pocket). Upon double reduction, Q_B is protonated by protons localised in the stroma and released from the pocket into the PQ pool as the PQH_2. The vacated space in the Q_B pocket after PQH_2 is re-occupied by its oxidised form from the PQ pool. The PQH_2 molecule moves within the PQ pool to the lumenal side of Cyt_{b6f}, where it is oxidised back to PQ with simultaneous electron transport into Cyt_{b6f} and release of two protons into the lumen. Cyt_{b6f} accepts two electrons from PQH_2, but only one of these is transported *via* the high-potential chain to the single-electron acceptor PC, and the other electron moves down the low-potential chain to participate in the so-called Q-cycle (for more detailed review, see Malone *et al.*, 2021). On the lumenal side, the PC molecule relocates electrons from Cyt_{b6f} to PSI, where analogous to PSII, the primary charge separation is initiated upon photon absorption in its primary electron donor, designated as P700. Similar to PSII, the potential composition of the primary electron donor of PSI is considered to be four Chl molecules (P_A, P_B, $AccChl_A$, $AccChl_B$), see, e.g. Holzwarth *et al.* (2006). The separated electrons are replenished by electrons from reduced PC. Through the electron acceptors, Chl (A_0), phylloquinone (A_1) and system of Fe-S centres (F_X, F_A, F_B), electrons are finally transported from PSI to Fd, further reducing Fd-$NAD(P)^+$-reductase (FNR). The double electron reduction of $NAD(P)^+$ by two electrons from FNR with simultaneous binding of one proton from the stroma leads to the formation of a reduced NAD(P)H molecule (reviewed, e.g. in Brettel, 1997).

Proton-coupled electron transport naturally leads to the formation of pH difference across the thylakoid membrane, ΔpH. To eliminate the pronounced positive charge of protons on the lumenal side of the thylakoid membrane, counter ions such as potassium, chloride and magnesium are simultaneously transported to the opposite side of the membrane, creating a time-dependent difference in electric potential across the membrane, also known as the membrane potential, $\Delta\psi$ (see, e.g. Lyu and Lazár, 2023). However, it is necessary to realise that the transient charges stored in the electron donors and acceptors in PSII, Cyt_{b6f} and PSI also contribute to the membrane potential (reviewed, e.g. in Bulychev and Vredenberg, 1999). The resulting proton motive force, composed of the thermodynamically equivalent electric potential $\Delta\psi$ and the ΔpH component, powers the ATP production from ADP and inorganic phosphate by the ATP synthase protein complex (CF_0-CF_1) (Mitchell, 1966).

1.3.2. Regulation of electron transport chain - rerouting of electrons

The paragraph above describes a schematic representation of the so-called Z scheme of the linear electron transport (LET) of photosynthesis. However, an increase in absorbed light energy leading to high ΔpH across the thylakoid membrane causes inhibition of LET (Kanazawa and Kramer, 2002; Tikkanen and Aro, 2014), and therefore other alternative electron transport pathways (alternative electron flow - AEF) must be activated to act as protective and regulatory mechanisms. These involve CET and pseudo-CET (Alric and Johnson, 2017). Otherwise, the excited Chls in a singlet state with no possibility of being quenched or no energy outflow could converse to long-lived Chl triplet states. Chl in the triplet state can interact with oxygen molecule to form reactive singlet oxygen ($^1O_2$), which has a harmful effect on the photosynthetic apparatus and membrane lipids (Gruber *et al.*, 2015).

CET is characterised by the return of electrons from Fd back to the Cyt_{b6f} complex, resulting in a closed cycle. It functions either as a form of photoprotection by reducing photoinhibition of both photosystems caused by over-reduction of stroma, or it is pronounced in plants when the ratio of ATP:NAD(P)H production needs to be altered in favour of ATP (Alric and Johnson, 2017).

Pseudo-CET redirects electrons either: i) from PSI to O_2 (Mehler-reaction) (Mehler, 1951), ii) from PQH_2 to O_2 by plastid terminal oxidase (PTOX) (Josse *et al.*, 2003; Yu *et al.*, 2014), or iii) in plants possessing flavodiiron (see, e.g. Ilík *et al.*, 2017; Alboresi *et al.*, 2019) from Fd (Sétif *et al.*, 2020) (originally thought to be from NAD(P)H) (Helman *et al.*, 2003; Allahverdiyeva *et al.*, 2011) to O_2. Ultimately, all reactions lead to water production, i.e. pseudo-CET, and are hypothesised to be directly involved in stress signalling, most probably via reactive oxygen species (ROS) as intermediates (see, e.g. Nawrocki *et al.*, 2015; Li and Kim, 2022). These regulatory mechanisms, among others, adjust the optimal energy use according to the plant's needs or protect the photosynthetic apparatus and are significantly controlled by the redox state of thioredoxins (Buchanan, 2016; Cejudo *et al.*, 2019; Nikkanen and Rintamäki, 2019; Yoshida *et al.*, 2019).

1.3.2.1. Cyclic electron transport and other alternative electron flows

There are two main types of CET, one involving the NDH-like complex and the other involving the PGR5/PGRL1 proteins (Shikanai, 2007; Suorsa *et al.*, 2012). It is hypothesised that the NDH-like pathway could be activated in stressed plants growing under LL intensity (Ueda *et al.*, 2012; Yamori *et al.*, 2015) and function as a safety valve preventing over-reduction of their chloroplast stroma (Shikanai, 2007). However, as previous studies have shown, spruce and other genera from *Pinaceae*, *Welwitschiaceae*, and *Gnetaceae* lack the *NDH-like* genes (Braukmann *et al.*, 2009; Nystedt *et al.*, 2013). It is important to note that the loss of *NDH-like* genes is not exclusive to gymnosperms, as the same loss has been confirmed in a few angiosperms (Blazier *et al.*, 2011; Peredo *et al.*, 2013; Ruhlman *et al.*, 2015).

The functional and essential type of CET for photosynthesis in conifers presumably uses PGR5/PGRL1 pathway (Munekage *et al.*, 2002, 2004), as PGR5 transcriptomes have been found in both families *Gnetaceae* and *Pinaceae*. Coping only with the PGR5/PGRL1 pathway could coincide with different conditions during the evolution of early gymnosperms and their younger gymnosperm successors. In a period of rising gymnosperm, plants needed to acclimate to the environment with HL intensity and therefore have no need for an NDH-like pathway activated at LL conditions (Shikanai, 2007; Yamori *et al.*, 2015). Contrary, evolutionary younger gymnosperms evolved in a less harsh environment already shaded by

the canopy of older trees (Engelmark and Hytterborn, 1999) and thus re-incorporate the NDH-like CET pathway (Yang *et al.*, 2020).

Although spruce lacks the NDH-like pathway, it possesses a different type of AEF involving FLAVODIIRON PROTEINS (FDPs) functioning as an electron safety valve. The C-class of FDP proteins are stromal proteins encoded by *FLVA and FLVB* genes (homologues of *FLV1* and *FLV3* in cyanobacteria) and form a heterodimer. Pseudo-CET, including FDP, is characterised by a very fast re-oxidation of PSI upon dark-to-light transition, which is much faster than in angiosperms (Helman *et al.*, 2003; Alboresi *et al.*, 2019). This oxygen-dependent reaction only works temporarily until the acceptor side of the PSI is fully activated, and its function is to transfer the electrons to oxygen (Franck and Houyoux, 2008). The functional FDP-mediated pseudo-CET was confirmed in gymnosperms and evolutionary older organisms down to cyanobacteria (Helman *et al.*, 2003; Ilík *et al.*, 2006; Franck and Houyoux, 2008; Grouneva *et al.*, 2009; Cruz *et al.*, 2011; Shirao *et al.*, 2013; Pavlovič *et al.*, 2016), but was not observed in angiosperms, which lack adequate genes. Until recently, it was assumed that the flavodiiron transfers electrons from NAD(P)H to oxygen (Allahverdiyeva *et al.*, 2011). However, more recent studies imply that the flavodiiron can accept electrons directly from Fd or even the FeS-centres of PSI and then transfers them to oxygen (Sétif *et al.*, 2020). Either way, the transfer of electrons via FDP does not lead to the detrimental side effect of producing ROS. There are several hypotheses as to why this pathway was not conserved in angiosperms, unlike gymnosperms, such as (i) disadvantageous dissipation of light energy for plants evolved under the light-limited conditions in the shade of their ancestors (Ilík *et al.*, 2017), (ii) redundancy due to compensation by increased CET efficiency, (iii) complementary activity of different AEFs (Wada *et al.*, 2018; Alboresi *et al.*, 2019), etc. Nevertheless, the distribution of FDP across photosynthetic organisms can be perceived as a division marker on the phylogenetic tree, highlighting the transition from gymnosperms to angiosperms.

To conclude, it should be emphasised that the different types of AEFs may be interdependent and, as such, may allow for more sensitive and precise regulation and better adaptation in response to changing environmental conditions.

1.3.3. Regulation of electron transport chain - energy redistribution and dissipation

To continue with functional regulations of the ETC, the aforementioned AEF mechanisms represent a simple and rapid way for plants how to redirect electrons and thus prevent the potential photooxidative damage. However, the plants must be able to adequately respond to changing light conditions over a longer period of time, and therefore they have evolved additional protective mechanisms, all at the level of the ETC. These include (i) state transitions, which allow the plants to balance the accepted light energy between the two photosystems (Lemeille and Rochaix, 2010; Pesaresi *et al.*, 2010, 2011), (ii) direct dissipation of the excess of light energy triggered by the induction of NPQ (Demmig-Adams and Adams, 1996; Horton *et al.*, 1996; de Bianchi *et al.*, 2010; Niyogi and Truong, 2013; Demmig-Adams *et al.*, 2014) or, (iii) the electron transport can be regulated by direct involvement of Cyt_{b6f} complex via photosynthetic control (Rumberg and Siggel, 1969; Kramer *et al.*, 2003; Tikhonov, 2014). The long-term regulations necessary for plant acclimation to biotic and abiotic changes in the environment are accompanied by up-or down-regulation of nuclear or chloroplast gene expression of proteins involved in photosynthesis (see, e.g. Pfannschmidt *et al.*, 1999, 2001).

1.3.3.1. Sustained NPQ – a rarity of overwintering evergreens

The effect of excessive light energy on the photosynthetic apparatus leads to the activation of NPQ. Based on the different recovery times of Chl fluorescence in the dark after previous illumination, three types of NPQ were originally distinguished, (i) a fast-recovered energy-dependent quenching (qE), a slowly-recovered quenching due to the state transition (qT), and the slowest-recovered quenching due to photoinhibition of PSII (qI) (see, e.g. Hodges *et al.*, 1989). However, qT does not actually represent a real quenching but rather reflects a reduction in antenna size and occurs only in LL conditions. In contrast to qT, qI occurs predominantly at HL illumination. Nevertheless, of the main importance is qE, which is triggered by the acidification of the lumen (Briantais *et al.*, 1979). The low pH causes protonation of PsbS and activation of violaxanthin de-epoxidase, which converts violaxanthin via antheraxanthin to zeaxanthin. Protonated PsbS and zeaxanthin are necessary conditions for full qE, which is realised by heat dissipation of the excess energy. In addition, the increased concentration of protons in the lumen simultaneously induces the aggregation of LHCII proteins, which are capable of energy dissipation due to conformational changes in their structure. However, the identification of the physical quencher and specification of either the direct or indirect involvement of each component in NPQ, together with the existence of other types of NPQ that have been reported, is still under debate. For a review, see, e.g. Bassi and Dall´Osto (2021).

In addition to the aforementioned NPQ, in overwintering spruce and other evergreens, a specific type of NPQ is induced to survive a combination of HL irradiation in parallel with freezing temperatures. Since low temperatures generally inhibit enzyme activity, the absorbed light energy cannot be used for eventual CO_2 assimilation and would instead lead to photooxidative damage. To prevent this, plants activate the S-NPQ that dissipates the excess of absorbed energy and releases part of it as a heat (Öquist and Huner, 2003; Demmig-Adams and Adams, 2006; Verhoven, 2014). The S-NPQ is a specific type of NPQ characterised as a state of prolonged energy dissipation emerging in plants as conifers under freezing temperatures with concurrent bright light. Compared to the relaxation kinetics of Chl fluorescence of qE NPQ in the dark after previous illumination, S-NPQ is characterised by a significant decrease in the maximum photochemical quantum yield of PSII (F_V/F_M), which relaxes really slowly (Verhoeven, 2013; Grebe *et al.*, 2020; Walter-McNeill *et al.*, 2021). When studying the specific properties of S-NPQ in spruce, Grebe *et al.* (2020) observed the presence of a triple phosphorylated N-terminus of LHCB1, specifically LHCB1_A (3p-LHCII) and phosphorylated PsbS protein (p-PsbS). It was concluded that three events interrelate with S-NPQ and are responsible for its initiation in spruce: i) freezing temperatures, which independently on light induce fast triple phosphorylation of LHCII that further initiates grana destacking due to electrostatic repulsion of adjacent membranes, ii) light- and temperature-dependent accumulation of p-PsbS and iii) limited PSII photoinhibition. The observed destacking of grana leads to concomitant linearisation of thylakoids, loss of the lateral heterogeneity of PSI and PSII distribution in the thylakoid membrane and increased PSII-PSI spillover (for a general overview, see Grebe *et al.*, 2020). Oppositely, relaxation of S-NPQ leads to 3p-LHCII dephosphorylation, re-stacking of the grana membranes, lateral segregation of PSI and PSII, and reduced spillover.

Focusing on PsbS, this protein is essential for the regulation of qE NPQ via changes in lumenal pH (Li *et al.*, 2000, 2004), together with increased conversion of violaxanthin to zeaxanthin (Ottander *et al.*, 1995; Verhoeven *et al.*, 1998) and LHCII aggregation (Johnson *et al.*, 2011; Ware *et al.*, 2015; Kress and Jahns, 2017). The major role of specifically phosphorylated p-PsbS in S-NPQ could hypothetically be the solidification of PsbS-

zeaxanthin-LHCII aggregates in the locked quenching state, where the acidification of lumen is no longer required to maintain S-NPQ in the dark (Johnson *et al.*, 2011; Ware *et al.*, 2015; Kress and Jahns, 2017; Grebe *et al.*, 2020).

It is important to mention that the S-NPQ is manifested by an increase in the quantum yield of non-regulated energy dissipation Y(NO) and a concomitant decrease in the quantum yield of non-photochemical quenching Y(NPQ) since S-NPQ does not relax during dark adaptation (Bag *et al.*, 2020; Grebe *et al.*, 2020). Moreover, the S-NPQ in spruce could also be triggered by PSII photodamage that over-exceeded the repair capacity of regulatory NPQ. Since the complete repair of PSII is light dependent (Aro *et al.*, 1993a, b), the lower level of F_V/F_M recovery during relaxation in the darkness in S-NPQ needles compared to the control needles without S-NPQ represents PSII photoinhibition.

Nevertheless, the exclusive presence of 3p-LHCII and p-PsbS is not sufficient to induce S-NPQ and thus, they mostly represent prerequisites, while partial PSII photoinhibition could function as a prompt trigger of S-NPQ. Although it is hypothesised that S-NPQ is "built on" the pre-existing components of regulatory qE NPQ (Grebe *et al.*, 2020), their interdependence has not yet been revealed, as there are strong indications for (i) their partial mutual sharing of components (increased levels of zeaxanthin, formation of LHCII aggregates, etc.), and (ii) combined regulation of these two molecular mechanisms (see, e.g. Porcar-Castell, 2011; Verhoeven, 2014).

The loss of grana stacking during S-NPQ is primarily the result of LHCII and PSII phosphorylation by STN7 and serine/threonine protein kinase 8 (STN8) (Pesaresi *et al.*, 2011; Rochaix *et al.*, 2012). The LHCII and PSII located in adjacent thylakoid membranes mediate the stacking of the membranes into grana (Trissl and Wilhelm, 1993; Anderson, 2012) and their destacking by reversible phosphorylation allows enormous quenching of excess light energy in PSI (Martin and Öquist, 1979; Öquist and Huner, 2003; Demmig-Adams *et al.*, 2015; Yang *et al.*, 2020). This phenomenon was further analysed in the analogous study by Bag *et al.* (2020), focusing on S-NPQ in pine. In this study, Bag *et al.* (2020) emphasised a direct link between the extensive grana destacking and the "static" quenching used by conifers. The structural rearrangements of thylakoid membranes and the loss of grana organisation observed in previous studies during the winter seasons (Martin and Öquist, 1979; Król *et al.*, 2002; Öquist and Huner, 2003) led to the reduction in lateral heterogeneity, randomisation of the PSI and PSII distribution, and thus enabled the direct energy transfer from PSII to PSI. According to Bag *et al.* (2020), the PSII-PSI spillover represents the major component of S-NPQ, which provides significantly stronger quenching than the regulatory NPQ and thus contributes to a multiple times lower risk of oxidative photodamage. A direct energy transfer from PSII to PSI would be in agreement with the observed, significantly higher limitation of the electron transport on the donor side of PSI than on its acceptor side.

The dynamic of grana destacking during S-NPQ is thought to be regulated by (i) triple phosphorylation of LHCII, which leads to an increase in negative charge between adjacent membranes, therefore promoting destacking (Grebe *et al.*, 2020), or it may also be facilitated by (ii) LHCB4/LHCB8, whose N-terminus is hypothesised to be responsible for mediating the interaction between adjacent membranes (Albanese *et al.*, 2017, 2020). The exclusive presence of LHCB8 with significantly higher sequence variability of its N-terminus compared to LHCB4 may then increase the flexibility of interactions between the grana in contact. To conclude, both of these factors may represent adaptive traits for overwintering evergreens and their regulation of energy dissipation (Grebe, 2022). Moreover, the high level of PSII-PSI spillover could be responsible for the putative independence of S-NPQ from delta-pH

(Gilmore and Ball, 2000; Öquist and Huner, 2003; Verhoeven, 2014), which is necessary for the initiation of regulatory NPQ.

1.3.4. Reactivation of photosynthesis in overwintering evergreens

Generally, overwintering evergreens need to alternate between dormancy during freezing winters and reactivation of photosynthesis in optimal conditions with precise timing for maximum growth. As an example, several frost-resistant plants have the ability to up-regulate metabolic sink capacity and down-regulate photochemical efficiency. In summary, they remodel primary carbon metabolism according to current needs, with CO_2 assimilation downregulated during winter and activation of alternative electron sinks to protect photosynthetic apparatus (Öquist and Huner, 2003; Ensminger *et al.*, 2006; Rochaix, 2013; Alric and Johnson, 2017). However, the efficiency of these mechanisms may vary considerably between conifers, as found by Yang *et al.* (2020) for pine and spruce.

Yang *et al.* (2020) revealed that pine is able to efficiently redirect electron flow to other acceptors during overwintering, leading to a change in the redox balance in the photosynthetic ETC, thereby preventing potential photooxidative damage. Oppositely, spruce lacks the ability to alternate between electron sinks or to adjust the CO_2 assimilation to current needs during critical periods. This leads to significant photodamage of the spruce photosynthetic apparatus associated with its higher lipid peroxidation.

It is suggested that the difference in adaptation mechanism of pine and spruce could coincide with their evolutionary ascent, with pine as a pioneer exposed to more intensive light radiation and spruce as its successor, partially shade-tolerant and hidden under dense canopy, with lower requirements for photoprotective mechanisms (Engelmark and Hytterborn, 1999). Ultimately, spruce is more sensitive to environmental changes and, with respect to global climate changes, has a lower capacity to acclimate its energetic metabolism compared to pine, which has the ability to balance photosynthesis and respiration in response to seasonal temperature changes and increasing atmospheric CO_2 levels (Kurepin *et al.*, 2018).

1.3.5. Chlorophyll synthesis in the darkness – an additional speciality of gymnosperms

In contrast to angiosperms, gymnosperms are able to synthesise Chl even in the dark, as the key step of their biosynthesis is catalysed by the light-independent dark-operative pchilide oxidoreductase (DPOR) instead of light-dependent POR (LPOR) present in angiosperms (Armstrong, 1998; Schoefs and Franck, 2003; Reinbothe *et al.*, 2010). This provides the spruce with additional plasticity of its photosynthetic apparatus. Another interesting feature is that PSI formed in the dark is fully active, while PSII is in a latent form with an inactive OEC (see, e.g. Oku *et al.*, 1974; Kamachi *et al.*, 1994). Upon illumination, part of the formed PSII scs starts to function due to the gradual assembly of OEC, while the rest of the PSII scs remains in the so-called Q_B-non-reduced inactive form. This mechanism has a logical rationale because the slow light-depended activation of PSII centres into the fully active mode preserves the low stoichiometry of PSI/PSII and prevents over-reduction of electron carriers leading to potential damage. This activation involves (i) formation and attachment of OEC proteins to PSII, (ii) synthesis and binding of LHCIIs and (iii) overall association of LHCIIs into PSII scs (Canovas *et al.*, 1993; Pavlovič *et al.*, 2016).

1.3.6. Photosynthesis and the experimental approach to its study

There are different approaches how to reveal the mysteries of photosynthesis. Since photochemistry and fluorescence are at significant levels competing processes in plants, biophysical methods aimed specifically at measuring fluorescence are most appropriate for determining the efficiency of photosynthesis. A wide range of fluorescence techniques, such as Chl fluorescence induction, fluorescence spectroscopy, etc., allow the study of photochemistry in real-time with the possibility of studying the effects of different biotic or abiotic stresses.

Although biochemical methods do not provide real-time data and are more destructive to the plant material, they are still irreplaceable due to the information provided about the qualitative and quantitative chemical composition of the photosynthetic apparatus with its specific modifications. These methods include optimised techniques for the isolation of DNA/RNA/proteins from biological material, separation techniques such as (non-)denaturing one- or two-dimensional electrophoresis, ultracentrifugation, high-pressure liquid chromatography (HPLC), liquid or gas chromatography combined with mass spectrometry, tandem mass spectrometry and others.

For detailed structural analysis of specific protein complexes of the photosynthetic apparatus and their final visualisation, techniques such as X-ray crystallography and cryo-EM/TEM are essential, with the latter becoming the dominant structural method in the study of large protein complexes in recent years.

In summary, it is inevitable to combine different approaches to achieve a comprehensive and complex picture of the structure and function of the photosynthetic apparatus. My research required the implementation and optimisation of biochemical methods for sample preparation (see Sections 3 and 4) and the use of EM, together with the application of computational methods for sample processing and structural analysis.

2. A deeper insight into the photosynthetic apparatus of spruce and its functional relevance

The two main objectives of my doctoral study were:

I) to study the photosynthetic apparatus of Norway spruce with a focus on a detailed structural analysis of its photosystem II using cryo-EM and,

II) to optimise the solubilisation conditions and separation methods for isolated thylakoid membranes (i) to obtain a homogeneous and highly concentrated sample of intact photosystem II supercomplex suitable for cryo-EM analysis and (ii) to isolate the transiently formed, but fragile, photosynthetic supercomplex PSI-LHCII$_{(n)}$ from Norway spruce.

Section 2 briefly summarises in four subsections the individual structural and functional studies carried out on the photosynthetic apparatus of spruce, which formed the basis of the individual publications. Section 4 summarises in detail the experimental approach used to optimise the separation of specific protein complexes from isolated thylakoid membranes that are starting points for structural or functional analysis.

2.1. Simulation of the loss of LHCB3 and LHCB6 proteins during spruce evolution in *Arabidopsis thaliana*

Spruce represents a rather unconventional model plant, and from one point of view, it is a relatively undemanding species for growing under controlled conditions and subsequent isolation and sample processing. However, on the other hand, any targeted gene manipulation in spruce represents quite an obstacle as its genome is more than 100 times bigger than that of *At* (Nystedt *et al.*, 2013). Therefore, there are strong ambitions to study its unique, photosynthesis-related traits indirectly, generally using "uncomplicated plants" with a small genome and known genome sequence, fast-growing rate and easier gene manipulation. This approach allows us to purposely mutate specific genes and to test the effect of individual modifications. The original idea of our project (Ilíková *et al.*, 2021) and our main objective was to simulate the characteristic spruce absence of LHCB3 and LHCB6 proteins in the model plant *At* by knock-outing the genes encoding both of these proteins. In this pilot study, we had a unique opportunity to observe the structural and functional effect of the loss of these proteins on the structure of *At* PSII sc. In addition, this study could shed light on the evolutionary advantage gained by spruce due to the absence of the LHCB3 and LHCB6 proteins. Complementary to the double mutant, we used already existing single-mutated *lhcb3* and *lhcb6* plants.

Electrophoretic separation of pigment-protein complexes showed that the double *lhcb3+lhcb6* mutant, which is characterised by lower fitness and reduced growth, is unable to form even larger scs than C_2S_2. Initially, we attributed the absence of C_2S_2M and $C_2S_2M_2$ to their lower stability and their possible disintegration during sample preparation. By structural analysis of the grana membranes of this mutant, we were able to rule out this possibility, as only smaller forms of C_2S_2 scs, organised into semi-crystalline domains, were observed in the membrane. The observed C_2S_2 scs arrangement in this mutant has a potential impact on the diffusion of PQ molecules and overall the fitness of photosynthetic apparatus and its function (de Bianchi *et al.*, 2008). Nevertheless, the formation of C_2S_2M/M_2 with shifted M-trimer in the *lhcb3+lhcb6* mutant could be unambiguously excluded.

However, an unexpected result was the observation of the so-called "spruce-type" PSII sc in the *At lhcb3* mutant. This "spruce-type" PSII sc was identified in the C_2S_2M fraction, with one missing M-trimer, with a minor abundance of 10 %. For the remaining 90% of the

particles in this fraction, their M-trimer had a characteristic binding to the PSII cc via LHCB4 and LHCB6 antennae (Caffarri *et al.*, 2009). Importantly, mass spectrometry analysis of thylakoid membranes of *lhcb3* mutant and wild type revealed comparable small amounts of LHCB8 protein, suggesting that the formation of the "spruce-type" PSII sc is not dependent on the presence of spruce-specific LHCB8.

2.2. Cryo-EM structure of the PSII supercomplex of Norway spruce

Until recently, the highest known resolution of the PSII-LHCII sc ($C_2S_2M_2$) in spruce was 14 Å, obtained from a negative stain projection map by SPA (Kouřil *et al.*, 2016). This structure was sufficient to reveal its unique architecture described above. However, the specific composition, mostly of the peripheral LHCII antennae and their interactions, still remained undescribed. However, the nearly atomic resolution at 2.8 Å of spruce C_2S_2 PSII sc obtained in our work using cryo-EM (Opatíková *et al.*, 2023) allowed us to study this structure in much greater detail with unique insight into the composition of its specific subunits and arrangement of pigment molecules. Comparing the spruce PSII structure with its evolutionary older or younger counterparts in green algae and angiosperms, respectively, allowed us to hypothesise about the functional impact and relevance of its unique attributes.

In our work, we aimed for the isolation and analysis of the larger spruce $C_2S_2M_2$ PSII sc, and for this purpose, we optimised the solubilisation conditions to achieve its higher yield. Since spruce is characterised by a higher occurrence of smaller forms of PSII scs compared to the land plants such as *At* (Kouřil *et al.*, 2016), we decided to extract fractions of PSII sc forms with one and two M-trimers together to achieve sufficiently high concentrated sample necessary for cryo-EM. However, the abundance of these forms in the primary data set was insufficient for image processing, most probably due to the lability of the M-trimer binding to the PSII cc and its disconnection during sample manipulation. Therefore, the homogeneous 2D classes of C_2S_2 were used for the final 3D reconstruction and generation of the electron density map.

The PSII cc in spruce is highly conservative and its subunit composition corresponds with that observed in green algae and angiosperms (subunit and pigment composition of spruce PSII sc see in Tab. 2). However, the presence of one additional low molecular mass subunit, specifically Ycf12, was confirmed similarly to the green algae *Cr* (Shen *et al.*, 2019; Sheng *et al.*, 2019). Oppositely, this subunit was not observed in the known structures from angiosperms, such as spinach, *At*, or pea, as they lack the *YCF12* gene (Wei *et al.*, 2016; Su *et al.*, 2017; van Bezouwen *et al.*, 2017). It is hypothesised that the Ycf12 subunit may play a role during acclimation to the HL intensity (Kashino *et al.*, 2007).

Within the light-harvesting antennae of spruce, specifically the S-trimer, we confirmed another previously unknown speciality of spruce, and that is the homotrimeric composition of its S-trimer. In land plants, the S-trimer is composed of a combination of LHCB1 and LHCB2 (and their various isoforms) (Minagawa and Takahashi, 2004) and is generally accepted that it forms either homo- or heterotrimers. In green algae *Cr*, the detailed composition of the S-trimer is known and includes LHCBM1, 2 and 3 (Sheng *et al.*, 2019) at specific positions, and thus always represents a heterotrimer. In spruce S-trimer, we were able to exclude the presence of all LHCB2 isoforms and even two LHCB1 isoforms (B1 and B2), and thus the S-trimer can be then assigned as a homotrimer of LHCB1_A (isoforms LHCB1_A1–3), oppositely to green algae and land plants. However, the physiological benefit of this specific aspect for spruce remains the subject of further studies (see the summary of this section). Moreover, since mass spectrometry analysis confirmed the presence of LHCB2 in the PSII sc fraction of spruce, and we ruled out its presence in the S-trimer, we assume that, unlike the

composition of *At*' M-trimer from LHCB1 and LHCB3, the spruce M-trimer composition could include the LHCB2 protein. Nevertheless, whether the M-trimer in spruce represents a homotrimer or a heterotrimer would require obtaining a detailed high-resolution structure of PSII sc with bound M-trimer.

The sole presence of LHCB8 in spruce provided a unique opportunity to study this protein in detail since it is not overshadowed by other isoforms, LHCB4.1 and LHCB4.2, in the final electron density map. In this protein, we evidenced the loss of two Chls compared with the PSII structures of land plants (Chl *a*613 and Chl *b*614) and one compared with *Cr* (Chl *b*614). The loss of two Chls in the LHCB8 protein of spruce compared to LHCB4.1 and LHCB4.2 present in land plants is attributed to its shorter C-terminus and related structural properties. The ability of *Cr* to maintain one extra Chl in its LHCB4.3 protein compared to spruce, even with its shorter terminus, is probably due to a clockwise rotation of its α-helix forming C-terminus (Shen *et al.*, 2019; Sheng *et al.*, 2019). As shown by calculations based on Förster's theory of resonant energy transfer, even with two missing Chls mentioned above, the main energetic pathways from LHCII antennae to PSI cc remained conserved in comparison with other known structures of PSII.

Nevertheless, the most unexpected discovery in spruce PSII structure was the presence of α-tocopherol/α-tocopherolquinone (α-Toc/α-TQ, second one is an oxidation product of α-Toc) localised between the inner core antenna CP43 and the Y/y chain (LHCB1 protein) of the S-trimer. Both α-Toc and α-TQ molecules were further confirmed in the purified PSII fraction by liquid chromatography with tandem mass spectrometry analysis (LC-MS/MS). It is important to mention that the identification of either of the two tocopherols was somewhat complicated since multiple molecules share similar structural features and have almost indistinguishable electron density at lower resolution, such as n-Dodecyl α-D-Maltopyranoside (α DDM), n-Dodecyl-β-D-Maltopyranoside (β DDM) or plastochromanol-8. Thus the identification or exclusion of such molecules depends mainly on the final level of resolution of the electron density map in the problematic regions of the obtained structures. Out of these molecules, α DDM was the most difficult to exclude because, in addition to its very similar electron density, its presence was justified in view of its use for sample preparation. Moreover, α DDM has already been fitted into several cryo-EM structures of PSI, e.g. in *Zm* (Pan *et al.*, 2018), or in *Cr* (Su *et al.*, 2019) and PSII (e.g. in diatoms (Nagao *et al.*, 2019), or in *Cr* (Sheng *et al.*, 2019). However, in our structure, the α DDM did not fully fit into the density map, which was confirmed by calculating the interaction energies ΔiG for the most relevant interaction interfaces.

We do not consider the presence of α-Toc/α-TQ in this specific position of the PSII structure to be exclusive to spruce, as we observed a similar density (more blurred so) in the density map of pea PSII structure. Even in the PSII structures from *At* and spinach, some traces of density were observed in the same position, although they are rather inconclusive. Oppositely, no such density was observed in *Cr*, nor could it be fitted, as the binding position in *Cr* is partly blocked due to the closer contact between its CP43 subunit and the S-trimer. Although at first glance, it seems that the presence of α-Toc/α-TQ is another feature of land plants that distinguishes them from green algae, this cannot be unambiguously concluded. Aside from high amino acid sequence variability between land plants and green algae at the critical positions of CP43 and LHCB1 (LHCBM1 from *Cr*), which mediate the contact with α-Toc/α-TQ in spruce, it is still possible that α-Toc/α-TQ molecule may have been originally present in *Cr* but was lost during sample preparation. Moreover, this loss may have eventually led to a shift in the PSII structure of *Cr*, resulting in closer contact between its CP43 and LHCBM1 subunits.

The hypothesis explaining the function of α-Toc/α-TQ can be built on the nature of the compound itself, which is known $^1O_2$ scavenger. $^1O_2$ ranks among the ROS with a high potential to cause oxidative damage. In plants, ROS are formed in high abundance upon exposure to excessive light irradiance (Foyer and Noctor, 2003, 2005; Apel and Hirt, 2004), and while carotenoids represent a primary protective barrier capable of quenching excessive energy uptake and thus preventing the $^1O_2$ formation, α-Tocs can be considered as a secondary protection (Edge and Truscott, 1999; Krieger-Liszkay and Trebst, 2006).

2.3. Formation of PSII supercomplexes and megacomplexes and their organisation into arrays

Compared to the higher plants, which are capable of forming various types of semi-crystalline arrays composed of all types of PSII scs ($C_2S_2M_2$, C_2S_2M and C_2S_2) (Boekema *et al.*, 2000; Yakushevska *et al.*, 2001; Kouřil *et al.*, 2013), no such arrays were observed in spruce (Kouřil *et al.*, 2016). This phenomenon could be the result of the spruce unique PSII structure with a potential functional impact on the regulation of its ETC. To avoid rash conclusions, however, it needs to be highlighted that the mechanisms and regulations standing behind arrays formation, together with their functional benefits, are still under debate. Nevertheless, the high structural similarity of PSII sc in spruce and *Cr* and their shared absence of LHCB3 and LHCB6 proteins led us to the conclusion that spruce may be able to potentially bind other trimers analogously to *Cr* (Drop *et al.*, 2014a). Thus in our work (Kouřil *et al.*, 2020), we focused on the possible formation of larger PSII scs in spruce and its organisation and mutual associations in the thylakoid membrane. Together with a parallel analysis in pine, we determined the potential impact of their unique PSII structure on the formation of larger PSII assemblies.

Due to the absence of the LHCB3 and LHCB6 proteins in both conifers, the $C_2S_2M_2$ PSII sc has a modified shape that more closely resembles the letter "S" compared to the characteristic rectangular shape of PSII sc in *At* (Fig. 4, adapted from Kouřil *et al.*, 2016). We showed that spruce also forms a much larger PSII scs with bound N-trimers (although they are rotated compared to those observed in *Cr*) and additional L-trimers compared to *At*. While it is hypothesised that the N-trimer in *Cr* is most probably composed of LHCBM1, 2, 3, 6 and 7 in different combinations (Drop *et al.*, 2014a; Shen *et al.*, 2019), in spruce, the main components of N-trimer would be LHCB1 and LHCB2, as they are the only LHCBs in spruce that are able to form trimers (Kouřil *et al.*, 2016). However, the participation of LHCB5 in N-trimer formation in spruce has lately been discussed (Grebe *et al.*, 2019). Interestingly, for some of the PSII scs from both studied conifers, the binding of the N-trimer did not require the presence of the M-trimer, as originally assumed, and the N-trimer binding was the same as for *Cr* with the M-trimer present. The origin of the different character of N-trimer binding in *Cr* and spruce is still unknown. However, it has been suggested that the PsbH and PsbX subunits, responsible for mediating the N-trimer interaction with the core in *Cr* (Shen *et al.*, 2019; Sheng *et al.*, 2019), may play the same role in spruce. Nevertheless, the difference in the angle at which the N-trimer binds to the core between spruce and *Cr* could affect the strength of the bond, which would be weaker in spruce and thus more easily disintegrated compared to *Cr*.

Furthermore, aside from the observed attachment of N-trimer in spruce PSII sc, we were able to identify PSII scs with two rows of connected LHCII trimers and experimentally confirm the existence of PSII scs with up to 7–8 LHCII trimers on one side of PSII sc. And since PSII scs have two-fold symmetry, it is logical to expect the existence of PSII sc with the ability to bind up to 18 LHCII trimers. It is important to note that according to the created

hypothetical model of these large PSII scs, the LHCII binding would still allow the necessary free flow of PQ into the RC of PSII (van Eerden *et al.*, 2017).

Megacomplexes are formed as a result of lateral interactions of PSII scs in the thylakoid membrane, and this association is mediated by LHCII and C_2 (Nosek *et al.*, 2017). However, PSII scs can also interact with each other from the stromal side of two adjacent membranes (Daum *et al.*, 2010; Albanese *et al.*, 2017; Su *et al.*, 2017). The characteristic features of the observed mcs were the composition of two PSII scs with variable interaction of $C_2S_2M_2$, C_2S_2M and C_2S_2 forms, which interacted either in parallel (70 %) or non-parallel (30 %) way. The S-trimer was the most involved part in the interaction, therefore it was considered as the main mediator of the association between two PSII scs, followed by involvements of LHCB5, LHCB4, dimeric core, L- and M-trimer, respectively. The same trend was also observed in pine (Kouřil *et al.*, 2020). Compared with the 13 types of PSII mcs observed in *At* by Nosek *et al.* (2017), in spruce and pine, we observed their lower structural variability, with 7 and 3 different types, respectively. Furthermore, the stability of formed PSII mcs was noticeably weaker in spruce compared with *At*. It is hypothesised that the origin of more firm binding in *At* is in the rectangular shape of its PSII sc, which may provide more stable side-by-side interactions (Kouřil *et al.*, 2020).

Although in spruce, we did not observe the typical arrangement of PSII scs into 2D arrays typical for land plants, we were able to identify specific interactions representing PSII mcs in the thylakoid membrane. As a result, we observed five different types of PSII mcs in spruce grana. However, these interactions did not match those observed in the isolated PSII mcs. This phenomenon could be then explained by the disproportion between the stability of specific PSII mc types and their abundance in membranes *in vivo*. The lower stability is additionally supported by the high occurrence of disintegrated intermediates of PSII mcs in the form of individual PSII scs in the PSII mc band (Kouřil *et al.*, 2020).

2.4. Acclimation to long-term changes in light intensity

Although there is more than one study addressing the survival tactics of overwintering evergreens in their photosynthetic adaptation and coping with high irradiance at freezing temperatures (Bag *et al.*, 2020; Grebe *et al.*, 2020; Yang *et al.*, 2020), there is a significant gap considering their adaptation to long-term light intensity changes under controlled conditions. The motivation for a more detailed study of the mechanisms involved originates in the early observation of light acclimation strategies of spruce compared to *At* since these initial studies already revealed quite significant differences between these two species (Kurasová *et al.*, 2003; Štroch *et al.*, 2008). Whereas a reduction in the size of their PSII antennae in response to intensive light is a common phenomenon in *At*, accompanied by downregulation of *LHCB1–3* and *LHCB6* and overexpression of *LHCB4.3* isoform, LHCIIs plasticity in spruce seems to be rather reduced. The reason for this phenomenon can be found in the nature of the plants, as *At* is typically a light-tolerant plant, while spruce is a shade-tolerant plant. In our work (Štroch *et al.*, 2022), we focused on characterising the different strategies of *At* and spruce with respect to their acclimation to different light intensities.

In detail, while the increasing light intensity leads to an increase in PSII/LHCII ratio in *At* due to a decrease in the fraction of bound LHCII antennae to PSII cc, and to a consequential increase in its Chl *a*/*b* ratio, no such phenomenon was observed in spruce. Rather oppositely, the PSII/LHCII ratio decreases in HL, while the Chl *a*/*b* ratio in spruce remains stable, with the most likely explanation being simultaneous and proportional degradation of PSII and PSI with concomitant preservation of released Chls. This hypothesis is further supported by increased levels of ELIPs (EARLY LIGHT-INDUCED PROTEINS)

in spruce samples acclimated to HL, which are responsible for binding released Chls as a way of protection from their oxidation.

Moreover, during long-term HL, *At* is able to sustain almost maximum F_V/F_M and the effective quantum yield of PSII photochemistry, Y(II), while the F_V/F_M in spruce is significantly decreased due to the already induced "locked-in" NPQ (described in detail in the following paragraph) and the preservation of de-epoxidised photoprotective xanthophylls and PsbS in the thylakoid membrane. Moreover, the effective PSII antennae size in *At* changes in response to the light intensity, while in spruce, it remains low regardless of the light intensity. Spruce seems to operate more with loosely bound LHCIIs that are present in high abundance under HL and are characterised by their weak interactions with PSII sc. Moreover, it is hypothesised that these weak interactions may be responsible for the minimal macro-organisation of PSII scs observed in spruce grana under HL.

Unlike in *At*, the significantly low NPQ parameter in HL-acclimated spruce is not a result of rapid adaptability, and its origin lies in the pre-existing specific type of NPQ in the dark-adapted spruce, namely "locked-in" NPQ. This "static" type of NPQ is reflected by an increase of Y(NO) and thus a decrease in the NPQ parameter, slow relaxation of NPQ parameter in the dark, formation of LHCII aggregates with strong quenching capacity and decrease in the Y(II), similarly to the S-NPQ observed in spruce in winter/early spring. However, to avoid misinterpretation, it is necessary to realise that the S-NPQ and "locked-in" NPQ differ primarily in their origin. The S-NPQ is attributed to the direct energy transfer from PSII to PSI (PSII-PSI spillover due to the reduced lateral segregation in the membrane) (Bag *et al.*, 2020) and is represented by a more significant decrease in F_V/F_M close to 0.2 values and quenching of PSII (Bag *et al.*, 2020; Grebe *et al.*, 2020). In the case of "locked-in" NPQ, its origin is in the zeaxanthin-dependent formation of LHCII aggregates, although their contribution to S-NPQ is still under debate (see, e.g. Kress and Jahns, 2017).

Moreover, the existence of "locked-in" NPQ is not exclusive to spruce, as the same response to the HL was observed in the angiosperm plant Monstera (Demmig-Adams *et al.*, 2006). Thereby, induction of this type of NPQ seems to be common for shade-tolerant evergreens.

2.5. Short summary

We used two independent approaches to reveal the origin of the unique structure of spruce PSII sc and the evolutionary benefit resulting from the loss of *LHCB3* and *LHCB6*. Our project Ilíková *et al*. (2021) involved gene manipulation of the model plant *At* and was aimed at simulating the loss of LHCB3 and LHCB6 proteins and its effect on the formation of its PSII scs. The main objective of our second project (Opatíková *et al.*, 2023) was to obtain a high-resolution structure of the PSII sc of spruce using cryo-EM. The integration of the results of these two projects has deepened our understanding of the structural and functional impact of the absence of the LHCB3 and LHCB6 proteins and shed light on specific aspects leading to the formation of the "spruce-type" PSII structure, which can be summarised as follows.

Firstly, the original hypothesis that considered the absence of LHCB3 and LHCB6 as the main cause responsible for the characteristic S shape of the spruce PSII sc was refuted because *lhcb3+lhcb6* double *At* mutants were unable to form scs even larger than C_2S_2. This suggests the contribution of other unknown factors to its structure, such as the exclusive presence of LHCB8 in spruce. However, because we observed the "spruce-type" PSII sc in the *lhcb3* mutant of *At* with a comparably minor abundance of LHCB4.3 (LHCB8) protein to that confirmed in the wild type, it was necessary to reconsider the possible involvement of this specific LHCB4 isoform (Ilíková *et al.*, 2021).

To rule out a possible role of LHCB8 in the formation of the "spruce-type" PSII sc, we prepared transgenic *At* lines, specifically a PENTA mutant knock-outed in *LHCB3*, *LHCB6*, and all isoforms of *LHCB4* (4.1, 4.2 and 4.3) genes, and supplemented them with *LHCB8* gene from spruce or *LHCB4.3* gene from *At* as a part of an ongoing study. Preliminary structural analysis of the PSII scs formed in these transgenic lines confirmed that neither LHCB8 nor LHCB4.3 are essential for the formation of "spruce-type" PSII sc (unpublished data).

A new indication of a key factor required for the formation of the S-shaped PSII sc provided the high-resolution structure of this sc that we obtained for spruce (Opatíková *et al.*, 2023). Based on our designation of the spruce S-trimer as a homotrimer composed of LHCB1_A proteins (isoforms 1–3), we concluded that this specific composition is most likely one of the conditions necessary for specific binding of the M-trimer to PSII cc. However, since the structure of the M-trimer is not yet known, a role of its specific composition in the formation of the S-shaped PSII sc cannot be ruled out either. Importantly, this hypothesis could be consistent with the observed presence of the S-shaped PSII sc in the *lhcb3 At* mutant. Since the S-trimer in *At* can be present either as homo- or a heterotrimer, the specific fraction resembling the "spruce-type" PSII sc could have an S-trimer composed exclusively of LHCB1s (like spruce) and thus would be able to bind the M-trimer at a different angle.

To confirm this hypothesis, we are currently working on the preparation of CRISPR *At* mutants with the main focus on the genes *LHCB1*, *LHCB2*, *LHCB3*, *LHCB4*, *LHCB6* and all their isoforms and simultaneous creation of transgenic lines to achieve the most authentic simulation of spruce PSII formation by modifying *At* genetic makeup. In parallel, we plan to use the optimised separation conditions presented in Section 4 to obtain a highly concentrated fraction of the intact $C_2S_2M_2$ PSII sc of spruce suitable for cryo-EM analysis and obtain its complete and detailed high-resolution structure that would reveal details of the M-trimer composition (unpublished data).

To continue with structural studies of the unique spruce PSII sc with rotated M-trimer, we determined its impact on the formation of larger PSII assemblies (scs and mcs), mutual PSII interaction and overall organisation in thylakoid membrane (Kouřil *et al.*, 2020). As a consequence, both conifers studied, spruce and pine, appeared to be able to form PSII scs with a greater LHCII trimer binding capacity and a wider range of their interactions with PSII than was observed for *At*. We hypothesise that the greater diversity in PSII scs and mcs in spruce and pine is indeed enabled by their unique S-shaped PSII structure.

The uniqueness of the photosynthetic apparatus of spruce is manifested during acclimation to changes in light conditions and, among other factors, its acclimation is closely related to the structure of its photosystems and their associated structural flexibility. Previous light acclimation studies by Kurasová *et al.* (2003) or Štroch *et al.* (2008), have already indicated that the acclimation strategies of spruce and *At* significantly differ and while *At* is characterised by a change of the size of its antennae during short-term light acclimation, spruce lacks this ability. Therefore the characteristic overabundance of the aforementioned loosely bound LHCIIs in spruce could act as quenching centres for the excess of absorbed energy. The highest demand for LHCIIs and the formation of their aggregates capable of quenching would be in the winter months, characterised by HL irradiation combined with freezing temperatures (Bailey *et al.*, 2001; Ballottari *et al.*, 2007; Kouřil *et al.*, 2013, Grebe *et al.*, 2020).

In our thorough study focused on long-term light acclimation (Štroch *et al.*, 2022) we proved that the optimisation of photosynthetic capacity in spruce is much lower than in *At* and is characterised by the induction of protective mechanisms at a relatively significant level,

including “locked-in” NPQ, photosynthetic control and CET around PSI, all of which lead to a decrease in its photosynthetic efficiency. Oppositely, *At* uses its adaptive capabilities with the main objective of increasing the LET capacity and thus photosynthetic efficiency at HL intensity and maintaining this state while minimising unnecessary involvement of regulatory processes represented by photosynthetic control and NPQ induction. In a brief comparison, it seems that the angiosperms are capable of faster and more efficient acclimation with precise regulation suitable even for sub-optimal conditions, but at the same time, they are not equipped to survive under extreme stress conditions. Oppositely, evolutionary older plants such as spruce seem to lack the regulatory precision evolved in evolutionary younger plants but are able to survive even under harsh environmental conditions.

In summary, spruce is an evolutionary enigma, and we are only at the beginning of discovering its evolutionary uniqueness. While on the one hand, it behaves as a shade-tolerant plant, on the other hand, it is able to withstand weather conditions of HL intensity combined with freezing temperatures. On closer inspection, however, this apparently highly adaptable plant uses rather sub-optimal protective mechanisms during the duration of stress conditions. This involves the induction and maintenance of the massive “locked-in” or S-NPQ at the high cost of a significantly lower PSII quantum yield and a higher rate of photooxidative damage than observed in angiosperms. The significance, or rather the impact of the evolutionary loss of LHCB3 and LHCB6 antennae combined with the exclusive presence of LHCB8 on the photosynthetic apparatus in spruce is not yet fully understood and would require further studies, both structural and functional. And although the results of our studies further characterised the specific features of this unique organism, such as the detailed composition of its C_2S_2 form of PSII sc with the additional presence of α-Toc/α-TQ in the structure, the absence of LHCB3, LHCB6 and the involvement of LHCB8 in the specific binding of M-trimer to PSII cc, the impact of unique PSII structure on the formation of larger PSII assemblies or long-term light acclimation strategies of this conifer, there are even more unanswered questions that would require further research.

3. Experimental methods

3.1. Plant material and growth conditions

Arabidopsis thaliana plants (wild type (Columbia), mutants *lhcb3* (SALK_020314c), *lhcb6* (SALK_077953) and double mutant *lhcb3+lhcb6* (Ilíková *et al.*, 2021) were grown under controlled conditions in a walk-in phytoscope (Photon Systems Instruments, Drásov, Czech Republic) for 6 to 7 weeks at 22 °C, 60 % humidity, light intensity of 120 μmol photons m^{-2} s^{-1} and with the 8-h light/16-h dark cycle. In the light acclimation studies, the pre-cultivated 32-days-old *At* plants were transferred to the growth chamber HGC1014 (Weiss, Germany) for 10–14 days and grown at three different light intensities of 20 μmol photons m^{-2} s^{-1} (low light (LL)), 100 μmol photons m^{-2} s^{-1} (normal light, (NL)) or 800 μmol photons m^{-2} s^{-1} (high light, (HL)). All other cultivation conditions were kept the same as in the pre-cultivation phase.

Norway spruce (*Picea abies* (L. Karst.)) and Scots pine (*Pinus sylvestris* (L.)) (Semenoles, Liptovský Hrádok, Slovakia) seedlings were grown under the same conditions as *At* plants, but with a 16-h light/8-h dark cycle. For the light acclimation studies, the pre-cultivated 11-weeks-old spruce seedlings were exposed to the same light conditions as for *At* mentioned in the previous paragraph.

3.2. Isolation of thylakoid membranes

Prior to isolation and depending on the main focus of the study, plants were either dark-adapted (DARK) for 30 min, harvested directly in the growth chamber either after one-hour acclimation to half intensity of growing light (1/2 LIGHT) or without acclimation under the growing light (LIGHT) and immediately transferred and processed under the green light. While for spruce seedlings, only the upper part, approx. 2 cm above the soil, was used for isolation, for *At*, whole rosettes were cut off and used. Thylakoid membranes were isolated according to the protocol described by Dau *et al.* (1995). If it was necessary to maintain the phosphorylation of the proteins in the sample in a given experiment, all buffers used for isolation were supplemented with 10 mM NaF, a phosphatase inhibitor. All isolations were performed under green light and samples were kept on ice throughout the whole procedure. The Chl content of the final thylakoid membrane suspension was determined spectrophotometrically by a pigment extraction in 80% acetone according to Lichtenthaler (1987). Aliquots containing 110 μg of Chls were shock-frozen in liquid nitrogen and further stored at -80 °C.

3.3. Clear-Native (CN), Blue-Native (BN) and 2D-SDS-Polyacrylamide gel electrophoresis (PAGE)

All protein complex separations by CN-PAGE reported in the attached publications were performed according to Nosek *et al.* (2017) with minor modifications. *At* thylakoid membranes were solubilised in an amount of 10 μg of Chls with α DDM prior to gel separation, using a detergent: Chl mass ratio of 15. Similarly, thylakoid membranes from spruce were solubilised using α DDM but with a higher mass ratio of detergent to Chl of 20. To obtain the final Chl concentration of 0.33 mg/ml, the sample was supplemented with buffer (50 mM HEPES (pH 7.2/NaOH), 0.4 M sucrose, 5 mM $MgCl_2$, 15 mM NaCl, 10 % glycerol) to a final volume of 30 μl. Thus, the final detergent concentration for *At* was 0.5% and for spruce 0.67%. After short, gentle mixing for less than one minute, the samples were immediately centrifuged at 20,000 g/4 °C for 10 min to remove un-solubilised membranes. The supernatant was loaded onto a gradient polyacrylamide gel (ranging from 4% to 8%)

(Wittig *et al.*, 2007) without the stacking gel. The electrophoretic separation was performed in a Bio-Rad Mini protean tetra cell system (Bio-Rad) under the following conditions: a constant current of 3.5 mA/15 min followed by a constant current of 7 mA until the visible front representing free LHCIIs reached the bottom of the gel (approx. 1.75 hours). The visualisation and analysis of the CN-PAGE gel were performed using an Amersham Imager 600RGB gel scanner (GE HealthCare Life Sciences, Tokyo, Japan), using both transmission mode with white light illumination for the visualisation of all bands and fluorescence mode with 460 nm excitation filter and an emission filter of Cy5 (705BP40 = 705 ± 20 nm).

Separations of protein complexes by CN-PAGE in Section 4 were performed either under the same conditions described in the previous paragraph or under the optimised conditions specified in the figure legend. The main optimisation conditions included the use of different detergents (or their combination), their concentration and solubilisation time. Standardly used non-optimised times for solubilisation were as follows: ~ 2-minute incubation for α DDM, ~ 1-minute incubation for β DDM and ~ 10–15-minute incubation for digitonin.

If used in the experiment, amphipol was added to the already solubilised sample after removal of un-solubilised membranes at a final concentration of 1% (with exceptions, see Subsection 4.2.) and incubated for 10–15 minutes on ice in the dark, while NaF was added to the solubilisation buffer with a final concentration of 10mM.

Buffer exchanges for solubilisation and separation by CN-PAGE were also tested as a part of the optimisation. HEPES buffer was replaced by MES as follows: 25mM MES (pH 6.5/NaOH), 10mM $MgCl_2$, 10mM $CaCl_2$ and 25% glycerol. Very mild solubilisation of protein scs with aminocaproic acid (ACA) in solubilisation buffer was tested using the buffer prepared according to Rantala *et al.* (2017) with the following composition: 50mM BisTris (pH 7/HCl), 375mM ACA, 1mM EDTA and 10mM NaF.

In addition to the 4–8% gradient gel, other various gradients were tested as well, either (i) self-prepared, specifically the 4–10% and 4–12% separating gel, both with 4% stacking gel, or (ii) the 4–15% pre-casted gradient gel from Bio-Rad. The specifications for the amount of Chl loaded per well and its final concentration are specified in the figure legends. The conditions for electrophoretic separation were the same as those described in the previous paragraph with the exclusion of pre-casted gel, where the conditions were as follows: 75 V/30 min => 100 V/30 min => 125 V/30 min => 150 V/1 hour => 175 V/30 min => 200 V/1.25 hours.

Conditions for protein separation using BN-PAGE were mostly identical with CN-PAGE with few changes. The gel was supplemented with critical micelle concentration (CMC) of α DDM of 0,008%, the upper buffer was composed of 0.05M Tricine, 0.015M Bis-Tris and supplemented with Coomassie Brilliant Blue-G (CBB-G) to a final concentration of 235μM. This buffer was replaced with the same buffer without CBB-G approx. one hour after separation was initiated. The loading buffer was the same as for CN-PAGE but was supplemented by CBB buffer composed of 0.75M ACA and 50mM CBB-G in a 1:9 ratio in the supernatant after solubilisation and centrifugation of the samples.

2D-SDS-PAGE was performed according to Laemmli (1970) with minor modifications. The gel was composed of 5% stacking gel (approx. height 2 cm) and 12% separating gel (see Tab. 4 for detailed composition and gel dimensions). The cathode (upper) buffer was composed of: 25mM Tris, 0.192M glycine and 3.5mM SDS, and the anode (lower) buffer was composed of 25mM Tris (pH 8.3/HCl).

After incubation of gel strips from the first dimension in SDS buffer (25mM Tris (pH7.5/HCl), 35mM SDS) for 30 min, the strips were applied on the stacking gel and fixed in

position by embedding in homogeneously dissolved 0.6% agarose in the upper buffer. The electrophoresis conditions were as follows: 10 mA/30 min => 20 mA/6.75 hours => 30 mA/0.75 hours => 40 mA/1.5 hours with continuous cooling at 4 °C.

Table 4: Composition of 2D-SDS-PAGE gel

Step	**separating gel** [12% acryl amid]	**stacking gel** [5% acryl amid]
Urea [g]	10.4	
Gel buffer 4x [ml] 2.8M Tris (pH 8.6/HCl)	5.67	2.4
Water [ml]	5.27	6.5
50% acrylamide [ml] 50% T, 2.6% C	6	1
TEMED [µl]	20	10
APS [µl]	200	50
Volume [ml]	~ 25	~ 10

Dimensions of the gel: width x height x thickness = 16.2 x 16 x 0.13 cm

3.4. Spontaneous elution and dialysis

Spontaneous elution of separated protein complexes and scs was performed from excised gel bands according to Kouřil *et al.* (2014) with two exceptions, (i) buffer was supplemented with the CMC concentration of α DDM and (ii) for less dense bands, the elution was carried out overnight rather than for 2–4 hours.

Dialysis of samples from the sucrose gradient ultracentrifugation fractions was performed in the cut lid of a 1.5ml Eppendorf tube (due to a small volume of 100–200 µl) through a one layer of dialysis membrane (molecular cut-off 14 kDa). The samples were dialysed for approx. 3–4 hours in the dark at 4 °C with the gentle stirring of the dialysis buffer. The composition of the buffer corresponded to that of the buffer used for ultracentrifugation except for sucrose.

3.5. Silver staining

Silver staining was carried out according to Blum (1987) with minor modifications (see Tab. 5). After stopping the development and a short wash with Milli-Q water, the gel was scanned with an Amersham Imager 600RGB gel scanner (GE HealthCare Life Sciences, Tokyo, Japan), using the transmission mode with white light illumination.

Table 5: Protocol used for silver staining of the gel

Step	Chemical/water	Solution (500 ml)	Time of incubation
Fixing (1)	30% ethanol	150 ml	1 h
	10% acetic acid	50 ml	
Washing (2)	20% ethanol	100 ml	15 min
Washing (3)	Milli-Q H_2O		15 min
Sensitisation (4)	$Na_2S_2O_3$ x 5 H_2O	0.1 g	90 s
Washing (5)	Milli-Q H_2O		2 x 20 s
Staining (6)	$AgNO_3$	1 g	30 min
Washing (7)	Milli-Q H_2O		2 x 10 s
Developing (8)	K_2CO_3	15 g	~ 5 min
	Formaldehyde	350 µl	
	Sensitisator (step 4)	25 ml	
Stopping (9)	Tris-base	25 g	2 min
	2.5% acetic acid	12,5 ml	

3.6. Ultracentrifugation

Separation of solubilised pigment-protein complexes on a sucrose gradient by ultracentrifugation reported in the attached publications was performed according to Caffarri *et al.* (2009) with slight modifications. An aliquot of thylakoid membranes containing 200 µg of Chls was centrifuged at 4,600 g/4 °C/4 min, and the pellet was resuspended in 10 mM HEPES (pH 7.5/NaOH) to a Chl concentration of 2 mg/ml. The membranes were then solubilised by α DDM in 10 mM HEPES (pH 7.5/NaOH) with a final concentration of 1% to 0.5 mg/ml of Chls (detergent: Chl mass ratio was 20) and gently vortexed for a few seconds. The sample was subsequently centrifuged at 18,000 g/4 °C/10 min to remove un-solubilised membranes residues and then separated by ultracentrifugation on a sucrose gradient at 284,000 g/4 °C/18 hours (P40ST Swinging Bucket Rotor, ultracentrifuge Hitachi, CP90WX). Gradients were formed directly in the tube by freezing at - 80 °C and subsequent thawing at 4 °C and of 0.65M sucrose solution in 10 mM HEPES (pH 7.5/NaOH) containing CMC of α DDM. The collected PSII fractions from each tube were combined and concentrated using a Millipore Amicon filter with a 50 kDa cut-off at 14,000 g/4 °C/5 min. The sample was then washed twice in 10 mM HEPES (pH 7.5/NaOH) buffer with CMC of α DDM to remove sucrose. The concentrated sample was used directly for specimen preparation for cryo-EM analysis.

In order to further optimise the ultracentrifugation on a sucrose gradient, different buffers with added stabilisers, solubilisation conditions and gradient preparation mechanism were used in addition to the above-mentioned protocol. Two commonly used biological buffers, HEPES (10mM, pH 7.5/NaOH) and MES (25mM, pH 6.5/NaOH), were tested. According to the sucrose gradient preparation method, in addition to the freeze/thaw method mentioned above, gradients were prepared using the Gradient Master device (Model 108, BioComp Instruments, Fredericton, Canada). Sucrose gradients of the required range were prepared by mixing a given amount of light and heavy sucrose solution. The light and heavy solutions consisted of 10% and 30%/40% sucrose, respectively, as well as a buffer component

(HEPES or MES) and the CMC of detergent used for solubilisation. An aliquot of the thylakoid membrane stock solution containing 200 μg of Chls was resuspended in a specific buffer (HEPES or MES) to a final Chl concentration of 1 mg/ml after a brief centrifugation at 4,600 g/4 min/4 °C. Subsequently, a buffer with a given concentration of detergent and optional additives was added to the samples, with a final Chl concentration of 0.5 mg/ml. Samples with α DDM were shortly vortexed and solubilised for a maximum of 2 minutes (1 min for β DDM); samples with digitonin were solubilised for approx. 10–15 minutes with gentle vortexing. Optional additives were used as follows: (i) 1M betaine was already included in the light and heavy solutions used to form the sucrose gradient, (ii) 10mM NaF was added into the solubilising buffer, and (iii) 1% amphipol was added into the already solubilised sample after centrifugation and incubated on ice for 10 minutes. Specifications of the loading amount of Chl and its final concentration are specified in the figure legends. The ultracentrifugation was performed at 284,000 g at 4 °C, with the total centrifugation time depending on the type of gradient (see figure legends for further specifications).

3.7. Western blot

Western blot was performed on proteins isolated from thylakoid membranes using the following procedure. A mixture with a ratio of 100 μg Chls per 1 ml of extraction buffer (14 mM DL-dithiothreitol, 28 mM Na_2CO_3, 175 mM sucrose, 5% (w/v) SDS, and 10 mM EDTA-Na_2) was properly mixed and incubated at 70 °C for 30 min followed by centrifugation at room temperature for 10 min/19,200 g. The supernatant containing the isolated proteins was supplemented with the sample buffer (Tricine Sample Buffer, Bio-Rad; 3x diluted) and dH_2O to a final volume of 20 μl with a final Chl concentration of 50 μg/ml (calculating with their hypothetical 100% extraction efficiency). After 10 minutes of incubation of this mixture at 70 °C, the entire volume was loaded onto a 10% gel (Mini-PROTEAN TGX Precast Protein Gel, Bio-Rad, Hercules, USA). The used running buffers were prepared according to Schägger (2006). The electrophoretic separation conditions were: constant voltage of 100 V/45 min. Separated proteins were transferred from the gel to the polyvinylidene fluoride membrane using Trans-Blot Turbo RTA Mini 0.2 mm PVDF Transfer Kit (Bio-Rad) and subsequently detected on the membrane by a system of two antibodies. The binding of the primary antibodies Anti-LHCB3 (AS01 002) and Anti-LHCB6 (AS01 010) (Agrisera) was detected by a secondary antibody with HRP-enzyme. (All antibodies used in this study were purchased from Agrisera (Vännäs, Sweden)). After incubation with Immobilon Western Chemiluminescent HRP Substrate (Merck, Darmstadt, Germany), the emitted chemiluminescent signal was visualised using chemiluminescence mode on the Amersham Imager 600RGB (GE HealthCare Life Sciences, Tokyo, Japan) gel scanner.

3.8. Electron microscopy - sample preparation, data processing

Specific PSII scs ($C_2S_2M_2$/C_2S_2M/C_2S_2) and PSII mcs separated by gel electrophoresis were, for structural analysis by electron microscopy and SPA or for sample quality verification, obtained from excised gel bands by spontaneous elution according to Kouřil *et al.* (2014) with modifications (see Subsection 3.4.). After overnight elution, the eluted protein complexes were applied on the glow-discharged, carbon-coated copper grid and negatively stained with a 2% aqueous solution of uranyl acetate. Electron microscopy was performed on an FEI Tecnai G2 F20 microscope (FEI, Eindhoven, The Netherlands) operated at 200 kV. Images were recorded with an Eagle 4K CCD camera (FEI, Eindhoven, The Netherlands) at

the final magnification of 134,028x, with the final pixel size of 2.24 Å at the specimen after binning the images to 2048 x 2048 pixels.

The recorded images were subjected to SPA using the Scipion3 image processing framework, which included a correction of the contrast transfer function (CTF) of the microscope in individual images, semi-automated particle selection and their classification into 2D classes.

The best-resolved classes representing projection maps of the most abundant types of PSII scs/mcs were fitted by a structural model of PSII scs from *At* (van Bezouwen *et al.*, 2017). The "spruce-type" PSII sc was fitted with the model of Kouřil *et al.* (2016).

Electron microscopy of isolated grana membranes from *At* and spruce, isolated according to Kouřil *et al.* (2013), was performed either on the FEI Tecnai G2 F20 microscope (FEI, Eindhoven, The Netherlands) with the Eagle 4K CCD camera ((FEI, Eindhoven, The Netherlands) or on a Jeol JEM2010 (Jeol, Tokyo, Japan) with a Quemesa CCD camera (EMSIS, Muenster, Germany).

4. Optimisation of the experimental approach to the structural analysis of spruce photosystem I and photosystem II

4.1. Optimal sample preparation - choice of solubilisation conditions and method of separation

The experimental approach of isolation procedure depends primarily on the character of the required protein complex that will be further analysed (in my case, PSII or PSI) and the natural environment from which the selected protein complex is going to be extracted (e.g. heterogeneous thylakoid membrane). Focusing on photosynthetic organisms, it is important to realise that evolutionary adaptation to a specific habitat led to the evolution of their own specific characteristics in addition to those generally shared within the plant kingdom. As a result, different organisms may contain or produce different chemical substances, enzymes, etc., which may affect the efficiency of the used experimental method. Thus, for almost every organism, the solubilisation conditions need to be carefully adjusted.

Sample quality and quantity are particularly important for high-throughput methods capable of providing detailed information about the analysed organism. An example is the cryo-EM method, which can provide high-resolution structures of proteins and their complexes, however, the quality of the final electron density map is highly dependent on the quality of the original sample. The most important sample properties are high concentration of the studied protein, purity and structural homogeneity. Moreover, extraction of a specific protein complex embedded in the thylakoid membrane while maintaining its intactness is quite challenging and specific approaches have to be used. For this purpose, mild solubilisation reagents are used for their gentle extraction from the thylakoid membrane, followed by non-denaturing separation methods for retrieval of the selected protein complex from its heterogeneous environment, including CN-PAGE or ultracentrifugation.

Thereby, in the following subsections, I discuss several obstacles encountered during sample processing with standard biochemical techniques, along with adequately designed solutions or improvements.

4.1.1. Solubilisation conditions and increase of protein complexes stability

An important step in customising the solubilisation is the choice of buffer necessary to maintain a defined pH that helps to preserve the integrity of the solubilised proteins of the thylakoid membrane. Although HEPES was initially preferred due to its ability to maintain a near-neutral pH of 7.5, later, it was shown that the scs might be more stable at lower pH (Crepin *et al.*, 2016). Our results from cryo-EM analysis revealed a significant loss of larger PSII scs due to their disintegration during sample processing, indicating their possible lower stability at pH 7.5. Therefore, we opted for another commonly used buffer, namely MES, with pH of 6.5. The lower pH was shown to better preserve the binding of peripheral subunits, hypothesising that this phenomenon has a physiological origin since these subunits play an important role during high lumen acidification. An example of such a subunit would be PsbP, functioning as a binding agent for calcium ions within OEC (Crepin *et al.*, 2016), which is more stably bound to PSII at lower pH.

Further, we optimised the conditions of solubilisation with the main objective to obtain the highest yield of specific protein sc while preserving its maximum intactness. The extraction and purification of native protein complexes embedded in bilayer membranes generally pose quite a hindrance. The reason is that while their extraction requires the usage of detergents, the options are significantly limited due to the simultaneous requirement for the

preservation of protein integrity. The generally used α DDM or β DDM, mild non-ionic detergents, provide the best alternative in most cases, with high yields of solubilised protein complexes without their excessive unfavourable rate of disintegration. The other most commonly used non-ionic detergent is digitonin with more than 50 % higher molecular weight than maltosides. However, due to the high toxicity of digitonin, this detergent has recently been replaced by its synthetic, non-toxic analogue, glyco-diosgenin (GDN). The amphiphilic character of the aforementioned detergents allows the extraction of membrane proteins from their constrained natural environment and, by providing them with a substitutional bilayer envelope, preserve them in a soluble form (Lichtenberg *et al.*, 2013). The optimal solubilisation conditions may vary for different photosynthetic organisms such as cyanobacteria, algae, vascular plants, etc., and the efficiency of solubilisation may vary even within a single plant division and need to be accordingly optimised.

In addition, another important attribute that determines the choice of solubilisation conditions is the main aim of the study. Whether the study focuses on the PSII or PSI, ATP synthase, PSII mcs, etc., it should always be taken into consideration that individual scs are extracted with different efficiency by different detergents. An example of different solubilisation efficiency and, thus different resulting pattern of protein complexes after CN-PAGE separation, can be illustrated by a comparison of four conifers: pine, spruce, larch and yew (Fig. 5). While pine and spruce show similar patterns after separation with only a small difference of easier disintegration of pine's PSII scs to smaller forms of C_2S_2/C_2SM than was observed in spruce, larch and yew show completely different pattern under the same solubilisation conditions. Larch is characterised by a relatively strong "resistance" to the used detergent, with only minor solubilisation of its PSII scs and the presence of additional bands of lower molecular weight localised under the PSII cc co-migrating with PSI sc. The absence of fluorescent signal in these low-molecular-weight bands at room temperature implies the presence of PSI in closely unspecified form. In comparison, yew is even more "resistant" to the same solubilisation conditions, with only minor extraction of PSI scs, whereas most of its membranes remained un-solubilised. The use of stronger detergent in the last two conifers led to preferential disintegration of the PSII scs into even smaller forms and overall denser bands in larch, while no improvement in solubilisation was observed in yew.

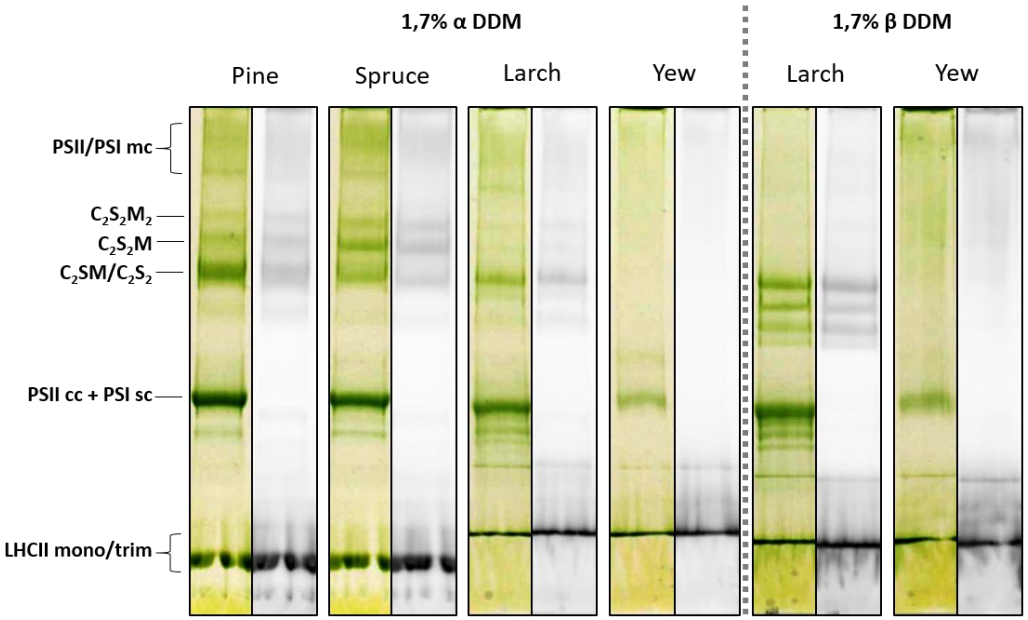

Figure 5: Different solubilisation efficiency of α DDM and β DDM and different patterns of separated photosynthetic complexes in selected conifers, division *Pinophyta*. Electrophoretic separation using CN-PAGE of solubilised thylakoid membranes from conifers (pine, spruce, larch and yew) solubilised with either 1.7% α DDM or 1.7% β DDM. Thylakoid membranes were isolated after 30 min of dark adaptation of plants. Images of selected lines from the gel were scanned at room temperature in transmission mode (green lines) and in fluorescence mode (black and white lines). *Abbreviations: PSII - photosystem II, PSI - photosystem I, LHCII - light-harvesting complex of photosystem II, mc - megacomplex, sc - supercomplex, cc - core complex, mono - monomer, trim - trimer.*

As previously mentioned, different plants are characteristic with variable protein composition and their abundance, the presence or absence of specific enzymes or substances and the overall organisation of thylakoid membranes. All these attributes may affect the final efficiency of thylakoid membrane isolation and the subsequent solubilisation of the protein complexes contained in the membrane. Moreover, due to the heterogeneous distribution of PSI and PSII in the thylakoid membrane, these photosystems are not equally solubilised under the same conditions, as their accessibility to a specific detergent may also differ.

The milder α DDM and the stronger detergent β DDM are commonly used to extract PSII scs from appressed grana, since their size is smaller than the size of digitonin, and they can easily fit between the grana. While the application of α DDM on *At* thylakoid membranes leads to preferential extraction of larger PSII scs and the presence of PSI and PSII mcs, the use of stronger β DDM leads to an almost complete disintegration of these mcs and preferential extraction of smaller PSII sc forms. This phenomenon is accompanied by the higher abundance of free LHCIIs in the form of monomers or trimers (Fig. 6).

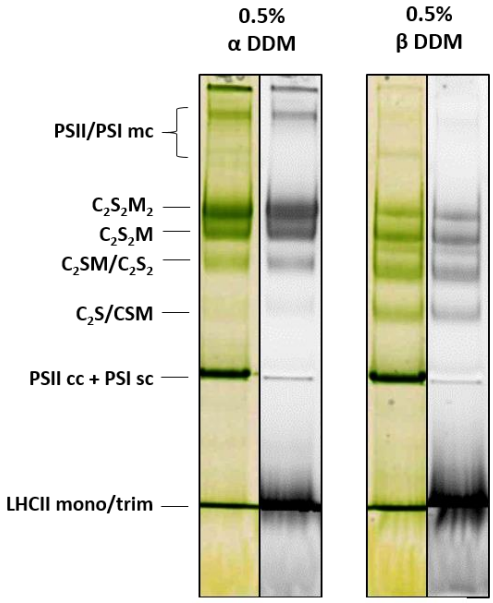

Figure 6: Different solubilisation efficiency of α and β DDM on *Arabidopsis thaliana* thylakoid membranes harvested for isolation after 30 min of dark adaptation. Electrophoretic separation using CN-PAGE of *At* thylakoid membranes solubilised with either 0.5% α DDM or 0.5% β DDM, final Chl concentration of 0.33 mg/ml. Images of selected lines from the gel were scanned at room temperature in the transmission mode (green lines) and in fluorescence mode (black and white lines). *Abbreviations: PSII - photosystem II, PSI - photosystem I, LHCII - light-harvesting complex of photosystem II, mc - megacomplex, sc - supercomplex, cc - core complex, mono - monomer, trim - trimer.*

Digitonin represents a mild detergent, milder than maltoside, and due to its size, it cannot fit into the appressed grana of the thylakoid membrane of higher plants. This fact makes the digitonin more suitable either (i) for extraction of the whole grana or (ii) for preferential extraction of PSI scs due to their localisation in the peripheral parts of grana, grana margins and stromal lamellae. For example, digitonin can be used to extract fragile scs such as PSI-LHCII sc (transition state 2) from *At*, spruce, barley, etc. Considering the above-mentioned potential non-uniform biochemical composition of plants, it is interesting to note that for spruce, a stronger detergent such as maltoside can also be used for PSI-LHCII extraction in addition to digitonin, whereas for *At*, the use of the same detergent would lead to the increased disintegration of its PSI-LHCII sc. It can be then concluded that the PSI-LHCII sc of spruce is more stable during extraction than that from *At*.

Moreover, using digitonin only, we were able to obtain the PSI-LHCII sc even from dark-adapted plants. This phenomenon was observable after the separation of solubilised thylakoid membranes either by electrophoresis or ultracentrifugation (Fig. 7, A and 8, IV). These results are consistent with the observations by Chukhutsina *et al.* (2020) and imply that plants are able to preserve the PSI-LHCII scs (state 2) even in the dark-adapted state *in vivo* for a closer unspecified period of time. We could hypothesise that their existence, even in the absence of light irradiation, is the consequence of their slower disassembly associated with slower dephosphorylation or that the stable pool of PSI-LHCII is deliberately preserved in plants and has functional relevance.

The main conditions optimised for detergents are their final concentration (or Chl to detergent ratio) and incubation time with the sample. Nevertheless, it is possible to also combine the detergents to achieve more efficient extraction. By combining detergents, lower concentrations of a stronger detergent can be used to mitigate its negative effect on the fragile

bonds between the individual subunits (Galka *et al.*, 2012; Crepin *et al.*, 2020). Application of low concentrations of digitonin in *At* thylakoid membranes promotes the preferential extraction of the PSI scs and only limited extraction of PSII scs even with longer incubation times. When samples solubilised in the first round with digitonin undergo solubilisation by two times higher concentration of α DDM that is standardly used, the characteristic pattern of separated PSII scs is clearly visible, whereas the yield of the PSI scs is lower due to their previous extraction by digitonin, and PSI-LHCII is absent (Fig. 7, A). The combination of digitonin and α DDM at low concentrations simultaneously supplemented with NaF allows for significantly more efficient extraction of PSI scs involving the fragile PSI-LHCII sc in both spruce and *At* (in *At* even PSI-6LHCI-LHCII sc, for more information see subsection 4.2.), while application of α DDM alone, even supplemented with NaF, leads to an enormous disintegration of this sc, more pronounced in *At* than in spruce (Fig. 7, B).

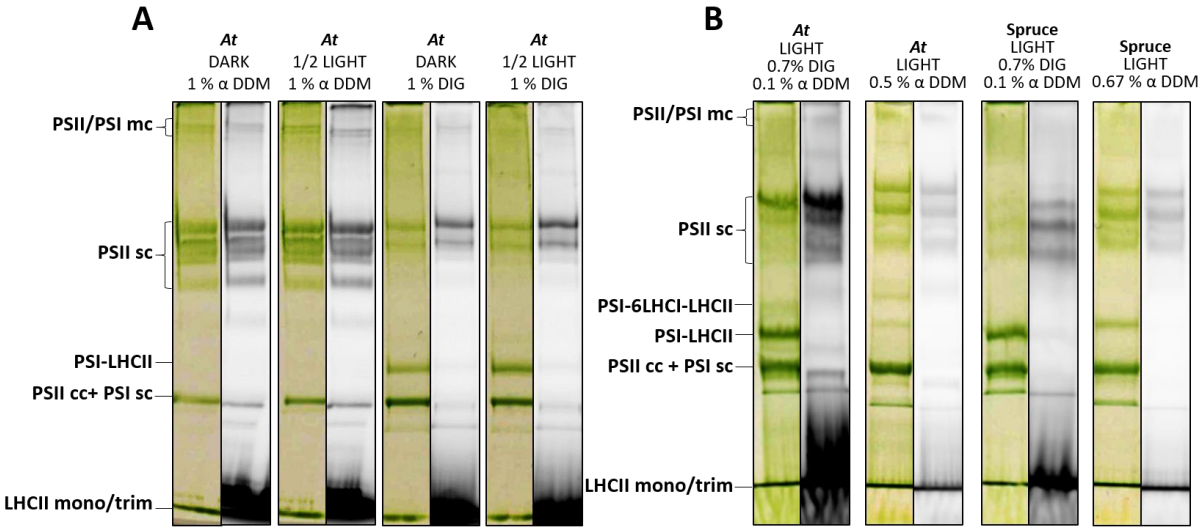

Figure 7: Different solubilisation efficiency of α DDM, digitonin and combination of α DDM and digitonin on *Arabidopsis thaliana* and spruce thylakoid membranes and stability of their PSI-LHCII supercomplex. Electrophoretic separation using CN-PAGE of *At* and spruce thylakoid membranes solubilised with A) 1% digitonin at Chl concentration of 0.33 mg/ml or 1% α DDM after previous solubilisation with 1% digitonin; B) combination of 0.7% digitonin with 0.1% α DDM at Chl concentration of 0.5 mg/ml or, solubilisation with 0.67% and 0.5% α DDM for spruce and *At*, respectively, both at Chl concentration of 0.33 mg/ml and supplemented with 10mM NaF. Membranes were harvested for isolation either after 30 min of dark adaptation (DARK), after one-hour adaptation to half intensity of growing light (1/2 LIGHT), or directly from growing light (LIGHT). Images of selected lines from the gel were scanned at room temperature in transmission mode (green lines) and in fluorescence mode (black and white lines). *Abbreviations: At - Arabidopsis thaliana, PSII - photosystem II, PSI - photosystem I, LHCII - light-harvesting complex of photosystem II, mc - megacomplex, sc - supercomplex, cc - core complex, mono - monomer, trim - trimer, DIG - digitonin.*

When working with fragile membrane protein complexes, the use of stabilisers should be considered. These complexes are particularly sensitive to their surroundings after extraction from the membrane, even though they are encased in a protective envelope consisting of detergent. Another reason for the application of stabilisers is that the detergent itself may not be suitable for further procedures and sample analysis. In optimising the

extraction of the PSI or PSII scs while maintaining their intactness, we opted for three stabilisers, namely amphipol, betaine and NaF.

I) Amphipols are surfactants that substitute the detergents used for membrane protein solubilisation and replace them in the surrounding envelope of extracted protein complexes. Amphipols increase the stability of proteins and prevent their thermodynamic dissociation during separation and aggregation in a detergent-free environment. The most commonly used amphipol A8-35 is suitable even for sample preparation for cryo-EM (see, e.g. Flötenmeyer *et al.*, 2007).

II) Betaine is a small, highly soluble osmolyte that neutralises differences in osmotic pressure, allowing organisms (at a lower level tissues) to adapt to changing environment and abiotic stress caused by salinity. Naturally present across all living organisms, betaine is also known to protect and stabilise the OEC against the dissociation of its subunits from PSII and to coordinate the included Mn cluster (Murata *et al.*, 1992; Papageorgiou and Murata, 1995).

III) NaF is an acid and serine/threonine phosphatase inhibitor, which preserves the phosphorylation state of extracted proteins. NaF is used throughout the entire sample preparation, including buffers used for the isolation of thylakoid membranes as well as buffers for solubilisation. The preservation of proteins in their phosphorylated state has important implications for protein analysis, as this type of modification often determines their function and associated structural characteristics. Adding NaF allows to study the activity of kinases or the effect of their absence in mutants, state transitions and other reactions or protein complexes, which function and structure are regulated by phosphorylation (Vener *et al.*, 1999, 2001).

4.1.2. Selection of suitable separation method and its optimisation

CN-PAGE is the ideal method for the separation of solubilised protein complexes of the photosynthetic apparatus. It finds its application, e.g. in (i) easy verification and determination of the most suitable solubilisation conditions for a specific sample, (ii) separation of individual scs that are further used for sample preparation for TEM and 2D structural analysis of native protein complexes or, (iii) the pre-separation of protein complexes that are further analysed in the second dimension, most often under denaturing conditions. The results from 2D separation provide information about the specific protein composition of the complexes separated in the first dimension, and the spots representing individual proteins can be further used for mass spectrometry analysis and protein quantification. However, it is disadvantageous to combine CN-PAGE with methods that require high concentration of specific protein complex, such as cryo-EM. Indeed, in our work, the extraction of protein complexes separated by CN-PAGE, which were further concentrated to be up to the standard for the cryo-EM requirements, led to their significant disintegration and aggregation. In addition, the final concentration of the extracted proteins was still insufficient for cryo-EM analysis.

Different separation method under non-denaturing conditions represents ultracentrifugation on a sucrose gradient. Ultracentrifugation currently represents the most suitable method for the separation of fragile complexes from thylakoid membranes that simultaneously reaches the cryo-EM standards.

The fractions of PSII scs from spruce in our work (Opatíková *et al.*, 2023) were obtained by ultracentrifugation, using gradient preparation by the freeze/thaw method as described by Caffarri *et al.* (2009). However, the separation was sub-optimal, as the fractions of individual scs, albeit separated, were mostly diffused. Hence, we have begun optimising

this method and looking for further improvements in how to preserve intact scs and increase their stability.

The first step was to change the method of gradient preparation, for which we used Gradient Master instead of the commonly used freeze/thaw protocol (for method specification, see Section 3). This way of preparation provided a significant breakthrough in the quality of separation of solubilised protein complexes. This device is designed to prepare the gradients with variable concentration ranges of the main gradient carrier. Its preparation is fast and precise, and the resulting gradient has smoother transitions, resulting in less diffused and less dispersed fractions with sharper edges.

Due to the optimisation of the solubilisation of thylakoid membranes and the following separation on the sucrose gradient, we were able to significantly improve the separation and subsequent collection of fractions of selected protein complexes. The improved separation manifested itself in more focused bands that were easier differentiated and partially also in the presence of protein complexes with a higher molecular weight representing fragile mcs (Fig. 8, 9). To a lesser extent, the results of ultracentrifugation reflect the influence of the used detergent and the presence of stabilisers on the efficiency of thylakoid membranes solubilisation. For example, the higher yield and concomitant higher stability of proteins are reflected by denser bands of individual scs and the lower presence or complete absence of their smaller forms, e.g. C_2S_2 scs of PSII (Fig. 8, II–IV). And although the gradient prepared by freezing and thawing provides sufficient separation, compared to the gradient prepared by Gradient Master, the fractions are more diffused and consequently less dense (Fig. 8).

The addition of 1M betaine increases the viscosity of the gradient solution, and therefore, the overall separation pattern of individual scs is characterised by their closer and overall higher localisation in the tube compared to the same gradient without betaine. This phenomenon was observable even when the separation took three hours longer compared to the separation without betaine (Fig. 8, II–III).

The addition of amphipol has the opposite effect on protein migration. By forming a protective envelope around the fragile scs, this stabiliser increases their molecular weight, and thus their position in the sucrose gradient is lower. However, this phenomenon is even better observed in the gel after electrophoretic separation, where the scs enveloped by amphipol are localised higher compared to their counterparts without amphipol (see next subsection, Fig. 13).

Nevertheless, the best way how to verify the stabilising effect of optimised buffer pH and added stabilisers such as NaF, betaine and amphipol is a detailed structural analysis of extracted proteins by cryo-EM. From our experience, we can conclude that the addition of betaine results in the preservation of OEC and that the added amphipol forms characteristic envelopes around the extracted proteins and remains stably bound, as even three hours of dialysis did not wash it out. The presence of NaF manifests in the higher yield of PSI-LHCII sc due to the preservation of LHCB2 phosphorylation (Fig. 7).

Furthermore, it is important to pinpoint that the separation on the sucrose gradient can have a significantly different pattern based on the detergent used. This can be well documented by comparing separations with digitonin and α DDM. Since the digitonin molecule is significantly larger, the separation pattern of the solubilised thylakoid membranes, even in the presence of betaine in the gradient, resembles that of samples solubilised with α DDM without the addition of betaine (Fig. 8, II–IV).

In addition to the changed separation pattern, the use of digitonin for thylakoid membrane solubilisation and their subsequent separation on sucrose gradient led to the extraction of fragile PSI-LHCII sc, with a higher abundance of extracted particles compared

to the electrophoretic separation. A feat, which was unachievable by α DDM (Fig. 8, IV). In the broader gradient of 10–40% instead of 10–30%, the scs are separated over a smaller area, resulting in the closer proximity of PSII scs. This fact presents a rather significant obstacle during the extraction of protein complexes as it increases the risk of their mutual contamination. Moreover, in a broader gradient range, the effect of betaine is even more pronounced with separated scs being even more appressed. (Fig. 9). Therefore, for optimal separation of protein complexes from thylakoid membranes while maintaining their intactness, it is advisable to use a lower gradient range, longer separation time and addition of stabilisers.

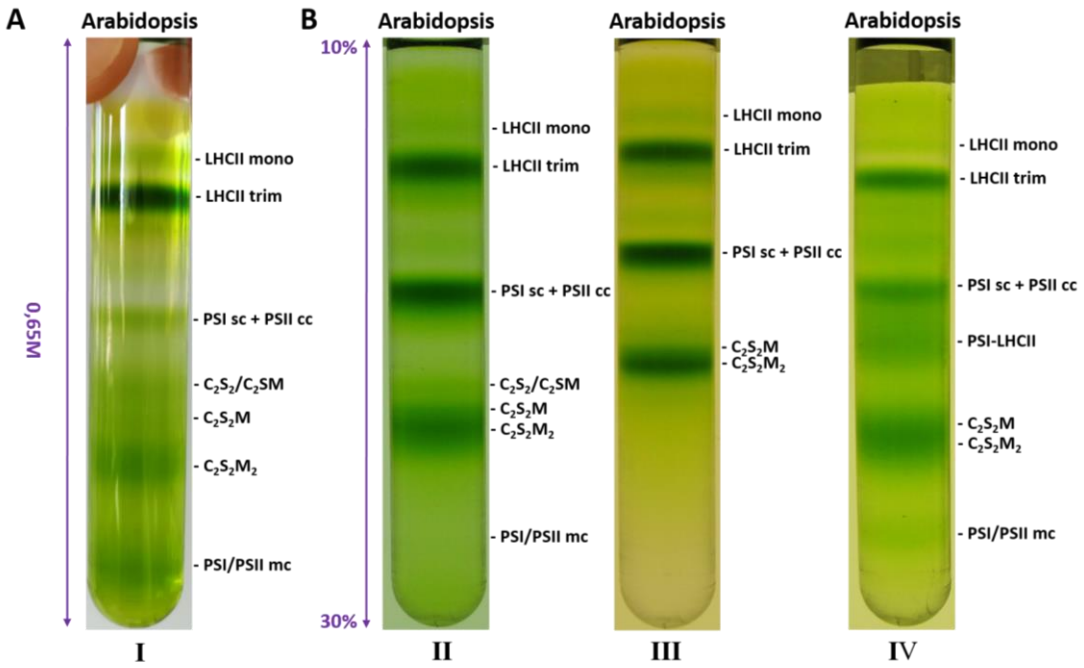

Figure 8: Optimisation of separation on sucrose gradient for solubilised thylakoid membranes from *Arabidopsis thaliana* harvested for isolation after 30 min of dark adaptation. Comparison of sucrose gradients prepared A) from 0.65M sucrose by freezing and consequential thawing at 4 °C and B) gradients prepared with Gradient Master in the range of 10 – 30% sucrose. Thylakoid membranes were solubilised and separated under different conditions as follows: I (0.75% α DDM, 10mM HEPES (pH 7.5/NaOH), Chl concentration of 0.5 mg/ml, 17 hours of separation); II (0.75% α DDM + 1% amphipol, 25mM MES (pH 6.5/NaOH), Chl concentration of 0.5 mg/ml, 13 hours of separation); III (0.75% α DDM + 1% amphipol, 25mM MES (pH 6.5/NaOH) + 1M betaine, Chl concentration of 0.5 mg/ml, 16 hours of separation); IV (1% digitonin + 1% amphipol, 25mM MES (pH 6.5/NaOH) + 1M betaine, Chl concentration of 0.33 mg/ml, 16 hours of separation). *Abbreviations: PSII - photosystem II, PSI - photosystem I, LHCII - light-harvesting complex of photosystem II, mc - megacomplex, sc - supercomplex, cc - core complex, mono - monomer, trim - trimer.*

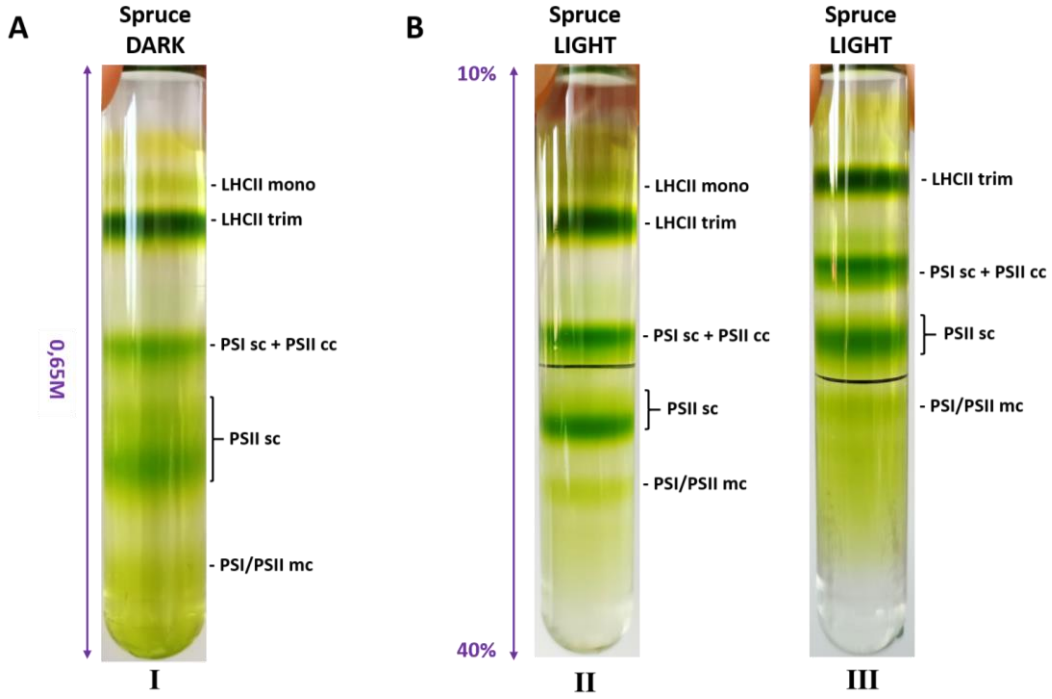

Figure 9: Optimisation of separation on sucrose gradient for solubilised thylakoid membranes from spruce harvested for isolation either after 30 min of dark adaptation (DARK) or directly from growing light (LIGHT). Comparison of sucrose gradients prepared A) from 0.65M sucrose by freezing and consequential thawing at 4 °C and B) gradients prepared with Gradient Master in the range of 10 – 40% sucrose. Thylakoid membranes were solubilised and separated under different conditions as follows: I (1% α DDM, 10mM HEPES (pH 7.5/NaOH), Chl concentration of 0.33 mg/ml, 17 hours of separation); II (1% α DDM + 10mM NaF, 10mM HEPES (pH 7.5/NaOH), Chl concentration of 0.5 mg/ml, 15 hours of separation); III (1% α DDM + 1% amphipol + 10mM NaF, 25mM MES (pH 6.5/NaOH) + 1M betaine, Chl concentration of 0.5 mg/ml, 14 hours of separation). *Abbreviations: PSII - photosystem II, PSI - photosystem I, LHCII - light-harvesting complex of photosystem II, mc - megacomplex, sc - supercomplex, cc - core complex, mono - monomer, trim - trimer.*

The necessity to optimise and improve the currently used methods is evident from the results obtained for spruce (Opatíková *et al.*, 2023). In spruce, the commonly abundant C_2S_2M and the slightly less populated $C_2S_2M_2$ forms, although present in our fraction from sucrose gradient, were underrepresented in the final data set after cryo-EM analysis, moreover, with the loss of two subunits from OEC and PsbJ subunit, all located at PSII periphery. We ascribed this loss to the suboptimal preparation conditions that increased the susceptibility of the extracted particles to the environment and made them more prone to disintegration.

4.2. State transitions in spruce

State transitions are characterised by the balancing of the energy absorption between the two photosystems. Upon preferential excitation of PSII, a significant reduction of PQ via thioredoxins leads to the activation of the specific kinase STN7/STT7 (in higher plants and green algae, respectively). Activated kinase phosphorylates LHCIIs (LHCB1 and LHCB2) (Bellaflore *et al.*, 2005), with the maximum phosphorylation observed under non-saturating light conditions (Rochaix *et al.*, 2014). Phosphorylated LHCII trimers bind to the PSI and effectively transfer the harvested energy to its RC.

The only high-resolution cryo-EM structure of the PSI-LHCII sc in higher plants has been solved for *Zm* at 3.3 Å resolution with one bound LHCII trimer (Pan *et al.*, 2018) and for the green alga *Cr* at 3.42 Å (Huang *et al.*, 2021) and 2.84 Å (Pan *et al.*, 2021) resolution with two bound LHCII trimers. The high-resolution structures provided detailed information of this sc composition and thus, in some cases, allowed to resolve previous discrepancies caused by limited resources. For example, original studies on *Cr* implied that the binding of LHCII trimer to the PSI is conditioned by simultaneous binding of the monomeric antenna CP29, along with the minor presence of CP26 (Kargul *et al.*, 2005; Tokutsu *et al.*, 2009; Drop *et al.*, 2014b; Takahashi *et al.*, 2014). However, since neither of these antennae were observed in both high-resolution structures of *Cr*, it is assumed that they were either only a contaminant of this fraction in previous studies (Pan *et al.*, 2021) or were present in negligible sub-stoichiometric amount (Drop *et al.*, 2014b; Huang *et al.*, 2021).

In addition to the high-resolution structures from *Zm* and *Cr*, the lower resolution of PSI-LHCII sc structures has been obtained for other land plants, with the *At* as a pioneer (Kouřil *et al.*, 2005a, Yadav *et al.*, 2017) or from other organisms such as *Pisum sativum* (Qin *et al.*, 2015; Mazor *et al.*, 2015, 2017) or the moss *Pp* (Yan *et al.*, 2021; Gorski *et al.*, 2022). Different studies focusing on state transitions in land plants have further characterised this sc and hypothesised about the essentiality of LHCII trimers phosphorylation for their attachment (see, e.g. Benson *et al.*, 2015), or emphasised their more complex regulation by an accompanying modification such as acetylation (see, e.g. Koskela *et al.*, 2020) (see the introduction for more details).

Moreover, the structural studies of this sc in land plants, combined with biochemical and fluorescence measurements data (see, e.g. Benson *et al.*, 2015; Yadav *et al.*, 2017; Schwartz *et al.*, 2018), strongly indicate the possibility of biding more than one LHCII trimer, as is characteristic for green algae. In *At*, specifically PSI-LHCII fraction obtained by interval zone free-flow electrophoresis, Yadav *et al.* (2017) observed attachment of a second LHCII trimer on the side of the LHCI belt of PSI in variable positions. However, the confirmation of PSI-LHCII$_{(n)}$ existence in higher plants remains controversial. The reason is that apart from the free-flow electrophoresis, where the separation efficiency of individual proteins is questionable, a specific fraction or band exclusive for this sc has not yet been obtained and visualised in land plants, neither by CN-PAGE nor ultracentrifugation. Moreover, the natural affinity of LHCII trimers for PSI extracted from the movement-limiting thylakoid membrane into the soluble buffer must be considered, as this only further supports the possible artificial origin of this sc in vascular plants. Any structural confirmation is then biochemically unsupported.

Looking under the surface, although the essential single phosphorylated N-terminus of LHCB2 (Thr3) and the surrounding amino acid region responsible for the binding of the LHCII trimer to PSI sc is conserved in algae and land plants, the variability in this sc has been observed. PSI-LHCII$_2$ in *Cr* is, for example, characterised by (i) a rotational shift of its first LHCII trimer within the membrane plane in comparison to the trimer in land plants and (ii) with the presence of the second bound LHCII trimer, both with highly dynamic binding (Huang *et al.*, 2021; Pan *et al.*, 2021). Interestingly, *Pp* is characterised by a lower level of LHCII phosphorylation compared to the levels observed in land plants and green algae (Busch *et al.*, 2013). Moreover, in plants, the LHCII trimer is pivoted to the stromal side, whereas in *Cr*, the situation is *vice versa*, and the first LHCII trimer is pivoted to the opposite side into the lumen. The rotational shift of the first LHCII trimer in *Cr* and different phosphorylation level in *Pp* suggest specific regulatory mechanisms evolved in plant species with respect to their environmental niche. Furthermore, in *Cr*, the second trimer stabilises the binding of the

first LHCII trimer and interacts with the core via the PsaH subunit. However, since the specific region of the PsaH subunit responsible for interaction with the second trimer considerably differs in the *Cr*, *Pp* and *Zm*, land plants are expected to lose the ability to bind the second LHCII trimer in the same manner as *Cr* and this binding is, therefore, specific only for *Cr* as a representative of green algae (Shang *et al.*, 2023).

It is interesting to pinpoint that although Crepin *et al.* (2020) also observed a larger form of the PSI-LHCII sc in *At*, this sc did not include the second attached LHCII trimer. Using a biochemical approach and electron microscopy, they revealed the existence of the PSI-LHII sc with an additional LHCA1/4 dimer, PSI-6LHCI-LHCII, previously considered to be exclusive to algae (Suga *et al.*, 2019). A similar phenomenon was also observed by Pinnola *et al.* (2018), who revealed the attachment of a closer unspecified dimer next to the LHCA1/4 dimer of PSI in *Pp* (according to the updated composition of LHCA belt in *Pp* by Gorski *et al.*, 2022, it is next to the dimer LHCA1/2b). And although its existence was originally thought to be dependent on the presence of LHCB9, a protein exclusive to this moss, the position of LHCB9 binding to the PSI (Iwai *et al.*, 2018) suggests otherwise. As the position of this dimer in *At* is shifted closer to the PsaH subunit of PSI compared to algae (Suga *et al.*, 2019), this dimer can easily interact with the bound LHCII trimer in its close proximity. Moreover, it is hypothesised that the binding of this dimer and LHCII trimer to PSI are mutually dependent. Nevertheless, whether the binding of the LHCII trimer is conditional for the binding of the LHCA1/4 dimer or it is *vice versa* is still unclear, although the former version is currently more preferred. The function of this additional dimer has been assigned to either stabilisation of LHCII trimer attachment to PSI, creation of a binding site for loosely bound LHCII trimers, or deliberate formation of the access' blockade for phosphatase to the phosphorylated threonine at the N-terminus of LHCB2 (Crepin *et al.*, 2020).

In relation to Yadav *et al.* (2017), we observed this larger PSI-LHCII$_2$ sc also in spruce as a contaminant of the PSI-LHCII fraction obtained by CN-PAGE. Nevertheless, due to its low abundance and the relatively substantial variability in the second trimer binding position (higher than observed for *At*, Yadav *et al.*, 2017), the resulting resolution was sufficient only for the characterisation of the different binding positions of the second LHCII trimer (Fig. 10), however insufficient for a more detailed structural analysis. We hypothesise that the high variability of the second trimer position towards the PSI cc is responsible for a non-uniform migration of the specific PSI-LHCII$_2$ sc forms and thus underlies the difficulty in achieving its unique, clearly visible band/fraction by standard separation. Therefore, in addition to obtaining a better resolution of PSI-LHCII$_2$ sc in spruce, we simultaneously aimed our efforts at obtaining a specific band/fraction where the PSI-LHCII$_2$ sc would represent the major moiety. In pursuit of this goal, we have put a considerable effort into optimising the protocol for its separation and extraction, and although the process is still ongoing, several selected experimental approaches and their results are listed below.

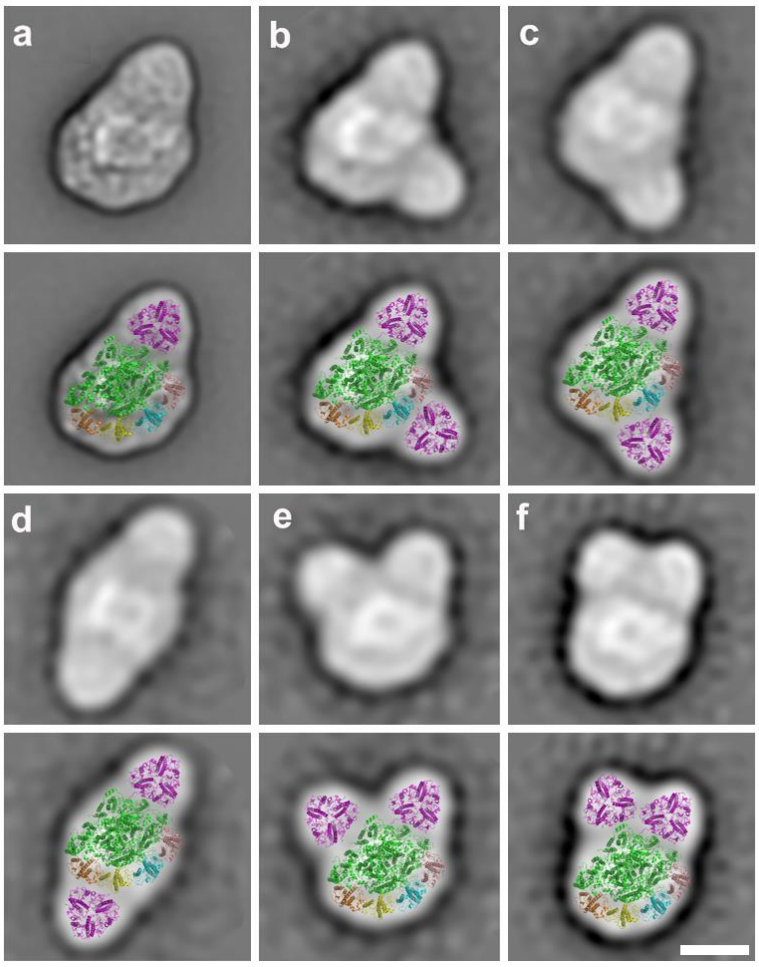

Figure 10: Projections maps of PSI-LHCII and PSI-LHCII$_{(2)}$ supercomplexes from spruce obtained by single particle electron microscopy. Projections were fitted with the known high-resolution structure of maize PSI-LHCII (Pan *et al.*, 2018, PDB identifier 5ZJI). A) Sc composed of PSI sc and one LHCII trimer attached to PSI cc subunits PsaA and PsaH, B–D) scs composed of PSI and two LHCII trimers with the second trimer attached in different positions within LHCA belt (via LHCA2/3 dimer, via both antennae LHCA2 and LHCA4 or via LHCA1/4 dimer), E–F) scs composed of one PSI and two LHCII trimers, the second trimer attached directly to the PSI cc. Structural assignment: PSI cc (green), LHCA1–4 (orange, blue, brown, yellow, respectively), LHCII trimer (magenta). The scale bar is 10 nm. Adapted from Arshad (2022).

Using our standardly optimised conditions for solubilisation (0.5% and 0.67% α DDM for *At* and spruce, respectively) and running 4–8% gradient CN-PAGE, the band with the major abundance of PSI-LHCII is clearly visible in both plants, localised above the band with co-migrating PSI sc and PSII cc. Moreover, a band representing PSI-6LHCI-LHCII is clearly visible in *At*, however, its abundance together with the abundance of PSI-LHCII is lower in *At* than in spruce due to the use of relatively strong detergent maltoside. In both samples, the three largest PSII scs ($C_2S_2M_2$, C_2S_2M and C_2S_2/C_2SM) form bands at the corresponding positions, with a visual difference in their ratio, resulting from (i) their different abundance *in vivo*, (ii) different solubilisation efficiency and, (iii) different stability after solubilisation. While in *At* the most abundant are the two largest PSII forms, in spruce, the most abundant form is the C_2S_2M (Fig. 11), a phenomenon that has been previously observed by our group (Kouřil *et al.*, 2016). It should be clarified that in the 4–8% gradient gel, the trimers and monomers of LHCII co-migrate and form a single band in the front of the gel.

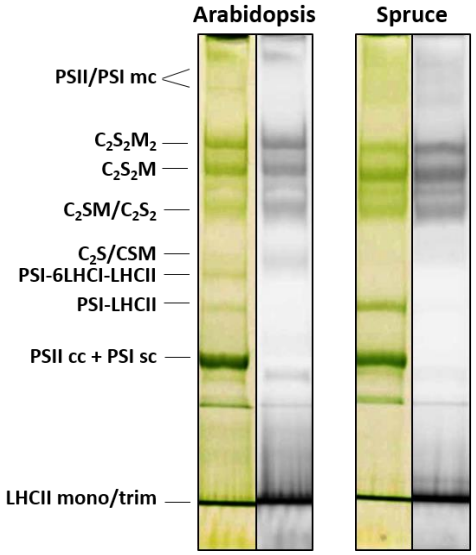

Figure 11: CN-PAGE of solubilised thylakoid membranes from spruce and *Arabidopsis thaliana* harvested for isolation directly from growing light. Electrophoretic separation of spruce and *At* thylakoid membranes solubilised with 0.67% and 0.5% α DDM, respectively, at a final Chl concentration of 0.33 mg/ml. Images of the selected lines from the gel were scanned at room temperature in transmission mode (green lines) and fluorescence mode (black and white lines). *Abbreviations: PSII - photosystem II, PSI - photosystem I, LHCII - light-harvesting complex of photosystem II, mc - megacomplex, sc - supercomplex, cc - core complex, mono - monomer, trim - trimer.*

To improve the PSI-LHCII$_2$ extraction from spruce, we focused on the optimisation of solubilisation conditions and separation. In addition to already tested different concentrations of α DDM and the time of its incubation with the sample, we tested: i) other detergents, specifically digitonin and β DDM, again at different concentrations, incubation times and their combination with α DDM, ii) MES buffer for the preservation of lower pH during solubilisation and separation, iii) buffer containing ACA, which loosens the appressed grana that are then more accessible to the milder detergent digitonin, while simultaneously preserving the stability of the scs, iv) different gradient of acrylamide gel or pre-casted gel, and, v) different separation method, namely ultracentrifugation on a sucrose gradient.

I) Simultaneous application of α DDM and digitonin for solubilisation confirmed the previously observed phenomenon that the combination of these two detergents has a milder negative effect on weaker bonds and significantly enhances the extraction of fragile PSI-LHCII scs (Galka *et al.*, 2012). However, we did not observe the presence of the unique PSI-LHCII$_2$ band (Fig. 12), although electron microscopy confirmed the presence of this particle in small amounts as a contaminant in the PSI-LHCII band. Extraction of PSII scs from the thylakoid membrane was strongly suppressed at lower concentration of α DDM, as reflected by their very low abundance in CN-PAGE, and only slightly increased at elevated concentrations of this detergent (Fig. 12). And while the 1–1.5% digitonin seems to be optimal for PSI extraction with concurrent preservation of their intactness, 2–2.5% digitonin proved to have a more disruptive effect (Fig. 12).

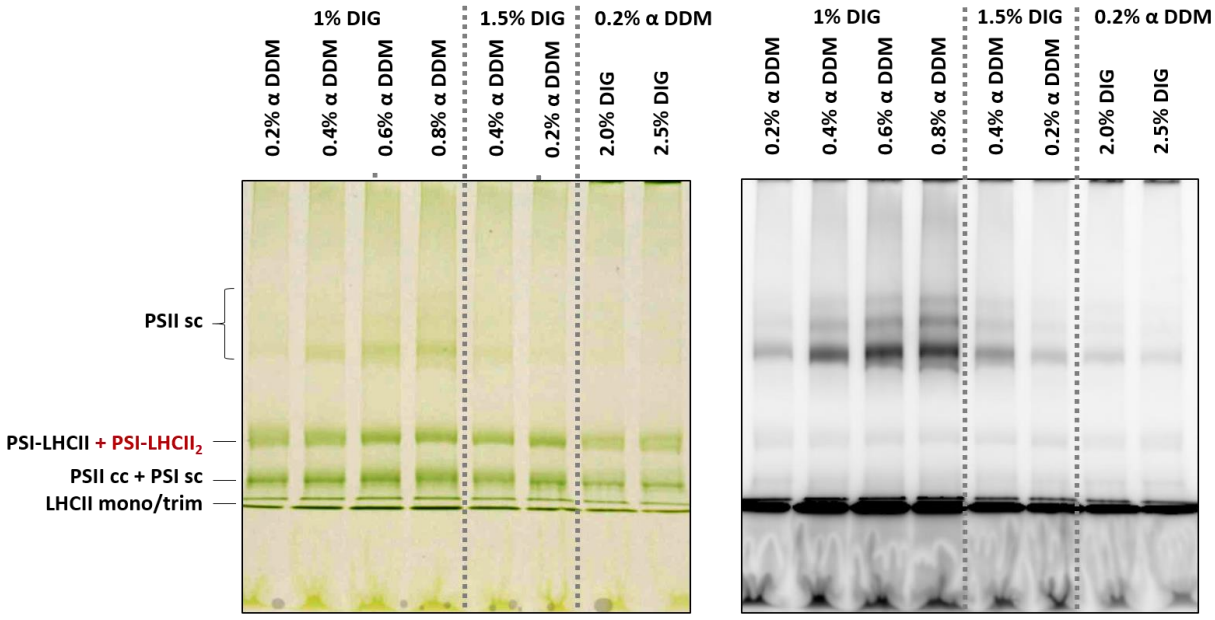

Figure 12: CN-PAGE of solubilised thylakoid membranes from spruce harvested for isolation directly from growing light. Electrophoretic separation of spruce thylakoid membranes solubilised with a combination of different concentrations of digitonin and α DDM (described in the line titles) at a final Chl concentration of 0.5 mg/ml. Images of the gel were scanned at room temperature in transmission mode (green image) and in fluorescence mode (black and white image). *Abbreviations: PSII - photosystem II, PSI - photosystem I, LHCII - light-harvesting complex of photosystem II, sc - supercomplex, cc - core complex, mono - monomer, trim - trimer, DIG - digitonin.*

I, II and IV) To increase the stability of this fragile complex, we tested lower pH of 6.5 preserved by MES buffer in combination with added amphipol a8-35. For separation, we opted for a broader acrylamide gradient of 4–10% or 4–12%, both with a 4% stacking gel, combined with a lower amount of loaded Chl per well to achieve sharper, denser bands, which may be otherwise diffused in the 4–8% gradient. And finally, we tested the solubilising effect of both α and β DDM.

While milder α DDM provides sufficient solubilisation of *At* thylakoid membranes, its solubilising effect on spruce is significantly lower (Fig. 13). Oppositely, use of β DDM on *At* leads to the increased degradation of its scs, while in spruce it allows more efficient solubilisation of the thylakoid membranes (Fig. 14). However, neither of these two separations resulted in a single specific band for PSI-LHCII$_2$ (Fig. 13 and 14).

Nevertheless, it is interesting to note that we could clearly observe the effect of amphipol in the gel, which enveloped the solubilised protein complexes and thus increased their molecular weight. This effect should be taken into consideration when evaluating the separation results for samples with and without amphipol. The expected increase in stability of scs due to added amphipol could be supported by a stronger signal (in transmission and fluorescent mode) of larger PSII scs in *At*. However, due to the low efficiency of solubilisation, the effect of amphipol in spruce cannot be evaluated.

Focusing on the overall separation, due to the broader gradient range, the PSII scs characterised by larger molecular weight are separated over a smaller area, which complicates their distinction, although the bands are sharper. In addition, the more efficient solubilisation of *At* thylakoid membranes (Fig. 13) and the overall higher amount of loaded sample (Fig. 14) led to Chl overloading. Combined with the longer separation time due to the broader gradient,

this led to the presence of characteristic ”fussy” bands, more pronounced in the gel with the wider range of gradient, probably caused by the depletion of ions in the running buffer. On the other hand, with increasing gradient ranges, complexes and subunits with lower molecular weight are separated with higher resolution over a larger area of the gel. This led to the discerning of the characteristic M-band (M-LHCII trimer-LHCB4-LHCB6 complex) in *At* (Bassi and Dainese, 1992), which is absent in spruce due to the loss of LHCB3 and LHCB6 (Fig. 14).

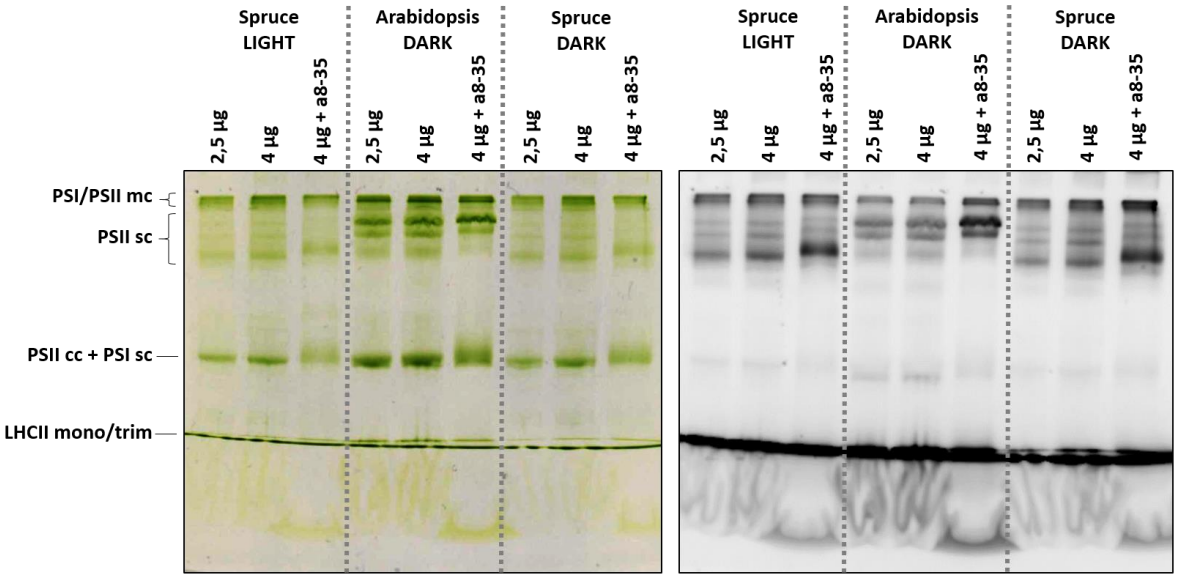

Figure 13: CN-PAGE of solubilised thylakoid membranes from spruce and *Arabidopsis thaliana* harvested for isolation either directly from growing light (LIGHT) or after 30 min of dark adaptation (DARK). Electrophoretic separation of spruce and *At* thylakoid membranes solubilised with 1% α DDM in MES buffer supplemented with 1% amphipol and 10mM NaF, in 4% stacking + 4–10% separating gradient gel. Labels represent the loaded amount of Chls (µg) per well (plus indicate the potentially added amphipol in three samples). Images of the gel were scanned at room temperature in transmission mode (green image) and in fluorescence mode (black and white image). *Abbreviations: PSII - photosystem II, PSI - photosystem I, LHCII - light-harvesting complex of photosystem II, mc - megacomplex, sc - supercomplex, cc - core complex, mono - monomer, trim - trimer, a8-35 - amphipol.*

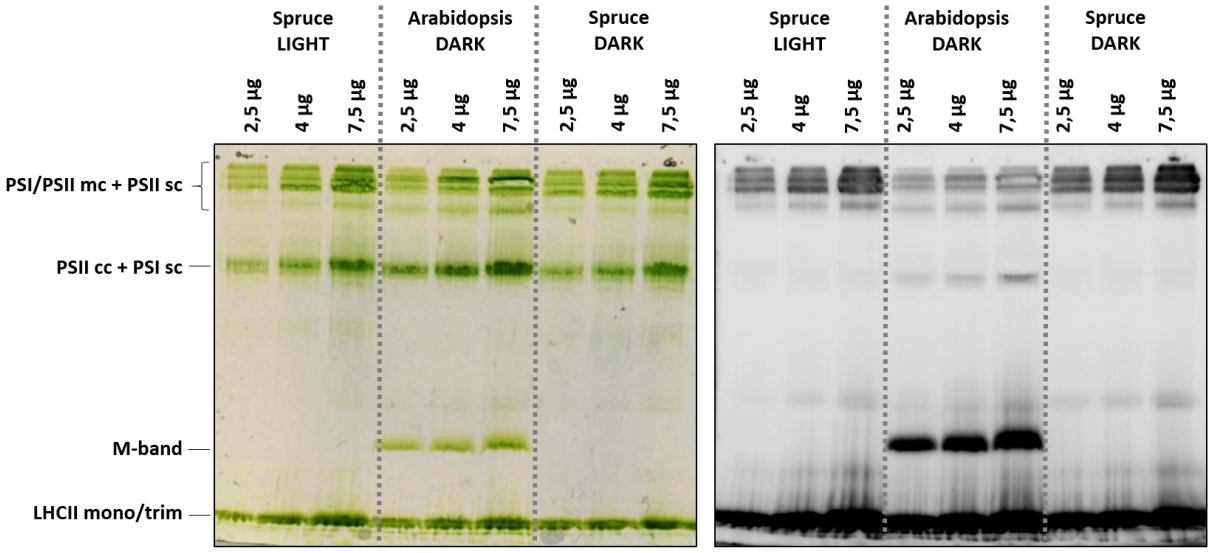

Figure 14: CN-PAGE of solubilised thylakoid membranes from spruce and *Arabidopsis thaliana* harvested for isolation either directly from growing light (LIGHT) or after 30 min of dark adaptation (DARK). Electrophoretic separation of spruce and *At* thylakoid membranes solubilised with 1% β DDM in MES buffer in 4% stacking + 4–12% separating gradient gel. Labels represent the loaded amount of Chls (µg) per well. Images of the gel were scanned at room temperature in transmission mode (green image) and in fluorescence mode (black and white image). *Abbreviations: PSII - photosystem II, PSI - photosystem I, LHCII - light-harvesting complex of photosystem II, mc - megacomplex, sc - supercomplex, cc - core complex, mono - monomer, trim - trimer, M-band – M-LHCII trimer-LHCB4-LHCB6.*

I, III and IV) To improve the extraction of PSI scs from membranes using only the milder detergent digitonin without maltoside, we tested ACA solubilisation buffer according to Rantala *et al.* (2017). Solubilised thylakoid membranes were then separated using the 4–15% pre-casted gel (Fig. 15) since we decided to test whether a commercially prepared gel would help with the separation and visualisation of fragile protein complexes extracted with low efficiency. The solubilisation conditions combining ACA and 1.5–2% digitonin were suitable for preferential extraction of labile PSI scs in high amounts, and this separation resulted in the clear and nicely separated band for PSI-LHCII. Since the position of the band localised directly above the PSI-LHCII band corresponded to the expected position of PSI-$LHCII_2$ sc, we verified its composition by TEM. However, analysis of this band revealed a major abundance of the C_2S_2 PSII sc with only low amounts of PSI-$LHCII_2$ sc, and therefore this separation cannot be considered to be a suitable method for its separation (Fig. 15).

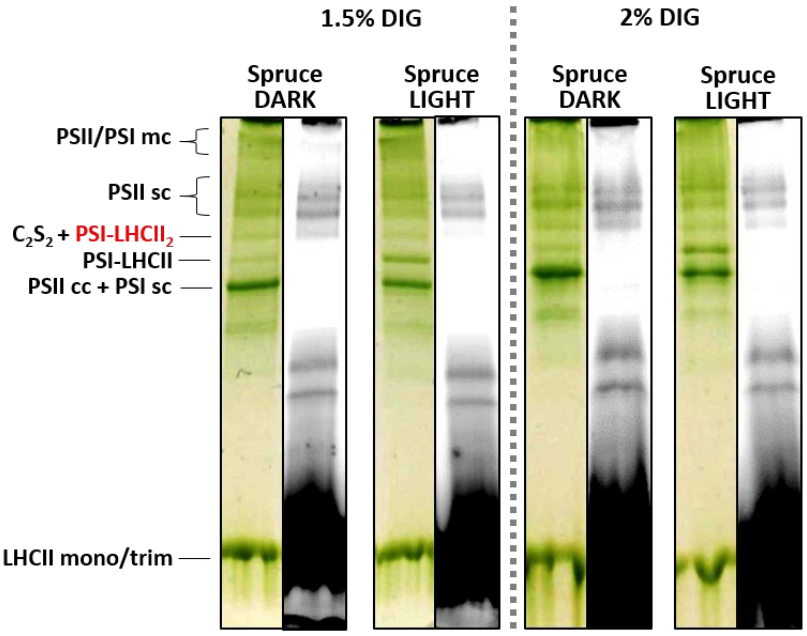

Figure 15: CN-PAGE of solubilised thylakoid membranes from spruce harvested for isolation either directly from growing light (LIGHT) or after 30 min of dark adaptation (DARK). Electrophoretic separation of spruce thylakoid membranes solubilised with 1.5 or 2% digitonin and final Chl concentration of 0.5 mg/ml with 10mM NaF in ACA buffer (loading of 25 µl per well), supplemented with 0.1% sodium deoxycholate after solubilisation, separated in 4–15% pre-casted gradient gel. Images of the selected lines from the gel were scanned at room temperature in transmission mode (green lines) and in fluorescence mode (black and white lines). *Abbreviations: PSII - photosystem II, PSI - photosystem I, LHCII - light-harvesting complex of photosystem II, mc - megacomplex, sc - supercomplex, cc - core complex, mono - monomer, trim - trimer, DIG - digitonin.*

V) Nevertheless, without any promising results from electrophoretic separation, we opted for separation on sucrose gradient, where we tested combinations of different (i) buffers (HEPES (pH 7.5/NaOH) or MES (pH 6.5/NaOH)), (ii) detergents (α DDM, digitonin), (iii) and different additives such as amphipol, betaine and NaF (Fig. 16). As discussed in the previous section, the gradient prepared by Gradient Master provides significantly higher resolution of the separated protein complexes, especially PSII scs and PSI/PSII mcs, under standard conditions compared to the separation on the gradient prepared by freezing at -80°C and thawing at 4°C (Fig. 16, I–II, VI). The combination of 0.5–1% digitonin with a low concentration of α DDM (0.1–0.2%) allows the prevalent extraction of PSI scs, with the main two bands of interest further analysed and designated as the PSI sc co-migrating with PSII cc (upper one, No. 3) and the fragile PSI-LHCII sc (lower one, No. 4) (Fig. 16, III–V and VII). The highest yield of PSI-LHCII fraction was obtained with a combination of 1% digitonin and 0.2% α DDM supplemented with 0.6% amphipol separated in MES buffer at pH 6.5 with the addition of 1M betaine (Fig. 16, VII). A higher concentration of α DDM (2.5%) combined with 1% digitonin led to the complete disintegration of the PSI-LHCII sc regardless of the addition of amphipol, NaF, betaine and lower pH (Fig. 16, VIII).

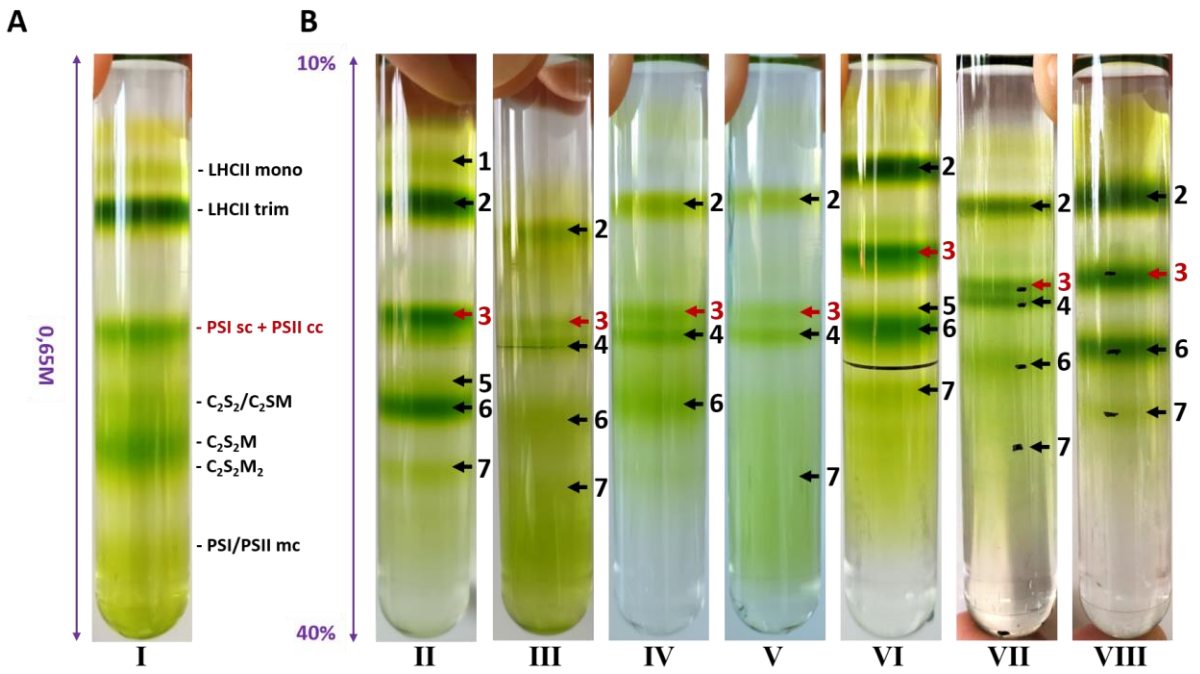

Figure 16: Optimisation of thylakoid membrane solubilisation, the preparation method of sucrose gradient, buffer composition, and addition of optional stabilisers to obtain PSI-LHCII$_2$ fraction from spruce. Thylakoid membranes were harvested for isolation directly from growing light. Images of solubilised thylakoid membranes from spruce, final Chl concentration of 0.5 mg/ml, separated by ultracentrifugation under different conditions: I and II (1% α DDM, 10mM HEPES (pH 7.5/NaOH)); III (0.1% α DDM + 0.5% digitonin, 10mM HEPES (pH 7.5/NaOH)); IV (0.2% α DDM + 1% digitonin + 10mM NaF + 1% amphipol, 10mM HEPES (pH 7.5/NaOH)); V (0.1% α DDM + 0.5% digitonin + 10mM NaF + 1% amphipol, 10mM HEPES (pH 7.5/NaOH)); VI (1% α DDM + 10mM NaF + 1% amphipol, 25mM MES (pH 6.5/NaOH) + 1M betaine); VII (0.2% α DDM + 1% digitonin + 10mM NaF + 0.6% amphipol, 25mM MES (pH 6.5/NaOH) + 1M betaine); VIII (2.5% α DDM + 1% digitonin + 10mM NaF + 0.7% amphipol, 25mM MES (pH 6.5/NaOH) + 1M betaine). Gradients I, VII and VIII: 17 hours of separation, II–V: 14 hours of separation and VI: 15 hours of separation. Protein complexes labelled with numbers as follows: 1 - LHCII monomers, 2 - LHCII trimers, 3 - PSI sc + PSII cc, 4 - PSI-LHCII, 5 - C_2S_2/ C_2SM, 6 - PSII scs ($C_2S_2M_2$ + C_2S_2M), 7 - PSI/PSII mcs. A) Gradient prepared from 0.65M sucrose by freezing and thawing and B) gradients prepared by Gradient Master in the range of 10 - 40% sucrose. Fractions representing PSI sc co-migrating with PSII cc are highlighted in red colour for easier orientation within the gradient. *Abbreviations: PSII - photosystem II, PSI - photosystem I, LHCII - light-harvesting complex of photosystem II, mc - megacomplex, sc - supercomplex, cc - core complex, mono - monomer, trim - trimer.*

However, since these experiments did not lead to any significant result in terms of the successful separation of PSI-LHCII$_2$ sc, we chose a different approach to extract this sc without detergents by styrene maleic acid (SMA) co-polymer, using a modified protocol originally designed by Lee *et al.* (2016). This method is based on the stabilisation of the extracted proteins by keeping them in their natural environment, encapsulated in their lipid bilayer surrounded by SMA. Despite its limitations as i) the maximum molecular weight of the extracted proteins is approximately 400 kDa or 36 transmembrane helices, ii) the pH-dependent solubility of SMA (insoluble below pH 6.5), and iii) the side effect of SMA as a divalent cations chelator resulting in an insoluble chelate, this method has its advantages, and we decided to test it in the separation of our PSI-LHCII$_2$ sc. We used two protocols: i) the

overnight incubation of spruce thylakoid membranes with the polymer at 4 °C, and ii) one-hour incubation with the polymer at 40 °C. Although we obtained three highly diffused fractions after separation on the sucrose gradient, none of them corresponded to the desired PSI-LHCII$_2$ fraction, but only to PSI-LHCII (data not shown).

To further biochemically reinforce the existence of PSI-LHCII$_2$ sc, we attempted to confirm its presence in the second dimension of electrophoresis, which is much more sensitive compared to native electrophoresis. The reason is that we did not manage to obtain one clear fraction or band of this sc, only its contaminant presence in another band (Fig. 12, 15). For the first dimension, we used BN-PAGE (Blue Native) instead of standard CN-PAGE to better visualise all separated bands. In the first dimension of BN-PAGE, the band corresponding to PSI-LHCII was clearly visible, but no band that could represent PSI-LHCII$_2$ was observed (Fig. 17, A). The most representative line from the first dimension was selected and used for electrophoresis in the second dimension under denaturing conditions. The separated proteins were then visualised by a silver staining technique characterised by high detection sensitivity. Interestingly, although no band corresponding to the PSI-LHCII$_2$ sc was observed above the PSI-LHCII in the first dimension as previously mentioned, a characteristic pattern of separated PsaA/PsaB and LHCAs proteins with a strong signal for LHCB1 and LHCB2 were observed below this apparently unoccupied region in the second dimension. Even though the separation in the second dimension was not optimal, as the dark horizontal lines representing partial lateral diffusion of the separated proteins are present, the LHCAs pattern is clearly discernible in the position of the PSI mcs and in additional three lower bands from the BN-PAGE strip, two of which represent the PSI sc co-migrating with PSII cc and PSI-LHCII (Fig. 17, B). This is further confirmation of a potentially formed PSI-LHCII$_2$ in spruce, undetectable in the first dimension, nevertheless supported in the second dimension. Admittedly, the presence of different PSI sc (with additionally attached, closely unspecified proteins) cannot be excluded without more detailed analysis, for example, by mass spectrometry. However, the position in the BN-PAGE gel derived from the characteristic pattern of PSI proteins in the 2D gel would be consistent with the expected position of PSI with two LHCII trimers based on its calculated molecular weight.

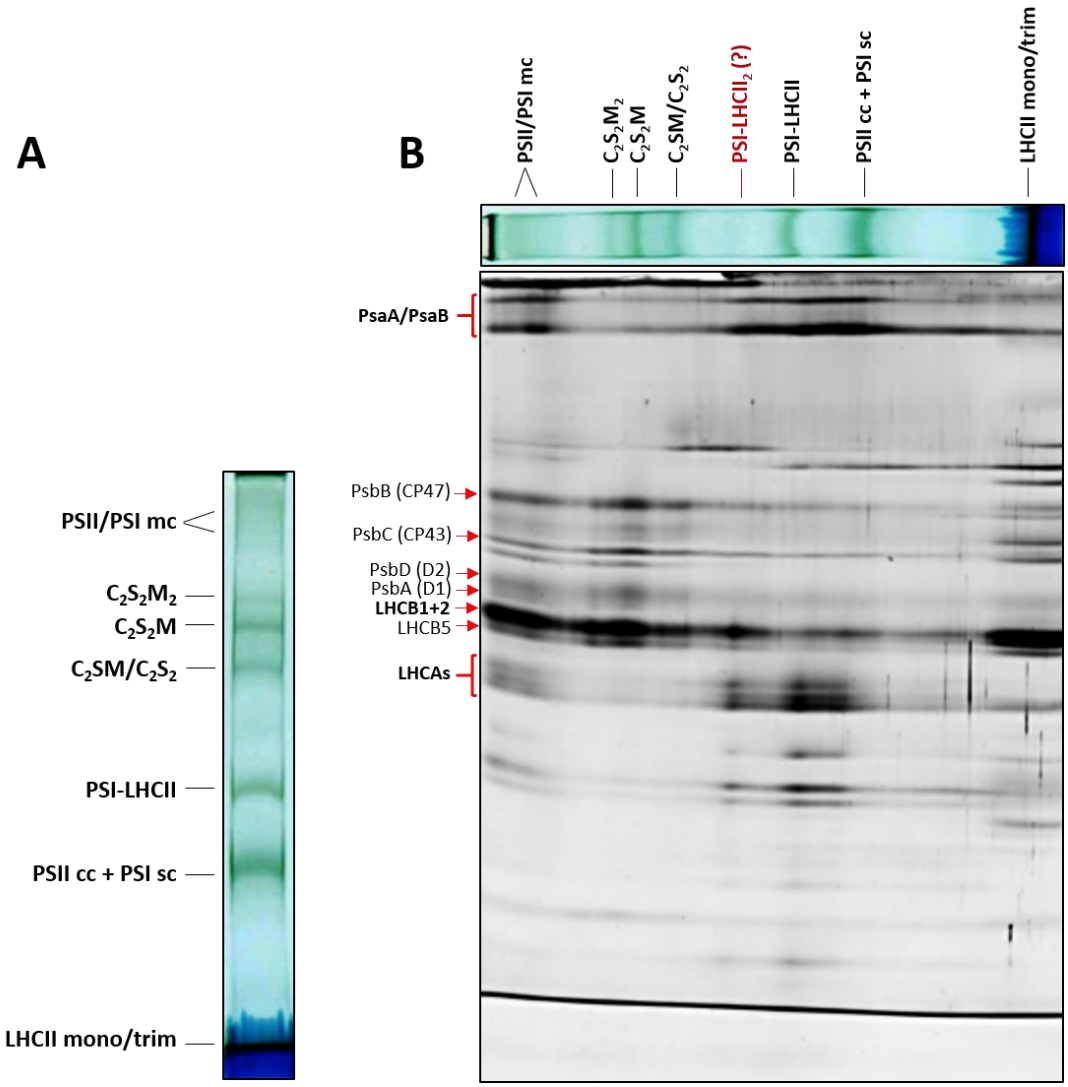

Figure 17: 2D-BN/SDS-PAGE of solubilised thylakoid membranes of spruce harvested for isolation directly from growing light. A) Electrophoretic separation of spruce thylakoid membranes solubilised with 0.7% α DDM in the gradient gel 4–8% and final Chl concentration of 0.5 mg/ml (loading of 16 µl per well). Image of the selected line from the gel scanned at room temperature in transmission mode. B) 2D-SDS-PAGE of thylakoid membrane protein complexes from spruce separated by BN-PAGE in the first dimension, applied on the gel as a gel strip, and subsequently separated in 5% stacking and 12% separating gel. A silver staining protocol was used to visualise the separated proteins, and the gel was scanned at room temperature in transmission mode. The individual protein spots are determined tentatively based on the available information from the literature and the expected molecular weight of proteins. *Abbreviations: PSII - photosystem II, PSI - photosystem I, LHCII - light-harvesting complex of photosystem II, mc - megacomplex, sc - supercomplex, cc - core complex, mono - monomer, trim - trimer, LHCAs - light-harvesting complexes of photosystem I.*

In addition to improving the separation and solubilisation conditions, we simultaneously attempted to eliminate the possibility of artificial formation of PSI-LHCII$_2$ by its forced induction. For this purpose, we combined eluates of gel bands representing free LHCII trimers or PSII scs with PSI-LHCII sc and subsequently analysed this mixture by (i) TEM (data not shown) or (ii) CN-PAGE re-electrophoresis. The purposeful complementation of PSI-LHCII

with either PSII scs or free LHCII trimers should represent a different source of the LHCII trimer's origin.

Neither the combination of PSI-LHCII sc and PSII sc (C_2S_2M) nor the combination of the PSI-LHCII sc and free LHCIIs led to the formation of the extra PSI-$LHCII_2$ band (Fig. 18). Separation of protein scs from control PSI-LHCII bands either from spruce or *At* on the second gel confirmed the previous observation that *At* PSI-LHCII sc is more fragile and easily disintegrate into the PSI sc and LHCII, whereas spruce counterpart is surprisingly stable and disintegrated only minimally. However, it should be pointed out that the original PSI-LHCII band from *At* has a significantly lower density than the same band from spruce. Control separation of PSII sc (C_2S_2M) as a position marker confirmed the expected high stability of this sc, however, we observed an additional band with higher molecular weight in the same line. Based on its position and supported by a strong fluorescent signal, this band could represent PSII aggregates or their artificially formed mcs, thus demonstrating their natural tendency to mutually adhere.

In conclusion, the forced induction of PSI-$LHCII_2$ scs formation by mixing the eluates from the specific gel bands further excluded the hypothesis about the artificial formation of this sc, as this form was not observed in any combination of the aforementioned gel bands.

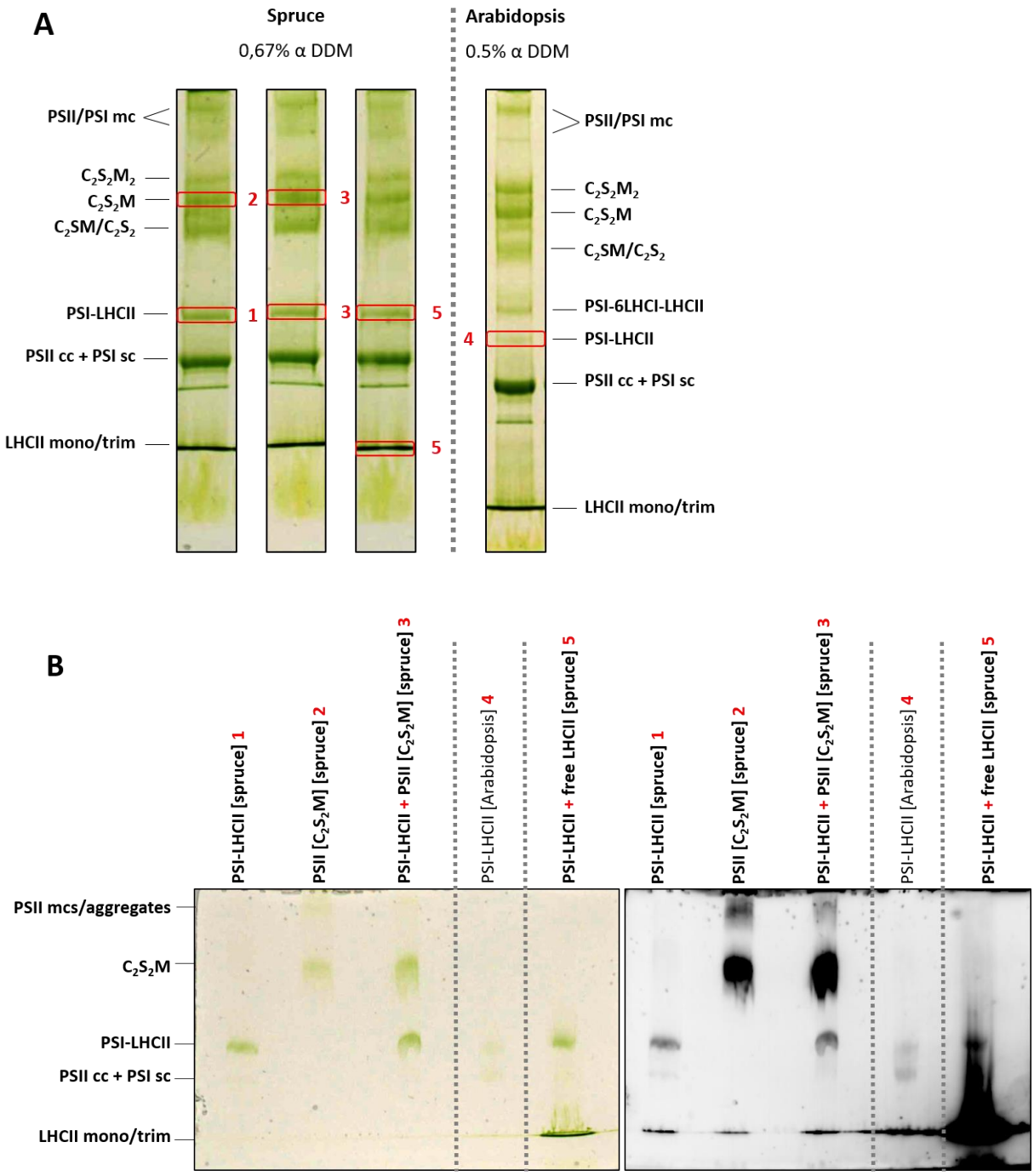

Figure 18: Re-electrophoresis of selected PSI and PSII supercomplexes and free LHCIIs from spruce and *Arabidopsis thaliana*. A) Electrophoretic separation of spruce and *At* thylakoid membranes harvested for isolation directly from growing light, solubilised with 0.67% and 0.5% α DDM, respectively, at a final Chl concentration of 0,33 mg/ml. Images of the selected lines from the gel were scanned at room temperature in transmission mode (green lines). The red boxes with numbers represent the gel bands used for re-electrophoresis. B) Re-electrophoresis of the gel bands from CN-PAGE, line labels designate the bands used from the first separation, fixed at a specific position in a second gel with 0.6% agarose in the upper buffer. Images of the gel were scanned at room temperature in transmission mode (green image) and in fluorescence mode (black and white image). *Abbreviations: PSII - photosystem II, PSI - photosystem I, LHCII - light-harvesting complex of photosystem II, mc - megacomplex, sc - supercomplex, cc - core complex, mono - monomer, trim - trimer.*

4.3. Conclusion of experimental approach - optimisation of supercomplexes extraction

In summary, the above-described biochemical experiments and their optimisations have brought a deeper insight into the plasticity of thylakoid membranes with respect to their solubilisation together with the effect of separation methods on the quality of the protein scs purification. Application of different modifications, such as (i) the use of different detergents, different concentrations or their combinations, (ii) the addition of stabilisers, or (iii) the implementation of different separation procedures, can all ensure favourable solubilisation and extraction of specific sc from the heterogeneous environment of thylakoid membranes. In addition, it can (i) improve the quality of the separation of different protein complexes through the higher resolution of individual CN-PAGE bands or sucrose gradient fractions, (ii) preserve the maximum intactness of the extracted protein complexes and keep them in the close to native state, and (iii) provide sufficient amounts of homogeneous sample for subsequent methods such as cryo-EM. The protein sample prepared in this way can be used to obtain a high-resolution structure close to its near-native state, thereby providing additional information needed to determine its function.

My primary goal in this part of my thesis was to optimise the separation protocol for the sucrose gradient ultracentrifugation to obtain homogeneous and concentrated fractions of specific protein scs suitable for analysis by cryo-EM. I was able to achieve this goal for the largest forms of the PSII sc present under standard conditions, specifically (i) $C_2S_2M_2$ observed in spruce and *At* and (ii) $C_2S_2M_2N_2$ observed in *Cr*. However, even this method cannot be universally applied to obtain arbitrary scs due to the co-migration of protein scs. This is a common drawback of separation methods that are based on the molecular weight of the separated proteins. Therefore, at least in the case of the study of photosynthetic protein scs, it is recommended to prepare, e.g. specific fragments of thylakoid membranes enriched in the protein sc of our interest before the actual separation.

Protein complexes that are too fragile or their inter-subunit binding is very labile due to their regulatory function, may be difficult to obtain in sufficient quantities. A low abundance of solubilised protein does not form a specific band or fraction during separation, which complicates or even prevents their structural analysis by EM. Such a protein sc, for example, is the transiently formed PSI-LHCII$_2$, where obtaining a pure, clearly visible PSI-LHCII$_2$ fraction remains elusive for now. The existence of this specific sc in higher plants is currently biochemically unprovable because the standard separation methods used in combination with different solubilisation conditions did not result in one unique fraction/band, even though this sc was observed by electron microscopy.

Focusing on induction of the state transitions in plants, obtaining a higher yield of characteristic PSI-LHCII$_2$ sc could be enhanced by fine-tuning of the light conditions in the growing chamber prior to isolation of the thylakoid membranes. The maximum level of phosphorylation of LHCB2, the conditional for the state 2 transition, does not occur under the growing light. It is known that in natural conditions, the maximal phosphorylation of LHCB2 occurs under non-saturating light (Rochaix *et al.*, 2014). It has been shown experimentally that maximum phosphorylation can be induced in plants exposed to light at half the intensity of the growing light. However, as discussed in the previous sections, a higher abundance of PSI-LHCII particles does not necessarily lead to a higher amount of PSI-LHCII$_2$, because the attachment of the second trimer in vascular plants is assumed to be independent of its phosphorylation. In conclusion, although there are numerous, more or less indirect indications for PSI-LHCII$_2$ formation in vascular plants, their structural validation and biochemical

confirmation would definitely require more creativity in the search for a non-standard optimal approach for their isolation.

As far as the experimental approach is concerned, the influence of the methods used on the results obtained must be taken into account when evaluating the structure of photosystems, especially when making hypotheses based on these results. With the increasing quality and resolution of the revealed structures of both photosystems (and a variety of their scs) or other protein complexes embedded in the membranes, we can simultaneously observe the influence of detergents and additives that were used for their extraction. On the one hand, they allow us to extract the intended protein in an "intact" state; on the other hand, the biochemical nature of these molecules may influence the final protein structure. An example could be α DDM, which was fitted in more than one electron density map of PSI sc (e.g. Pan *et al.*, 2018), even numerous molecules per one photosystem, or in the PSII sc (e.g. Sheng *et al.*, 2019), albeit with lower abundance. While the amphiphilic character of these molecules allows them to form an envelope around the extracted protein, at the same time, it allows them to expel a potentially present molecule, e.g. lipid, from the native structure and replace it with the potential effect on the final structure. However, the presence and conclusive identification of these detergent molecules in the structure is hard to achieve, as (i) the electron density map is insufficient or incomplete at some positions, most often due to the higher flexibility of the specific region in the structure, and (ii) there is a number of molecules with similar structure. Nevertheless, the presence of different molecules with physiological relevance to plants should also be considered.

A deeper insight into the effect of the used detergent on the final structure and its composition provided the study by Graca *et al.* (2021), in which they used digitonin for extraction of PSII sc from *At*. Since this detergent molecule has a relatively large molecular mass and a specific structure, its presence in the electron density map was easily detectable. And although, on the one hand, the authors emphasised its beneficial effect on the stability of PSII sc during extraction, they also highlighted the effect of its integration on the resulting structure, composition and integrity. The 22 molecules of digitonin identified in one structure of *At* PSII resulted in: i) changes in the inter-subunit distances, ii) destabilisation of the natural conformation that led to the release of molecules from the structure, for example, the loss of xanthophyll molecule from S-trimer or replacement of digalactosyldiacyl glycerol (DGD) leading to the loss of PsbJ subunit or, iii) changes in flexibility within individual PSII scs due to the induced loss of several interactions between the molecules. And although this disruptive effect of digitonin, or detergents in general, on the protein structures may seem inconvenient, the achieved findings can be used to study the importance of specific subunits, molecules or interactions (protein-protein, protein-ligand, ligand-ligand) on the function and stability of a protein complex or, to evaluate the consequences of using a particular detergent and thus provide important additional information. It is, thereby, very important to be aware of such an effect and to take it into consideration when studying the structural aspects of protein complexes.

In addition to detergents, the influence of other factors on the obtained results needs to be considered, such as the character of studied biological material. Taking spruce as an example, it is important whether we are studying few-weeks-old seedlings grown under control conditions or spruce in its natural habitat. Whether we process either a few-years-old needles or their fresh spring sprouts, which are further affected by fluctuating light conditions due to shading, etc. The influence of such a difference in the source material for study needs to be considered, and all influencing factors taken into account when hypothesising about the

photosynthetic apparatus and its regulation in particular photosynthetic organisms under selected controlled or natural conditions.

In conclusion, when researching a specific topic and performing the corresponding experiments, one has to be really careful when evaluating the obtained experimental data and, at the same time, to be aware that unknown attributes can influence the final results.

5. List of references

Akhtar, P., Lingvay, M., Kiss, T., Deák, R., Bóta, A., Ughy, B., Garab, G., Lambrev, P.H. (2016) Excitation energy transfer between Light-harvesting complex II and Photosystem I in reconstituted membranes. *Biochim. Biophys. Acta (BBA) - Bioenerg.* **1857**, 462–472.

Albanese, P., Manfredi, M., Meneghesso, A., Marengo, E., Saracco, G., Barber, J., Morosinotto, T., Pagliano, C. (2016) Dynamic reorganization of photosystem II supercomplexes in response to variations in light intensities. *Biochim Biophys Acta – Bioenerg.* **1857,** 1651–1660.

Albanese, P., Melero, R., Engel, B.D., Grinzato, A., Berto, P., Manfredi, M., Chiodoni, A., Vargas, J., Sorzano, C.Ó.S., Marengo, E., Saracco, G., Zanotti, G., Carazo, J.-M., Pagliano, C. (2017) Pea PSII-LHCII supercomplexes form pairs by making connections across the stromal gap. *Sci. Rep*. **7**, 10067.

Albanese, P., Tamara, S., Saracco, G., Scheltema, R.A., Pagliano, C. (2020) How paired PSII–LHCII supercomplexes mediate the stacking of plant thylakoid membranes unveiled by structural mass-spectrometry. *Nat. Commun.* **11**, 1361.

Alboresi, A., Caffarri, S., Nogue, F., Bassi, R., Morosinotto, T. (2008) *In silico* and biochemical analysis of *Physcomitrella patens* photosynthetic antenna: identification of subunits which evolved upon land adaptation. *PLoS ONE* **3**, e2033.

Alboresi, A., Storti, M., Cendron, L., Morosinotto, T. (2019) Role and regulation of class-C flavodiiron proteins in photosynthetic organisms. *Biochem. J.* **476**, 2487–2498.

Allahverdiyeva, Y., Ermakova, M., Eisenhut, M., Zhang, P., Richaud, P., Hagemann, M., Cournac, L., Aro, E.-M. (2011) Interplay between flavodiiron proteins and photorespiration in Synechocystis sp. PCC 6803. *J. Biol. Chem.* **286**, 24007–24014.

Allen, J.F. (2003) Botany. State transitions--a question of balance. *Science.* **299**, 1530-1532.

Alric, J. and Johnson, X. (2017) Alternative electron transport pathways in photosynthesis: a confluence of regulation. *Curr. Opin. Plant Biol.* **37**, 78–86.

Anderson, J. M. (2012) Lateral heterogeneity of plant thylakoid protein complexes: Early reminiscences. *Philos. Trans. R. Soc. Lond. B: Biol. Sci.* **367**, 3384–3388.

Andersson, I. and Backlund, A. (2008) Structure and function of Rubisco. *Plant Physiol. Biochem.* **46**, 275–291.

Apel, K. and Hirt, H. (2004) Reactive oxygen species: metabolism, oxidative stress, and signal transduction. *Annu. Rev. Plant Biol.* **55**, 373–399.

Armstrong, G.A. (1998) Greening in the dark:light-independent chlorophyll biosynthesis from anoxygenic photosynthetic bacteria to gymnosperms. *J. Photochem. Photobiol. B: Biol.* **43**, 87–100.

Aro, E.-M., McCaffery, S., Anderson, J.M. (1993b) Photoinhibition and D1 protein degradation in peas acclimated to different growth irradiances. *Plant Physiol.* **103**, 835–843.

Aro, E.-M., Virgin, I., Andersson, B. (1993a) Photoinhibition of Photosystem II. Inactivation, protein damage and turnover. *Biochim. Biophys. Acta – Bioenerg.* **1143**, 113–134.

Arshad, R. (2022) Supramolecular structures of thylakoid membrane protein complexes: supercomplex organization under different environmental conditions. [Thesis fully internal (DIV), University of Groningen]. *University of Groningen*. https://doi.org/10.33612/diss.199785099

Bag, P., Chukhutsina, V., Zhang, Z., Paul, S., Ivanov, A.G., Shutova, T., Croce, R., Holzwarth, A.R., Jansson, S. (2020) Direct energy transfer from photosystem II to photosystem I confers winter sustainability in Scots Pine. *Nat. Commun.* **11**, 6388.

Bailey, S., Walters, R.G., Jansson, S., Horton, P. (2001) Acclimation of Arabidopsis thaliana to the light environment: the existence of separate low light and high light responses. *Planta* **213**, 794–801.

Ballottari, M., Dall'Osto, L., Morosinotto, T., Bassi, R. (2007) Contrasting behavior of higher plant photosystem I and II antenna systems during acclimation. *J. Biol. Chem.* **282**, 8947–8958.

Ballottari, M., Girardon, J., Dall'Osto, L., Bassi, R. (2012) Evolution and functional properties of Photosystem II light harvesting complexes in eukaryotes, *Biochim. Biophys. Acta (BBA) - Bioenerg*. **1817**, 143–157.

Bassi, R. and Dainese, P. (1992) A supramolecular light-harvesting complex from chloroplast photosystem-II membranes. *Eur. J. Biochem.* **204**, 317–326.

Bassi, R. and Dall'Osto, L. (2021) Dissipation of light energy absorbed in excess: the molecular mechanisms. *Annu. Rev. Plant Biol*. **72**, 47–76.

Bellafiore, S., Barneche, F., Peltier, G., Rochaix, J.-D. (2005) State transitions and light adaptation require chloroplast thylakoid protein kinase STN7. *Nature* **433**, 892–895.

Ben-Shem, A., Frolow, F., Nelson, N. (2003) Crystal structure of plant photosystem I. *Nature* **426**, 630–635.

Benson, S.L., Maheswaran, P., Ware, M.A., Hunter, C.N., Horton, P., Jansson, S., Ruban, A.V., Johnson, M.P. (2015) An intact light harvesting complex I antenna system is required for complete state transitions in Arabidopsis. *Nat. Plants* **1**, 15176.

Betterle, N., Ballottari, M., Zorzan, S., de Bianchi, S., Cazzaniga, S., Dall'osto, L., Morosinotto, T., Bassi, R. (2009) Light-induced dissociation of an antenna hetero-oligomer is needed for non-photochemical quenching induction. *J. Biol. Chem.* **284**, 15255–15266.

Bielczynski, L.W., Schansker, G., Croce, R. (2016) Effect of light acclimation on the organization of photosystem II super- and sub-complexes in *Arabidopsis thaliana*. *Front. Plant Sci.* **7**, 1–12.

Blazier, J.C., Guisinger, M.M., Jansen, R.K. (2011) Recent loss of plastid-encoded ndh genes within *Erodium* (Geraniaceae) *Plant Mol. Biol.* **76**, 263–72.

Blum, H., Beier, H., Gross, H.J. (1987) Improved silver staining of plant proteins, RNA and DNA in polyacrylamide gels. *Electrophoresis* **8**, 93–99.

Boekema, E.J., Dekker, J.P., Vanheel, M.G., Rogner, M., Saenger, W., Witt, I., Witt, H.T. (1987) Evidence for a trimeric organization of the photosystem-i complex from the thermophilic cyanobacterium Synechococcus sp. *Febs Lett*. **217**, 283–286.

Boekema, E.J., Jensen, P.E., Schlodder, E., van Breemen, J.F.L., van Roon, H., Scheller, H.V., Dekker, J.P. (2001) Green plant photosystem I binds light-harvesting complex I on one side of the complex. Biochem. **40**, 1029–1036.

Boekema, E.J., van Breemen, J.F.L., van Roon, H., Dekker, J.P. (2000) Arrangement of photosystem II supercomplexes in crystalline macrodomains within the thylakoid membrane of green plant chloroplasts. *J. Mol. Biol*. **301**, 1123–1133.

Boekema, E.J., van Roon, H., Breemen, J. F. L., Dekker, J. P. (1999b) Supramolecular organization of photosystem II and its light-harvesting antenna in partially solubilized photosystem II membranes. *Eur. J. Biochem*. **266**, 444–452.

Boekema, E.J., van Roon, H., Calkoen, F., Bassi, R., Dekker, J.P. (1999a) Multiple types of association of photosystem II and its light-harvesting antenna in partially solubilized photosystem II membranes. *Biochem.* **38**, 2233–2239.

Bos, I., Bland, K.M., Tian, L.J., Croce, R., Frankel, L.K., van Amerongen, H., Bricker, T.M., Wientjes, E. (2017) Multiple LHCII antennae can transfer energy efficiently to a single Photosystem I. *Biochim. Biophys. Acta – Bioenerg.* **1858**, 371–378.

Braukmann, T.W.A., Kuzmina, M., Stefanovic, S. (2009) Loss of all plastid ndh genes in Gnetales and conifers: extent and evolutionary significance for the seed plant phylogeny. *Curr. Gen.* **55**, 323–337.

Bressan, M., Bassi, R., Dall'Osto, L. (2018) Loss of LHCI system affects LHCII re-distribution between thylakoid domains upon state transitions. *Photosynth. Res.* **135**, 251–261.

Brettel, K. (1997) Electron transfer and arrangement of the redox cofactors in photosystem I, *Biochim. Biophys. Acta* **1318**, 322–373.

Briantais, J.-M., Vernotte, C., Picaud, M., Krause, G.H. (1979) A quantitative study of the slow decline of chlorophyll a fluorescence in isolated chloroplasts. *Biochim. Biophys. Acta - Bioenerg.* **548**, 128–138.

Buchanan, B.B. (2016) The path to thioredoxin and redox regulation in chloroplasts. *Annu. Rev. Plant Biol.* **67**, 1–24.

Bulychev, A.A. and Vredenberg, W.J. (1999) Light-triggered electrical events in the thylakoid membrane of plant chloroplasts. *Physiol. Plant.* **105**, 577–584.

Busch, A., Petersen, J., Webber-Birungi, M.T., Powikrowska, M., Lassen, L.M., Naumann-Busch, B., Nielsen, A.Z., Ye, J., Boekema, E.J., Jensen, O.N., Lunde, C., Jensen, P.E. (2013) Composition and structure of photosystem I in the moss *Physcomitrella patens*. *J. Exp. Bot.* **64**, 2689–2699.

Caffarri, S., Croce, R., Cattivelli, L., Bassi, R. (2004) A look within LHCII: differential analysis of the LHCB1−3 complexes building the major trimeric antenna complex of higher-plant photosynthesis. *Biochemistry* **43**, 9467–9476.

Caffarri, S., Kouřil, R., Kereiche, S., Boekema, E. J., Croce, R. (2009) Functional architecture of higher plant photosystem II supercomplexes. *EMBO J.* **28**, 3052–3063.

Caffarri, S., Tibiletti, T., Jennings, R.C. (2014) A comparison between plant photosystem I and photosystem II architecture and functioning. *Curr. Protein Pept. Sci.* **15**, 296–331.

Canovas, F., McLarney, B., Silverthorne, J. (1993) Light-independent synthesis of LHCIIb polypeptides and assembly of the major pigmented complexes during the initial stages of *Pinus palustris* seedling development. *Photosynth. Res.* **38**, 89–97.

Cao, P., Bracun, L., Yamagata, A., Christianson, B.M., Negami, T., Zou, B., Terada, T., Canniffe, D.P., Shirouzu, M., Li, M., Liu, L.N. (2022) Structural basis for the assembly and quinone transport mechanisms of the dimeric photosynthetic RC-LH1 supercomplex. *Nat. Commun.* **13**, 1977.

Cao, P., Su, X., Pan, X., Liu, Z., Chang, W., Li, M. (2018) Structure, assembly and energy transfer of plant photosystem II supercomplex. *Biochim. Biophys. Acta - Bioenerg*. **1859**, 633–644.

Cariti, F., Chazaux, M., Lefebvre-Legendre, L., Longoni, P., Ghysels, B., Johnson, X., Goldschmidt-Clermont, M. (2020) Regulation of light harvesting in *Chlamydomonas reinhardtii* two protein phosphatases are involved in state transitions. *Plant Physiol.* **183**, 1749–1764.

Caspy, I. and Nelson, N. (2018) Structure of the plant photosystem. *Biochem. Soc. Trans.* **46**, 285–294.

Caspy, I., Malavath, T., Klaiman, D., Fadeeva, M., Shkolnisky, Y., Nelson, N. (2020) Structure and energy transfer pathways of the *Dunaliella Salina* photosystem I supercomplex. *Biochim. Biophys. Acta - Bioenerg.* **1861**, 148253.

Cejudo, F.J., Ojeda, V., Delgado-Requerey, V., González, M., Pérez-Ruiz, J.M. (2019) Chloroplast redox regulatory mechanisms in plant adaptation to light and darkness. *Front. Plant Sci*. **10**, 1–11.

Chitnis, V.P., and Chitnis, P.R. (1993) PsaL subunit is required for the formation of photosystem-I trimers in the cyanobacterium Synechocystis sp pcc-6803. *Febs Lett.* **336**, 330–334.

Chukhutsina, V.U., Liu, X., Xu, P., Croce, R. (2020) Light-harvesting complex II is an antenna of photosystem I in dark-adapted plants. *Nat. Plants* **6**, 860–868.

Clarke, J.T., Warnock, R.C.M., Donoghue, P.C.J. (2011) Establishing a time-scale for plant evolution. *New Phytol.* **192**, 266–301.

Crepin A, Santabarbara S, Caffarri S. (2016) Biochemical and spectroscopic characterization of highly stable photosystem II supercomplexes from Arabidopsis. *J. Biol. Chem.* **291**, 19157–19171.

Crepin, A. and Caffarri, S. (2015) The specific localizations of phosphorylated Lhcb1 and Lhcb2 isoforms reveal the role of Lhcb2 in the formation of the PSI-LHCII supercomplex in Arabidopsis during state transitions. *Biochim. Biophys. Acta - Bioenerg.* **1847**, 1539–1548.

Crepin, A. and Caffarri, S. (2018) Functions and evolution of LHCB isoforms composing LHCII, the major light harvesting complex of photosystem II of green eukaryotic organisms. *Curr. Protein Pept. Sci.* **19**, 699–713.

Crepin, A., Kučerová, Z., Kosta, A., Durand, E., Caffarri, S. (2020) Isolation and characterization of a large photosystem I-light-harvesting complex II supercomplex with an additional Lhca1-a4 dimer in Arabidopsis. *Plant J.* **102**, 398–409.

Croce, R. and van Amerongen, H. (2011) Light-harvesting and structural organization of Photosystem II: From individual complexes to thylakoid membrane. *J. Photochem. Photobiol. B: Biol.* **104**, 142–153.

Croce, R. and van Amerongen, H. (2013) Light-harvesting in photosystem I. *Photosynth. Res.* **116**, 153–166.

Croce, R. and van Amerongen, H. (2020) Light harvesting in oxygenic photosynthesis: Structural biology meets spectroscopy. *Science* **369**, eaay2058.

Cruz, S., Goss, R., Wilhelm, C., Leegood, R., Horton, P., Torsten, J. (2011) Impact of chlororespiration on non-photochemical quenching of chlorophyll fluorescence and on the regulation of the diadinoxanthin cycle in the diatom *Thalassiosira pseudonana*, *J. Exp. Bot.* **62**, 509–519.

Dainese, P. and Bassi, R. (1991) Subunit stoichiometry of the chloroplast photosystem-II antenna system and aggregation state of the component chlorophyll-a /b binding proteins. *J. Biol. Chem.* **266**, 8136–8142.

Damkjær, J.T., Kereiche, S., Johnson, M.P., Kovács, L., Kiss, A.Z., Boekema, E.J., Ruban, A.V., Horton, P., Jansson, S. (2009) The photosystem II light-harvesting protein LHCB3 affects the macrostructure of photosystem II and the rate state transitions in Arabidopsis. *Plant Cell* **21**, 3245–3256.

Dau, H., Andrews, J.C., Roelofs, T.A., Latimer, M.J., Liang, W.C., Yachandra, V.K., Sauer, K., Klein, M.P. (1995) Structural consequences of ammonia binding to the manganese center of the photosynthetic oxygen-evolving complex - an x-ray-absorption spectroscopy study of isotropic and oriented photosystem-II particles. *Biochem*. **34**, 5274–5287.

Daum, B., Nicastro, D., Austin, J., McIntosh, J., Kühlbrandt, W. (2010) Arrangement of photosystem II and ATP synthase in chloroplast membranes of spinach and pea. *Plant Cell* **22**, 1299–1312.

de Bianchi, S., Ballottari, M., Dall'Osto, L., Bassi, R. (2010) Regulation of plant light harvesting by thermal dissipation of excess energy. *Biochem. Soc. Trans*. **38**, 651–660.

de Bianchi, S., Betterle, N., Kouřil, R., Cazzaniga, S., Boekema, E., Bassi, R., Dall'Osto, L. (2011) Arabidopsis mutants deleted in the light-harvesting protein LHCB4 have a disrupted photosystem II macrostructure and are defective in photoprotection. *Plant Cell*. **23**, 2659–2679.

de Bianchi, S., Dall'Osto, L., Tognon, G., Morosinotto, T., Bassi, R. (2008) Minor antenna proteins CP24 and CP26 affect the interactions between photosystem II subunits and the electron transport rate in grana membranes of Arabidopsis. *Plant Cell* **20**, 1012–1028.

Dekker, J.P. and Boekema, E.J. (2005) Supramolecular organization of thylakoid membrane proteins in green plants. *Biochim. Biophys. Acta – Bioenerg.* **1706**, 12–39.

Dekker, J.P. and Van Grondelle, R. (2000) Primary charge separation in photosystem II. *Photosynth. Res*. **63**, 195–208.

Demmig-Adams, B. and Adams, W.W. (1996) The role of xanthophyll cycle carotenoids in the protection of photosynthesis. *Trends Plant Sci*. **1**, 21–26.

Demmig-Adams, B. and Adams, W.W. (2006) Photoprotection in an ecological context: the remarkable complexity of thermal energy dissipation. *New Phytol.* **172**, 11–21.

Demmig-Adams, B., Ebbert, V., Mellman, D.L., Mueh, K.E., Schaffer, L., Funk, C., Zarter, C.R., Adamska, I., Jansson, S., Adams, W.W. III (2006) Modulation of PsbS and flexible vs sustained energy dissipation by light environment in different species. *Physiol. Plant.* **127**, 670–680.

Demmig-Adams, B., Garab, G., Adams III, W., Govindjee (2014) Non-photochemical quenching and energy dissipation in plants, algae and cyanobacteria. *Advances in photosynthesis and respiration*, volume **40**, *Springer, Dordrecht*.

Demmig-Adams, B., Muller, O., Stewart, J.J., Cohu, C.M., Adams, W.W. (2015) Chloroplast thylakoid structure in evergreen leaves employing strong thermal energy dissipation. J. *Photochem. Photobiol. B*: *Biol.* **152**, 357–366.

Depege, N., Bellafiore, S., Rochaix, J.-D. (2003) Role of chloroplast protein kinase Stt7 in LHCII phosphorylation and state transition in Chlamydomonas. *Science* **299**, 1572–1575.

Drop, B., Webber-Birungi, M., Yadav, S. K. N., Filipowicz-Szymanska, A., Fusetti, F., Boekema, E. J., Croce, R. (2014a) Light-harvesting complex II (LHCII) and its supramolecular organization in *Chlamydomonas reinhardtii*. *Biochim. Biophys. Acta* **1837**, 63–72.

Drop, B., Yadav, K. N. S., Boekema, E. J., Croce, R. (2014b) Consequences of state transitions on the structural and functional organization of photosystem I in the green alga *Chlamydomonas reinhardtii. Plant J.* **78**, 181–191.

Edge, R. and Truscott, T.G. (1999) Carotenoid radicals and the interaction of carotenoids with active oxygen species. In: Frank, H.A., Young, A.J., Britton, G., Cogdell, R.J. (eds.) The photochemistry of carotenoids. *Advances in photosynthesis and respiration*, volume **8**, 223–234, *Springer, Dordrecht*.

Engelmark, O. and Hytterborn, H. (1999) Coniferous forest. In: Rydin, H. (ed.) Swedish plant geography, 55–74, *Svenska växtgeografiska sällskapet, Uppsala*.

Ensminger, I., Busch, F., Huner, N. (2006). Photostasis and cold acclimation: Sensing low temperature through photosynthesis. *Physiol. Plant.* **126**, 28–44.

Flötenmeyer, M., Weiss, H., Tribet, C., Popot, J.L., Leonard, K. (2007) The use of amphipathic polymers for cryo electron microscopy of NADH:ubiquinone oxidoreductase (complex I). *J Microsc.* **227**, 229–35.

Foyer, C.H. and Noctor, G. (2003) Redox sensing and signaling associated with reactive oxygen in chloroplasts, peroxisomes and mitochondria. *Physiol. Plant.* **119**, 355–364.

Foyer, C.H. and Noctor, G. (2005) Redox homeostasis and antioxidant signaling: a metabolic interface between stress perception and physiological responses. *Plant Cell* **17**, 1866–75.

Franck, F. and Houyoux, P.-A. (2008) The Mehler reaction in Chlamydomonas during photosynthetic induction and steady-state photosynthesis in wild-type and a mitochondrial mutant. In: Allen, J.F, Gantt, E., Golbeck, J.H., Osmond, B. (eds.) Photosynthesis. Energy from the sun, 581–584, *Springer, Dordrecht*.

Galka, P., Santabarbara, S., Thi, T.H.K., Degand, H., Morsomme, P., Jennings, R.C., Boekema, E.J., Caffarri, S. (2012) Functional analyses of the plant photosystem I-light-harvesting complex II supercomplex reveal that light-harvesting complex II loosely bound to photosystem II is a very efficient antenna for photosystem I in state II. *Plant Cell* **24**, 2963–2978.

Garber, M.P., and Steponkus, P.L. (1976). Alterations in chloroplast thylakoids during cold-acclimation. *Plant Physiol.* **57**, 681–686.

Gauthier, S., Bernier, P., Kuuluvainen, T., Shvidenko, A. Z., Schepaschenko, D. G. (2015) Boreal forest health and global change. *Science* **349**, 819–822.

George, D.M., Vincent, A.S., Mackey, H.R. (2020) An overview of anoxygenic phototrophic bacteria and their applications in environmental biotechnology for sustainable Resource recovery. *Biotech. Rep.* **28**, e00563.

Gilmore, A. M. and Ball, M. C. (2000) Protection and storage of chlorophyll in overwintering evergreens. *Proc. Natl. Acad. Sci. U. S. A.* **97**, 11098–11101.

Gisriel, C.J., Wang, J., Liu, J., Flesher, D.A., Reiss, K.M., Huang, H.L., Yang, K.R., Armstrong, W.H., Gunner, M.R., Batista, V.S., Debus, R.J., Brudvig, G.W. (2022) High-resolution cryo-electron microscopy structure of photosystem II from the mesophilic cyanobacterium, Synechocystis sp. PCC 6803. *Proc. Natl. Acad. Sci. U. S. A.* **119**, e2116765118.

Goldschmidt-Clermont, M. and Bassi, R. (2015) Sharing light between two photosystems: mechanism of state transitions. *Curr. Opin. Plant Biol.* **25**, 71–78.

Gorski, C., Riddle, R., Toporik, H., Da, Z., Dobson, Z., Williams, D., Mazor, Y. (2022) The structure of the *Physcomitrium patens* photosystem I reveals a unique Lhca2 paralogue replacing Lhca4. *Nat. Plants* **8**, 307–316.

Graça, A.T., Hall, M., Persson, K., Schröder, W.P. (2021) High-resolution model of Arabidopsis Photosystem II reveals the structural consequences of digitonin-extraction. *Sci. Rep.* **11**, 15534.

Grebe, S. (2022) Photosynthetic characteristics of *Pinaceae* –from evolution to environmental acclimation. [Doctoral thesis, *University of Turku*] UTUPub: https://urn.fi/URN:ISBN:978-951-29-8924-9.

Grebe, S., Trotta, A., Bajwa, A., Mancini, I., Bag, P., Jansson, S., Tikkanen, M., Aro, E.-M. (2020) Specific thylakoid protein phosphorylations are prerequisites for overwintering of Norway spruce (*Picea abies*) photosynthesis. *Proc. Natl. Acad. Sci. U. S. A.* **117**, 17499–17509.

Grebe, S., Trotta, A., Bajwa, A.A., Suorsa, M., Gollan, P.J., Jansson, S., Tikkanen, M., Aro, E.-M. (2019) The unique photosynthetic apparatus of *Pinaceae*: analysis of photosynthetic complexes in *Picea abies*. *J. Exp. Bot.* **70**, 3211–3225.

Grieco, M. Suorsa, M., Jajoo, A., Tikkanen, M., Aro, E.-M. (2015) Light-harvesting II antenna trimers connect energetically the entire photosynthetic machinery - including both photosystems II and I. *Biochim. Biophys. Acta - Bioenerg.* **1847**, 607–619.

Grouneva, I., Jakob, T., Wilhelm, C., Goss, R. (2009) The regulation of xanthophyll cycle activity and of non-photochemical fluorescence quenching by two alternative electron flows in the diatoms *Phaeodactylum tricornutum* and *Cyclotella meneghiniana*. *Biochim. Biophys. Acta*. **1787**, 929–938.

Gruber, M.J., Chmeliov, J., Krüger, T.P.J., Valkunas, L., van Grondelle, R. (2015) Singlet–triplet annihilation in single LHCII complexes. *Phys. Chem. Chem. Phys.* **17**, 19844–19853.

Guardini, Z., Gomez, R.L., Caferri, R., Dall'Osto, L., Bassi, R. (2022) Loss of a single chlorophyll in CP29 triggers re-organization of the Photosystem II supramolecular assembly. *Biochim. Biophys. Acta – Bioenerg.* **1863**, 148555.

Hamel, P., Olive, J., Pierre, Y., Wollman, F.-A., de Vitry, C. (2000) A new subunit of cytochrome b6f complex undergoes reversible phosphorylation upon state transition. *J. Biol. Chem.* **275**, 17072–17079.

He, T., Pausas, J.G., Belcher, C.M., Schwilk, D.W., Lamont, B.B. (2012) Fire-adapted traits of Pinus arose in the fiery Cretaceous. *New Phytol.* **194**, 751–759.

He, W.Z. and Malkin, R. (1992) Specific release of a 9-kDa extrinsic polypeptide of photosystem I from spinach chloroplasts by salt washing. *FEBS Lett.* **308**, 298–300.

Helman, Y., Tchernov, D., Reinhold, L., Shibata, M., Ogawa, T., Schwarz, R., Ohad, I., Kaplan, A. (2003) Genes encoding A-type flavoproteins are essential for photoreduction of O_2 in cyanobacteria. *Curr. Biol.* **13**, 230–235.

Hodges, M., Cornic, G., Briantais, J.-M. (1989) Chlorophyll fluorescence from spinach leaves: resolution of non-photochemical quenching. *Biochim. Biophys. Acta* **974**, 289–293.

Holzwarth, A.R., Müller, M.G., Niklas, J., Lubitz, W. (2006) Ultrafast transient absorption studies on photosystem I reaction centers from *Chlamydomonas reinhardtii*. 2: mutations near the P700 reaction center chlorophylls provide new insight into the nature of the primary electron donor. *Biophys. J.* **90**, 552–565.

Horton, P., Ruban, A. V., Walters, R.G. (1996) Regulation of light harvesting in green plants. *Annu. Rev. Plant Physiol. Plant Mol. Biol.* **47**, 655–684.

Huang, Z., Shen, L., Wang, W., Mao, Z., Yi, X., Kuang, T., Shen, J.R., Zhang, X., Han, G. (2021) Structure of photosystem I-LHCI-LHCII from the green alga *Chlamydomonas reinhardtii* in state 2. *Nat. Commun.* **12**, 1100.

Ifuku, K., Ishihara, S., Sato, F. (2010) Molecular functions of oxygen-evolving complex family proteins in photosynthetic electron flow. *J. Integr. Plant Biol.* **52**, 723–734.

Ilík, P., Pavlovič, A., Kouřil, R., Alboresi, A., Morosinotto, T., Allahverdiyeva, Y., Aro, E.-M., Yamamoto, H., Shikanai, T. (2017) Alternative electron transport mediated by flavodiiron proteins is operational in organisms from cyanobacteria up to gymnosperms. *New Phytol.* **214**, 967–972.

Ilík, P., Schansker, G., Kotabová, E., Váczi, P., Strasser, R.J., Barták, M. (2006) A dip in the chlorophyll fluorescence induction at 0.2–2 s in Trebouxia-possessing lichens reflects a fast reoxidation of photosystem I. A comparison with higher plants. *Biochim. Biophys. Acta – Bioenerg.* **1757**, 12–22.

Ilíková I., Ilík P., Opatíková M., Arshad R., Nosek L., Karlický V., Kučerová Z., Roudnický P., Pospíšil P., Lazár D., Bartoš J., Kouřil R. (2021) Towards spruce-type photosystem II supercomplex: consequences of the loss of LHCB3 and LHCB6 in Arabidopsis. *Plant Physiol.* **187**, 2691–2715.

Iwai, M. and Yokono, M. (2017) Light-harvesting antenna complexes in the moss *Physcomitrella patens*: implications for the evolutionary transition from green algae to land plants. *Curr. Opin. Plant Biol*. **37**, 94–101.

Iwai, M., Grob, P., Iavarone, A.T., Nogales, E., Niyogi, K.K. (2018) A unique supramolecular organization of photosystem I in the moss *Physcomitrella patens. Nat. Plants* **4**, 904–909.

Iwai, M., Takizawa, K., Tokutsu, R., Okamuro, A., Takahashi, Y., Minagawa, J. (2010) Isolation of the elusive supercomplex that drives cyclic electron flow in photosynthesis. *Nature* **464**, 1210–1213.

Jackowski, G., Kacprzak, K., Jansson, S. (2001) Identification of LHCB1/LHCB2/LHCB3 heterotrimers of the main light-harvesting chlorophyll a/b-protein complex of Photosystem II (LHC II). *Biochim. Biophys. Acta* **1504**, 340–345.

Jansson, S. (1999) A guide to the Lhc genes and their relatives in Arabidopsis. *Trends Plant Sci.* **4**, 236–240.

Jansson, S., Andersen, B., Scheller, H.V. (1996). Nearest-neighbor analysis of higher plant photosystem I holocomplex. *Plant Physiol.* **112**, 409–420.

Johnson M.P. (2016) Photosynthesis. *Essays in Biochem.* **60**, 255–273.

Johnson, M.P., Goral, T.K., Duffy, C.D.P., Brain, A.P.R., Mullineaux, C.W., Ruban, A. V. (2011) photoprotective energy dissipation involves the reorganization of photosystem II light-harvesting complexes in the grana membranes of spinach chloroplasts. *Plant Cell*. **23**, 1468–1479.

Jordan, P., Fromme, P., Witt, H.T., Klukas, O., Saenger, W., Krauss, N. (2001) Three dimensional structure of cyanobacterial photosystem I at 2.5 angstrom resolution. *Nature* **411**, 909–917.

Josse, E.-M., Alcaraz, J.-P., Laboure, A.-M., Kuntz, M. (2003) In vitro characterization of a plastid terminal oxidase (PTOX). *Eur. J. Biochem*. **270**, 3787–3794.

Kamachi, H., Tamura, N., Yoshihira, T., Oku, T. (1994) Photoactivation of the latent wateroxidizing complex in photosystem II membranes isolated from dark-grown spruce seedlings. *Physiol. Plant.* **91**, 747–753.

Kanazawa, A. and Kramer, D.M. (2002) In vivo modulation of nonphotochemical exciton quenching (NPQ) by regulation of the chloroplast ATP synthase. *Proc. Natl. Acad. Sci. U. S. A.* **99**, 12789–12794.

Kargul, J., Turkina, M.V., Nield, J., Benson, S., Vener, A.V., Barber, J. (2005) Light-harvesting complex II protein CP29 binds to photosystem I of *Chlamydomonas reinhardtii* under state 2 conditions. *FEBS J.* **272**, 4797–4806.

Kashino, Y., Takahashi, T., Inoue-Kashino, N., Ban, A., Ikeda, Y., Satoh, K., Sugiura, M. (2007) Ycf12 is a core subunit in the photosystem II complex. *Biochim. Biophys. Acta* **1767**, 1269–1275.

Ke, B. (2001) Photosynthesis – photobiochemistry and photobiophysics. *Advances in photosynthesis and respiration,* volume **10**, *Kluwer, Dordrecht.*

Kern, J. and Renger, G. (2007) Photosystem II: Structure and mechanism of the water:plastoquinone oxidoreductase. *Photosynth. Res.* **94**, 183–202.

Kim, E., Yokono, M., Tsugane, K., Ishii, A., Noda, C., Minagawa, J. (2023) Formation of a stable PSI-PSII megacomplex in rice that conducts energy spillover. *Plant Cell Physiol.* pcad037.

Kirchhoff, H. (2008) Significance of protein crowding, order and mobility for photosynthetic membrane functions. *Biochem. Soc. Trans*. **36**, 967–970.

Kirchhoff, H., Haase, W., Wegner, S., Danielsson, R., Ackermann, R., Albertsson, P.-A. (2007) Low-light-induced formation of semicrystalline photosystem II arrays in higher plant chloroplast. *Biochem.* **46**, 11169-11176.

Kirchhoff, H., Hall, C., Wood, M., Herbstová, M., Tsabari, O., Nevo, R., Charuvi, D., Shimoni, E., Reich, Z. (2011) Dynamic control of protein diffusion within the granal thylakoid lumen. *Proc. Natl. Acad. Sci. U. S. A.* **108**, 20248–20253.

Klimmek, F., Sjödin, A., Noutsos, C., Leister, D., Jansson, S. (2006) Abundantly and rarely expressed Lhc protein genes exhibit distinct regulation patterns in plants. *Plant Physiol.* **140**, 793–804.

Koskela, M.M., Brünje, A., Ivanauskaite, A., Lopez, L.S., Schneider, D., DeTar, R.A., Kunz, H.-H., Finkemeier, I., Mulo, P. (2020) Comparative analysis of thylakoid protein complexes in state transition mutants nsi and stn7: focus on PSI and LHCII. *Photosynth. Res.* **145**, 15–30.

Kouřil, R., Dekker, J.P., Boekema, E.J. (2012) Supramolecular organization of photosystem II in green plants. *Biochim. Biophys. Acta-Bioenerg.* **1817**, 2–12.

Kouřil, R., Nosek, L., Bartoš, J., Boekema, E.J., Ilík, P. (2016) Evolutionary loss of light-harvesting proteins LHCB6 and LHCB3 in major land plant groups - break-up of current dogma. *New Phytol*. **210**, 808–814.

Kouřil, R., Nosek, L., Opatíková, M., Arshad, R., Semchonok, D.A., Chamrád, I., Lenobel, R., Boekema, E.J., and Ilík, P. (2020). Unique organization of photosystem II supercomplexes and megacomplexes in Norway spruce. *Plant J.* **104**, 215–225.

Kouřil, R., Nosek, L., Semchonok, D., Boekema, E.J., Ilík, P. (2018) Organization of plant photosystem II and photosystem I supercomplexes. In Harris, J.R., Boekema, E.J. (eds.) Membrane proteincomplexes: structure and function. *Subcellular Biochemistry*, volume **87**, 259–286, *Springer, Singapore*.

Kouřil, R., Strouhal, O., Nosek, L., Lenobel, R., Chamrád, I., Boekema, E.J., Šebela, M., Ilík, P. (2014) Structural characterization of a plant photosystem I and NAD(P)H dehydrogenase supercomplex. *Plant J.* **77**, 568–576.

Kouřil, R., van Oosterwijk, N., Yakushevska, A.E., Boekema, E.J. (2005b) Photosystem I: a search for green plant trimers. *PPS* **4**, 1091–1094.

Kouřil, R., Wientjes, E., Bultema, J. B., Croce, R., Boekema, E. J. (2013) High-light vs. low-light: Effect of light acclimation on photosystem II composition and organization in *Arabidopsis thaliana*. *Biochim. Biophys. Acta – Bioenerg.* **1827**, 411–419.

Kouřil, R., Zygadlo, A., Arteni, A.A., de Wit, C.D., Dekker, J.P., Jensen, P.E., Scheller, H.V., Boekema, E.J. (2005a) Structural characterization of a complex of photosystem I and light-harvesting complex II of *Arabidopsis thaliana. Biochem.* **44**, 10935–10940.

Kovács, L., Damkjær, J., Kereïche, S., Ilioaia, C., Ruban, A.V., Boekema, E.J., Jansson, S., Horton, P. (2006) Lack of the light-harvesting complex CP24 affects the structure and function of the grana membranes of higher plant chloroplasts. *Plant Cell* **18**, 3106–3120.

Koziol, A.G., Borza, T., Ishida, K., Keeling, P., Lee, R.W., Durnford, D.G. (2007) Tracing the evolution of the light-harvesting antennae in chlorophyll a/b-containing organisms. *Plant Phys.* **143**, 1802–1816.

Kramer, D.M., Cruz, J.A., Kanazawa, A. (2003) Balancing the central roles of the thylakoid proton gradient. *Trends Plant Sci.* **8**, 27–32.

Kress, E. and Jahns, P. (2017) The dynamics of energy dissipation and xanthophyll conversion in Arabidopsis indicate an indirect photoprotective role of zeaxanthin in slowly inducible and relaxing components of non-photochemical quenching of excitation energy. *Front. Plant Sci.* **8**, 2094.

Krieger-Liszkay, A. and Trebst, A. (2006) Tocopherol is the scavenger of singlet oxygen produced by the triplet states of chlorophyll in the PSII reaction centre. *J. Exp. Bot.* **57**, 1677–1684.

Król, M., Hurry, V., Maxwell, D., Malek, L., Ivanov, A., Huner, N. (2002). Low growth temperature inhibition of photosynthesis in cotyledons of jack pine seedlings (*Pinus banksiana*) is due to impaired chloroplast development. *Can. J. Bot.* **80**, 1042−1051.

Kurasová, I., Kalina, J., Urban, O., Štroch, M., Špunda, V. (2003) Acclimation of two distinct plant species, spring barley and Norway spruce, to combined effect of various irradiance and CO2 concentration during cultivation in controlled environment. *Photosynthetica* **41,** 513–523.

Kurepin, L.V., Stangl, Z.R., Ivanov, A.G., Bui, V., Mema, M., Hüner, N.P.A., Öquist, G., Way, D., Hurry, V. (2018) Contrasting acclimation abilities of two dominant boreal conifers to elevated CO_2 and temperature. *Plant Cell Environ.* **41**, 1331–1345.

Laemmli, U. K. (1970). Cleavage of structural proteins during the assembly of the head of bacteriophage T4. *Nature* **227**, 680–685.

Le Quiniou, C., van Oort, B., Drop, B., van Stokkum, I.H.M., Croce, R. (2015) The high efficiency of Photosystem I in the green alga *Chlamydomonas reinhardtii* is maintained after the antenna size is substantially increased by the association of light-harvesting complexes II. *J. Biol. Chem.* **290**, 30587–30595.

Lee, S.C., Knowles, T.J., Postis, V.L., Jamshad, M., Parslow, R.A., Lin, Y.P., Goldman, A., Sridhar, P., Overduin, M., Muench, S.P., Dafforn, T.R. (2016) A method for detergent-free isolation of membrane proteins in their local lipid environment. *Nat. Protoc.* **11**, 1149–62.

Lemeille, S. and Rochaix, J.D. (2010) State transitions at the crossroad of thylakoid signalling pathways. *Photosynth. Res.* **106**, 33–46.

Li, M. and Kim, C. (2022) Chloroplast ROS and stress signaling. *Plant Communications*. **3**, 100264.

Li, X.P., Björkman, O., Shih, C., Grossman, A.R., Rosenquist, M., Jansson, S., Niyogi, K.K. (2000) A pigment-binding protein essential for regulation of photosynthetic light harvesting. *Nature* **403**, 391–395.

Li, X.P., Gilmore, A.M., Caffarri, S., Bassi, R., Golan, T., Kramer, D., Niyogi, K.K. (2004) Regulation of photosynthetic light harvesting involves intrathylakoid lumen pH sensing by the PsbS protein. *J. Biol. Chem*. **279**, 22866–22874.

Lichtenberg, D., Ahyayauch, H., Goñi, F.M. (2013) The mechanism of detergent solubilization of lipid bilayers. *Biophys. J.* **105**, 289–299.

Lichtenthaler, H.K. (1987) Chlorophylls and carotenoids - pigments of photosynthetic biomembranes. *Meth. Enzymol*. **148**, 350–382.

Lunde, C., Jensen, P.E., Haldrup, A., Knoetzel, J., Scheller, H.V. (2000) The PSI-H subunit of photosystem I is essential for state transitions in plant photosynthesis. *Nature* **408**, 613–615.

Lundin, B., Hansson, M., Schoefs, B., Vener, A.V., Spetea, A. (2007) The Arabidopsis PsbO2 protein regulates dephosphorylation and turnover of the photosystem II reaction centre D1 protein. *Plant J. Cell Mol. Biol.* **49**, 528–539.

Lyu, H. and Lazár, D. (2023) Effect of ion fluxes on regulating the light-induced transthylakoid electric potential difference. *Plant Physiol. Biochem.* **194**, 60–69.

Ma, M., Liu, Y., Bai, C., Yang, Y., Sun, Z., Liu, X., Zhang, S., Han, X., Yong, J.W.H. (2021) The physiological functionality of PGR5/PGRL1-dependent cyclic electron transport in sustaining photosynthesis. *Front. Plant Sci.* **7**, 702196.

Malavath, T., Caspy, I., Netzer-El, S.Y., Klaiman, D., Nelson, N. (2018) Structure and function of wild-type and subunit-depleted photosystem I in *Synechocystis. Biochim. Biophys. Acta - Bioenerg*. **1859**, 645–654.

Malone, L.A., Proctor, M.S., Hitchcock, A., Hunter, C.N., Johnson, M.P. (2021) Cytochrome b6f – Orchestrator of photosynthetic electron transfe. *Biochim. Biophys. Acta – Bioenerg.* **1862**, 148380.

Martin, B. and Öquist, G. (1979) Seasonal and experimentally induced changes in the ultrastructure of chloroplasts of *Pinus silvestris*. *Physiol. Plant*. **46**, 42–49.

Mazor, Y., Borovikova, A., Caspy, I., Nelson, N. (2017) Structure of the plant photosystem I supercomplex at 2.6 Å resolution. *Nat. Plants* **3**, 17014.

Mazor, Y., Borovikova, A., Nelson, N. (2015) The structure of plant photosystem I super-complex at 2.8 Å resolution. *Elife* **4**, e07433.

Mehler, A.H. (1951) Studies on reactions of illuminated chloroplasts. *Arch. Biochem. Biophys.* **33**, 65–77.

Miller, C.N. (1999) Implications of fossil conifers for the phylogenetic relationships of living families. *Bot. Rev.* **65**, 239–277.

Minagawa, J. (2011) State transitions - The molecular remodeling of photosynthetic supercomplexes that controls energy flow in the chloroplast. *Biochim. Biophys. Acta − Bioenerg.* **1807**, 897–905.

Minagawa, J. and Takahashi, Y. (2004) Structure, function and assembly of photosystem II and its light-harvesting proteins. *Photosyn. Res.* **82**, 241–263.

Mitchell, P. (1966) Chemiosmotic coupling in oxidative and photosynthetic phosphorylation. *Biol. Rev.* **41**, 445–502.

Müh, F., Renger, T., Zouni, A. (2008) Crystal structure of cyanobacterial photosystem II at 3.0 A resolution: a closer look at the antenna system and the small membrane-intrinsic subunits. *Plant Physiol. Biochem.* **46**, 238–64.

Mullineaux, C.W. (2008) Factors controlling the mobility of photosynthetic proteins. *Photochem. Photobiol.* **84**, 1310–1316.

Munekage, Y., Hashimoto, M., Miyake, C., Tomizawa, K.I., Endo, T., Tasaka, M., Shikanai, T. (2004) Cyclic electron flow around photosystem I is essential for photosynthesis. *Nature* **429**, 579–582.

Munekage, Y., Hojo, M., Meurer, J., Endo, T., Tasaka, M., Shikanai, T. (2002) PGR5 is involved in cyclic electron flow around photosystem I and is essential for photoprotection in Arabidopsis. *Cell* **110**, 361–371.

Murata, N., Mohanty, P.S., Hayashi, H., Papageorgiou, G.C. (1992) Glycinebetaine stabilizes the association of extrinsic proteins with the photosynthetic oxygen-evolving complex. *FEBS Lett.* **296** , 187–189.

Nagao, R., Kato, K., Kumazawa, M., Ifuku, K., Yokono, M., Suzuki, T., Dohmae, N., Akita, F., Akimoto, S., Miyazaki, N., Shen, J.R. (2022) Structural basis for different types of hetero-tetrameric light-harvesting complexes in a diatom PSII-FCPII supercomplex. *Nat. Commun.* **13**, 1764.

Nagao, R., Kato, K., Suzuki, T., Ifuku, K., Uchiyama, I., Kashino, Y., Dohmae, N., Akimoto, S., Shen, J.-R., Miyazaki, N., Akita, F. (2019) Structural basis for energy harvesting and dissipation in a diatom PSII–FCPII supercomplex. *Nat. Plants* **5**, 890–901.

Nanba, O. and Satoh, K. (1987) Isolation of a photosystem II reaction center consisting of D-1 and D-2 polypeptides and cytochrome b-559, *Proc. Natl. Acad. Sci. U. S. A.* **84**, 109–112.

Naschberger, A., Mosebach, L., Tobiasson, V., Kuhlgert, S., Scholz, M., Perez-Boerema, A., Ho, T.T.H., Vidal-Meireles, A., Takahashi, Y., Hippler, M., Amunts, A. (2022) Algal photosystem I dimer and high-resolution model of PSI-plastocyanin complex. *Nat. Plants* **8**, 1191–1201.

Natali, A. and Croce, R. (2015) Characterization of the major light-harvesting complexes (LHCBM) of the green alga *Chlamydomonas reinhardtii*. *PLoS ONE* **10**, e0119211.

Nawrocki, W.J., Tourasse, N.J., Taly, A., Rappaport, F., Wollman, F.-A. (2015) The plastid terminal oxidase: its elusive function points to multiple contributions to plastid physiology. *Annu. Rev. Plant Biol.* **66**, 49–74.

Nelson, N. (2009) Plant photosystem I - the most efficient nano-photochemical machine. *J. Nanosci. Nanotech.* **9**, 1709–1713.

Nelson, N. and Ben-Shem, A. (2004) The complex architecture of oxygenic photosynthesis. *Nature Rev. Mol. Cell Biol.* **5**, 971–982.

Nelson, N. and Junge, W. (2015) Structure and energy transfer in photosystems of oxygenic photosynthesis. *Annu. Rev. Biochem.* **84**, 659–683.

Nelson, N. and Yocum, C.F. (2006) Structure and function of photosystems I and II. *Annu. Rev. Plant Biol.* **57**, 521–565.

Nikkanen, L. and Rintamäki, E. (2019) Chloroplast thioredoxin systems dynamically regulate photosynthesis in plants. *Biochem. J.* **476**, 1159–1172.

Niyogi, K. K. and Truong, T. B. (2013) Evolution of flexible non-photochemical quenching mechanisms that regulate light harvesting in oxygenic photosynthesis. *Curr. Opin. Plant Biol.* **16**, 307–314.

Nosek, L., Semchonok, D., Boekema, E.J., Ilík, P., Kouřil, R. (2017) Structural variability of plant photosystem II megacomplexes in thylakoid membranes. *Plant J.* **89**, 104–111.

Nystedt, B., Street, N.R., Wetterbom, A., Zuccolo, A., Lin, Y.C., Scofield, D.G., Vezzi, F., Delhomme, N., Giacomello, S., Alexeyenko, A., Vicedomini, R., Sahlin, K., Sherwood, E., Elfstrand, M., Gramzow, L., Holmberg, K., Hällman, J., Keech, O., Klasson, L., Koriabine, M., Kucukoglu, M., Käller, M., Luthman, J., Lysholm, F., Niittylä, T., Olson, A., Rilakovic, N., Ritland, C., Rosselló, J.A., Sena, J., Svensson, T., Talavera-López, C., Theißen, G., Tuominen, H., Vanneste, K., Wu, Z.Q., Zhang, B., Zerbe, P., Arvestad, L., Bhalerao, R., Bohlmann, J., Bousquet, J., Garcia Gil, R., Hvidsten, T.R., de Jong, P., MacKay, J., Morgante, M., Ritland, K., Sundberg, B., Thompson, S.L., Van de Peer, Y., Andersson, B., Nilsson, O., Ingvarsson, P.K., Lundeberg, J., Jansson, S. (2013) The Norway spruce genome sequence and conifer genome evolution. *Nature* **497**, 579–584.

Oku, T., Sugahara, K., Tomita, G. (1974) Functional development of photosystem I and II in dark-grown pine seedlings. *Plant Cell Physiol*. **15**, 175–178.

Opatíková M., Semchonok, D.A., Kopečný D., Ilík P., Pospíšil P., Ilíková I., Roudnický P., Zeljković S.Ć., Tarkowski P., Kyrilis F.L., Hamdi F., Kastritis P.L., Kouřil R. (2023) Cryo-EM structure of plant photosystem II supercomplex with light-harvesting protein LHCB8 and α-tocopherol. *Nat. Plants* (in press).

Öquist, G. and Huner, N. P. (2003) Photosynthesis of overwintering evergreen plants. *Annu. Rev. Plant Biol.* **54**, 329–355.

Otani, T., Kato, Y., Shikanai, T. (2018) Specific substitutions of light harvesting complex I proteins associated with photosystem I are required for supercomplex formation with chloroplast NADH dehydrogenase-like complex. *Plant J.* **94**, 122–130.

Ottander, C., Campbell, D., Öquist, G. (1995) Seasonal changes in photosystem-II organization and pigment composition in *Pinus sylvestris. Planta* **197**, 176–183.

Ozawa, S., Onishi, T., Takahashi, Y. (2010) Identification and characterization of an assembly intermediate subcomplex of photosystem I in the green alga *Chlamydomonas reinhardtii. J. Biol. Chem.* **285**, 20072–20079.

Pagliano, C., Nield, J., Marsano, F., Pape, T., Barera, S., Saracco, G., Barber, J. (2014) Proteomic characterization and three-dimensional electron microscopy study of PSII-LHCII supercomplexes from higher plants. *Biochim. Biophys. Acta.* **1837**, 1454-1462.

Pan, X., Ma, J., Su, X., Cao, P., Chang, W., Liu, Z., Zhang, X., Li, M. (2018) Structure of the maize photosystem I supercomplex with light-harvesting complexes I and II. *Science.* **360**, 1109–1113.

Pan, X., Tokutsu, R., Li, A., Takizawa, K., Song, C., Murata, K., Yamasaki, T., Liu, Z., Minagawa, J., Li, M. (2021) Structural basis of LHCBM5-mediated state transitions in green algae. *Nat. Plants* **7**, 1119–1131.

Pan, Y., Birdsey, R.A., Fang, J., Houghton, R., Kauppi, P.E., Kurz, W.A., Phillips, O.L., Shvidenko, A., Lewis, S.L., Canadell, J.G., Ciais, P., Jackson, R.B., Pacala, S.W., McGuire, A.D., Piao, S., Rautiainen, A., Sitch, S., Hayes, D. (2011) A large and persistent carbon sink in the World's Forests. *Science* **333**, 988–993.

Papageorgiou, G.C, and Murata, N. (1995) The unusually strong stabilizing effects of glycine betaine on the structure and function of the oxygen-evolving Photosystem II complex. *Photosynth Res.* **44**, 243–52.

Pavlovič, A., Stolárik, T., Nosek, L., Kouřil, R., Ilík, P. (2016) Light-induced gradual activation of photosystem II in dark-grown Norway spruce seedlings. *Biochim. Biophys. Acta – Bioenerg.* **1857**, 799–809.

Peers, G., Truong, T.B., Ostendorf, E., Busch, A., Elrad, D., Grossman, A.R., Hippler, M., Niyogi, K.K. (2009) An ancient light-harvesting protein is critical for the regulation of algal photosynthesis. *Nature* **462**, 518–521.

Peng, L., Shimizu, H., Shikanai, T. (2008) The chloroplast NAD(P)H dehydrogenase complex interacts with photosystem I in Arabidopsis. *J. Biol. Chem.* **283**, 34873–34879.

Peng, L.W., Fukao, Y., Fujiwara, M., Takami, T., Shikanai, T. (2009) Efficient operation of NAD(P)H dehydrogenase requires supercomplex formation with photosystem I via minor LHCI in Arabidopsis. *Plant Cell* **21**, 3623–3640.

Peredo, E.L., King, U.M., Les, D.H. (2013) The plastid genome of Najas flexilis: Adaptation to submersed environments is accompanied by the complete loss of the NDH complex in an aquatic angiosperm. *PLoS One*. **8**, e68591.

Pesaresi, P., Hertle, A., Pribil, M., Schneider, A., Kleine, T., Leister, D. (2010) Optimizing photosynthesis under fluctuating light: the role of the Arabidopsis STN7 kinase. *Plant Signal. Behav.* **5**, 21–25.

Pesaresi, P., Pribil, M., Wunder, T. and Leister, D. (2011) Dynamics of reversible protein phosphorylation in thylakoids of flowering plants: The roles of STN7, STN8 and TAP38. *Biochim. Biophys. Acta – Bioenerg.* **1807**, 887–896.

Peter, G.F. and Thornber, J.P. (1991) Biochemical composition and organization of higher plant photosystem II light-harvesting pigment - proteins. *J. Biol. Chem.* **266**, 16745–16754.

Peterson, R.B. and Schultes, N.P. (2014) Light-harvesting complex B7 shifts the irradiance response of photosynthetic light-harvesting regulation in leaves of *Arabidopsis thaliana*. *J. Plant Physiol.* **171**, 311–318.

Pfannschmidt, T., Nilsson, A., Allen, J.F. (1999) Photosynthetic control of chloroplast gene expression. *Nature* **397**, 625–628.

Pfannschmidt, T., Schutze, K., Brost, M., Oelmuller, R. (2001) A novel mechanism of nuclear photosynthesis gene regulation by redox signals from the chloroplast during photosystem stoichiometry adjustment. *J. Biol. Chem*. **276**, 36125–36130.

Pinnola, A., Alboresi, A., Nosek, L., Semchonok, D., Rameez, A., Trotta, A., Barozzi, F., Kouřil, R., Dall'Osto, L., Aro, E.-M., Boekema, E.J., Bassi, R. (2018) A LHCB9-dependent photosystem I megacomplex induced under low light in *Physcomitrella patens*. *Nat. Plants* **4**, 910–919.

Poolman, M.G. and Fell, D.A. (2000) Modelling photosynthesis and its control. *J. Exp. Bot.* **51**, 319–328.

Porcar-Castell, A. (2011) A high-resolution portrait of the annual dynamics of photochemical and non-photochemical quenching in needles of *Pinus sylvestris*. *Physiol. Plant.* **143**, 139–153.

Pribil, M., Pesaresi, P., Hertle, A., Barbato, R., Leister, D. (2010) Role of plastid protein phosphatase TAP38 in LHCII dephosphorylation and thylakoid electron flow. *PLoS Biol.* **8**, e1000288.

Qin, X., Pi, X., Wang, W., Han, G., Zhu, L., Liu, M., Cheng, L., Shen, J.-R., Kuang, T., Sui, S.-F. (2019) Structure of a green algal photosystem I in complex with a large number of light-harvesting complex I subunits. *Nat. Plants* **5**, 263–272.

Qin, X., Suga, M., Kuang, T., Shen, J.R. (2015) Photosynthesis. Structural basis for energy transfer pathways in the plant PSI-LHCI supercomplex. *Science* **348**, 989–995.

Rantala, M., Rantala, S., Aro, E-M. (2020) Composition, phosphorylation and dynamic organisation of photosynthetic protein complexes in plant thylakoid membrane. *Photochem. Photobiol. Sci.* **19**, 604-619.

Rantala, M., Tikkanen, M. Aro, E.-M. (2017) Proteomic characterization of hierarchical megacomplex formation in Arabidopsis thylakoid membrane. *Plant J.* **92**, 951–962.

Raymond, J. and Blankenship, R.E. (2004) Biosynthetic pathways, gene replacement and the antiquity of life. *Geobiol.* **2**, 199–203.

Reinbothe, C., El Bakkouri, M., Buhr, F., Muraki, N., Nomata, J., Kurisu, G., Fujita, Y., Reinbothe, S. (2010) Chlorophyll biosynthesis: spotlight on protochlorophyllide reduction. *Trends Plant Sci.* **15**, 614–624.

Rintamäki, E., Martinsuo, P., Pursiheimo, S. and Aro, E.-M. (2000) Cooperative regulation of lightharvesting complex II phosphorylation via the plastoquinol and ferredoxin-thioredoxin system in chloroplasts. *Proc. Natl. Acad. Sci. U. S. A.* **97**, 11644–11649.

Rochaix, J.-D. (2007) Role of thylakoid protein kinases in photosynthetic acclimation. *FEBS Lett.* **581**, 2768–2775.

Rochaix, J.-D. (2013) Fine-tuning photosynthesis. *Science* **342**, 50–51.

Rochaix, J.-D. (2014) Regulation and dynamics of the light-harvesting system. *Annu. Rev. Plant Biol.* **65**, 287–309.

Rochaix, J.-D., Lemeille, S., Shapiguzov, A., Samol, I., Fucile, G., Willig, A., Goldschmidt-Clermont, M. (2012) Protein kinases and phosphatases involved in the acclimation of the photosynthetic apparatus to a changing light environment. *Philos. Trans. R. Soc. Lond. B Biol. Sci.* **367**, 3466–3474.

Ruhlman, T.A., Chang, W.-J., Chen, J.J.W., Huang, Y.-T., Chan, M.-T., Zhang, J., Liao, D.-C., Blazier, J.C., Jin, X., Shih, M.-C., Jansen, R.K. and Lin, C.-S. (2015) NDH expression marks major transitions in plant evolution and reveals coordinate intracellular gene loss. *BMC Plant Biol*. **15**, 100.

Rumberg, B. and Siggel, U. (1969) pH changes in the inner phase of the thylakoids during photosynthesis. *Naturwissenschaften* **56**, 130–132.

Sawchuk, M.G., Donner, T.J., Head, P., Scarpella, E. (2008) Unique and overlapping expression patterns among members of photosynthesis associated nuclear gene families in Arabidopsis. *Plant Physiol.* **148**, 1908–1924.

Schägger, H. (2006) Tricine-SDS-PAGE. *Nat Protoc*. **1**, 16-22.

Schiphorst, C., Achterberg, L., Gómez, R., Koehorst, R., Bassi, R., van Amerongen, H., Dall'Osto, L. Wientjes, E. (2022) The role of light-harvesting complex I in excitation energy transfer from LHCII to photosystem I in Arabidopsis. *Plant Physiol.* **188**, 2241–2252.

Schoefs, B. and Franck, F. (2003) Protochlorophyllide reduction: mechanisms and evolution. *Photochem. Photobiol*. **78**, 543–557.

Schwarz, E.M., Tietz, S., Froehlich, J.E. (2018) Photosystem I-LHCII megacomplexes respond to high light and aging in plants. *Photosynth. Res.* **136**, 107–124.

Semchonok, D.A., Mondal, J., Cooper, C.J., Schlum, K., Li, M., Amin, M., Sorzano, C.O.S., Ramírez-Aportela, E., Kastritis, P.L., Boekema, E.J., Guskov, A., Bruce, B.D. (2021) Cryo-EM structure of a tetrameric photosystem I from Chroococcidiopsis TS-821, a thermophilic, unicellular, non-heterocyst-forming cyanobacterium. *Plant Commun*. **3**, 100248.

Semenova, G.A. (1995). Particle regularity on thylakoid fracture faces is influenced by storage-conditions. *Canad. J. Bot.* **73**, 1676–1682.

Sétif, P., Shimakawa, G., Krieger-Liszkay, A., Miyake, C. (2020) Identification of the electron donor to flavodiiron proteins in Synechocystis sp. PCC 6803 by in vivo spectroscopy. *Biochim. Biophys. Acta – Bioenerg.* **1861**, 148256.

Shang, H., Li, M., Pan, X. (2023) Dynamic Regulation of the Light-Harvesting System through State Transitions in Land Plants and Green Algae. *Plants (Basel)* **12**, 1173.

Shapiguzov, A., Ingelsson, B., Samol, I., Andres, C., Kessler, F., Rochaix, J.-D., Vener, A.V., Goldschmidt-Clermont, M. (2010) The PPH1 phosphatase is specifically involved in LHCII dephosphorylation and state transitions in Arabidopsis. *Proc. Natl. Acad. Sci. U. S. A.* **107**, 4782–4787.

Shen, L., Huang, Z., Chang, S., Wang, W., Wang, J., Kuang, T., Han, G., Shen, J.R., Zhang, X. (2019) Structure of a $C_2S_2M_2N_2$-type PSII–LHCII supercomplex from the green alga *Chlamydomonas reinhardtii*. *Proc. Natl. Acad. Sci. U. S. A.*, **116**, 21246−21255.

Shen, L., Tang, K., Wang, W., Wang, C., Wu, H., Mao, Z., An, S., Chang, S., Kuang, T., Shen, J.R., Han, G., Zhang, X. (2022) Architecture of the chloroplast PSI-NDH supercomplex in *Hordeum vulgare. Nature* **601**, 649–654.

Sheng, X., Watanabe, A., Li, A., Kim, E., Song, Ch., Murata, K., Song, D., Minagawa, J., Liu, Z. (2019) Structural insight into light harvesting for photosystem II in green algae. *Nat. Plants* **5**, 1320–1330.

Shi, L.X. and Schroder, W.P. (2004) The low molecular mass subunits of the photosynthetic supracomplex, photosystem II. *Biochim. Biophys. Acta – Bioenerg.* **1608**, 75–96.

Shikanai, T. (2007) Cyclic electron transport around photosystem I: genetic approaches. *Annu. Rev. Plant Biol.* **58**, 199–217.

Shikanai, T. (2014) Central role of cyclic electron transport around photosystem I in the regulation of photosynthesis. *Curr. Opin. Biotech.* **26**, 25–30.

Shikanai, T. (2020) Regulation of photosynthesis by cyclic electron transport around photosystem I. *Adv. Bot. Res.* **96**, 177–204.

Shirao, M., Kuroki, S., Kaneko, K., Kinjo, Y., Tsuyama, M., Förster, B., Takahashi, S., Badger, M.R. (2013) Gymnosperms have increased capacity for electron leakage to oxygen (Mehler and PTOX reactions) in photosynthesis compared with angiosperms. *Plant Cell Physiol.* **54**, 1152–1163.

Shorohova, E., Kneeshaw, D., Kuuluvainen, T., Gauthier, S. (2011) Variability and dynamics of old-growth forests in the circumboreal zone: Implications for conservation, restoration and management. *Silva Fenn.* **45**, 785–806.

Stirbet, A., Lazár, D., Guo, Y., Govindjee, G. (2020) Photosynhesis: basics, history, and modeling. *Ann. Bot*. **126**, 511-537.

Storf, S., Jansson, S., Schmid, V.H. (2005) Pigment binding, fluorescence properties, and oligomerization behavior of Lhca5, a novel light-harvesting protein. *J Biol Chem.* **18**, 5163–5168.

Štroch, M., Karlický, V., Ilík, P., Ilíková, I., Opatíková, M., Nosek, L., Pospíšil, P., Svrčková, M., Rác, M., Roudnický, P., Zdráhal, Z., Špunda, V., Kouřil, R. (2022) Spruce versus Arabidopsis: different strategies of photosynthetic acclimation to long-term light intensity changes. *Photosynth. Res.* **154**, 21–40.

Štroch, M., Kuldová, K., Kalina, J., Špunda, V. (2008) Dynamics of the xanthophyll cycle and non-radiative dissipation of absorbed light energy during exposure of Norway spruce to high irradiance. *J. Plant Physiol.* **165,** 612–622.

Su, X., Cao, D., Pan, X., Shi, L., Liu, Z., Dall'Osto, L., Bassi, R., Zhang, X., Li, M. (2022) Supramolecular assembly of chloroplast NADH dehydrogenase-like complex with photosystem I from *Arabidopsis thaliana*. *Mol. Plant* **15**, 454–467.

Su, X., Ma, J., Pan, X., Zhao, X., Chang, W., Liu, Z., Zhang, X., Li, M. (2019) Antenna arrangement and energy transfer pathways of a green algal photosystem-I–LHCI supercomplex. *Nat. Plants* **5**, 273–281.

Su, X., Ma, J., Wei, X., Cao, P., Zhu, D., Chang, W., Liu, Z., Zhang, X., Li, M. (2017) Structure and assembly mechanism of plant C2S2M2-type PSII-LHCII supercomplex. *Science* **357**, 815–820.

Suga, M., Ozawa, S.I., Yoshida-Motomura, K., Akita, F., Miyazaki, N., Takahashi, Y. (2019) Structure of the green algal photosystem I supercomplex with a decameric light-harvesting complex I. *Nat. Plants* **5**, 626–636.

Sun, H., Shang, H., Pan, X., Li, M. (2023) Light-harvesting complex Lhcb9 confers a green alga-type photosystem I supercomplex to the moss Physcomitrella patens

Suorsa, M., Järvi, S., Grieco, M., Nurmi, M., Pietrzykowska, M., Rantala, M., Kangasjärvi, S., Paakkarinen, V., Tikkanen, M., Jansson, S., Aro, E.-M. (2012) PROTON GRADIENT REGULATION5 is essential for proper acclimation of Arabidopsis photosystem I to naturally and artificially fluctuating light conditions. *Plant Cell* **24**, 2934–2948.

Suorsa, M., Rantala, M., Mamedov, F., Lespinasse, M., Trotta, A., Grieco, M., Vuorio, E., Tikkanen, M., Järvi, S., Aro, E.-M. (2015) Light acclimation involves dynamic re-organization of the pigment–protein megacomplexes in non-appressed thylakoid domains. *Plant J.* **84**, 360–373.

Svensson, P. and Albertsson, P.-Å. (1989) Preparation of highly enriched photosystem II membrane vesicles by a nondetergent method. *Photosynth. Res*. **20**, 249–259.

Takahashi, H., Okamuro, A., Minagawa, J., Takahashi, Y. (2014) Biochemical characterization of photosystem I-associated light-harvesting complexes I and II isolated from state 2 cells of *Chlamydomonas reinhardtii*. *Plant Cell Physiol*. **55**, 1437–1449.

Tietz, S., Puthiyaveetil, S., Enlow, H.M., Yarbrough, R., Wood, M., Semchonok, D. A., Lowry, T., Li, Z., Jahns, P., Boekema, E.J., Lenhert, S., Niyogi, K.K., Kirchhoff, H. (2015) Functional implications of photosystem II crystal formation in photosynthetic membranes. *J. Biol. Chem.* **290**, 14091–14106.

Tikhonov, A.N. (2014) The cytochrome b6f complex at the crossroad of photosynthetic electron transport pathways. *Plant Physiol. Biochem*. **81**, 163–83.

Tikkanen, M. and Aro, E.-M. (2014). Integrative regulatory network of plant thylakoid energy transduction. *Trends Plant Sci*. **19**, 10–17.

Tokutsu, R., Iwai, M., Minagawa, J. (2009) CP29, a monomeric light-harvesting complex II protein, is essential for state transitions in *Chlamydomonas reinhardtii. J. Biol. Chem.* **284**, 7777–7782.

Tokutsu, R., Kato, N., Bui, K. H., Ishikawa, T., Minagawa, J. (2012) Revisiting the supramolecular organization of photosystem II in *Chlamydomonas reinhardtii*. *J. Biol. Chem.* **287**, 31574–31581

Trissl, H.-W. and Wilhelm, C. (1993) Why do thylakoid membranes from higher plants form grana stacks? *Trends Biochem. Sci.* **18**, 415–419.

Ueda, M., Kuniyoshi, T., Yamamoto, H., Sugimoto, K., Ishizaki, K., Kohchi, T., Nishimura, Y. and Shikanai, T. (2012) Composition and physiological function of the chloroplast NADH dehydrogenase-like complex in Marchantia polymorpha. *Plant J.* **72**, 683–693.

van Bezouwen, L.S., Caffarri, S., Kale, R.S., Kouřil, R., Thunnissen, A.-M.W.H., Oostergetel, G.T., Boekema, E.J. (2017) Subunit and chlorophyll organization of the plant photosystem II supercomplex. *Nat. Plants* **3**, 17080.

van Eerden, F.J., Melo, M.N., Frederix, P.W.J.M., Periole, X., Marrink, S.J. (2017) Exchange pathways of plastoquinone and plastoquinol in the photosystem II complex. *Nat. Commun.* **8**, 15214.

Vener, A.V., Harms, A., Sussman, M.R., Vierstra, R.D. (2001) Mass spectrometric resolution of reversible protein phosphorylation in photosynthetic membranes of *Arabidopsis thaliana. J. Biol. Chem.* **276**, 6959–6966.

Vener, A.V., Rokka, A., Fulgosi, H., Andersson, B., Herrmann, R.G. (1999) A cyclophilin-regulated PP2A-like protein phosphatase in thylakoid membranes of plant chloroplasts. *Biochem.* **38**, 14955–14965.

Verhoeven, A. (2014) Sustained energy dissipation in winter evergreens. *New Phytol.* **201**, 57–65.

Verhoeven, A.S. (2013) Recovery kinetics of photochemical efficiency in winter stressed conifers: the effects of growth light environment, extent of the season and species. *Physiol. Plant.* **147**, 147–158.

Verhoeven, A.S., Adams, W.W., Demmig-Adams, B. (1998) Two forms of sustained xanthophyll cycle-dependent energy dissipation in overwintering *Euonymus kiautschovicus. Plant Cell Environ*. **21**, 893–903.

Wada, S., Yamamoto, H., Suzuki, Y., Yamori, W., Shikanai, T., Makino, A. (2018) Flavodiiron protein substitutes for cyclic electron flow without competing CO2 assimilation in rice. *Plant Physiol.* **176**, 1509–1518.

Walter-McNeill, A., Garcia, M.A., Logan, B.A., Bombard, D.M., Reblin, J.S., Lopez, S., Southwick, C.D., Sparrow, E.L. and Bowling, D.R. (2021) Wide variation of winter-induced sustained thermal energy dissipation in conifers: a common-garden study. *Oecologia* **197**, 589–598.

Ware, M.A., Giovagnetti, V., Belgio, E., Ruban, A. V. (2015) PsbS protein modulates nonphotochemical chlorophyll fluorescence quenching in membranes depleted of photosystems. *J. Photochem. Photobiol. B: Biol.* **152**, 301–307.

Webber, A.N., Packman, L., Chapman, D.J., Barber, J., Gray, J.C. (1989) A fifth chloroplast-encoded polypeptide is present in the photosystem II reaction centre complex, *FEBS Lett.* **242**, 259–262.

Wei, X., Su, X., Cao, P., Liu, X., Chang, W., Li, M., Zhang, X., Liu, Z. (2016) Structure of spinach photosystem II–LHCII supercomplex at 3.2 Å resolution. *Nat. Cell Biol.* **534**, 69–74.

Wientjes, E., Drop, B., Kouril, R., Boekema, E.J., Croce, R. (2013) During state 1 to state 2 transition in *Arabidopsis thaliana*, the photosystem II supercomplex gets phosphorylated but does not disassemble. *J. Biol. Chem.* **288**, 32821–32826.

Wientjes, E., Oostergetel, G.T., Jansson, S., Boekema, E.J., and Croce, R. (2009) The role of Lhca complexes in the supramolecular organization of higher plant photosystem I. *J. Biol. Chem.* **284**, 7803–7810.

Wittig, I., Karas, M., Schägger, H. (2007) High resolution clear native electrophoresis for in-gel functional assays and fluorescence studies of membrane protein complexes. *Mol. Cell. Proteomics.* **6**, 1215–1225.

Xu, C., Pi, X., Huang, Y., Han, G., Chen, X., Qin, X., Huang, G., Zhao, S., Yang, Y., Kuang, T., Wang, W., Sui, S.F., Shen, J.R. (2020) Structural basis for energy transfer in a huge diatom PSI-FCPI supercomplex. *Nat. Commun.* **11**, 5081.

Yadav, K.N., Semchonok, D.A., Nosek, L., Kouřil, R., Fucile, G., Boekema, E.J., Eichacker, L.A. (2017) Supercomplexes of plant photosystem I with cytochrome b6f, light-harvesting complex II and NDH. *Biochim. Biophys. Acta – Bioenerg.* **1858**, 12-20.

Yakushevska, A.E., Jensen, P.E., Keegstra, W., van Roon, H., Scheller, H.S., Boekema, E.J., Dekker, J.P. (2001) Supermolecular organization of photosystem II and its associated light-harvesting antenna in *Arabidopsis thaliana*. *Eur. J. Biochem.* **268**, 6020–6028.

Yamori, W. and Shikanai, T. (2016) Physiological functions of cyclic electron transport around photosystem I in sustaining photosynthesis and plant growth. *Annu. Rev. Plant Biol.* **67**, 81–106.

Yamori, W., Shikanai, T., Makino, A. (2015) Photosystem I cyclic electron flow via chloroplast NADH dehydrogenase-like complex performs a physiological role for photosynthesis at low light. *Sci. Rep.* **5**, 13908.

Yan, Q., Zhao, L., Wang, W., Pi, X., Han, G., Wang, J., Cheng, L., He, Y.K., Kuang, T., Qin, X., Sui, S.-F., Shen, J.-R. (2021) Antenna arrangement and energy-transfer pathways of PSI-LHCI from the moss *Physcomitrella patens*. *Cell Discov.* **7**, 10.

Yang, Q., Blanco, N. E., Hermida-Carrera, C., Lehotai, N., Hurry, V., Strand, Å. (2020) Two dominant boreal conifers use contrasting mechanisms to reactivate photosynthesis in the spring. *Nat. Commun.* **11**, 128.

Yoshida, K., Yokochi, Y., Hisabori, T. (2019) New light on chloroplast redox regulation: molecular mechanism of protein thiol oxidation. *Front. Plant Sci.* **10**, 1–6.

You, X., Zhang, X., Cheng, J., Xiao, Y., Ma, J., Sun, S., Zhang, X., Wang, H.W., Sui, S.F. (2023) In situ structure of the red algal phycobilisome-PSII-PSI-LHC megacomplex. *Nature* **616**, 199–206.

Yu, Q., Feilke, K., Krieger-Liszkay, A., Beyer, P. (2014) Functional and molecular characterization of plastid terminal oxidase from rice (Oryza sativa). *Biochim. Biophys. Acta – Bioenerg.* **1837**, 1284–1292.

Zhang, C., Shuai, J., Ran, Z., Zhao, J., Wu, Z., Liao, R., Wu, J., Ma, W., Lei, M. (2020) Structural insights into NDH-1 mediated cyclic electron transfer. *Nat. Commun.* **11**, 888.

Zhang, S., Tang, K., Yan, Q., Li, X., Shen, L., Wang, W., He, Y.K., Kuang, T., Han, G., Shen, J.R., Zhang, X. (2023) Structural insights into a unique PSI-LHCI-LHCII-Lhcb9 supercomplex from moss *Physcomitrium patens*. *Nat. Plants* **9**, 832–846.

6. Appendix

Opatíková M., Semchonok, D.A., Kopečný D., Ilík P., Pospíšil P., Ilíková I., Roudnický P., Zeljković S.Ć., Tarkowski P., Kyrilis F.L., Hamdi F., Kastritis P.L., Kouřil R. (2023) Cryo-EM structure of plant photosystem II supercomplex with light-harvesting protein LHCB8 and α-tocopherol. *Nat. Plants* (in press).

Štroch M., Karlický V., Ilík P., Ilíková I., **Opatíková M.**, Nosek L., Pospíšil P., Svrčková M., Rác M., Roudnický P., Zdráhal Z., Špunda V., Kouřil R. (2022) Spruce versus Arabidopsis: different strategies of photosynthetic acclimation to light intensity change. *Photosynth. Res.* **154**, 21–40.

Ilíková I., Ilík P., **Opatíková M.**, Arshad R., Nosek L., Karlický V., Kučerová Z., Roudnický P., Pospíšil P., Lazár D., Bartoš J., Kouřil R. (2021) Towards spruce-type photosystem II supercomplex: consequences of the loss of LHCB3 and LHCB6 in Arabidopsis. *Plant Physiol.* **187**, 2691–2715.

Kouřil R., Nosek L., **Opatíková M.**, Arshad R., Semchonok D.A., Chamrád I., Lenobel R., Boekema E.J., Ilík P. (2020) Unique organization of photosystem II supercomplexes and megacomplexes in Norway spruce. *Plant J.* **104**, 215–225.

Cryo-EM structure of a plant photosystem II supercomplex with light-harvesting protein Lhcb8 and α-tocopherol

Monika Opatíková[1,*] (https://orcid.org/0000-0002-3833-6971), Dmitry A. Semchonok[2,*] (https://orcid.org/0000-0003-1622-9443), David Kopečný[3] (https://orcid.org/0000-0002-4309-4284), Petr Ilík[1] (https://orcid.org/0000-0002-8929-8290), Pavel Pospíšil[1] (https://orcid.org/0000-0001-9126-2011), Iva Ilíková[4] (https://orcid.org/0000-0002-3547-3110), Pavel Roudnický[5] (https://orcid.org/0000-0002-6904-7646), Sanja Ćavar Zeljković[6,7] (https://orcid.org/0000-0002-8534-3146), Petr Tarkowski[6,7] (https://orcid.org/0000-0002-7581-7686), Fotis L. Kyrilis[2] (https://orcid.org/0000-0002-4040-6289), Farzad Hamdi[2] (https://orcid.org/0000-0002-2155-5000), Panagiotis L. Kastritis[2,8,9] (https://orcid.org/0000-0002-1463-8422), Roman Kouřil[1,#] (https://orcid.org/0000-0001-8211-3348)

[1]Department of Biophysics, Faculty of Science, Palacký University, Šlechtitelů 27, 783 71 Olomouc, Czech Republic

[2]Interdisciplinary Research Center HALOmem, Charles Tanford Protein Center, Martin Luther University Halle-Wittenberg, Kurt-Mothes-Straße 3a, Halle/Saale, Germany

[3]Department of Experimental Biology, Faculty of Science, Palacký University, Šlechtitelů 27, 783 71 Olomouc, Czech Republic

[4]Institute of Experimental Botany of the Czech Academy of Sciences, Centre of Plant Structural and Functional Genomics, Šlechtitelů 31, 783 71 Olomouc, Czech Republic

[5]Central European Institute of Technology, Masaryk University, 625 00 Brno, Czech Republic

[6]Czech Advanced Technology and Research Institute, Palacký University, Šlechtitelů 27, 78371 Olomouc, Czech Republic

[7]Centre of the Region Haná for Biotechnological and Agricultural Research, Department of Genetic Resources for Vegetables, Medicinal and Special Plants, Crop Research Institute, Šlechtitelů 29, 77900 Olomouc, Czech Republic

[8]Institute of Biochemistry and Biotechnology, Martin Luther University Halle-Wittenberg, Kurt-Mothes-Straße 3, and Biozentrum, Weinbergweg 22, Halle/Saale, Germany

[9]Institute of Chemical Biology, National Hallenic Research Foundation, Leof. Vasileos Konstantinou 48, 116 35 Athens, Greece

* these authors contributed equally

corresponding author: roman.kouril@upol.cz

Dedicated to Professor Emeritus Jan Nauš for his outstanding contribution to the development of biophysics at Palacký University.

Abstract

The heart of oxygenic photosynthesis is the water-splitting photosystem II (PSII), which forms supercomplexes with a variable amount of peripheral trimeric light-harvesting complexes (LHCII). Our knowledge of the structure of green plant PSII supercomplex is based on findings obtained from several representatives of green algae and flowering plants, however, data from a non-flowering plant are currently missing. Here we report a cryo-electron microscopy (cryo-EM) structure of PSII supercomplex from spruce, a representative of non-flowering land plants, at 2.8 Å resolution. Compared to flowering plants, PSII supercomplex in spruce contains an additional Ycf12 subunit, Lhcb4 protein is replaced by Lhcb8, and trimeric LHCII is present as a homotrimer of Lhcb1. Unexpectedly, we have found α-tocopherol (α-Toc)/α-tocopherolquinone (α-TQ) at the boundary between the LHCII trimer and the inner antenna CP43. The molecule of α-Toc/α-TQ is located close to chlorophyll *a*614 of one of the Lhcb1 proteins and its chromanol/quinone head is exposed to the thylakoid lumen. The position of α-Toc in PSII supercomplex makes it an ideal candidate for the sensor of excessive light, as α-Toc can be oxidized to α-TQ by high-light-induced singlet oxygen at low lumenal pH. The molecule of α-TQ appears to shift slightly into the PSII supercomplex, which could trigger important structure-functional modifications in PSII supercomplex. Inspection of the previously reported cryo-EM maps of PSII supercomplexes indicates that α-Toc/α-TQ can be present at the same site also in PSII supercomplexes from flowering plants, but its identification in the previous studies has been hindered by insufficient resolution.

Introduction

Photosynthesis is essential for the majority of organisms living on Earth. This process, employed by (cyano-)bacteria, algae, and land plants, is crucial for the conversion of water and carbon dioxide molecules into oxygen and organic substances and is enabled by the cooperative function of two pigment-protein complexes - photosystem (PS) II and I.

PSII is a supramolecular pigment-protein complex embedded in the thylakoid membrane. Upon absorption of light, it splits water molecules into oxygen, electrons, and protons, and creates the proton gradient across the thylakoid membrane, which is the driving power for ATP-synthase. Over the past few years, an extensive effort of several research groups in the field of cryo-electron microscopy (cryo-EM) has led to the description of the structure of eukaryotic

PSII supercomplexes at near-atomic resolution in representatives of green algae (*Chlamydomonas reinhardtii* (*Cr*))[1,2] and flowering plants (angiosperms)[3-5]. All the PSII structures known so far confirm the dimeric nature of the PSII core (C_2). The structure of C_2 is highly conserved across photosynthetic species and its pigment-protein composition arrangement is strikingly similar to its evolutionarily older counterpart in thermophilic cyanobacteria[6-8]. Unlike C_2, the light-harvesting complexes (LHCII) that bind to C_2 in the form of LHCII trimers and monomers are the source of significant variability of PSII structure in different organisms. For instance in *Cr*, the LHCII trimers consist of a combination of LHCBM1-9 proteins[9], while in land plants they are formed by a variable combination of only three proteins Lhcb1-3[10].

Differences in the type and number of LHCII trimers attached to C_2 result in different forms of PSII supercomplexes. Three types of LHCII trimers are recognized, based on the strength of their attachment to C_2 – Strongly (S), Moderately (M), and Loosely (L) bound trimers. The most abundant form of PSII supercomplex in land plants is the $C_2S_2M_2$ supercomplex, where two copies of each S and M trimers are bound to C_2 via monomeric antenna proteins Lhcb4, Lhcb5, and Lhcb6 (see below for exceptions). In *Cr*, however, the Lhcb6 protein is missing, which results in a slightly altered binding position of LHCII trimers in the PSII supercomplex[11,12]. This modification may also be the reason why large $C_2S_2M_2L_2$ supercomplexes are common in *Cr*, whereas in land plants they are usually very rare. Different organization of PSII supercomplexes in *Cr* and land plants has a direct impact on the major excitation energy transfer (EET) pathways between chlorophyll (Chl) molecules from LHCII to the reaction center of C_2[13], which can have significant consequences for the adjustment of the absorption cross-section of PSII in the dynamic light environment.

Recently, we have found that the composition and arrangement of PSII supercomplexes in land plant species are not as conserved and uniform as initially hypothesized. The gymnosperm genera *Picea* and *Pinus* (family Pinaceae) and *Gnetum* (clade Gnetales) have lost light-harvesting proteins Lhcb3 and Lhcb6 during evolution. As a consequence, the organization of their PSII supercomplexes is different from other land plants and shares some common features with the supercomplex from the green alga *Cr*[14,15]. In addition, these genera have retained only one isoform of the Lhcb4 protein, namely Lhcb4.3, also referred to as Lhcb8[16]. Lhcb8 is a specific isoform of Lhcb4 that has been observed so far only in a subgroup of dicotyledonous plants and only under high-light conditions[17], suggesting its important role in plants coping with excess light[18]. However, even the exposure of plants to high light intensity does not lead to a complete replacement of Lhcb4 by Lhcb8 in the PSII supercomplex, and their simultaneous

presence does not allow a structural study focused purely on the structure and role of Lhcb8 in the organization of the PSII supercomplex[19].

Here we present a cryo-EM density map and structural model of the PSII C_2S_2 supercomplex from Norway spruce (*Picea abies*, hereinafter referred to as spruce) at 2.8 Å resolution. The obtained model with near-atomic resolution provides structural insight into subunit composition and pigment arrangements, enabling analysis of EET pathways within the supercomplex. The PSII structure from a gymnosperm representative partially fills the gap between the known PSII structures from green algae and angiosperm species and enables their detailed structural and functional comparison. Analysis of the cryo-EM density map of the PSII supercomplex revealed a specific density at the boundary between the LHCII trimer and the inner antenna CP43, which was assigned to α-tocopherol (α-Toc)/α-tocopherolquinone (α-TQ). The possible role of α-Toc in the protection of PSII against photo-oxidative damage is discussed.

Results and Discussion

Overall structure

The structure of the PSII supercomplex from Norway spruce, a model organism of gymnosperms, was studied using single-particle cryo-EM. PSII supercomplexes were purified from solubilized thylakoid membranes by sucrose gradient ultracentrifugation. A gradient fraction of PSII supercomplexes was collected (Fig. 1a), concentrated, and used for cryo specimen preparation and data acquisition (Fig. 1b). A visual analysis of 2D classes of aligned particle projections showed that the best-resolved densities were obtained for the C_2S_2 form of the PSII supercomplex (Supplementary Fig. 1). The larger forms of PSII supercomplexes (i.e. $C_2S_2M_2$ and C_2S_2M) were underrepresented in the obtained data set, leading to the absence of their homogeneous classes with well-resolved projections. This is in agreement with our previous report indicating a higher abundance of smaller forms of PSII supercomplexes (C_2S_2) in spruce[14] compared to other plant species, e.g. *Arabidopsis thaliana* (*At*). The best resolved 2D classes of C_2S_2 supercomplexes were used for the 3D reconstruction, which generated a final map of the PSII C_2S_2 supercomplex at 2.8 Å resolution (FSC=0.143, Fig. 1c, d; Supplementary Fig. 2; Supplementary Table 1).

Spruce PSII C_2S_2 supercomplex consists of the dimeric core complex, which binds two S-LHCII trimers and two of each minor antenna proteins Lhcb5 and Lhcb8 (Fig. 1c, d). It binds 204 chlorophylls, 4 pheophytins, 56 carotenoids, and a number of lipids and cofactor molecules

(Supplementary Table 2). The calculated root-mean-square deviation (RMSD) values between the spruce PSII C_2S_2 supercomplex and supercomplexes from other plant species[1-5,19] ranged from 1.4 Å to 2.4 Å, indicating similar structural features between spruce PSII and PSII from other organisms (Supplementary Table 3). The structural similarities are also apparent from the superposition of the structural model of the spruce PSII C_2S_2 supercomplex with those from other photosynthetic organisms, including *Cr*, *At*, spinach, and pea (Supplementary Fig. 3).

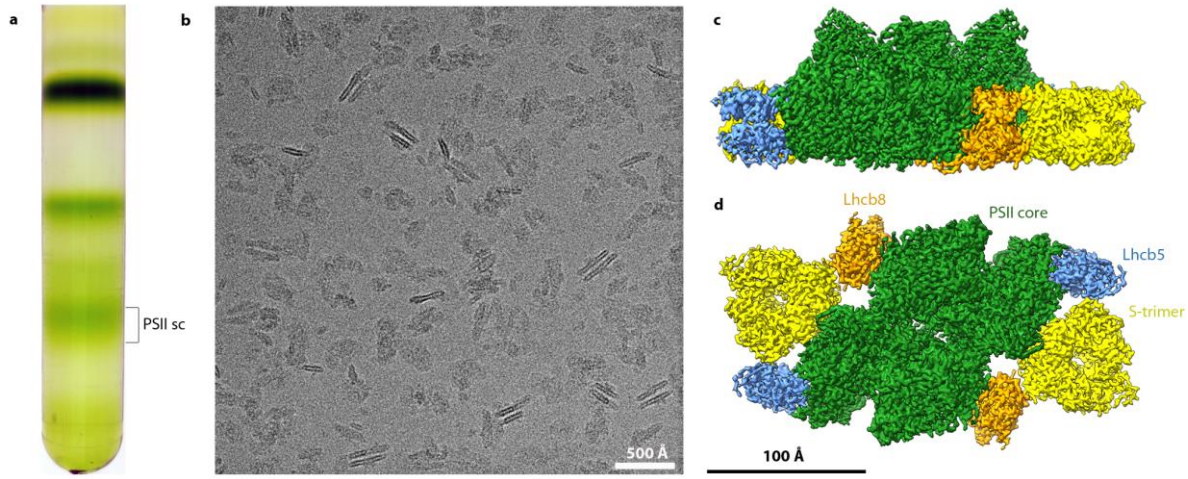

Fig. 1 | Separation and single-particle cryo-EM analysis of spruce photosystem II C_2S_2 supercomplex. a, Separation of the PSII supercomplexes using sucrose gradient ultracentrifugation of solubilized thylakoid membranes from spruce. The fraction marked "PSII sc" was used for the cryo specimen preparation. The experiment was repeated nine times independently with similar results. **b,** Representative electron micrograph of a cryo-EM specimen of the spruce PSII supercomplexes. In total, 2392 electron micrographs were recorded. **c, d,** 3D cryo-EM density map of the spruce C_2S_2 supercomplex side view (along the membrane plane) (c), and top view (lumenal side) (d). The PSII dimeric core complex C_2 is shown in green, Lhcb5 in light blue, Lhcb8 in orange, and the S-LHCII trimer in yellow.

Structure of the core complex of PSII

As in other plant species, the core complex of spruce forms a homodimer with characteristic two-fold symmetry (Fig. 2). Each monomer is composed of four major intrinsic subunits PsbA (D1), PsbB (CP47), PsbC (CP43), and PsbD (D2). The rest of the core complex is formed by smaller low-molecular-weight subunits, namely PsbE, PsbF (cytochrome b_{559} alpha and beta subunit, respectively), PsbH, PsbI, PsbK-M, PsbO, $PsbT_c$, $PsbT_n$, Ycf12, PsbW, PsbX, and PsbZ (Fig. 2c). A comparison of the subunit composition of the core complex from spruce and its counterparts from angiosperm species (Arabidopsis, pea, spinach) revealed the presence of one subunit specific for the spruce core complex, Ycf12. This protein has so far been found only in the PSII structure from green alga *Cr*[1,2], as the corresponding gene is missing in angiosperms[20]. The position of Ycf12 in spruce closely corresponds with its position in *Cr*. It strongly interacts with PsbK and PsbZ with an interface area of 446 $Å^2$ and 347 $Å^2$, respectively.

On the stromal side, the C-terminal tail of Ycf12 interacts with the N-terminus of PsbC. In *Cr*, Ycf12 is also in contact with PsbJ[1,2], which is, however, missing in our structure, together with PsbP and PsbQ subunits. PsbJ is a low-molecular-mass subunit represented by a single transmembrane α-helix localized at the periphery of the core complex close to the cyt b_{559}. PsbP and PsbQ are extrinsic subunits of the oxygen-evolving complex (OEC). As the mass spectrometry analysis has confirmed the presence of these three protein subunits in the fraction of purified spruce PSII supercomplexes (Supplementary Table 4), their absence in the obtained PSII supercomplex structure is most likely caused by their loose binding to the core complex. The absence of these labile subunits has also been observed to some extent in other PSII structures from *At*, pea, and *Cr* (PDB ID 5mdx, 6yp7, and 6kad, respectively). These subunits thus either dissociate from the supercomplexes during sample handling before/during cryo-EM specimen preparation or are bound to the supercomplex sub-stoichiometrically, and thus their presence in the density map is suppressed during image analysis.

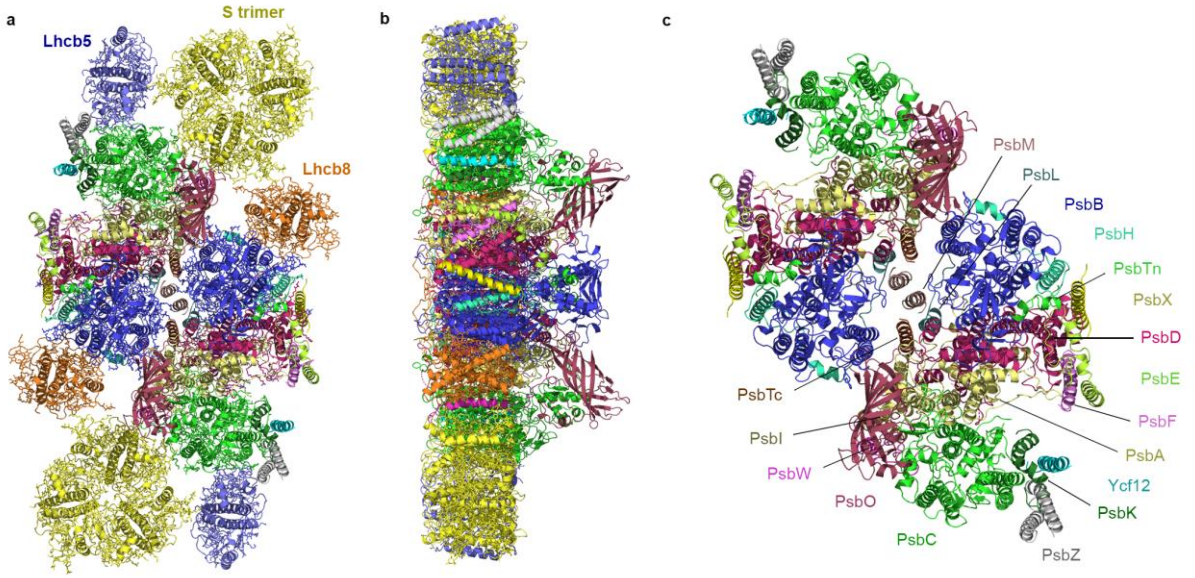

Fig. 2 | Overall architecture of the spruce photosystem II C_2S_2 supercomplex. a, The view of the C_2S_2 supercomplex from the lumenal side with indicated subunits of light-harvesting antenna, Lhcb5, Lhcb8, and the S-LHCII trimer, bound to the dimeric core complex. **b,** The side-view of the C_2S_2 supercomplex along the membrane plane. **c,** Assigned subunits of the core complex.

Structure of the PSII peripheral antenna

Light-harvesting antenna of the spruce PSII C_2S_2 supercomplex consists of two S-LHCII trimers bound to the PSII core complex via two monomeric antennae, Lhcb5 and Lhcb8 (Fig. 2). The spruce S-LHCII trimer shows similar structural features as LHCII trimers from other representatives of land plants or green algae. It has identical pigment composition, and the

localization of the pigment molecules is also very similar to other species (Supplementary Fig. 4). In each monomer, we have identified 14 Chl binding sites (8 Chl *a*, 6 Chl *b*) and 4 carotenoid binding sites (two luteins, one violaxanthin, one neoxanthin) (Supplementary Table 2).

In land plants, the S-LHCII trimer is formed by various combinations of Lhcb1 and Lhcb2 proteins, forming either homotrimers or heterotrimers[10]. Moreover, both Lhcb1 and Lhcb2 are usually present in several isoforms[21] with very high homology, and the separation of PSII supercomplexes with S-LHCII with different isoform composition is virtually impossible. Therefore, the samples for cryo-EM analysis always contain the sum of PSII complexes with various types of the S-LHCII trimers, i.e., the structure of the S-LHCII trimer in the resulting cryo-EM density maps represents a superposition of all present Lhcb1 and Lhcb2 isoforms. This in turn lowers the resolution at the isoform-specific amino acid positions and thus the distinction of present isoforms is impossible. This effect, however, was not observed in the case of spruce S-LHCII trimer. Its cryo-EM density map has unusually high resolution, which indicates that its isoform composition is rather uniform.

Based on the detailed comparison of the cryo-EM structure with the amino acid composition of the trimer-forming proteins Lhcb1 and Lhcb2, we were able to identify the spruce S-LHCII trimer as a homotrimer, composed solely of Lhcb1. In spruce, Lhcb1 protein can be present in 5 isoforms (Lhcb1-A1, A2, A3; Lhcb1-B1, B2) and Lhcb2 in 3 isoforms (Lhcb2-A1, A2, A3)[16]. By tracing the amino acid densities of individual monomers in the S-LHCII trimer, we were able to exclude the presence of all isoforms of Lhcb2 (Supplementary Fig. 5). Namely, Glu64 and Leu171 of Lhcb2 do not fit the corresponding densities in any of the three proteins/monomers forming the S-LHCII trimer (chain G/g, N/n, and Y/y in the structure file, respectively) (see Supplementary Fig. 6 for sequence comparison). Instead, these densities in all three monomers were reliably fitted by amino acids from the sequence of Lhcb1 (Gly73 and Ala180) (Supplementary Fig. 5a, b). Using this approach, we were able to narrow the number of possible isoforms even further. The presence of both Lhcb1-B1 and -B2 isoforms in the S-LHCII trimer was excluded as Leu174 (present in Lhcb1-B1 and Lhcb1-B2) does not fit the corresponding density in the map, whereas Trp171 (present in Lhcb1-A1, -A2 and A-3) matches it perfectly. The presence of isoform Lhcb1-A3 is also unlikely, at least in chain G, as there is no corresponding density for Tyr253, whereas Ala253 fits nicely. Nevertheless, as the same confirmation cannot be achieved for the chains N & Y, the presence of this isoform in the S-LHCII trimer cannot be excluded. According to the systematic annotation by model refinement, the EM map was best matched by the Lhcb1-A1/A2 isoforms, and the Lhcb1-A1 isoform was used in the structural model. Thus, to our knowledge, this is the first specific

identification of a LHCII homotrimer as a component of PSII supercomplex in any photosynthetic organism studied up to date. As the mass spectrometry analysis of the fraction of PSII supercomplexes also revealed the presence of Lhcb2 protein (Supplementary Table 4), it can be deduced that Lhcb2 is a building component of the M-LHCII trimer, because the PSII supercomplexes with M-LHCII trimers were also partially present in the isolated PSII fraction (Supplementary Fig. 1). However, the question of whether the spruce M-LHCII trimer is a homotrimer of Lhcb2 or a heterotrimer composed of Lhcb1/Lhcb2 can only be answered by detailed structural analysis of spruce $C_2S_2M_2$ supercomplex.

Spruce Lhcb5 antenna protein exhibits typical structural features of Lhcb5 in other land plants and has identical pigment composition. It binds 9 Chl a, 4 Chl b, and 3 carotenoids (Supplementary Table 2). The comparison of Lhcb5 from spruce and *Cr* shows that the algal Lhcb5 protein has longer loops between the helixes C and A and the helixes E and C, allowing it to bind one extra Chl *a* (Supplementary Fig. 7).

The structure of the monomeric antenna protein found at the binding position between the S-LHCII trimer and CP47 in spruce is different from other land plants. While this position in the C_2S_2 supercomplex from spinach and pea is occupied by the Lhcb4[3,5], in spruce Lhcb4 is replaced by Lhcb8 (formerly known as Lhcb4.3 isoform), the only Lhcb4-type protein present in spruce (Fig. 3a). Lhcb8 has a slightly different amino acid sequence from Lhcb4, but its most distinctive feature is its shorter C-terminus (Fig. 3b, c). Lhcb8 binds 9 Chl *a*, 3 Chl *b*, and three carotenoids (Supplementary Table 2), and the binding positions and orientations of these pigment molecules are very similar to land plant Lhcb4 protein. However, due to its shorter C-terminus, Lhcb8 has lost two Chl molecules that are present in land plant Lhcb4 (Supplementary Fig. 8), namely Chl *a*613 and *b*614 (Fig. 3b). It is interesting to note that Lhcb4 from green alga *Cr*[1,2] also has a shorter C-terminus (Supplementary Fig. 8 d, e), but its C-terminal α-helix is rotated slightly clockwise compared to spruce, which probably allows the binding of one extra Chl *a* molecule compared to Lhcb8. The exclusive presence of Lhcb8 is probably connected with the evolutionary loss of Lhcb3 and Lhcb6 proteins in spruce and other representatives of the Pinaceae and Gnetales families[14], as in other land plants, the longer C-terminus of Lhcb4 is involved in the direct interaction with Lhcb3 and Lhcb6[22].

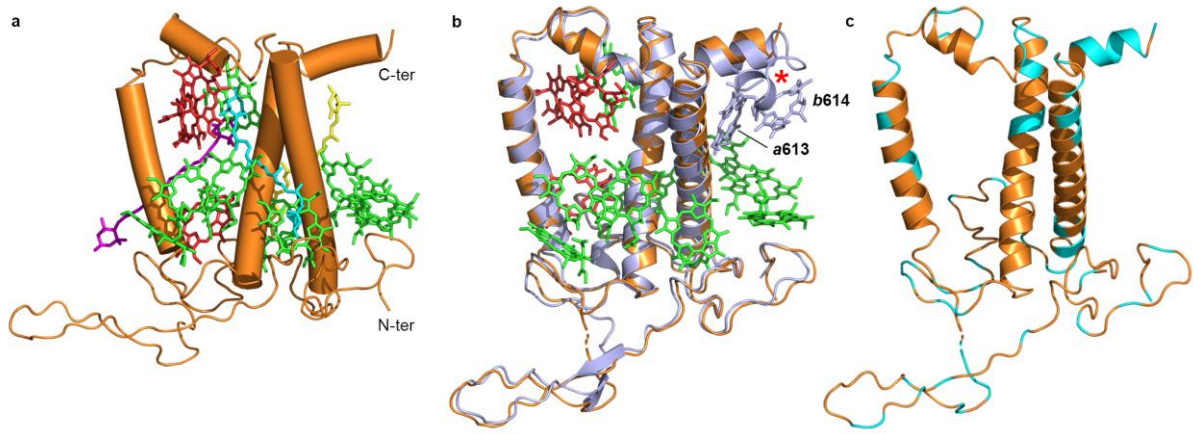

Fig. 3 | Structure of the Lhcb8 subunit. a, A cartoon representation of spruce Lhcb8 with bound pigments (Chl *a* – green, Chl *b* – red, lutein – yellow, violaxanthin – cyan, neoxanthin – magenta). **b,** A structural comparison of spruce Lhcb8 (orange) and Lhcb4 (light blue) from pea (PDB code: 5xnl). Chlorophylls of spruce Lhcb8 are shown in green (Chl *a*) and red (Chl *b*). The red asterisk indicates a longer C-terminus of pea Lhcb4, which supports the binding of two additional chlorophylls, Chl *a* (*a*613) and Chl *b* (*b*614) (in light blue). **c,** Spruce Lhcb8 with highlighted regions of amino acid sequence (cyan) that differ from pea Lhcb4 (PDB code: 5xnl).

Antenna-core interactions

The binding of light–harvesting proteins in the spruce PSII C_2S_2 supercomplex is similar to other known PSII structures from land plant species and a green alga. The binding of Lhcb5 to the PSII core is supported mainly by PsbZ subunit with an interface area of 295Å^2. The association is supported by a salt bridge between Asp100 (Lhcb5) and Lys37 (PsbZ) on the stromal side and a hydrogen bond between Leu290 (Lhcb5) and Ser59 (PsbZ) on the lumenal side. The interface area of Lhcb5 with CP43 is 189Å^2. Interestingly, the interaction of Lhcb5 with the S-LHCII trimer is apparently weaker compared to other plant species, as the interface area is only about 100Å^2, i.e. approx. 1/3 of the interface area observed in other plant PSII structures. The binding of Lhcb8 to the PSII core is similar to that of Lhcb4 in plant and algal PSII C_2S_2 supercomplex. It involves interactions with PsbB, PsbH, PsbA, and PsbL subunits via several specific hydrogen bonds and a salt bridge (Supplementary Table 5). The attachment of the S-LHCII trimer to the core complex is controlled mainly by the PsbW subunit and CP43 with interaction areas of 116Å^2 and 41Å^2, respectively. The precise position of the S-LHCII is also supported by Lhcb8 with an interface area of 86Å^2.

Analysis of the density map between CP43 and S-LHCII (Y/y chain) revealed a specific density not described in any previous cryo-EM structures of PSII. The first possible candidate for this density could be the detergent molecule n-dodecyl α-D-maltoside (α-DDM), which has already been detected in several cryo-EM structures, including PSII C_2S_2 supercomplex from *Cr*[2]. However, when α-DDM is refined to the corresponding density, it is clear that the hydroxyl groups

and carbon atoms of the pyranose ring of the second glucose of the maltoside protrude from the density map (Supplementary Fig. 9). Since we are not aware of any lipid molecules that could match the density map, we fitted the density map with the molecule of α-Toc (Fig. 4) and refined. Its presence in the fraction containing PSII C_2S_2 supercomplexes was confirmed by LC-MS/MS analysis (Supplementary Fig. 10). The molecule of α-Toc is fully embedded in the thylakoid membrane with its chromanol ring facing the lumenal side. It interacts with CP43 (Leu204-Pro206, Phe210, Val238, Trp239, Ser242, Ile243, Phe246), Lhcb1 of the S-LHCII (Leu256-Val260), and linolenic acid ($LNL526_{CP43}$), and is close to two chlorophylls $a506_{CP43}$ and $a614_{S\text{-}LHCII}$ (Fig. 4a).

In order to support the attribution of the electron density to α-Toc, we calculated the interaction energies Δ^iG for the most relevant interaction interface (based on the interface area) of both α-Toc and α-DDM with adjacent surroundings in the PSII supercomplex. The calculations resulted in the interaction with CP43 for both molecules. However, whereas the major surface area buried by α-Toc was predicted to be favourable (Δ^iG = -2.0 kcal/mol), the opposite was true for both possible conformations of α-DDM (Δ^iG = 1.7 kcal/mol and Δ^iG = 2.3 kcal/mol).

Except of α-Toc, the LC-MS/MS analysis of the fraction of spruce PSII C_2S_2 supercomplexes also revealed the presence of a significant amount of α-TQ (Supplementary Fig. 10). α-TQ is the oxidation product of α-Toc, which has been previously identified in chloroplasts and thylakoid membrane[23,24]. The relative amount of α-TQ was slightly lower compared to α-Toc (45% and 55%, respectively). The quantification analysis of the PSII fraction also shows that the ratio of the sum of α-Toc and α-TQ per C_2S_2 supercomplex is approximately 0.9. Although this quantitative estimation indicates that in our sample, α-Toc with α-TQ were present at a sub-stoichiometric amount with respect to C_2S_2 supercomplex, the occupancy of the binding site by these molecules was still high enough to enable the detection of this specific density in the PSII structure. The shape and the fitting of the density map suggest that the α-Toc is more abundant in our sample, but α-TQ can be fitted as well (Fig.4b).

The inspection of the cryo-EM density 3D maps of PSII supercomplexes from other organisms revealed that α-Toc at this position might not be unique to spruce, as we have observed a trace of similar density in the pea PSII supercomplex[5] (EMD-6741) as well. A striking similarity between the shapes of these spruce and pea density maps could indicate their common origin in α-Toc/α-TQ molecules (Supplementary Fig. 11). The resolution of the cryo-EM density 3D maps from *At* (EMD-3491) and spinach (EMD-6617) was insufficient for the analysis of the same area with a representable outcome. On the other hand, the inspection of PSII supercomplexes from *Cr* (EMD-9955, EMD-9956, EMD-9957) revealed the unequivocal absence of this density, which results in a closer contact between the S-LHCII trimer with the CP43 subunit. Nevertheless, it is

impossible to draw any firm conclusion about the absence of α-Toc/α-TQ in *Cr*. Both molecules could have been lost during the isolation procedure, which probably happened in a recent structural study of the PSII supercomplex from *At*[25]. The analysis of amino acid sequence, however, suggests that the regions of CP43 and S-LHCII (Lhcb1 or LhcbM1) that are involved in the interaction with α-Toc are relatively conserved in spinach, pea, and *At*, whereas in *Cr* there are more substantial changes (Supplementary Fig. 12, 13). These findings could indicate that the presence of α-Toc/α-TQ at the interface between S-LHCII and CP43 might be specific to land plants.

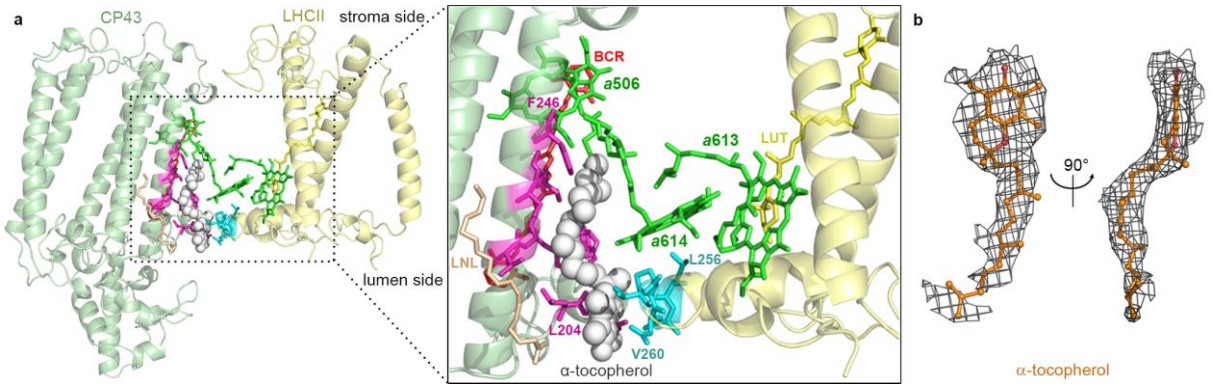

Fig. 4 | Localization of α-tocopherol in spruce photosystem II C_2S_2 supercomplex. a, α-tocopherol (α-Toc) is localized between the S-LHCII trimer and CP43, the inner antenna of the core complex, close to the lumenal side of the thylakoid membrane. α-Toc interacts with CP43 via several specific amino acids in the region between Leu204 to Phe246 (magenta), Chl *a*506, and linolenic acid (LNL), and with one monomer of the S-LHCII trimer through the amino acid region from Leu256 to Val260 (cyan) and Chl *a*614. Lutein (LUT) is shown in yellow, and β-carotene (BCR) in red. **b,** The density identified in the cryo-EM density map of the spruce PSII supercomplex fitted by α-tocopherol (α-Toc) (orange) and α-tocopherolquinone (α-TQ) (magenta), respectively.

Excitation energy transfer pathways

Localization and assignments of chlorophyll molecules in the spruce PSII allow a calculation of the excitation energy transfer (EET) pathways in the C_2S_2 supercomplex. We have used a recently proposed approach[13], based on the calculation of EET between the entire individual light-harvesting proteins (Lhcb5, Lhcb8, and S-LHCII trimer) and the inner antenna of the PSII core complex (CP43 and CP47). When calculating the main pathway for EET, this approach considers the contribution of all chlorophylls of given light-harvesting proteins, but at the same time, it allows the identification of key pairs of chlorophylls that mediate EET between the subunits.

As expected, the calculated FRET rates show that EET from monomeric antennae Lhcb5 and Lhcb8 to S-LHCII trimer is highly improbable (Supplementary Table 6). The main EET pathways from these minor antenna proteins are directed to inner antenna complexes CP43 and CP47, respectively (Fig. 5). The energy absorbed by S-LHCII trimer is directed mainly to inner antenna CP43 (Fig. 5), and EET to Lhcb5 and Lhcb8 is negligible (Supplementary Table 6).

Similar pathways of the main EET have been described in PSII supercomplexes of other land plants and green algae, but our data indicate that the majority of FRET rates of spruce EET pathways are slightly slower (Supplementary Table 6). This is most likely due to the subtle changes in the positions of participating chlorophylls, as the FRET rate is inversely proportional to the sixth power of the distance between them.

A detailed inspection of the chlorophylls that mediate EET from the peripheral antenna proteins (Lhcb5, Lhcb8, trimer S-LHCII) to the internal antenna complexes (CP43 and CP47) shows that, as in other plants, EET is mediated primarily through chlorophylls localized on the stromal side of the thylakoid membrane. This is due to their closer contact compared to chlorophylls localized on the lumenal side. Detailed information about chlorophylls involved in the main EET pathways, their localization, orientation, and mutual distances can be found in Fig. 5b-d.

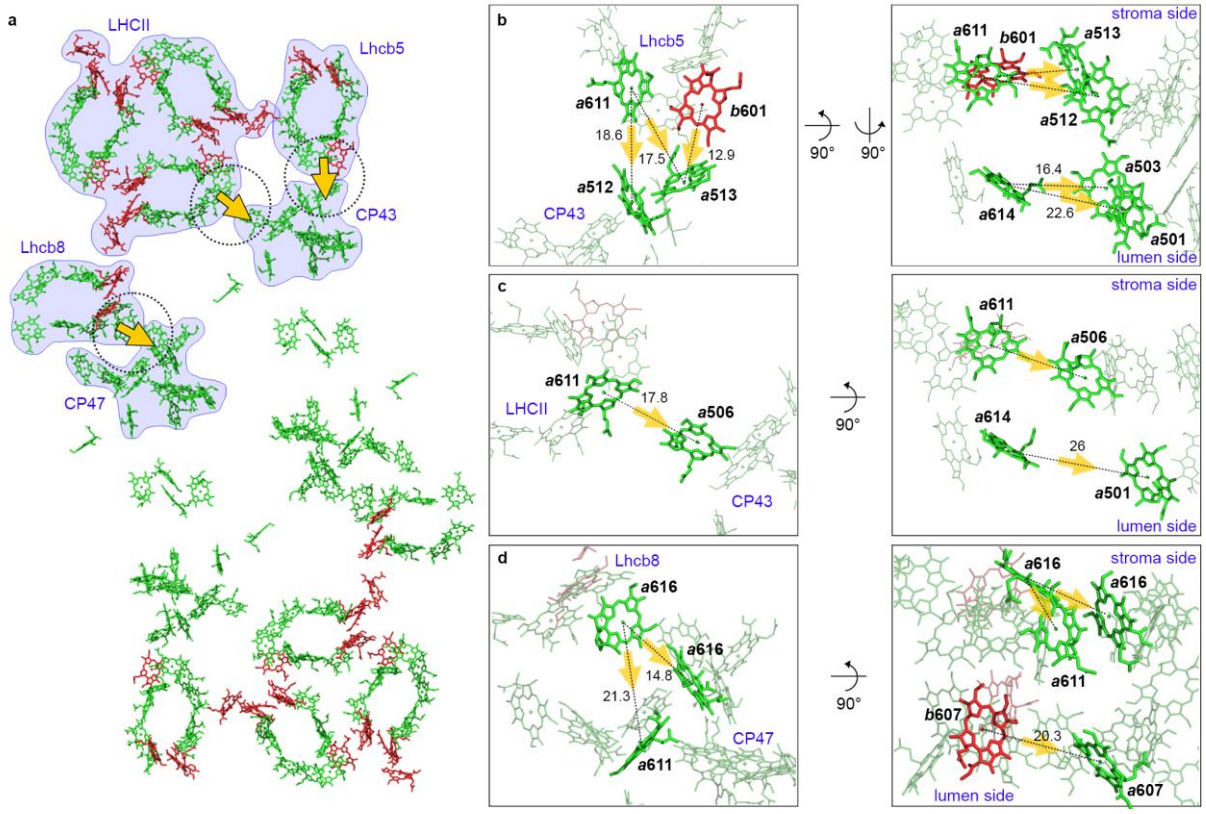

Fig. 5 | Major energy transfer pathways within the spruce PSII C_2S_2 supercomplex. a, Overview of all chlorophylls in the spruce C_2S_2 supercomplex shown from the stromal side, Chl *a* in green, Chl *b* in red. Major energy transfer pathways between the highlighted LHCII subunits (Lhcb5, Lhcb8, S-LHCII trimer) and the core complex (CP43 and CP47) are indicated by yellow arrows. **b-d,** Chlorophylls involved in the energy transfer from Lhcb5 to CP43 (b), S-LHCII trimer to CP43 (c), and Lhcb8 to CP47 (d). Chlorophylls, which are the most prominent in the EET, are highlighted. The numbers at the dotted lines indicate the Mg-to-Mg distances in Å between two adjacent chlorophylls. The left figures in b-d show the view from the stromal side.

What is the role of α-tocopherol(quinone) in PSII?

It is well known that $^1O_2$ formed in photosynthetic organisms exposed to excessive light is most effectively eliminated by carotenoids[26]. However, they are not the only $^1O_2$–detoxifying compounds in plants. The second line of defence against $^1O_2$ is represented by tocopherols, namely α-tocopherol (α-Toc), which can react with $^1O_2$ forming hydroperoxide (α-Toc-OOH). This compound can be either regenerated back to α-Toc by reducing agents (e.g. ascorbate), or irreversibly converted to α-tocopherolquinone (α-TQ). This conversion is known to be promoted under acidic conditions, i.e. conditions typically present in the lumen of light-exposed thylakoids[27].

In light of these facts, it is very interesting to note that the chromanol head of the α-Toc molecule newly identified in the PSII supercomplex of spruce is exposed to the lumen. This position indicates that whenever this α-Toc is oxidized by $^1O_2$ produced by PSII (in excessive light), it can be readily regenerated by ascorbate present in the lumen. At the same time, when the lumenal pH becomes acidic, this regeneration pathway could be surpassed by the irreversible conversion of the hydroperoxide α-Toc-OOH to α-TQ. It appears that a minor shift occurs between the two-ring chromanol head and quinone head when refined as α-TQ or α-Toc, respectively, in the PSII supercomplex (Fig. 6). We hypothesize that the conversion of α-Toc to α-TQ can lead to conformational changes in PSII supercomplex with possible functional consequences. The conversion of α-Toc to α-TQ could be, for example, sensed by the neighboring PSII subunit PsbW, which is known to be crucial for the proper assembly of proteins into PSII supercomplexes[28,29], and could therefore act as a molecular switch triggering the high-light adjustment of PSII.

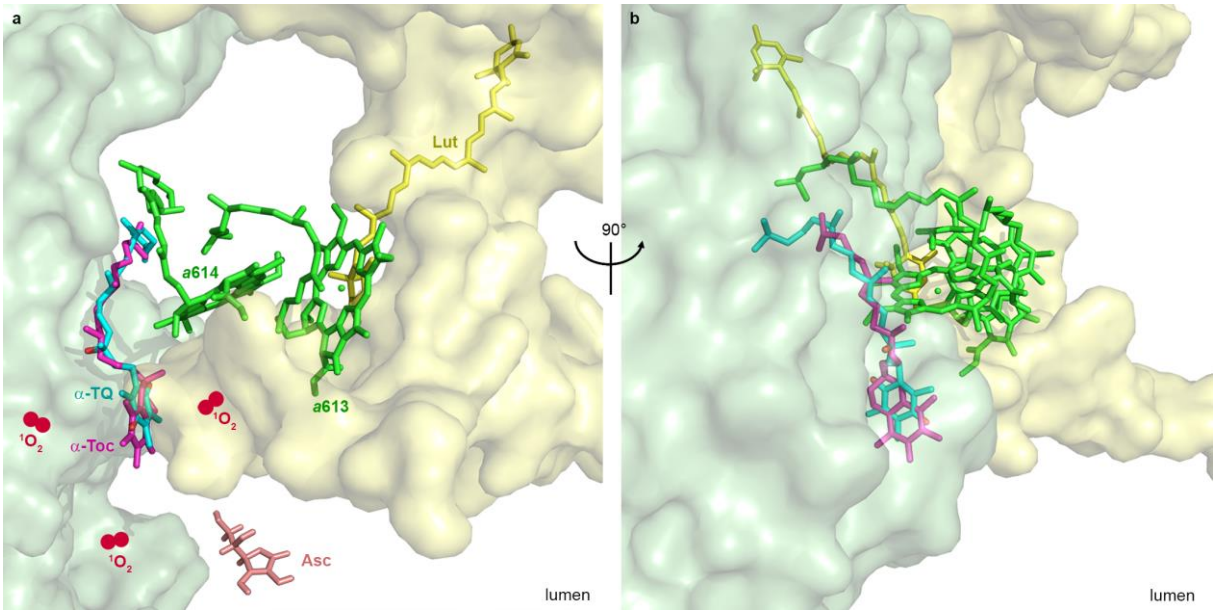

Fig. 6 | Position of α-tocopherol (α-Toc)/α-tocopherolquinone (α-TQ) in the structure of spruce PSII supercomplex. A detail of membrane side view (a) and the same detail rotated by 90°(b) with embedded α-Toc/α-TQ in PSII supercomplex. A cluster of chlorophylls a614, a613, and lutein (Lut) in the Lhcb1 protein of trimeric LHCII is close to the α-Toc/α-TQ. Ascorbate (Asc) molecule in the thylakoid lumen can reach and reduce the chromanol head of the α-Toc oxidized by singlet oxygen ($^1O_2$) (for details, see the text).

The molecule of α-TQ itself is an effective quencher of chlorophyll fluorescence from PSII[30] and therefore it can contribute to the quenching of excessive excitations in the PSII supercomplex. However, the involvement of α-Toc/α-TQ in the frequently discussed quenching of excitations in PSII supercomplex[31] can also be indirect. The molecule is localized in the proximity of the Chl*a*614-Chl*a*613 cluster in the Lhcb1 antenna of the S-trimer of LHCII (Fig. 6). In the context of LHCII, the chlorophylls in this cluster are of middle energy[32] and therefore this cluster is not likely to act as a quenching center, although it is well coupled with the carotenoid lutein. However, it is tempting to suggest that the oxidation of α-Toc to α-TQ induced by lumen acidification under excessive light can lead to a conformation change of the supercomplex, which could lower the energy levels of the Chl*a*614-Chl*a*613 cluster and turn the cluster into an effective quenching site in PSII supercomplex. Indeed, recent *in silico* predictions suggest that the Chl*a*614-Chl*a*613 cluster might serve as a quenching center upon protonation of the D-helix in the Lhcb1 antenna[33].

Our hypothesis that α-Toc/α-TQ has not only structural, but also functional role in PSII supercomplex is supported by the analysis of Arabidopsis *vte1* mutant, defective in the synthesis of α-Toc. It has been reported that this mutant has probably impaired turnover of D1 protein both at high[34] and low[35] irradiation, which supports that the α-Toc/α-TQ localized within the supercomplex could be important for the proper function of PSII.

Material and Methods

Plant material and isolation of thylakoid membranes. Seedlings of Norway spruce (*Picea abies* L. Karst.) were grown in a growth chamber for 3 weeks at 120 µmol photons $m^{-2}s^{-1}$, 22 °C, with a 16 h light/8 h dark cycle. Before the isolation procedure, spruce seedlings were dark-adapted for 30 min. Subsequently, seedlings were cut approximately 2 cm above the soil, and thylakoid membranes were isolated according to the protocol described by Dau et al.[36] with one modification. All buffers used for the isolation were complemented with phosphatase inhibitor sodium fluoride (NaF) at a final concentration of 10 mM. The isolation was performed under green light and samples were kept on ice during the whole procedure. The chlorophyll content in the final thylakoid membrane suspension was determined spectrophotometrically by a pigment extraction in 80% acetone[37].

Ultracentrifugation and sample preparation for cryo-EM. Ultracentrifugation was performed according to Caffarri et al.[38] with minor modifications. For the preparation of the PSII supercomplexes fraction, thylakoid membranes (corresponding to 200 µg of chlorophyll a+b) were centrifuged at 4,600 *g* (4 °C, 4 min). The resulting pellet was resuspended in 10 mM Hepes (pH 7.5) to a chlorophyll concentration of 2 mg/ml and solubilized by adding α-DDM in 10 mM Hepes (pH 7.5) to the final detergent concentration of 1% and final chlorophyll concentration of 0.5 mg/ml (final detergent/chlorophyll mass ratio of 20) and vortexed gently for a few seconds. The solubilized thylakoid membranes were immediately centrifuged at 18,000 *g* (4 °C, 10 min) to remove insolubilized membranes and then fractionated by ultracentrifugation on a sucrose gradient at 284,000 *g* (4 °C, 18 hours). The sucrose gradients were prepared in tubes containing 0.65 M sucrose solution in 10 mM Hepes (pH 7.5) with critical micelle concentration (CMC) of α-DDM (0.008%). Tubes were frozen (- 80 °C) and subsequently thawed at 4 °C. A total volume of 5.4 ml of the sucrose fraction with PSII supercomplexes was collected from nine tubes (0.6 ml from each tube) and concentrated using a 50 kDa cut-off Millipore Amicon filter at 14,000 g (4 °C, 5 min) and washed twice in 400 µl of 10 mM Hepes (pH 7.5) buffer with a CMC concentration of α-DDM to remove sucrose. The obtained fraction with a chlorophyll concentration of 3 mg/ml was directly used for cryo specimen preparation.

Sample preparation for electron microscopy. Aliquots (3.5 µl) containing PSII supercomplexes were applied to the glow-discharged (PELCO easiGlow™, 15 mA, 25s) Quantifoil holey carbon-supported copper grids (R 2/1, 200 mesh). The sample excess was

blotted away (TFS 595 type Φ55/20 filter paper, blot force 2, blotting time of 6 sec) and plunge-frozen in liquid ethane using a TFS Vitrobot Mark IV at 4 °C and 95% humidity.

Electron microscopy data acquisition. Image acquisition was performed on the Thermo Fisher Scientific Glacios cryogenic electron microscope equipped with a field emission gun (ThermoFisher X-FEG) and operated at 200 kV in bright field imaging mode. In total, 2,392 movies were recorded using a Thermo Scientific Falcon 3EC Direct electron Detector in linear mode at a nominal magnification of 150,000 X and a true magnification of 145,641 X at the camera level, corresponding to a pixel size of 0.96127 Å/pix with 120 frames at a dose of 0.9215 $e^-/Å^2$ per frame and an exposure time of 108 s per movie. The acquisition was performed using TFS EPU2 (Supplementary Table 1).

Image processing. The raw movies were imported into SCIPION 3.0[39]. The motion correction for drift correction and dose weighting was performed with MotionCor2-plugin[40] and GCTF-plugin[41] for contrast transfer function estimation. During the previous step, the 2,100 micrographs with well-estimated parameters were further subjected to the manual/auto Xmipp particle picking[42]. Extracted 202,251 particles were 2D classified using cryoSPARC-plugin[43] and the best classes were selected for *ab initio* map generation with cryoSPARC-plugin. Then 118,509 particles from the best 2D class averages were taken for 3D classification using Relion 3.1-plugin[44] with 2 classes. The best resulting 3D class containing C_2S_2 supercomplexes was further taken to 3D non-uniformed refinement in cryoSPARC-plugin, resulting in a 3D map of 3.32 Å resolution. The subsequent particles have undergone Bayesian polishing using Relion 3.1-plugin[44] and further 3D non-uniformed refinement with cryoSPARC-plugin[43] resulting in a 2.785 Å resolution 3D map (Supplementary Fig. 2, Supplementary Table 1).

Modeling, structure, and FRET analysis. Initial fitting of the subunits in the cryo-EM map was performed by rigid body real-space refinement in Chimera[45], using the high-resolution crystal structure of PSII from *Spinacia oleracea* (PDB code 3JCU). Several linear-shaped electron densities were fitted with linolenic acid (LNL) in line with its high abundance among fatty acid esters identified in the PSII supercomplex fraction (Supplementary Fig. 14). Fatty acids in the final model are assumed to belong to membrane lipids, which were not possible to model fully due to a poor density. Local fitting of the subunits in the cryo-EM map was performed using the program Coot. Refinement was performed at 2.8 Å resolution (equal to Fourier Shell Correlation at 0.143) in Phenix using the Real-space refinement module and

applying geometry, secondary structure, rotamer, and Ramachandran plot restraints. A model of chain V was obtained by fitting a polyalanine α-helix into the empty density for a transmembrane helix and side chains were subsequently updated to the protein sequence (UniProt accession R4ZGY5_PICAB). The validation statistics calculated by MolProbity provided the final score value of 1.6, the overall clash score of 8, Ramachandran outliers of 0.06 %, and the CC (mask) value of 0.85 (Supplementary Table 1). Images were prepared with PyMOL[46].

To evaluate the structural similarity between spruce and other plant PSII supercomplexes, the average deviation between the corresponding atoms of two superimposed proteins/supercomplexes (RMSD values) was calculated from structural files[47, 48] using CCP4 software. The interface area between specific protein subunits and between cofactors and $\Delta^{i}G$, (the solvation free energy gain upon interface formation) was calculated from structural files using the Pisa software[49]. FRET analysis was performed according to Sheng et al.[2] and Croce and Amerongen[13]. Multiple sequence alignments were performed with BioEdit software using ClustalW algoritm.

Analysis of separated PSII supercomplexes from spruce by MS. Isolated photosystem II (PSII) supercomplexes from spruce (*P. abies*) seedlings were subjected to filter-aided sample preparation based on Wisniewski et al.[50]. The resulting peptides were analyzed by liquid chromatography-tandem mass spectrometry (LC-MS/MS) performed using UltiMate 3000 RSLCnano system (Thermo Fisher Scientific) on-line coupled with Orbitrap Exploris 480 spectrometer (Thermo Fisher Scientific) using Thermo Scientific Xcalibur software. The sample was processed and measured in technological triplicates. See supplemental material for complete details regarding the analyses and data evaluation.

Detection of α-Toc and α-TQ by LC-MS/MS. *n*-Hexane (200 µl) was added into a fraction of isolated PSII supercomplexes (10 µl, chlorophyll concentration of 3.075 mg/ml), sonicated for 3 min at 25 °C, and the upper layer was transferred into a new vial. Extraction was repeated three times, and collected *n*-hexane extracts were evaporated to dryness under a vacuum at 40 °C and redissolved in 40 µl of acetonitrile. For the quantification, UHPLC-MS/MS analysis was performed using Nexera X2 UHPLC (Shimadzu Handels GmbH, Kyoto, Japan), coupled with MS-8050 (Shimadzu Handels GmbH, Kyoto, Japan). Chromatographic separation was performed on an Acquity UPLC BEH C18 (50 × 2.1 mm; 1.7 µm particle size; Waters, Milford, MA, USA) with the corresponding pre-column. Target compounds were separated using a

binary gradient consisting of 15 mM formic acid, pH 3 (adjusted with NH_4OH) (component A), and 0.1% formic acid in acetonitrile (component B) at a flow rate of 0.4 ml/min. The column temperature was maintained at 40 °C. The linear gradient consisted of 75 % B for 2 min, 75–100 % B for 9 min, isocratic for 0.3 min, back to 75 % B within 0.2 min, and equilibration for 2 min. Injected volume was 5 µl. The effluent was introduced into an electrospray source (interface temperature of 300 °C, heat block temperature of 400 °C, and interface capillary voltage of 5.0 kV). Argon was used as the collision gas, and nitrogen was used as the nebulizing gas. To achieve high specificity in addition to the high sensitivity, the analysis was performed in the multiple reaction monitoring (MRM) mode alternating the following transitions 431.30>165.10, 431.30>134.05, and 431.30>68.95 for α-tocopherol, and 429.00>164.95, 429.00>163.20, and 429.00>191.20 for α-tocopherolquinone. The calculated amount of α-Toc and α-TQ in the analyzed PSII fraction was 100 pmol and 81 pmol, respectively, indicating that the chls/(α-Toc+α-TQ) ratio in the fraction is 188/1. Both data collection and data analysis were performed via Lab Solutions software (Shimadzu corporation 2008-2019).

Fatty acid composition. Extraction solvent [$CHCl_3$:MeOH (2:1, v:v)] was added into membrane extract and sonicated for 10 min at room temperature. The extract was centrifuged for 5 min at 14,500 *g* and the supernatant was evaporated at 40 °C under a vacuum. Methylation of fatty acids was performed with 1 M NaOMe/MeOH for 5 min at room temperature. After the addition of 200 µl of saturated NaCl, fatty acid methyl esters (FAME) were extracted with 2 x 500 µl of *n*-hexane. The solvent was evaporated under a vacuum and the residuum was dissolved into 20 µl of *n*-hexane. The resulting FAMEs were analyzed via gas-chromatography –mass spectrometry using the Agilent system (GC 7890 A; MSD 5975C series II) on a fused silica HP-5MS UI column (30 m × 0.25 mm × 0.25 mm) and carrier gas He (1.1 ml/min). The temperature was programmed at 120 °C for 3 min, 5 °C/min to 180 °C, then held for 10 min, 10 °C/min to 220 °C, and finally 2 °C/min to 250 °C and held for 5 min. The temperature of the injection port and detector was 230 °C. Ionization was performed in the EI mode (70 eV). Injection (1 µl) was done in splitless mode. Identification was performed by comparing retention times, indices, and mass spectra with the mixture of authentic standards (Supelco 37 Component FAME Mix, Merck, Czech Republic). Pinolenic acid (Cayman, USA) was also derivatized using the above protocol. All compounds' linear retention indices (RI) were determined via the Kovats method by injecting homologous series of C8-C40 *n*-alkanes (Merck, Czech Republic) in *n*-hexane solution. Other compounds detected in the sample were identified by comparison of their mass spectra with those found in the database (NIST/EPA/NIH Mass

Spectral Library v.2.0, USA). Results are presented as percentage content calculated according to the area of the chromatographic peaks. Both data collection and data analysis were performed via MSD ChemStation software (Agilent Technologies, Inc. 1989-2011).

Data Availability

The mass spectrometry proteomic data have been deposited to the ProteomeXchange Consortium via the PRIDE partner repository with the identifiers: PXD035272. The cryo-EM map of the spruce PSII supercomplex has been deposited in the Electron Microscopy Data Bank with accession
code EMD-16389. The corresponding structure model has been deposited in the Protein Data Bank under PDB code 8C29.

Acknowledgements

This work was supported by the Grant Agency of the Czech Republic (project no. 21-05497S to M.O., P.I., P.P., I.I., R.K.) and the European Regional Development Fund (ERDF) project "Plants as a tool for sustainable global development" (no. CZ.02.1.01/0.0/0.0/16_019/0000827 to M.O., P.I., P.P., R.K., S.Ć.Z., P.T.). We acknowledge support by the Federal Ministry for Education and Research (BMBF, ZIK program) (Grant nos. 03Z22HN23, 03Z22HI2, and 03COV04 to P.L.K.), Horizon Europe ERA Chair "hot4cryo" project number 101086665 to P.L.K., the European Regional Development Funds for Saxony-Anhalt (grant no. EFRE: ZS/2016/04/78115 to P.L.K.), funding by the Deutsche Forschungsgemeinschaft (DFG) (project number 391498659 and RTG 2467 to P.L.K.), and the Martin-Luther University of Halle-Wittenberg. This work was also funded by project No. RO0423 to S.Ć.Z. and P.T. (Sustainable systems and technologies, improving crop production for higher quality of production of food, feed, and raw materials, under conditions of changing climate) funded by the Ministry of Agriculture, Czechia. CIISB, Instruct-CZ Centre of Instruct-ERIC EU consortium, funded by MEYS CR infrastructure project LM2023042 and European Regional Development Fund-Project „UP CIISB" (No. CZ.02.1.01/0.0/0.0/18_046/0015974), is gratefully acknowledged for the financial support of the measurements at the CEITEC Proteomics Core Facility. We thank Lucie Hloušková and Jan Bartoš for help with FRET rate calculation.

Author contributions

M.O., D.K., P.I., P.P, P.L.K., R.K. designed the study. M.O., D.A.S., F.L.K., F.H. sample preparation for cryo-electron microscopy. D.A.S. image analysis of cryo-EM data. D.K., R.K. model building. M.O., I.I. amino acid sequence analysis. P.R. mass spectrometry analysis. P.T., S.Ć.Z. fatty acid composition. P.T., S.Ć.Z. α-tocopherol(quinone) analysis. M.O., D.K., P.I., P.P. I.I., R.K. data interpretation. M.O., D.A.S., P.I., I.I., and R.K. wrote the main body of the manuscript and all authors revised and approved it.

Competing interests

The authors declare no competing interests.

References

1. Shen, L. et al. Structure of a $C_2S_2M_2N_2$-type PSII–LHCII supercomplex from the green alga *Chlamydomonas reinhardtii*. *Proc. Natl. Acad. Sci. USA* **116**, 21246–21255 (2019).
2. Sheng, X. et al. Structural insight into light harvesting for photosystem II in green algae. *Nat. Plants* **5**, 1320–1330 (2019).
3. Wei, X. et al. Structure of spinach photosystem II–LHCII supercomplex at 3.2 Å resolution. *Nature* **534**, 69–74 (2016).
4. van Bezouwen, L.S. et al. Subunit and chlorophyll organization of the plant photosystem II supercomplex. *Nat. Plants* **3**, 17080 (2017).
5. Su, X. et al. Structure and assembly mechanism of plant C2S2M2-type PSII-LHCII supercomplex. *Science* **357**, 815–820 (2017).
6. Kamiya N. & Shen, J.-R. Crystal structure of oxygen-evolving photosystem II from *Thermosynechococcus vulcanus* at 3.7-Å resolution. *Proc. Natl. Acad. Sci. USA* **100**, 98–103 (2003).
7. Ferreira, K.N., Iverson, T.|M., Maghlaoui, K., Barber, J., & Iwata, S. Architecture of the photosynthetic oxygen-evolving center. *Science* **303**, 1831-1838 (2004).
8. Loll, B., Kern, J., Saenger, W., Zouni, A. & Biesiadka, J. Towards complete cofactor arrangement in the 3.0 Å resolution structure of photosystem II. *Nature* **438**, 1040–1044 (2005).
9. Minagawa, J. & Takahashi, Y. Structure, function and assembly of photosystem II and its light-harvesting proteins. *Photosynth. Res.* **82**, 241–263 (2004).
10. Jansson, S. The light-harvesting chlorophyll a/b-binding proteins. *Biochim. Biophys. Acta* **1184**, 1–19 (1994).
11. Kouřil, R., Nosek, L., Semchonok, D., Boekema, E.J. & Ilík, P. Organization of Plant Photosystem II and Photosystem I Supercomplexes. *Subcell. Biochem.* **87**, 259–286 (2018).
12. Cao, P., pan, X., Su, X., Liu, Z. & Li, M. Assembly of eukaryotic photosystem II with diverse light-harvesting antennas. *Curr. Opin. Struct. Biol.* **63**, 49–57 (2020).
13. Croce, R. & van Amerongen, H. Light harvesting in oxygenic photosynthesis: Structural biology meets spectroscopy. *Science* **369**, eaay2058 (2020).
14. Kouřil, R., Nosek, L., Bartoš, J., Boekema, E.J. & Ilík, P. Evolutionary loss of light-harvesting proteins Lhcb6 and Lhcb3 in major land plant groups - break-up of current dogma. *New Phytol.* **210**, 808–814 (2016).

15. Kouřil, R. et al. Unique organization of photosystem II supercomplexes and megacomplexes in Norway spruce. *Plant J.* **104**, 215–225 (2020).
16. Grebe, S. et al. The unique photosynthetic apparatus of Pinaceae: analysis of photosynthetic complexes in *Picea abies. J. Exp. Bot.* **70**, 3211–3225 (2019).
17. Klimmek, F., Sjödin, A., Noutsos, C., Leister, D. & Jansson, S. Abundantly and rarely expressed Lhc protein genes exhibit distinct regulation patterns in plants. *Plant Physiol.* **140**, 793–804 (2006).
18. Albanese, P. et al. Dynamic reorganization of photosystem II supercomplexes in response to variations in light intensities. *Biochim. Biophys. Acta-Bioenerg.* **1857**, 1651–1660 (2016).
19. Grinzato, A. et al. High-light versus low-light: effects on paired photosystem II supercomplex structural rearrangement in pea plants. *Int. J. Mol. Sci.* **21**, 8643 (2020).
20. Kashino, Y. et al. Ycf12 is a core subunit in the photosystem II complex. *Biochim. Biophys. Acta* **1767**, 1269–1275 (2007).
21. Crepin, A. & Caffarri, S. Functions and evolution of Lhcb isoforms composing LHCII, the major light harvesting complex of photosystem II of green eukaryotic organisms. *Curr. Protein Pept. Sci.* **19**, 699–713 (2018).
22. Guardini, Z., Gomez, R.L., Caferri, R., Dall'Osto, L. & Bassi, R. Loss of a single chlorophyll in CP29 triggers re-organization of the Photosystem II supramolecular assembly. *Biochim. Biophys. Acta (BBA) - Bioenerg.* **1863**, 148555 (2022).
23. Kruk, J. & Srzałka, K. Occurrence and function of alpha-tocopherol quinone in plants. *J. Plant Physiol.* **145**, 405–409 (1995).
24. Kumar, A., Prasad, A. & Pospíšil, P. Formation of α-tocopherol hydroperoxide and α-tocopheroxyl radical: relevance for photooxidative stress in Arabidopsis. *Sci. Rep.* **10**, 19646 (2020).
25. Graça, A.T., Hall, M., Persson, K. & Schröder, W.P. High-resolution model of Arabidopsis Photosystem II reveals the structural consequences of digitonin-extraction. *Sci. Rep.* **11**, 15534 (2021).
26. Triantaphylides, C. & Havaux, M. Singlet oxygen in plants: production, detoxification and signaling. *Trends Plant Sci.* **14**, 219–228 (2009).
27. Krieger-Liszkay, A. & Trebst, A. Tocopherol is the scavenger of singlet oxygen produced by the triplet states of chlorophyll in the PSII reaction centre. *J. Exp. Bot.* **57**, 1677–1684 (2006).

28. Shi, L.X., Lorkovic, Z.J., Oelmuller, R. & Schroder, W.P. The low molecular mass PsbW protein is involved in the stabilization of the dimeric photosystem II complex in Arabidopsis thaliana. *J. Biol. Chem.* **275**, 37945–37950 (2000).
29. Granvogl, B., Zoryan, M., Plöscher, M. & Eichacker, L.A. Localization of 13 one-helix integral membrane proteins in photosystem II subcomplexes. *Anal. Biochem.* **383**, 279–288 (2008).
30. Kruk, J., Schmid, G.H. & Strzałka, K. Interaction of α-tocopherol quinone, α-tocopherol and other prenyllipids with photosystem II. *Plant Physiol. Biochem.* **38**, 271−277 (2000).
31. Bielczynski, L.W., Xu, P. & Croce, R. PSII supercomplex disassembly is not needed for the induction of energy quenching (qE). *Photosynth. Res.* **152**, 275–281 (2022).
32. Novoderezhkin, V., Marin, A. & van Grondelle, R. Intra- and inter-monomeric transfers in the light harvesting LHCII complex: the Redfield–Förster picture. *Phys. Chem. Chem. Phys*. **13**, 17093–17103 (2011).
33. Papadatos, S., Charalambous, A.C. & Daskalakis, V. A pathway for protective quenching in antenna proteins of Photosystem II. *Sci. Rep.* **7**, 2523 (2017).
34. Hakala-Yatkin, M. et al. Magnetic field protects plants against high light by slowing down production of singlet oxygen. *Physiol. Plant.* **42**, 26–34 (2011).
35. Niewiadomska, E. et al. Lack of tocopherols influences the PSII antenna and the functioning of photosystems under low light. *J. Plant Physiol.* **223**, 57–64 (2018).
36. Dau, H. et al. Structural consequences of ammonia binding to the manganese center of the photosynthetic oxygen-evolving complex: an X-ray absorption spectroscopy study of isotropic and oriented photosystem II particles. *Biochemistry* **34**, 5274–5287 (1995).
37. Lichtenthaler, H.K. Chlorophylls and carotenoids: Pigments of photosynthetic biomembranes. *Methods Enzymol.* **148**, 350–382 (1987).
38. Caffari, S., Kouřil, R., Kereiche, S., Boekema, E. J. & Croce, R. Functional architecture of higher plant photosystem II supercomplexes. *EMBO J.* **28**, 3052–3063 (2009).
39. Sorzano, C.O.S. et al. A new algorithm for high-resolution reconstruction of single particles by electron microscopy. *J. Struct. Biol.* **204**, 329–337 (2018).
40. Zheng, A.Q. et al. MotionCor2: anisotropic correction of beam-induced motion for improved cryo-electron microscopy. *Nat. Methods* **4**, 331-332 (2017).
41. Zhang, K. Gctf: Real-time CTF determination and correction. *J. Struct. Biol.* **193**, 1-12 (2016).

42. de la Rosa Tevín, J.M. et al. Xmipp 3.0: An improved software suite for image processing in electron microscopy. *J. Struct. Biol.* **184**, 321–328 (2013).
43. Punjani, A., Rubinstein, J.L., Fleet, D.J. & Brubaker, M.A. cryoSPARC: algorithms for rapid unsupervised cryo-EM structure determination. *Nat. Methods* **14**, 290–296 (2017).
44. Scheres, S.H. RELION: implementation of a Bayesian approach to cryo-EM structure determination. *J. Struct. Biol.* **180**, 519–30 (2012).
45. Pettersen, E.F. et al. UCSF Chimera—A visualization system for exploratory research and analysis. *J. Comput. Chem.* **25**, 1605–1612 (2004).
46. DeLano, W.L. The PyMOL Molecular Graphics System. San Carlos, CA: DeLano Scientific (2002).
47. Winn, M.D. et al. Overview of the CCP4 suite and current developments. *Acta Crystallogr. D.* **67**, 235–242 (2011)
48. Krissinel, E. & Henrick, K. Secondary-structure matching (SSM), a new tool for fast protein structure alignment in three dimensions. *Acta Crystallogr. D.* **60**, 2256–2268 (2004).
49. Krissinel, E. & Henrick, K. Inference of macromolecular assemblies from crystalline state. *J. Mol. Biol.* **372**, 774–797 (2007).
50. Wiśniewski, J.R., Zougman, A., Nagaraj, N. & Mann, M. Universal sample preparation method for proteome analysis. *Nat. Methods* **6**, 359–362 (2009).

Supplementary Methods

MS identification of proteins in separated PSII supercomplexes from spruce

A sample of PSII supercomplexes obtained from multiple spruce seedlings was equally divided into 3 parts prior to sample preparation to form 3 technological replicates. These were lysed in SDT buffer (4% SDS, 0.1M DTT, 0.1M Tris/HCl, pH 7.6) in a thermomixer (Eppendorf ThermoMixer® C, 30 min, 95°C, 750 rpm). After that, a sample was centrifuged (15 min, 20,000 g) and the supernatant used for filter-aided sample preparation as described elsewhere[51] using 0.5 μg of trypsin (sequencing grade; Promega) and 0.5 μg of chymotrypsin (sequencing grade; Sigma-Aldrich). In parallel, part of the samples were digested only by chymotrypsin. Resulting peptides were analyzed by LC-MS/MS.

LC-MS/MS analyses of all peptides were done using the UltiMate 3000 RSLCnano system (Thermo Fisher Scientific) connected to Orbitrap Exploris 480 spectrometer (Thermo Fisher Scientific). Prior to LC separation, tryptic digests were on-line concentrated and desalted using a trapping column (μPrecolumn, 300 μm × 5 mm; C18 PepMap100, 5 μm particles, 100 A; P/N 160,454; Thermo Fisher Scientific). After washing of trapping column with 0.1% FA, the peptides were eluted in backflush mode (flow 300 $nl.min^{-1}$) from the trapping column onto an analytical column (EASY spray column, emitter part of the column, Acclaim PepMap RSLC C18 column, 2 μm particles, 75 μm × 250 mm; P/N ES902; Thermo Fisher Scientific) by 98 min gradient program (3-80% of mobile phase B; mobile phase A: 0.1% FA in water; mobile phase B: 0.1% FA in 80% ACN). Equilibration of the trapping and analytical column was done prior to sample injection into the sample loop. FAIMS module was not installed.

MS data were acquired in a data-dependent cycle time mode (2s) strategy. The intensity threshold required to trigger the data-dependent scan was set to 5.0e3. The resolution of the survey scan was 120,000 with a range m/z 350-2000 and a maximum injection time of 500 ms. HCD MS/MS spectra were acquired with a resolution of 15,000 (first mass m/z 120). The maximum injection time for MS/MS was 50 ms. Dynamic exclusion was enabled for 45 s after one MS/MS spectra acquisition. The isolation window for MS/MS fragmentation was set to 1.2 m/z.

For data evaluation, we used MaxQuant software (v1.6.17)[52] with an in-built Andromeda search engine[53]. Samples were searched against databases of spruce thylakoid protein database (66,989 protein sequences, based on database S2[54]) and cRAP contaminants. Modifications were set as follows for database search: oxidation (M), deamination (N, Q), and acetylation (Protein N-term) as variable modifications, with carbamidomethylation (C) as a

fixed modification. Enzyme specificity was tryptic and chymotryptic, with four permissible miscleavages. Only three permissible miscleavages were set for samples' data after chymotrypsin digestion. Only peptides and proteins with a false discovery rate threshold under 0.01 were considered. Relative protein abundance was assessed using protein intensities calculated by MaxQuant. Intensities of reported proteins were further evaluated using a software container environment (https://github.com/OmicsWorkflows/KNIME_docker_vnc; version 4.1.3a). Processing workflow is available upon request: it covers reverse hits and contaminant protein groups (cRAP) removal, protein group intensities log2 transformation and normalisation (median). For this article, protein groups reported by MaxQuant are referred to as proteins.

Mass spectrometry proteomics data were deposited to the ProteomeXchange Consortium via the PRIDE[55] partner repository under dataset identifier PXD035272.

Supplementary Figures

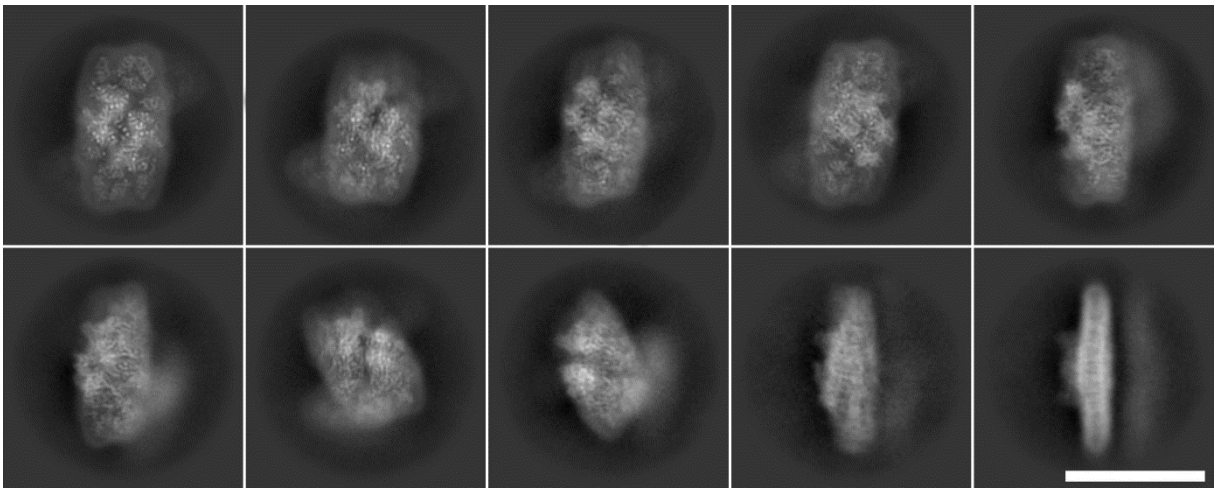

Supplementary Fig. 1 | A gallery of 2D class averages of spruce PSII supercomplexes. Class-averaged projections of different angular views of PSII supercomplexes used for the 3D reconstruction of the final cryo-EM map. The scale bar equals 200 Å.

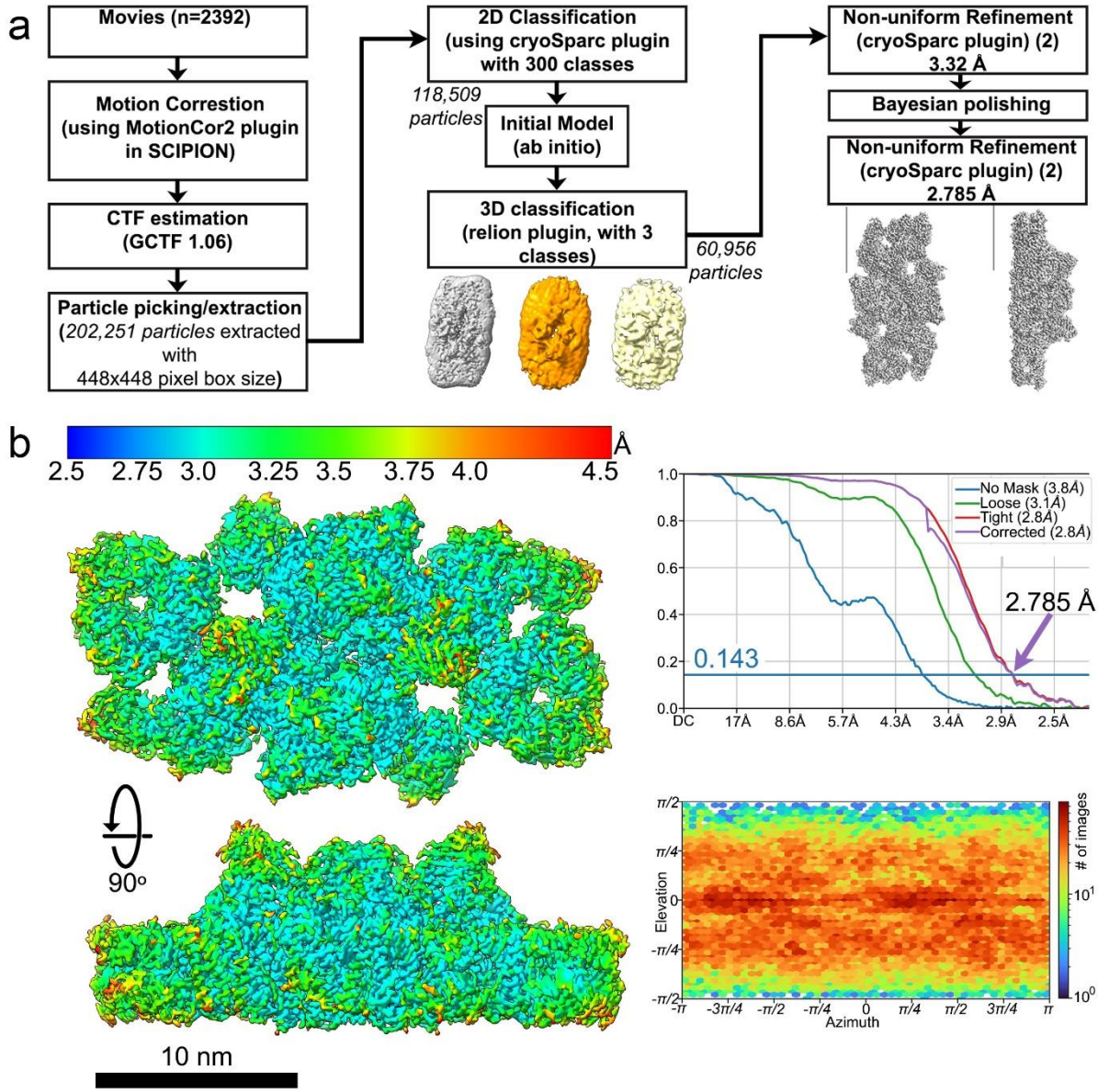

Supplementary Fig. 2 | Single particle cryo-EM workflow and estimation of the resolution of the cryo-EM map. (a) Overview of cryo-EM data processing workflow for spruce photosystem II C_2S_2 supercomplex dataset. (b) Local resolution and Fourier Shell Correlation (FSC) resolution curve of the cryo-EM density map. Local resolution of the cryo-EM map estimated by cryoSparc 3.1 (resMap). The colour bar indicates the resolution range from 2.5 to 4.5 Å. The views are as follows: the upper one – lumenal view, and the lower one – view parallel to the thylakoid membrane plain. FSC curves as implemented in cryoSparc 3.1. with C2 rotational symmetry applied. The overall resolution of the corrected density map was determined as 2.785 Å at 0.143 Gold Standard FSC cut-off.

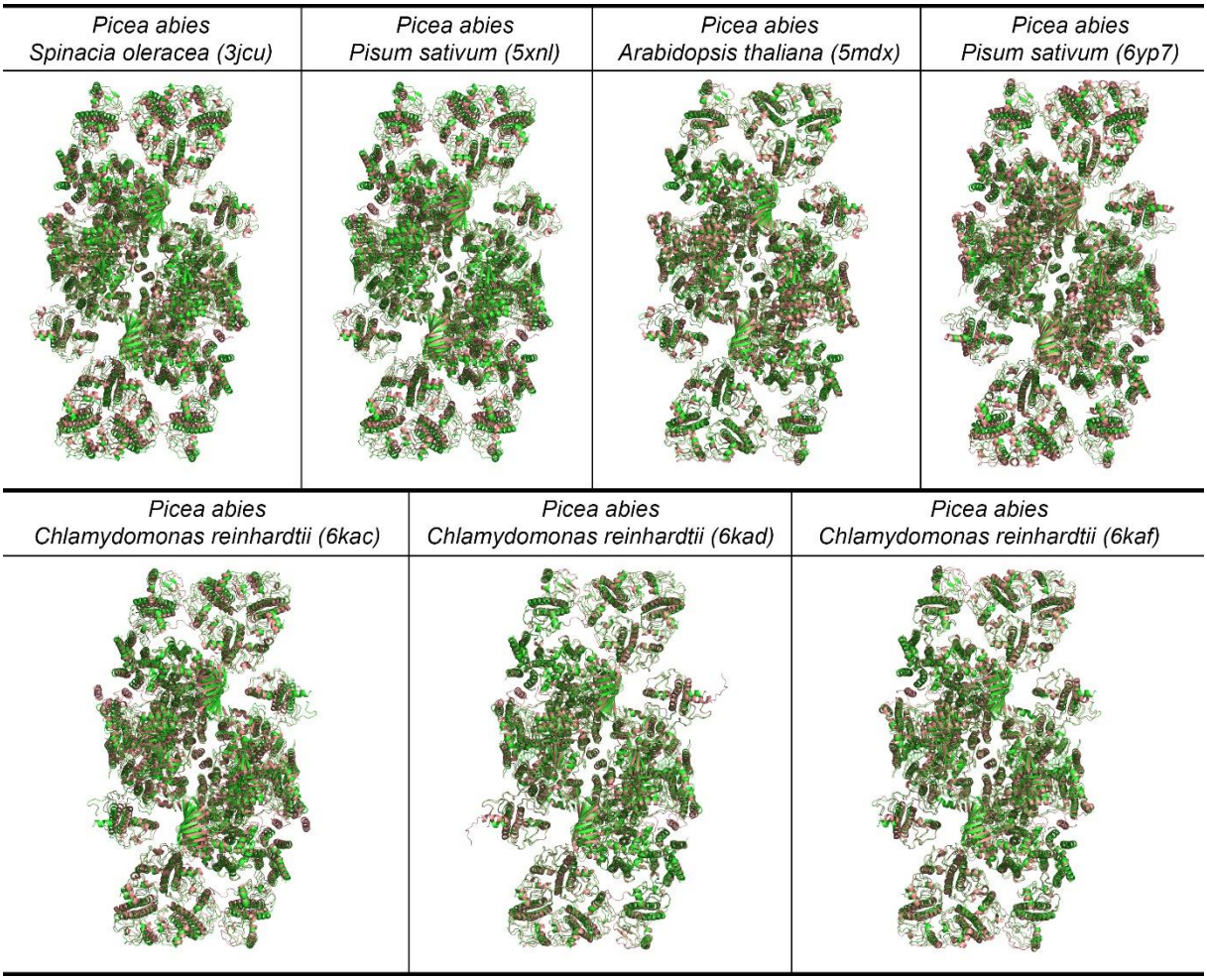

Supplementary Fig. 3 | Structural comparison of the spruce PSII C_2S_2 supercomplex with the same type of supercomplexes of other photosynthetic organisms. Superposition of the cryo-EM structure of the C_2S_2 supercomplex from spruce (green) and from other plant species (salmon) viewed from the lumenal side. The four-digit codes indicate PDB ID of the particular structure.

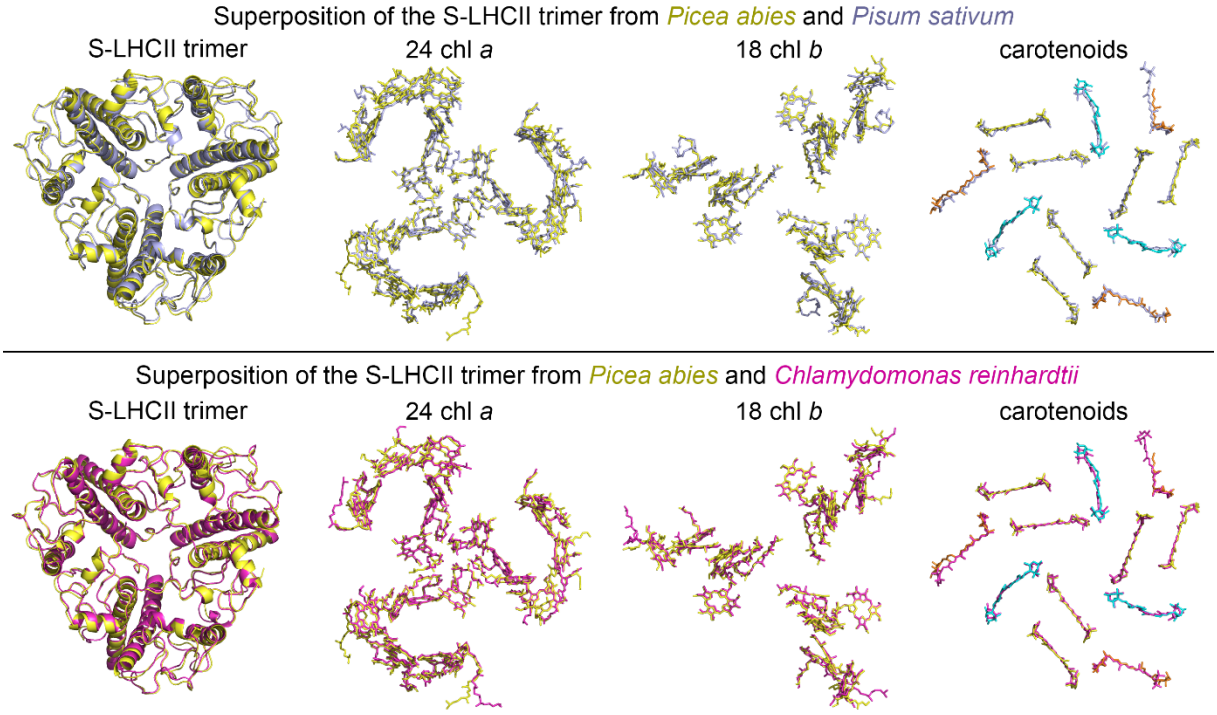

Supplementary Fig. 4 | Structural comparison of the S-LHCII trimers from *Picea abies*, *Pisum sativum* and *Chlamydomonas reinhardtii*. Superposition of the cryo-EM structures of the S-type of LHCII trimers and bound pigments from spruce with those from pea (PDB code: 5xnl) and *Chlamydomonas reinhardtii* (*Cr*) (PDB code: 6kac) viewed from the lumenal side. Colour coding: S-LHCII trimer: spruce (yellow), pea (light blue), *Cr* (magenta); Chl *a*: spruce (yellow), pea (light blue), *Cr* (magenta); Chl *b*: spruce (yellow), pea (light blue), *Cr* (magenta); carotenoids: spruce (lutein – yellow, violaxanthin – cyan, neoxanthin – orange), pea (all carotenoids in light blue), *Cr* (all carotenoids in magenta).

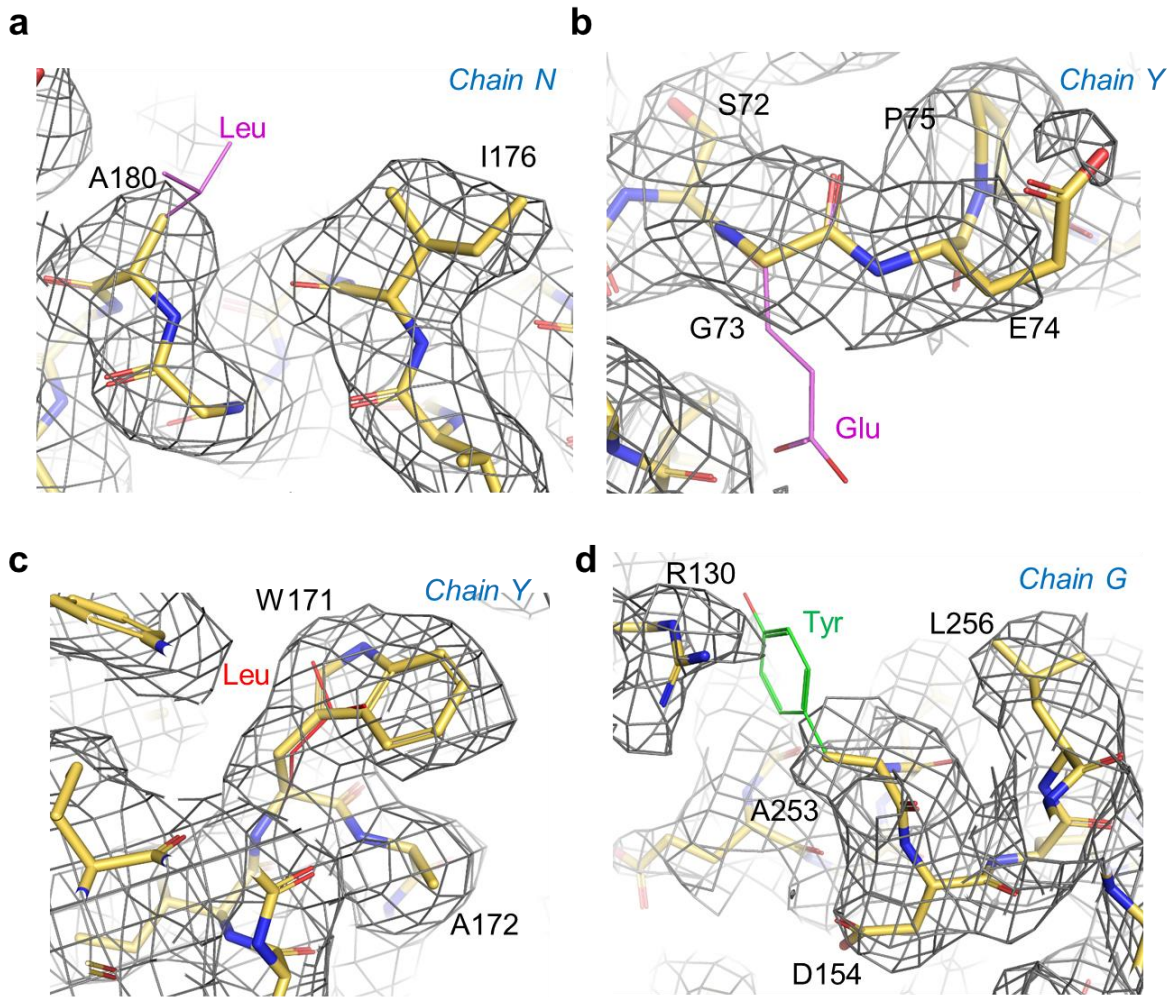

Supplementary Fig. 5 | Identification of S-LHCII as a homotrimer composed of Lhcb1-A isoforms based on amino acid tracing in the electron density map. (a, b) Maps (contoured at 3 sigma level) confirm the presence of A180 and G73 and exclude the presence of Leu and Glu at the equivalent positions found in Lhcb2 proteins (coloured in magenta). (c) Electron density maps of W171 exclude the presence of the equivalent Leu in Lhcb1-B1, -B2 proteins (coloured in red). (d) Map of A253 exclude the presence of the equivalent Tyr (coloured in green) found in Lhcb1-A3 and Lhcb2-A3 proteins. This systematic annotation suggests that the S-LHCII homotrimer consists preferentially of the Lhcb1-A1/A2 isoforms, but the presence of the Lhcb1-A3 isoform cannot be excluded for the N and Y chains.

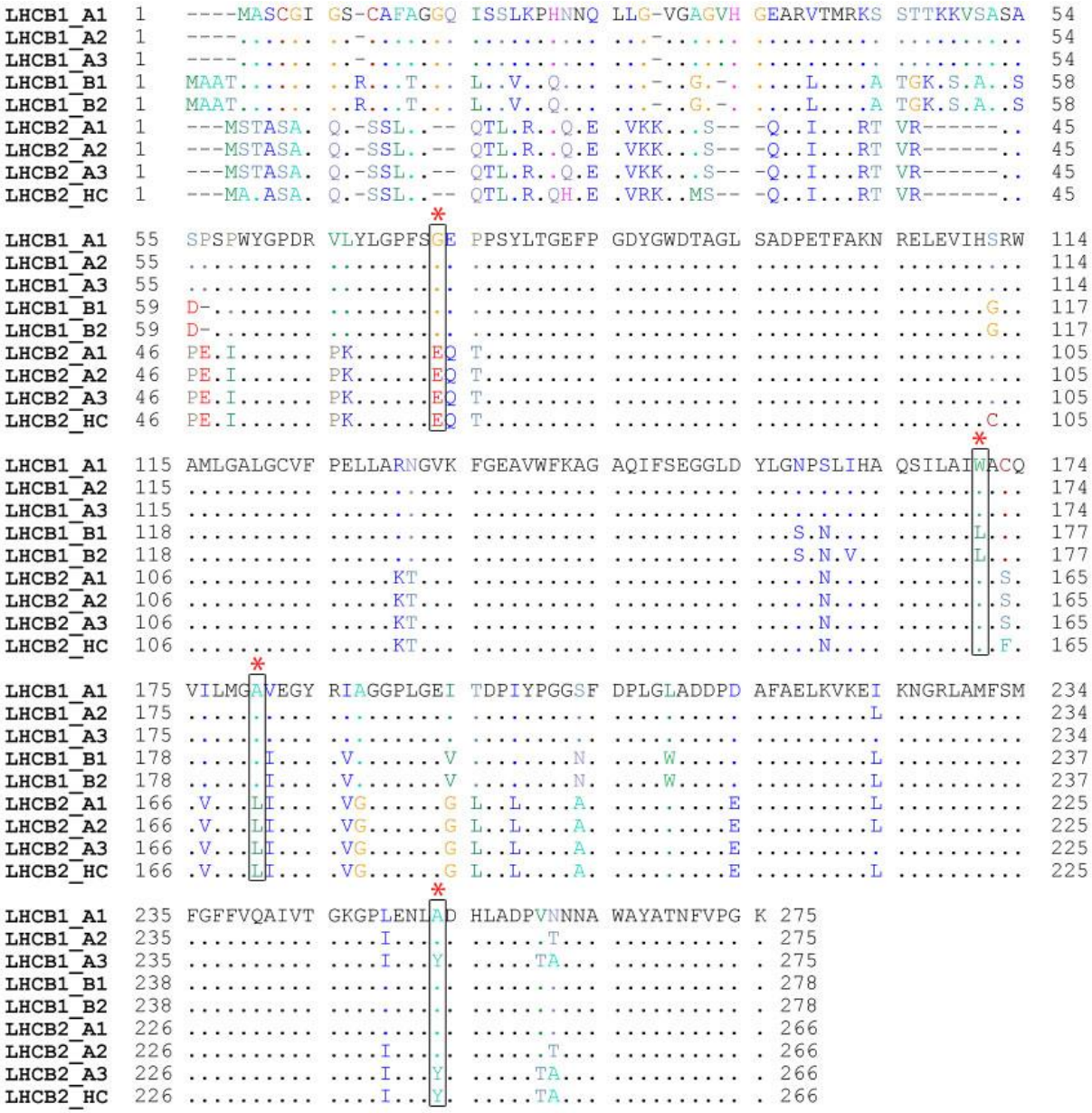

Supplementary Fig. 6 | Sequence alignment of light-harvesting proteins of photosystem II from *Picea abies*. Multiple sequence alignment of isoforms of Lhcb1 and Lhcb2 amino acid sequences from *Picea abies* run by ClustalW algorithm (scoring matrix BLOSUM62). Used source: database S2[54]; LHCB2_HC sequence: MA_10431300g0020 (HC as high confidence, designation of another isoform of Lhcb2 confirmed in spruce, adapted from Grebe et al. 2019). Amino acids in rectangles marked by asterisk represent selected positions with critical variability in sequences of Lhcb1 & Lhcb2 isoforms used for determining the S-trimer of PSII as homotrimer based on their distinct characteristics features in electron density map. Identic amino acids in specific positions of alignment are in black colour in the reference sequence (first row) and plotted as dots in the remaining sequences.

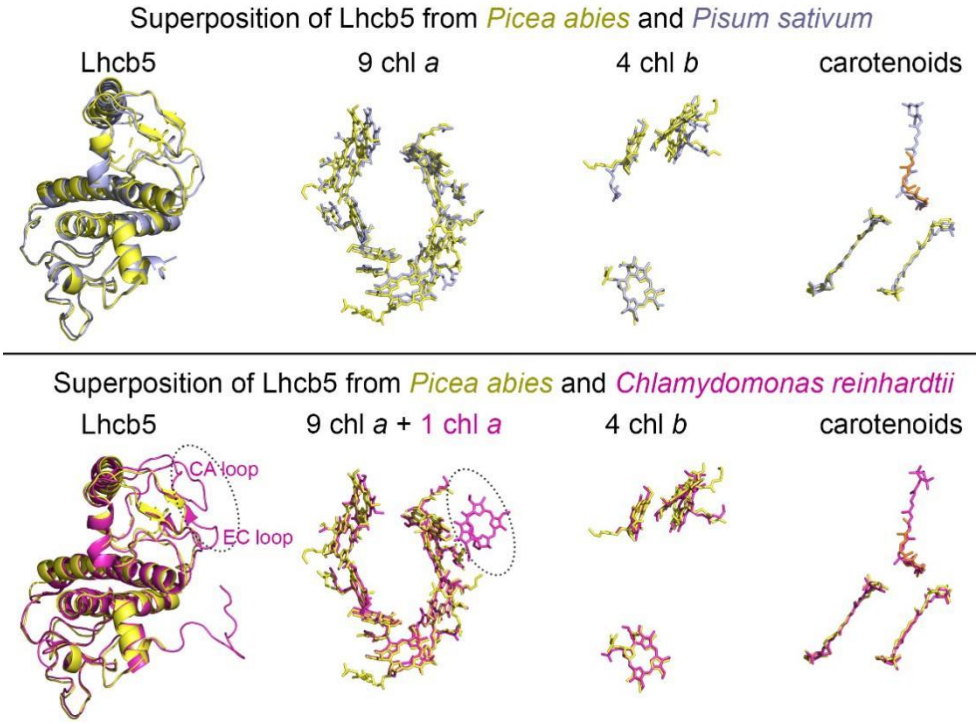

Supplementary Fig. 7 | Structural comparison of Lhcb5 from *Picea abies*, *Pisum sativum* and *Chlamydomonas reinhardtii*. Superposition of the cryo-EM structures of monomeric antenna proteins Lhcb5 and bound pigments from spruce with those from pea (PDB code: 5xnl) and *Chlamydomonas reinhardtii* (*Cr*) (PDB code: 6kac) viewed from the lumenal side. Colour coding: Lhcb5: spruce (yellow), pea (light blue), *Cr* (magenta); Chl *a*: spruce (yellow), pea (light blue), *Cr* (magenta); Chl *b*: spruce (yellow), pea (light blue), *Cr* (magenta); carotenoids: spruce (lutein – yellow, neoxanthin – orange), pea (all carotenoids in light blue), *Cr* (all carotenoids in magenta).

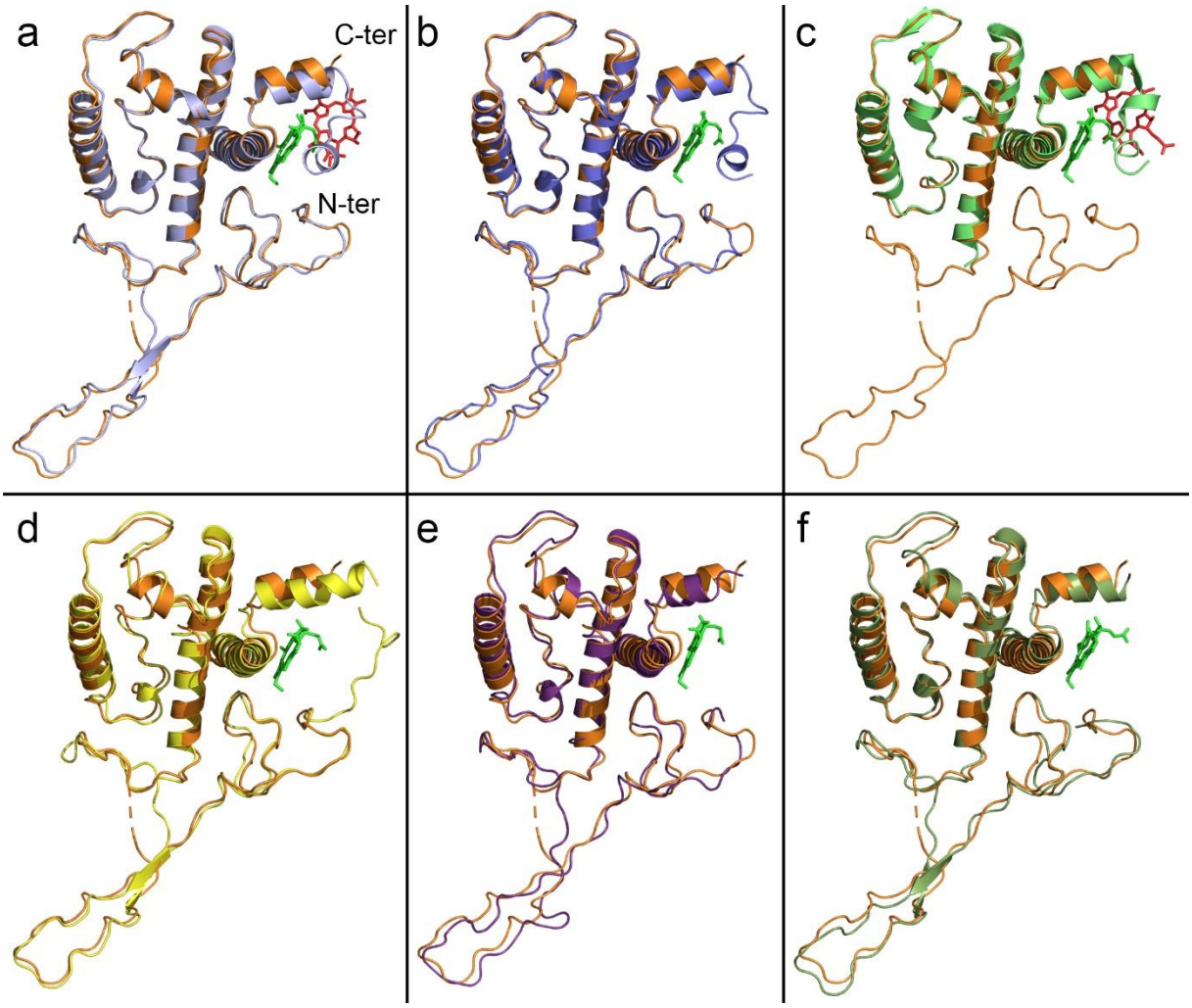

Supplementary Fig. 8 | Structural comparison of spruce Lhcb8 with Lhcb4/8 from other photosynthetic organisms. a-f, Comparison of spruce Lhcb8 (orange) with Lhcb4/8 from different photosynthetic organisms: (a) pea (PDB code: 5xnl), (b) spinach (PDB codes: 3jcu), (c) spinach (PDB code: 3pl9), (d) Chlamydomonas (PDB code: 6kad), (e) Chlamydomonas (PDB code: 6kaf), (f) Lhcb8 of high-light acclimated pea (PDB code: 6yp7). Visualized Chl *a* (green) and Chl *b* (red) represent chlorophylls, which are missing in spruce Lhcb8, but present in the Lhcb4/8 of a given organism. In the cryo-EM structure of Lhcb4 from spinach (b), Chl *b* was probably lost during purification[56]. In high-light acclimated pea (f), the structure of Lhcb8 was predicted by the fit of amino acid sequence of Lhcb8 to low resolution density map[57].

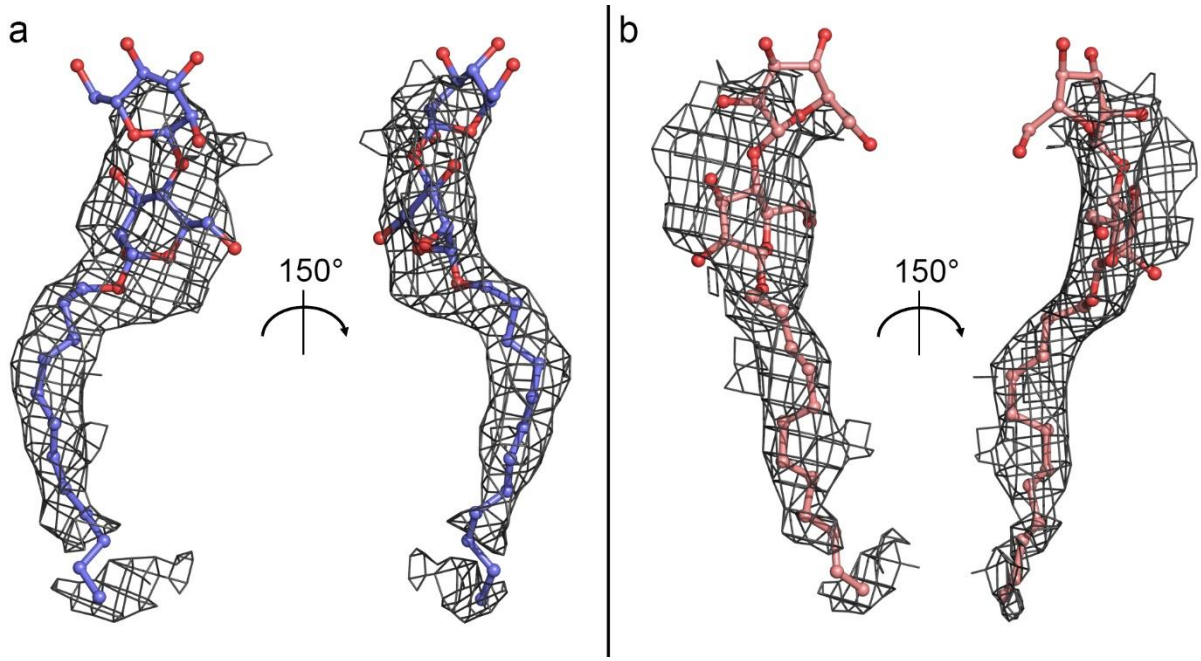

Supplementary Fig. 9 | Elimination of the detergent molecule n-dodecyl-α-D-maltoside as a possible candidate for the originally uncharacterised density revealed in the structure of the spruce photosystem II C_2S_2 supercomplex. a, b, Fitting the density map by n-dodecyl α-D-maltoside shows that the density cannot fully accommodate the second glucose molecule of the maltoside. Considering the free rotation between the two glucose molecules of maltoside, the fit was performed for two conformations of glucose rings - position 1 (blue) (a) and position 2 (salmon) (b).

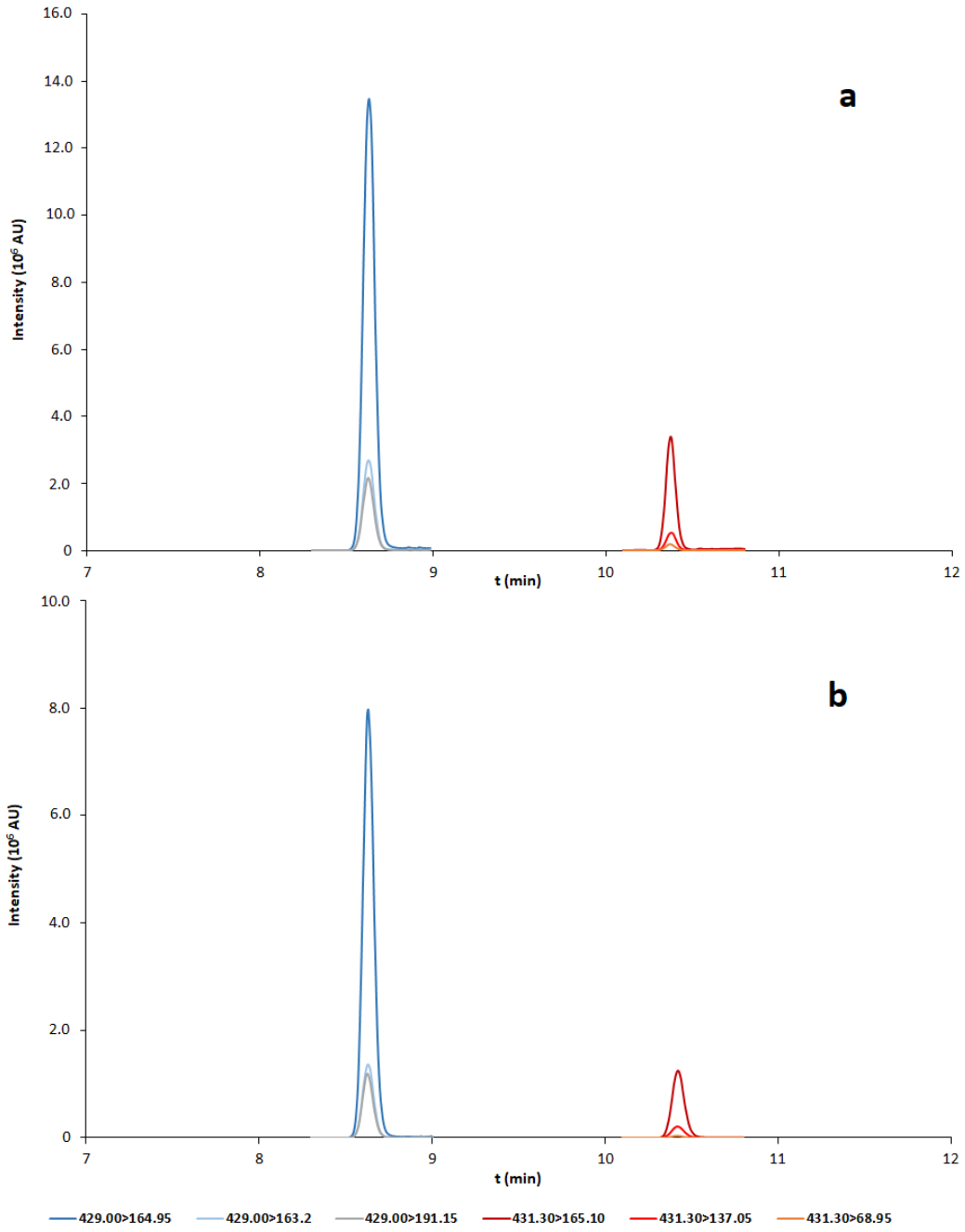

Supplementary Fig. 10 | Detection of α-tocopherol and α-tocopherolquinone in photosystem II supercomplexes using liquid chromatography-tandem mass spectrometry (LC-MS/MS) with multiple reaction monitoring (MRM) mode. The MRM chromatograms of α-tocopherolquinone (blue) and α-tocopherol (red) of 1μM standard mixture (a) and the MRM chromatogram of a concentrated "PSII sc" fraction (b). The LC-MS/MS analysis was repeated twice independently with similar results.

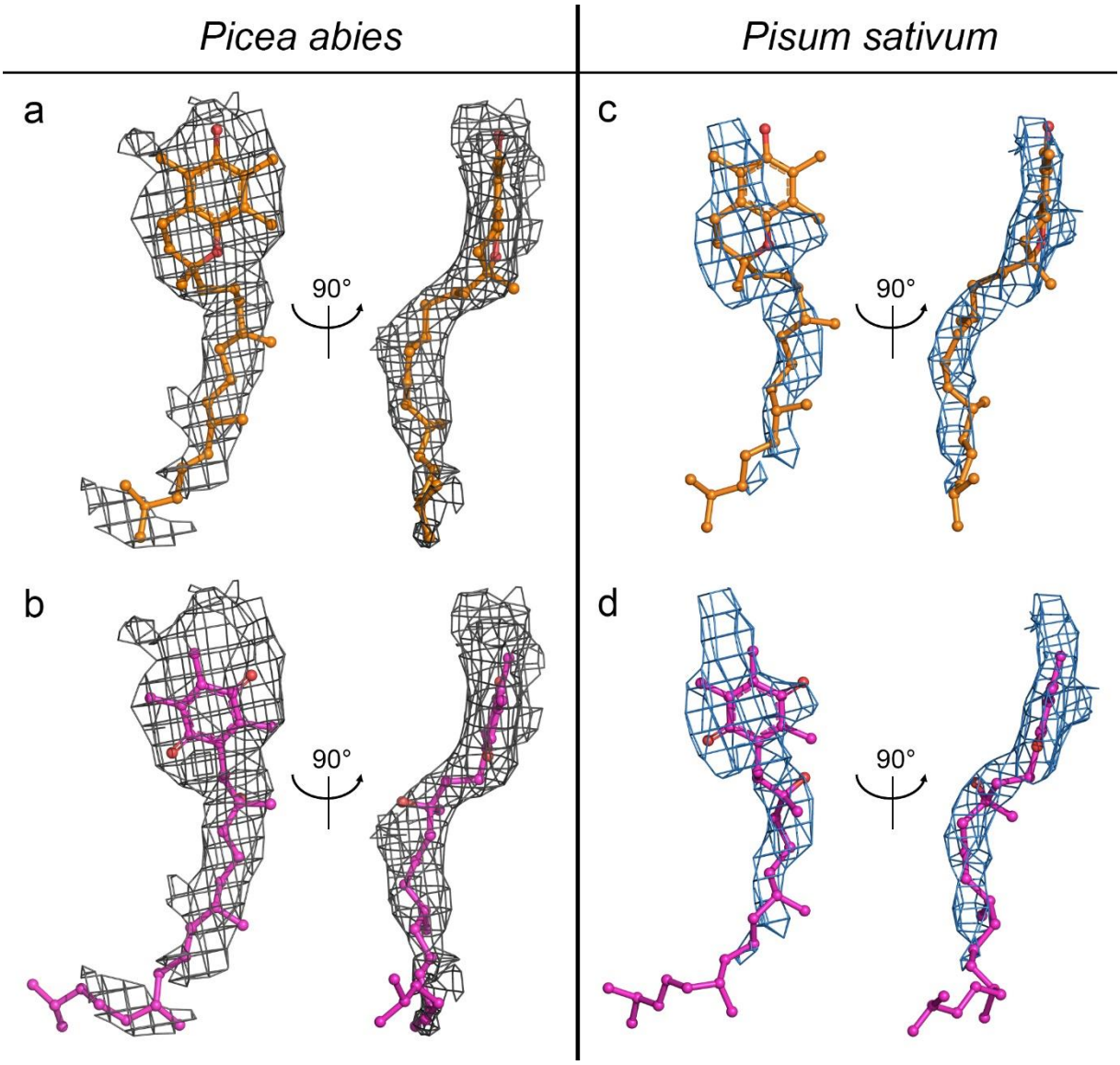

Supplementary Fig. 11 | Cryo-EM density of α-tocopherol bound in the spruce photosystem II C_2S_2 supercomplex. a, b, The density map revealed in the structure of the spruce PSII supercomplex fitted by α-tocopherol (orange) and α-tocopherolquinone (magenta), respectively. **c, d,** The corresponding density found in the structure of the PSII supercomplex from pea[58] fitted by α-tocopherol (orange) and α-tocopherolquinone (magenta), respectively.

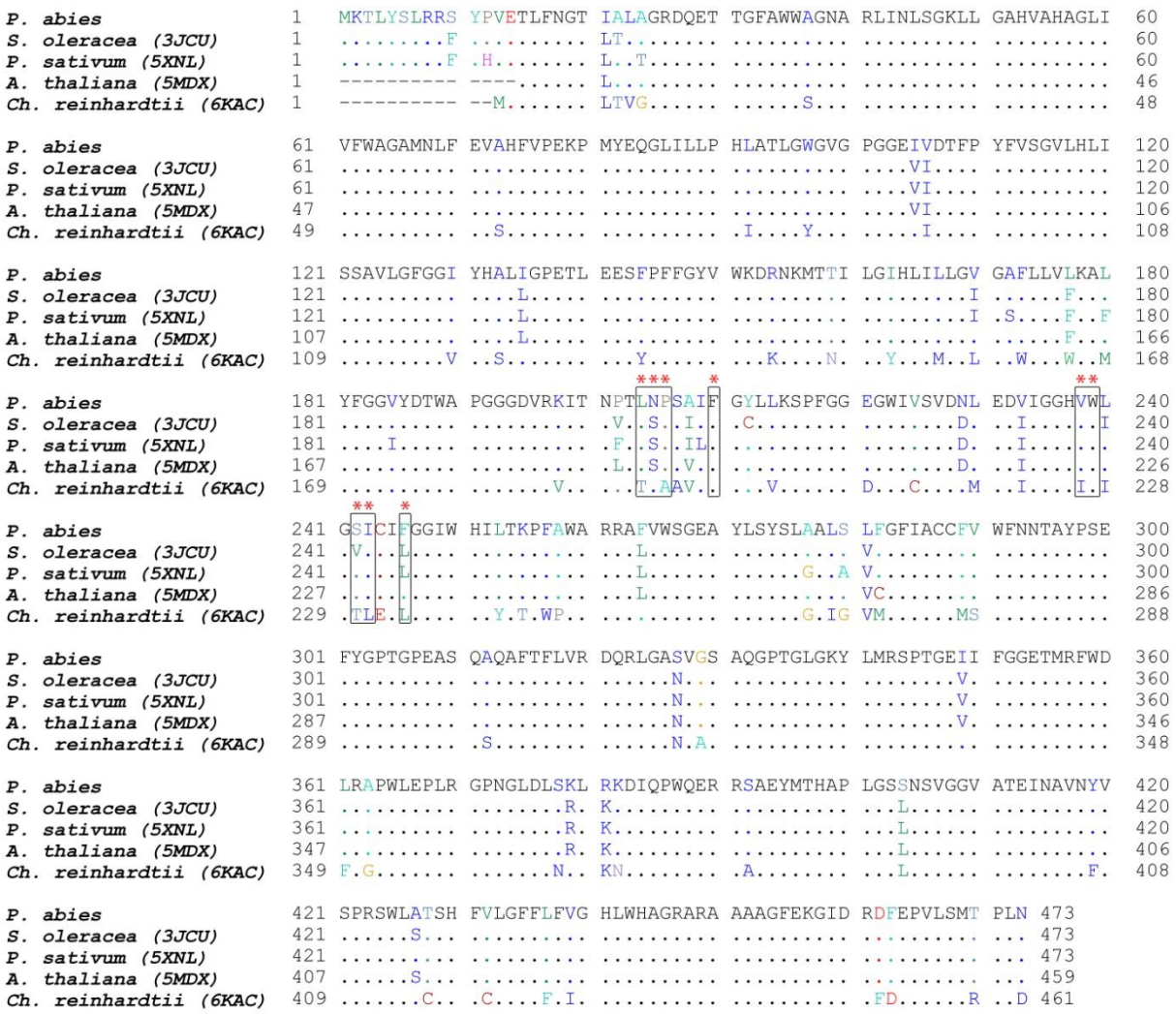

Supplementary Fig. 12 | Sequence alignment of photosystem II reaction center subunit CP43 from different organisms. Multiple sequence alignment by ClustalW algorithm (scoring matrix BLOSUM62) of CP43 amino acid sequences from *Picea abies* (YP_008082859.1), *Spinacia oleracea* (3JCU), *Pisum sativum* (5XNL), *Arabidopsis thaliana* (5MDX), and *Chlamydomonas reinhardtii* (6KAC). Selected amino acid sequence positions in rectangles marked by red asterisks represent contact areas of the CP43 subunit with α-tocopherol in *Picea abies*. Source of sequences: RCSB PDB, for *P. abies* database S2[54]. Identic amino acids in specific alignment positions are in black in the reference sequence (first row) and plotted as dots in the remaining sequences.

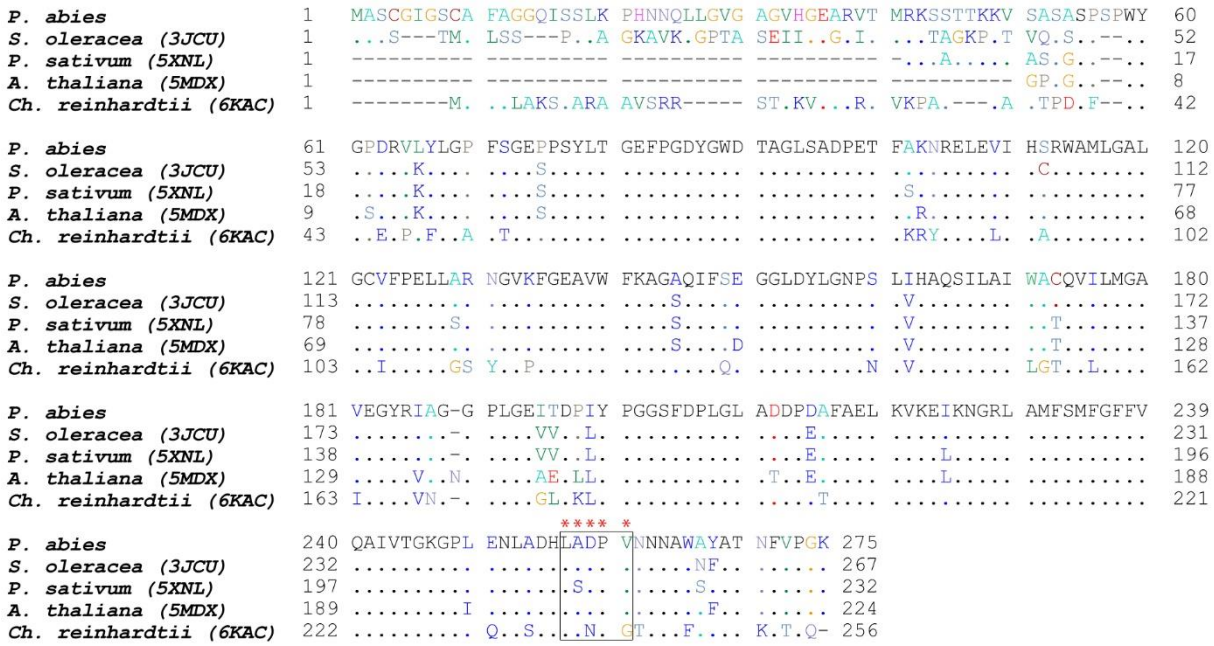

Supplementary Fig. 13 | Sequence alignment of chlorophyll a-b binding protein Lhcb1 from different organisms. Multiple sequence alignment by ClustalW algorithm (scoring matrix BLOSUM62) of Lhcb1 amino acid sequences from *Picea abies* (comp94480_c0_seq6), *Spinacia oleracea* (3JCU), *Pisum sativum* (5XNL), *Arabidopsis thaliana* (5MDX) & *Chlamydomonas reinhardtii* (6KAC). All sequences represent the Lhcb1 isoform except *Cr*, which is represented by LhcbM1. Selected positions in rectangle marked by red asterisks represent region in amino acids sequence involved in binding α-tocopherol/α-tocopherolquinone. Source of sequences: RCSB PDB, for *P. abies* database S2[54]. Identic amino acids in specific alignment positions are in black in the reference sequence (first row) and plotted as dots in the remaining sequences.

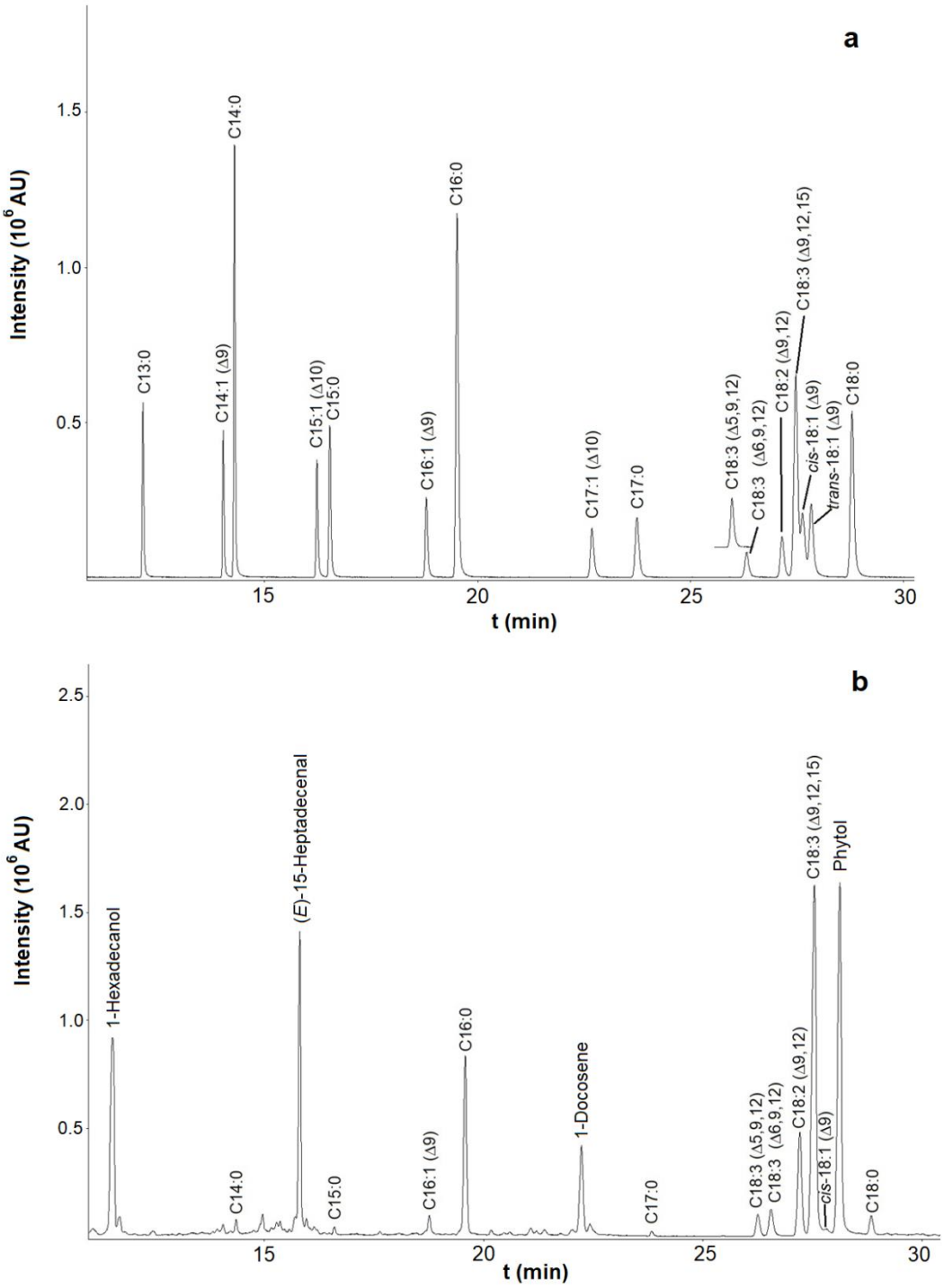

Supplementary Fig. 14 | Detection of fatty acid composition in photosystem II C_2S_2 supercomplex fraction. The GCMS chromatograms of FAME (fatty acid methyl esters) standard mixture (a), and sample (b). C13:0 – tridecanoate; C14:1(Δ9) – *cis*-9-tetradecenoate; C14:0 – tetradecanoate; C15:1(Δ10) – *cis*-10-pentadecenoate; C15:0 – pentadecanoate; C16:1(Δ9) – palmitoleate; C16:0 – palmitate; C17:1(Δ10) – *cis*-10-heptadecenoate; C17:0 – heptadecanoate; C18:3(Δ5,9,12) – pinolenate; C18:3(Δ6,9,12) – *γ*-linolenate; C18:2 (Δ9,12) –

linoleate; C18:3(Δ9,12,15) – α-linolenate; C18:1(Δ9)-*cis* – oleate; C18:1(Δ9)-*trans* – elaidate; C18:0 – stearate. Peaks, which are not annotated, do not represent fatty acids but phytol or other derivatives. The analysis was repeated twice independently (each time in technological triplicates) with similar results.

Supplementary Tables

Supplementary Table 1 | Cryo-EM data collection, refinement and validation statistics for the structural model of the spruce PSII C_2S_2 supercomplex.

Data collection	
Magnification	150 000 x
Voltage (kV)	200
Focal length/Cs (mm)	3.4/2.7
Objective aperture (μm)	100
Number of movies collected	2392
Electron exposure ($e^-/Å^2$)	120 (30 at the Bayesian polishing step)
Defocus range (μm)	-0.5 to -2.0
Pixel size (Å)	0.96127
Data Processing	
Symmetry imposed	C2
Initial particle images (no.)	202251
Final particle images (no.)	60956
Map resolution (Å)/FSC threshold	2.785/0.143
Map sharpening B-factor ($Å^2$)	-87.3
Refinement	
Resolution (Å)	2.80
Mask CC	0.858
Volume CC	0.827
Initial model (PDB)	3JCU
Model composition	
Non-hydrogen atoms	71184
Protein residues	6773
Ligands	358
Water molecules	280
Average B factors ($Å^2$)	
Overall	56.2
Protein	53.7
Ligands	63.6
R.M.S. deviations	
Bond lengths (Å)	0.007
Bond angles (°)	0.780
Validation	
MolProbity score	1.58
Clash score	8.54
Rotamer outliers (%)	0.07
Ramachandran plot	
Favored (%)	97.37
Allowed (%)	2.63
Disallowed (%)	0.00

Supplementary Table 2 | Cofactors bound by each monomeric subunit of the dimeric spruce PSII C_2S_2 supercomplex.

Subunit	Chlorophylls	Carotenoids	Lipids	Others
PsbA	4 Chl a 2 Pheo	1 β-carotene	1 MGDG 1 SQDG 1 3PH 1 LNL	1 bicarbonate ion 1 Cl^- ion 1 Fe^{3+} ion 1 plastoquinone
PsbB	16 Chl a	3 β-carotenes	1 MGDG 1 SQDG 2 3PH 1 PAM 5 LNL 1 PG	
PsbC	13 Chl a	4 β-carotenes	1 DGDG 1 3PH 6 LNL	1 Mg^{2+} ion
PsbD	2 Chl a	1 β-carotene	1 MGDG 1 diacylglycerol 1 3PH 2 PG 1 LNL	1 plastoquinone
PsbE				
PsbF				1 heme
PsbH		1 β-carotene	1 DGDG	
PsbI				
PsbK				
PsbL			1 PG	
PsbM				
PsbO				
PsbTc				
PsbTn				
Ycf12				
PsbW				
PsbX				
PsbZ				
Lhcb5	9 Chl a 4 Chl b	2 Luteins 1 Neoxanthin	1 3PH 1 PG	
Lhcb8	9 Chl a 3 Chl b	1 Lutein 1 Neoxanthin 1 Violaxanthin	2 MGDG 1 PG	
S-LHCII trimer	24 Chl a 18 Chl b	6 Luteins 3 Neoxanthins 3 Violaxanthins	1 MGDG 3 PG	
Total	102 Chls, 2 Pheo	28	40	7

Abbreviations: 3PH, phosphatidic acid; Chl, chlorophyll; DGDG, digalactosyldiacyl glycerol; LNL, alpha-linolenic acid; MGDG, monogalactosyldiacyl glycerol; PAM, palmitoleic acid; PG, phosphatidyl glycerol; Pheo, pheophytin; SQDG, sulfoquinovosyldiacyl glycerol.

Supplementary Table 3 | Structural deviations between different structures of PSII C_2S_2 supercomplexes and dimeric core complexes (C_2) from different organisms expressed by the RMSD values. The upper and lower values represent the RMSD of the backbone C-alpha atoms of the C_2S_2 supercomplex and C_2, respectively. The four-digit codes indicate the PDB ID of the particular structure.

RMSD [Å]	spruce	pea 5xnl	spinach 3jcu	*At* 5mdx	pea 6yp7	*Cr* 6kac	*Cr* 6kad	*Cr* 6kaf
spruce	-	2.365 1.863	2.161 1.587	1.671 1.545	1.929 1.895	2.296 2.058	1.488 1.273	1.414 1.301
pea 5xnl	2.365 1.863	-	0.923 0.827	2.465 2.526	3.325 3.296	2.749 2.597	2.72 1.839	2.466 1.673
spinach 3jcu	2.161 1.587	0.923 0.827	-	2.302 2.29	3.142 3.123	2.455 2.31	2.531 2.087	2.213 2.313
At 5mdx	1.671 1.545	2.465 2.526	2.302 2.29	-	2.223 2.109	2.262 2.032	1.797 1.518	1.513 1.449
pea 6yp7	1.929 1.895	3.325 3.296	3.142 3.123	2.223 2.109	-	2.896 2.83	1.9 1.839	1.611 1.673
Cr 6kac	2.296 2.058	2.749 2.597	2.455 2.31	2.262 2.032	2.896 2.83	-	1.704 1.457	2.212 1.668
Cr 6kad	1.488 1.273	2.72 2.352	2.531 2.087	1.797 2.032	1.9 2.83	1.704 1.457	-	1.033 0.825
Cr 6kaf	1.414 1.301	2.466 2.604	2.213 2.313	1.513 1.449	1.611 1.673	2.212 1.668	1.033 0.825	-

Abbreviations: RMSD - root mean square deviations; *At* – *Arabidopsis thaliana*; *Cr* – *Chlamydomonas reinhardtii*.

Supplementary Table 4 | MS analysis of the purified fraction of photosystem II C_2S_2 supercomplexes used for cryo-EM analysis. The photosystem II subunits identified in the purified fraction after simultaneous digestion with trypsin and chymotrypsin are listed. PsbF and Lhcb2 were detected only after chymotrypsin digestion. A and B letters stand for a designation of isoforms. *Identification according to Grebe et al.[54].

Protein		Accession	Peptides (all/unique)	Sequence coverage (%)
PsbA (D1)		YP_008082796.1	20/20	38.8
PsbB (CP47)		YP_008082835.1	39/39	46.5
PsbC (CP43)		YP_008082859.1	32/32	33.6
PsbD (D2)		YP_008082860.1	29/29	36.8
PsbE		YP_008082810.1	6/6	42.2
PsbF		YP_008082811.1	4/4	66.7
PsbH		YP_008082838.1	6/6	41.3
PsbJ		YP_008082813.1	1/1	17.5
PsbL		YP_008082812.1	3/3	36.8
PsbO		comp75415_c0_seq1	62/6	62.5
PsbP		MA_3005g0010	6/6	27.9
PsbQ		MA_218996g0010	13/13	35.9
PsbR	A1	MA_282g0010	12/7	26.4
	A4	PUT-175a-Picea_abies-6379	9/5	31.5
PsbTn		MA_17217g0020	3/3	37.9
PsbW		MA_10431532g0010	2/2	11.6
PsbX		UCPabies_isotig10782	1/1	20.9
Lhcb1	A1	comp94480_c0_seq6	43/0	61.1
	A2	MA_131587g0010	42/0	61.1
	A3	comp94480_c0_seq2	43/0	61.1
	B2	UCPabies_isotig06275	32/5	57.6
Lhcb2*		MA_10431300g0020	57/1	79.2
Lhcb5		MA_176279g0010	27/27	50.2
Lhcb8		comp95233_c3_seq1	15/3	33.7

Supplementary Table 5 | Interactions between light-harvesting proteins and subunits of the photosystem II core complex from spruce. Interface area and specific bonds (hydrogen bonds and salt bridges) between amino acids are indicated.

Subunit interactions	Interface area [Å^2]	H bonds	Salt bridge
Lhcb5 – CP43	189		
Lhcb5 – S-LHCII	101		
Lhcb5 – PsbZ	295	Leu290 - Ser59	Asp100 - Lys37
S-LHCII – CP43	41		
S-LHCII – PsbW	116		
S-LHCII – Lhcb8	86		
Lhcb8 – PsbA	245	Gln122 – Asn230 Asn123 – Asn230 Leu124 – Glu229 Asn127 – Glu229	
Lhcb8 – PsbB	828	Gln122 – Thr10 Tyr115 – Gln223 Tyr115 – Arg127	Asp116 – Arg127
Lhcb8 – PsbH	524	Leu113 – Val33 Gln114 – Tyr30 Tyr115 – Gly31 Asp118 – Tyr30 Gln147 – Glu29 Ser150 – Lys32	
Lhcb8 - PsbL	75	Asn123 – Gln9	

Supplementary Table 6 | Calculated FRET rates for the excitation energy transfer from the S-LHCII trimer, Lhcb5, and Lhcb8/Lhcb4 to adjacent antenna subunits and the core complex of photosystem II in spruce and other selected organisms. The lifetime (τ) is defined as $1/k_{FRET}$. Interacting subunits in bold represent the main pathways for energy transfer. The four-digit codes indicate the PDB ID of the particular structure.

Interacting subunits	spruce		pea (5xnl)		spinach (3jcu)		chlamydomonas (6kac)	
	FRET rate k_{FRET} (ps^{-1})	lifetime τ (ps)	FRET rate k_{FRET} (ps^{-1})	lifetime τ (ps)	FRET rate k_{FRET} (ps^{-1})	lifetime τ (ps)	FRET rate k_{FRET} (ps^{-1})	lifetime τ (ps)
S-LHCII → CP43	0.054	18.5	0.077	12.9	0.067	14.8	0.066	15.1
S-LHCII → Lhcb5	0.007	140.8	0.009	117.3	0.009	113.9	0.016	63.6
S-LHCII → Lhcb8/4	0.003	400.0	0.003	346.8	0.003	303.4	0.003	387.7
Lhcb5 → CP43	0.107	9.3	0.135	7.4	0.125	8.0	0.085	11.7
Lhcb5 → S-LHCII	0.007	153.8	0.008	127.5	0.008	123.8	0.013	76.5
Lhcb8/4 → CP47	0.220	4.6	0.275	3.6	0.255	3.9	0.213	4.7
Lhcb8/4 → S-LHCII	0.002	434.8	0.002	417.1	0.003	361.0	0.002	461.3

References (supplement)

51. Wiśniewski, J.R., Zougman, A., Nagaraj, N. & Mann, M. Universal sample preparation method for proteome analysis. *Nat. Methods* **6**, 359–362 (2009).
52. Cox, J. & Mann, M. MaxQuant enables high peptide identification rates, individualized p.p.b.-range mass accuracies and proteome-wide protein quantification. *Nat. Biotechnol.* **26**, 1367–1372 (2008).
53. Cox, J. et al. A Peptide Search Engine Integrated into the MaxQuant Environment. *J. Proteome Res.* **10**, 1794–1805 (2011).
54. Grebe, S. et al. The unique photosynthetic apparatus of Pinaceae: analysis of photosynthetic complexes in *Picea abies. J. Exp. Bot.* **70**, 3211–3225 (2019).
55. Perez-Riverol, Y. et al. The PRIDE database and related tools and resources in 2019: improving support for quantification data. *Nucleic Acids Res.* **47**, D442–D450 (2019).
56. Wei, X. et al. Structure of spinach photosystem II–LHCII supercomplex at 3.2 Å resolution. *Nature* **534**, 69–74 (2016).
57. Grinzato, A. et al. High-light versus low-light: effects on paired photosystem II supercomplex structural rearrangement in pea plants. *Int. J. Mol. Sci.* **21**, 8643 (2020).
58. Su, X. et al. Structure and assembly mechanism of plant C2S2M2-type PSII-LHCII supercomplex. *Science* **357**, 815–820 (2017).

Photosynthesis Research (2022) 154:21–40
https://doi.org/10.1007/s11120-022-00949-0

ORIGINAL ARTICLE

Spruce versus Arabidopsis: different strategies of photosynthetic acclimation to light intensity change

Michal Štroch[1,2] · Václav Karlický[1,2] · Petr Ilík[3] · Iva Ilíková[4] · Monika Opatíková[3] · Lukáš Nosek[3] · Pavel Pospíšil[3] · Marika Svrčková[3] · Marek Rác[3] · Pavel Roudnický[5] · Zbyněk Zdráhal[5] · Vladimír Špunda[1,2] · Roman Kouřil[3]

Received: 22 April 2022 / Accepted: 30 July 2022 / Published online: 18 August 2022

Abstract

The acclimation of higher plants to different light intensities is associated with a reorganization of the photosynthetic apparatus. These modifications, namely, changes in the amount of peripheral antenna (LHCII) of photosystem (PS) II and changes in PSII/PSI stoichiometry, typically lead to an altered chlorophyll (Chl) *a/b* ratio. However, our previous studies show that in spruce, this ratio is not affected by changes in growth light intensity. The evolutionary loss of PSII antenna proteins LHCB3 and LHCB6 in the Pinaceae family is another indication that the light acclimation strategy in spruce could be different. Here we show that, unlike Arabidopsis, spruce does not modify its PSII/PSI ratio and PSII antenna size to maximize its photosynthetic performance during light acclimation. Its large PSII antenna consists of many weakly bound LHCIIs, which form effective quenching centers, even at relatively low light. This, together with sensitive photosynthetic control on the level of cytochrome b_6f complex (protecting PSI), is the crucial photoprotective mechanism in spruce. High-light acclimation of spruce involves the disruption of PSII macro-organization, reduction of the amount of both PSII and PSI core complexes, synthesis of stress proteins that bind released Chls, and formation of "locked-in" quenching centers from uncoupled LHCIIs. Such response has been previously observed in the evergreen angiosperm *Monstera deliciosa* exposed to high light. We suggest that, in contrast to annuals, shade-tolerant evergreen land plants have their own strategy to cope with light intensity changes and the hallmark of this strategy is a stable Chl *a/b* ratio.

Keywords Light acclimation · Photoprotection · *Picea abies* · *Arabidopsis thaliana* · Thylakoid membrane · Non-photochemical quenching · LHCII antenna · Photosynthetic control

Introduction

Light intensity is the most important factor affecting plant photosynthetic performance. Although light is indispensable for plants as the driving force for photosynthetic electron transport, it is also potentially damaging to the photosynthetic apparatus. To cope with changing light intensity, plants have developed a number of regulatory mechanisms which enable them to adjust the function and composition of their photosynthetic apparatus to a particular light environment. The responses to fast changes in light conditions include state transitions and non-photochemical quenching (NPQ). State transitions enable the optimization of the distribution of excitation energy between photosystem I (PSI) and II (PSII) via the reversible phosphorylation of light-harvesting complex II (LHCII), especially under low-light conditions (for a recent review, see Allen 2017). On the

Michal Štroch, Václav Karlický, and Petr Ilík have contributed equally to this work.

✉ Michal Štroch
michal.stroch@osu.cz

1 Department of Physics, Faculty of Science, University of Ostrava, 710 00 Ostrava, Czech Republic

2 Global Change Research Institute, Czech Academy of Sciences, 603 00 Brno, Czech Republic

3 Department of Biophysics, Faculty of Science, Palacký University, 783 71 Olomouc, Czech Republic

4 Institute of Experimental Botany, Czech Academy of Sciences, Centre of the Region Haná for Biotechnological and Agricultural Research, 779 00 Olomouc, Czech Republic

5 Mendel Centre for Plant Genomics and Proteomics, Central European Institute of Technology, Masaryk University, 625 00 Brno, Czech Republic

other hand, NPQ is active mainly in high-light conditions and allows safe dissipation of the excess of absorbed light energy within PSII and LHCII. This prevents overexcitation of PSII reaction centers and protects the photosynthetic apparatus against photooxidative damage (de Bianchi et al. 2010; Bassi and Dall'Osto 2021; Ruban and Wilson 2021). The response of plants to longer-term changes in light conditions (acclimation response) involves specific modifications of the photosynthetic apparatus at the protein level, which lead to structural and functional changes of PSI and PSII (Anderson 1986; Walters 2005; Eberhard et al. 2008; Schöttler and Tóth 2014).

PSII–LHCII of a typical higher plant is composed of a dimeric core complex (C_2) and a variable number of light-harvesting proteins (LHCB1–6). A major part of the plant LHCII is formed by LHCII trimers, which consist of three proteins (LHCB1–3) and which are specifically associated with the core complex via monomeric antenna proteins LHCB4–6. According to the character of their bond to the C_2, LHCII trimers have been designated as "S" and "M" (strongly and moderately bound LHCII, respectively) (Dekker and Boekema 2005; Kouřil et al. 2018). The S trimer is formed by variable combinations of LHCB1 and LHCB2 proteins, whereas the M trimer contains also LHCB3. The binding of the S trimer to the C_2 is mediated by LHCB4 and LHCB5, while the binding of the M trimer is facilitated by the interactions between LHCB3, a constituent of the M trimer (Dainese and Bassi 1991), and LHCB4 and LHCB6 (Caffarri et al. 2009; van Bezouwen et al. 2017; Su et al. 2017). Under normal light (100 µmol photons m^{-2} s^{-1}, NL) conditions, the most abundant type of PSII–LHCII supercomplex is the $C_2S_2M_2$, where two copies of the S and M trimers are bound to the C_2 (Kouřil et al. 2013). In contrast to PSII, the plant PSI complex is monomeric and consists of the PSI core complex which binds four monomeric LHCA1–4 proteins forming LHCI (for a recent review, see Bai et al. 2021).

At light intensity that is limiting to photosynthesis, light energy must be captured and utilized by plants with the highest possible efficiency. Therefore, higher plants respond to low-light (LL) exposure by two main adjustments of their photosynthetic apparatus. The first is an enlargement of LHCII via upregulation of LHCB1 and LHCB2 proteins, which in turn leads to a lower chlorophyll (Chl) *a*/*b* ratio. The second is a decrease in the abundance of PSII, which is reflected in the increase in the PSI/PSII ratio (Bailey et al. 2001; Ballottari et al. 2007; Kouřil et al. 2013; Albanese et al. 2016). These modifications lead to an enlarged absorption cross section of PSII complexes, thereby compensating for the potentially detrimental effects of LL conditions on the photosynthetic performance of plants.

Under high-light (HL) conditions, on the other hand, plants have to cope with a surplus of absorbed light energy, which exceeds the utilization capacity of photosynthetic electron transport. The amount of absorbed light energy is downregulated by a reduction of the antenna size. This is achieved by a selective and coordinated downregulation of LHCB1–3 proteins and the downregulation of the LHCB6 protein, which is crucial for the binding of the M trimer to the C_2 (Bailey et al. 2001; Ballottari et al. 2007; Kouřil et al. 2013; Albanese et al. 2016). At the same time, LHCB4.3, one of the isoforms of minor antenna LHCB4, is strongly upregulated by HL (Floris et al. 2013). This isoform, sometimes also referred to as LHCB8, was found to have reduced affinity to LHCB6 and to weaken the binding of the M trimer to the C_2 (Albanese et al. 2016, 2018, 2019). Acclimation of higher plants to HL is thus typically accompanied by a gradual transformation of the $C_2S_2M_2$ supercomplex to its smaller forms—C_2S_2M and C_2S_2 (Kouřil et al. 2013; Albanese et al. 2016). This reduction of the antenna size is directly manifested as an increase in the Chl *a*/*b* ratio (Bailey et al. 2001; Ballottari et al. 2007; Kouřil et al. 2013; Albanese et al. 2016). In contrast to LHCII, LHCI does not change significantly in HL, and the regulation at the level of PSI is ensured by changes in the PSI/PSII ratio and the amount of LHCII proteins associated with PSI (Ballottari et al. 2007; Wientjes et al. 2013a).

Recently, we have found that the structure and composition of PSII supercomplexes are not conserved among higher plants; the gymnosperm genera *Picea* and *Pinus* (family Pinaceae) and *Gnetum* (order Gnetales) lack functional *lhcb6* and *lhcb3* genes (Kouřil et al. 2016). Structural analysis of the PSII supercomplexes from Norway spruce (*Picea abies*) revealed that the absence of LHCB3 and LHCB6 proteins changes the binding of the M trimer to the C_2, leading to the formation of a PSII supercomplex configuration that is unique among land plants (Kouřil et al. 2016). In addition, Grebe et al. (2019) revealed that genes coding for LHCB4.1 and LHCB4.2 proteins have also been lost from the genome of *Picea abies*, while the gene for LHCB4.3 has been retained. Interestingly, this evolutionarily modified protein composition of the PSII–LHCII complex from *Picea abies* has a striking resemblance to the protein composition of PSII–LHCII of higher plants acclimated to HL conditions (Kouřil et al. 2013). The evolutionary modification of LHCB proteins composition in PSII–LHCII in Pinaceae and Gnetales could be one of the factors contributing to the reduced plasticity of LHCII (stable Chl *a*/*b* ratio) in spruce grown under LL and HL conditions observed in our previous studies (Kurasová et al. 2003; Štroch et al. 2008).

In the present work, we studied the acclimation response of Norway spruce seedlings and *Arabidopsis thaliana* (model organisms of Pinaceae and angiosperms, respectively) to different light intensities under well-defined conditions (i.e., in growth chambers). We focused on acclimation-related changes in the stoichiometry of protein complexes

involved in primary photosynthetic reactions and on the consequences of these changes for the regulation of electron transport in thylakoid membranes. This approach allowed us to identify distinct strategies in the acclimation response in these two species. We suggest that these different strategies may generally represent light acclimation strategies of shade-tolerant and shade-intolerant species across the land plant kingdom.

Materials and methods

Plant material and acclimation conditions

Arabidopsis thaliana wild type (accession Columbia) and transgenic *A. thaliana* expressing *flvA* and *flvB* genes from *Physcomitrella patens* (Yamamoto et al. 2016) were pre-grown in a walk-in phytoscope (Photon Systems Instruments, Drásov, Czech Republic) at a light intensity of 100 µmol photons m^{-2} s^{-1} (with an 8-h light/16-h dark cycle), air temperature of 21 °C, 50% relative air humidity, and atmospheric CO_2 concentration. Norway spruce (*Picea abies* [L.] Karst.) was grown from seeds (Semenoles, Liptovský Hrádok, Slovakia) under the same conditions, but with a 16-h light/8-h dark cycle. Arabidopsis and spruce seedlings were grown in soil substrate Potgrond H (Klasmann-Deilmann GmbH, Geeste, Germany) in separated pots to avoid overlapping and shading of leaves/needles, and were regularly watered with drinking water. The seedlings were transferred (Arabidopsis after 32 days and spruce after 11 weeks) to three spatially homogeneous light intensities: low light (LL; 20 µmol photons m^{-2} s^{-1}), control normal light (NL; 100 µmol photons m^{-2} s^{-1}), and high light (HL; 800 µmol photons m^{-2} s^{-1}) inside the growth chamber HGC1014 (Weiss, Germany). All other cultivation conditions were kept the same as in the pre-cultivation phase. The illumination module of the HGC1014 growth chamber consisted of halogen lamps (POWERSTAR HQI-BT 400 W/D Daylight, Osram, Germany) and was shielded by a UV-absorbing filter (Lee 226 UV filter), which blocks UV radiation emitted from the halogen lamps. Plants exposed to each acclimation regime were kept in separate growth chambers for 10–14 days. After the light acclimation phase, fully developed Arabidopsis leaves and primary needles of spruce were used for all measurements.

Isolation of thylakoid membranes, estimation of Chl *a/b* and de-epoxidation state of xanthophyll cycle pigments

Thylakoid membranes were isolated from Arabidopsis leaves and spruce needles after 30 min of dark adaptation using the protocol described by Dau et al. (1995). All procedures were performed under dim green light on ice or at 4 °C. The chlorophyll content of the final thylakoid membrane suspension was determined spectrophotometrically (Unicam UV 500, Thermo Spectronics, UK) by a pigment extraction in 80% acetone (Lichtenthaler 1987). Thylakoid membrane suspensions were used for estimating the Chl *a/b* ratio and de-epoxidation state of xanthophyll cycle pigments [$DEPS_{dark} = (A + Z)/(V + A + Z)$, where V, A, and Z represent the concentrations of violaxanthin, antheraxanthin, and zeaxanthin, respectively]. The Chl *a/b* ratio was determined spectrophotometrically according to Lichtenthaler (1987). Quantification of xanthophyll cycle pigments was performed by reversed-phase high-performance liquid chromatography (HPLC) using Alliance e 2695 HPLC System (Waters, Milford, MA, USA). The separation was carried out using a gradient system (1.5 ml min^{-1} at 25 °C) on a LiChrospher 100 RP-18 (5 µm) LiChroCART 250-4 (Merck, Darmstadt, Germany) with acetonitrile:methanol:Tris (pH 8) (87:10:3; v/v) and methanol:*n*-hexane (80:20; v/v) as solvent systems. Quantification of the xanthophylls was based on a comparison of their absorbance (441, 446, and 454 nm for *V*, *A,* and *Z*, respectively) with corresponding standards purchased from DHI Lab Products (Hørsholm, Denmark).

Mass spectrometry analysis of thylakoid proteins

Thylakoid membranes from Arabidopsis leaves and spruce needles were subjected to filter-aided sample preparation as described in Wiśniewski et al. (2009). The resulting peptides were analyzed by liquid chromatography–tandem mass spectrometry (LC–MS/MS) performed using UltiMate 3000 RSLCnano system (Thermo Fisher Scientific) online coupled with an Orbitrap Elite hybrid spectrometer (Thermo Fisher Scientific). See Supplementary Information for full details regarding the analyses and data evaluation.

Low temperature (77 K) chlorophyll fluorescence spectra

Chl *a* fluorescence spectra of thylakoid membranes at 77 K were recorded using a Fluorolog 3–22 spectrofluorometer (Horiba Jobin Yvon, Paris, France) equipped with a Dewar-type optical cryostat as described by Dlouhý et al. (2021). Fluorescence spectra were measured on a freshly prepared suspension of thylakoid membranes in a 2 mm capillary tube. Chl content was adjusted to 5 µg ml^{-1} to avoid reabsorption. The emission spectra were recorded at the preferential excitation of Chl *b* at 475 nm with 3 and 2 nm slit widths of excitation and emission monochromators, respectively. The emission spectra were corrected for the spectral sensitivity of the detection system. The excitation spectra of PSII and PSI were detected at emission wavelengths 685 nm and 735 nm, respectively, with 2 and 3 nm slit widths of

the excitation and emission monochromators, respectively. The excitation spectra were automatically corrected for the output of the excitation source, the efficiency of the excitation monochromator, and the sensitivity of the reference photomultiplier.

Circular dichroism spectroscopy

Circular dichroism (CD) spectra were recorded in the range of 400–750 nm with a J-815 spectropolarimeter (Jasco, Tokyo, Japan) as described earlier (Karlický et al. 2016, 2021). The spectra were recorded in 0.5 nm steps with an integration time of 1 s, a 2 nm band-pass, and a scanning speed of 100 nm min^{-1}. CD spectra of freshly prepared thylakoid membranes were recorded in the cell with an optical path length of 1 cm. Thylakoid membranes were prepared by resuspending isolated membranes at a Chl content of 20 µg ml^{-1} in a medium containing 50 mM Tricine (pH 7.5), 0.4 M sorbitol, 5 mM KCl, and 5 mM $MgCl_2$.

Chlorophyll fluorescence and P700 redox state measurements

The function of PSII and PSI was simultaneously assessed using a Dual-PAM100 measuring system (Heinz Walz, Effeltrich, Germany). Plants were sampled no earlier than 2 h after the start of the light phase in the growth chamber and were dark adapted for 30 min prior to the measurement. First, minimal Chl fluorescence (F_0), maximal Chl fluorescence (F_M), maximum quantum yield of PSII photochemistry [$F_V/F_M = (F_M - F_0)/F_M$], and maximal level of $P700^+$ (P_M) were measured using 300 ms saturating red light (635 nm) pulses with an intensity of 10 000 µmol photons m^{-2} s^{-1} [after pre-illumination with far-red light (720 nm) for P_M determination]. Then, actinic red light (635 nm) with an intensity of 20, 100, 400, or 800 µmol photons m^{-2} s^{-1} was switched on and saturation light pulses were applied after 10 s, 30 s, 1 min, 2 min, and further in 1-min intervals. After 15 min of illumination, the actinic light was switched off and the recovery phase in darkness was monitored for 15 min using saturation light pulses at 1-min intervals. Blue measuring light (460 nm) and near infra-red dual-wavelength (830 and 875 nm) P700 measuring light were used for excitation of Chl fluorescence and measurement of $P700^+$ transmittance, respectively.

PSII function was assessed by non-photochemical quenching of F_M, $NPQ = (F_M - F_M')/F_M'$ (F_M' is maximal Chl fluorescence under illumination) (Bilger and Björkman 1990), non-photochemical quenching of F_0, $SV_0 = (F_0 - F_0')/F_0'$ (F_0' is minimal Chl fluorescence under illumination) (Gilmore and Yamamoto 1991), quantum yield of PSII photochemistry, $Y(II) = (F_M' - F)/F_M'$ (F is Chl fluorescence level induced by actinic light) (Genty et al. 1989), and the fraction of open PSII reaction centers, $qL = [(F_M' - F)/(F_M' - F_0')]\cdot(F_0'/F)$ (Kramer et al. 2004). The complementary PSI quantum yields were determined according to Klughammer and Schreiber (2008): quantum yield of PSI photochemistry [$Y(I) = (P_M' - P)/P_M$] (in analogy to Chl fluorescence levels, P and P_M' are $P700^+$ signals induced by actinic light and a saturation pulse with background actinic light, respectively), quantum yield of non-photochemical energy dissipation due to PSI donor side limitation [$Y(ND) = P/P_M$], and quantum yield of non-photochemical energy dissipation due to PSI acceptor side limitation [$Y(NA) = (P_M - P_M')/P_M$].

Thermoluminescence measurements

Thermoluminescence curves were measured with a Thermoluminescence TL 6000/ST (Photon Systems Instruments, Ltd, Drásov, Czech Republic). Thylakoid membrane suspension (400 µl, corresponding to 27.5 µg of Chl) in a buffer (50 mM HEPES, pH 7.2, 5 mM $MgCl_2$, 15 mM NaCl) was placed on a metallic disk and cooled from room temperature to 0 °C, followed by one single turnover flash prior to the measurement. The thermoluminescence curves were recorded while the sample was warmed up to 85 °C at a heating rate of 0.5 °C s^{-1}.

Data and statistical analysis

Spectroscopic data were processed and analyzed using MatLAB software (MathWorks, Natick, MA, USA) with implemented Spectr-O-Matic toolbox (Dr. Petar H. Lambrev, Szeged, Hungary), which is available at the MatLAB File Exchange and homebuilt routines. Before statistical analysis, the normality of data distribution and homogeneity of variances were checked using the Kolmogorov–Smirnov test and Levene's test, respectively, that were performed using Origin 8.6 (OriginLab, Northampton, USA). All data confirmed a normal distribution and for the data that did not meet the assumption of homogeneity of variances, logarithmic or power transformations were applied. Then one-, two-, or three-way ANOVA (level of significance $p < 0.05$) was applied to analyze statistical differences. Tukey's post hoc tests were used to identify those means with significant differences. ANOVA and Tukey's post hoc tests were performed using MatLAB (MathWorks, Natick, MA, USA). The values presented in figures are means ± standard deviations (S.D.). The numbers of samples, from which the means were calculated, are 20 for F_0, F_M, and F_V/F_M and 3–5 for other characteristics (see figure captions).

Results

Light acclimation of spruce is characterized by unusually low plasticity of its electron transport protein complexes

In Arabidopsis, we observed a typical light acclimation response previously described for higher plants (e.g., Anderson 1986; Anderson et al. 1988; Ballottari et al. 2007; Kouřil et al. 2013). With increasing acclimation light intensity there was a corresponding increase in the Chl *a/b* ratio (Fig. 1a), as well as an increase in the relative abundance of PSII, cytochrome *f* (Cyt *f*), and ATP synthase compared to PSI (Fig. 1b, e, and f). The peripheral light-harvesting system of PSII (LHCII) was reduced with increasing acclimation light intensity (higher PSII/LHCII ratio, Fig. 1c), which results mainly from decreased relative abundances of LHCB1, LHCB2, and LHCB3 antenna proteins—the building blocks of trimeric LHCIIs (Fig. S1a). Contrary to PSII, the relative extent of the PSI antenna system did not change in response to light acclimation (Figs. 1d and S2a), which was expected as LHCI (LHCA1–4) is strongly bound to the PSI core and the PSI-LHCI complex usually behaves as a single unit (Ballottari et al. 2007).

Surprisingly, spruce seedlings showed much lower plasticity of electron transport protein complexes. We found virtually no effect of light acclimation on the Chl *a/b*, PSII/PSI, and Cyt *f*/PSI ratios (Fig. 1a, b, and e). However, after HL acclimation we observed about a 30% decrease in the PSII/LHCII ratio, an opposite trend to what was found in Arabidopsis (Fig. 1c). The composition of the PSII core in spruce was not affected by HL acclimation (Fig. S1b). Thus,

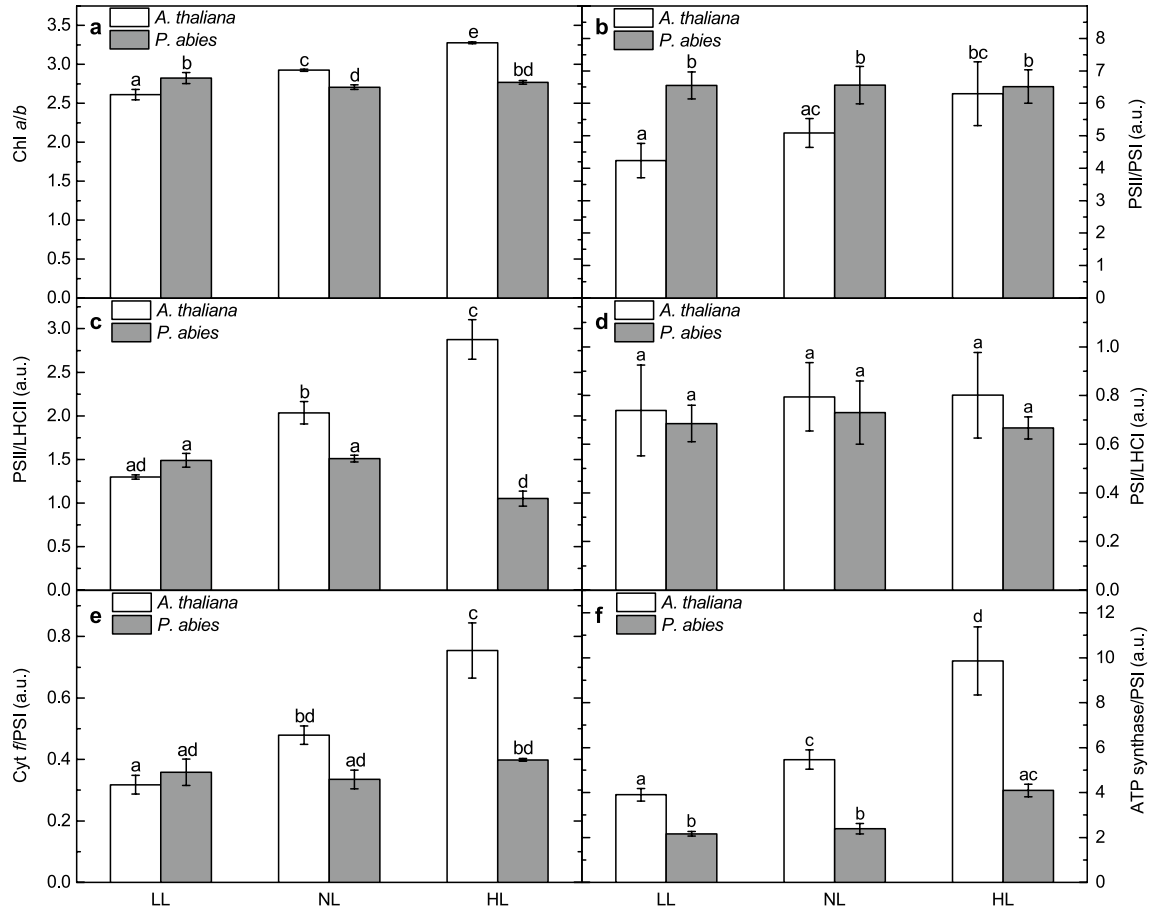

Fig. 1 Chl *a/b* ratios and relative amounts of electron transport protein complexes and ATP synthase in light-acclimated Arabidopsis (*A. thaliana*) and spruce (*P. abies*). **a** Chl *a/b*, **b** PSII/PSI, **c** PSII/LHCII, **d** PSI/LHCI, **e** Cyt *f*/PSI, **f** ATP synthase/PSI ratios for low-light-acclimated (LL), non-acclimated (NL), and high-light-acclimated (HL) Arabidopsis and spruce. The relative content of protein complexes (proteins) was determined by mass spectrometry; *PSII* represents the sum of relative PG intensities of D1, D2, CP43, and CP47 proteins, *LHCII* LHCB1–3 proteins, *PSI* PSAA and PSAB proteins, *LHCI* LHCA1–4 proteins, *ATP synthase* α and β subunits of CF_1. The presented values are means ± S.D. from five replicates for Chl *a/b* and from four replicates for other ratios. Different letters represent statistically significant differences ($p < 0.05$, two-way ANOVA followed by Tukey's post hoc test)

the simplest explanation of the decrease in PSII/LHCII, although physiologically difficult to interpret, would be an increase in the abundance of LHCB1 and LHCB2 proteins. However, this is largely contradicted by the unchanged Chl *a/b* ratio at HL (2.77), as the preferential synthesis of trimeric LHCII (which have Chl *a/b* ~ 1.3, see, e.g., Su et al. 2017) would lower the Chl *a/b* ratio. The observed phenomenon can be explained only by a proportional degradation of both PSII and PSI-LHCI, accompanied by storage of released chlorophylls. This explanation would justify the lower PSII/LHCII and unchanged PSII/PSI and Chl *a/b* ratios in HL spruce.

To test the possibility of the retention of released chlorophylls, we analyzed the level of stress proteins called ELIPs (Early Light-Induced Proteins), which are able to bind free chlorophylls and protect them against oxidation within the thylakoid membrane (Adamska et al. 2001; Hutin et al. 2003). Indeed, in HL-acclimated spruce, we observed a dramatic increase in ELIPs, whereas in all Arabidopsis samples as well as in LL- and NL-acclimated spruce, the ELIPs were very close to (or even below) the mass spectrometry (MS) detection limit (Fig. 2a). Aside from ELIPs, two other protein groups have been suggested to have possible roles in the binding of released chlorophylls in the thylakoid membrane—OHPs (One Helix Proteins) and LIL3s (LHC-like 3 proteins) (Rochaix and Bassi 2019). The relative abundance of these proteins also increased in spruce with increasing acclimation light intensity, although the changes were much less pronounced than in the case of ELIPs (Fig. 2b, c).

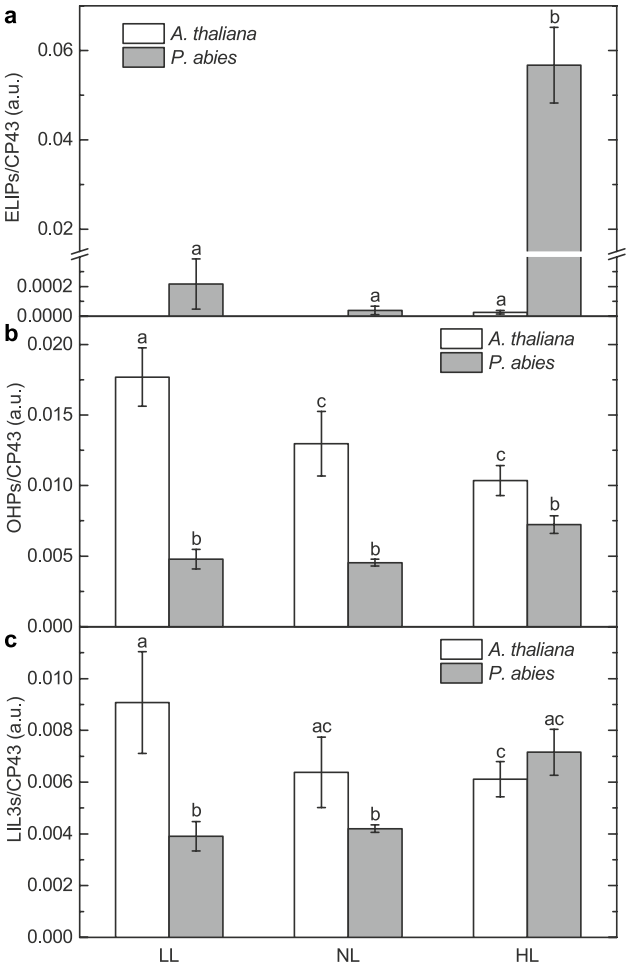

Fig. 2 Relative amounts of stress-induced proteins in light-acclimated Arabidopsis (*A. thaliana*) and spruce (*P. abies*). **a** ELIPs/CP43, **b** OHPs/CP43, **c** LIL3s/CP43 for low-light-acclimated (LL), non-acclimated (NL), and high-light-acclimated (HL) Arabidopsis and spruce. Relative amounts of proteins were calculated as a ratio of relative PG intensities for the proteins from MS analysis. ELIPs contents in LL and NL Arabidopsis were below the detection limit. The presented values are means ± S.D. from four replicates. Different letters represent statistically significant differences ($p < 0.05$, two-way ANOVA followed by Tukey's post hoc test)

PSII photochemistry is considerably downregulated in HL-acclimated spruce due to "locked-in" NPQ

In Arabidopsis grown at NL conditions, the maximum quantum yield of PSII photochemistry (F_V/F_M) was 0.82 (Fig. 3a), which is a typical value for non-stressed plants (Björkman and Demmig 1987). The LL acclimation of Arabidopsis led to a small decrease of F_V/F_M (0.78), which is consistent with data from Ware et al. (2015). After HL acclimation, the F_V/F_M value was 0.8, which implies that the acclimation strategy of Arabidopsis ensured successful adjustment of the PSII function to HL conditions.

In spruce, however, HL acclimation resulted in a significant decrease in F_V/F_M, as its value dropped from 0.79 in LL and NL plants to only 0.53 in HL plants (Fig. 3a). A similar effect was observed in our previous studies with 1-year-old needles of 5-year-old spruce acclimated to very high light intensities (≥ 1000 µmol photons m^{-2} s^{-1}) (Kurasová et al. 2003; Štroch et al. 2008). Figure 3b shows that in HL spruce, the increase in the F_0 level, reflecting a disconnection of LHCII antenna from PSII core (e.g., Ware et al. 2015), played a minor role in this phenomenon, and that the drop of F_V/F_M was caused mainly by the decrease of the F_M level.

The pronounced decrease of F_M during HL acclimation was shown to be associated with the induction of "locked-in" NPQ in some representatives of evergreen angiosperms (e.g., Demmig-Adams et al. 2006, 2014). This type of NPQ appeared to be connected with the retention of de-epoxidized xanthophylls and PSBS protein (for a review, see Demmig-Adams et al. 2012, 2014). To test whether the HL-induced decrease of F_M in spruce could also be a result of such "locked-in" NPQ, we determined the de-epoxidation state of xanthophylls ($DEPS_{dark}$) and PSBS content.

As expected, $DEPS_{dark}$ in Arabidopsis was found to be zero for LL and NL plants and about 13% for HL plants (due to the *A*; *Z* was absent). In spruce, $DEPS_{dark}$ was

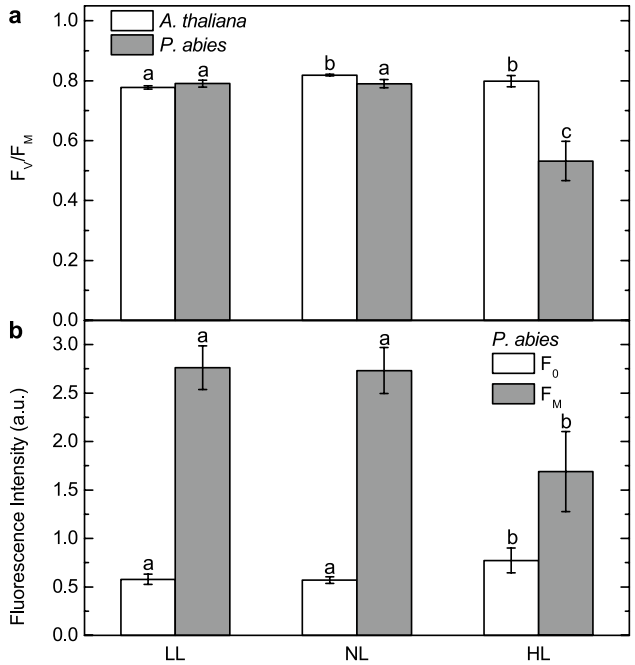

Fig. 3 Maximum quantum yield of PSII photochemistry (F_V/F_M) in light-acclimated Arabidopsis (*A. thaliana*) and spruce (*P. abies*). **a** F_V/F_M ratio and **b** minimal (F_0) and maximal (F_M) Chl fluorescence levels for low-light-acclimated (LL), non-acclimated (NL), and high-light-acclimated (HL) Arabidopsis and spruce. Measurements were performed with seedlings dark adapted for 30 min. The presented values are means ± S.D. from 20 replicates. Different letters represent statistically significant differences ($p < 0.05$, two-way ANOVA followed by Tukey's post hoc test). F_0 and F_M mean values (panel **b**) were analyzed separately

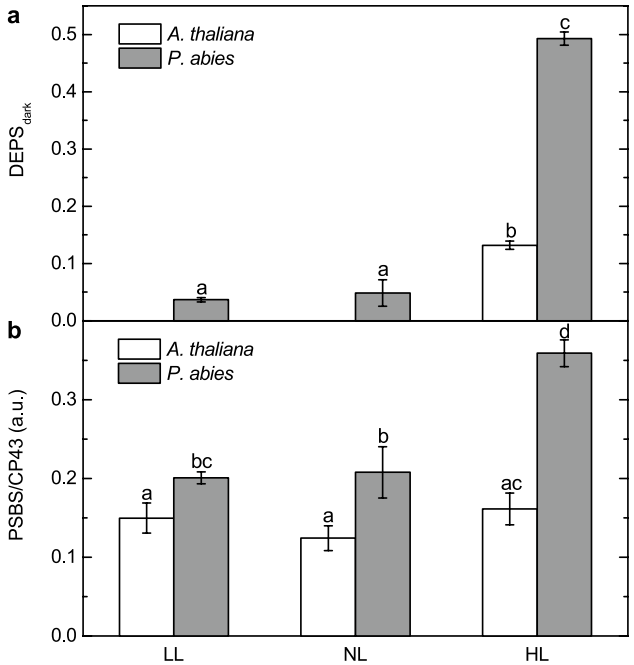

Fig. 4 De-epoxidation state of xanthophyll cycle pigments (DEPS) and relative amount of PSBS protein in light-acclimated Arabidopsis (*A. thaliana*) and spruce (*P. abies*). **a** $DEPS_{dark}$ determined in the thylakoid membranes isolated after 30-min dark adaptation of the seedlings (mean ± S.D., $n = 5$) and **b** the relative content of PSBS protein (PSBS/CP43) (mean ± S.D., $n = 4$). Measurements were performed for low-light-acclimated (LL), non-acclimated (NL), and high-light-acclimated (HL) Arabidopsis and spruce. DEPS is equal to $(A + Z)/(V + A + Z)$, where V, A, and Z represent the concentrations of violaxanthin, antheraxanthin, and zeaxanthin, respectively. PSBS amount was calculated as a ratio of relative PG intensities of the proteins from MS analysis. Different letters represent statistically significant differences ($p < 0.05$, two-way ANOVA followed by Tukey's post hoc test)

above zero even for LL and NL plants (4–5%, due to the A; Z was absent) and in HL plants it reached a very pronounced level, about 50% [$Z/(V + A + Z) = 0.22 \pm 0.01$; $A/(V + A + Z) = 0.27 \pm 0.01$] (Fig. 4a). The relative amount of PSBS (PSBS/CP43) in HL spruce was more than 70% higher compared to LL and NL plants, whereas in Arabidopsis the level of PSBS was not affected by light acclimation (Fig. 4b). These data indicate that HL acclimation of spruce shares common features with HL acclimation of angiosperm evergreens (Demmig-Adams and Adams 2006; Demmig-Adams et al. 2006) and that indeed, the "locked-in" NPQ appears to be operational in HL-acclimated spruce.

Absorption cross section of PSII in spruce is not affected by light acclimation

The slight increase in F_0 level observed in HL spruce (Fig. 3b) suggests that some of the LHCII antennae might be weakly bound to PSII. The possible partial disconnection of LHCII was further analyzed using the measurement of 77 K steady-state Chl *a* fluorescence emission spectra, which can detect the presence of uncoupled LHCII as the emission peaking at 680 nm (Belgio et al. 2012). The emission spectra of thylakoid membranes show three typical bands (Fig. 5a). Two of them are attributed to the emission from PSII (at wavelengths of 685 and 695 nm, i.e., F685 and F695) and one to emission from PSI (at 735 nm, i.e., F735) (van Grondelle et al. 1994). The emission from PSII in Arabidopsis is dominated by the F685 band, whereas in spruce by the F695 band. This phenomenon has been observed previously (Weis 1985; Karlický et al. 2016), but its origin or physiological significance has yet to be elucidated.

Light acclimation led to changes in the emission bands F680 and F700, which are known to be related to emission from free and aggregated forms of LHCII, respectively (e.g., Miloslavina et al. 2008; Chmeliov et al. 2016; Ostroumov et al. 2020). The HL–NL difference spectra clearly showed that in HL spruce, the relative intensities of F680 and F700 bands were significantly higher than in HL Arabidopsis (Fig. 5a, insets). Thus, in HL spruce, a larger fraction of LHCII had only a weak connection to the PSII core antenna,

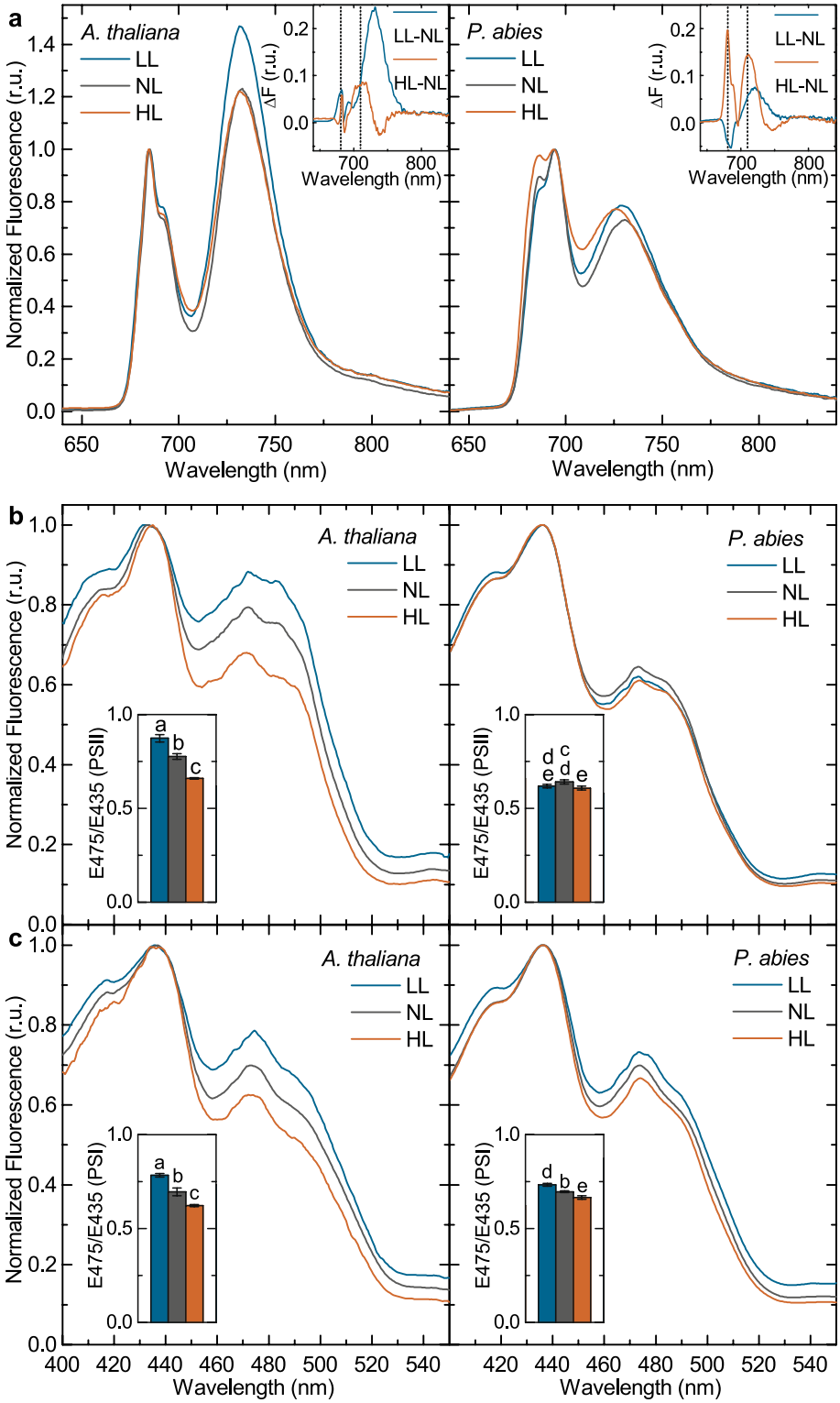

Fig. 5 Low-temperature Chl fluorescence spectra in light-acclimated Arabidopsis (*A. thaliana*) and spruce (*P. abies*). **a** Normalized 77 K fluorescence emission spectra, **b** excitation spectra of PSII, and **c** excitation spectra of PSI measured in thylakoid membranes isolated from low-light-acclimated (LL), non-acclimated (NL), and high-light-acclimated (HL) Arabidopsis and spruce. Emission spectra were collected at excitation wavelength of 475 nm; excitation spectra were detected at wavelength of 685 nm and 735 nm for PSII and PSI, respectively. Average spectra from three to five replicates are presented. Insets in **a** show HL–NL and LL–NL difference spectra calculated from emission spectra in corresponding panels; the dotted lines highlight the wavelengths of 680 nm (F680) and 707 nm (F700). Insets in **b** and **c** show fluorescence excitation ratios E475/E435 determined from excitation spectra in corresponding panels. The presented values in insets are means ± S.D. from three to five replicates. Different letters in insets of panels **b** and **c** represent statistically significant differences ($p < 0.05$, two-way ANOVA followed by Tukey's post hoc test)

which is consistent with a higher F_0 level (Fig. 3b). The enhanced F700 emission band for HL-acclimated spruce indicates that a part of LHCIIs form aggregates. The LL–NL difference spectra for spruce showed a negative peak at 680 nm, implying that NL spruce had more LHCIIs weakly bound to PSII than in LL spruce. In Arabidopsis, the situation is the opposite, as the LL–NL difference spectrum showed a positive peak at 680 nm. This indicates that LL

acclimation of Arabidopsis led to the appearance of weakly bound LHCIIs, which is in agreement with a slight decrease in F_V/F_M in LL plants (Fig. 3a).

Analysis of the 77 K excitation spectra allowed us to examine the changes in the absorption cross sections of both photosystems. The changes in energy transfer from LHCIIs to PSII and PSI can be evaluated from the relative changes in excitation bands corresponding to Chl *b* and carotenoids (E475/E435) for emission wavelengths typical for PSII (685 nm) and PSI (735 nm) (Tikkanen et al. 2008; Jajoo et al. 2014). In Arabidopsis, the E475/E435 ratio for PSII emission gradually decreased with increasing acclimation light intensity (Fig. 5b), which corresponds with a reduction of PSII antenna (increase in PSII/LHCII ratio, Fig. 1c). Interestingly, no such changes were observed in the PSII excitation spectrum of spruce, indicating that the PSII absorption cross section remained the same in spruce during all light acclimation regimes. The PSII absorption cross section in spruce was kept notably low (Fig. 5b), much lower than for LL Arabidopsis, which had a comparably large LHCII antenna (similar PSII/LHCII, Fig. 1c). This indicates that in spruce, a substantial part of this large LHCII was weakly bound to PSII. A population of partially disconnected LHCII was present also in LL Arabidopsis (Fig. 5a, inset); however, in spruce the fraction of loosely bound LHCII appears to be much larger. The absorption cross section of PSI in Arabidopsis decreased with increasing acclimation light intensity, as in the case of the absorption cross section of PSII (Fig. 5c), although its decrease was smaller. This decreasing absorption cross section thus coincides with the decreasing amount of LHCIIs (Fig. 1c) that can partially transfer excitation energy to PSI (Chukhutsina et al. 2020; Croce 2020). On the other hand, in spruce, the absorption cross section of PSI was found to be much more stable under different acclimation light intensities, which reflects the fact that the amount of LHCIIs in spruce did not significantly change.

PSII–LHCII macro-organization is lost in HL-acclimated spruce

Circular dichroism (CD) spectroscopy of thylakoid membranes provides information on the chiral macro-organization of PSII–LHCII, which is connected to the appearance of intensive Ψ-type CD bands (+)685, (−)673, and (+)505 nm (Barzda et al. 1994; Dobrikova et al. 2003). The intensity of positive (+) bands depends on the LHCII content and carries information mainly about the long-distance lateral macro-organization of PSII–LHCII supercomplexes (Kovács et al. 2006; Tóth et al. 2016), whereas the negative (−)673 nm band reflects mostly the degree of grana stacking (Garab et al. 1991).

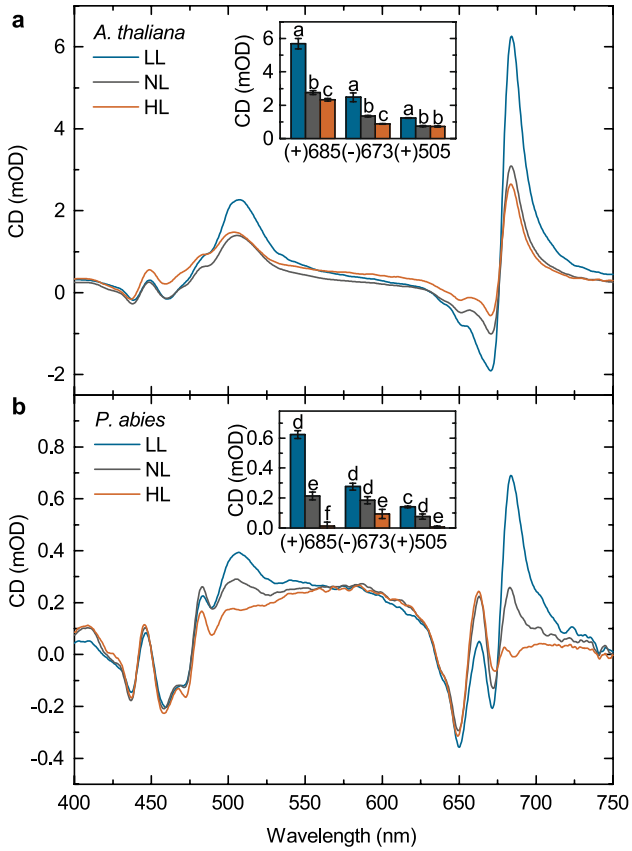

Fig. 6 Circular dichroism (CD) spectra in light-acclimated Arabidopsis (*A. thaliana*) and spruce (*P. abies*). Room temperature CD spectra for **a** Arabidopsis and **b** spruce measured in thylakoid membranes isolated from low-light-acclimated (LL), non-acclimated (NL), and high-light-acclimated (HL) plants. Spectra are normalized to the Q_y absorbance maximum. Averaged spectra from three to five replicates are presented. Insets show amplitudes of Ψ-type CD bands at around (+)685 nm, (−)673 nm, and (+)505 nm with reference wavelengths at 730 nm or 550 nm. The presented values in insets are means ± S.D. from three to five replicates. Different letters in insets represent statistically significant differences ($p < 0.05$, two-way ANOVA followed by Tukey's post hoc test)

In Arabidopsis, the height of all the Ψ-type CD bands decreased with increasing acclimation light intensity (Fig. 6a), which corresponds with the decrease in the relative amount of LHCII (Fig. 1c). In spruce, the extent of PSII–LHCII macro-organization was much smaller than in Arabidopsis, as indicated by approximately ten times lower amplitudes of the Ψ-type CD bands (compare Fig. 6a, b). This result is consistent with our previous study (Karlický et al. 2016), where we hypothesized that the smaller macrodomains of PSII–LHCII in spruce, leading to smaller Ψ-type CD bands, could be the result of different PSII supercomplex structure (Kouřil et al. 2016). Although the MS data suggest

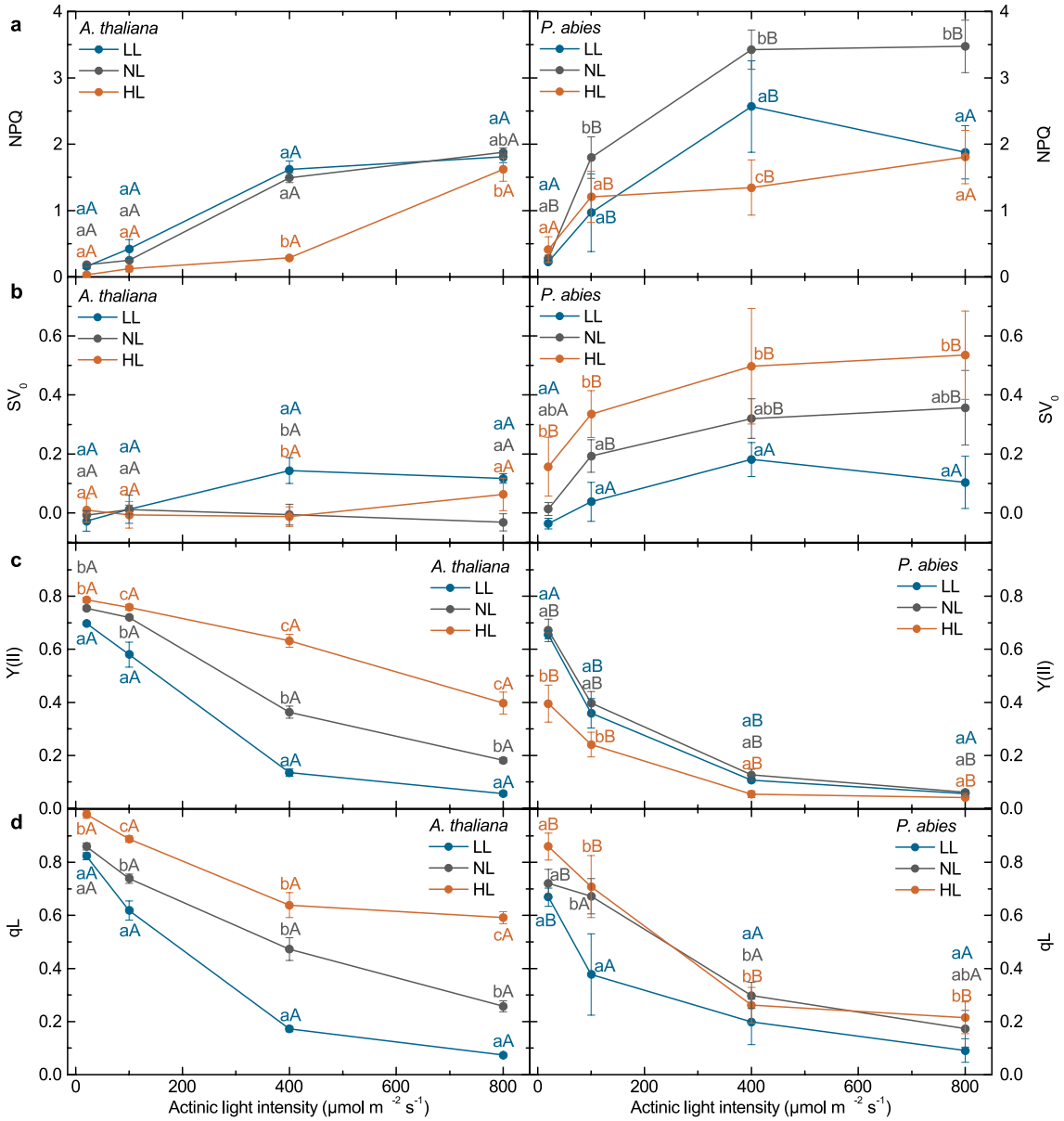

Fig. 7 Steady-state PSII parameters after exposure of light-acclimated Arabidopsis (*A. thaliana*) and spruce (*P. abies*) to different light intensities. **a** Non-photochemical quenching of maximal Chl fluorescence F_M (NPQ), **b** non-photochemical quenching of minimal Chl fluorescence F_0 (SV_0), **c** quantum yield of PSII photochemistry [Y(II)], and **d** the fraction of open PSII reaction centers (qL) for low-light-acclimated (LL), non-acclimated (NL), and high-light-acclimated (HL) Arabidopsis and spruce. Parameters were determined after 15-min exposure to different light intensities (20, 100, 400, and 800 µmol photons m^{-2} s^{-1}). The presented values are means ± S.D. from four to five replicates. The different lowercase letters represent statistically significant differences between light acclimation regimes for the same plant species and the same actinic light intensity, whereas the different uppercase letters represent differences between plant species for the same light acclimation intensity and the same actinic light intensity ($p < 0.05$, three-way ANOVA followed by Tukey's post hoc test)

that LL acclimation of spruce did not lead to significant changes in the protein composition of its Chl-containing complexes (Fig. 1), their macro-organization was increased compared to NL (Fig. 6b). In HL-acclimated spruce, by contrast, the macrodomain organization was almost completely lost. This finding is probably associated with the weakening of PSII–LHCII interaction, as indicated by the increases in F680 emission at 77 K (Fig. 5a) and in F_0 (Fig. 3b).

A pronounced non-photochemical quenching in spruce

To assess the functional consequences of the different photosynthetic complex structural adjustments observed in HL- and LL-acclimated spruce and Arabidopsis, we analyzed Chl fluorescence kinetics and P700 redox state at various intensities of actinic light and subsequent dark recovery (Figs. 7, 8, and S3–S6). The key photoprotective regulatory mechanism that prevents the overexcitation of PSII reaction centers is light-induced thermal dissipation of absorbed light energy, which can be monitored as non-photochemical Chl fluorescence quenching of F_M (i.e., the NPQ parameter) (Bilger and Björkman 1990).

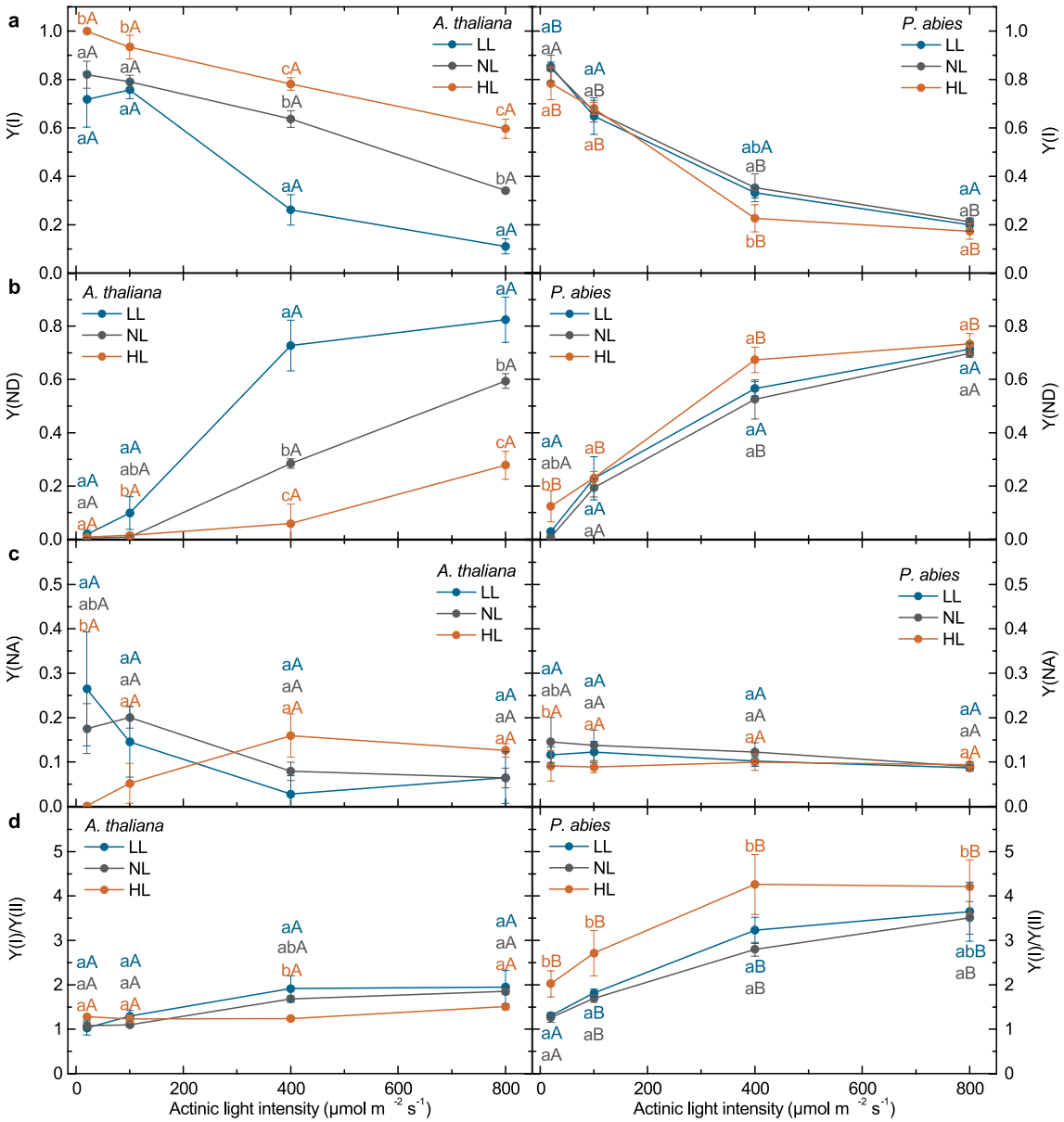

Fig. 8 Steady-state PSI parameters after exposure of light-acclimated Arabidopsis (*A. thaliana*) and spruce (*P. abies*) to different light intensities. **a** Quantum yield of PSI photochemistry [Y(I)], **b** quantum yield of non-photochemical energy dissipation due to PSI donor side limitation [Y(ND)], **c** PSI acceptor side limitation [Y(NA)], and **d** the ratio of quantum yield of PSI photochemistry to quantum yield of PSII photochemistry [Y(I)/Y(II)] for low-light-acclimated (LL), non-acclimated (NL), and high-light-acclimated (HL) Arabidopsis and spruce. Parameters were determined after 15-min exposure to different light intensities (20, 100, 400, and 800 µmol photons m^{-2} s^{-1}). The presented values are means ± S.D. from four to five replicates. The different lowercase letters represent statistically significant differences between light acclimation regimes for the same plant species and the same actinic light intensity, whereas the different uppercase letters represent differences between plant species for the same light acclimation intensity and the same actinic light intensity ($p < 0.05$, three-way ANOVA followed by Tukey's post hoc test)

As expected, in all acclimation variants of Arabidopsis, the steady-state level of NPQ increased with increasing intensity of actinic light (Fig. 7a). The actinic light intensity profile of NPQ was very similar for LL and NL plants, whereas in HL Arabidopsis the substantial NPQ was induced at the highest used actinic light intensity (800 µmol photons m^{-2} s^{-1}). In spruce, we observed overall higher NPQ compared to Arabidopsis. For example, the actinic light intensity corresponding to NL (100 µmol photons m^{-2} s^{-1}) induced 7 times higher NPQ level in NL spruce than in NL Arabidopsis (Fig. 7a). The unexpectedly low level of NPQ detected for HL spruce (lower than for NL spruce) is associated with the previously described pre-existing "locked-in" NPQ. As this NPQ is active already in dark-adapted spruce, it lowers the measurable value of F_V/F_M (Fig. 3a), which in turn leads to the underestimation of the real NPQ level. The measured NPQ parameter reflects only the non-photochemical quenching that is induced by the actinic light and does not reflect the dark level of NPQ in HL spruce.

As mentioned above, the results of the measurement of the F_0 level (Fig. 3b) and 77 K emission spectra (Fig. 5a) suggest that there were loosely bound LHCIIs in HL spruce. It is known that weakly bound LHCIIs can form aggregates that are strongly quenched, which often leads to F_0 quenching and slow relaxation of NPQ in the subsequent dark period (see, e.g., Belgio et al. 2012; Ware et al. 2015). Therefore, we evaluated non-photochemical quenching of the F_0 level using the parameter SV_0 (Gilmore and Yamamoto 1991), which can be used for the estimation of the light-induced non-photochemical quenching localized in the weakly bound LHCIIs (Belgio et al. 2012; Karlický et al. 2021).

In Arabidopsis, the induction of SV_0 was very low and appeared significantly only in LL plants at higher actinic light intensities (400 and 800 µmol photons m^{-2} s^{-1}) (Fig. 7b). This corresponds with the appearance of LHCIIs loosely coupled to PSII (see LL–NL difference spectrum in Fig. 5a, inset). In spruce, we observed much higher SV_0 values. In LL spruce, the actinic light intensity profile of SV_0 was similar to LL Arabidopsis (Fig. 7b), which may indicate that these plants have a roughly similar amount of LHCII loosely coupled to PSII core. For NL and especially HL spruce, however, the SV_0 values were found to be much higher. This corresponds to a higher amount of loosely bound LHCII, which agrees with 77 K difference emission spectra (Fig. 5a) and weaker PSII–LHCII macroorganization (Fig. 6b).

A pronounced "photosynthetic control" in spruce

As the photochemical activity of PSII and electron transport in thylakoid membranes are the most important factors affecting the induction of NPQ, it was necessary to analyze them in detail to correctly interpret the differences in spruce and Arabidopsis acclimation strategy. We evaluated the steady-state values of Chl fluorescence parameters Y(II) and qL, which reflect the actual quantum yield of PSII photochemistry and a fraction of open PSII reaction centers, respectively (Genty et al. 1989; Kramer et al. 2004) (Fig. 7c, d).

In spruce, Y(II) decreased with increasing actinic light intensity more steeply than in Arabidopsis (Fig. 7c), which corresponds with a pronounced induction of NPQ (Fig. 7a). The seeming exception is HL spruce, where the measured NPQ is, however, strongly underestimated due to the pre-existing "locked-in" NPQ in the dark (see above). At higher actinic light intensities, PSII photochemistry in spruce is thus downregulated due to high NPQ, which should keep PSII reaction centers more open. Nevertheless, qL values were very low also for NL and HL spruce at higher intensities of actinic light.

To understand why PSII reaction centers in spruce were closed despite the strong NPQ, we decided to analyze the redox state of PSI (Figs. 8 and S3–S6). We determined PSI-related complementary quantum yields, i.e., the quantum yield of PSI photochemistry Y(I), non-photochemical energy dissipation due to PSI donor side limitation Y(ND), and acceptor side limitation Y(NA). For all acclimation variants of Arabidopsis, the actinic light intensity profiles of Y(I) (Fig. 8a) were similar to those of Y(II) (Fig. 7c). Furthermore, the decrease of Y(I), irrespective of the acclimation variant, was always connected with the increase in Y(ND), i.e., with the limitation in electron transport at the donor side of PSI (Fig. 8b). It is not surprising, as at higher actinic light intensities the concomitant higher lumen acidification activates the so-called "photosynthetic control," i.e., the slowing down of electron transport on the level of Cyt b_6f complex (for a recent comprehensive study, see Yamamoto and Shikanai 2019). Activation of photosynthetic control leads to a higher reduction of the plastoquinone (PQ) pool, which in turn lowers Y(II). In Arabidopsis, photosynthetic control was pronounced in the LL variant (Fig. 8b), which probably reflects its large LHCII antenna system (Fig. 1c) and consequent high excitation pressure in PSII reaction centers (Fig. 7d). On the other hand, in HL Arabidopsis, photosynthetic control was low, which can be an indication that the generation of the trans-thylakoid proton gradient by photosynthetic electron transport and its utilization by ATP synthase were optimized and thus well balanced.

In NL and HL spruce, Y(I) decreased more steeply with increasing actinic light intensity than the corresponding Arabidopsis acclimation variants (Fig. 8a). Similarly to Arabidopsis, the decrease in Y(I) can be entirely ascribed to an increase in Y(ND) (Fig. 8b), which implies that in

spruce the photosynthetic control is much more pronounced than in Arabidopsis. In spruce, the Y(I)/Y(II) ratio progressively increased with the increasing intensity of actinic light, reaching the values 3–4 (Fig. 8d). Such high ratios indicate highly imbalanced photochemistry of both photosystems and the involvement of cyclic electron transport around PSI (CET), which may increase lumen acidification to the level that causes both pronounced photosynthetic control and induction of high NPQ.

Very fast induction and slow relaxation of NPQ in HL-acclimated spruce

The kinetics of PSII and PSI parameters during exposure to actinic light and a subsequent dark period revealed further details on the regulation of NPQ and electron transport (Figs. S3–S6). For actinic light intensities ≥ 400 µmol photons m^{-2} s^{-1}, the induction of NPQ in LL and NL Arabidopsis was rather monotonic (i.e., without a peak), as a result of actinic light intensity exceeding the acclimation light intensity. In LL Arabidopsis, the induction as well as relaxation of NPQ was slower compared to NL. The slow recovery of NPQ together with its elevated steady-state level in the dark period indicate a partial formation of "locked-in" quenching centers. This finding coincides with the existence of loosely bound LHCIIs (Fig. 5a) and the induction of relatively high SV_0 in LL Arabidopsis (Fig. 7b). On the other hand, the induction of NPQ in HL Arabidopsis for the intensities ≥ 400 µmol photons m^{-2} s^{-1} was biphasic, with a peak at the initial phase of induction when the photosynthetic control was relatively high [low Y(II), Y(I), and high Y(ND)]. The subsequent NPQ decay phase in the light period most probably reflects a decrease in lumen acidity (and thus also a decrease in photosynthetic control) due to the high activity of ATP synthase (Fig. 1f).

In LL and NL spruce, the kinetics of NPQ induction for actinic light intensities ≥ 400 µmol photons m^{-2} s^{-1} was also monotonic and relatively slow, similar to LL Arabidopsis. In HL spruce, however, the NPQ induction kinetics was very fast, reaching the saturation within the first minute. The relaxation kinetics of NPQ in the dark was relatively slow for all acclimation variants, again comparable to LL Arabidopsis. In all acclimation variants of spruce, PSI parameters as well as Y(II) were also similar to those for LL Arabidopsis. The difference was found in the first two minutes of induction. While in LL Arabidopsis, the establishment of photosynthetic control took 1–2 min, in spruce it required less than 10 s (Figs. S3e and S4e). This phenomenon is probably associated with the activity of pseudocyclic electron transport to molecular oxygen, mediated by the flavodiiron enzyme. This pathway is operational in all non-flowering plants on the acceptor side of PSI within a second after the onset of light (Ilík et al. 2017). This alternative electron transport chain contributes to rapid acidification of the thylakoid lumen and thus is probably responsible for the very fast establishment of photosynthetic control (Yamamoto et al. 2016; Yamamoto and Shikanai 2019). It is also of note that the fast lumen acidification in spruce due to the flavodiiron-dependent pathway may be involved in the very fast induction of NPQ in HL spruce.

To find out whether the flavodiiron-dependent pathway could participate in the unusually high steady-state Y(I)/Y(II) ratio observed in spruce (Fig. 8d), we performed the measurements of the PSII and PSI parameters in transgenic Arabidopsis with flavodiiron enzyme from *Physcomitrella patens* (Yamamoto et al. 2016) (Fig. S7). The results showed that although the flavodiiron enzyme can indeed significantly speed up the establishment of photosynthetic control, it did not affect the steady-state Y(I)/Y(II) ratio in Arabidopsis. It thus seems likely that in spruce, the steady-state Y(I)/Y(II) ratio was not affected by the flavodiiron-dependent pathway and the most probable explanation of high Y(I)/Y(II) ratios is the high activity of CET.

Discussion

Acclimation of spruce to different light intensities does not modulate LHCII antenna size

Acclimation of the photosynthetic apparatus of Arabidopsis plants to different light intensities proceeded via mechanisms considered typical for higher plants. The acclimation involved modulation of the amount of LHCII trimers, which is directly reflected by changes in Chl *a/b* ratio (Fig. 1a) (Bailey et al. 2001; Ballottari et al. 2007; Kouřil et al. 2013; Wientjes et al. 2013b; Bielczynski et al. 2016).

LL acclimation of Arabidopsis led to an almost 40% decrease in the PSII/LHCII ratio (Fig. 1c), which is a result of two simultaneous processes—enlargement of LHCII due to upregulation of LHCB1, LHCB2, and LHCB3 proteins (Fig. S1a), and reduction of the number of PSII core complexes (decrease in the PSII/PSI ratio, Fig. 1b) (Ballottari et al. 2007; Kouřil et al. 2013). Under NL conditions, the dominant form of PSII supercomplexes is $C_2S_2M_2$, which binds four LHCII trimers. An increase in the number of LHCII trimers under LL conditions increases the pool of trimers, which are loosely bound to the PSII–LHCII supercomplexes. These weakly bound LHCIIs are functionally connected to PSII and they provide excitation energy to the reaction center, which increases the light-harvesting capacity. However, as the transfer of excitation energy from these trimers to PSII is slower than from the more tightly attached S or M trimers (Wientjes et al. 2013b), the presence of weakly bound LHCIIs simultaneously lowers the quantum yield of PSII photochemistry. In agreement with

this, LL-acclimated Arabidopsis had lower F_V/F_M (Fig. 3a; Wientjes et al. 2013b; Ware et al. 2015), a parameter used for the approximation of the quantum efficiency of PSII photochemistry (Baker 2008). Due to the presence of these two counteracting effects (better light-harvesting and lower PSII photochemical yield), there appears to be an upper limit of the amount of LHCII that is still advantageous and that leads to a maximally effective light harvesting. Any further increase in LHCII content would not substantially improve the light-harvesting function (Wientjes et al. 2013b).

Acclimation of Arabidopsis to HL conditions induced an inverse response to what was observed for LL acclimation. In HL Arabidopsis, the relative extent of LHCII antenna was lowered by more than 50% compared to LL Arabidopsis (Fig. 1c). This results from a combination of at least three processes—downregulation of the LHCB proteins forming the L and M trimers, downregulation of the monomeric antenna protein LHCB6, and an increase in the PSII/PSI ratio (Figs. 1b and S1a; Ballottari et al. 2007; Kouřil et al. 2013; Wientjes et al. 2013b; Bielczynski et al. 2016). In addition, HL acclimation was found to upregulate the LHCB4.3 protein, which is thought to partially replace the other two protein isoforms LHCB4.1/4.2 that are present in the PSII–LHCII supercomplex under NL and LL conditions (Floris et al. 2013; Albanese et al. 2016, 2018). All these regulatory mechanisms lead to a greater abundance of smaller forms of the PSII–LHCII supercomplexes (C_2S_2M, C_2S_2) upon HL acclimation (Kouřil et al. 2013; Albanese et al. 2016, 2018).

The acclimation strategy of Norway spruce seedlings appears to be noticeably different. Our MS analysis indicates that in spruce, both the protein composition and the relative amount of LHCII per PSII did not significantly change during acclimation to different light conditions. This fact is reflected in the stable value of the Chl *a/b* ratio (Fig. 1), a phenomenon described in our previous studies on HL-acclimated spruce saplings (Kurasová et al. 2003; Štroch et al. 2008). The hypothesis that the light intensity used in our HL conditions (i.e., 800 µmol photons m^{-2} s^{-1}) is insufficient to induce Chl *a/b* increase can be ruled out on the basis of the fact that no change in Chl *a/b* was observed even in 1-year-old spruce needles acclimated to 1200 µmol photons m^{-2} s^{-1} (Kurasová et al. 2003).

The size of the LHCII antenna in spruce was considerably larger, irrespective of the applied acclimation light intensity, and its extent was comparable to LL-acclimated Arabidopsis, as can be judged from the similar PSII/LHCII ratios (Fig. 1c). This raises a question about the functional role of LHCII and its possible involvement in the formation of PSII–LHCII supercomplexes under different light acclimation conditions. Our recent work indicates that spruce can form unusually large PSII–LHCII supercomplexes with multiple binding sites for LHCII trimers. Hypothetically, up to 18 LHCII trimers can bind in two rows around the PSII complex (Kouřil et al. 2020), which by far exceeds the size of other currently known large PSII–LHCII supercomplexes observed, e.g., in green alga *Chlamydomonas reinhardtii* (Shen et al. 2019; Sheng et al. 2019). Such a large LHCII antenna ensures efficient light harvesting under light-limiting conditions and makes spruce LL-tolerant species; however, it represents a burden for spruce grown in NL or even HL conditions. Without the ability to regulate the size of its LHCII, spruce has to utilize different mechanisms of coping with the potentially dangerous surplus of excitation energy.

One of these mechanisms may be regulated LHCII reorganization, which is detectable as a change in the long-range macro-organization of LHCII and PSII–LHCII supercomplexes in the thylakoid membrane. CD spectroscopy suggests that the long-range macro-organization of PSII–LHCII in spruce was generally very low compared to Arabidopsis (Fig. 6). A low degree of organization is usually connected with high variability in the PSII–LHCII interaction, which corresponds to our earlier finding that the random distribution of PSII complexes dominates in the grana membranes of spruce. In spruce, PSII complexes are not arranged into the 2D crystalline arrays (Kouřil et al. 2020), which are often present in other higher plant species (Kouřil et al. 2012; Kirchhoff 2013) and which are one of the probable sources of the Ψ-type signal bands in CD spectra (Tóth et al. 2016). Interestingly, despite the almost unchanged composition of protein complexes in the thylakoid membrane of LL and NL spruce, the acclimation to LL revealed a certain degree of adjustment, manifested as an increase in macrodomain organization (Fig. 6b). We hypothesize that this could reflect the strengthening of interactions between LHCII trimers and PSII, which is associated with a decrease in Chl fluorescence emission from weakly bound LHCIIs (Fig. 5a). On the contrary, HL-acclimated spruce revealed a strongly limited macrodomain organization, which could be related to a weakening of these interactions. Similarly, a drastic reduction in macrodomain organization was previously observed in HL-grown cells of *C. reinhardtii* (Nama et al. 2019) and was explained mainly by the severely reduced formation of PSII–LHCII supercomplexes.

Interestingly, the PSII/LHCII ratio was the lowest for HL spruce (Fig. 1c). This is the exact opposite of what is typical for HL-acclimated angiosperms (e.g., Kouřil et al. 2013; Albanese et al. 2016; Bielczynski et al. 2016), which tend to reduce large antenna and thus increase the PSII/LHCII ratio in HL. The low PSII/LHCII ratio in HL spruce likely results from partial degradation of the PSII core (see "Results" section), which is further evidenced by the decrease in the intensity of the B band occurring at around 30 °C in thermoluminescence curves (Fig. S8). The degradation of the PSII core in HL spruce was not accompanied by changes in Chl *a/b* and PSII/PSI ratios (Fig. 1a, b), which implies that PSI

was degraded proportionally to PSII and that Chls released during the degradation of pigment-protein complexes were somehow preserved. We propose that the light-stress-related proteins, ELIPs and OHPs, could have a crucial role in this process. These proteins, which were significantly upregulated in HL spruce (Fig. 2a, b), are known to be associated with PSII core degradation and repair (Rochaix and Bassi 2019) and have been proposed to play an important photoprotective role. Whereas ELIPs are able to transiently bind released Chl *a* and thus prevent the formation of reactive oxygen species (Hutin et al. 2003), OHPs are important for the delivery of Chl *a* to PSII reaction centers during PSII repair cycle (Li et al. 2019).

Functional consequences of the acclimation of spruce photosynthetic apparatus to different light intensities

Our results confirmed that Arabidopsis, a representative of angiosperms, follows the well-known strategy of higher plants for coping with changes in light intensity on the thylakoid membrane level. Apart from the increase in the PSII/LHCII ratio with increasing acclimation light intensity discussed above, this strategy involves increases in PSII/PSI, Cyt *f*/PSI, and ATP synthase/PSI ratios (Fig. 1) (e.g., Anderson 1986; Bailey et al. 2001; Ballottari et al. 2007). All these adjustments serve to increase the capacity of photosynthetic linear electron transport at higher light intensities. These changes were reflected in the balanced and coordinated increase in the photochemical yield of both PSII and PSI and in the minimization of regulatory processes involvement—photosynthetic control and induction of NPQ (Figs. 7, 8, and S3–S6).

In contrast, spruce showed a completely different acclimation strategy to the changes in light intensity. We observed no adjustment in the stoichiometry of PSI, PSII, and Cyt *f* (Fig. 1) with increasing acclimation light intensity. Upon LL acclimation, there was also no change in ATP synthase and LHCII levels. These results show that, unlike Arabidopsis, spruce does not adjust its photosynthetic capacity through the adjustment of the relative amounts of protein complexes involved in primary photosynthetic reactions. In line with these results, the yields of PSII and PSI photochemistry were very similar in spruce acclimated to all light intensities, which was evident mainly at higher intensities of actinic light (Figs. 7, 8, and S3–S6). The unavoidable disadvantage of this strategy is, however, the necessity of permanent and massive involvement of regulatory processes.

Another interesting finding came from the comparison of relative amounts of photosynthetic protein complexes in spruce and Arabidopsis (Fig. 1). In spruce, the antenna size of PSII (PSII/LHCII ratio) and Cyt *f*/PSI ratio were close to the levels for LL Arabidopsis, suggesting that under all light acclimation conditions, the light-harvesting antenna of spruce stayed "adjusted" to light-limiting conditions. However, the PSII/PSI ratio in spruce was constantly high (Fig. 1b)—its value was similar to that of HL Arabidopsis. This could imply that there might be a considerable imbalance between PSII and PSI function in spruce, which could lead to an overreduction of the PQ pool and consequent rapid closure of PSII reaction centers at higher actinic light intensities.

To verify this assumption, we analyzed the steady-state levels of PSII reaction center openness (qL) in all acclimation variants of spruce (Fig. 7d) and compared them to LL Arabidopsis, which had a similar PSII/LHCII ratio to spruce. In LL Arabidopsis, the PSII reaction centers were gradually closed with increasing actinic light intensity. Considering the higher PSII/PSI ratio in spruce, one might expect that the PSII closure in spruce would be even more pronounced than in LL Arabidopsis due to the faster supply of electrons to PQ pool. However, our data show rather an opposite trend, suggesting that some regulatory process maintains more open PSII reaction centers in spruce at higher intensities of actinic light. We suggest that this process is the non-photochemical quenching of F_M and F_0, which alleviates the excitation pressure at PSII and dramatically reduces PSII photochemical yield Y(II) (Fig. 7c). For LL spruce, all the monitored PSII parameters (NPQ, SV_0, Y(II), and qL) were very similar to LL Arabidopsis. However, in NL spruce, we observed a much higher level of NPQ than in NL Arabidopsis, as it reached values up to 3–4 at actinic light intensities ≥ 400 µmol photons m^{-2} s^{-1}. The induction of such high NPQ requires high lumen acidification, which, in general, can be achieved by low ATP synthase activity (Rott et al. 2011) and/or by highly active CET (Miyake et al. 2005). In spruce, it appears that both these mechanisms acted in unison, when compared to Arabidopsis, as spruce had a markedly lower amount of ATP synthase per PSI (Fig. 1f) and higher Y(I)/Y(II) ratio (Fig. 8d).

In LL Arabidopsis, the kinetics of NPQ induction and its dark recovery was very slow (at actinic light intensities ≥ 400 µmol photons m^{-2} s^{-1}) and a similar phenomenon was observed in LL and NL spruce (Figs. S3a and S4a). In all these plants, a part of light-induced NPQ did not recover even after 15 min dark adaptation and we ascribe this to the formation of "locked-in" NPQ. The origin of this type of quenching seems to be related to the existence of loosely bound LHCIIs (Fig. 5a) and the induction of relatively high SV_0 (Fig. 7b). Similarly slow NPQ relaxation, as well as the appearance of the "locked-in" NPQ, has been described earlier on various systems where LHCIIs were weakly bound to PSII (Belgio et al. 2012, 2018; Ware et al. 2015; Karlický et al. 2021).

In HL spruce, the high "locked-in" NPQ was permanent and led to persistently low maximum Y(II) (i.e., low

F_V/F_M value). The maintenance of this highly quenched state requires not only high amount of loosely bound/detached LHCII (Fig. 5a) but also a persistently high dark level of DEPS (Fig. 4a), i.e., high amount of zeaxanthin, which is crucial for the formation of quenching centers. The "locked-in" NPQ observed in HL spruce partially resembles the "sustained NPQ," which is induced in spruce in winter. However, during the "sustained NPQ," the quenching was attributed to a direct energy transfer from PSII to PSI (the so-called spillover) and was connected with a much more pronounced decrease of F_V/F_M (e.g., down to 0.2) and with dramatic quenching of PSII emission in 77 K emission spectra (Bag et al. 2020; Grebe et al. 2020). As we did not observe these characteristics in our study, the mechanism of the "locked-in" NPQ in our HL spruce is probably different. It is most likely based on the zeaxanthin-dependent formation of aggregates from LHCIIs, which are characterized by fluorescence emission at about 700 nm in 77 K emission spectra (Fig. 5a).

The analysis of the PSI function in LL Arabidopsis showed that, for higher actinic light intensities, there was a pronounced limitation of electron transport at the donor side of PSI, i.e., high Y(ND) (Fig. 8b). As this increase in Y(ND) coincided with the decrease in qL (Fig. 7d), this response reflects the induction of pronounced photosynthetic control on the level of Cyt b_6f complex. This regulatory process slows down the electron transport from the PQ pool to PSI (for a review see, e.g., Tikhonov 2013) and keeps P700 oxidized, which is crucial for the photoprotection of PSI, as $P700^+$ acts as a non-photochemical quencher of absorbed light energy (e.g., Bukhov and Carpentier 2003). In spruce, the photosynthetic control at the level of Cyt b_6f was less pronounced and was partially substituted by the strong NPQ, which by itself slows down the linear electron transport.

Conclusion

In this study, we found that spruce seedlings follow the characteristics of shade-tolerant plants, i.e., they have a large LHCII antenna (similar to LL-acclimated Arabidopsis). In Arabidopsis, a shade-intolerant plant, acclimation to HL conditions results in a massive reduction of LHCII, which appears to be necessary for optimizing its photosynthetic capacity and balancing the functions of PSII and PSI. In spruce, however, there is no such reduction of LHCII in HL conditions. This raises an interesting question of how spruce is able to tolerate HL, despite the fact that its light-harvesting apparatus appears permanently adjusted to LL. We propose that the answer may lie in the ability of spruce to induce massive NPQ in its antenna system (Fig. 7)—much higher than what was observed for LL Arabidopsis with a similarly large PSII antenna. We suggest that one of the reasons for the unusually strong NPQ is higher acidification of thylakoid lumen because spruce has more active CET and a lower relative amount of ATP synthase than Arabidopsis (Figs. 1f and 8d). In Arabidopsis plants, which optimize their light-harvesting antenna size to particular light conditions, the induction of extremely high NPQ (i.e., strong lumen acidification) is not necessary. This allows them to increase the relative amount of ATP synthase and thus improve their overall photosynthetic performance, which represents a substantial evolutionary advantage in HL environments.

Beyond the strong induction of NPQ, we revealed that spruce also has other mechanisms to help it to cope with long-term exposure to excessive light. When the light intensity exceeds the capacity of the energy-dependent NPQ, spruce downregulates the amount of PSII and PSI complexes and induces "locked-in" NPQ. Although the latter might appear disadvantageous as it permanently lowers the photochemical yield of PSII (low F_V/F_M ratio), it is probably crucial for the survival of spruce during long-term exposure to HL. The formation of "locked-in" quenching centers (aggregated LHCII, probably with zeaxanthin) coincides with the synthesis of stress proteins, which can bind Chls released from degraded photosystems.

An interesting question is whether the loss of LHCB3 and LHCB6 proteins in spruce somehow affects its light acclimation strategy. The shade-tolerant tropical evergreen angiosperm *Monstera deliciosa* has been reported to have a similar response to HL as spruce—formation of high "locked-in" NPQ, synthesis of stress proteins (Demmig-Adams et al. 2006). As Monstera belongs to Araceae family, whose representative has been shown to possess genes for both LHCB3 and LHCB6 (Michael et al. 2017), it seems that their absence is not a prerequisite of these phenomena. Nevertheless, the loss of LHCB3 and LHCB6 can be a result of evolutionary pressure imposed on spruce by exposure to HL conditions (Kouřil et al. 2016). It is possible that this unique feature, observed only in Pinaceae and Gnetales, contributes to better photoprotection in these plants. As the absence of LHCB3 and LHCB6 appears to weaken the binding of LHCII trimers to PSII (Ilíková et al. 2021), it is possible that the loss of these proteins leads to a higher number of weakly bound LHCIIs, which in turn enables a stronger induction of NPQ and the formation of more "locked-in" quenching centers.

It is possible that the formation of "locked-in" quenching centers and the induction of massive NPQ (associated with weakly bound LHCIIs and a higher level of photosynthetic control) is a common response to HL in all shade-tolerant evergreen plants. These plants, which include a large group of non-flowering plants and perennial angiosperms, appear to have a low ability to regulate LHCII size, i.e., they have stable Chl *a/b* ratios (see Ferroni et al. 2016 for lycophytes, Gerotto et al. 2011 for bryophytes, and Murchie and Horton 1997 for shade-tolerant angiosperms). The specific light

acclimation strategy we described in spruce may be common to many shade-tolerant plants, even from evolutionarily distant plant groups in the land plant kingdom. This phenomenon deserves to be thoroughly studied.

Supplementary Information The online version contains supplementary material available at https://doi.org/10.1007/s11120-022-00949-0.

Acknowledgements This work was supported by the Grant Agency of the Czech Republic (Projects No. 18-12178S and 21-05497S) and the European Regional Development Fund (ERDF) Projects "Plants as a tool for sustainable global development" (no. CZ.02.1.01/0.0/0.0/16_019/0000827) and "SustES—Adaptation strategies for sustainable ecosystem services and food security under adverse environmental conditions" (CZ.02.1.01/0.0/0.0/16_019/0000797). CIISB, Instruct-CZ Centre of Instruct-ERIC EU consortium, funded by MEYS CR infrastructure Project LM2018127, is gratefully acknowledged for the financial support of the measurements at the CEITEC Proteomics Core Facility. The authors thank prof. Toshiharu Shikanai for providing us with seeds of transgenic *Arabidopsis thaliana* expressing flavodiiron genes *flvA* and *flvB* from the moss *Physcomitrella patens*, Běla Piskořová for technical assistance, and Lena Hunt for language editing of the manuscript.

Author contributions RK, MŠ, VK, VŠ, and PI planned and designed the research; all the authors performed experiments and/or analyzed the data. MŠ, VK, PI, II, and RK wrote the manuscript with input from all the authors, and all the authors revised and approved it.

Data availability All relevant data can be found within the manuscript and its supporting materials. Mass spectrometry proteomics data were deposited to the ProteomeXchange Consortium via PRIDE partner repository under dataset identifier PXD029868.

Declarations

Conflict of interest The authors declare that there is no conflict of interest.

References

Adamska I, Kruse E, Kloppstech K (2001) Stable insertion of the early light-induced proteins into etioplast membranes requires chlorophyll *a*. J Biol Chem 276:8582–8587. https://doi.org/10.1074/jbc.M010447200

Albanese P, Manfredi M, Meneghesso A, Marengo E, Saracco G, Barber J, Morosinotto T, Pagliano C (2016) Dynamic reorganization of photosystem II supercomplexes in response to variations in light intensities. Biochim Biophys Acta Bioenerg 1857:1651–1660. https://doi.org/10.1016/j.bbabio.2016.06.011

Albanese P, Manfredi M, Re A, Marengo E, Saracco G, Pagliano C (2018) Thylakoid proteome modulation in pea plants grown at different irradiances: quantitative proteomic profiling in a non-model organism aided by transcriptomic data integration. Plant J 96:786–800. https://doi.org/10.1111/tpj.14068

Albanese P, Manfredi M, Marengo E, Saracco G, Pagliano C (2019) Structural and functional differentiation of the light-harvesting protein Lhcb4 during land plant diversification. Physiol Plant 166:336–350. https://doi.org/10.1111/ppl.12964

Allen JF (2017) Why we need to know the structure of phosphorylated chloroplast light-harvesting complex II. Physiol Plant 161:28–44. https://doi.org/10.1111/ppl.12577

Anderson JM (1986) Photoregulation of the composition, function, and structure of thylakoid membranes. Annu Rev Plant Physiol Plant Mol Biol 37:93–136. https://doi.org/10.1146/annurev.arplant.37.1.93

Anderson JM, Chow WS, Goodchild DJ (1988) Thylakoid membrane organization in sun/shade acclimation. Aust J Plant Physiol 15:11–26. https://doi.org/10.1071/PP9880011

Bag P, Chukhutsina V, Zhang ZS, Paul S, Ivanov AG, Shutova T, Croce R, Holzwarth AR, Jansson S (2020) Direct energy transfer from photosystem II to photosystem I confers winter sustainability in Scots Pine. Nat Commun 11:6388. https://doi.org/10.1038/s41467-020-20137-9

Bai TY, Guo L, Xu MY, Tian LR (2021) Structural diversity of Photosystem I and its light-harvesting system in eukaryotic algae and plants. Front Plant Sci 12:781035. https://doi.org/10.3389/fpls.2021.781035

Bailey S, Walters RG, Jansson S, Horton P (2001) Acclimation of *Arabidopsis thaliana* to the light environment: the existence of separate low light and high light responses. Planta 213:794–801. https://doi.org/10.1007/s004250100556

Baker NR (2008) Chlorophyll fluorescence: a probe of photosynthesis in vivo. Annu Rev Plant Biol 59:89–113. https://doi.org/10.1146/annurev.arplant.59.032607.092759

Ballottari M, Dall'Osto L, Morosinotto T, Bassi R (2007) Contrasting behavior of higher plant photosystem I and II antenna systems during acclimation. J Biol Chem 282:8947–8958. https://doi.org/10.1074/jbc.M606417200

Barzda V, Mustardy L, Garab G (1994) Size dependency of circular-dichroism in macroaggregates of photosynthetic pigment-protein complexes. Biochemistry 33:10837–10841. https://doi.org/10.1021/bi00201a034

Bassi R, Dall'Osto L (2021) Dissipation of light energy absorbed in excess: the molecular mechanisms. Annu Rev Plant Biol 72:47–76. https://doi.org/10.1146/annurev-arplant-071720-015522

Belgio E, Johnson MP, Juric S, Ruban AV (2012) Higher plant photosystem II light-harvesting antenna, not the reaction center, determines the excited-state lifetime-both the maximum and the nonphotochemically quenched. Biophys J 102:2761–2771. https://doi.org/10.1016/j.bpj.2012.05.004

Belgio E, Trsková E, Kotabová E, Ewe D, Prášil O, Kaňa R (2018) High light acclimation of *Chromera velia* points to photoprotective NPQ. Photosynth Res 135:263–274. https://doi.org/10.1007/s11120-017-0385-8

Bielczynski LW, Schansker G, Croce R (2016) Effect of light acclimation on the organization of photosystem II super- and sub-complexes in *Arabidopsis thaliana*. Front Plant Sci 7:105. https://doi.org/10.3389/fpls.2016.00105

Bilger W, Björkman O (1990) Role of the xanthophyll cycle in photoprotection elucidated by measurements of light-induced absorbance changes, fluorescence and photosynthesis in leaves of *Hedera canariensis*. Photosynth Res 25:173–185. https://doi.org/10.1007/BF00033159

Björkman O, Demmig B (1987) Photon yield of O_2 evolution and chlorophyll fluorescence characteristics at 77 K among vascular plants of diverse origins. Planta 170:489–504. https://doi.org/10.1007/BF00402983

Bukhov NG, Carpentier R (2003) Measurement of photochemical quenching of absorbed quanta in photosystem I of intact leaves using simultaneous measurements of absorbance changes at 830 nm and thermal dissipation. Planta 216:630–638. https://doi.org/10.1007/s00425-002-0886-2

Caffarri S, Kouřil R, Kereiche S, Boekema EJ, Croce R (2009) Functional architecture of higher plant photosystem II supercomplexes. EMBO J 28:3052–3063. https://doi.org/10.1038/emboj.2009.232

Chmeliov J, Gelzinis A, Songaila E, Augulis R, Duffy CDP, Ruban AV, Valkunas L (2016) The nature of self-regulation in photosynthetic light-harvesting antenna. Nat Plants 2:16045. https://doi.org/10.1038/NPLANTS.2016.45

Chukhutsina VU, Liu X, Xu P, Croce R (2020) Light-harvesting complex II is an antenna of photosystem I in dark-adapted plants. Nat Plants 6:860–868. https://doi.org/10.1038/s41477-020-0693-4

Croce R (2020) Beyond 'seeing is believing': the antenna size of the photosystems *in vivo*. New Phytol 228:1214–1218. https://doi.org/10.1111/nph.16758

Dainese P, Bassi R (1991) Subunit stoichiometry of the chloroplast photosystem II antenna system and aggregation state of the component chlorophyll a/b binding proteins. J Biol Chem 266:8136–8142. https://doi.org/10.1016/S0021-9258(18)92952-2

Dau H, Andrews JC, Roelofs TA, Latimer MJ, Liang WC, Yachandra VK, Sauer K, Klein MP (1995) Structural consequences of ammonia binding to the manganese center of the photosynthetic oxygen-evolving complex: an X-ray absorption spectroscopy study of isotropic and oriented photosystem II particles. Biochemistry 34:5274–5287. https://doi.org/10.1021/bi00015a043

de Bianchi S, Ballottari M, Dall'Osto L, Bassi R (2010) Regulation of plant light harvesting by thermal dissipation of excess energy. Biochem Soc Trans 38:651–660. https://doi.org/10.1042/BST0380651

Dekker JP, Boekema EJ (2005) Supramolecular organization of thylakoid membrane proteins in green plants. Biochim Biophys Acta Bioenerg 1706:12–39. https://doi.org/10.1016/j.bbabio.2004.09.009

Demmig-Adams B, Adams WW (2006) Photoprotection in an ecological context: the remarkable complexity of thermal energy dissipation. New Phytol 172:11–21. https://doi.org/10.1111/j.1469-8137.2006.01835.x

Demmig-Adams B, Ebbert V, Mellman DL, Mueh KE, Schaffer L, Funk C, Zarter CR, Adamska I, Jansson S, Adams WW III (2006) Modulation of PsbS and flexible vs sustained energy dissipation by light environment in different species. Physiol Plant 127:670–680. https://doi.org/10.1111/j.1399-3054.2006.00698.x

Demmig-Adams B, Cohu CM, Muller O, Adams WW III (2012) Modulation of photosynthetic energy conversion efficiency in nature: from seconds to seasons. Photosynth Res 113:75–88. https://doi.org/10.1007/s11120-012-9761-6

Demmig-Adams B, Koh SC, Cohu CM, Muller O, Stewart JJ, Adams WW III (2014) Non-photochemical fluorescence quenching in contrasting plant species and environments. In: Demmig-Adams B, Garab G, Adams WW III, Govindjee (eds) Non-photochemical quenching and energy dissipation in plants, algae and cyanobacteria. Advances in photosynthesis and respiration 40. Springer, Dordrecht, pp 531–552

Dlouhý O, Karlický V, Arshad R, Zsiros O, Domonkos I, Kurasová I, Wacha AF, Morosinotto T, Bóta A, Kouřil R, Špunda V, Garab G (2021) Lipid polymorphism of the subchloroplast-granum and stroma thylakoid membrane-particles. II Structure and functions. Cells 10:2363. https://doi.org/10.3390/cells10092363

Dobrikova AG, Varkonyi Z, Krumova SB, Kovacs L, Kostov GK, Todinova SJ, Busheva MC, Taneva SG, Garab G (2003) Structural rearrangements in chloroplast thylakoid membranes revealed by differential scanning calorimetry and circular dichroism spectroscopy. Thermo-optic effect. Biochemistry 42:11272–11280. https://doi.org/10.1021/bi034899j

Eberhard S, Finazzi G, Wollman FA (2008) The dynamics of photosynthesis. Annu Rev Genet 42:463–515. https://doi.org/10.1146/annurev.genet.42.110807.091452

Ferroni L, Suorsa M, Aro EM, Baldisserotto C, Pancaldi S (2016) Light acclimation in the lycophyte *Selaginella martensii* depends on changes in the amount of photosystems and on the flexibility of the light-harvesting complex II antenna association with both photosystems. New Phytol 211:554–568. https://doi.org/10.1111/nph.13939

Floris M, Bassi R, Robaglia C, Alboresi A, Lanet E (2013) Post-transcriptional control of light-harvesting genes expression under light stress. Plant Mol Biol 82:147–154. https://doi.org/10.1007/s11103-013-0046-z

Garab G, Kieleczawa J, Sutherland JC, Bustamante C, Hind G (1991) Organization of pigment protein complexes into macrodomains in the thylakoid membranes of wild-type and chlorophyll *b*-less mutant of barley as revealed by circular dichroism. Photochem Photobiol 54:273–281. https://doi.org/10.1111/j.1751-1097.1991.tb02016.x

Genty B, Briantais JM, Baker NR (1989) The relationship between the quantum yield of photosynthetic electron transport and quenching of chlorophyll fluorescence. Biochim Biophys Acta 990:87–92. https://doi.org/10.1016/S0304-4165(89)80016-9

Gerotto C, Alboresi A, Giacometti GM, Bassi R, Morosinotto T (2011) Role of PSBS and LHCSR in *Physcomitrella patens* acclimation to high light and low temperature. Plant Cell Environ 34:922–932. https://doi.org/10.1111/j.1365-3040.2011.02294.x

Gilmore AM, Yamamoto HY (1991) Zeaxanthin formation and energy-dependent fluorescence quenching in pea chloroplasts under artificially mediated linear and cyclic electron transport. Plant Physiol 96:635–643. https://doi.org/10.1104/pp.96.2.635

Grebe S, Trotta A, Bajwa AA, Suorsa M, Gollan PJ, Jansson S, Tikkanen M, Aro EM (2019) The unique photosynthetic apparatus of Pinaceae: analysis of photosynthetic complexes in *Picea abies*. J Exp Bot 70:3211–3225. https://doi.org/10.1093/jxb/erz127

Grebe S, Trotta A, Bajwa AA, Mancini I, Bag P, Jansson S, Tikkanen M, Aro EM (2020) Specific thylakoid protein phosphorylations are prerequisites for overwintering of Norway spruce (*Picea abies*) photosynthesis. Proc Natl Acad Sci USA 117:17499–17509. https://doi.org/10.1073/pnas.2004165117

Hutin C, Nussaume L, Moise N, Moya I, Kloppstech K, Havaux M (2003) Early light-induced proteins protect Arabidopsis from photooxidative stress. Proc Natl Acad Sci USA 100:4921–4926. https://doi.org/10.1073/pnas.0736939100

Ilík P, Pavlovič A, Kouřil R, Alboresi A, Morosinotto T, Allahverdiyeva Y, Aro EM, Yamamoto H, Shikanai T (2017) Alternative electron transport mediated by flavodiiron proteins is operational in organisms from cyanobacteria up to gymnosperms. New Phytol 214:967–972. https://doi.org/10.1111/nph.14536

Ilíková I, Ilík P, Opatíková M, Arshad R, Nosek L, Karlický V, Kučerová Z, Roudnický P, Pospíšil P, Lazár D, Bartoš J, Kouřil R (2021) Towards spruce-type photosystem II: consequences of the loss of light-harvesting proteins LHCB3 and LHCB6 in Arabidopsis. Plant Physiol 187:2691–2715. https://doi.org/10.1093/plphys/kiab396

Jajoo A, Mekala NR, Tongra T, Tiwari A, Grieco M, Tikkanen M, Aro EM (2014) Low pH-induced regulation of excitation energy between the two photosystems. FEBS Lett 588:970–974. https://doi.org/10.1016/j.febslet.2014.01.056

Karlický V, Kurasová I, Ptáčková B, Večeřová K, Urban O, Špunda V (2016) Enhanced thermal stability of the thylakoid membranes from spruce. A comparison with selected angiosperms. Photosynth Res 130:357–371. https://doi.org/10.1007/s11120-016-0269-3

Karlický V, Kmecová Materová Z, Kurasová I, Nezval J, Štroch M, Garab G, Špunda V (2021) Accumulation of geranylgeranylated chlorophylls in the pigment-protein complexes of *Arabidopsis thaliana* acclimated to green light: effects on the organization of light-harvesting complex II and photosystem II

functions. Photosynth Res 149:233–252. https://doi.org/10.1007/s11120-021-00827-1
Kirchhoff H (2013) Architectural switches in plant thylakoid membranes. Photosynth Res 116:481–487. https://doi.org/10.1007/s11120-013-9843-0
Klughammer C, Schreiber U (2008) Saturation pulse method for assessment of energy conversion in PSI. PAM Appl Notes 1:11–14
Kouřil R, Dekker JP, Boekema EJ (2012) Supramolecular organization of photosystem II in green plants. Biochim Biophys Acta Bioenerg 1817:2–12. https://doi.org/10.1016/j.bbabio.2011.05.024
Kouřil R, Wientjes E, Bultema JB, Croce R, Boekema EJ (2013) High-light vs. low-light: Effect of light acclimation on photosystem II composition and organization in *Arabidopsis thaliana*. Biochim Biophys Acta Bioenerg 1827:411–419. https://doi.org/10.1016/j.bbabio.2012.12.003
Kouřil R, Nosek L, Bartoš J, Boekema EJ, Ilík P (2016) Evolutionary loss of light-harvesting proteins Lhcb6 and Lhcb3 in major land plant groups - break-up of current dogma. New Phytol 210:808–814. https://doi.org/10.1111/nph.13947
Kouřil R, Nosek L, Semchonok D, Boekema EJ, Ilík P (2018) Organization of plant photosystem II and photosystem I supercomplexes. Subcell Biochem 87:259–286. https://doi.org/10.1007/978-981-10-7757-9_9
Kouřil R, Nosek L, Opatíková M, Arshad R, Semchonok DA, Chamrád I, Lenobel R, Boekema EJ, Ilík P (2020) Unique organization of photosystem II supercomplexes and megacomplexes in Norway spruce. Plant J 104:215–225. https://doi.org/10.1111/tpj.14918
Kovács L, Damkjær J, Kereïche S, Ilioaia C, Ruban AV, Boekema EJ, Jansson S, Horton P (2006) Lack of the light-harvesting complex CP24 affects the structure and function of the grana membranes of higher plant chloroplasts. Plant Cell 18:3106–3120. https://doi.org/10.1105/tpc.106.045641
Kramer DM, Johnson G, Kiirats O, Edwards GE (2004) New fluorescence parameters for the determination of Q_A redox state and excitation energy fluxes. Photosynth Res 79:209–218. https://doi.org/10.1023/B:PRES.0000015391.99477.0d
Kurasová I, Kalina J, Urban O, Štroch M, Špunda V (2003) Acclimation of two distinct plant species, spring barley and Norway spruce, to combined effect of various irradiance and CO_2 concentration during cultivation in controlled environment. Photosynthetica 41:513–523. https://doi.org/10.1023/B:PHOT.0000027515.05641.fd
Li YH, Liu B, Zhang J, Kong FN, Zhang L, Meng H, Li WJ, Rochaix JD, Li D, Peng LW (2019) OHP1, OHP2, and HCF244 form a transient functional complex with the Photosystem II reaction center. Plant Physiol 179:195–208. https://doi.org/10.1104/pp.18.01231
Lichtenthaler HK (1987) Chlorophylls and carotenoids: pigments of photosynthetic biomembranes. In: Douce R, Packer L (eds) Methods in enzymology. Academic Press Inc., New York, pp 350–382
Michael TP, Bryant D, Gutierrez R, Borisjuk N, Chu P, Zhang HZ, Xia J, Zhou JF, Peng H, El Baidouri M et al (2017) Comprehensive definition of genome features in *Spirodela polyrhiza* by high-depth physical mapping and short-read DNA sequencing strategies. Plant J 89:617–635. https://doi.org/10.1111/tpj.13400
Miloslavina Y, Wehner A, Lambrev PH, Wientjes E, Reus M, Garab G, Croce R, Holzwarth AR (2008) Far-red fluorescence: a direct spectroscopic marker for LHCII oligomer formation in non-photochemical quenching. FEBS Lett 582:3625–3631. https://doi.org/10.1016/j.febslet.2008.09.044
Miyake C, Miyata M, Shinzaki Y, Tomizawa K (2005) CO_2 response of cyclic electron flow around PSI (CEF-PSI) in tobacco leaves—relative electron fluxes through PSI and PSII determine the magnitude of non-photochemical quenching (NPQ) of Chl fluorescence. Plant Cell Physiol 46:629–637. https://doi.org/10.1093/pcp/pci067
Murchie EH, Horton P (1997) Acclimation of photosynthesis to irradiance and spectral quality in British plant species: chlorophyll content, photosynthetic capacity and habitat preference. Plant Cell Environ 20:438–448. https://doi.org/10.1046/j.1365-3040.1997.d01-95.x
Nama S, Madireddi SK, Yadav RM, Subramanyam R (2019) Non-photochemical quenching-dependent acclimation and thylakoid organization of *Chlamydomonas reinhardtii* to high light stress. Photosynth Res 139:387–400. https://doi.org/10.1007/s11120-018-0551-7
Ostroumov EE, Gotze JP, Reus M, Lambrev PH, Holzwarth AR (2020) Characterization of fluorescent chlorophyll charge-transfer states as intermediates in the excited state quenching of light-harvesting complex II. Photosynth Res 144:171–193. https://doi.org/10.1007/s11120-020-00745-8
Rochaix JD, Bassi R (2019) LHC-like proteins involved in stress responses and biogenesis/repair of the photosynthetic apparatus. Biochem J 476:581–593. https://doi.org/10.1042/BCJ20180718
Rott M, Martins NF, Thiele W, Lein W, Bock R, Kramer DM, Schöttler MA (2011) ATP synthase repression in tobacco restricts photosynthetic electron transport, CO_2 assimilation, and plant growth by overacidification of the thylakoid lumen. Plant Cell 23:304–321. https://doi.org/10.1105/tpc.110.079111
Ruban AV, Wilson S (2021) The mechanism of non-photochemical quenching in plants: localization and driving forces. Plant Cell Physiol 62:1063–1072. https://doi.org/10.1093/pcp/pcaa155
Schöttler MA, Tóth SZ (2014) Photosynthetic complex stoichiometry dynamics in higher plants: environmental acclimation and photosynthetic flux control. Front Plant Sci 5:188. https://doi.org/10.3389/fpls.2014.00188
Shen LL, Huang ZH, Chang SH, Wang WD, Wang JF, Kuang TY, Han GY, Shen JR, Zhang X (2019) Structure of a $C_2S_2M_2N_2$ type PSII-LHCII supercomplex from the green alga *Chlamydomonas reinhardtii*. Proc Natl Acad Sci USA 116:21246–21255. https://doi.org/10.1073/pnas.1912462116
Sheng X, Watanabe A, Li AJ, Kim E, Song CH, Murata K, Song DF, Minagawa J, Liu ZF (2019) Structural insight into light harvesting for photosystem II in green algae. Nat Plants 5:1320–1330. https://doi.org/10.1038/s41477-019-0543-4
Štroch M, Kuldová K, Kalina J, Špunda V (2008) Dynamics of the xanthophyll cycle and non-radiative dissipation of absorbed light energy during exposure of Norway spruce to high irradiance. J Plant Physiol 165:612–622. https://doi.org/10.1016/j.jplph.2007.03.013
Su XD, Ma J, Wei XP, Cao P, Zhu DJ, Chang WR, Liu ZF, Zhang XZ, Li M (2017) Structure and assembly mechanism of plant $C_2S_2M_2$-type PSII-LHCII supercomplex. Science 357:815–520. https://doi.org/10.1126/science.aan0327
Tikhonov AN (2013) pH-dependent regulation of electron transport and ATP synthesis in chloroplasts. Photosynth Res 116:511–534. https://doi.org/10.1007/s11120-013-9845-y
Tikkanen M, Nurmi M, Kangasjärvi S, Aro EM (2008) Core protein phosphorylation facilitates the repair of photodamaged photosystem II at high light. Biochim Biophys Acta Bioenerg 1777:1432–1437. https://doi.org/10.1016/j.bbabio.2008.08.004
Tóth TN, Rai N, Solymosi K, Zsiros O, Schröder WP, Garab G, van Amerongen H, Horton P, Kovács L (2016) Fingerprinting the macro-organisation of pigment-protein complexes in plant thylakoid membranes in vivo by circular-dichroism spectroscopy. Biochim Biophys Acta Bioenerg 1857:1479–1489. https://doi.org/10.1016/j.bbabio.2016.04.287

van Bezouwen LS, Caffarri S, Kale RS, Kouřil R, Thunnissen A, Oostergetel GT, Boekema EJ (2017) Subunit and chlorophyll organization of the plant photosystem II supercomplex. Nat Plants 3:17080. https://doi.org/10.1038/nplants.2017.80

Van Grondelle R, Dekker JP, Gillbro T, Sundstrom V (1994) Energy-transfer and trapping in photosynthesis. Biochim Biophys Acta Bioenerg 1187:1–65. https://doi.org/10.1016/0005-2728(94)90166-X

Walters RG (2005) Towards an understanding of photosynthetic acclimation. J Exp Bot 56:435–447. https://doi.org/10.1093/jxb/eri060

Ware MA, Belgio E, Ruban AV (2015) Photoprotective capacity of non-photochemical quenching in plants acclimated to different light intensities. Photosynth Res 126:261–274. https://doi.org/10.1007/s11120-015-0102-4

Weis E (1985) Chlorophyll fluorescence at 77 K in intact leaves—characterization of a technique to eliminate artifacts related to self-absorption. Photosynth Res 6:73–86. https://doi.org/10.1007/BF00029047

Wientjes E, van Amerongen H, Croce R (2013a) LHCII is an antenna of both photosystems after long-term acclimation. Biochim Biophys Acta Bioenerg 1827:420–426. https://doi.org/10.1016/j.bbabio.2012.12.009

Wientjes E, van Amerongen H, Croce R (2013b) Quantum yield of charge separation in photosystem II: functional effect of changes in the antenna size upon light acclimation. J Phys Chem B 117:11200–11208. https://doi.org/10.1021/jp401663w

Wiśniewski JR, Zougman A, Nagaraj N, Mann M (2009) Universal sample preparation method for proteome analysis. Nat Methods 6:359–362. https://doi.org/10.1038/NMETH.1322

Yamamoto H, Shikanai T (2019) PGR5-dependent cyclic electron flow protects photosystem I under fluctuating light at donor and acceptor sides. Plant Physiol 179:588–600. https://doi.org/10.1104/pp.18.01343

Yamamoto H, Takahashi S, Badger MR, Shikanai T (2016) Artificial remodelling of alternative electron flow by flavodiiron proteins in Arabidopsis. Nat Plants 2:16012. https://doi.org/10.1038/NPLANTS.2016.12

Supplementary Information

Photosynthesis Research

Spruce versus Arabidopsis: different strategies of photosynthetic acclimation to light intensity change

Michal Štroch[1,2], Václav Karlický[1,2], Petr Ilík[3], Iva Ilíková[4], Monika Opatíková[3], Lukáš Nosek[3], Pavel Pospíšil[3], Marika Svrčková[3], Marek Rác[3], Pavel Roudnický[5], Zbyněk Zdráhal[5], Vladimír Špunda[1,2], Roman Kouřil[3]

[1] Department of Physics, Faculty of Science, University of Ostrava, 710 00 Ostrava, Czech Republic

[2] Global Change Research Institute, Czech Academy of Sciences, 603 00 Brno, Czech Republic

[3] Department of Biophysics, Faculty of Science, Palacký University, 783 71 Olomouc, Czech Republic

[4] Institute of Experimental Botany, Czech Academy of Sciences, Centre of the Region Haná for Biotechnological and Agricultural Research, 779 00 Olomouc, Czech Republic

[5] Mendel Centre for Plant Genomics and Proteomics, Central European Institute of Technology, Masaryk University, 625 00 Brno, Czech Republic

Michal Štroch, Václav Karlický, and Petr Ilík have contributed equally to this work.

Corresponding Author: Michal Štroch, michal.stroch@osu.cz

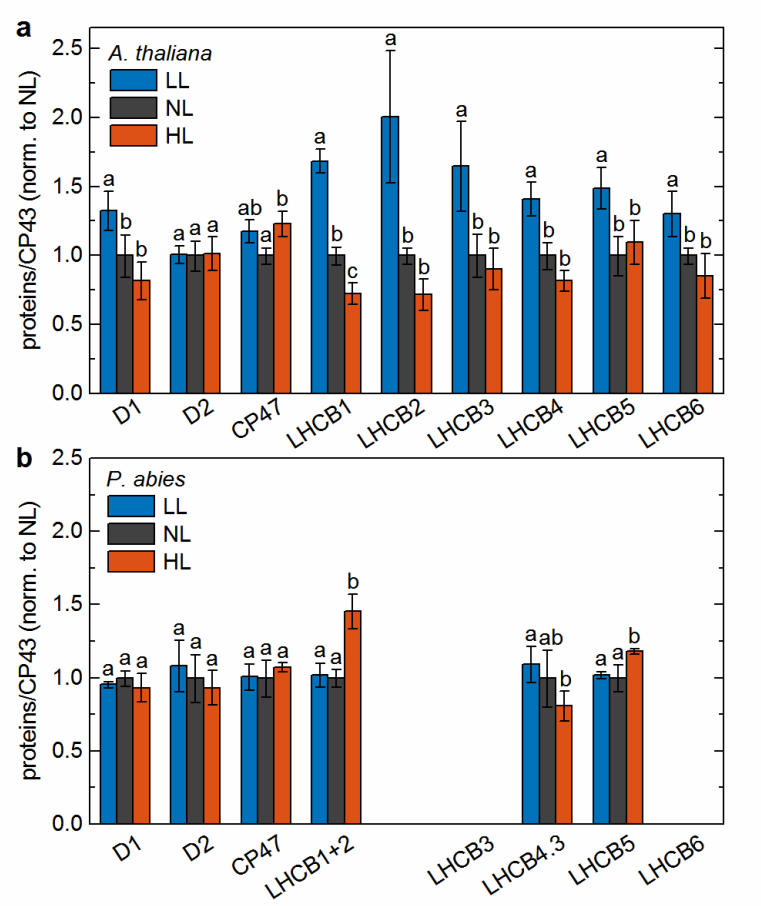

Fig. S1 Relative amounts of PSII proteins in light-acclimated Arabidopsis (*A. thaliana*) and spruce (*P. abies*). Relative amounts of PSII core proteins (D1, D2, CP47) and light-harvesting complexes LHCB1-6 in low-light-acclimated (LL), non-acclimated (NL) and high-light-acclimated (HL) Arabidopsis (**a**) and spruce (**b**). CP43 protein was used as reference and data were normalized to the values obtained for the NL variant. In spruce, it was not possible to reliably distinguish LHCB1 and LHCB2 proteins from each other, thus their amount is presented as a sum (LHCB1+2). Proteins LHCB3 and LHCB6 are missing in spruce. Relative protein amount were calculated as a ratio of relative PG intensities for the proteins from MS analysis. The presented values are means ± S.D. from four replicates. Different letters represent statistically significant differences ($p < 0.05$, one-way ANOVA followed by Tukey's post hoc test).

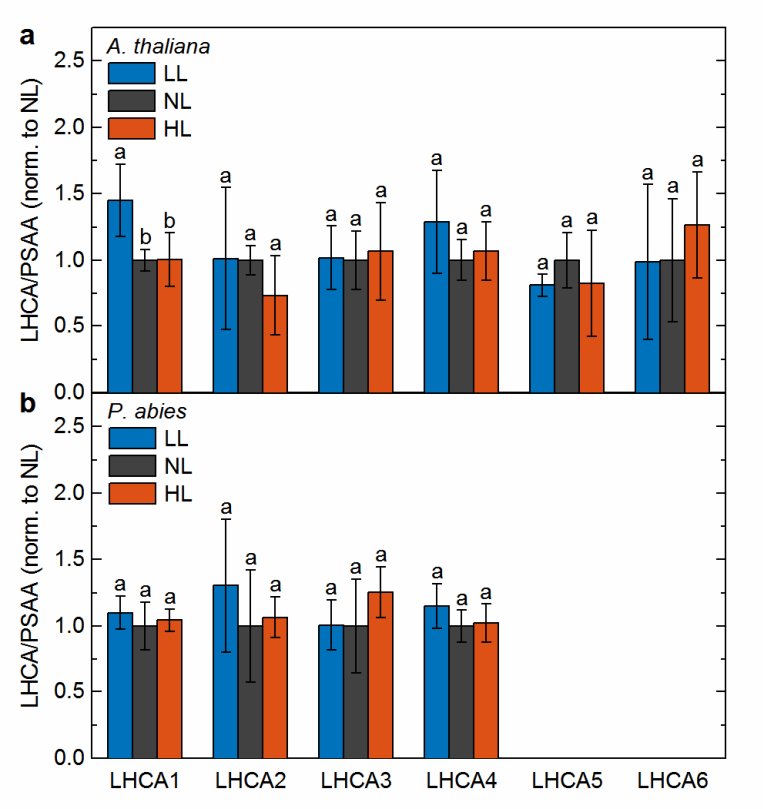

Fig. S2 Relative amounts of PSI light-harvesting proteins in light-acclimated Arabidopsis (*A. thaliana*) and spruce (*P. abies*). Relative amounts of LHCA1-6 proteins in low-light-acclimated (LL), non-acclimated (NL) and high-light-acclimated (HL) Arabidopsis (**a**) and spruce (**b**). Protein PSAA was used as reference and data were normalized to the values obtained for the NL variant. Proteins LHCA5 and LHCA6 are missing in spruce. Relative amounts of proteins were calculated as a ratio of relative PG intensities for the proteins from MS analysis. The presented values are means ± S.D. from four replicates. Different letters represent statistically significant differences ($p < 0.05$, one-way ANOVA followed by Tukey's post hoc test).

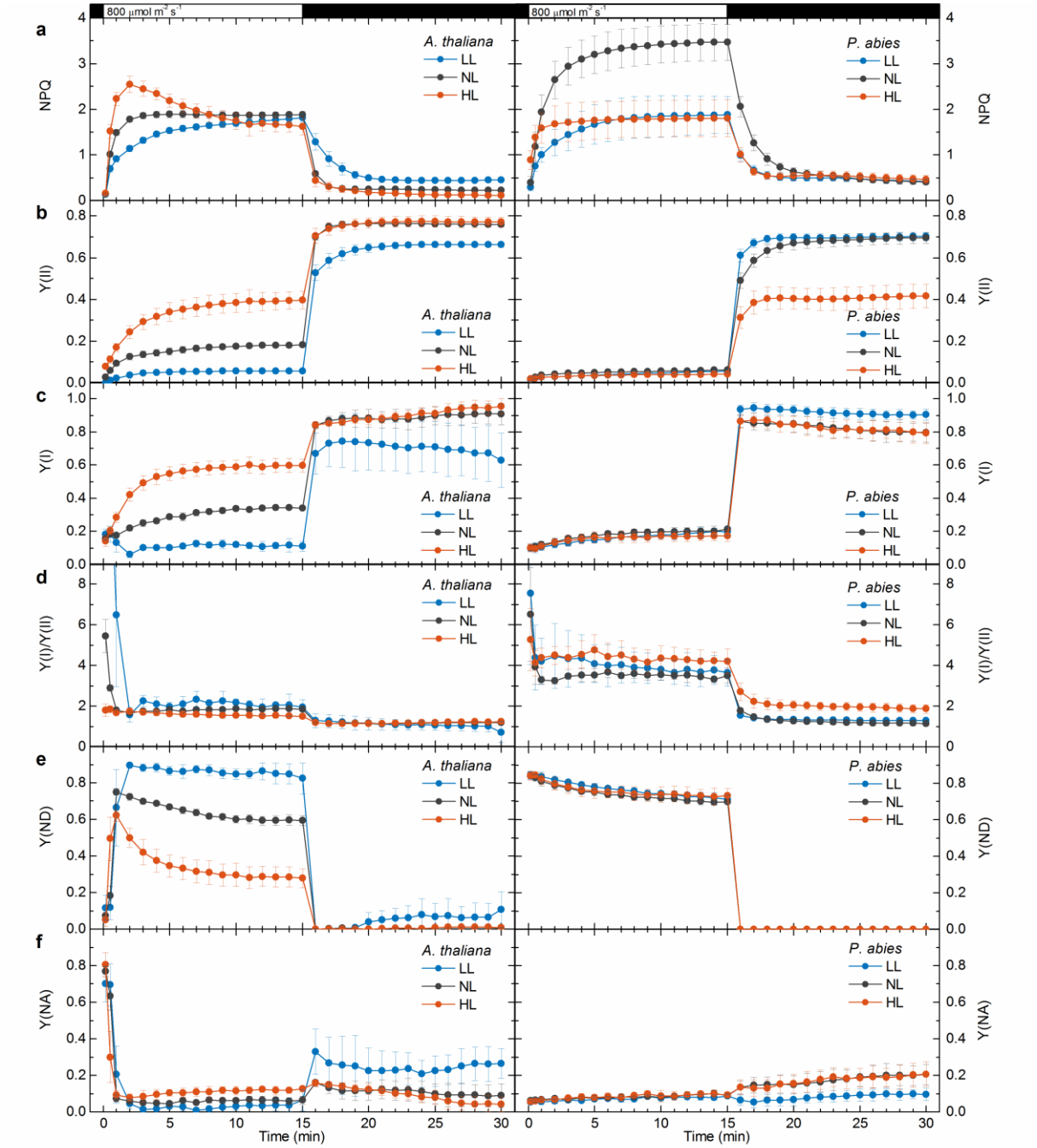

Fig. S3 Kinetics of PSII and PSI parameters during light exposure (800 µmol photons $m^{-2} s^{-1}$) and subsequent darkening of light-acclimated Arabidopsis (*A. thaliana*) and spruce (*P. abies*). (**a**) Non-photochemical quenching of maximal Chl fluorescence (NPQ), (**b**) quantum yield of PSII photochemistry [Y(II)] and (**c**) PSI photochemistry [Y(I)], (**d**) Y(I)/Y(II) ratio, (**e**) quantum yield of non-photochemical energy dissipation due to PSI donor side limitation [Y(ND)] and (**f**) PSI acceptor side limitation [Y(NA)] for low-light-acclimated (LL), non-acclimated (NL) and high-light-acclimated (HL) Arabidopsis and spruce. Leaves/needles were exposed to actinic light 800 µmol photons $m^{-2} s^{-1}$ for 15 min and subsequently kept in darkness for 15 min. The presented values are means ± S.D. from four to five replicates.

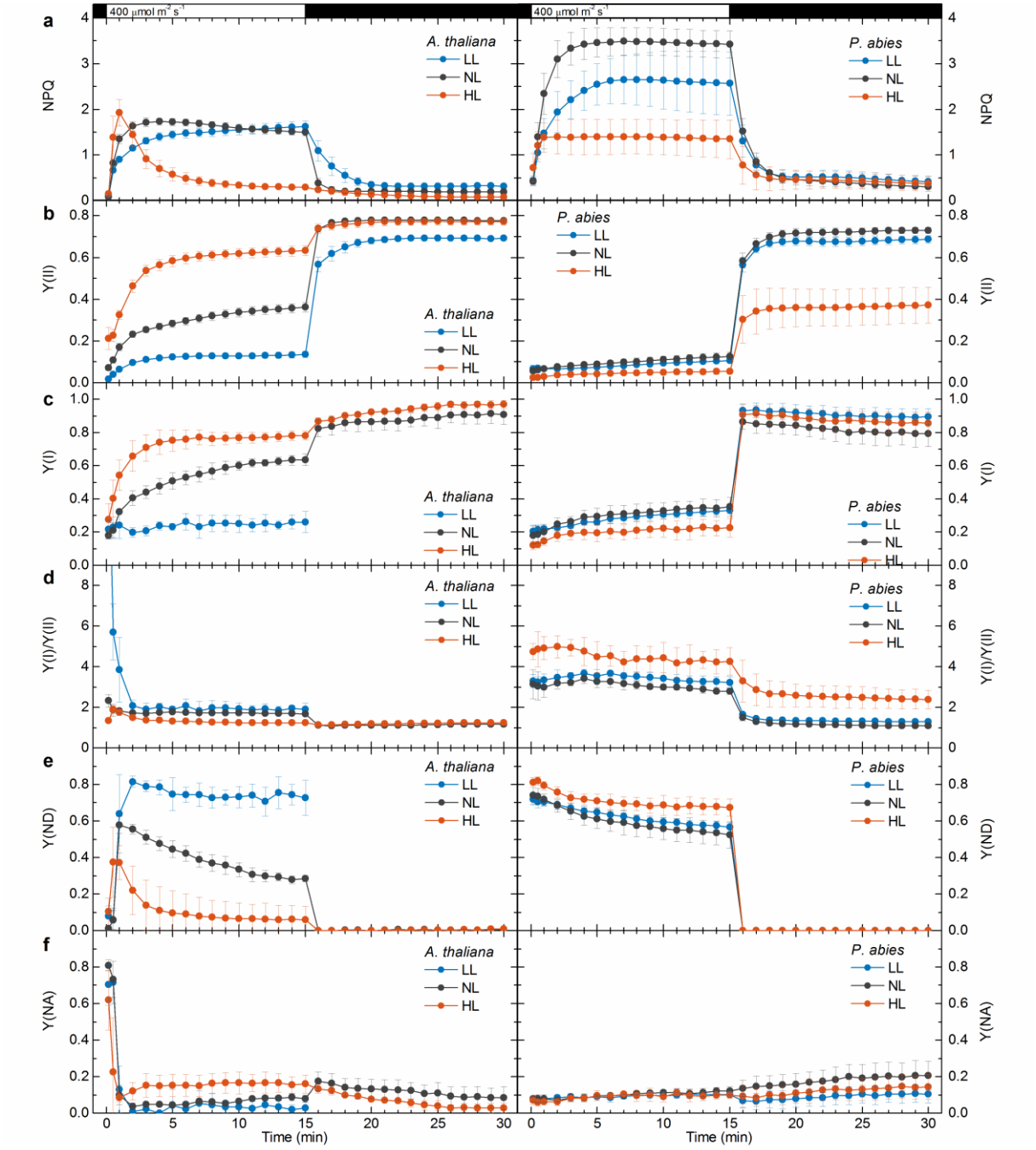

Fig. S4 Kinetics of PSII and PSI parameters during light exposure (400 µmol photons $m^{-2} s^{-1}$) and subsequent darkening of light-acclimated Arabidopsis (*A. thaliana*) and spruce (*P. abies*). (**a**) Non-photochemical quenching of maximal Chl fluorescence (NPQ), (**b**) quantum yield of PSII photochemistry [Y(II)] and (**c**) PSI photochemistry [Y(I)], (**d**) Y(I)/Y(II) ratio, (**e**) quantum yield of non-photochemical energy dissipation due to PSI donor side limitation [Y(ND)] and (**f**) PSI acceptor side limitation [Y(NA)] for low-light-acclimated (LL), non-acclimated (NL) and high-light-acclimated (HL) Arabidopsis and spruce. Leaves/needles were exposed to actinic light 400 µmol photons $m^{-2} s^{-1}$ for 15 min and subsequently kept in darkness for 15 min. The presented values are means ± S.D. from four to five replicates.

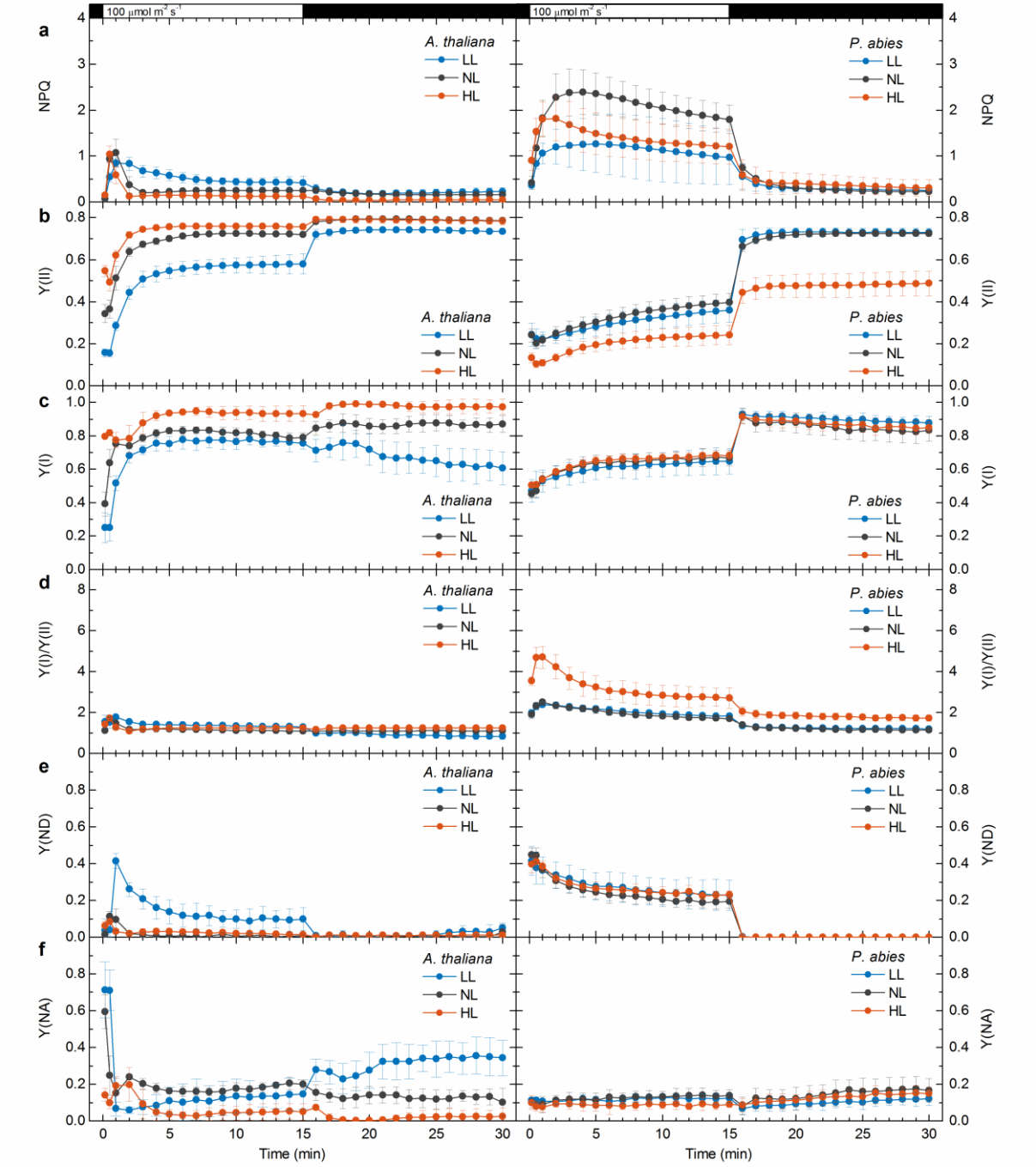

Fig. S5 Kinetics of PSII and PSI parameters during light exposure (100 µmol photons $m^{-2} s^{-1}$) and subsequent darkening of light-acclimated Arabidopsis (*A. thaliana*) and spruce (*P. abies*). (**a**) Non-photochemical quenching of maximal Chl fluorescence (NPQ), (**b**) quantum yield of PSII photochemistry [Y(II)] and (**c**) PSI photochemistry [Y(I)], (**d**) Y(I)/Y(II) ratio, (**e**) quantum yield of non-photochemical energy dissipation due to PSI donor side limitation [Y(ND)] and (**f**) PSI acceptor side limitation [Y(NA)] for low-light-acclimated (LL), non-acclimated (NL) and high-light-acclimated (HL) Arabidopsis and spruce. Leaves/needles were exposed to actinic light 100 µmol photons $m^{-2} s^{-1}$ for 15 min and subsequently kept in darkness for 15 min. The presented values are means ± S.D. from four to five replicates.

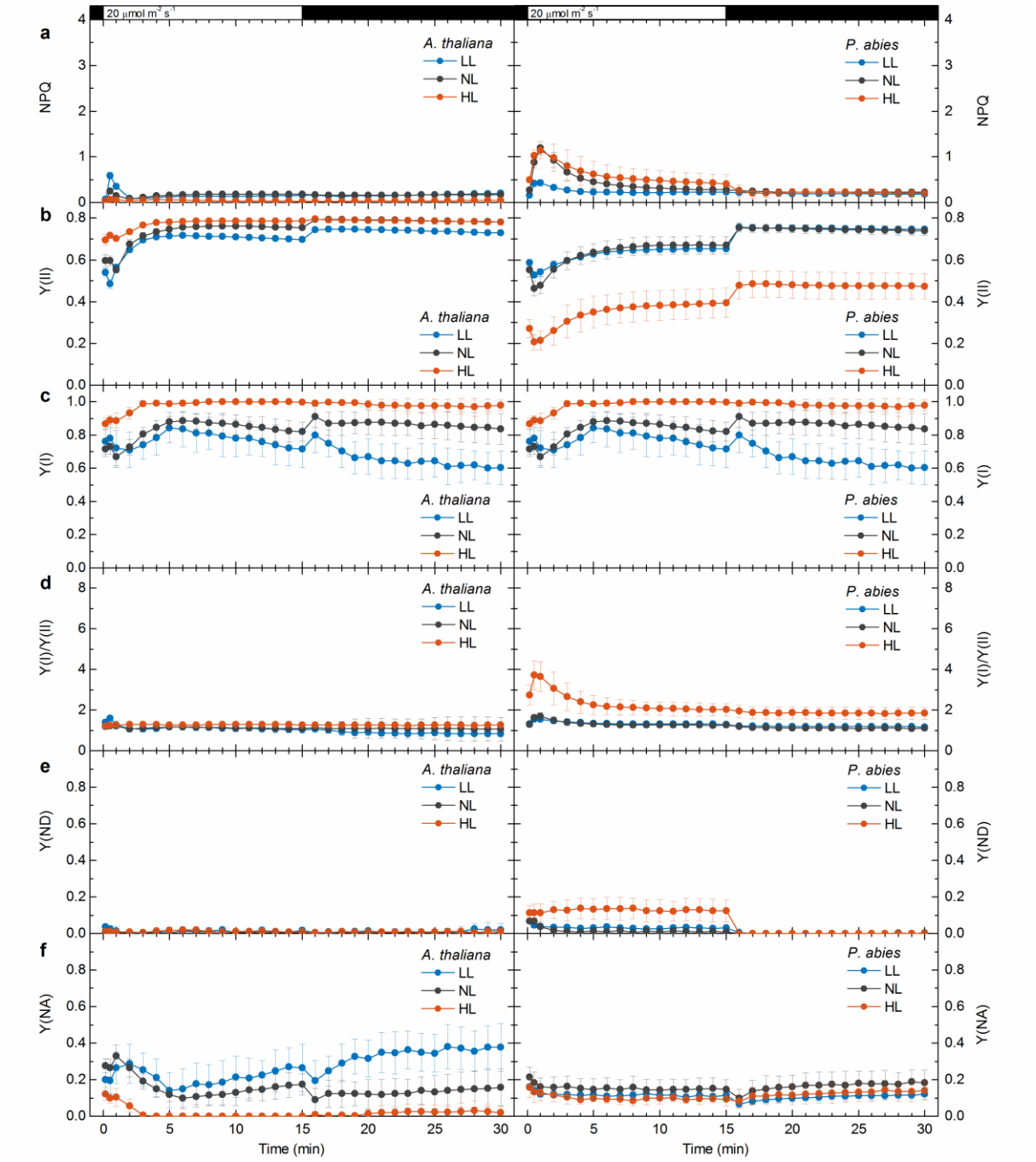

Fig. S6 Kinetics of PSII and PSI parameters during light exposure (20 µmol photons $m^{-2} s^{-1}$) and subsequent darkening of light-acclimated Arabidopsis (*A. thaliana*) and spruce (*P. abies*). (**a**) Non-photochemical quenching of maximal Chl fluorescence (NPQ), (**b**) quantum yield of PSII photochemistry [Y(II)] and (**c**) PSI photochemistry [Y(I)], (**d**) Y(I)/Y(II) ratio, (**e**) quantum yield of non-photochemical energy dissipation due to PSI donor side limitation [Y(ND)] and (**f**) PSI acceptor side limitation [Y(NA)] for low-light-acclimated (LL), non-acclimated (NL) and high-light-acclimated (HL) Arabidopsis and spruce. Leaves/needles were exposed to actinic light 20 µmol photons $m^{-2} s^{-1}$ for 15 min and subsequently kept in darkness for 15 min. The presented values are means ± S.D. from four to five replicates.

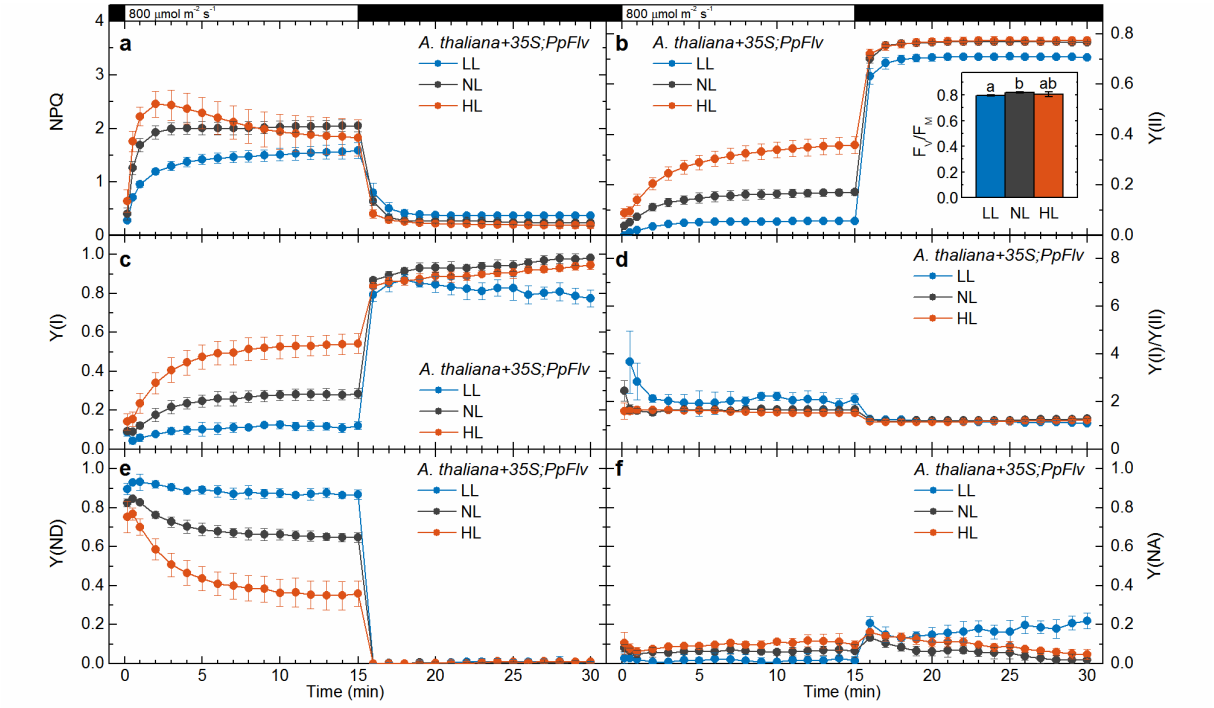

Fig. S7 Kinetics of PSII and PSI parameters during light exposure (800 µmol photons $m^{-2} s^{-1}$) and subsequent darkening of light-acclimated transgenic Arabidopsis *(A. thaliana+35S;PpFlv)*. (**a**) Non-photochemical quenching of maximal Chl fluorescence (NPQ), (**b**) quantum yield of PSII photochemistry [Y(II) and F_V/F_M in inset] and (**c**) PSI photochemistry [Y(I)], (**d**) Y(I)/Y(II) ratio, (**e**) quantum yield of non-photochemical energy dissipation due to PSI donor side limitation [Y(ND)] and (**f**) PSI acceptor side limitation [Y(NA)] for low-light-acclimated (LL), non-acclimated (NL) and high-light-acclimated (HL) transgenic Arabidopsis expressing flavodiiron genes *flvA* and *flvB* from the moss *Physcomitrella patens* (Yamamoto et al. 2016). Leaves were exposed to actinic light 800 µmol photons $m^{-2} s^{-1}$ for 15 min and subsequently kept in darkness for 15 min. The presented values are means ± S.D. from five to seven replicates. Different letters in inset of panel **b** represent statistically significant differences ($p < 0.05$, one-way ANOVA followed by Tukey's post hoc test).

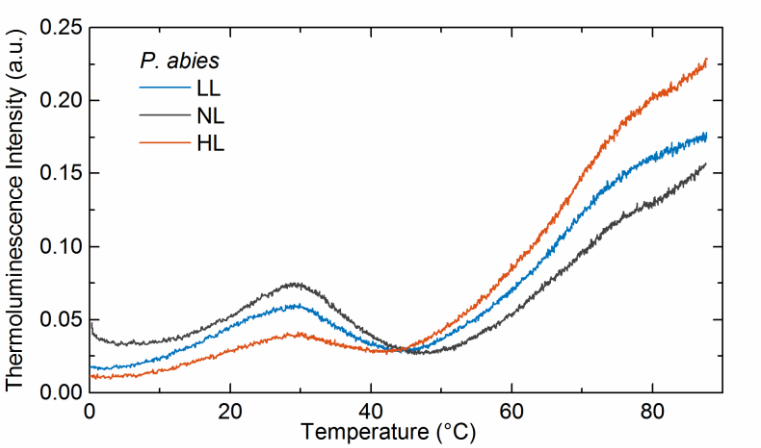

Fig. S8 Thermoluminescence curves in light-acclimated spruce (*P. abies*). Suspensions of thylakoid membranes prepared from low-light-acclimated (LL), non-acclimated (NL) and high-light-acclimated (HL) spruce were cooled from room temperature to 0°C, followed by one single turnover flash. Thermoluminescence curves were recorded while the samples were warmed up. Representative curves are presented.

Methods S1

All samples of Arabidopsis and spruce thylakoid membranes were lysed in SDT buffer (4% SDS, 0.1M DTT, 0.1M Tris/HCl, pH 7.6) in a thermomixer (Eppendorf ThermoMixer® C, 30 min, 95°C, 750 rpm). After that, samples were centrifuged (15 min, 20,000 x g) and the supernatant was used for filter-aided sample preparation as described in Wiśniewski et al. (2009) using 0.5 µg of trypsin (sequencing grade; Promega). The resulting peptides were analyzed by LC-MS/MS.

LC-MS/MS analyses of all peptides were performed using an UltiMate 3000 RSLCnano system (Thermo Fisher Scientific) connected to an Orbitrap Elite hybrid spectrometer (Thermo Fisher Scientific). Prior to LC separation, tryptic digests were online concentrated and desalted using a trapping column (Acclaim™ PepMap™ 100 C18, dimensions 300 µm × 5 mm, 5 µm particles; Thermo Fisher Scientific, part number 160454). After washing the trapping column with 0.1% formic acid (FA), the peptides were eluted in backflush mode (flow 300 $nl.min^{-1}$) from the trapping column onto an analytical column (Acclaim™ PepMap™ 100 C18, 3 µm particles, 75 µm × 500 mm; Thermo Fisher Scientific, part number 164570) by 100 min gradient program (3-80% of mobile phase B; mobile phase A: 0.1% FA in water; mobile phase B: 0.1% FA in 80% ACN). Equilibration of the trapping and analytical column was done prior to sample injection to the sample loop. The analytical column outlet was directly connected to the Digital PicoView 550 (New Objective) ion source with a sheath gas option and SilicaTip emitter (New Objective; FS360-20-15-N-20-C12) utilization. ABIRD (Active Background Ion Reduction Device, ESI Source Solutions) was installed.

MS data were acquired in a data-dependent strategy, selecting up to the top 10 precursors based on precursor abundance in the survey scan (*m/z* 350–2,000). The resolution of the survey scan was 60,000 (at *m/z* 400) with a target value of 1×10^6 ions and a maximum injection time of 1,000 ms. HCD MS/MS spectra were acquired with a target value of 50,000 and resolution of 15,000 (at *m/z* 400). The maximum injection time for MS/MS was 500 ms. Dynamic exclusion was enabled for 45 s after one MS/MS spectra acquisition. The isolation window for MS/MS fragmentation was set to *m/z* 2.0.

For data evaluation, we used MaxQuant software (v1.6.17) (Cox and Mann 2008) with a built in Andromeda search engine (Cox et al. 2011). Searches of samples from Arabidopsis and spruce were done separately. Arabidopsis samples were searched against protein databases of *Arabidopsis thaliana* (27,500 protein sequences, version from 12-08-2020, downloaded from ftp://ftp.uniprot.org/pub/databases/uniprot/current_release/knowledgebase/reference_proteomes/Eukaryota/UP000006548_3702.fasta.gz) and cRAP contaminants (112 sequences, version from 22-11-2018, downloaded from http://www.thegpm.org/crap). Spruce samples were searched against databases of spruce thylakoid proteins (66,989 protein sequences, based on database S2, Grebe et al. 2019) and cRAP contaminants. Modifications were set as follows for database search: oxidation (M), deamidation (N, Q), and acetylation (Protein N-term) as variable modifications, with carbamidomethylation (C) as a fixed modification. Enzyme specificity was tryptic with two permissible miscleavages. Only peptides and proteins with a false discovery rate threshold under 0.01 were considered. Relative protein abundance was assessed using protein intensities calculated by MaxQuant. Intensities of reported proteins were further evaluated using a software container environment (https://github.com/OmicsWorkflows/KNIME_docker_vnc; version 4.1.3a). Processing workflow is available upon request: it covers reverse hits and contaminant protein groups (cRAP) removal, protein group intensities log2 transformation and normalization (loessF). For the purpose of this article, protein groups reported by MaxQuant are referred to as proteins. Mass spectrometry

proteomics data were deposited to the ProteomeXchange Consortium via PRIDE (Perez-Riverol et al. 2019) partner repository under dataset identifier *PXD029868*.

References

Cox J, Mann M (2008) MaxQuant enables high peptide identification rates, individualized p.p.b.-range mass accuracies and proteome-wide protein quantification. Nat Biotechnol 26:1367–1372. https://doi.org/10.1038/nbt.1511

Cox J, Neuhauser N, Michalski A, Scheltema RA, Olsen JV, Mann M (2011) Andromeda: A Peptide Search Engine Integrated into the MaxQuant Environment. J Proteome Res 10:1794–1805. https://doi.org/10.1021/pr101065j

Grebe S, Trotta A, Bajwa AA, Suorsa M, Gollan PJ, Jansson S, Tikkanen M, Aro EM (2019) The unique photosynthetic apparatus of Pinaceae: analysis of photosynthetic complexes in *Picea abies*. J Exp Bot 70:3211-3225. https://doi.org/10.1093/jxb/erz127

Perez-Riverol Y, Csordas A, Bai JW, Bernal-Llinares M, Hewapathirana S, Kundu DJ, Inuganti A, Griss J, Mayer G, Eisenacher M, et al (2019) The PRIDE database and related tools and resources in 2019: improving support for quantification data. Nucleic Acids Res 47:D442–D450. https://doi.org/10.1093/nar/gky1106

Stejskal K, Potěšil D, Zdráhal Z (2013) Suppression of peptide sample losses in autosampler vials. J Proteome Res 12:3057–3062. https://doi.org/10.1021/pr400183v

Wiśniewski JR, Zougman A, Nagaraj N, Mann M (2009) Universal sample preparation method for proteome analysis. Nat Methods 6:359-362. https://doi.org/10.1038/NMETH.1322

doi:10.1093/plphys/kiab396 PLANT PHYSIOLOGY 2021: 187: 2691–2715

Plant Physiology®

Research Article

Towards spruce-type photosystem II: consequences of the loss of light-harvesting proteins LHCB3 and LHCB6 in Arabidopsis

Iva Ilíková [1], Petr Ilík [2], Monika Opatíková [2], Rameez Arshad [2,3], Lukáš Nosek [2], Václav Karlický [4,5], Zuzana Kučerová [2], Pavel Roudnický [6], Pavel Pospíšil [2], Dušan Lazár [2], Jan Bartoš [1] and Roman Kouřil [2,†,*]

1 Institute of Experimental Botany of the Czech Academy of Sciences, Centre of the Region Haná for Biotechnological and Agricultural Research, 783 71 Olomouc, Czech Republic
2 Department of Biophysics, Centre of the Region Haná for Biotechnological and Agricultural Research, Palacký University, 783 71 Olomouc, Czech Republic
3 Electron Microscopy Group, Groningen Biomolecular Sciences and Biotechnology Institute, University of Groningen, Nijenborgh 7, 9747 AG Groningen, The Netherlands
4 Department of Physics, Faculty of Science, University of Ostrava, 710 00 Ostrava, Czech Republic
5 Global Change Research Institute of the Czech Academy of Sciences, 603 00 Brno, Czech Republic
6 Central European Institute of Technology, Masaryk University, 625 00 Brno, Czech Republic

*Author for communication: roman.kouril@upol.cz
†Senior author.

R.K., I.I., and P.I. planned and designed the research. All authors performed experiments and analyzed the data. I.I., R.K., and P.I. wrote the manuscript with input from all authors, and all authors revised and approved it.
The author responsible for distribution of materials integral to the findings presented in this article in accordance with the policy described in the Instructions for Authors (https://academic.oup.com/plphys/pages/General-Instructions) is: Iva Ilíková (ilikova@ueb.cas.cz).

Abstract

The largest stable photosystem II (PSII) supercomplex in land plants ($C_2S_2M_2$) consists of a core complex dimer (C_2), two strongly (S_2) and two moderately (M_2) bound light-harvesting protein (LHCB) trimers attached to C_2 via monomeric antenna proteins LHCB4–6. Recently, we have shown that LHCB3 and LHCB6, presumably essential for land plants, are missing in Norway spruce (*Picea abies*), which results in a unique structure of its $C_2S_2M_2$ supercomplex. Here, we performed structure–function characterization of PSII supercomplexes in Arabidopsis (*Arabidopsis thaliana*) mutants *lhcb3*, *lhcb6*, and *lhcb3 lhcb6* to examine the possibility of the formation of the "spruce-type" PSII supercomplex in angiosperms. Unlike in spruce, in Arabidopsis both LHCB3 and LHCB6 are necessary for stable binding of the M trimer to PSII core. The "spruce-type" PSII supercomplex was observed with low abundance only in the *lhcb3* plants and its formation did not require the presence of LHCB4.3, the only LHCB4-type protein in spruce. Electron microscopy analysis of grana membranes revealed that the majority of PSII in *lhcb6* and namely in *lhcb3 lhcb6* mutants were arranged into C_2S_2 semi-crystalline arrays, some of which appeared to structurally restrict plastoquinone diffusion. Mutants without LHCB6 were characterized by fast induction of non-photochemical quenching and, on the contrary to the previous *lhcb6* study, by only transient slowdown of electron transport between PSII and PSI. We hypothesize that these functional changes, associated with the arrangement of PSII into C_2S_2 arrays in thylakoids, may be important for the photoprotection of both PSI and PSII upon abrupt high-light exposure.

Received June 07, 2021. Accepted July 26, 2021. Advance access publication September 1, 2021

Introduction

Photosynthesis is a very complex process that relies on a synergistic function of large multi-subunit pigment–protein complexes of photosystem II (PSII) and photosystem I (PSI), which are embedded in specific regions of the thylakoid membrane called grana and stroma lamellae, respectively. Photosystems mediate a light-driven electron transport from water molecules across the thylakoid membrane, leading to the reduction of $NADP^+$ to NADPH and generation of a proton gradient across the membrane, subsequently utilized by ATP-synthase in the production of ATP. The basic concepts of photosynthesis are shared by the majority of photosynthesizing organisms and the individual photosynthetic proteins and their organization into higher complexes are usually highly conserved.

In land plants, PSII is present in the form of supercomplexes, consisting of a dimeric core complex (C_2) and light-harvesting antenna (LHC) II. The light-harvesting system is formed by a variable amount of antenna proteins organized into LHCII trimers (LHCB1–3), which are functionally attached to the core via minor antennae (LHCB4–6). The most abundant light-harvesting protein in land plants is LHCB1, its content being about two-fold and eight-fold higher compared with the other two trimer-forming proteins, LHCB2 and LHCB3 (Peter and Thornber, 1991). LHCB1 and LHCB2 can form both homo- and heterotrimers, while LHCB3 is present only in heterotrimers together with two copies of LHCB1/LHCB2 (Caffarri et al., 2004; Standfuss and Kühlbrandt, 2004). The monomeric LHCB4–6 proteins, which represent a minor fraction of LHCII, mediate a specific association of LHCII trimers to the PSII core complex and are crucial for the formation of the PSII supercomplex. The LHCII trimers are designated as "S" and "M" based on the strength of their binding to the core dimer (strongly and moderately bound, Dekker and Boekema, 2005; Kouřil et al., 2018). The S trimers bind to the core complex with the help of LHCB5 and LHCB4, whereas the binding of the M trimers is mediated by LHCB4 and LHCB6. Apart from the different binding sites, the trimers also differ in their protein composition, as the M trimer specifically contains one copy of LHCB3 monomer (Caffarri et al., 2009; Su et al., 2017; van Bezouwen et al., 2017). The largest stable form of PSII in land plants is the $C_2S_2M_2$ supercomplex, where C_2 binds two copies of both the S and M trimers (Dekker and Boekema, 2005; Kouřil et al., 2018). Occasionally, the binding of the "L" (loosely bound) and "N" (naked) trimers can further extend the size of the light-harvesting antenna (Boekema et al., 1999; Kouřil et al., 2020). Our knowledge about the composition and architecture of the $C_2S_2M_2$ supercomplex has gradually improved and we have gained substantial information about the structural details of interactions between individual subunits and pigment arrangements within the supercomplex monomer (Caffarri et al., 2009; Su et al., 2017; van Bezouwen et al., 2017).

A generally accepted dogma that the composition and structure of PSII supercomplexes is uniform and strongly conserved in all land plants was refuted by our finding that LHCB3 and LHCB6 proteins, which had been considered as essential components of LHCII in land plants, are missing in gymnosperm families Pinaceae and Gnetales (Kouřil et al., 2016). In these plants, in the absence of LHCB3 and LHCB6, the M trimer binds to the C_2 in a different orientation, which results in a specific form of PSII supercomplex that is unique among land plants (henceforth, termed "spruce-type" in this work; Kouřil et al., 2016). It is currently difficult to speculate what was the evolutionary factor that led to the loss of LHCB3 and LHCB6 in these plant families, as we do not have enough information about the physiological consequences of the absence of these two important proteins. Norway spruce (*Picea abies*) and other representatives of Pinaceae and Gnetales are not very convenient model plants and therefore their photosynthetic performance and characteristics have not been extensively analyzed yet. At the same time, even if such study had been performed, it would be extremely difficult to decipher which features of the photosynthetic response of these plants are linked to the loss of LHCB3 and LHCB6 (i.e. linked to the unique structure of their PSII supercomplex) and which are related to other specific properties of these plant groups, including the loss of LHCB4.1/4.2 (Grebe et al., 2019), the loss of the NDH complex (Nystedt et al., 2013), and the presence of flavodiiron protein (Allahverdiyeva et al., 2015; Ilík et al., 2017). To investigate the putative physiological benefits and drawbacks of the unique composition of the light-harvesting system in Norway spruce, we have attempted to create a first approximation of the "spruce-type" PSII supercomplex in Arabidopsis (*Arabidopsis thaliana*) by preparing a double mutant *lhcb3 lhcb6* line.

Arabidopsis single mutant lines lacking either LHCB6 or LHCB3 have already been characterized and the studies have revealed some interesting properties of these mutants. Analysis of the Arabidopsis *lhcb3* mutant has shown that the absence of LHCB3 is compensated by LHCB1 and/or LHCB2 proteins and that the $C_2S_2M_2$ supercomplexes can be formed in this mutant, as electron microscopy (EM) of *lhcb3* grana membrane fragments revealed semi-crystalline arrays of $C_2S_2M_2$ supercomplexes (Damkjær et al., 2009). Even though the resolution of the PSII supercomplex structure in this study was very low, the analysis of these arrays suggested that the position of the M trimer in $C_2S_2M_2$ is modified, but that its binding to C_2 is probably still mediated by LHCB6 (Damkjær et al., 2009).

The loss of LHCB6 appears to have a much stronger detrimental effect on the photosynthetic performance of Arabidopsis plants than the loss of LHCB3, as strong reduction of plant growth, permanent limitation of electron transport, and impairment of non-photochemical quenching (NPQ) has been reported in *lhcb6* (Kovács et al., 2006; de Bianchi et al., 2008). The analysis of the *lhcb6* mutant revealed

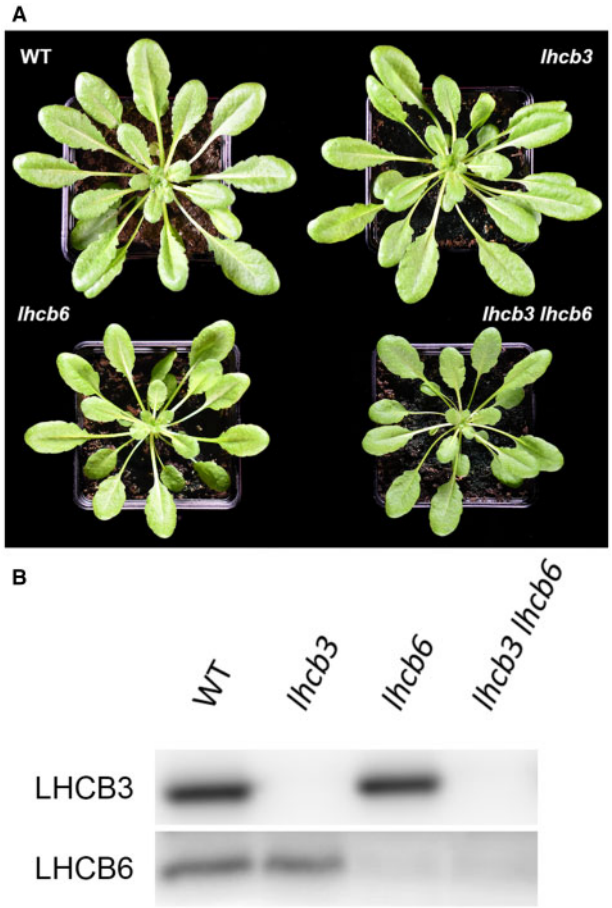

Figure 1 Phenotype and immunoblot analysis. A, Phenotype of *A. thaliana* WT and mutant plants (*lhcb3*, *lhcb6*, *lhcb3 lhcb6*) grown in control conditions for 6 weeks (120 µmol photons m^{-2} s^{-1}, 22 °C, 8/16 h day/night, and 60% humidity). B, Immunoblot analysis of thylakoid membranes of WT and mutant plants (*lhcb3*, *lhcb6*, *lhcb3 lhcb6*) with antibodies directed against minor light-harvesting proteins LHCB3 and LHCB6.

that in Arabidopsis, LHCB6 might be important for the binding of the M trimer to C_2, as no $C_2S_2M_2$ supercomplexes were observed in the *lhcb6* mutant (Kovács et al., 2006; Caffarri et al., 2009).

It has been suggested that the strong impairment of photosynthesis in *lhcb6* is not primarily caused by the loss of LHCB6 per se, but that it results from the relatively high proportion of PSII arranged into so-called PSII semi-crystalline arrays, which in turn may result in severe and permanent limitation of plastoquinone (PQ) diffusion between PSII and PSI (de Bianchi et al., 2008). The ability of PSII complexes to form semi-crystalline arrays has been known for a long time, the early evidence coming from freeze-fracture experiments. In one of the first studies, Park and Biggins (1964) have reported that the "quantasomes" (i.e. PSII supercomplexes) could exist in thylakoids in a variety of arrangements, from random through linear arrays to crystalline arrays, although the crystals were reported to be rather rare. Despite the lack of any structural details and limited knowledge on the structure and composition of PSII particles at that time, there have already been data suggesting that there are various types of semi-crystals (Miller et al., 1976; Simpson, 1979; Tsvetkova et al., 1995; Semenova, 1995). Currently, we know that all types of PSII supercomplexes observed in land plants ($C_2S_2M_2$, C_2S_2M, and C_2S_2) are able to form semi-crystalline arrays (Boekema et al., 2000; Yakushevska et al., 2001), but the mechanism and regulation of their formation, as well as their physiological function, importance, and putative benefits, are still very poorly understood.

In our study, we have prepared Arabidopsis double mutant line lacking LHCB3 and LHCB6 in an attempt to reproduce the unique "spruce-type" PSII supercomplex in Arabidopsis, which would help us to obtain valuable information about the possible physiological benefits of this type of supercomplex. From the published studies, we already know that in the absence of LHCB6, the "regular" M trimer containing LHCB3 is not able to bind to the supercomplex. Our primary question thus was whether the additional loss of LHCB3 in *lhcb6* mutant line can facilitate the binding of the M trimer to C_2S_2 and if not, what could be the possible factors preventing its appearance in Arabidopsis. It appears that indeed, in Arabidopsis the loss of both LHCB3 and LHCB6 is not sufficient for the stable formation of "spruce-type" supercomplex. At the same time, we have found that in the Arabidopsis double mutant *lhcb3 lhcb6*, the majority of PSII are arranged into C_2S_2 semi-crystalline arrays. Therefore, we have used this mutant for an extensive analysis of its primary photosynthetic reactions in order to shed some light on the possible physiological/regulatory role of PSII ordering into C_2S_2 semi-crystalline arrays.

Results

The additional loss of LHCB3 does not change the phenotype of Arabidopsis *lhcb6* mutant

Arabidopsis *lhcb3 lhcb6* double mutant was prepared via the crossing of two SALK T-DNA insertion lines, SALK_020314c (*lhcb3*) and SALK_077953 (*lhcb6*), which were already used in several previous studies. Western blot analysis confirmed a complete absence of LHCB3 in both *lhcb3* and *lhcb3 lhcb6* mutants (Figure 1, B), which agrees with the findings of other authors and confirms that the SALK_020314c is indeed a knockout line (Damkjær et al., 2009; Adamiec et al., 2015). However, in the case of LHCB6, we were able to observe a weak antibody signal in the Western blots, suggesting either cross-reactivity of the used antibody or the presence of some residual amount of LHCB6 in both *lhcb6* and *lhcb3 lhcb6* mutants (Figure 1, B). Closer examination of the T-DNA insertion site in the SALK_077953 line reveals that the T-DNA insertion is localized in the 5′-UTR region of the lhcb6 gene (AT1G15820), which frequently leads to knockdowns rather than knockouts (Wang, 2008). Other authors who have previously used this insertion line and performed Western blots either failed to detect this residual amount of LHCB6 (de Bianchi et al., 2008; Chen et al., 2018), or observed it but disregarded it as

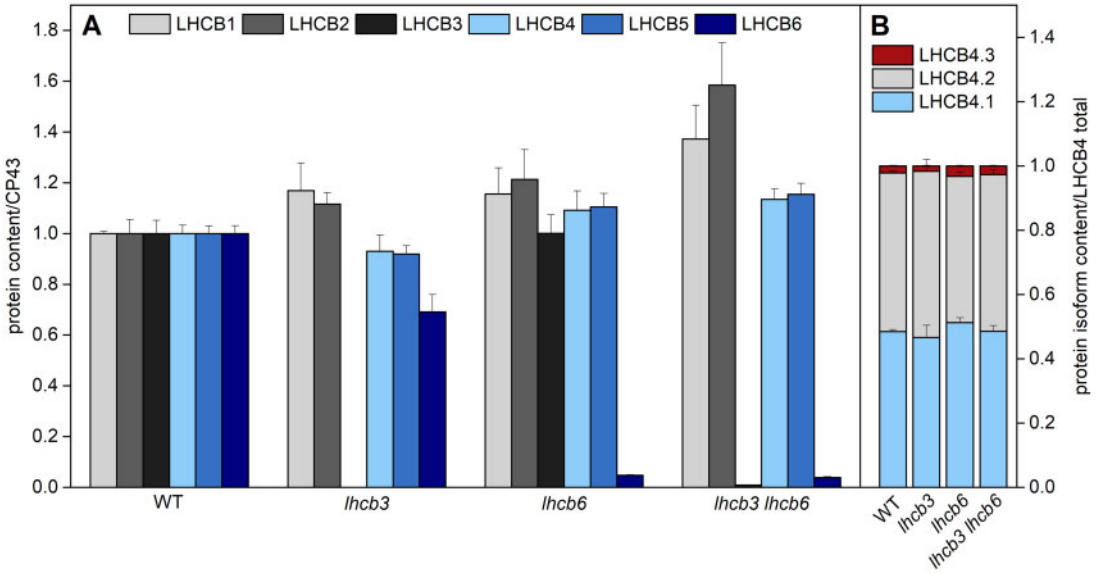

Figure 2 Relative content of light-harvesting proteins in thylakoid membranes of WT and mutant plants (*lhcb3*, *lhcb6*, *lhcb3 lhcb6*). A, The content of individual light-harvesting proteins LHCB1-6 evaluated relatively to the content of chlorophyll protein 43 (CP43, the inner antenna of PSII), and subsequently normalized to WT. B, The content of individual LHCB4 isoforms (LHCB4.1, LHCB4.2, LHCB4.3) related to the sum of all LHCB4 isoforms. The protein content was determined in isolated thylakoid membranes by LC–MS/MS. The presented values are means ± SD from four replicates.

Table 1 Growth parameter and pigment content

	Fresh weight (g)	Chl *a* + *b*	Chl *a*/*b*	Car	Vio	Ant	Zea
WT	1.4 ± 0.2	960 ± 190	2.79 ± 0.09	169 ± 26	15 ± 4	2.0 ± 0.5	ND
lhcb3	1.4 ± 0.3	910 ± 73	2.84 ± 0.04	165 ± 8	18 ± 2	2.4 ± 0.4	ND
lhcb6	0.6 ± 0.2	820 ±85	2.94 ± 0.07	149 ± 14	18 ± 2	3.1 ± 0.2	ND
lhcb3 lhcb6	0.7 ± 0.2	800 ± 68	2.96 ± 0.05	148 ± 12	17 ± 2	3.1 ± 2.1	ND

Notes: Presented values are means ± SD. Fresh weight of individual rosettes was measured (n = 13–15). Pigment content is expressed in μg g^{-1} fresh weight (n = 4). Chl, chlorophyll; Car, carotenoids; Vio, violaxanthin; Ant, antheraxanthin; Zea, zeaxanthin; and ND, not detectable.

non-detectable (3% ± 1% of wild-type (WT) level, Kovács et al., 2006), and therefore the insertion line has been widely used as a knockout mutant for LHCB6. Nevertheless, we have confirmed the presence of the residual amount of LHCB6 in the presumed knockout line also by the mass spectrometry analysis, which revealed a low, but unequivocally detectable amount of LHCB6 in both *lhcb6* and *lhcb3 lhcb6* (4%–5% of WT level, Figure 2, A). Thus, unlike *lhcb3* (SALK_020314c), *lhcb6* (SALK_077953) is a strong knockdown line rather than a complete knockout.

In agreement with a previous study (Damkjær et al., 2009), a phenotypic characterization of mutant plants lacking LHCB3 did not show any distinct changes compared with WT, either in growth rate or pigment composition (Figure 1, A and Table 1). Plants of *lhcb6* line were visibly smaller (Figure 1, A), but their chlorophyll and carotenoid content did not significantly differ from WT and *lhcb3* (Table 1). The double mutant *lhcb3 lhcb6* plants grown under controlled conditions in the phytotron were indistinguishable from the *lhcb6* plants (Figure 1, A), indicating that the additional loss of LHCB3 did not have a substantial effect on the plant visual phenotype.

The changes in LHCB protein levels in individual mutant lines were assessed using mass spectrometry and expressed relative to protein levels in WT. The loss of LHCB3 in *lhcb3* led to a slight increase in the amount of LHCB1 and LHCB2 proteins (Figure 2, A), which probably replace LHCB3 in the M trimer. At the same time, the amount of LHCB6 decreased to approximately 70% of WT level (Figure 2, A), which has not been observed on Western blots from *lhcb3* plants in previous studies (Damkjær et al., 2009; Adamiec et al., 2015). In *lhcb6* mutant plants, we have found again a slight increase in the amount of LHCB1 and LHCB2 (Figure 2, A), which is in agreement with previously observed trends (Kovács et al., 2006; de Bianchi et al., 2008). The level of LHCB3 did not change (Figure 2, A), although literature suggests a decrease to 70% (Kovács et al., 2006; Chen et al., 2018) or even 25% (de Bianchi et al., 2008) of the WT level. LHCB4 and LHCB5 did not show any distinct change in abundance (Figure 2, A). Mass spectrometry analysis confirmed the presence of a residual amount of LHCB6 protein in the *lhcb6* line (less than 5% of the WT level, Figure 2, A), which was already observed in immunoblots (Figure 1, B). The protein composition of the

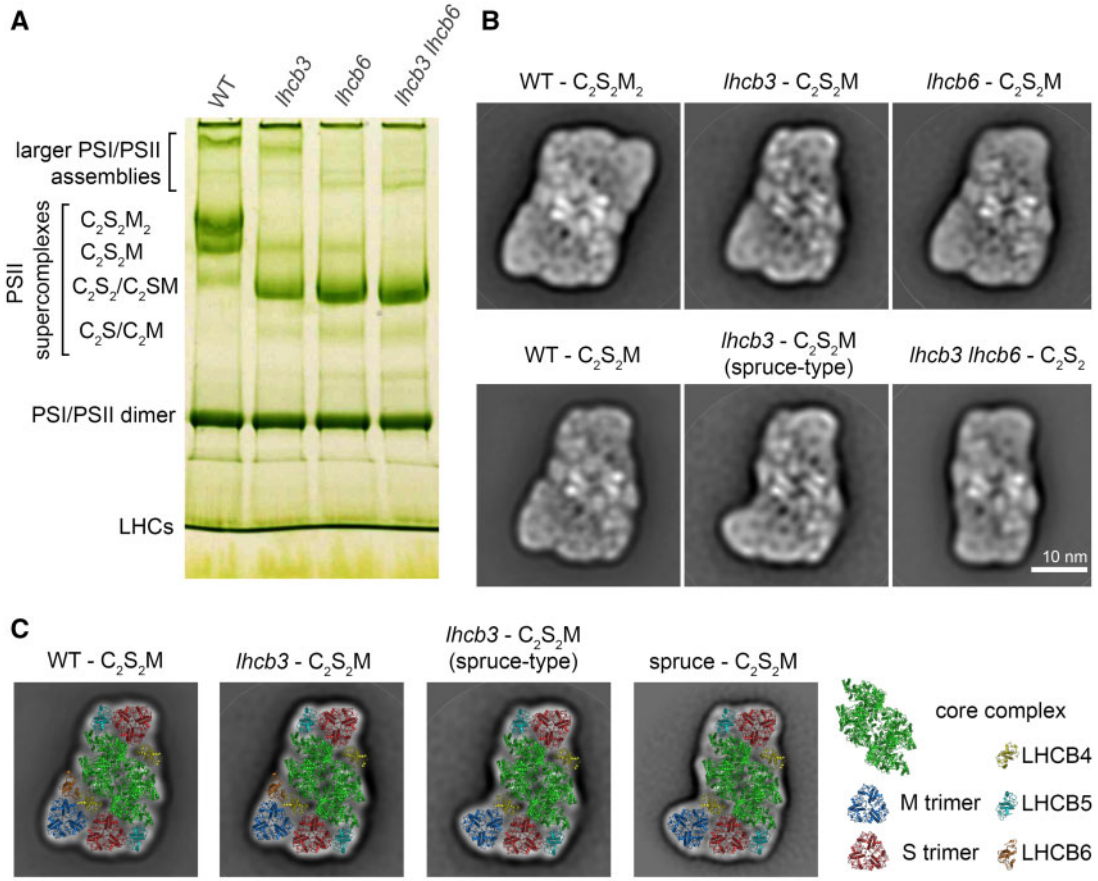

Figure 3 Separation and structural characterization of PSII (PSII) supercomplexes from WT and mutant plants (*lhcb3*, *lhcb6*, *lhcb3 lhcb6*). A, CN polyacrylamide gel electrophoresis separation of pigment–protein complexes from thylakoid membranes from *A. thaliana* WT, *lhcb3*, *lhcb6*, and *lhcb3 lhcb6* mutants solubilized by *n*-dodecyl α-D-maltoside. Different forms of separated PSII supercomplexes consist of PSII core dimer (C_2) and one and/or two copies of strongly (S) and moderately (M) bound light-harvesting trimers. B, Structural characterization of the largest forms of PSII supercomplexes revealed in WT and *lhcb3*, *lhcb6*, and *lhcb3 lhcb6* mutants. In WT, the gel bands designated as $C_2S_2M_2$ and C_2S_2M were analyzed. In *lhcb3* and *lhcb6*, the C_2S_2M gel bands, and the C_2S_2 gel band in *lhcb3 lhcb6* were analyzed. C, Structural models of C_2S_2M PSII supercomplexes from WT and *lhcb3* mutant shown in (B) supplemented with the model of C_2S_2M separated from thylakoid membranes of spruce (Kouřil et al. 2016). The models were obtained by a fit of the high-resolution structure from van Bezouwen et al. (2017). Individual PSII subunits are color-coded.

double mutant plants *lhcb3 lhcb6* was similar to *lhcb6* plants, except for the absence of LHCB3 and a slightly more pronounced increase in LHCB1 and LHCB2 abundance (Figure 2, A).

Out of all assessed LHCB proteins, LHCB4 and LHCB5 were affected the least. It is of note that these two proteins can be considered as a part of the "functional core" of the PSII antenna system in all organisms from the green lineage (Alboresi et al., 2008), and unlike the rest of the LHCB proteins, their content is not readily affected by environmental conditions (Ballottari et al., 2007). As LHCB4 is known to be present in Arabidopsis in three isoforms (LHCB4.1, LHCB4.2, and LHCB4.3), we used mass spectrometry to analyze the relative contribution of individual isoforms to the total amount of LHCB4. In WT, LHCB4.1 and LHCB4.2 isoforms were present in approximately equimolar amounts, which agrees with the recently published data (McKenzie et al., 2020), and the loss of LHCB3 and/or LHCB6 did not significantly change this ratio (Figure 2, B). The relative contribution of the third isoform, LHCB4.3, was very low in all analyzed plants (Figure 2, B).

C_2S_2 is the main stable form of PSII supercomplex in Arabidopsis *lhcb3 lhcb6* mutant

To analyze the impact of the loss of LHCB3 and/or LHCB6 proteins on the formation and structure of PSII supercomplexes in Arabidopsis, we have used clear-native PAGE (CN-PAGE), which enabled us to separate individual photosynthetic protein complexes from thylakoid membranes mildly solubilized with *n*-dodecyl α-D-maltoside (α-DDM). The separation profile of PSII supercomplexes from WT (Figure 3, A) agrees with our previously published data (Nosek et al., 2017) and confirms that $C_2S_2M_2$ is the most abundant form of PSII supercomplex present

in Arabidopsis plants grown under normal light conditions (Kouřil et al., 2013). Other forms (C_2S_2M and namely C_2S_2/C_2SM) are not so frequent and may also originate from the disassembly of the $C_2S_2M_2$ complex during sample preparation.

In plants lacking LHCB3, we did not observe any distinct band that would correspond to $C_2S_2M_2$, instead, the dominant form appeared to be the small C_2S_2 supercomplex (Figure 3, A). However, the presence of a faint, but clearly visible band at the position corresponding to C_2S_2M supercomplexes suggests that even in the absence of LHCB3, the M trimer is able to bind to C_2S_2. The data obtained by Damkjær et al. (2009) on fragments of granal membranes with crystalline arrays indicate that the $C_2S_2M_2$ supercomplex is indeed present in *lhcb3* in vivo. It seems that in the absence of LHCB3, the binding of the M trimer to C_2S_2 is very weak and the fragile $C_2S_2M_2$ supercomplexes are easily disrupted to smaller supercomplexes during the solubilization. In the previous report, where sucrose gradient fractionation was used instead of CN-PAGE to analyze *lhcb3* PSII supercomplexes, even the C_2S_2M supercomplexes were not detectable and C_2S_2/C_2SM was the only detected form of PSII supercomplex (Caffarri et al., 2009).

The separation profile of PSII supercomplexes isolated from *lhcb6* is very similar to *lhcb3* (Figure 3, A). In agreement with a previous study (Caffarri et al., 2009), we have found out that the band corresponding to $C_2S_2M_2$ is absent and that the major form of PSII supercomplex in this mutant is C_2S_2. However, in addition to this, we were able to observe also a faint band at the position of C_2S_2M supercomplexes. This again suggests the superiority of our CN-PAGE purification approach, as this form of PSII supercomplexes was not detectable in *lhcb6* via sucrose gradient fractionation (Caffarri et al., 2009). We have assumed that the formation of a small amount of C_2S_2M was enabled by the presence of the residual amount of LHCB6 (Figures 1, B, 2, A) in the *lhcb6* mutant. This hypothesis has been indeed confirmed by mass spectrometry analysis of this band, as it contained LHCB6 and had the same protein composition as C_2S_2M from WT plants (Supplemental Figure S1). In contrast to *lhcb3*, in *lhcb6*, the $C_2S_2M_2$ supercomplexes are probably not present even in the membrane, as the previous EM analysis of PSII supercomplexes in *lhcb6* thylakoids revealed more than 95% of C_2S_2 (Kovács et al., 2006). Thus, in the absence of LHCB6, the only stable form of PSII supercomplex appears to be C_2S_2 (Figure 3, A).

CN-PAGE analysis of PSII supercomplexes from the double mutant *lhcb3 lhcb6* revealed only one strong PSII band, corresponding to C_2S_2 (Figure 3, A). This is interesting in the light of the data obtained from Norway spruce. This representative of Pinaceae lacks both LHCB3 and LHCB6 (Kouřil et al., 2016), but at the same time, the CN-PAGE separation of its thylakoid membranes provides clear evidence of the presence of large forms of PSII supercomplexes (Kouřil et al., 2016, 2020). However, based solely on electrophoretic analysis, it was not possible to decide whether the larger forms of PSII supercomplexes are absent in *lhcb3 lhcb6* mutant or whether they are just too unstable to be isolated via CN-PAGE as in the case of *lhcb3*.

The appearance of "spruce-type" PSII supercomplex in Arabidopsis *lhcb3* mutant

The largest forms of PSII supercomplexes separated by CN-PAGE from thylakoid membranes of individual lines were analyzed using single-particle EM. The analysis of the supercomplexes from $C_2S_2M_2$ and C_2S_2M WT bands showed the presence of typical forms of supercomplexes (Figure 3, B; Caffarri et al., 2009), which was also confirmed by the fitting of our projection maps with a structural model of PSII supercomplex from Arabidopsis (van Bezouwen et al., 2017) and by detailed protein analysis of individual supercomplexes (Supplemental Figure S1).

The analysis of a faint CN-PAGE band from *lhcb3* that is present at the tentative position of C_2S_2M confirmed that it indeed contained C_2S_2M supercomplexes. The proteomic data suggest that the absence of LHCB3, normally present in the LHCII trimer at M position, is in *lhcb3* compensated by increased amounts of LHCB1/LHCB2 (Figure 2, A). Detailed single particle EM image analysis revealed the presence of two different forms of the C_2S_2M supercomplex in *lhcb3*. About 90% of the particles were represented by a C_2S_2M supercomplex where the M trimer binds to the PSII core complex with the help of both LHCB4 and LHCB6 subunits (Figure 3, B and C). This type of supercomplex is similar to the C_2S_2M present in WT, the only difference being a slight change in the position of the M trimer with respect to the S trimer (rotation by ca 10°, Figure 3, B and C). This result is in agreement with the previous report, where the change in the orientation of the M trimer was suggested from the analysis of semi-crystalline arrays of $C_2S_2M_2$ supercomplexes in *lhcb3* granal membranes (Damkjær et al., 2009). In the second type of C_2S_2M present in *lhcb3*, however, the M trimer is attached to the core complex only via LHCB4, without the participation of LHCB6. Single particle analysis revealed that in this type of supercomplex, the position normally occupied by LHCB6 is empty (Figure 3, B and C). In this case, the structure closely resembles the C_2S_2M supercomplex observed previously in Norway spruce (Kouřil et al., 2016); therefore, we term it "spruce-type." Although this "spruce-type" supercomplex represents only about 10% of all the analyzed supercomplexes from the *lhcb3* C_2S_2M band, it is not possible to draw any reliable conclusions about its natural abundance in *lhcb3* thylakoids. PSII supercomplexes appear to be very fragile in the absence of LHCB3, as evidenced by the disruption of $C_2S_2M_2$ supercomplexes from *lhcb3* by even very mild solubilization (Figure 3, A). Therefore, any differences in the stability of the two forms of C_2S_2M during the preparation of the sample for

CN-PAGE and EM can easily distort the estimation of their relative abundance in intact thylakoids. However, irrespective of its relative occurrence in vivo, our finding demonstrates that even in Arabidopsis, the absence of LHCB3 and LHCB6 can lead to the formation of the "spruce-type" C_2S_2M supercomplexes. The presence of this LHCB6-less "spruce-type" C_2S_2M supercomplex could contribute to the observed decrease in the relative amount of LHCB6 in *lhcb3* thylakoids (Figure 2, A).

Single particle analysis of the C_2S_2M band from *lhcb6* revealed a typical form of the C_2S_2M supercomplex observed in WT, without any structural modification (Figure 3, B). The projection map shows a density at the position of LHCB6, which could in theory indicate that there is a replacement of LHCB6 by some other LHC protein. However, the mass spectrometry analysis of supercomplexes eluted from this *lhcb6* CN-PAGE band unequivocally confirmed that these C_2S_2M supercomplexes indeed contain LHCB6 (Supplemental Figure S1) and that the appearance of the faint C_2S_2M band is a direct consequence of the presence of the residual amount of LHCB6. This band would probably be absent in a complete LHCB6 knockout and the only stable form of PSII supercomplex would be C_2S_2.

The analysis of the C_2S_2 band from *lhcb3 lhcb6* revealed a typical form of C_2S_2 (Figure 3, B). Although we have confirmed the ability of Arabidopsis to form "spruce-type" C_2S_2M (see above, Figure 3, B and C), these larger forms of PSII supercomplexes were completely absent in the CN-PAGE of the thylakoids from the double mutant. We have concluded that either $C_2S_2M_{(2)}$ supercomplexes are not formed in this mutant at all, or are present in thylakoid membranes, but are too fragile to be isolated by CN-PAGE. To resolve this issue, it was necessary to perform EM analysis of granal thylakoid membranes.

The majority of PSII supercomplexes in Arabidopsis *lhcb3 lhcb6* mutant are organized into C_2S_2 semi-crystalline arrays

EM analysis of isolated grana membranes of individual Arabidopsis mutant lines can bring additional information about the arrangement of PSII supercomplexes in vivo. In WT plants, the arrangement of PSII supercomplexes in thylakoid membranes is mostly random (Supplemental Figure S2, A), but supercomplexes can also specifically interact to form various megacomplexes (e.g. Nosek et al., 2017). Some of these megacomplexes could originate from the disassembly of semi-crystalline arrays of $C_2S_2M_2$, which are occasionally present in WT thylakoids (Supplemental Figure S2, A; e.g. Kouřil et al., 2013). The arrangement of PSII supercomplexes into semi-crystalline arrays was observed also in grana membranes isolated from *lhcb3* (Supplemental Figure S2, B). Previously, it has been shown that these arrays have slightly higher abundance in *lhcb3* and that they also consist of $C_2S_2M_2$ (Damkjær et al., 2009).

In *lhcb6*, the PSII arrays are formed by C_2S_2 rather than $C_2S_2M_2$ supercomplexes (Kovács et al., 2006; de Bianchi et al., 2008) and their abundance is relatively high (Supplemental Figure S2, C). Based on the analysis of freeze–fracture electron micrographs of *lhcb6* thylakoids, the fraction of PSII present in arrays has been previously estimated to be 25% (Goral et al., 2012). Our EM data, however, suggest that the arrays are much more frequent. In the majority of electron micrographs randomly selected for analysis, semi-crystalline arrays were present in 60%–90% of the area of granal thylakoid membranes of *lhcb6* (Figure 4). The remaining membrane areas without arrays were usually represented by low PSII density regions, where randomly oriented PSII complexes were surrounded by seemingly free space (low PSII density areas, Supplemental Figure S2, C). These parts of the granal membrane most likely contained free LHCII trimers, which could not be directly resolved in the membrane by EM due to their low contrast.

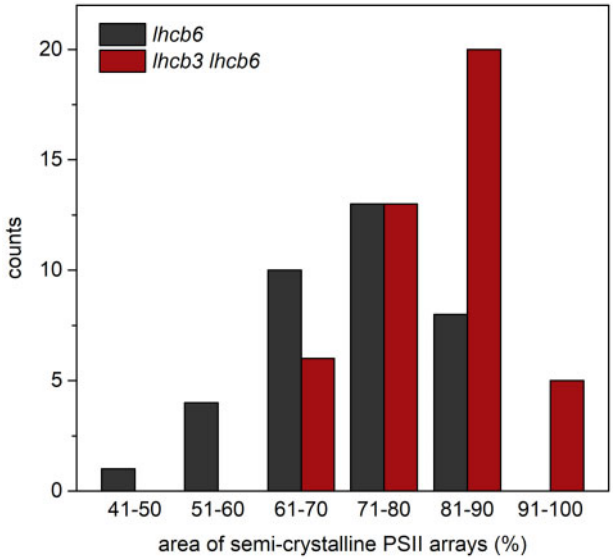

Figure 4 Histogram of a relative representation of two-dimensional semi-crystalline arrays of PSII in the grana membranes from *lhcb6* and *lhcb3 lhcb6* mutants. Area of semi-crystalline arrays of PSII per a total area of the grana membranes was determined in 30 electron micrographs of grana membranes from each type of mutants.

In the grana membranes isolated from the double mutant *lhcb3 lhcb6*, the degree of the arrangement of PSII supercomplexes into arrays was very high, with only a minor representation of LHCII-rich regions (Supplemental Figure S3). In most of the analyzed granal membranes, 80%–100% of the area was occupied by semi-crystalline arrays and we did not observe any membrane where the relative contribution of the arrays was lower than 60% (Figure 4). The average parameters of the lattice unit cell of these arrays, calculated from the analyzed crystals, were $(243 \pm 4) \times (165 \pm 3)$ Å with lattice angles 82° or $98° \pm 2°$. Very similar lattice parameters were reported for C_2S_2 arrays in PSI-less *viridis zb63* barley (*Hordeum vulgare*) mutant (250 × 165 Å, angles 80° and 100°; Morosinotto et al., 2006), and also the C_2S_2 arrays observed in *lhcb6* appear to be of the same type (de Bianchi et al., 2008). Indeed, fitting of the arrays in *lhcb3*

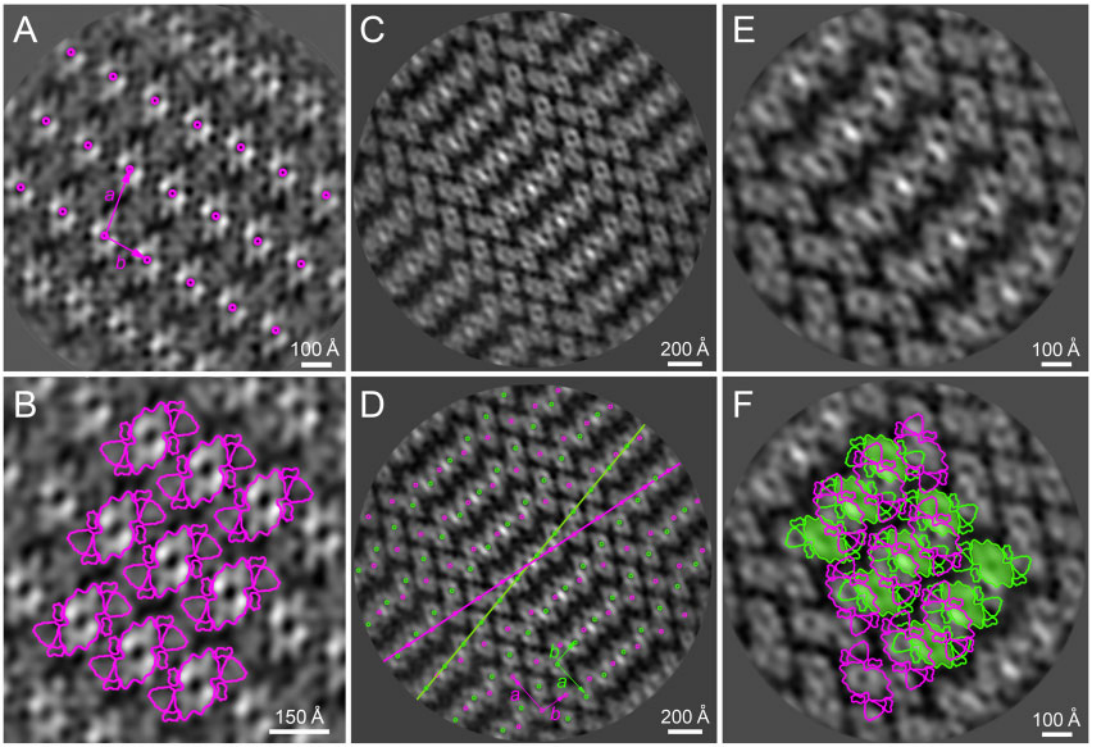

Figure 5 Different types of the two-dimensional semi-crystalline arrays of PSII in the grana membranes from *lhcb3 lhcb6* mutant. A, Image analysis of grana membrane sub-areas (1,320 × 1,320 Å) with semi-crystalline array of PSII complexes revealed a projection map of one layer of PSII complexes ordered into the regular array viewed from the lumen side. The centers of the PSII core complexes represent the lattice points of the PSII arrays (magenta). The unit cell is defined by the *a* and *b* parameters. B, Enlarged central parts of the PSII arrays shown in A. The cartoon model shows that the semi-crystalline array is formed by PSII C_2S_2 supercomplexes viewed from the lumen side. C, Image analysis of larger sub-areas (2,160 × 2,160 Å) of another type of semi-crystalline array, a carpet-like motive, of PSII complexes revealed a projection map of two translationally and rotationally shifted layers of ordered PSII complexes. D, The lattice points of the PSII arrays viewed from the lumen and stroma sides are indicated by magenta and green points, respectively. A mutual rotation of the two layers is indicated by the two magenta and green lines and it is about 17°. The unit cells are defined by the *a* and *b* parameters. E, Image analysis focused on smaller sub-areas (1,230 × 1,230 Å) of the semi-crystalline array presented in (C) revealed interactions between the two PSII layers in more details. F, A cartoon model shows variable interactions between PSII C_2S_2 supercomplexes from the two adjacent layers viewed from the lumen and stroma sides (in magenta and green, respectively).

lhcb6 (Figure 5) by a cartoon model of PSII supercomplex (Figure 6) confirms that they consist of C_2S_2. Based on this observation, we can conclude that the absence of the $C_2S_2M_2$ band in CN-PAGE of *lhcb3 lhcb6* (Figure 3, A) cannot be ascribed to the disintegration of the large supercomplexes during sample preparation and that, on the contrary to *lhcb3*, the $C_2S_2M_{(2)}$ supercomplexes are not present even in the granal membranes of *lhcb3 lhcb6*.

Previously, it has been shown that in barley *viridis zb63* mutant, PSII can be arranged in several crystal forms (Stoylova et al., 2000), and therefore we have performed a detailed analysis of crystalline arrays in order to find out whether such variability exists also in *lhcb3 lhcb6* mutant. Indeed, we have identified at least three types of C_2S_2 arrays, which differ in the dimensions and angle of the lattice unit cell, whereas the tilting of the C_2S_2 with respect to the vector of the lattice cell was similar in all three types (Figure 6 and Table 2). The models of individual crystal forms clearly show that although all of them consist of C_2S_2, the different tightness of supercomplex packing is likely to have different consequences for the diffusion rate of PQ molecules. Therefore, different types of C_2S_2 crystal arrangement can have different effects on PSII photochemical activity.

The analysis of EM micrographs of granal thylakoid membranes from *lhcb3 lhcb6* (Supplemental Figures S3–S5) also revealed the presence of membrane stacks consisting of pairs of membrane layers interacting through their stromal sides. The layers are attached to each other via two types of interactions between PSII supercomplexes—regular and variable. Regular interactions between PSII supercomplexes in adjacent layers lead to a regular pattern in EM micrographs (Figure 5, A and B and Supplemental Figure S4), which closely resembles the pattern already observed in *viridis zb63* barley mutant (Morosinotto et al., 2006). It remains an open question which component mediates the interaction of PSII supercomplexes over the stromal gap. Unfortunately, in the regular arrays, the mutual orientation of PSII supercomplexes in the interacting layers is difficult to analyze because the interacting supercomplexes vertically overlap each other. It has been suggested that the stacking might be mediated by interactions between adjacent PSII core complexes (PSII sandwiches, Albanese et al., 2016b, 2017) or between

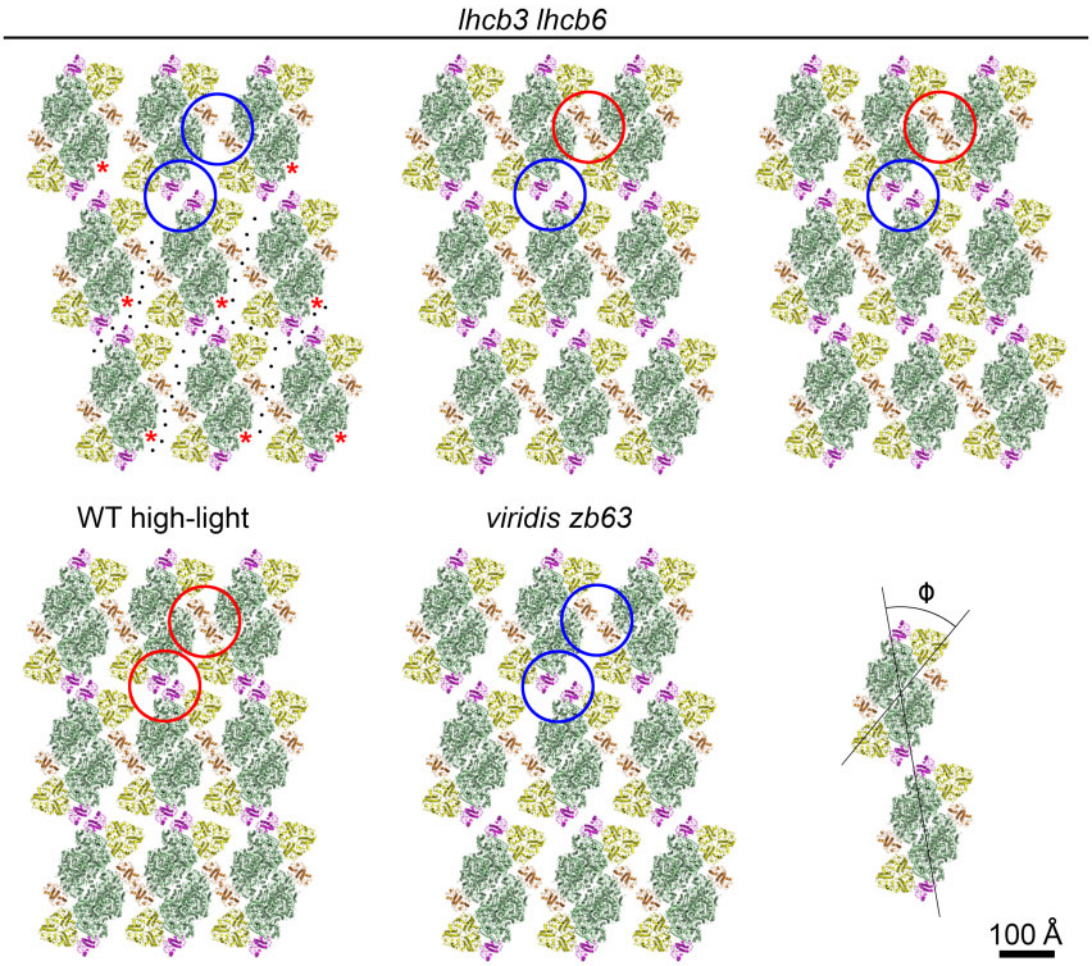

Figure 6 Structural models of different types of packing of PSII C_2S_2 complexes into two-dimensional semi-crystalline arrays. A–C, Structural models of C_2S_2 arrays in grana membranes of Arabidopsis *lhcb3 lhcb6* mutant with different lattice unit cell parameters (Table 2). The model (A) represents an open conformation with a larger distance between LHCB4 and LHCB5 proteins of neighboring C_2S_2 supercomplexes (see blue circles), which is favorable for free diffusion of PQ molecules (black on-scale dots) to/from the Q_B binding pockets (indicated by red asterisks). On the contrary, the models (B) and (C) show a closer contact between the neighboring C_2S_2 supercomplexes, especially between LHCB4 proteins (see red circles), which can hamper a free diffusion of PQ molecules. D, Structural model of C_2S_2 arrays in Arabidopsis WT acclimated to high-light intensity indicates even closer contact between neighboring C_2S_2 supercomplexes (adopted from Kouřil et al., 2013). E, Structural model of C_2S_2 arrays in barley mutant, *viridis zb63*, grown under optimal light conditions shows an open conformation similar to the open conformation (A) in Arabidopsis *lhcb3 lhcb6*. F, Determination of the ϕ angle, which is defined as the angle between the vector *a* of the lattice unit cell and the diagonal of the C_2S_2 supercomplex. Lattice unit cell parameters of all presented models are shown in Table 2. Structural model of the C_2S_2 supercomplex was obtained from Wei et al. (2016). Individual PSII subunits are color-coded: dark green, core complex; yellow, S trimer; magenta, LHCB5; and orange, LHCB4.

overlapping S trimers (Grinzato et al., 2020). Except for the regular arrays, where all PSII supercomplexes in one layer appear to interact in a periodically repeating manner with their counterparts in the second layer, we have also observed "variable" arrays. In these arrays, the interactions between PSII supercomplexes in the adjacent membrane layers are less specific, as the vertically overlapping (i.e. potentially interacting) proteins are variable. These arrays originate via interaction of two translationally and rotationally (about 17°) shifted layers of PSII complexes and are recognizable through the appearance of a "carpet-like" motive in electron micrographs (Figure 5, B–E and Supplemental Figure S5).

C_2S_2 arrays are present in vivo in Arabidopsis *lhcb6* and *lhcb3 lhcb6* mutants

Higher organization of photosynthetic complexes can be sometimes affected by isolation procedures, which are necessary for the preparation of samples for EM. Therefore, we have complemented our study by circular dichroism (CD) spectroscopy, a method that can be used to assess the macroorganization of pigment–protein complexes in thylakoid membrane in vivo (Garab and van Amerongen, 2009). Complex systems such as granal thylakoid membranes provide a complex CD spectrum, consisting of a superposition of signals induced by the intrinsic asymmetry of molecules, excitonic short-range interactions, and so-called psi-type

Table 2 Lattice unit cell parameters of C_2S_2 arrays in Arabidopsis *lhcb3 lhcb6*, Arabidopsis WT acclimated to high light and barley *vir-zb63* mutant

Plant	*a* (Å)	*b* (Å)	α (°)	ϕ (°)[a]	Type of C_2S_2 double layer	Source
Arabidopsis *lhcb3 lhcb6*	244	170	80	50	Carpet	This study, Figure 6, A
	233	162	84	51	Regular	This study, Figure 6, B
	245	155	83	50	Regular	This study, Figure 6, C
Arabidopsis WT (high light)	234 ± 5[b]	154 ± 1[b]	86 ± 1[b]	48	–	This study, Figure 6, D (data from Kouřil et al. 2013)
Barley *vir-zb63*	250	165	80	–	–	Morosinotto et al. (2006)
	244 ± 3[b]	170 ± 3[b]	82 ± 0[b]	51	–	This study, Figure 6, E
Barley *vir-zb63* (far-red light)	234 ± 0.3[b]	162 ± 0.2[b]	81.2 ± 1.9[b]	–	–	Stoylova et al. (2000)
	243 ± 0.4[b]	162 ± 0.2[b]	81.1 ± 1.9[b]	–	–	Stoylova et al. (2000)
	235 ± 0.4[b]	158 ± 0.3[b]	80.5 ± 2.0[b]	–	–	Stoylova et al. (2000)
	215 ± 0.7[b]	175 ± 0.5[b]	87.1 ± 1.7[b]	–	–	Stoylova et al. (2000)

Notes: The *a* and *b* are lengths of vectors of lattice unit cells, α is the angle between these vectors, and ϕ is the angle between the *a* vector and the diagonal of C_2S_2 supercomplex (see Figure 6, F). Data for the evaluation of the lattice unit cell parameters for Arabidopsis acclimated to high light (800 μmol photons m^{-2} s^{-1}) was taken from Kouřil et al. (2013). For other details, see the legend to Figure 6 and Materials and Methods.
[a]Evaluated from the models presented in Figure 6.
[b]Values ± SD.

signals (polymer and salt-induced; Garab and van Amerongen, 2009). We are mostly interested in the psi-type signals, as they originate from three-dimensional aggregates, which contain a high number of interacting chromophores and whose dimensions are comparable to the wavelength of measuring light.

The main spectral features of the CD spectra of WT leaves (Figure 7) are three bands at wavelengths around (+)685, (−)673, and (+)505 nm, which are of psi-type origin and thus reflecting the supramolecular organization of pigment–protein complexes (Barzda et al., 1994; Dobrikova et al., 2003). It is well established that the (+)685 and (−)673 nm psi-type CD bands are associated with chlorophyll molecules while the (+)505 psi-type CD band mainly originates from a β-carotene bound to PSII core complexes (Kovács et al., 2006; Tóth et al., 2016). The psi-type CD (−)673 nm band is mostly associated with grana stacking (Garab et al., 1991), whereas the (+)505 and (+)685 nm bands are not linked directly to the granal stacking, but rather to the lateral supramolecular organization of PSII–LHCII supercomplexes (Kovács et al., 2006; Tóth et al., 2016).

In agreement with EM microscopy analysis, the absence of LHCB3 did not lead to a substantial change in long-range macroorganization of the thylakoid membranes compared with WT, which is evidenced by a very similar psi-type signal (Figure 7). On the other hand, the depletion of LHCB6 (in both *lhcb6* and *lhcb3 lhcb6*) led to an almost complete loss of the main positive psi-type band at 685 nm, whereas the 505-nm band was unaffected (Figure 7). This change, which agrees with previously published data obtained on *lhcb6* (Kovács et al., 2006; Tóth et al., 2016), was even more pronounced in leaves of *lhcb3 lhcb6* (Figure 7). The ratio CD_{685}/CD_{505}, suggested to be proportional to PSII nearest neighbor distance (Tóth et al., 2016), is also lower in the double mutant compared with *lhcb6* (Figure 7). CD data thus support our finding from EM analysis that the *lhcb3 lhcb6* mutants have an exceptionally high abundance of C_2S_2 semi-crystalline arrays in their granal thylakoid membranes.

C_2S_2 arrays transiently slow down the electron flow from PSII to PSI

To examine the functional state of the donor and acceptor sides of the PSII complex in the LHCB mutants, the kinetics of the Q_A^- reoxidation after a single-turnover saturating flash was measured on intact leaves (Supplemental Figure S6). For WT and mutant leaves, we have observed very similar multiphasic fluorescence decay kinetics of variable fluorescence, which could be deconvoluted into three different exponential decays (Supplemental Table S1). The fast decay component (time constant ∼460–490 μs, relative amplitude ∼ 62%–65%), which arises from Q_A^- to Q_B/Q_B^- electron transfer (Vass et al., 1999), was similar in all plants, which indicates that the redox gap between the two quinone acceptors is largely unaffected in the studied LHCB mutants. The middle decay phase (∼70–80 ms, 14%–16%), reflecting the Q_A^- reoxidation in the PSII centers with an empty Q_B pocket (Deák et al., 2014), was also unchanged, suggesting a very similar redox state of PQ in the dark in WT and the mutants. Only very minor differences were observed in the slow phase of the decay (∼3.6–4 s, 20%–23%), arising from $S_2(Q_AQ_B)^-$ charge recombination, indicating that also the donor side of PSII in the mutants is not substantially different from WT. Thus, we can conclude that no substantial changes in the properties of both the acceptor and donor side of PSII were observed.

Although the function of PSII per se was not affected by the loss of LHCB3 and/or LHCB6 or by the arrangement of PSII into C_2S_2 arrays, the mesoscopic arrangement of PSII has important consequences for the functionality of the electron transport chain. To analyze the electron transport balance between PSII and PSI, we have simultaneously measured chlorophyll fluorescence and P700 oxidation, reflecting the photochemical activity of PSII and PSI (Figure 8). Upon switching on the actinic light, P700 is gradually oxidized due to PSI photochemistry and subsequent outflow of electrons from the acceptor side of PSI, but at the same time, it is reduced by electrons from PSII or cyclic electron flow around PSI. The balance between these processes shapes the final P700 signal.

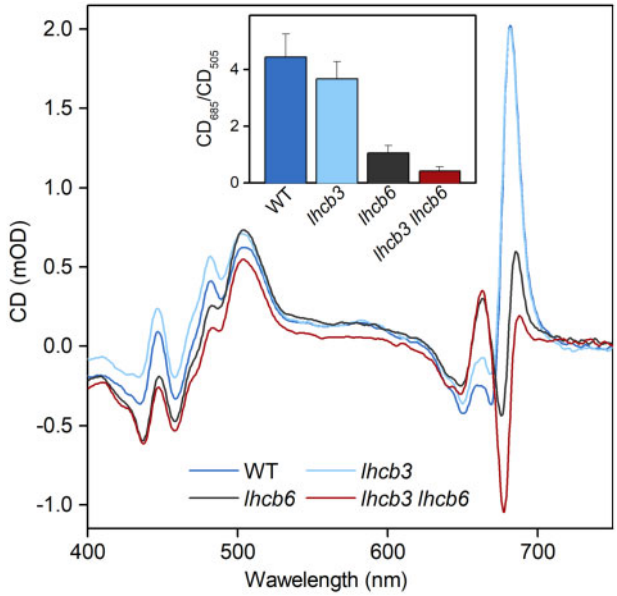

Figure 7 CD Spectra of intact leaves of WT and mutant plants (*lhcb3*, *lhcb6*, *lhcb3 lhcb6*). Averaged spectra from four leaves of each genotype (WT, *lhcb3*, *lhcb6*, *lhcb3 lhcb6*) are shown, for each leaf three scans were collected and averaged. CD spectra were normalized to the Chl Q_y absorption band. The inset presents the ratio of amplitudes of positive psi-type CD bands (CD_{685}/CD_{505}), mean ± SD is shown (n = 4).

In WT leaves, the full stable oxidation of P700 is reached after ca 60 s of light exposure (Figure 8, A). Within this period, the limitation of electron flow at the acceptor side of PSI is replaced by the limitation of electron flow at the donor side of PSI (Figure 9, D and E). This response probably reflects the induction of so-called photosynthetic control, that is the slowing of electron flow on the level of the cytochrome b_6f complex due to lumen acidification induced by cyclic electron flow around PSI (Yamamoto and Shikanai, 2019). The P700 kinetics is the same in the leaves of *lhcb3* mutants (Figure 8, B), indicating that the electron transport is similar to WT plants. In *lhcb6* and *lhcb3 lhcb6* mutants, however, the light-induced oxidation of P700 is much faster, as P700 is fully oxidized already within the first ca 15 s of illumination (Figure 8, C and D). Although in principle this type of response can result from faster activation of electron outflow from the acceptor side of PSI, the most likely explanation of this phenomenon is the limited supply of electrons to PSI. A very similar acceleration of P700 oxidation upon transition to high light was observed also in *pgr1* Arabidopsis mutant (Yamamoto and Shikanai, 2019), in which the sensitivity of the activation of photosynthetic control to lumen acidification is enhanced due to a mutation of the Rieske protein in the cytochrome b_6f complex (Munekage et al., 2001).

The fast activation of photosynthetic control in mutants without LHCB6 is supported by the highly retarded electron transport rate through PSI (ETR-I, Figure 9, C), accompanied by a strong limitation of electron transport on the donor side of PSI (Y(ND), Figure 9, D). Chlorophyll fluorescence data used for the monitoring of the PSII functioning show that in the first minutes of light exposure, the electron transport rate of PSII is reduced (ETR-II, Figure 9, B). Taking into account that the PSII function per se is not affected by the mutations (see above), these lower values of ETR-II indicate a higher reduction of the PQ pool. In principle, the lower ETR-II could also reflect a lower supply of excitations to PSII due to the smaller light-harvesting capacity of the mutants, but this was not confirmed (see below). The higher values of the parameter 1–*qP* (reflecting higher reduction of PQ pool) in the first minutes of light exposure in *lhcb6* and *lhcb3 lhcb6* (Figure 10) further support the view that in this time range, the PQ pool in thylakoid membranes of *lhcb6* and *lhcb3 lhcb6* is more reduced than in WT and *lhcb3*. The discrepancy between the transient higher reduction of PQ pool and the pronounced limitation of PSI electron transport due to a shortage of electrons on the donor side of PSI in *lhcb6* and *lhcb3 lhcb6* could be a result of the organization of PSII into C_2S_2 arrays in these mutants. However, it is important to stress that this restriction is only transient, as the PSII and PSI electron transport rates reach the WT values after several minutes of light exposure (Figure 9, B and C). This result agrees with the results by Chen et al. (2018), who observed WT level of ETR-II at steady-state conditions in *lhcb6* mutant, but disagrees with the results by de Bianchi et al. (2008), who observed in *lhcb6* mutant a permanent restriction of electron transport.

The induction of NPQ of excitations in *lhcb6* and *lhcb3 lhcb6* mutants was different from the WT and *lhcb3*. The absence of LHCB6 resulted in fast induction of NPQ in the first 30 s of light exposure, even faster than in WT and *lhcb3*, followed by a slow rise in NPQ till the end of light exposure (Figure 9, A), at which point its value reached 80%–85% of the WT and *lhcb3* value. Again, these findings correspond with the results by Chen et al. (2018), who observed similar level of the steady-state NPQ in *lhcb6* and WT, but disagrees with the results obtained by de Bianchi et al. (2008), who have reported much lower NPQ values. de Bianchi et al. (2008) explained their NPQ data by permanent restriction in electron transport leading to lower lumen acidification. However, our NPQ data indicate that there is only transient limitation in electron transport rates upon the dark-to-light transition described above.

The effective antenna size of PSII is not reduced in the mutants

The data from CN-PAGE and EM show that PSII supercomplexes in *lhcb6* and *lhcb3 lhcb6* lack the M trimer, that is the supercomplexes have smaller apparent antenna compared with WT. However, at the same time, our mass spectrometry data clearly indicate that in all mutants, the relative amount of light-harvesting proteins per RC PSII is very similar to WT (Figure 2, A). We can thus ask where these unbound LHCII trimers are located and whether they are functionally connected to PSII. As they cannot be present within the C_2S_2 arrays in *lhcb6* and *lhcb3 lhcb6*, they

Table 3 Chlorophyll fluorescence induction parameters

	F_V/F_M	F_O (r.u.)	F_M (r.u.)	ACS PSII (r.u.)	TR_0/RC (r.u.)
WT	0.836 ± 0.003	1.00 ± 0.03	1.00 ± 0.03	1.00 ± 0.03	1.00 ± 0.06
lhcb3	0.819 ± 0.011	1.07 ± 0.01	0.97 ± 0.05	0.97 ± 0.06	1.04 ± 0.05
lhcb6	0.749 ± 0.014	1.33 ± 0.04	0.87 ± 0.06	1.00 ± 0.07	1.06 ± 0.09
lhcb3 lhcb6	0.731 ± 0.011	1.41 ± 0.01	0.86 ± 0.05	1.15 ± 0.11	1.19 ± 0.05

Notes: Absorption cross-section of PSII was estimated using the area above the chlorophyll fluorescence induction curve in DCMU-treated leaves (ACS PSII) and the initial slope of the O–J rise in the chlorophyll fluorescence induction normalized to the fluorescence intensity at the J step (TR_0/RC). The parameters, except for the F_V/F_M, are normalized to the values of WT. Presented values are means ± SD (n = 5–8).

are most probably concentrated in areas with low PSII density sometimes observed at the edge of the arrays (low PSII density area, see Supplemental Figures S2, C, S3). The question is whether they are functionally attached to PSII in crystalline arrays.

To resolve this issue, we have decided to estimate the effective antenna size of PSII via the measurement of chlorophyll fluorescence induction curves. The maximal quantum yield of PSII photochemistry for dark-adapted samples, expressed as the F_V/F_M ratio (Kitajima and Butler, 1975; Lazár, 1999), is ≈0.83, which is a typical value for healthy leaves (Björkman and Demmig, 1987; Lazár and Nauš, 1998). The mutants without LHCB6 have lower values of the quantum yield, which is caused by a simultaneous increase in minimal chlorophyll fluorescence (F_O) and a decrease in maximal fluorescence (F_M) (Table 3). The effective antenna size, estimated from the O–J phase of the O–J–I–P chlorophyll fluorescence induction curves (TR_0/RC parameter), was unexpectedly slightly higher in the mutants, and the increase was the highest for the *lhcb3 lhcb6* mutant (119% of WT, Table 3). Similar results have been obtained using estimation of PSII absorption cross-section based on chlorophyll fluorescence induction measured with electron-blocking agent DCMU (ACS PSII). Also, this method indicates that the absorption cross-section of the *lhcb3 lhcb6* mutant is slightly higher than in WT (115% of WT, Table 3).

Based on our data we can conclude that the domains of unbound LHCII, which we assume to be present at grana margins in *lhcb3 lhcb6*, are most likely responsible for the mild increase in the minimal fluorescence F_O. However, considering the supposed large number of unbound LHCII, they are either very effectively quenched, or are functionally connected to PSII arrays. The estimation of absorption cross-section indicates that the latter possibility is more likely. If only S trimers were involved in light-harvesting, the absorption cross-section should be considerably smaller than in WT, where the predominant form of PSII is $C_2S_2M_2$. The fact that the absorption cross-section in the mutants without LHCB6 did not decrease compared with WT is a clear indication that the pool of unbound LHCII can supply excitations to PSII in the arrays. The existence of a large fraction of LHCII weakly connected to PSII in thylakoid membranes of the *lhcb6* mutant is also supported by fluorescence lifetime measurements at different excitation wavelengths performed earlier for *lhcb6* mutant by van Oort et al. (2010). These weakly bound LHCIIs characterized by high fluorescence lifetime are probably the reason for the observed higher F_O values in *lhcb6* and *lhcb3 lhcb6* mutants, which can lower the F_V/F_M ratio and thus underestimate the real maximum yield of PSII photochemistry.

As the effective antenna of PSII, as well as the functionality of RC PSII, are very similar in WT and all mutants, the transient retardation of the electron transport observed in *lhcb6* and *lhcb3 lhcb6* is most likely a result of limited mobility of electron carriers involved in the transfer of electrons to PSI. In our case, cytochrome b_6f complex is most likely localized at grana margins (it is probably not a part of arrays) and thus it seems unlikely that the transfer from cytochrome b_6f complex to PSI via plastocyanin would be largely affected. The most probable electron carrier that would be affected by the arrangement of PSII into semi-crystalline arrays is PQ (Morosinotto et al., 2006; de Bianchi et al., 2008).

Lateral separation of LHCII results in faster state transitions

It can be expected that the lateral separation of PSII supercomplexes from a substantial part of LHCII trimers would have functional consequences, namely on processes that largely involve LHCII. Assuming that free LHCII trimers are preferentially localized at the periphery of the PSII arrays, likely at grana margins, this localization should affect the process of state transitions. To verify this assumption, we have measured both the extent and rate of state transitions in WT as well as in all the mutants. State transitions were successfully induced in all plants (Supplemental Figure S7) and the changes of absorption cross-sections of PSII upon State I to State II transition were similar in all genotypes (Table 4).

However, the rate of state transitions (characterized by $t_{1/2}$ of the fluorescence decay upon switching off far-red light) was significantly different in individual mutants. In *lhcb3*, the rate was almost two times faster compared with WT (Table 4). This is in agreement with the previous study, where higher phosphorylation of LHCII (due to the replacement of LHCB3 by LHCB1/2) was identified as a possible cause of faster state transitions (Damkjær et al., 2009). In the *lhcb6* and *lhcb3 lhcb6* mutants, we have found that the rates were about four times faster compared with WT (Table 4), which agrees with faster state transitions in *lhcb6* reported by de Bianchi et al. (2008).

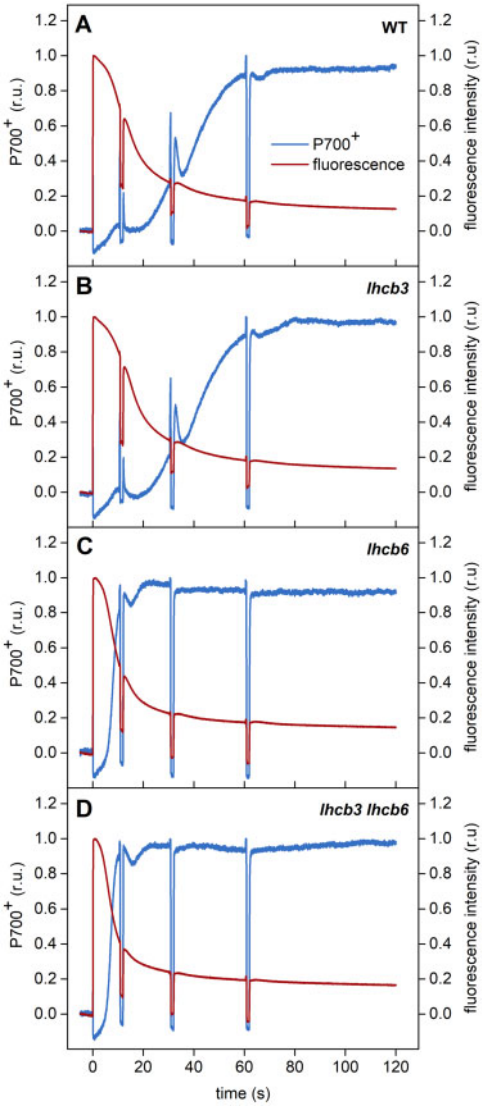

Figure 8 Representative P700 oxidation and chlorophyll fluorescence induction curves of WT and mutant plants (*lhcb3*, *lhcb6*, *lhcb3 lhcb6*). The induction curves were recorded in leaves dark-adapted for 30 min and then exposed to actinic light (800 μmol photons m^{-2} s^{-1}). The induction curves were interrupted by saturating red light pulses (300 ms, 10,000 μmol photons m^{-2} s^{-1}) followed by switching off the actinic light for 1 s, which were necessary for the calculation of PSII and PSI activity parameters presented in Figure 9. Representative curves are shown.

As similarly fast state transitions were observed in *lhcb6* and *lhcb3 lhcb6*, it is not likely that the effect is related to the replacement of LHCB3. The reason for such substantially faster state transition in *lhcb6* and *lhcb3 lhcb6* might be the involvement of free LHCII trimers localized at the periphery of the PSII arrays. Due to their peripheral location, they would have a substantially shorter migration distance to PSI than free trimers in WT, where they are probably dispersed in the whole area of the granum. At the same time, the free LHCIIs are most likely co-localized with the cytochrome b_6f complex, which is required for the activation of the kinase responsible for state transitions. Therefore, once activated, it can directly phosphorylate LHCII located conveniently at its vicinity and the phosphorylated LHCII then can quickly attach to PSI which is located nearby.

Discussion

"Spruce-type" C_2S_2M supercomplex appears in Arabidopsis lacking LHCB3

Since the emergence of LHCB3 and LHCB6 proteins at the dawn of plant land colonization, the structure of the $C_2S_2M_2$ supercomplex had been thought to be highly conserved. However, recently we have broken this dogma and have shown that LHCB3 and LHCB6 proteins, whose presence had been considered as a fingerprint of all land plants, are absent in several gymnosperm families. The loss of these two light-harvesting proteins is reflected in a unique structure of PSII supercomplex in these plant species ("spruce-type" $C_2S_2M_2$ supercomplex). In this supercomplex, the position usually occupied by LHCB6 is empty and the binding of the M trimer to the PSII core complex is modified, resulting in its tighter association with the S trimer (Kouřil et al., 2016).

It is not clear why such specific photosynthetic adaptation has developed in this group of plants. As LHCB3 and LHCB6 proteins are known to be downregulated during high light stress (Kouřil et al., 2013), it is possible that this adaptation could be connected with environmental conditions in which the ancestors of these plant groups have evolved. This would also partially explain the unusual responses of spruce photosynthetic apparatus to changes in light intensity, some of them being typical for high-light adapted plants (Kurasova et al., 2003).

To shed some light on the evolutionary and physiological implications of the "spruce-type" form of PSII supercomplex, we have prepared a double mutant of *A. thaliana* lacking LHCB3 and LHCB6 proteins. It has been shown that in the absence of LHCB3, the M trimer can bind to C_2S_2, but in a slightly different rotational position than in WT (Damkjær et al., 2009). Nevertheless, this change does not correspond with the binding mode of the M trimer within the "spruce-type" $C_2S_2M_2$ (Kouřil et al., 2016). At the same time, in Arabidopsis, the $C_2S_2M_2$ supercomplex with LHCB3-less M trimer is very fragile, a feature not observed in the "spruce-type" supercomplex. The loss of LHCB6 is known to induce much more serious disturbance of photosynthetic apparatus of Arabidopsis than the loss of LHCB3 (Kovács et al., 2006; de Bianchi et al., 2008). It has been shown that the absence of LHCB6 leads to the dissociation of the M trimer, leaving C_2S_2 as the main form of supercomplex in the *lhcb6* mutant (Kovács et al., 2006). By creating a double *lhcb3 lhcb6* mutant, we wanted to find out whether the modified LHCII trimer without LHCB3 is able to bind to C_2S_2 in the absence of LHCB6 and whether the resulting supercomplex will mimic the structure of the "spruce-type" $C_2S_2M_2$.

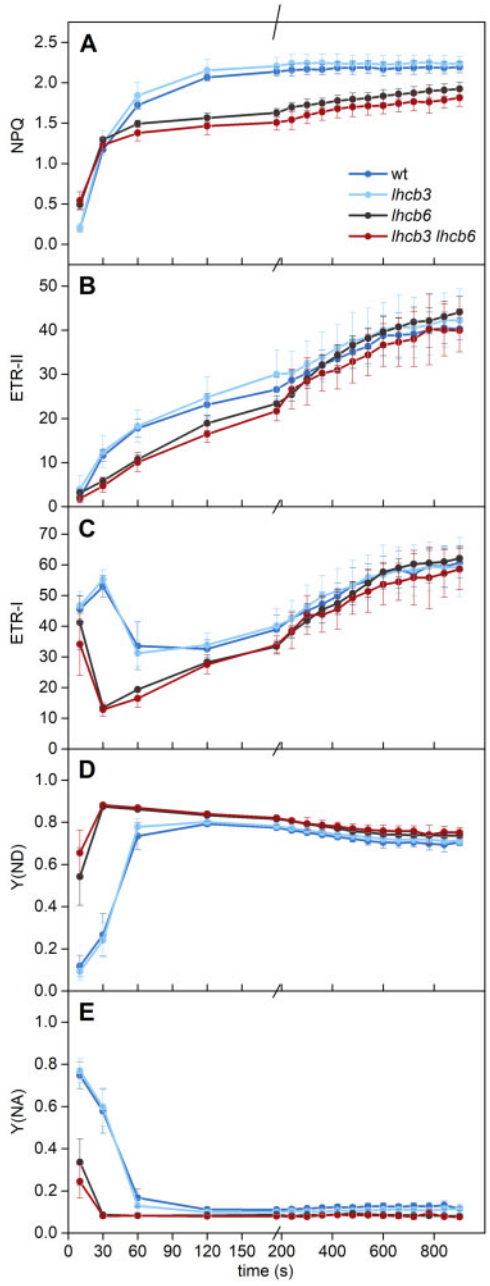

Figure 9 Photosynthetic control parameters in WT and mutant plants (*lhcb3*, *lhcb6*, *lhcb3 lhcb6*) during light exposure. The parameters of (A) NPQ in PSII, electron transport rates through (B) PSII and (C) PSI (ETR-II and ETR-I), and quantum yields of non-photochemical energy dissipation in PSI due to (D) donor and (E) acceptor side limitation (Y(ND) and Y(NA)) were recorded in leaves dark-adapted for 30 min and then exposed to actinic light (800 μmol photons m^{-2} s^{-1}). The parameters were calculated using saturating red light pulses (300 ms, 10,000 μmol photons m^{-2} s^{-1}) applied during 16-min actinic light exposure. The presented values are means ± SD from four plants.

Our results revealed that the "spruce-type" supercomplex without LHCB3 and LHCB6 can be formed even in in Arabidopsis (Figure 3, B), but at the same time, it appears that there are other important factors that are playing role in its formation and stability. Nevertheless, we were able to observe and identify the "spruce-type" supercomplex in an angiosperm plant, in particular in the *lhcb3* mutant. It is obvious that this type of supercomplex can be formed only when LHCB6 is absent along with LHCB3 (Figure 3, B), whereas in the presence of LHCB6, the LHCB3-less supercomplex closely resembles the supercomplex from WT. It is difficult to make any estimation of the abundance of "spruce-type" supercomplex in *lhcb3* in vivo, as the results of CN-PAGE and single particle analysis can be distorted by different stabilities of individual types of supercomplexes. However, the mass spectrometry data show that thylakoid membranes from *lhcb3* have a lower relative amount of LHCB6 (70% of WT, Figure 2, A), so it is tempting to hypothesize that in vivo, the fraction of supercomplexes that lack LHCB6 might correspond to the fraction of "spruce-type" supercomplexes.

We have confirmed that in Arabidopsis, "spruce-type" supercomplexes without LHCB3 and LHCB6 can be formed, but why these supercomplexes are not found in the double mutant *lhcb3 lhcb6*? As has been mentioned, it appears that without LHCB3, the attachment of the M trimer to C_2S_2 is much weaker than in WT—in the CN-PAGE of mildly solubilized *lhcb3* thylakoids we did not see any $C_2S_2M_2$ band (Figure 3, A), although we know that this type of supercomplex is present in vivo in this mutant (Damkjær et al., 2009). No such disassembly was observed for WT $C_2S_2M_2$ (Figure 3, A). The combined absence of LHCB3 and LHCB6 may lead to so strong destabilization of the M trimer, that the resulting structure is not advantageous. It might be possible that the binding of the M trimer to C_2S_2 is so weak that it cannot ensure efficient energy transfer and in such situation, the formation of C_2S_2 arrays functionally connected to a large pool of unbound LHCII trimers might represent a preferable, more efficient arrangement.

There is, however, an inevitable question—what is the factor that makes this particular form of supercomplex stable in spruce? It is possible that the key to its different stability in Arabidopsis and spruce is the type of minor antenna protein LHCB4. Due to its prominent position in the PSII supercomplex, LHCB4 is responsible for proper binding of the S and M trimers to the PSII core dimer (de Bianchi et al., 2011; van Bezouwen et al., 2017; Su et al., 2017) and plays a key role in both the energy transfer and PSII photoprotection (de Bianchi et al., 2011). Recently, it has been found that the Pinaceae and Gnetales families lack not only LHCB3 and LHCB6, but also the LHCB4.1/4.2 proteins, which have so far been thought to be the dominant isoforms of LHCB4 in land plants (Grebe et al., 2019). It appears that in spruce, only the gene for the isoform LHCB4.3 (later renamed LHCB8) is present, which has for a long time been considered as a peculiar, rarely expressed gene restricted only to angiosperm clade Eurosids (Klimmek et al., 2006). In spruce PSII, LHCB8 replaces LHCB4.1/4.2 at its binding site in the $C_2S_2M_2$, which could contribute to the stability of the "spruce-type" supercomplex.

In Arabidopsis, LHCB4 is present in three isoforms coded by three separate genes—LHCB4.1 (AT5G01530), LHCB4.2

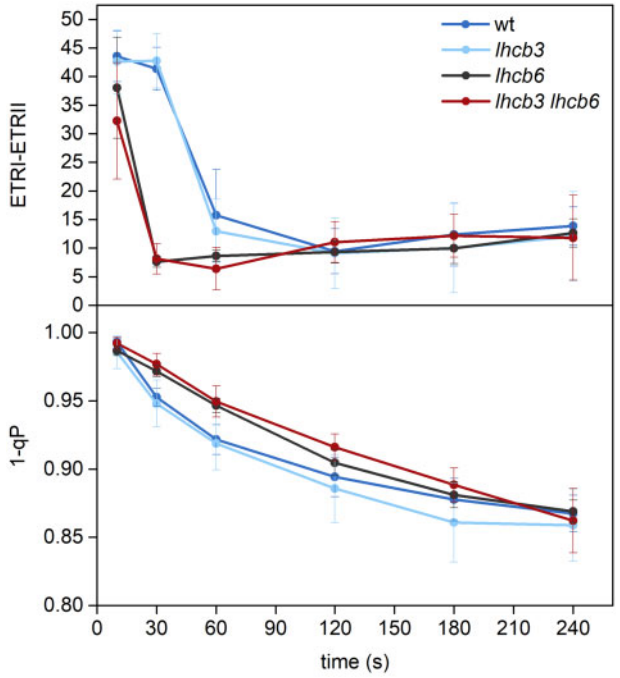

Figure 10 Cyclic electron flow around PSI and redox state of the PQ pool in WT and mutant plants (*lhcb3*, *lhcb6*, *lhcb3 lhcb6*). The extent of cyclic electron flow around PSI was estimated as a difference between ETR-I and ETR-II shown in Figure 9. The fraction of reduced PQ pool in thylakoid membranes was evaluated as 1–qP, where qP is the photochemical quenching coefficient calculated as $(F_M'-F)/(F_M'-F_O')$. The intensity of actinic light was 800 μmol photons m^{-2} s^{-1}. The presented values are means ± SD from four plants.

(AT3G08940), and LHCB4.3 (AT2G40100). All LHCB4.1/4.2 proteins from various plants have a strictly conserved 15-amino-acid motif at their C-terminus (WxTHLxDPLHTTIxD; Grebe et al., 2019). This motif has been proposed as the site of the interaction of LHCB4.1/4.2 with LHCB6 and LHCB3 (i.e. the M trimer; Su et al., 2017). This C-terminal motif is completely absent in LHCB4.3, which could explain why the evolution pressure in plant species without LHCB3 and LHCB6 led to the loss of LHCB4.1/4.2, whereas LHCB4.3 has been retained. The proteins LHCB4.1 and LHCB4.2 have high sequence homology (89% identity) and similar structure, function, and regulation (Jansson, 1999; de Bianchi et al., 2011), whereas there are strong indications that LHCB4.3 is functionally different from LHCB4.1/4.2, at least in angiosperms (Klimmek et al., 2006).

To explore possible changes in the relative amount of individual LHCB4 isoforms in the mutants, we have performed a detailed analysis of the mass spectrometry data. The amount LHCB4.3 was not increased in any of the mutants compared with WT, which indicates that in Arabidopsis, the loss of LHCB3 and/or LHCB6 does not stimulate the synthesis of LHCB4.3 (Figure 2, B). Even in a very detailed proteomic analysis of the supercomplexes eluted from the *lhcb3* $C_2S_2M_2$ band, which contains a fraction of "spruce-type" C_2S_2M, we did not see any change in the relative LHCB4.3 content (Figure 11). It seems that in Arabidopsis, the regulation of gene expression of *LHCB4.3* is completely different from spruce. The main role of LHCB4.3 in Eurosids is probably related to photoprotection, as there is an up-regulation of the LHCB4.3 gene expression under high-light conditions (Klimmek et al., 2006; Albanese et al., 2016a, 2018, 2019).

We can thus hypothesize that the reason why we were not able to observe "spruce-type" PSII supercomplexes in Arabidopsis *lhcb3 lhcb6* double mutant is the presence of LHCB4.1/4.2 proteins, which are replaced by LHCB4.3 (LHCB8) in spruce. Analysis of the double mutant grown under specific conditions leading to the accumulation of LHCB4.3 might clarify whether LHCB4.3 is indeed the key to the stability of "spruce-type" PSII supercomplex or whether some other factors stabilize this unusual PSII supercomplex structure in spruce (e.g. differences in amino-acid composition of PSII proteins in spruce and Arabidopsis, different phosphorylation pattern, etc.). Physiological characterization of Arabidopsis plants with high abundance of "spruce-type" PSII would be important for our understanding of the specifics of photosynthesis in spruce and could provide valuable clues about the possible evolutionary advantage of the loss of LHCB3 and LHCB6 in some gymnosperm groups.

Semi-crystalline arrays of PSII supercomplexes

Today we have a lot of information about photosynthetic complexes at the level of individual proteins or protein complexes (high-resolution crystal structures). However, their organization into higher order assemblies and their cooperation within them is still poorly understood, although it is clear that these processes play a key role in the highly organized and strongly regulated process of photosynthesis.

It has been known for a very long time that PSII supercomplexes in granal membranes are able to spontaneously order into semi-crystalline arrays. However, only after solving the PSII supercomplex crystal structure, it was possible to identify particular types of supercomplexes that are involved in array formation. In an extensive study, Boekema et al. (2000) were able to unequivocally distinguish two types of crystals in spinach thylakoids. The more abundant crystals with wider spacing (27.3 × 18.3 nm, 74.5°, unit area 481 nm^2) were shown to consist of the array of C_2S_2M, whereas the rare (1% abundance), more tightly packed crystals (23 × 16.9 nm, unit area of 389 nm^2) were formed by C_2S_2. On the contrary to spinach, the analysis of thylakoid membranes in Arabidopsis revealed only one type of semi-crystalline arrays, which have a bigger unit cell (25.6 × 21.4 nm, 77°, 534 nm^2) that has been identified as $C_2S_2M_2$ (Yakushevska et al., 2001). These data indicate that all forms of PSII supercomplexes (i.e. C_2S_2, C_2S_2M, and $C_2S_2M_2$) are capable of forming semi-crystalline arrays, although different types of arrays may have different properties and function. Since then, a number of studies have described the presence of the arrays in several plant species grown under various conditions (Kirchhoff et al., 2007; Daum et al., 2010; Sznee et al., 2011; Kouřil et al., 2013; Wientjes et al., 2013; Charuvi et al., 2015) or in various mutants (Ruban et al., 2003; Yakushevska et al., 2003;

Table 4 State transition parameters

	$t_{1/2}$ (s)	qT (%)
WT	124 ± 14	11.7 ± 0.4
lhcb3	75 ± 12	12.9 ± 0.4
lhcb6	26 ± 1	8.7 ± 1.3
lhcb3 lhcb6	28 ± 1	9.2 ± 1

Notes: The rate of state transition from State I to State II was characterized as the half-time ($t_{1/2}$) of a gradual fluorescence decay upon switching off far-red light according to Damkjær et al. (2009). Parameter qT, which reflects the decrease in the LHCII antenna size, was calculated as $(F_M'-F_M'')/F_M'$. Presented values are means ± SD (n = 5).

Morosinotto et al., 2006; Kovács et al., 2006; de Bianchi et al., 2008; Damkjær et al., 2009; Kereïche et al., 2010; Goral et al., 2012; Onoa et al., 2014; Tietz et al., 2015). Thus, it appears that the formation of PSII arrays is a relatively widespread phenomenon.

The heterogeneity in PSII packing, that is the simultaneous existence of "random" and "arrayed" PSII in thylakoid membranes, makes it difficult to analyze the specific properties of PSII in the arrays. The proportion of PSII present in the crystal phase is usually relatively low (around or below 10%), although there are some mutants where the fraction of arrays is reported to be higher (Morosinotto et al., 2006; Goral et al., 2012; Tietz et al., 2015). The double mutant *lhcb3 lhcb6* prepared in this study is unique as it has the majority of PSII supercomplexes packed into C_2S_2 semi-crystalline arrays (Figure 4), that is it represents a very good model for the investigation of formation, regulation, and properties of C_2S_2 PSII arrays.

It has been suggested that one of the functions of C_2S_2 arrays might be related to more efficient energy transfer among different supercomplexes (Morosinotto et al., 2006). As high protein density is a prerequisite for efficient energy transfer (Haferkamp et al., 2010), it can be speculated that the tight packing of C_2S_2 supercomplexes improves energy equilibration within interconnected antenna and makes the distribution of excitations to PSII more efficient. As the relative amount of LHCII per reaction center in both *lhcb6* and *lhcb3 lhcb6* is approximately the same as in WT (Figure 2 and Table 1), the LHCII trimers, which in WT are bound within $C_2S_2M_2$, have to contribute to the pool of "free" LHCII in the mutants. As the free trimers are not part of the arrays, they most likely create LHCII-only areas outside the arrays at the grana margins. The presence of these unattached LHCII is probably responsible for slightly higher minimal fluorescence F_O observed in the mutants (Table 3). However, it appears that this pool of LHCII has to be functionally connected with PSII in the arrays, as the effective absorption cross-section of PSII in *lhcb6* and *lhcb3 lhcb6* is comparable, or even slightly higher than in WT (Table 3). We can hypothesize that the packing of C_2S_2 supercomplexes into arrays and their functional attachment to the pool of free LHCII might represent a compensatory mechanism, which can substitute the binding of M trimers to individual PSII in the form of $C_2S_2M_2$.

The "separation" of the pool of free LHCII at the grana margins can also explain faster kinetics of state transitions. Due to space restrictions, it is obvious that the cytochrome b_6f complex is not a part of the arrays and thus it is probably located close to the LHCII pool at grana margins. It has been suggested that the kinase involved in state transitions cannot enter the closely stacked areas in the grana and that it is able to phosphorylate only LHCII in stroma or on the interface between grana and stroma (Dekker and Boekema, 2005). The activation of the kinase thus probably takes place in the same area (or very close) to the pool of free LHCII and, once phosphorylated, LHCII will have a short diffusion distance from the grana margins to stromal thylakoids. As a result, we can expect significantly faster state transition kinetics, which is indeed a phenomenon we have observed in both mutants without LHCB6 (Table 4).

Another of the frequently discussed issues related to PSII arrays is their large effect on the mobility of PQ and thus on the overall electron transport rate. There is an emerging evidence that different types of PSII arrays ($C_2S_2M_2$ and C_2S_2) may actually have the opposite effect on the effectivity of PQ diffusion. It is well known that the granal membrane is highly crowded by proteins (70%–80% of the membrane area, Kirchhoff, 2008) and that the protein concentration is very close to a critical threshold above which the long-range diffusion coefficient drops to zero (Tremmel et al., 2003). It has been proposed that the arrangement of $C_2S_2M_2$ PSII supercomplexes into crystalline arrays can lead to the formation of a kind of lipidic channel, which might be viewed as a diffusion highway facilitating fast diffusion of PQ molecules to the cytochrome b_6f complex localized outside the arrays (Tietz et al., 2015). However, on the other hand, it has been argued that in C_2S_2 arrays the packing is so tight that there is very limited space for PQ diffusion. Indeed, plants with extensive C_2S_2 arrays (Arabidopsis *lhcb6*, barley *viridis zb63*) have been previously reported to suffer from retarded linear electron transport, lower PSII yield, and impaired NPQ (Kovács et al., 2006; Morosinotto et al., 2006; de Bianchi et al., 2008).

However, the situation appears to be much more complex, as a detailed analysis of multiple crystalline arrays in the *lhcb3 lhcb6* mutant revealed that there is a substantial degree of variability in the types of C_2S_2 arrays (Table 2). It appears that while some of the C_2S_2 arrays are indeed very tightly packed, leaving very small space for the diffusion of PQ, there are also other types of arrays where the diffusion restriction is not so severe. As in all types of the observed crystals the Q_B pocket (red asterisk, Figure 6) is freely accessible to PQ (black dots, Figure 6), the main factor affecting the PQ diffusion appears to be the spatial "bottleneck" between LHCB4 and LHCB5 in the neighboring supercomplexes (red and blue circles, Figure 6). Figure 6, A shows a type of crystal where the packing of C_2S_2 supercomplexes is relatively loose, with enough space left between individual protein complexes to enable diffusion of PQ in all directions. A similar type of crystal was observed in barley mutant without PSI (*viridis zb63*) (Figure 6, E). However, in *lhcb3*

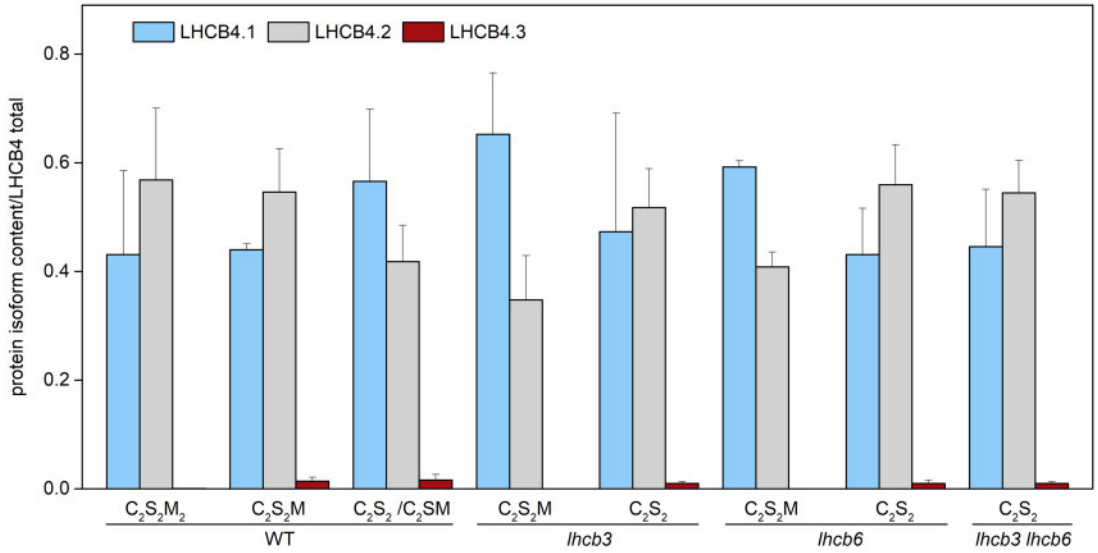

Figure 11 Content of individual LHCB4 isoforms in PSII supercomplexes isolated from *A. thaliana* WT and mutant plants (*lhcb3*, *lhcb6*, *lhcb3 lhcb6*). The relative content of individual LHCB4 isoforms was determined by LC–MS/MS in samples prepared from gel bands excised from CN-PAGE (see Figure 3, A). The contribution of LHCB4.1, 4.2 and 4.3 isoforms, evaluated from normalized PG intensities, is shown relatively to the overall content of LHCB4. The presented values are means ± SD from four replicates. Different forms of separated PSII supercomplexes consist of PSII core dimer (C_2) and one and/or two copies of strongly (S) and moderately (M) bound light-harvesting trimers.

lhcb6, we have also found crystals with smaller lattice units (Table 2), where the PQ diffusion pathway was partially closed due to the very close contact between LHCB4 subunits of neighboring C_2S_2 supercomplexes (red circle, Figure 6, B and C). As a result, the PQ diffusion is more restricted in these types of crystals as PQ can move only in one direction (horizontally, considering the crystal orientation shown in Figure 6, B and C). An example of an extremely tightly packed C_2S_2 crystal is shown in Figure 6, D. In this PSII arrangement, previously sporadically observed in high-light acclimated WT Arabidopsis (Kouřil et al., 2013), the diffusion of PQ is completely restricted, as the possible pathways are closed in both directions by a tight contact between LHCB4 and LHCB5 antennae (red circles, Figure 6, D). It can be assumed that the PSII supercomplexes arranged into this type of crystal do not contribute to linear electron transport and could represent an operative storage structure of PSII with their own quenching mechanism.

Our data indicate that there is a variety of C_2S_2 crystal types, which largely vary with respect to the degree of the restriction of PQ diffusion. It appears that a very small rearrangement of the PSII crystalline arrays can have a large effect on their photochemical activity, as it can lead to the opening or closing of two apparent "bottlenecks" for PQ diffusion, localized between LHCB4 and LHCB5 subunits of the neighboring supercomplexes. It is possible that such crystal rearrangement can be a part of the fine-tuning mechanism by which plants regulate and optimize electron transport under various conditions.

Formation of C_2S_2 arrays—a strategy for the protection of both PSI and PSII upon abrupt high light exposure?

Analysis of the photosynthetic response of *lhcb6* and *lhcb3 lhcb6* mutants revealed significant retardation of the electron transport rate in the first minutes of light exposure. Interestingly, after this transient slow-down, the electron transport parameters in both mutants reached the values of WT and *lhcb3* (Figure 9). This finding contradicts the result obtained by de Bianchi et al. (2008), who have reported that considerable suppression of the PSII electron transport rate of *lhcb6* persists even at steady-state conditions. The reason for the discrepancy is not clear, but it could be associated with different growth conditions leading to substantially higher overall fitness of our *lhcb6* (and *lhcb3 lhcb6*) mutants, which is evidenced by, for example better growth (Figure 1, A), higher F_V/F_M ratio (Table 3) or NPQ values (Figure 9, A). Obviously, in our case, the transient retardation of electron flow between PSII and PSI in mutants without LHCB6 cannot be attributed to any permanent damage of the electron transport pathway, but seems to be rather a result of altered dynamics of regulatory processes. One of the feasible hypotheses that could possibly explain the dynamic changes in electron transport restriction is the light-induced rearrangement/disordering of the C_2S_2 arrays.

It has been shown that immediately after the exposure of dark-adapted plants to light, when the outflow of electrons from the acceptor side of PSI is restricted, the cyclic electron transport (CET) around PSI is highly stimulated (Joliot and Joliot, 2002). As a result, P700 becomes gradually fully oxidized (Figure 8), which is crucial for the protection of PSI against photoinhibition (for a recent review, see Miyake, 2020). The lumen acidification induced by CET then leads to the suppression of electron transport from PSII to PSI on the level of the cytochrome b_6f complex (photosynthetic control, see Yamamoto and Shikanai, 2019), which, together with the gradual activation of electron outflow at the acceptor side of PSI, leads to the suppression of CET. The activity

of CET can be estimated from the difference between electron transport rates ETR I and ETR II and the evaluation of this parameter revealed that the activation and dynamics of CET are the same in WT and *lhcb3* mutant (Figure 10). However, in *lhcb6* and *lhcb3 lhcb6* mutants, the suppression of CET was much faster, within the first 30 s of illumination (Figure 10). The reason for this result is not clear, but could be somehow associated with the transient limitation of PQ diffusion due to the arrangement of PSII into C_2S_2 arrays. As the over-reduction of the PQ pool is thought to suppress CET (Allen, 2003; Miyake, 2010), the higher reduction of the PQ pool observed in the first minutes of illumination in *lhcb6* and *lhcb3 lhcb6* (Figure 10) can be connected with the faster inactivation of CET in these mutants. However, it is important to stress that even when CET is activated for a substantially shorter time in *lhcb6* and *lhcb3 lhcb6* mutants, P700 is oxidized in these plants much faster than in WT (Figure 8). It is tentative to speculate that the transient restriction of PQ diffusion, likely resulting from the packing of PSII into C_2S_2 arrays, can substitute CET in the photoprotection of PSI.

Another interesting phenomenon that might be connected with the arrangement of PSII in C_2S_2 arrays is related to the dynamics of the induction of NPQ. In both *lhcb6* and *lhcb3 lhcb6*, the induction of NPQ in the first seconds of light exposure was faster compared with WT and *lhcb3* (Figure 9, A). The light-induced induction of energy-dependent NPQ (qE) in plants is a strictly regulated and complex process triggered by lumen acidification. Lowering lumen pH leads to several processes, including the dissociation of LHCIIs from PSII supercomplexes, activation of xanthophyll cycle (deepoxidation of violaxanthin (Vio) to zeaxanthin (Zea) by violaxanthin deepoxidase (VDE)), and formation of quenching centers in the aggregated LHCIIs (for a recent review, see Ruban and Wilson, 2020). It has been proposed that the light-induced dissociation of LHCIIs from PSII supercomplexes is represented by a detachment of the M trimer and LHCB6 from the $C_2S_2M_2$ supercomplex and that this process is induced by protonated PsbS (Betterle et al., 2009; Dall'Osto et al., 2017). As the pK_a of PsbS protonation is relatively low (about 5.2, Li et al., 2002), considerably pronounced lumen acidification is necessary for the light-induced disassembly of $C_2S_2M_2$, that is for the induction of NPQ in plants where $C_2S_2M_2$ is the major form of PSII supercomplex. As the dissociation of LHCIIs from PSII supercomplexes is necessary to make Vio in LHCIIs available for the conversion to Zea by activated VDE (for a review, see Morosinotto et al., 2003), pronounced lumen acidification (inducing LHCII dissociation) is also required for the effective function of the xanthophyll cycle, although VDE itself is activated already at higher luminal pH (pKa about 6, Günther et al., 1994; Bratt et al., 1995). Therefore, the dynamics of LHCII detachment appears to be the main factor determining the dynamics/kinetics of NPQ.

Recent findings evidenced that only separated LHCIIs and light-induced lumen acidification are the crucial factors that are necessary for qE (Johnson, 2020; Saccon et al., 2020). Therefore, it is natural to expect that in plants exposed to stress factors that lead to the detachment of LHCII from PSII supercomplexes, the dynamics of qE will be affected. Indeed, faster induction of qE has been observed for example in plants preheated in the dark (Ilík et al., 2010), where the disassembly of PSII supercomplexes is well known (e.g. Lípová et al., 2010). This scenario matches also the results obtained in this work for the *lhcb6* and *lhcb3 lhcb6* Arabidopsis mutants. As the $C_2S_2M_2$ supercomplexes are replaced by C_2S_2 and a large pool of separated LHCII trimers, the dissociation is already achieved and therefore we can observe very fast qE induction in the first seconds of illumination, even though the overall rate of electron transport is retarded. These results are supported by a paper by Townsend et al. (2018), who have observed pronounced initial phase of qE induction in Arabidopsis mutants NoM that lack minor PSII antenna complexes and have a large pool of free LHCIIs. Taking into account the facts above, it appears that PSII arranged into C_2S_2 arrays with a pool of detached LHCII trimers at the array margins represents the arrangement that is "pre-prepared" for the formation of quenching centers and thus is beneficial for very fast induction of NPQ.

Conclusions

Our experiments have shown that the loss of LHCB3 has surprisingly strong destabilizing effect on $C_2S_2M_2$ supercomplexes, as the binding of the LHCB3-less M trimer to C_2S_2 is very weak. A very small part of the PSII supercomplexes in Arabidopsis *lhcb3* mutant appeared to adopt unique structure previously observed only in Norway spruce ("spruce-type" supercomplex), where LHCB6 is missing but the LHCB3-less M trimer is still attached to the PSII core. The absence of the "spruce-type" PSII supercomplexes in the *lhcb6* and *lhcb3 lhcb6* mutants indicates that on the contrary to spruce, in Arabidopsis both LHCB3 and LHCB6 proteins are needed for stable binding of the M trimer to PSII core. As the minor antenna LHCB4 is in direct contact with both the M trimer and LHCB6, we can speculate that the clue to the different stability of the "spruce-type" PSII supercomplex in Arabidopsis and spruce could be different isoform of this protein. The only isoform of LHCB4 in spruce is of LHCB4.3 type (renamed LHCB8), which is characteristic by the loss of a highly conserved motif at its C-terminus. On the other hand, in WT Arabidopsis as well as in all the analyzed mutants, the most populated isoforms were LHCB4.1 and LHCB4.2, with only negligible contribution of LHCB4.3. Further studies are needed to identify factors that are crucial for the formation and stabilization of PSII supercomplex with "spruce-like" structure in Arabidopsis. We are just beginning to understand the unique physiological benefits of the "spruce-like" PSII structure and more effort will be necessary to fully fathom the reasons that led a group of plants to "abandon" the widely conserved and evolutionary optimized PSII structure adopted by all other land plants.

PSII supercomplexes in Arabidopsis *lhcb6* and *lhcb3 lhcb6* mutants were present almost exclusively in the C_2S_2 form, which in WT plants appears primarily at high light conditions when LHCB3 and LHCB6 are downregulated. The C_2S_2 supercomplexes were arranged into very large semi-crystalline arrays, which can be connected with some interesting physiological features we have observed in *lhcb6* and *lhcb3 lhcb6* plants. These mutants showed fast activation of photosynthetic control of electron transport in thylakoid membranes, which can protect PSI against photoinhibition upon a sudden rise in light intensity, and even faster induction of NPQ, protecting PSII against overexcitation. Both these responses, which would be especially helpful in fluctuating light conditions, are probably associated with the restriction of electron transport between PSII and PSI resulting from the semi-crystalline arrangement of C_2S_2. However, on the contrary to the previous study on the *lhcb6* mutant (de Bianchi et al., 2008), we show that this restriction is only transient, as both PSI and PSII electron transport rates in *lhcb6* and *lhcb3 lhcb6* reach WT values after approximately 4 min of continuous illumination. It is tempting to hypothesize that this transient slowdown in electron transport between PSII and PSI could be controlled by light-dependent rearrangement of C_2S_2 semi-crystalline arrays, which would also explain the considerable variability in the types of C_2S_2 arrays we have observed in grana membranes of *lhcb3 lhcb6* mutants. Detailed structural analysis of the dynamics of C_2S_2 arrays in response to light could further contribute to the uncovering of the still enigmatic function of PSII crystalline arrangement in plants.

Material and methods

Plant material and growth conditions

Arabidopsis (*A. thaliana*) WT (accession Columbia) and T-DNA insertion lines *lhcb3* (SALK_020314c), *lhcb6* (SALK_077953) were obtained from Arabidopsis Biological Resource Center collection. Plants carrying double mutation (*lhcb3 lhcb6*) were prepared by crossing homozygous *lhcb3* and *lhcb6* plants. Plants from the F_1 generation were self-fertilized and double homozygous plants were selected from the F_2 generation via PCR genotyping (Thermo Scientific Phire Plant Direct PCR Kit) using the combination of gene-specific primers and universal T-DNA primer LBb1. Primer sequences were as follows: lhcb3_FP: AGAATTCCCTG GCGATTATGG; lhcb3_RP: ATAAAGGTCGTCACCGGA AATG; lhcb6_FP: GGTGAGGAACGAAGAACCAA; lhcb6_RP: CCAAACTCCCGACTTTACCA; and LBb1: GCGTGGACC GCTTGCTGCAACT. Arabidopsis plants were grown in a walk-in phytoscope (Photon Systems Instruments, Drásov, Czech Republic) at 22 °C, with an 8-h light/16-h dark cycle (light intensity 120 µmol photons m^{-2} s^{-1}), and 60% humidity. All experiments were performed with 6–7-week-old plants. Barley (*H. vulgare*) mutant *viridis zb63* was grown hydroponically (Knop solution) in a growth chamber (PGC-40L2, Percival Scientific, USA) at 21 °C, with a 16-h light/8-h dark cycle (light intensity 100 µmol photons m^{-2} s^{-1}) and 50% humidity for 2 weeks.

Fresh weight determination and isolation of thylakoid membranes

Prior to isolation, plants were dark-adapted for 30 min. Arabidopsis rosettes or primary leaves of barley were cut and used for the determination of fresh weight. Subsequently, thylakoid membranes were isolated using the protocol described by Dau et al. (1995). All procedures were performed under green light on ice or at 4 °C. The chlorophyll content in the final thylakoid membrane suspension was determined spectrophotometrically by a pigment extraction in 80% acetone (Lichtenthaler, 1987).

Pigment analysis

Leaves were collected from dark-adapted plants (30 min), weighed, and frozen in liquid nitrogen. After homogenization in 80% acetone with a small amount of $MgCO_3$ and centrifugation (3,600 *g*, 5 min, 4°C), the obtained supernatant was used for spectrophotometric (Unicam UV 500, Thermo Spectronics, UK) determination of chlorophyll and carotenoid content (Lichtenthaler, 1987). Quantification of xanthophyll content (violaxanthin, antheraxanthin, zeaxanthin) was performed by a reversed-phase high-performance liquid chromatography (HPLC) using Alliance e 2695 HPLC System (Waters, Milford, MA, USA) equipped with 2,998 Photodiode Array detectors. The separation was carried out using a gradient system (1.5 mL min^{-1} at 25 °C) on a LiChrospher 100 RP-18 (5 µm) LiChroCART 250-4 (Merck, Darmstadt, Germany) with acetonitrile:methanol:water (87:10:3; v/v) and methanol:*n*-hexane (80:20; v/v) as solvent systems. Quantification of the xanthophylls was based on the comparison of their absorbance (441 nm violaxanthin, 446 nm antheraxanthin, and 454 nm zeaxanthin) with corresponding standards purchased from DHI Lab Products (Hørsholm, Denmark).

Western blot analysis

Thylakoid membranes (100 µg of chlorophyll) were mixed with 1 mL of extraction buffer (14 mM DL-dithiothreitol, 28 mM Na_2CO_3, 175 mM sucrose, 5% (w/v) SDS, and 10 mM EDTA-Na_2), incubated at 70 °C for 30 min, and centrifuged for 10 min at 19,200 g. The supernatant containing isolated proteins was used for blotting. Isolated proteins (corresponding to 1 µg of chlorophyll) were supplemented with sample buffer (Tricine Sample Buffer, BioRad; 3× diluted) and dH_2O to a total volume of 20 µL. After 10 min incubation at 70 °C, samples were loaded onto 10% gel (Mini-PROTEAN TGX Precast Protein Gel, Bio Rad, Hercules, USA). Electrophoretic buffers were prepared according to Schägger (2006). Electrophoresis was performed at RT with a constant voltage of 100 V for 45 min.

The separated proteins were transferred to a polyvinylidene fluoride membrane using Trans-Blot Turbo RTA Mini 0.2 µm PVDF Transfer Kit (Bio Rad) and detected using specific antibodies. All antibodies used in the

present study were purchased from Agrisera (Vännäs, Sweden). The presence of primary antibodies Anti-LHCB3 (AS01 002) and Anti-LHCB6 (AS01 010) was detected with a secondary antibody with conjugated HRP enzyme and a chemiluminescent signal was recorded after developing with Immobilon Western Chemiluminescent HRP Substrate (Merck, Darmstadt, Germany) and visualized using gel scanner Amersham Imager 600RGB (GE HealthCare Life Sciences, Tokyo, Japan).

CN-PAGE

CN-PAGE (CN-page) was performed according to Nosek et al. (2017) with minor modifications. Thylakoid membranes (10 μg of chlorophyll) were solubilized with *n*-dodecyl α-D-maltoside using a detergent:chlorophyll mass ratio of 15, and supplemented with sample buffer (50 mM HEPES/NaOH, pH 7.2, 0.4 M sucrose, 5 mM $MgCl_2$, 15 mM NaCl, 10% glycerol) to a final volume of 30 μL. After short gentle mixing (approximately for 2 s), samples were immediately centrifuged at 20,000 g/4 °C for 10 min to remove non-solubilized membranes. The supernatant was loaded onto a polyacrylamide gel with 4%–8% gradient (Wittig et al., 2007), stacking gel was not used. The electrophoretic separation was conducted in a Bio-Rad Mini protean tetra cell system (Bio Rad), starting with a constant current of 3.5 mA for 15 min and then continuing with a constant current of 7 mA until the front reached the bottom of the gel. The CN-PAGE gel was analyzed using a gel scanner Amersham Imager 600RGB (GE HealthCare Life Sciences, Tokyo, Japan). Transmission mode using white light illumination was used for the visualization of all bands.

Mass spectrometry analysis

Isolated thylakoid membranes were subjected to filter-aided sample preparation as described elsewhere (Wiśniewski et al., 2009). The resulting peptides were analyzed by liquid chromatography–tandem mass spectrometry (LC–MS/MS) performed using UltiMate 3000 RSLCnano system (Thermo Fisher Scientific, Waltham, USA) on-line coupled with Orbitrap Elite hybrid spectrometer (Thermo Fisher Scientific).

Bands with desired PSII supercomplexes separated by CN-PAGE were excised and after washing procedures, each gel band was incubated with trypsin. LC–MS/MS analysis was performed using UltiMate 3000 RSLCnano system (Thermo Fisher Scientific) on-line coupled with Orbitrap Q Exactive HF-X spectrometer (Thermo Fisher Scientific). See the section Supplemental Methods S1 for full details regarding the analyses and data evaluation.

EM and single particle analysis

Elution of isolated PSII supercomplexes from the gel and preparation of specimens for single particle EM was performed according to a procedure described by Kouřil et al. (2014). Electron micrographs were collected using a Tecnai G2 F20 microscope (FEI Technologies, Hillsboro, USA) with an Eagle 4K CCD camera (FEI Technologies) at 133,000× magnification. The pixel size at the specimen level after binning the images to 2,048 × 2,048 pixels was 0.218 nm. Approximately 92.000, 293.000, 42.000, 33.000, and 61.000 PSII projections were picked in semi-automated mode from 2,128, 7,642, 4,447, 2,311, and 1,925 micrographs of specimens prepared from the gel bands assigned as WT $C_2S_2M_2$, WT C_2S_2M, *lhcb3* C_2S_2M, *lhcb6* C_2S_2M, and *lhcb3 lhcb6* C_2S_2, respectively. Individual datasets were subjected to reference-free two-dimensional classification using SCIPION image processing framework (de la Rosa-Trevín et al., 2016). The structure of the $C_2S_2M_2$ supercomplex (van Bezouwen et al., 2017) was used to fit the projection maps of analyzed PSII supercomplexes.

EM of isolated grana membranes from *A. thaliana* WT, *lhcb3*, *lhcb6*, and *lhcb3 lhcb6* mutants, isolated according to Kouřil et al. (2013), was performed on a Jeol JEM2010 (Jeol, Tokyo, Japan) with a Quemesa CCD camera (EMSIS, Muenster, Germany) and a Jeol 2100 (Jeol, Japan) with a Tengra CCD camera (EMSIS, Muenster, Germany). Sub-areas (1,320 × 1,320 Å, 2,160 × 2,160 Å) of two-dimensional crystalline arrays of PSII C_2S_2 supercomplexes from *lhcb3 lhcb6* were analyzed using a single particle approach using RELION software (Scheres, 2012). The structure of the C_2S_2 supercomplex (Wei et al., 2016) was used to fit the two-dimensional arrays. Lattice parameters of the crystalline arrays and a ratio of the area of semi-crystalline PSII arrays per total area of the grana membranes were analyzed using ImageJ software (Schneider et al., 2012).

Chlorophyll fluorescence and P700 measurements

Minimal chlorophyll fluorescence F_O, maximal chlorophyll fluorescence F_M, and maximum quantum yield of PSII photochemistry F_V/F_M (where $F_V = F_M - F_O$) for the dark-adapted state were evaluated from a fast chlorophyll fluorescence induction transients measured for 5 s on pre-darkened (30 min) Arabidopsis leaves using a Plant Efficiency Analyzer—PEA (Hansatech, King's Lynn, Norfolk, UK). The parameters were calculated using Biolyzer software (R.M. Rodriguez, University of Geneva, Switzerland). Chlorophyll fluorescence was excited using red light adjusted to the relative intensity of 45%.

PSII and PSI functions were simultaneously recorded on whole leaves (pre-darkened for 30 min) using a Dual-PAM100 measuring system (Heinz Walz, Effeltrich, Germany) during light exposure by red actinic light (800 μmol photons m^{-2} s^{-1}) for 16 min and using 300 ms saturating red light pulses (10,000 μmol photons m^{-2} s^{-1}). PSII function and induction of NPQ in PSII were detected and calculated as the effective yield of PSII photochemistry for light-adapted state $Y(II) = (F_M' - F)/F_M'$ (F_M' is the maximum chlorophyll fluorescence intensity at a light-adapted state and F is related chlorophyll fluorescence level at the state induced by the actinic light) and $NPQ = (F_M - F_M')/F_M'$ (F_M is the maximum chlorophyll fluorescence intensity at dark-adapted state; Genty et al., 1989; Bilger and Björkman, 1990). Parameters related to PSI function, Y(I), Y(ND), and Y(NA), that is the effective quantum yield of PSI photochemistry, and the quantum yields of non-

photochemical energy dissipation due to donor and acceptor side limitation, respectively, were calculated using the Dual-PAM100 software according to Klughammer and Schreiber (2008). The electron transport rate through PSII and PSI (ETR-II and ETR-I) are directly related to Y(II) a Y(I), respectively (= PAR × Y(II) or Y(I) × 0.84 × 0.5, where PAR is the irradiation level at 400–700 nm and the constants represent the assumed average leaf absorptance of PAR and the fraction of the light absorbed by given photosystem). The fraction of reduced PQ pool in thylakoid membranes was estimated as 1–qP, where qP is the photochemical quenching coefficient calculated as $(F_M'-F)/(F_M'-F_O')$. F_O' represents related minimal chlorophyll fluorescence level during the light exposure and was calculated according to Oxborough and Baker (1997).

Estimation of effective antenna size of PSII

Chlorophyll fluorescence induction was measured with a Dual-PAM100 system (Heinz Walz) on leaves that were excised from dark-adapted (30 min) Arabidopsis plants and subsequently infiltrated with 50 μM 3-(3,4-dichlorophenyl)-1,1-dimethylurea (DCMU) using five low-pressure shockwaves. This treatment was sufficient to block the PSII electron transport from Q_A to Q_B. The fluorescence induction was excited by red light (12 μmol photons $m^{-2}s^{-1}$) according to Belgio et al. (2014). Evaluation of effective absorption cross-section (σ, denoted as ACS PSII in Table 3) of PS II in the samples was estimated from fluorescence induction curves measured for 450 ms and double-normalized to obtain relative variable Chl fluorescence $V(t)$ as

$$V(t) = \big(F(t)-F_0\big)/(F_M-F_0),$$

where F_0 and F_M are minimal and maximal Chl fluorescence, respectively, and $F(t)$ is Chl fluorescence at time t.

According to the theory of Malkin et al. (1981), the complementary area (CA, area between the $V(t)$ measured with DCMU-treated samples and the horizontal line at the F_M level) of dark-adapted sample is related to σ as follows:

$$\mathrm{CA} = 1/\sigma I,$$

where I is the incident light intensity. Since I was the same for all measured samples, we get

$$\sigma \approx 1/\mathrm{CA}.$$

The CA has been calculated using Microsoft Excel.

Another estimation of effective antenna size of PSII of the samples was performed from the measurement of chlorophyll fluorescence curves of dark-adapted (30 min) leaves (without DCMU) measured using a PEA (Hansatech) under high intensity of incident light (adjusted to 45%). Under these conditions, a typical O–J–I–P Chl fluorescence induction curve is measured (Strasser and Srivastava, 1995; Lazár, 2006). According to the theory of energy fluxes and the JIP test (Strasser et al., 2004; Stirbet et al., 2018), maximal trapping flux at time zero TR_0/RC (corresponding to the rate by which an incident light is trapped by the reaction centers of PSII resulting in the reduction of Q_A) can be expressed as $TR_0/RC = M_0/V_J$, where M_0 and V_J are defined as follows:

$$M_0 = 4(F_{300\mu s}-F_{50\mu s})/(F_M-F_0)$$

$$V_J = (F_J-F_0)/(F_M-F_0),$$

where $F_{50\mu s}$, $F_{300\mu s}$, and F_J are values of Chl fluorescence signal at 50 and 300 μs and at the position of the J step (at 2 ms), respectively, of the O–J–I–P curve. Since the initial rate of Q_A reduction reflects the effective antenna size of PSII of the sample (Lazár et al., 2001), TR_0/RC was used as another way to estimate the effective antenna size of PSII. The TR_0/RC was calculated using Biolyzer software (R.M. Rodriguez, University of Geneva, Switzerland).

Measurement of state transitions

State transitions were induced and monitored via the measurement of chlorophyll fluorescence using a Dual-PAM100 (Heinz Walz) according to de Bianchi et al. (2008) with modifications. A measurement protocol started with a preferential excitation of PSII by illumination with red light (13 μmol photons m^{-2} s^{-1}) for 15 min. Then PSI was excited by far-red light for 15 min simultaneously with the red light, which was followed by 800 ms saturating red light pulse (10,000 μmol photons m^{-2} s^{-1}) to determine the F_M' level in State I. A transition from State I to State II was achieved by red light illumination for 15 min, followed by a saturating light pulse to determine the F_M'' level in State II. The half-time of state transition from State I to State II was evaluated as the half-time of a gradual fluorescence decay upon switching off far-red light according to Damkjær et al. (2009). Parameter qT, which reflects the decrease in the LHCII antenna size, was calculated as $(F_M'-F_M'')/F_M'$ according to Ruban and Johnson (2009).

CD spectroscopy

Room temperature CD spectra of intact leaves were recorded in the range of 400–750 nm with a J-815 spectropolarimeter (Jasco, Tokyo, Japan). Intact leaves were supported by a flat cell and CD spectra were measured perpendicularly to the optical path. Measurements were carried out at room temperature with 0.5 nm step, 1 s integration time, 3 nm band-pass, and scanning speed 100 nm min^{-1}. To improve the signal-to-noise ratio, leaves were infiltrated with distilled water prior to the measurements using a 2-min interval at low pressure, and three scans were collected and averaged. CD spectra were normalized to the Chl Q_y absorption band. In order to minimize the influences of the overlapping excitonic CD bands, the amplitudes of the (+)685 nm and (+)505 nm psi-type CD bands were calculated as the difference between the CD signal at 685 and 750 nm and between 505 and 620 nm, respectively.

Chlorophyll fluorescence decay after a single-turnover saturating flash

The kinetics of the Chl fluorescence decay after a single-turnover saturating flash was monitored using Joliot-type kinetic spectrometer JTS-100 (Biologic, Seyssinet-Pariset, France). Arabidopsis plants were dark-adapted for 30 min, individual leaves were detached and immediately used for the measurement. Single turnover saturating (0.5 J) actinic flashes of 2 μs duration at half-peak intensity were provided by a xenon lamp (Hamamatsu LF1 L-11730-04-01-1, Shimokanzo, Japan) with Schott BG39 filter (Schott, Mainz, Germany), whereas the instruments LED system with a narrow bandpass filter centered at 650 nm (XHQA650; FWHM of 12 nm) provided measuring flashes. Fluorescence decay was recorded in the time range 15 μs to 50 s. Multicomponent deconvolution of the obtained fluorescence decay curves was achieved by fitting the experimental data with two exponential components (fast and middle phase) and one hyperbolic component (slow phase) as described earlier (Vass et al., 1999):

$$F_V = A_0 + A_1 \cdot e^{\frac{-t}{T_1}} + A_2 \cdot e^{\frac{-t}{T_2}} + \frac{A_3}{1 + \frac{t}{T_3}}$$

where $F_V = F(t) - F_0$, $F(t)$ is the fluorescence yield at time t, F_0 is the basic fluorescence level before the flash, A_1–A_3 are the amplitudes, T_1–T_3 are the time constants and A_0 describe non-decaying fluorescence component in the time span of the measurement.

Accession numbers

The accession numbers are as follows: LHCB3 (AT5G54270), LHCB6 (AT1G15820), LHCB4.1 (AT5G01530), LHCB4.2 (AT3G08940), and LHCB4.3 (AT2G40100). The mass spectrometry proteomic data have been deposited to the ProteomeXchange Consortium via the PRIDE partner repository with the identifiers: PXD023071 (thylakoid membranes) and PXD026019 (PSII supercomplexes).

Supplemental data

Supplemental Figure S1. Relative content of light-harvesting proteins in PSII supercomplexes separated by CN-PAGE.

Supplemental Figure S2. Gallery of electron micrographs of grana membranes isolated from Arabidopsis WT, *lhcb3* and *lhcb6* mutants.

Supplemental Figure S3. Electron micrograph of grana membranes isolated from Arabidopsis *lhcb3 lhcb6* mutant.

Supplemental Figure S4. Electron micrograph of grana membranes isolated from Arabidopsis *lhcb3 lhcb6* mutant—regular arrays.

Supplemental Figure S5. Electron micrograph of grana membranes isolated from Arabidopsis *lhcb3 lhcb6* mutant—carpet-like motive.

Supplemental Figure S6. Kinetics of Q_A^- reoxidation following a single turnover saturating flash.

Supplemental Figure S7. Measurements of state transitions in WT and mutant plants (*lhcb3*, *lhcb6*, *lhcb3 lhcb6*).

Supplemental Table S1. Decay kinetics of flash-induced variable fluorescence in Arabidopsis leaves.

Supplemental Methods S1. Mass spectrometry analysis of isolated thylakoid membranes and PSII supercomplexes.

Acknowledgments

We thank Pavla Ocvirková for a technical assistance.

Funding

This work was supported by the Grant Agency of the Czech Republic (projects no. 18-12178S and 21-05497S) and the European Regional Development Fund (ERDF) projects "Plants as a tool for sustainable global development" (no. CZ.02.1.01/0.0/0.0/16_019/0000827) and "SustES—Adaptation strategies for sustainable ecosystem services and food security under adverse environmental conditions" (CZ.02.1.01/0.0/0.0/16_019/0000797). CIISB, Instruct—CZ Centre of Instruct—ERIC EU consortium, funded by MEYS CR infrastructure project LM2018127, is gratefully acknowledged for the financial support of the measurements at the CEITEC Proteomics Core Facility.

Conflict of interest statement. The authors declare that there is no conflict of interest.

References

Adamiec M, Gibasiewicz K, Luciński R, Giera W, Chełminiak P, Szewczyk S, Sipińska W, van Grondelle R, Jackowski G (2015) Excitation energy transfer and charge separation are affected in *Arabidopsis thaliana* mutants lacking light-harvesting chlorophyll a/b binding protein Lhcb3. J Photochem Photobiol B **153:** 423–428

Albanese P, Manfredi M, Meneghesso A, Marengo E, Saracco G, Barber J, Morosinotto T, Pagliano C (2016a) Dynamic reorganization of photosystem II supercomplexes in response to variations in light intensities. Biochim Biophys Acta **1857:** 1651–1660

Albanese P, Nield J, Tabares JAM, Chiodoni A, Manfredi M, Gosetti F, Marengo E, Saracco G, Barber J, Pagliano C (2016b) Isolation of novel PSII-LHCII megacomplexes from pea plants characterized by a combination of proteomics and electron microscopy. Photosynth Res **130:** 19–31.

Albanese PMelero REngel BDGrinzato ABerto PManfredi MChiodoni AVargas JSorzano CÓSMarengo E, et al. (2017) Pea PSII–LHCII supercomplexes form pairs by making connections across the stromal gap. Sci Rep. **7:** 10067.

Albanese P, Manfredi M, Re A, Marengo E, Saracco G, Pagliano C (2018) Thylakoid proteome modulation in pea plants grown at different irradiances: quantitative proteomic profiling in a non-model organism aided by transcriptomic data integration. Plant J **96:** 786–800

Albanese P, Manfredi M, Marengo E, Saracco G, Pagliano C (2019) Structural and functional differentiation of the light-harvesting protein Lhcb4 during land plant diversification. Physiol Plant **166:** 336–350

Alboresi A, Caffarri S, Nogue F, Bassi R, Morosinotto T (2008) *In silico* and biochemical analysis of *Physcomitrella patens* photosynthetic antenna: Identification of subunits which evolved upon land adaptation. PLoS ONE **3:** e2033

Allahverdiyeva Y, Isojärvi J, Zhang P, Aro E-M (2015) Cyanobacterial oxygenic photosynthesis is protected by flavodiiron proteins. Life Basel Switz **5:** 716–743

Allen JF (2003) Cyclic, pseudocyclic and noncyclic photophosphorylation: New links in the chain. Trends Plant Sci **8:** 15–19

Ballottari M, Dall'Osto L, Morosinotto T, Bassi R (2007) Contrasting behavior of higher plant photosystem I and II antenna systems during acclimation. J Biol Chem **282:** 8947–8958

Barzda V, Mustárdy L, Garab G (1994) Size dependency of circular dichroism in macroaggregates of photosynthetic pigment–protein complexes. Biochemistry **33:** 10837–10841

Belgio E, Kapitonova E, Chmeliov J, Duffy CDP, Ungerer P, Valkunas L, Ruban AV (2014) Economic photoprotection in photosystem II that retains a complete light-harvesting system with slow energy traps. Nat Commun **5:** 4433.

Betterle N, Ballottari M, Zorzan S, de Bianchi S, Cazzaniga S, Dall'Osto L, Morosinotto T, Bassi R (2009) Light-induced dissociation of an antenna hetero-oligomer is needed for non-photochemical quenching induction. J Biol Chem **284:** 15255–15266

van Bezouwen LS, Caffarri S, Kale RS, Kouřil R, Thunnissen A-MWH, Oostergetel GT, Boekema EJ (2017) Subunit and chlorophyll organization of the plant photosystem II supercomplex. Nat. Plants **3:** 17080

de Bianchi S, Betterle N, Kouril R, Cazzaniga S, Boekema E, Bassi R, Dall'Osto L (2011) Arabidopsis mutants deleted in the light-harvesting protein Lhcb4 have a disrupted photosystem II macrostructure and are defective in photoprotection. Plant Cell **23:** 2659–2679

de Bianchi S, Dall'Osto L, Tognon G, Morosinotto T, Bassi R (2008) Minor antenna proteins CP24 and CP26 affect the interactions between photosystem II subunits and the electron transport rate in grana membranes of Arabidopsis. Plant Cell **20:** 1012–1028

Bilger W, Björkman O (1990) Role of the xanthophyll cycle in photoprotection elucidated by measurements of light-induced absorbance changes, fluorescence and photosynthesis in leaves of *Hedera canariensis*. Photosynth Res **25:** 173–185

Björkman O, Demmig B (1987) Photon yield of O_2 evolution and chlorophyll fluorescence characteristics at 77 K among vascular plants of diverse origins. Planta **170:** 489–504

Boekema EJ, van Roon H, Calkoen F, Bassi R, Dekker JP (1999) Multiple types of association of photosystem II and its light-harvesting antenna in partially solubilized photosystem II membranes. Biochemistry **38:** 2233–2239

Boekema EJ, van Breemen JFL, van Roon H, Dekker JP (2000) Arrangement of photosystem II supercomplexes in crystalline macrodomains within the thylakoid membrane of green plant chloroplasts. J Mol Biol **301:** 1123–1133

Bratt CE, Arvidsson PO, Carlsson M, Akerlund HE (1995) Regulation of violaxanthin de-epoxidase activity by pH and ascorbate concentration. Photosynth Res **45:** 169–175

Caffarri S, Croce R, Cattivelli L, Bassi R (2004) A look within LHCII: Differential analysis of the Lhcb1 – 3 complexes building the major trimeric antenna complex of higher-plant photosynthesis. Biochemistry **43:** 9467–9476

Caffarri S, Kouřil R, Kereïche S, Boekema EJ, Croce R (2009) Functional architecture of higher plant photosystem II supercomplexes. EMBO J **28:** 3052–3063

Charuvi D, Nevo R, Shimoni E, Naveh L, Zia A, Adam Z, Farrant JM, Kirchhoff H, Reich Z (2015) Photoprotection conferred by changes in photosynthetic protein levels and organization during dehydration of a homoiochlorophyllous resurrection plant. Plant Physiol **167:** 1554–1565

Chen Y-E, Ma J, Wu N, Su Y-Q, Zhang Z-W, Yuan M, Zhang H-Y, Zeng X-Y, Yuan S (2018) The roles of Arabidopsis proteins of Lhcb4, Lhcb5 and Lhcb6 in oxidative stress under natural light conditions. Plant Physiol Biochem **130:** 267–276

Dall'Osto L, Cazzaniga S, Bressan M, Paleček D, Židek K, Niyogi KK, Fleming GR, Zigmantas D, Bassi R (2017) Two mechanisms for dissipation of excess light in monomeric and trimeric light-harvesting complexes. Nat Plants **3:** 17033.

Damkjær JT, Kereiche S, Johnson MP, Kovács L, Kiss AZ, Boekema EJ, Ruban AV, Horton P, Jansson S (2009) The photosystem II light-harvesting protein Lhcb3 affects the macrostructure of photosystem II and the rate of state transitions in Arabidopsis. Plant Cell **21:** 3245–3256.

Dau H, Andrews JC, Roelofs TA, Latimer MJ, Liang W, Yachandra VK, Sauer K, Klein MP (1995) Structural consequences of ammonia binding to the manganese center of the photosynthetic oxygen-evolving complex: An X-ray absorption spectroscopy study of isotropic and oriented photosystem II particles. Biochemistry **34:** 5274–5287

Daum B, Nicastro D, Austin J, McIntosh JR, Kühlbrandt W (2010) Arrangement of photosystem II and ATP synthase in chloroplast membranes of spinach and pea. Plant Cell **22:** 1299–1312

Deák Z, Sass L, Kiss É, Vass I (2014) Characterization of wave phenomena in the relaxation of flash-induced chlorophyll fluorescence yield in cyanobacteria. Biochim Biophys Acta **1837:** 1522–1532

Dekker JP, Boekema EJ (2005) Supramolecular organization of thylakoid membrane proteins in green plants. Biochim Biophys Acta **1706:** 12–39

Dobrikova AG, Várkonyi Z, Krumova SB, Kovács L, Kostov GK, Todinova SJ, Busheva MC, Taneva SG, Garab G (2003) Structural rearrangements in chloroplast thylakoid membranes revealed by differential scanning calorimetry and circular dichroism spectroscopy. Thermo-optic effect. Biochemistry **42:** 11272–11280

Garab G, Kieleczawa J, Sutherland JC, Bustamante C, Hind G (1991) Organization of pigment–protein complexes into macrodomains in the thylakoid membranes of wild-type and chlorophyll-b less mutant of barley as revealed by circular dichroism. Photochem Photobiol **54:** 273–281

Garab G, van Amerongen H (2009) Linear dichroism and circular dichroism in photosynthesis research. Photosynth Res **101:** 135–146

Genty B, Briantais J-M, Baker NR (1989) The relationship between the quantum yield of photosynthetic electron transport and quenching of chlorophyll fluorescence. Biochim Biophys Acta **990:** 87–92

Goral TK, Johnson MP, Duffy CDP, Brain APR, Ruban AV, Mullineaux CW (2012) Light-harvesting antenna composition controls the macrostructure and dynamics of thylakoid membranes in Arabidopsis. Plant J **69:** 289–301

Grebe S, Trotta A, Bajwa AA, Suorsa M, Gollan PJ, Jansson S, Tikkanen M, Aro E-M (2019) The unique photosynthetic apparatus of Pinaceae: Analysis of photosynthetic complexes in *Picea abies*. J Exp Bot **10:** 3211–3225

Grinzato A, Albanese P, Marotta R, Swuec P, Saracco G, Bolognesi M, Zanotti G, Pagliano C (2020) High-light versus low-light: Effects on paired photosystem II supercomplex structural rearrangement in pea plants. Int J Mol Sci **21:** 8643

Günther G, Thiele A, Laasch H (1994) A new method for the determination of the transthylakoid pH gradient in isolated chloroplasts: The pH-dependent activity of violaxanthin de-epoxidase. Plant Sci **102:** 19–30.

Haferkamp S, Haase W, Pascal AA, van Amerongen H, Kirchhoff H (2010) Efficient light harvesting by photosystem II requires an optimized protein packing density in grana thylakoids. J Biol Chem **285:** 17020–17028

Ilík P, Kotabová E, Spundová M, Novák O, Kana R, Strzałka K (2010) Low-light-induced violaxanthin de-epoxidation in shortly preheated leaves: uncoupling from Delta pH-dependent nonphotochemical quenching. Photochem Photobiol **86:** 722–726

Ilík P, Pavlovič A, Kouřil R, Alboresi A, Morosinotto T, Allahverdiyeva Y, Aro E-M, Yamamoto H, Shikanai T (2017) Alternative electron transport mediated by flavodiiron proteins is operational in organisms from cyanobacteria up to gymnosperms. New Phytol **214:** 967–972

Jansson S (1999) A guide to the Lhc genes and their relatives in Arabidopsis. Trends Plant Sci **4:** 236–240

Johnson MP (2020) Just the essentials: Photoprotective energy dissipation pared-down. J Exp Bot **71:** 3380–3382

Joliot P, Joliot A (2002) Cyclic electron transfer in plant leaf. Proc Natl Acad Sci USA **99:** 10209–10214

Kereïche S, Kiss AZ, Kouřil R, Boekema EJ, Horton P (2010) The PSBS protein controls the macro-organisation of photosystem II complexes in the grana membranes of higher plant chloroplasts. FEBS Lett **584:** 759–764

Kirchhoff H (2008) Significance of protein crowding, order and mobility for photosynthetic membrane functions. Biochem Soc Trans **36:** 967–970

Kirchhoff H, Haase W, Wegner S, Danielsson R, Ackermann R, Albertsson P-A (2007) Low-light-induced formation of semicrystalline photosystem II arrays in higher plant chloroplasts. Biochemistry **46:** 11169–11176

Kitajima M, Butler WL (1975) Quenching of chlorophyll fluorescence and primary photochemistry in chloroplasts by dibromothymoquinone. Biochim Biophys Acta **376:** 105–115

Klimmek F, Sjödin A, Noutsos C, Leister D, Jansson S (2006) Abundantly and rarely expressed LHC protein genes exhibit distinct regulation patterns in plants. Plant Physiol **140:** 793–804

Klughammer C, Schreiber U (2008) Saturation pulse method for assessment of energy conversion in PS I. PAM Appl Notes **1:** 11–14.

Kouřil R, Wientjes E, Bultema JB, Croce R, Boekema EJ (2013) High-light vs. low-light: Effect of light acclimation on photosystem II composition and organization in *Arabidopsis thaliana*. Biochim Biophys Acta **1827:** 411–419

Kouřil R, Strouhal O, Nosek L, Lenobel R, Chamrád I, Boekema EJ, Šebela M, Ilík P (2014) Structural characterization of a plant photosystem I and NAD(P)H dehydrogenase supercomplex. Plant J **77:** 568–576

Kouřil R, Nosek L, Bartoš J, Boekema EJ, Ilík P (2016) Evolutionary loss of light-harvesting proteins Lhcb6 and Lhcb3 in major land plant groups—break-up of current dogma. New Phytol **210:** 808–814

Kouřil R, Nosek L, Semchonok D, Boekema EJ, Ilík P (2018) Organization of plant photosystem II and photosystem I supercomplexes. *In* JR Harris, EJ Boekema, eds, Membrane Protein Complexes: Structure and Function, Vol. Subcellular Biochemistry. Springer, Singapore, pp 259–286

Kouřil R, Nosek L, Opatíková M, Arshad R, Semchonok DA, Chamrád I, Lenobel R, Boekema EJ, Ilík P (2020) Unique organization of photosystem II supercomplexes and megacomplexes in Norway spruce. Plant J **104:** 215–225

Kovács L, Damkjær J, Kereiche S, Ilioaia C, Ruban AV, Boekema EJ, Jansson S, Horton P (2006) Lack of the light-harvesting complex CP24 affects the structure and function of the grana membranes of higher plant chloroplasts. Plant Cell **18:** 3106–3120

Kurasova I, Kalina J, Urban O, Stroch M, Spunda V (2003) Acclimation of two distinct plant species, Spring Barley and Norway Spruce, to combined effect of various irradiance and CO_2 concentration during cultivation in controlled environment. Photosynthetica **41:** 513–523

Lazár D (1999) Chlorophyll a fluorescence induction 1. Biochim Biophys Acta **1412:** 1–28

Lazár D (2006) The polyphasic chlorophyll a fluorescence rise measured under high intensity of exciting light. Funct Plant Biol **33:** 9–30.

Lazár D, Nauš J (1998) Statistical properties of chlorophyll fluorescence induction parameters. Photosynthetica **35:** 121–127

Lazár D, Tomek P, Ilík P, Nauš J (2001) Determination of the antenna heterogeneity of photosystem II by direct simultaneous fitting of several fluorescence rise curves measured with DCMU at different light intensities. Photosynth Res **68:** 247–257

Li X-P, Gilmore AM, Niyogi KK (2002) Molecular and global time-resolved analysis of a psbS gene dosage effect on pH- and xanthophyll cycle-dependent nonphotochemical quenching in photosystem II. J Biol Chem **277:** 33590–33597

Lichtenthaler HK (1987) Chlorophylls and carotenoids: Pigments of photosynthetic biomembranes. *In:* R Douce and L Packer, eds, Methods in Enzymology, Academic Press Inc., New York, pp 350–382

Lípová L, Krchnák P, Komenda J, Ilík P (2010) Heat-induced disassembly and degradation of chlorophyll-containing protein complexes in vivo. Biochim Biophys Acta **1797:** 63–70

Malkin S, Armond PA, Mooney HA, Fork DC (1981) Photosystem II photosynthetic unit sizes from fluorescence induction in leaves: Correlation to photosynthetic capacity. Plant Physiol **67:** 570–579

McKenzie SD, Ibrahim IM, Aryal UK, Puthiyaveetil S (2020) Stoichiometry of protein complexes in plant photosynthetic membranes. Biochim Biophys Acta **1861:** 148141

Miller KR, Miller GJ, McIntyre KR (1976) The light-harvesting chlorophyll–protein complex of photosystem II. Its location in the photosynthetic membrane. J Cell Biol **71**: 624–638

Miyake C (2010) Alternative electron flows (water–water cycle and cyclic electron flow around PSI) in photosynthesis: Molecular mechanisms and physiological functions. Plant Cell Physiol **51:** 1951–1963

Miyake C (2020) Molecular mechanism of oxidation of P700 and suppression of ROS production in photosystem I in response to electron–sink limitations in C3 plants. Antioxidants **9:** 230

Morosinotto T, Caffarri S, Dall'Osto L, Bassi R (2003) Mechanistic aspects of the xanthophyll dynamics in higher plant thylakoids. Physiol Plant **119:** 347–354

Morosinotto T, Bassi R, Frigerio S, Finazzi G, Morris E, Barber J (2006) Biochemical and structural analyses of a higher plant photosystem II supercomplex of a photosystem I-less mutant of barley. FEBS J **273:** 4616–4630

Munekage Y, Takeda S, Endo T, Jahns P, Hashimoto T, Shikanai T (2001) Cytochrome b(6)f mutation specifically affects thermal dissipation of absorbed light energy in Arabidopsis. Plant J **28:** 351–359

Nosek L, Semchonok D, Boekema EJ, Ilík P, Kouřil R (2017) Structural variability of plant photosystem II megacomplexes in thylakoid membranes. Plant J **89:** 104–111

Nystedt BStreet NRWetterbom AZuccolo ALin Y-CScofield DGVezzi FDelhomme NGiacomello SAlexeyenko A, et al. (2013) The Norway spruce genome sequence and conifer genome evolution. Nature **497:** 579–584

Onoa B, Schneider AR, Brooks MD, Grob P, Nogales E, Geissler PL, Niyogi KK, Bustamante C (2014) Atomic force microscopy of photosystem II and its unit cell clustering quantitatively delineate the mesoscale variability in Arabidopsis thylakoids. PLoS ONE **9:** e101470

van Oort B, Alberts M, de Bianchi S, Dall'Osto L, Bassi R, Trinkunas G, Croce R, van Amerongen H (2010) Effect of antenna-depletion in photosystem II on excitation energy transfer in *Arabidopsis thaliana*. Biophys J **98:** 922–931

Oxborough K, Baker NR (1997) Resolving chlorophyll a fluorescence images of photosynthetic efficiency into photochemical and non-photochemical components—calculation of qP and F_v'/F_m'; without measuring F_o'. Photosynth Res **54:** 135–142

Park RB, Biggins J (1964) Quantasome: size and composition. Science **144:** 1009–1011

Peter GF, Thornber JP (1991) Biochemical composition and organization of higher plant photosystem II light-harvesting pigment–-proteins. J Biol Chem **266:** 16745–16754

de la Rosa-Trevín JMQuintana ADel Cano LZaldívar AFoche IGutiérrez JGómez-Blanco JBurguet-Castell JCuenca-Alba JAbrishami V, et al. (2016) Scipion: A software framework toward integration, reproducibility and validation in 3D electron microscopy. J Struct Biol **195:** 93–99

Ruban AV, Johnson MP (2009) Dynamics of higher plant photosystem cross-section associated with state transitions. Photosynth Res **99:** 173–183

Ruban AV, Wentworth M, Yakushevska AE, Andersson J, Lee PJ, Keegstra W, Dekker JP, Boekema EJ, Jansson S, Horton P (2003)

Plants lacking the main light-harvesting complex retain photosystem II macro-organization. Nature **421:** 648–652

Ruban AV, Wilson S (2020). The mechanism of non-photochemical quenching in plants: Localisation and driving forces. Plant Cell Physiol (doi: 10.1093/pcp/pcaa155)

Saccon F, Giovagnetti V, Shukla MK, Ruban AV (2020) Rapid regulation of photosynthetic light harvesting in the absence of minor antenna and reaction centre complexes. J Exp Bot **71:** 3626–3637

Schägger H (2006) Tricine-SDS-PAGE. Nat Protoc **1:** 16–22.

Scheres SHW (2012) RELION: Implementation of a Bayesian approach to cryo-EM structure determination. J Struct Biol **180:** 519–530

Schneider CA, Rasband WS, Eliceiri KW (2012) NIH Image to ImageJ: 25 years of image analysis. Nat Methods **9:** 671–675

Semenova GA (1995) Particle regularity on thylakoid fracture faces is influenced by storage conditions. Can J Bot **73:** 1676–1682

Simpson DJ (1979) Freeze–fracture studies on barley plastid membranes. III. Location of the light-harvesting chlorophyll-protein. Carlsberg Res Commun **44:** 305–336

Standfuss J, Kühlbrandt W, (2004) The three isoforms of the light-harvesting complex II: Spectroscopic features, trimer formation, and functional roles. J Biol Chem **279:** 36884–36891

Stirbet A, Lazár D, Kromdijk J, Govindjee (2018) Chlorophyll a fluorescence induction: Can just a one-second measurement be used to quantify abiotic stress responses? Photosynthetica **56:** 86–104.

Stoylova S, Flint TD, Ford RC, Holzenburg A (2000) Structural analysis of photosystem II in far-red-light-adapted thylakoid membranes: New crystal forms provide evidence for a dynamic reorganization of light-harvesting antennae subunits. Eur J Biochem **267:** 207–215

Strasser RJ, Srivastava A (1995) Polyphasic chlorophyll a fluorescence transient in plants and cyanobacteria. Photochem Photobiol **61:** 32–42

Strasser RJ, Tsimilli-Michael M, Srivastava A (2004) Analysis of the chlorophyll a fluorescence transient. *In* GC Papageorgiou and Govindjee, eds, Chlorophyll a Fluorescence: A Signature of Photosynthesis. Advances in Photosynthesis and Respiration. Springer, Dordrecht, Netherlands, pp 321–362

Su X, Ma J, Wei X, Cao P, Zhu D, Chang W, Liu Z, Zhang X, Li M (2017) Structure and assembly mechanism of plant $C_2S_2M_2$-type PSII–LHCII supercomplex. Science **357:** 815–820

Sznee K, Dekker JP, Dame RT, van Roon H, Wuite GJL, Frese RN (2011) Jumping mode atomic force microscopy on grana membranes from Spinach. J Biol Chem **286:** 39164–39171

Tietz S., Puthiyaveetil SEnlow HMYarbrough RWood MSemchonok DALowry TLi ZJahns PBoekema EJ, et al. (2015) Functional implications of photosystem II crystal formation in photosynthetic membranes. J Biol Chem **290:** 14091–14106

Tóth TN, Rai N, Solymosi K, Zsiros O, Schröder WP, Garab G, van Amerongen H, Horton P, Kovács L (2016) Fingerprinting the macro-organisation of pigment–protein complexes in plant thylakoid membranes in vivo by circular-dichroism spectroscopy. Biochim Biophys Acta **1857:** 1479–1489

Townsend AJ, Saccon F, Giovagnetti V, Wilson S, Ungerer P, Ruban AV (2018) The causes of altered chlorophyll fluorescence quenching induction in the Arabidopsis mutant lacking all minor antenna complexes. Biochim Biophys Acta **1859:** 666–675

Tremmel IG, Kirchhoff H, Weis E, Farquhar GD (2003) Dependence of plastoquinol diffusion on the shape, size, and density of integral thylakoid proteins. Biochim Biophys Acta **1607:** 97–109

Tsvetkova NM, Apostolova EL, Brain APR, Patrick Williams W, Quinn PJ (1995) Factors influencing PS II particle array formation in *Arabidopsis thaliana* chloroplasts and the relationship of such arrays to the thermostability of PS II. Biochim Biophys Acta **1228:** 201–210.

Vass I, Kirilovsky D, Etienne AL (1999) UV-B radiation-induced donor- and acceptor-side modifications of photosystem II in the cyanobacterium *Synechocystis* sp. PCC 6803. Biochemistry **38:** 12786–12794

Wang YH (2008) How effective is T-DNA insertional mutagenesis in Arabidopsis? J Biochem Technol **1:** 11–20.

Wei X, Su X, Cao P, Liu X, Chang W, Li M, Zhang X, Liu Z (2016) Structure of spinach photosystem II—LHCII supercomplex at 3.2 Å resolution. Nature **534:** 69–74

Wientjes E, Drop B, Kouřil R, Boekema EJ, Croce R (2013) During state 1 to state 2 transition in *Arabidopsis thaliana*, the photosystem II supercomplex gets phosphorylated but does not disassemble. J Biol Chem **288:** 32821–32826

Wiśniewski JR, Zougman A, Nagaraj N, Mann M (2009) Universal sample preparation method for proteome analysis. Nat Methods **6:** 359–362

Wittig I, Karas M, Schägger H (2007) High resolution clear native electrophoresis for in-gel functional assays and fluorescence studies of membrane protein complexes. Mol Cell Proteomics **6:** 1215–1225

Yakushevska AE, Jensen PE, Keegstra W, van Roon H, Scheller HV, Boekema EJ, Dekker JP (2001) Supermolecular organization of photosystem II and its associated light-harvesting antenna in *Arabidopsis thaliana*: Supermolecular organization of photosystem II. Eur J Biochem **268:** 6020–6028.

Yakushevska AE, Keegstra W, Boekema EJ, Dekker JP, Andersson J, Jansson S, Ruban AV, Horton P (2003) The structure of photosystem II in *Arabidopsis:* localization of the CP26 and CP29 antenna complexes. Biochemistry **42:** 608–613

Yamamoto H, Shikanai T (2019) PGR5-dependent cyclic electron flow protects photosystem I under fluctuating light at donor and acceptor sides. Plant Physiol **179:** 588–600

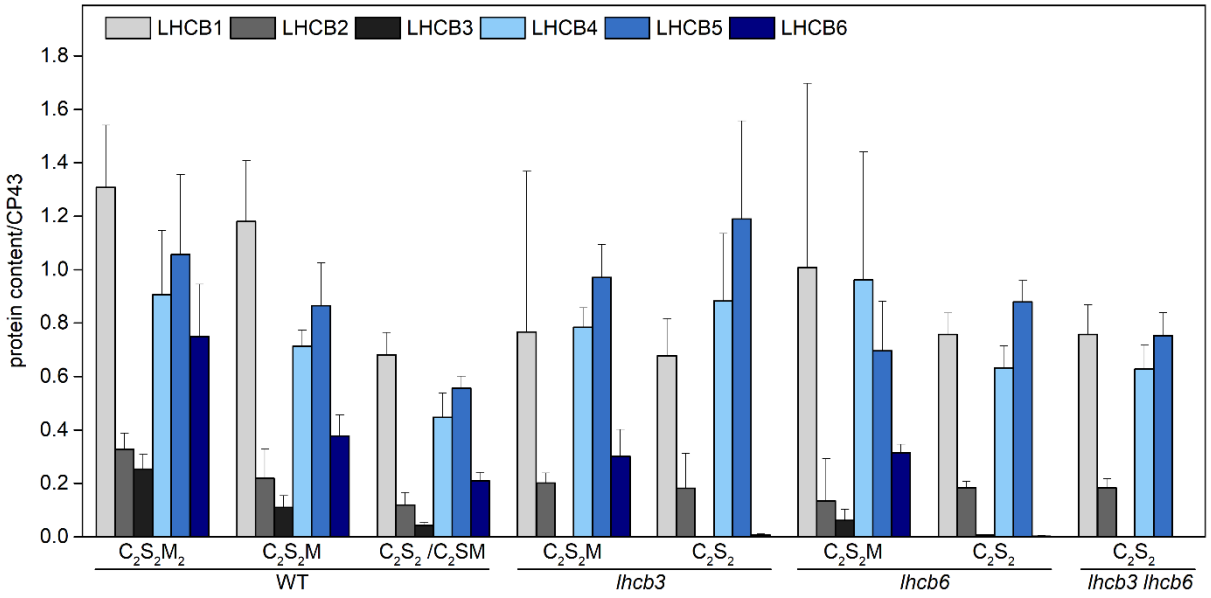

Supplemental Figure S1. Relative Content of Light-harvesting Proteins in PSII supercomplexes separated by CN-PAGE

The content of individual light-harvesting proteins Lhcb1-6 was determined in samples prepared via the elution of excised gel bands separated from wild type (WT) and mutant plant (*lhcb3, lhcb6, lhcb3 lhcb6*) thylakoids via CN-PAGE (see Figure 3A). The content of individual proteins was analyzed using liquid chromatography-tandem mass spectrometry (LC-MS/MS) and evaluated based on relative PG intensities relatively to the content of chlorophyll protein 43 (CP43, the inner antenna of PSII). The presented values are means ± SD from 4 replicates. These data complement Figure 11 from the main text. Different forms of separated PSII supercomplexes consist of PSII core dimer (C_2) and one and/or two copies of strongly (S) and moderately (M) bound light-harvesting trimers.

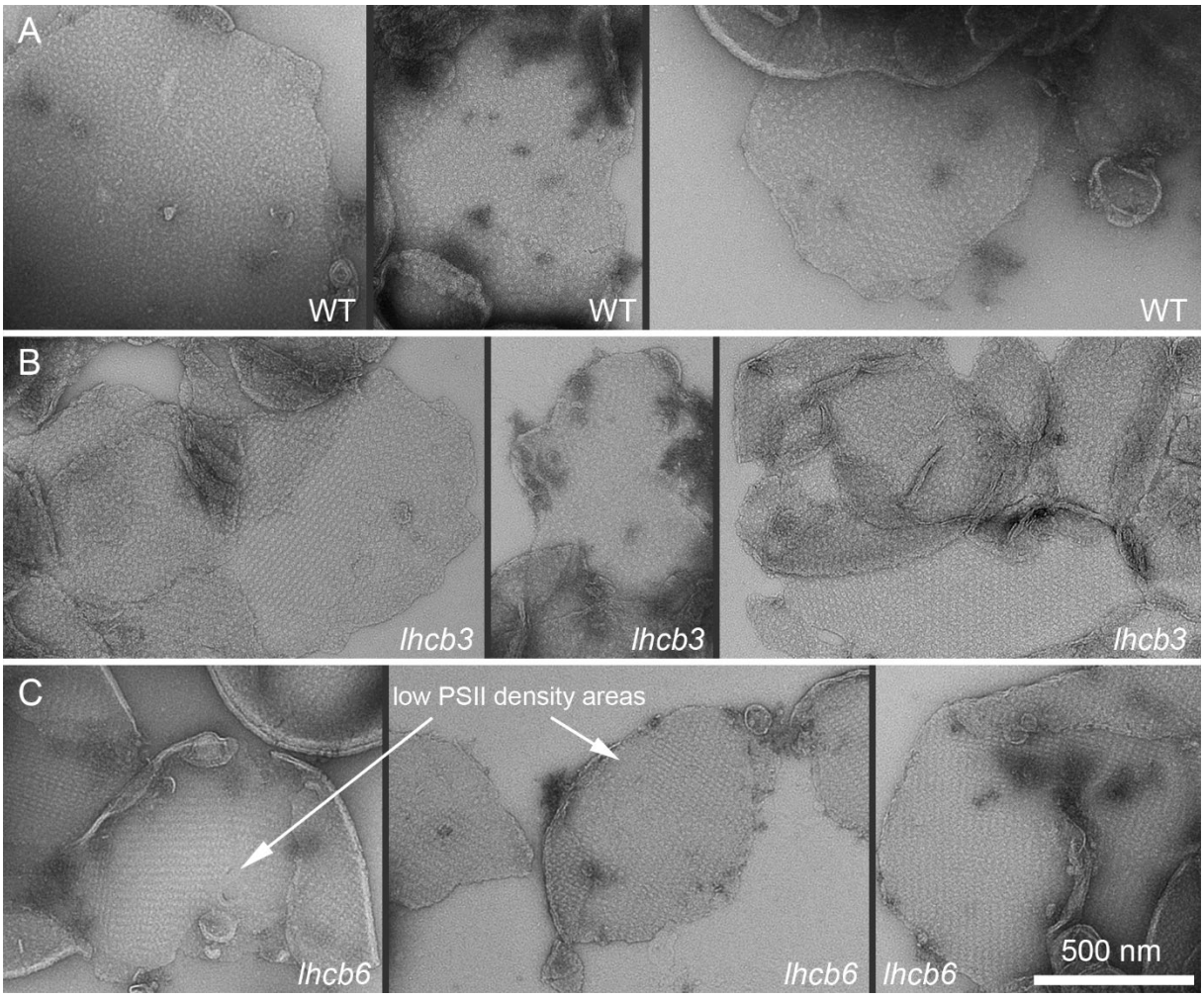

Supplemental Figure S2. Gallery of Electron Micrographs of Grana Membranes Isolated from Arabidopsis WT, *lhcb3* and *lhcb6* Mutants

(A, B) Organization of PSII complexes in the grana membranes from Arabidopsis WT and *lhcb3* mutant is predominantly random. Occasionally, PSII complexes are organized into semi-crystalline arrays.

(C) PSII complexes in the grana membranes from Arabidopsis *lhcb6* mutant are organized into semi-crystalline arrays. In addition, there are often areas at the periphery of the arrays, where PSII complexes are less ordered and their density is lower, likely due to a presence of free LHCII. This gallery supports Figure 7 from the main text.

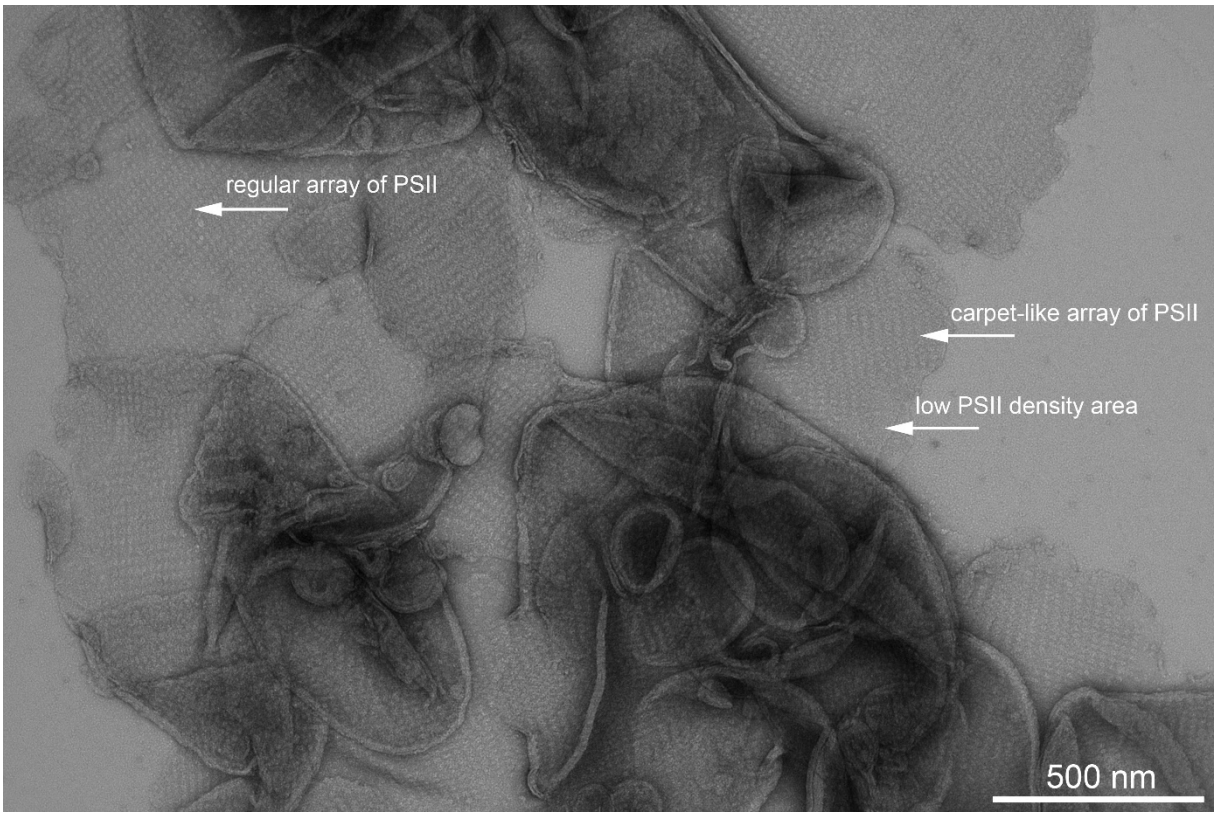

Supplemental Figure S3. Electron Micrograph of Grana Membranes Isolated from Arabidopsis *lhcb3 lhcb6* Mutant

The image shows that PSII complexes are almost exclusively organized into large semi-crystalline arrays. Two types of arrays can be distinguished - regular and carpet-like arrays. Rarely, there are regions in the membrane, where PSII complexes are less ordered and their density is lower, likely due to a presence of free LHCII. This figure complements Figure 5 from the main text.

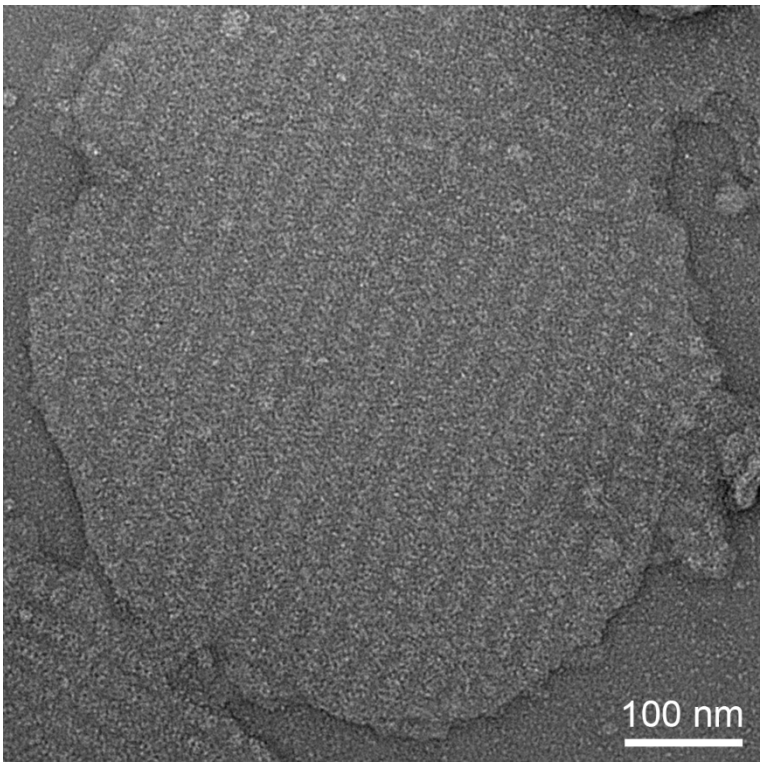

Supplemental Figure S4. Electron Micrograph of Grana Membranes Isolated from Arabidopsis *lhcb3 lhcb6* Mutant – Regular Arrays

A raw electron micrograph, which was used for image analysis of selected sub-areas (1320x1320 Å) of ordered arrays of PSII complexes. The result of image analysis, which revealed the regular array of C_2S_2 supercomplexes, is presented in the Figure 5A, B.

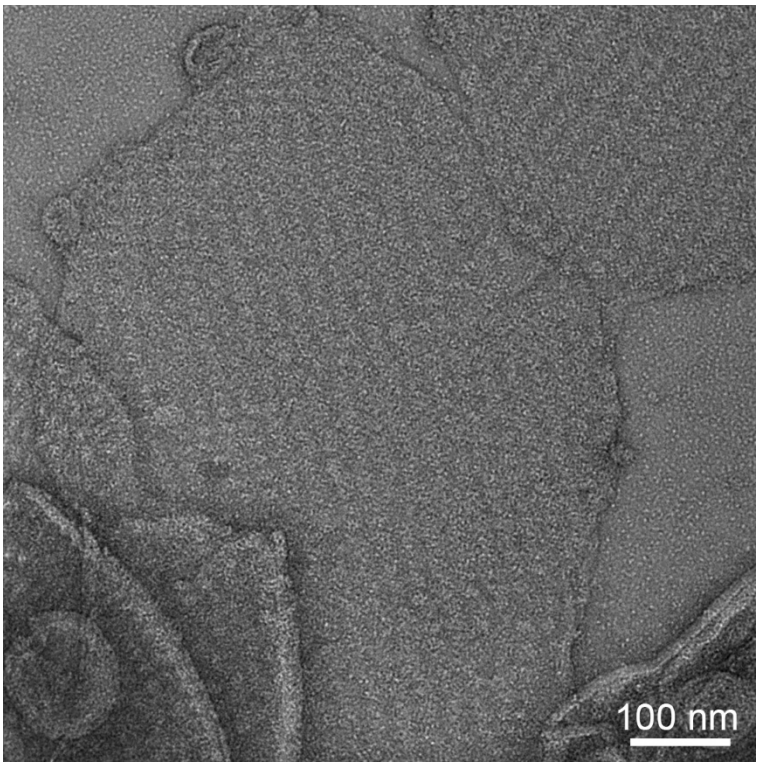

Supplemental Figure S5. Electron Micrograph of Grana Membranes Isolated from Arabidopsis *lhcb3 lhcb6* Mutant – Carpet-Like Motive

A raw electron micrograph, which was used for image analysis of selected sub-areas (2160x2160 Å and 1230x1230 Å) of ordered arrays of PSII complexes. Results of image analysis, which revealed the array of C_2S_2 supercomplexes with carpet-like motive, are presented in the Figure 5C-F.

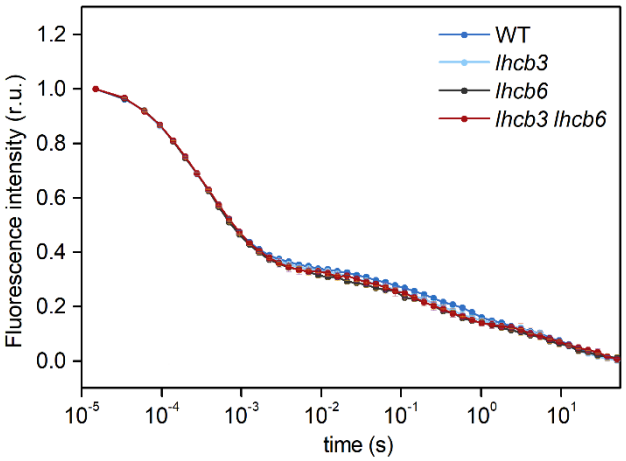

Supplemental Figure S6. Kinetics of Q_A^- Reoxidation Following a Single Turnover Saturating Flash

Fluorescence decay kinetics were measured in dark-adapted leaves (30 min) in wild type (WT) and *lhcb3*, *lhcb6* and *lhcb3 lhcb6* mutants. In order to facilitate a comparison of the kinetics, the fluorescence signal was subtracted by F_0 level detected before the measurement and then normalized to the maximum fluorescence level at 15μs (the first detected fluorescence value after the single turnover flash). This fluorescence decay reflects Q_A^- reoxidation in PSII after a single turnover saturating flash. Averaged curves for given sample type are presented including ± SD and calculated from 4-6 replicates. The measured kinetics were deconvoluted by three decay components (see Supplemental Table S1). The data complement 6th paragraph of Results.

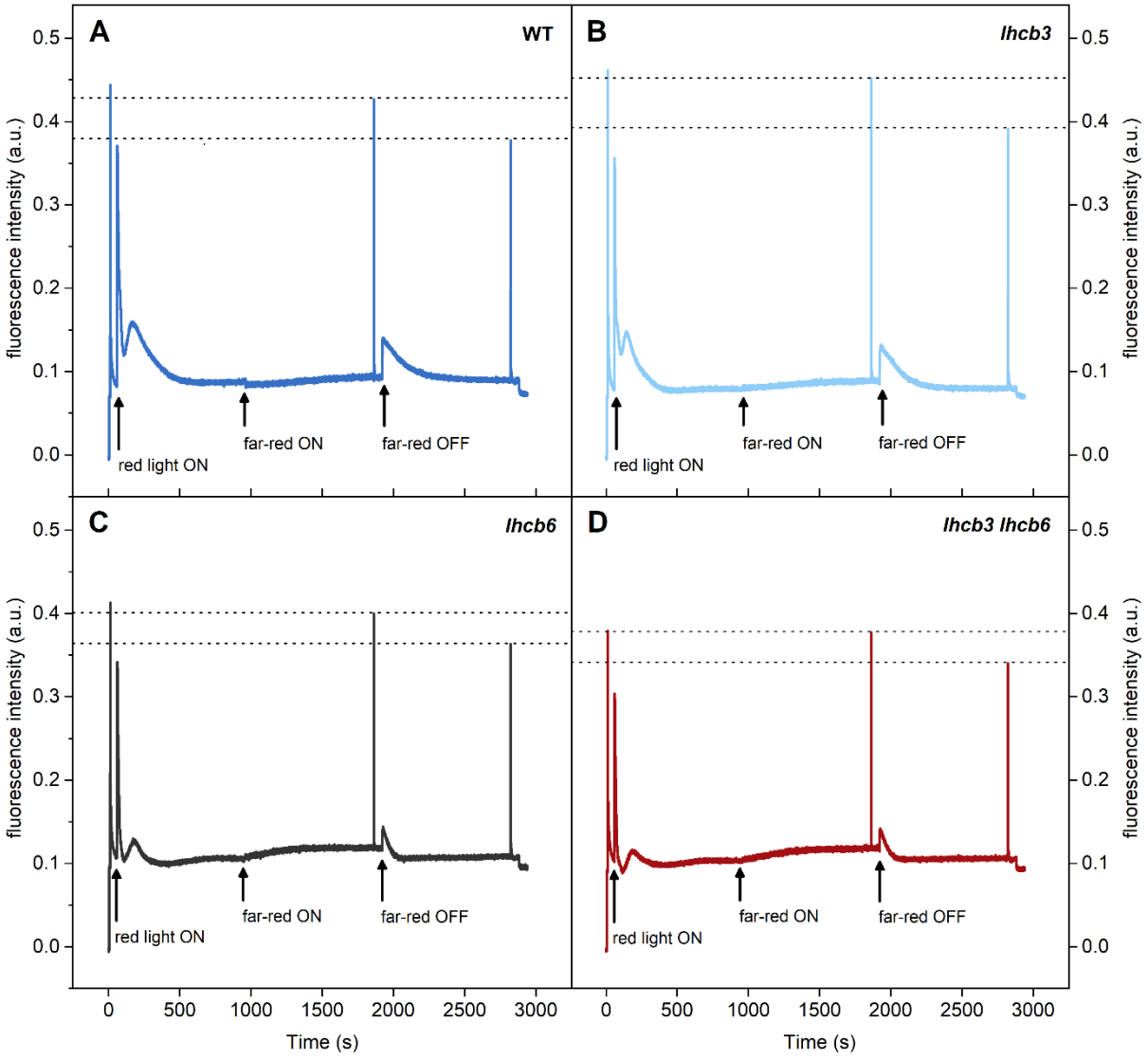

Supplemental Figure S7. Measurements of State Transitions in Wild Type (WT) and Mutant Plants (*lhcb3, lhcb6, lhcb3 lhcb6*)

State transitions were induced in dark-adapted leaves of Arabidopsis WT **(A)**, *lhcb3* **(B)**, *lhcb6* **(C)**, and *lhcb3 lhcb6* **(D)** by illumination with red light (13 µmol photons m^{-2} s^{-1}). State I was induced by additional illumination with far-red light, transition to State II was induced by switching off the far-red light. Maximum fluorescence F_M in the dark-adapted state, $F_{M'}$ in State I, and $F_{M''}$ in State II were induced by saturation light pulses (10.000 µmol photons m^{-2} s^{-1}, 800 ms). The data supplement Table 4 from the main text.

Supplemental Table S1. Decay Kinetics of Flash-Induced Variable Fluorescence in Arabidopsis Leaves

Multicomponent deconvolution of the fluorescence decay curves presented in Supplemental Figure S6. The kinetics was fitted by two exponential components (fast and middle phase) and one hyperbolic component (slow phase). For each component, T is the characteristic time constant and A is the corresponding amplitude. Presented values are means ± SD (n = 4–6). The data complement 6th paragraph of Results.

	Fast phase T_1(µs)/A_1(%)	Middle phase T_2(ms)/A_2(%)	Slow phase T_3(s)/A_3(%)
WT	459 ± 25/62.7 ± 0.5	80 ± 11/14.7 ± 0.4	3.63 ± 0.18/22.6 ± 0.4
lhcb3	459 ± 7/63.1 ± 0.5	70 ± 5/15.6 ± 1.1	3.48 ± 0.42/21.2 ± 1.1
lhcb6	477 ± 21/64.4 ± 0.7	69 ± 8/15.8 ± 0.7	3.92 ± 0.79/19.8 ± 1.4
lhcb3 lhcb6	486 ± 10/63.8 ± 1.4	81 ± 5/16.2 ± 0.7	4.04 ± 0.37/20.0 ± 1.6

Supplemental Methods S1: Mass spectrometry analysis of isolated thylakoid membranes and PSII supercomplexes

Thylakoid membranes were lysed in SDT buffer (4% SDS, 0.1M DTT, 0.1M Tris/HCl, pH 7.6) in a thermomixer (Eppendorf ThermoMixer® C, 30 min, 95°C, 750 rpm). The sample was centrifuged (15 min, 20,000 x g) and the supernatant used for filter-aided sample preparation as described elsewhere (Wisniewski et al., 2009) using 1 µg of trypsin (sequencing grade; Promega). Resulting peptides were analysed by LC-MS/MS. LC-MS/MS analyses of all peptides were done using UltiMate 3000 RSLCnano system (Thermo Fisher Scientific) connected to Orbitrap Elite hybrid spectrometer (Thermo Fisher Scientific). Prior to LC separation, tryptic digests were online concentrated and desalted using trapping column (Acclaim™ PepMap™ 100 C18, dimensions 300 µm × 5 mm, 5 µm particles; Thermo Fisher Scientific, part number 160454). After washing of the trapping column with 0.1% formic acid, the peptides were eluted in backflush mode (flow 300 nl.min^{-1}) from the trapping column onto an analytical column (Acclaim™ PepMap™ 100 C18, 3 µm particles, 75 µm × 500 mm; Thermo Fisher Scientific, part number 164570) by 100 min gradient program (3-80% of mobile phase B; mobile phase A: 0.1% formic acid in water; mobile phase B: 0.1% formic acid in 80% acetone). The equilibration of the trapping and analytical column was done prior to sample injection to the sample loop. The analytical column outlet was directly connected to the Digital PicoView 550 (New Objective) ion source with sheath gas option and SilicaTip emitter (New Objective; FS360-20-15-N-20-C12). ABIRD (Active Background Ion Reduction Device, ESI Source Solutions) was installed. MS data were acquired in a data-dependent strategy selecting up to top 10 precursors based on precursor abundance in the survey scan (*m/z* 350–2,000). The resolution of the survey scan was 60,000 (at *m/z* 400) with a target value of 1×10^6 ions and maximum injection time of 1,000 ms. HCD MS/MS spectra were acquired with a target value of 50,000 and resolution of 15,000 (at *m/z* 400). The maximum injection time for MS/MS was 500 ms. Dynamic exclusion was enabled for 45 s after one MS/MS spectra acquisition. The isolation window for MS/MS fragmentation was set to 2.0 *m/z*.

Photosystem II supercomplexes were manually excised from CN-PAGE gels and after washing procedures, each band was subjected to protein reduction (10mM DTT in 25mM $NaHCO_3$, 45 min, 56°C, 750 rpm) and alkylation (55mM IAA in 25mM $NaHCO_3$; 30 min, RT, 750 rpm) step. After further washing by 50% acetone/$NaHCO_3$ and pure acetone, the gel pieces were incubated with 125 ng trypsin (sequencing grade;

Promega) in 50mM $NaHCO_3$. The digestion was performed for 2 h at 40 °C in a thermomixer (Eppendorf ThermoMixer® C, 750 rpm). Tryptic peptides were extracted into LC-MS vials by 2.5% formic acid in 50% acetone with addition of polyethylene glycol (20,000; final concentration 0.001%) (Stejskal et al., 2013) and concentrated in a SpeedVac concentrator (Thermo Fisher Scientific). LC-MS/MS analyses of all peptides were done using RSLCnano system (UltiMate™ 3000, Thermo Fisher Scientific) connected to Orbitrap Q Exactive HF-X spectrometer (Thermo Fisher Scientific) as described above. MS data were acquired in a data-dependent strategy selecting up to top 15 precursors based on precursor abundance in the survey scan (*m/z* 350–2,000). The resolution of the survey scan was 120,000 (at *m/z* 200) with a target value of 3×10^6 ions and maximum injection time of 250 ms. MS/MS spectra were acquired with a target value of 50,000 and resolution of 15,000 (at *m/z* 200). The maximum injection time for MS/MS was 250 ms. Dynamic exclusion was enabled for 30 s after one MS/MS spectra acquisition. The isolation window for MS/MS fragmentation was set to 1.2 *m/z*.

For data evaluation, we used MaxQuant software (v1.6.17) (Cox and Mann 2008) with inbuild Andromeda search engine (Cox et al., 2011). Searches for samples of thylakoid membranes and photosystem II supercomplexes were done separately against protein databases of *Arabidopsis thaliana* (27,500 protein sequences, version from 12-08-2020, downloaded from ftp://ftp.uniprot.org/pub/databases/uniprot/current_release/knowledgebase/reference_proteomes/Eukaryota/UP000006548_3702.fasta.gz) and cRAP contaminants (112 sequences, version from 22-11-2018, downloaded from http://www.thegpm.org/crap). Modifications for all database searches were set as follows: oxidation (M), deamidation (N, Q), and acetylation (Protein N-term) as variable modifications, with carbamidomethylation (C) as a fixed modification. Enzyme specificity was tryptic with two permissible miscleavages. Only peptides and proteins with false discovery rate threshold under 0.01 were considered. Relative protein abundance was assessed using protein intensities calculated by MaxQuant. Intensities of reported proteins were further evaluated using software container environment (https://github.com/OmicsWorkflows/KNIME_docker_vnc; version 4.1.3a). Processing workflow is available upon request: it covers reverse hits and contaminant protein groups (cRAP) removal, protein group intensities log2 transformation and normalization (median). For the purpose of this article, protein groups reported by

MaxQuant are referred to as proteins. Mass spectrometry proteomics data were deposited to the ProteomeXchange Consortium via PRIDE (Perez-Riverol et al 2019) partner repository under dataset identifiers: PXD023071 (Thylakoid membranes) and PXD026019 (PSII Supercomplexes).

Supplemental References

Cox, J. and Mann, M. (2008). MaxQuant enables high peptide identification rates, individualized p.p.b.-range mass accuracies and proteome-wide protein quantification. Nat Biotechnol. **26**: 1367–1372.

Cox, J., Neuhauser, N., Michalski, A., Scheltema, R.A., Olsen, J.V. and Mann, M. (2001). Andromeda: A Peptide Search Engine Integrated into the MaxQuant Environment. J. Proteome Res. **10**: 1794–1805.

Perez-Riverol, Y., Csordas, A., Bai, J., Bernal-Llinares, M., Hewapathirana, S., Kundu, D.J., et al. (2019). The PRIDE database and related tools and resources in 2019: improving support for quantification data. Nucleic Acids Res. **47**: D442–D450.

Stejskal, K., Potěšil, D. and Zdráhal, Z. (2013). Suppression of Peptide sample losses in autosampler vials. J. Proteome Res. **12**: 3057–3062.

Wiśniewski, J.R., Zougman, A., Nagaraj, N. and Mann, M. (2009). Universal sample preparation method for proteome analysis. Nat. Methods **6**: 359–362.

the plant journal

SEB SOCIETY FOR EXPERIMENTAL BIOLOGY

The Plant Journal (2020) **104,** 215–225 doi: 10.1111/tpj.14918

Unique organization of photosystem II supercomplexes and megacomplexes in Norway spruce

Roman Kouřil[1,*], Lukáš Nosek[1], Monika Opatíková[1], Rameez Arshad[1,2], Dmitry A. Semchonok[2], Ivo Chamrád[3], René Lenobel[3], Egbert J. Boekema[2] and Petr Ilík[1]

[1]*Department of Biophysics, Centre of the Region Haná for Biotechnological and Agricultural Research, Faculty of Science, Palacký University, Šlechtitelů 27, Olomouc 783 71, Czech Republic,*

[2]*Electron Microscopy Group, Groningen Biomolecular Sciences and Biotechnology Institute, University of Groningen, Nijenborgh 7, Groningen 9747 AG, The Netherlands, and*

[3]*Department of Protein Biochemistry and Proteomics, Centre of the Region Haná for Biotechnological and Agricultural Research, Faculty of Science, Palacký University, Šlechtitelů 27, Olomouc 783 71, Czech Republic*

Received 19 December 2019; accepted 26 June 2020; published online 11 July 2020.
*For correspondence (e-mail roman.kouril@upol.cz).

SUMMARY

Photosystem II (PSII) complexes are organized into large supercomplexes with variable amounts of light-harvesting proteins (Lhcb). A typical PSII supercomplex in plants is formed by four trimers of Lhcb proteins (LHCII trimers), which are bound to the PSII core dimer via monomeric antenna proteins. However, the architecture of PSII supercomplexes in Norway spruce[*Picea abies* (L.) Karst.] is different, most likely due to a lack of two Lhcb proteins, Lhcb6 and Lhcb3. Interestingly, the spruce PSII supercomplex shares similar structural features with its counterpart in the green alga *Chlamydomonas reinhardtii* [Kouřil *et al.* (2016) *New Phytol.* 210, 808–814]. Here we present a single-particle electron microscopy study of isolated PSII supercomplexes from Norway spruce that revealed binding of a variable amount of LHCII trimers to the PSII core dimer at positions that have never been observed in any other plant species so far. The largest spruce PSII supercomplex, which was found to bind eight LHCII trimers, is even larger than the current largest known PSII supercomplex from *C. reinhardtii*. We have also shown that the spruce PSII supercomplexes can form various types of PSII megacomplexes, which were also identified in intact grana membranes. Some of these large PSII supercomplexes and megacomplexes were identified also in *Pinus sylvestris*, another representative of the Pinaceae family. The structural variability and complexity of LHCII organization in Pinaceae seems to be related to the absence of Lhcb6 and Lhcb3 in this family, and may be beneficial for the optimization of light-harvesting under varying environmental conditions.

Keywords: clear native polyacrylamide electrophoresis, *Picea abies*, *Pinus sylvestris*, photosystem II, megacomplex, supercomplex, single-particle electron microscopy, grana membrane.

INTRODUCTION

Photosystem II (PSII) is a large multi-subunit pigment–protein complex embedded in the thylakoid membrane of cyanobacteria, algae and plants. It is a key player in light reactions of photosynthesis due to its ability to split water into oxygen, protons and electrons, which are further utilized in photosynthetic reactions (Barber, 2003).

A core complex of PSII forms a dimer (C_2), which contains pigments and redox cofactors necessary for the photochemical reactions. In land plants, C_2 associates with light-harvesting complex II (LHCII), consisting of a variable number of membrane-embedded light-harvesting proteins (Lhcb1–6). The variability of LHCII composition and size is important for the optimization of the absorption cross-section of the PSII core complex under different light conditions (Bailey *et al.*, 2001; Ballottari *et al.*, 2007; Kouřil *et al.*, 2013; Albanese *et al.*, 2016). Lhcb1–3 proteins are present only in the trimeric form (Jansson, 1994). Lhcb1 and Lhcb2 can form homotrimers, but they are also able to form heterotrimers with each other or with Lhcb3. These trimers specifically bind to C_2 core with the help of monomeric proteins Lhcb4–6 (also called CP29, CP26 and CP24, respectively).

Depending on the strength of the association of the trimers to C_2, we distinguish between strongly (S), moderately (M) and loosely (L) bound LHCII trimers (Dekker and

Boekema, 2005; Kouřil *et al.*, 2012, 2018; see also Figure 5). The S trimer consists of Lhcb1 and Lhcb2 proteins at different ratios and is attached to C_2 via Lhcb5 and Lhcb4 proteins. The M trimer is formed by one copy of Lhcb3 and two Lhcb1/2 proteins (Caffarri *et al.*, 2004, 2009; Su *et al.*, 2017; Crepin and Caffarri, 2018). Lhcb3 is a structurally important component of the M trimer (Caffarri *et al.*, 2009; Su *et al.*, 2017), as it can interact with Lhcb6, one of the minor antenna proteins. Lhcb6, together with Lhcb4, plays a crucial role in the binding of M trimer to C_2 (Kovács *et al.*, 2006; de Bianchi *et al.*, 2008, 2011).

In plants grown under optimal light conditions, the most abundant form of PSII is the $C_2S_2M_2$ supercomplex, containing two strongly and two moderately bound trimers (Kouřil *et al.*, 2013). Namely in plants grown under high light conditions, the size of the supercomplex can be reduced to C_2S_2, the smallest physiologically relevant form of PSII that binds just two S trimers (Morosinotto *et al.*, 2006; Ballottari *et al.*, 2007; Kouřil *et al.*, 2013; Albanese *et al.*, 2016). On the other hand, the $C_2S_2M_2$ supercomplex can be occasionally further extended by the presence of an L trimer; however, the $C_2S_2M_2L_{1\text{-}2}$ supercomplexes are very rare. Up to today, they have been found only in spinach and only as a very minor fraction of all supercomplexes (Boekema *et al.*, 1999a,b). Recently, an additional LHCII trimer was found to be associated with $C_2S_2M_2$ in Arabidopsis as well, but in a different position than in spinach and only as a part of PSII megacomplexes (Nosek *et al.*, 2017).

Our understanding of the assembly and structure of plant PSII supercomplexes has significantly increased during the last 10 years. High-resolution structures uncovered details of subunit positions and arrangement of pigment molecules, which are crucial for the identification of possible energy transfer pathways within the PSII supercomplex (Caffarri *et al.*, 2009; Wei *et al.*, 2016; van Bezouwen *et al.*, 2017; Su *et al.*, 2017). At the same time, the generally accepted hypothesis that the architecture of the PSII supercomplex is uniform in land plants has been recently disproved by our work showing the surprising absence of Lhcb3 and Lhcb6 proteins in some gymnosperm genera (Kouřil *et al.*, 2016). The lack of these proteins, which had been considered as essential components of LHCII in all land plants, has apparent consequences for the structure of PSII supercomplex in these species, including Norway spruce (*Picea abies*; Kouřil *et al.*, 2016).

Structural analysis of PSII supercomplex from spruce provided direct evidence that the M trimer (or rather the pseudo-M trimer without Lhcb3) can bind to C_2 even in the absence of Lhcb6 (Kouřil *et al.*, 2016). However, the absence of Lhcb3 and Lhcb6 changes the orientation of the M trimer with respect to the C_2 core, and this unique position of the M trimer has never been observed in any other land plant species. Interestingly, the orientation of the M trimer in spruce is similar to the position of the M trimer in the PSII supercomplex from the green alga *Chlamydomonas reinhardtii* (Kouřil *et al.*, 2016). Compared with spruce, however, the PSII supercomplexes from *C. reinhardtii* are larger, because they contain two additional LHCII trimers and form $C_2S_2M_2N_2$ supercomplexes (Tokutsu *et al.*, 2012; Drop *et al.*, 2014; Shen *et al.*, 2019; Sheng *et al.*, 2019). The two additional trimers attached to the $C_2S_2M_2$ in the alga were designated as N (naked) trimers, because – unlike S and M trimers – they bind directly to C_2 core without the involvement of any monomeric antenna (Drop *et al.*, 2014). Actually, the N trimers bind to C_2 at the position that is in land plants occupied by Lhcb6 (CP24; Drop *et al.*, 2014). Therefore, as the absence of Lhcb6 seems to be a prerequisite of the binding of this additional trimer, it is reasonable to ask whether the N trimer can be found in the spruce PSII supercomplex as well.

Plant PSII supercomplexes exhibit variability not only in their composition and structure, but they can also form variable higher order structures in the thylakoid membrane. Neighboring individual supercomplexes can interact with each other, forming so-called PSII megacomplexes, which can be isolated from thylakoid membranes using mild solubilization conditions. Different types of interactions then result in different long-distance arrangement of supercomplexes within the thylakoids (Kirchhoff *et al.*, 2004, 2008; Nosek *et al.*, 2017). Random PSII organization, as well as highly ordered (crystalline) arrays of PSII, have been observed, each characterized by different interactions between the supercomplexes (for reviews, see Kouřil *et al.*, 2012; Kirchhoff, 2013). Structural analysis revealed that pairs of neighboring PSII supercomplexes can interact in two ways. The first one involves interaction between stromal sides of PSII supercomplexes located in two adjacent grana membranes (Daum *et al.*, 2010; Albanese *et al.*, 2016, 2017; Su *et al.*, 2017), the second one takes place in the membrane plane and is mediated by the interaction between LHCII and C_2 (Nosek *et al.*, 2017). The physiological relevance of the formation of PSII megacomplexes *in vivo* was supported by their identification on the level of the thylakoid membrane (Daum *et al.*, 2010; Nosek *et al.*, 2017).

In the present work, we study the consequences of the loss of Lhcb3 and Lhcb6 proteins for the organization of PSII supercomplexes and megacomplexes in Norway spruce. As the spruce $C_2S_2M_2$ supercomplex shares some structural features with the PSII supercomplex from *C. reinhardtii*, we focused on the question whether the additional N trimers typical for this alga could attach also to spruce PSII supercomplex. As we have shown, the absence of the Lhcb6 and Lhcb3 proteins also results in a loss of a rectangular shape of the $C_2S_2M_2$ supercomplex, which is typical for other land plants (Kouřil *et al.*, 2016). We were thus interested in how the modified shape of spruce

supercomplexes affects their ability to form megacomplexes and higher order assemblies in thylakoid membranes.

RESULTS

Separation of large spruce PSII assemblies

A necessary prerequisite of our search for larger assemblies of PSII complexes in Norway spruce was the optimization of the solubilization and separation protocols. The solubilization was achieved using detergent α-DDM, which is milder than β-DDM used in our previous study (Kouřil *et al.*, 2016). The concentration of α-DDM was optimized to maximize the yield of high-molecular-mass bands (PSII megacomplexes and larger PSII supercomplexes) in clear native–polyacrylamide gel electrophoresis (CN–PAGE). Interestingly, the optimal detergent: chlorophyll ratio (w/w) for spruce appeared to be 50, whereas similar optimization performed for separation of larger PSII assemblies from *Arabidopsis thaliana* led to a ratio of 20 (Nosek *et al.*, 2017). Therefore, the solubilization protocol is not universal and should be optimized for each plant species separately.

Figure 1 shows a typical separation profile of mildly solubilized thylakoid membranes from Norway spruce using CN–PAGE. Most PSII supercomplexes were separated into three dense bands in the central part of the gel. They differed in their antenna size and were assigned as the $C_2S_2M_2$, C_2S_2M and C_2S_2 supercomplexes, in analogy with our previous paper (Kouřil *et al.*, 2016). The use of mild detergent α-DDM and optimized solubilization conditions allowed us to observe two additional high-molecular-weight bands in the upper part of the gel (the bands I and II; Figure 1). These bands contain larger PSII supercomplexes and megacomplexes, as mass spectrometry (MS) analysis revealed a high abundance of the proteins related to PSII and LHCII in these bands (Table S1). Both bands were excised from the gel, protein content was extracted by spontaneous elution and the obtained protein solution was subjected to structural analysis by single-particle electron microscopy.

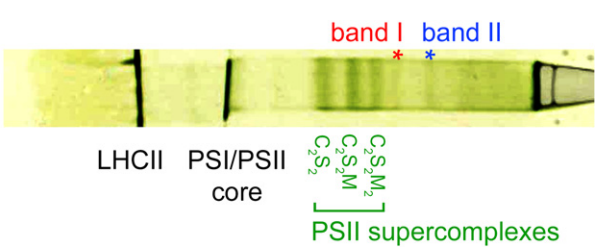

Figure 1. Separation of photosystem II (PSII) supercomplexes and megacomplexes from Norway spruce using clear native–polyacrylamide gel electrophoresis (CN–PAGE).
Isolated thylakoid membranes were mildly solubilized by *n*-dodecyl α-D-maltoside. The red and blue asterisks (the bands I and II) indicate the high-molecular-weight bands containing large PSII supercomplexes and megacomplexes, which were subjected to structural analysis by single-particle electron microscopy. The bands of lower molecular weight represent different forms of PSII supercomplexes, PSI complex and PSII core complex, and LHCII proteins, respectively.

Structural characterization of PSII supercomplexes

Image analysis of particle projections selected from electron micrographs revealed that PSII supercomplexes are present in both high-molecular-weight CN–PAGE bands (the bands I and II; Figure 1). Although various forms of large supercomplexes were found predominantly in band I, the largest PSII supercomplexes were so big that they co-migrated with PSII megacomplexes in band II.

Single-particle analysis of the samples prepared from band I resulted in the selection of 163 447 particle projections that were subsequently classified into 80 classes (Figure S1). In addition to the standard spruce $C_2S_2M_2$ supercomplex, where the core complex C_2 binds four LHCII trimers (Figure 2a), we observed novel types of PSII supercomplexes with up to six LHCII trimers (Figure 2b,c,g,h). The identified forms of PSII supercomplexes (Figure S1) differ significantly in their size, although they were obtained from the same highly focused band after CN–PAGE. Thus, it is probable that the smaller supercomplexes in Figure S1 (e.g. C_2S_2) are degradation products of the larger supercomplexes, which disintegrated during the elution of supercomplexes from the gel and/or during the preparation of samples for electron microscopy.

The samples obtained from band II (Figure 1) contained mainly PSII megacomplexes (Figure S2, detailed analysis follows), but a substantial part of the dataset contained various types of PSII supercomplexes. Except for several smaller PSII supercomplexes (C_2S_2, C_2S_2M and $C_2S_2M_2$), which probably originate from the break-up of less stable megacomplexes during the elution step and/or the specimen preparation, we observed very unique very large PSII supercomplexes that contain up to seven–eight LHCII trimers (Figure 2d–f), and have not been observed in any other plant species yet.

To examine the architecture of the large PSII supercomplexes and especially to analyze novel binding positions of LHCII trimers in detail, we fitted the electron microscopy projection maps with a recent molecular model of the PSII supercomplex (van Bezouwen *et al.*, 2017). Structural models show the organization of LHCII trimers within the supercomplexes (Figure 2i–p). In addition to the standard S and M trimers (Figure 2i), in some supercomplexes we were able to identify the N trimers, typical for supercomplexes from *C. reinhardtii* (Figure 2j,l–p). The orientation of the N trimer with respect to C_2 core was determined in the best-resolved projection map of the $C_2S_2M_2N$ supercomplex (Figure 2b,j), and this orientation seems to be the same in all other supercomplexes but one (Figure 2l–o).

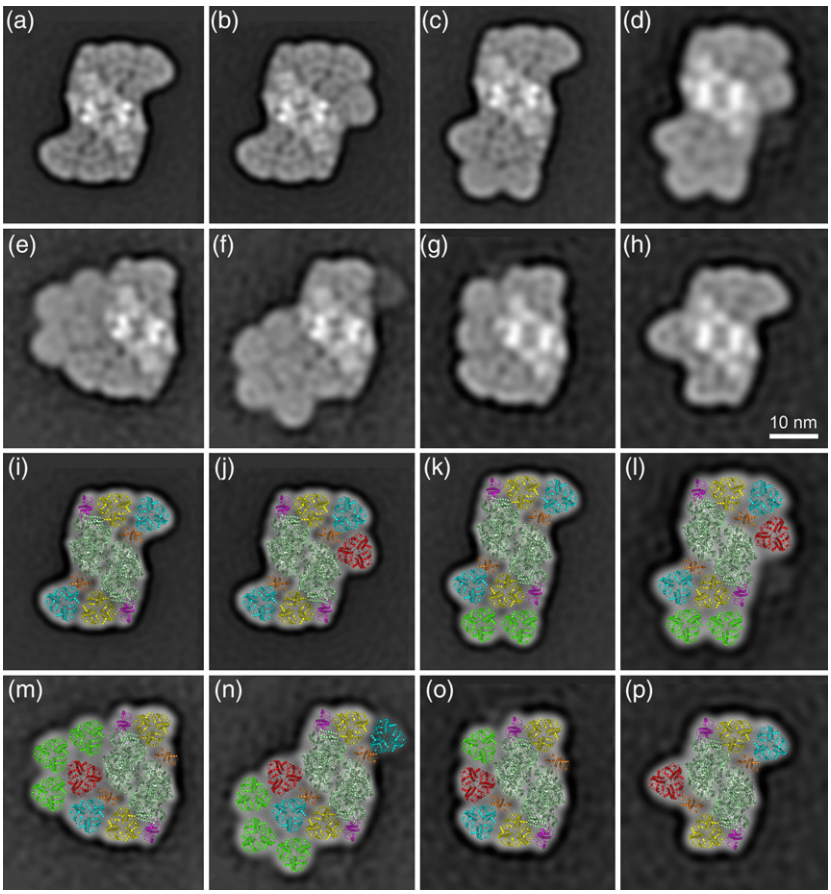

Figure 2. The large photosystem II (PSII) supercomplexes from Norway spruce.
The supercomplexes were eluted from the band I (a–c, g, h) and the band II (d–f) in Figure 1. Projection maps of individual types of the PSII supercomplexes represent the best class averages of: (a) 12 015; (b) 9847; (c) 6356; (d) 622; (e) 1298; (f) 1018; (g) 1554; (h) 1219 particles.
(i–p) Structural models of PSII supercomplexes were obtained by a fit of the high-resolution structure (van Bezouwen *et al.*, 2017). Individual PSII subunits are color-coded: dark green – core complex; yellow – S trimer; cyan – M trimer; red – N trimer; green – L trimer; magenta – Lhcb5; orange – Lhcb4.

The exception is the C_2S_2MN supercomplex (Figure 2p), where the orientation of the N trimer is different, probably due to the absence of the M trimer in the vicinity of the N trimer. Our analysis also revealed the presence of the L trimer in some of the supercomplexes (Figure 2m,o), and we were even able to see supercomplexes where there was a row of four LHCII trimers (S, M, N and L) around one side of the PSII core complex (Figure 2m,o). Moreover, our data show that the spruce PSII supercomplex has a unique ability to extend the antenna size even more by binding additional LHCII trimers. These trimers, which we term as the L_a trimers (additional loosely bound trimers), bind to the supercomplexes at different positions via the S, M, N and L trimers, and form the second row of LHCII trimers around the PSII core complex (Figure 2k–n).

To investigate whether the presence of larger PSII supercomplexes is a unique feature of Norway spruce or whether these structures can be found also in other members of the Pinaceae family (lacking the Lhcb3 and Lhcb6 proteins), we performed an analogical structural analysis of PSII supercomplexes isolated from Scots pine (*Pinus sylvestris*; Figure S3). Single-particle image analysis revealed several larger forms of pine PSII supercomplexes (Figure S4a–f), which were identical to their counterparts in spruce (Figure 2a–d,h). This finding indicates that the unique ability to form larger antenna around the PSII core complex is likely a general property of the species from the Pinaceae family.

Structural characterization of PSII megacomplexes

The inspection of electron micrographs of the sample prepared from the high-molecular-weight band depicted as band II (Figure 1) resulted in the selection of 66 650 particle projections, which were subjected to image analysis and classification into 64 classes (Figure S2). Visual analysis of the classification file (Figure S2) allowed us to estimate that the PSII megacomplexes account for about 30% of the whole dataset. Approximately half of the dataset contained various types of PSII supercomplexes (see above). The rest of the structures (about 20%) in Figure S2 contained other types of unspecific protein complexes (e.g. dimers/monomers of ATP synthase), which co-migrated with the PSII megacomplexes in the gel.

Figure 3 shows the best-resolved classes of PSII megacomplexes. Each megacomplex consists of two copies of PSII supercomplexes, which associate with each other through their antenna complexes. Based on the orientation of PSII cores, the associations of the pairs of PSII

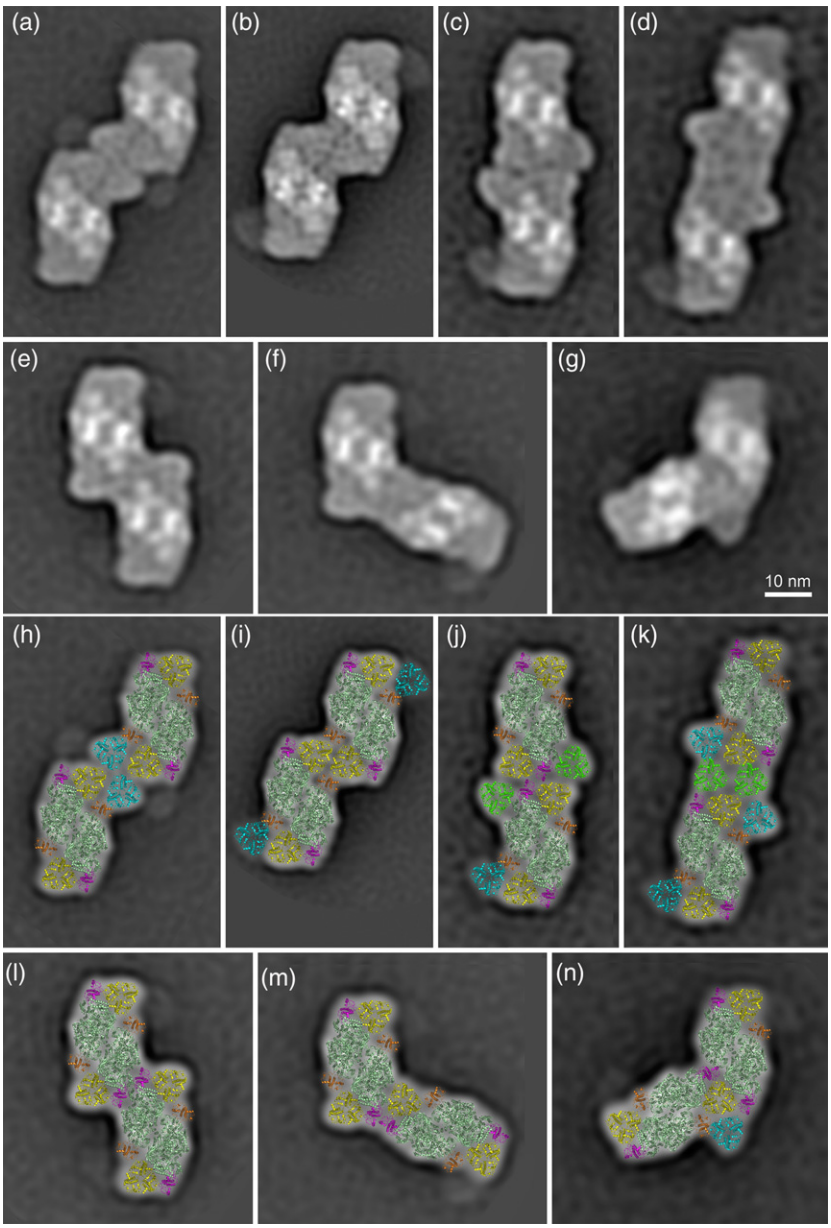

Figure 3. Various photosystem II (PSII) megacomplexes from Norway spruce.
The megacomplexes were eluted from the band II (Figure 1). Projection maps of individual types of the PSII megacomplexes represent the best class averages of: (a) 1549; (b) 3118; (c) 1095; (d) 724; (e) 1178; (f) 915; (g) 1103 particles.
(h–n) Structural models of the PSII megacomplexes obtained by a fit of the high-resolution structure of PSII (van Bezouwen *et al.*, 2017). Individual PSII subunits are color-coded: dark green – core complex; yellow – S trimer; cyan – M trimer; green – L trimer; magenta – Lhcb5; orange – Lhcb4.

supercomplexes were either parallel (Figure 3a–e) or non-parallel (Figure 3f,g). The parallel associations were more abundant (70%) than the non-parallel ones (30%).

Structural models of the projection maps of the PSII megacomplexes show that the megacomplexes are formed by variable interactions between $C_2S_2M_2$ (Figure 3k), C_2S_2M (Figure 3h–k) and C_2S_2 (Figure 3j,l,m) supercomplexes. In some cases, PSII megacomplexes are formed with the help of the additional L trimers (Figure 3j,k). A closer view at the models of the identified megacomplexes (Figure 3) shows that the S trimer is most frequently involved in the megacomplex formation. Thus, the S trimer mediates probably the strongest binding between PSII supercomplexes within the PSII megacomplexes. However, also other subunits were found to participate in the association of supercomplexes into megacomplexes – Lhcb5 (CP26), Lhcb4 (CP29), C_2, L and M trimers (in order of decreasing importance). Similar forms of PSII megacomplexes were also observed in Scots pine (Figure S4g–i).

Interaction between PSII complexes in grana membranes

Isolated grana membranes were analyzed using electron microscopy in order to characterize the organization and interaction between the neighboring PSII supercomplexes in the membrane. Visual screening of the electron micrographs revealed a random distribution of PSII complexes in the grana membranes (Figure 4a). The organization of PSII complexes into 2D crystalline arrays was not observed

in analyzed micrographs, which is somewhat surprising as the array formation is quite common in other plant species (Kouřil *et al.*, 2012). In order to confirm the physiological relevance of the PSII megacomplexes, which were observed after CN–PAGE separation, we investigated specific interactions between individual PSII complexes in the grana membranes. Indeed, image analysis of the PSII projections revealed several conserved mutual positions of PSII core complexes (Figure 4b). These pairs can be considered as PSII megacomplexes as the projection maps can be fitted with the model of the $C_2S_2M_2$ supercomplex with tight interactions between the LHCII trimers or PSII core complexes (Figure 4c).

DISCUSSION

Structural characterization of large spruce PSII supercomplexes

Our previous study showed that the absence of Lhcb6 and Lhcb3 in the PSII complex of spruce results in a specific assembly of $C_2S_2M_2$, which has never been found in land plants before (Kouřil *et al.*, 2016). Here we show that the unique organization of the $C_2S_2M_2$ supercomplex seems to be characteristic for the Pinaceae family, as we have found the identical architecture of this supercomplex also in Scots pine (Figure S4a). This unique organization of the PSII supercomplex brought several questions about the possible consequences for the attachment of additional LHCII trimers and the formation of larger super- and megacomplexes.

As the spruce PSII supercomplex shares some features with PSII supercomplex in *C. reinhardtii* (Kouřil *et al.*, 2016), the first hypothesis we wanted to verify was whether the spruce $C_2S_2M_2$ supercomplex is able to bind additional LHCII trimer (N trimer) in the same way as *C. reinhardtii* (Tokutsu *et al.*, 2012; Drop *et al.*, 2014; Shen *et al.*, 2019; Sheng *et al.*, 2019). The outcome of single-particle analysis unequivocally confirmed that the $C_2S_2M_2$ supercomplex is indeed able to bind the N trimer; however, its precise orientation depends on the presence of the M trimer. In supercomplexes where both the N and M trimers are present (Figure 2j,l–o), the N trimer is rotated clockwise by 63° compared with *C. reinhardtii*. This rotation could be most probably explained by the differences in the structure of the M and N trimers themselves. While the LHCII trimers in Norway spruce are formed by Lhcb1 and Lhcb2 proteins (Kouřil *et al.*, 2016) with possible involvement of Lhcb5 (Grebe *et al.*, 2019), the LHCII trimers in *C. reinhardtii* are formed by Lhcbm1/2/3/6/7 proteins (Drop *et al.*, 2014; Shen *et al.*, 2019). In Scots pine, the orientation of the N trimer in PSII supercomplexes is the same as in spruce (Figure S4b,e). Interestingly, in both spruce and pine, we have also found supercomplex where the N trimer is bound to the PSII core without the presence of the M trimer (Figures 2p and S4f, respectively). In this case, the N trimer binds to the PSII core complex in the same orientation as in *C. reinhardtii* (Figure 5). This finding indicates that the mutual interaction between the M and N trimer determines the orientation of the N trimer in PSII supercomplexes in Pinaceae. However, due to the lack of high-resolution structural details of the spruce and pine PSII supercomplexes, we cannot exclude the possibility that some PSII core subunits are involved in the binding of the N trimer – namely PsbH and PsbX, which are involved in the binding of the N trimer in *C. reinhardtii* (Shen *et al.*, 2019; Sheng *et al.*, 2019). A high-resolution cryo-electron microscopy structure of spruce/pine supercomplex will be necessary to unequivocally resolve this question.

The optimization of the separation procedure allowed us not only to find supercomplexes with attached N trimer, but also PSII supercomplexes that are even larger than the $C_2S_2M_2N$. In some of these supercomplexes from Norway spruce, another LHCII trimer binds in the vicinity of the N trimer (Figure 2m,o). As the position of this trimer is similar to the position of the L trimer observed in the very small fraction of isolated PSII supercomplexes from spinach (Boekema *et al.*, 1999a,b; see also Figure 5), we tentatively named it as the L trimer. Such a large PSII supercomplex with four LHCII trimers (S, M, N, L) bound around the PSII core has never been found in any plant species so far. There are some indications that this structure might exist in *C. reinhardtii*, as Kawakami *et al.* (2019) recently found that there are four types of LHCII trimers in *C. reinhardtii*. Nevertheless, their work was based on biochemical methods, and the attachment of the L trimer to the $C_2S_2M_2N_{1\text{-}2}$ supercomplex in *C. reinhardtii* is yet to be confirmed experimentally. It is possible that the difference in the orientation of the N trimer in spruce and in *C. reinhardtii* affects the strength of the binding of the L trimer, making it more labile and thus more prone to dissociation in the latter.

Surprisingly, we have found out that even the large PSII supercomplex with attached S, M, N and L trimers is not the largest one that could be found in spruce. Our structural analysis revealed for the first time that the PSII supercomplex is able to bind LHCII trimers in two rows. The LHCII trimers of the second (outer) row, which we named L_a (additional L) trimers, can bind to PSII at five specific positions along the inner row of the S, M, N and L trimers. The largest spruce PSII supercomplex identified in our study binds seven or eight LHCII trimers (Figure 2l–n), which exceeds the antenna size of $C_2S_2M_2N_2$ supercomplex in *C. reinhardtii*, currently considered to be the largest known PSII supercomplex. Considering the twofold symmetry of the PSII supercomplex, we can hypothesize that the most complete spruce PSII supercomplex would have the ability to bind up to 18 LHCII trimers (Figure 5). The hypothetical model can be applied also for Scots pine,

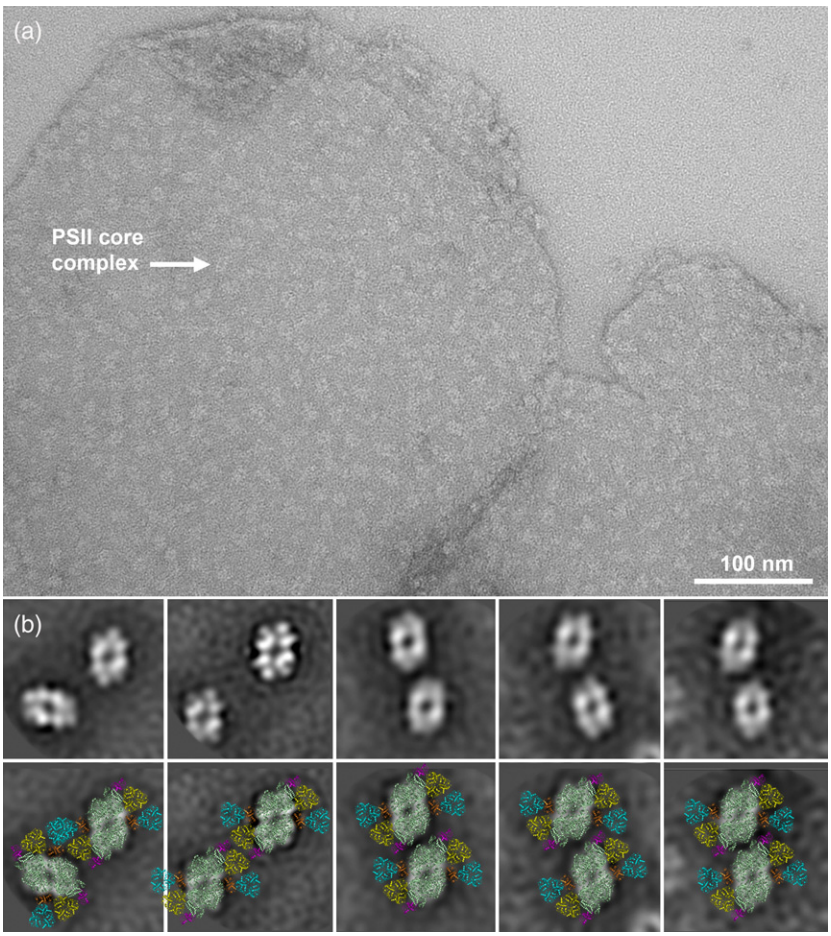

Figure 4. Distribution of photosystem II (PSII) complexes and their association into megacomplexes in isolated grana membranes.
(a) An example of the electron micrograph of negatively stained grana membranes isolated from Norway spruce showing a density and distribution of PSII complexes. White arrow indicates a typical density of the PSII core complex.
(b) Most abundant associations of PSII complexes into different types of megacomplexes found within the grana membranes after image analysis.
(c) Structural models of the PSII megacomplexes obtained by a fit of the high-resolution structure (van Bezouwen *et al.*, 2017). Individual PSII subunits are color-coded: dark green – core complex; yellow – S trimer; cyan – M trimer; magenta – Lhcb5; orange – Lhcb4.

where the largest identified form of the PSII supercomplex binds seven LHCII trimers (Figure S4e). Interestingly, the antenna organization in this large PSII supercomplex would still keep free the path for plastoquinone to the acceptor sites in the PSII core complex (van Eerden *et al.*, 2017), which gives the hypothetical model a physiological relevance.

Structural characterization of spruce PSII megacomplexes

It is well known that plant PSII supercomplexes can further associate into larger assemblies, forming PSII megacomplexes. Our work shows that the species from Pinaceae family are no exception. Single-particle electron microscopy analysis revealed several distinct types of spruce and pine PSII megacomplexes, which were formed either by parallel or non-parallel associations between two PSII supercomplexes (Figures 3 and S4g–i). The main distinctive feature of the spruce and pine PSII megacomplexes, when compared with those from Arabidopsis (Nosek *et al.*, 2017), is their lower structural variability. While we found only seven types of megacomplexes in spruce and three in pine, their number in Arabidopsis was significantly higher (13; Nosek *et al.*, 2017). This finding can be simply explained by the lower stability of PSII megacomplexes in Pinaceae. This explanation is supported, for example, by our finding that during the image analysis of the sample from the high-molecular-weight band II (Figure 1), we have observed classes of the C_2S_2, C_2S_2M and $C_2S_2M_2$ PSII supercomplexes, which are the building blocks of the megacomplexes (Figure S2). As these supercomplexes cannot co-migrate in the gel with megacomplexes, which have roughly twice the size and weight, the only feasible explanation of the presence of these supercomplexes in this sample is that they originate from the break-up of megacomplexes during the elution step and specimen preparation for electron microscopy.

In our previous study with Arabidopsis, we have successfully identified some forms of megacomplexes also on the level of the thylakoid membrane (Nosek *et al.*, 2017), and therefore we have employed this approach also for spruce. Image analysis of the PSII distribution in thylakoid membranes from spruce revealed five well-resolved specific associations between the adjacent PSII supercomplexes (Figure 4b,c), which strongly indicates that PSII megacomplexes in spruce exist *in vivo*. The proposed structural models of these megacomplexes show that they can be

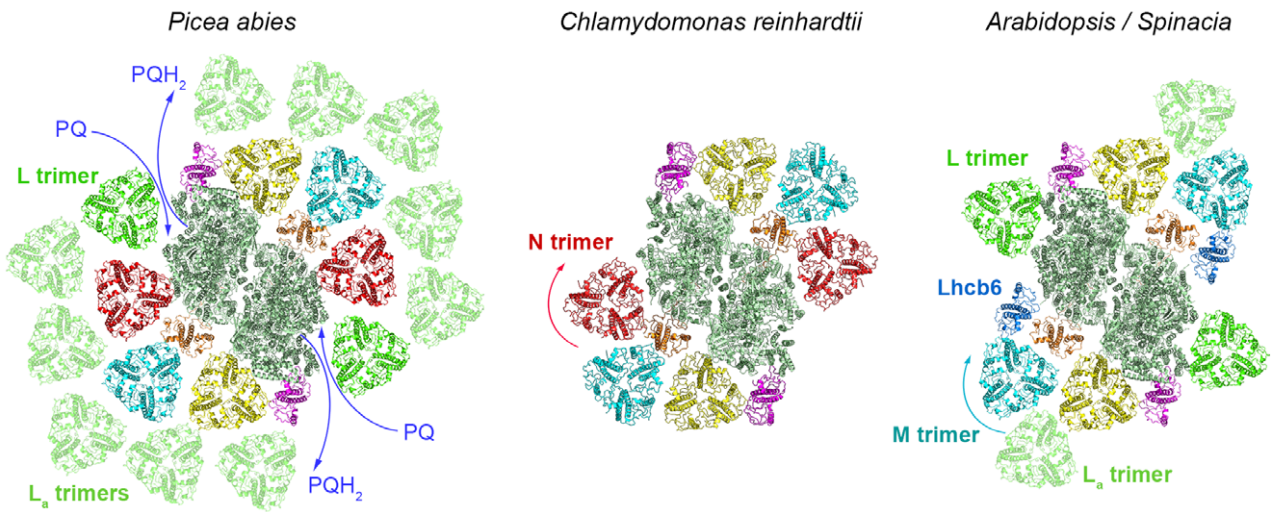

Figure 5. A hypothetical model of photosystem II (PSII) supercomplex from Norway spruce (*Picea abies*) and its comparison with evolutionary different organisms.

The model of the complete PSII supercomplex in Norway spruce is based on the structures of different forms of PSII supercomplexes revealed by single-particle electron microscopy. The specific orientation of the N trimer in Norway spruce probably enables a stable binding of the L trimer and formation of the second row of additional L_a trimers along the PSII core complex, but still keeps the path for plastoquinone molecules free. Different orientation of the N trimer in *Chlamydomonas reinhardtii* (Shen *et al.*, 2019) likely does not support the binding of the L trimer. In the majority of land plants, the binding site for the N trimer is occupied by the Lhcb6 protein, which probably modifies the binding of the M trimer. The L trimer can very occasionally bind to the PSII core complex (e.g. in spinach; Boekema *et al.*, 1999a,b) or additional L_a trimers can associate with PSII at the site of the S/M trimers (e.g. Arabidopsis; Nosek *et al.*, 2017). Individual PSII subunits are color-coded: dark green – core complex; yellow – S trimer; cyan – M trimer; red – N trimer; green – L trimer; light green – L_a trimers; magenta – Lhcb5; orange – Lhcb4.

formed, for example, by $C_2S_2M_2$ supercomplexes (Figure 4c), but we cannot exclude the involvement of even larger forms of the PSII supercomplexes. Three types of the megacomplexes represent an almost parallel association of the PSII supercomplexes along the core complex, which is similar to the megacomplex formations observed in Arabidopsis (Nosek *et al.*, 2017).

It is, however, important to note that - unlike in Arabidopsis (Nosek *et al.*, 2017) – in spruce the PSII associations observed in thylakoid membranes do not correspond to any spruce PSII megacomplexes that we were able to isolate and separate. The interactions between the neighboring PSII supercomplexes in the membrane seem to be too weak to keep the megacomplexes intact during the separation procedure and/or specimen preparation for electron microscopy analysis. Thus, it is likely that the separated PSII megacomplexes (Figure 3) represent the most stable megacomplex forms, but they do not represent the most frequent type of megacomplexes found in the thylakoid membrane.

We assume that the lower stability of the bigger PSII megacomplexes could be closely related to the overall architecture of individual PSII supercomplexes. While a majority of the isolated spruce and pine megacomplexes are formed by pairs of smaller forms of PSII supercomplexes (C_2S_2 or C_2S_2M; Figures 3 and S4g–i), in Arabidopsis the megacomplexes are formed by the larger, $C_2S_2M_2$, supercomplexes. Considering a different shape of the $C_2S_2M_2$ supercomplexes in spruce and Arabidopsis (Figure 5), it becomes obvious that the rectangular shape of the $C_2S_2M_2$ in Arabidopsis can provide more stable interaction between adjacent supercomplexes. Indeed, a majority of the Arabidopsis megacomplexes were formed by parallel associations of two PSII supercomplexes along their longer sides, which probably represents a relatively stable configuration. The shape of the $C_2S_2M_2$ supercomplex in Pinaceae, modified by the absence of Lhcb3 and Lhcb6 proteins (Kouřil *et al.*, 2016), cannot provide the same interaction interface, which could potentially explain the lower stability of the PSII megacomplexes.

In summary, the structural analysis of PSII from two species from the Pinaceae family, Norway spruce and Scots pine, further extended our knowledge about the architecture of PSII supercomplexes. Our results clearly show that there are more binding sites for LHCII trimers than it was originally thought. We suggest that the evolutionary loss of Lhcb6 in Pinaceae resulted in the ability of PSII core to bind the N trimer as in the case of green alga *C. reinhardtii* (Figure 5). A unique orientation of the N trimer in Pinaceae probably supports the binding of the L trimer and additional L_a trimers, thus leading to the formation of larger PSII supercomplexes. A different orientation of the N trimer in *C. reinhardtii* or the absence of the N trimer in other land plant species (e.g. Arabidopsis, spinach) likely results in a loose binding of the L trimer to the PSII core (Figure 5).

The interesting question to answer is what environmental conditions would lead to a formation of such giant PSII supercomplexes, hypothetically up to the $C_2S_2M_2N_2L_2L_{a10}$ supercomplex. Formation of these giant supercomplexes would require LHCII trimers to be in great excess of PSII core complexes. Acclimation of land plants to low light intensity is well known to induce a higher LHCII/PSII core ratio (Bailey *et al.*, 2001; Ballottari *et al.*, 2007; Kouřil *et al.*, 2013); however, for example Norway spruce does not follow this strategy, as the antenna size remains almost unchanged during acclimation (Kurasová *et al.*, 2003; Štroch *et al.*, 2008). Nevertheless, there are indications that the acclimation of conifers to winter conditions can lead to the enhanced LHCII/PSII core ratio (Verhoeven, 2014), which may create favorable conditions for the formation of large PSII supercomplexes.

EXPERIMENTAL PROCEDURES

Plant material and isolation of PSII megacomplexes and supercomplexes

Norway spruce [*Picea abies* (L.) Karst.] and Scots pine [*Pinus sylvestris* (L.); Semenoles, Liptovský Hrádok, Slovakia] seedlings were grown in a growth chamber with 16 h: 8 h, light: dark photoperiod at 21°C for 4 weeks. Plants were illuminated with white light at 100 μmol photons m^{-2} sec^{-1} (400–700 nm). Isolation of thylakoid membranes and electrophoretic separation of solubilized membranes using CN–PAGE were performed according to a protocol described by Nosek *et al.* (2017) with one modification in the solubilization condition, that is spruce and pine thylakoid membranes with 10 μg of chlorophylls were solubilized with *n*-dodecyl α-D-maltoside (α-DDM) using a detergent: chlorophyll mass ratio of 50.

Spruce PSII membranes were isolated using mild solubilization of thylakoid membranes with digitonin (0.5 mg of chlorophylls per ml and 0.5% digitonin) in a buffer containing 20 mM HEPES, pH 7.5, 5 mM $MgCl_2$ and 15 mM NaCl. Solubilization was performed for 20 min at 4°C with slow stirring, and was followed by centrifugation (5 min, 12 000 ***g***, 4°C). The pellet with the non-solubilized PSII grana membranes was washed twice with the buffer mentioned above, spun down again for 5 min (12 000 ***g***, 4°C) and then used for electron microscopy analysis.

Single-particle electron microscopy and image analysis

The PSII megacomplexes and supercomplexes were eluted from excised CN–PAGE gel bands according to Kouřil *et al.* (2014). Obtained protein solutions were directly used for electron microscopy specimen preparations by negative staining with 2% uranyl acetate on glow-discharged carbon-coated copper grids. Electron microscopy of spruce PSII supercomplexes and megacomplexes was performed on a Tecnai G2 F20 microscope (FEI) equipped with a LaB_6 cathode, operated at 200 kV. Images were recorded with an UltraScan 4000 UHS CCD camera (Gatan, Pleasanton, CA, USA) at 130 000 × magnification with a pixel size of 0.224 nm at the specimen level after binning the images to 2048 × 2048 pixels. GRACE software (Oostergetel *et al.*, 1998) was used for semi-automated acquisition of 14 000 and 11 000 images of PSII complexes eluted from the bands I and II, respectively, and two datasets of approx. 163 447 (band I) and 66 650 (band II) single-particle projections were selected and subjected to several rounds of single-particle image analysis and classification (Boekema *et al.*, 2009) using RELION software (Scheres, 2012) and reference-free 2D classification using SCIPION image processing framework (De La Rosa-Trevín *et al.*, 2016). Pseudo-atomic models of obtained PSII projection maps were created using PYMOL (DeLano, 2002).

Electron microscopy of isolated grana membranes from Norway spruce and eluted PSII megacomplexes and supercomplexes from Scots pine was performed on a Tecnai G2 F20 microscope (FEI) equipped with a field emission gun operated at 200 kV. Images were recorded with an Eagle 4K CCD camera (FEI) at 83 000 × magnification with a pixel size of 0.36 nm (spruce grana membrane), and at 130 000 × magnification with a pixel size of 0.226 nm (pine PSII super-/megacomplexes) at the specimen level after binning the images to 2048 × 2048 pixels. In total, 150 micrographs were recorded and about 13 000 manually selected projections of PSII particles were analyzed using RELION software (Scheres, 2012) to reveal the specific formation of PSII megacomplexes in the spruce grana membrane. Two datasets of approx. 73 000 and 310 000 single-particle projections were selected from 8000 and 7000 electron micrographs of pine PSII megacomplexes and PSII supercomplexes, respectively, and analyzed using reference-free 2D classification using SCIPION image processing framework (de la Rosa-Trevín *et al.*, 2016).

Proteomic characterization of spruce PSII supercomplexes and megacomplexes

The electroeluted PSII super- and megacomplexes were first concentrated and transferred to a denaturing buffer using a centrifugal filter unit with 3K cut-off. Next, in-solution protein digestion was performed with commercially available trypsin, as described previously (León *et al.*, 2013). The tryptic peptides were desalted and fractionated with the use of a custom reversed-phase (C18) microcolumn (Franc *et al.*, 2012) and subsequently analyzed by LC-MS (Simerský *et al.*, 2017). The acquired MS data were searched against *P. abies*-specific protein database (Grebe *et al.*, 2019) employing MaxQuant software v.1.6.10.43 (Beck *et al.*, 2015; Tyanova *et al.*, 2016) with Andromeda search engine (Cox *et al.*, 2011). To evaluate the abundances of the identified proteins, the well-established iBAQ method (Schwanhäusser *et al.*, 2011) was applied. Missing protein annotations were assigned by pBLAST homology searches. Details for all described methods can be found in the Supporting Information (Methods S1).

ACKNOWLEDGEMENTS

This work was supported by the Grant Agency of the Czech Republic (project no. 18-12178S/P501) to R.K., L.N. and P.I., the European Regional Development Fund (ERDF) project 'Plants as a tool for sustainable global development' (no. CZ.02.1.01/0.0/0.0/16_019/0000827) to R.K., L.N., P.I. and M.O., and the Marie Curie Actions Initial Training Networks SE2B (under grant agreement no. 675006) to R.K., R.A. and E.J.B. CIISB research infrastructure project LM2015043 funded by MEYS CR is gratefully acknowledged for the financial support of the measurements at the CF Cryo-electron Microscopy and Tomography. The authors thank Dr Iva Ilíková for editing of the manuscript.

AUTHOR CONTRIBUTIONS

RK, LN, PI planned and designed the research. RK, LN, MO, RA, DS, IC, RL performed experiments. RK, LN, MO, RA, DS, IC, R.L., EJB and PI analyzed the data. RK and PI wrote the manuscript, and all authors revised and approved it.

CONFLICT OF INTEREST

The authors have no conflict of interest to declare.

DATA AVAILABILITY STATEMENT

All relevant data can be found within the manuscript and its supporting materials. The mass spectrometry proteomics data have been deposited to the ProteomeXchange Consortium via the PRIDE (Perez-Riverol *et al.*, 2019) partner repository with the dataset identifier PXD020138.

SUPPORTING INFORMATION

Additional Supporting Information may be found in the online version of this article.

Figure S1. Single-particle image analysis and classification of PSII supercomplexes from Norway spruce extracted from CN–PAGE band I.

Figure S2. Single-particle image analysis and classification of PSII supercomplexes and megacomplexes from Norway spruce extracted from CN–PAGE band II.

Figure S3. Separation of pigment–protein complexes from Scots pine using CN–PAGE.

Figure S4. Structural characterization of PSII supercomplexes and megacomplexes from Scots pine.

Data S1. Complete protein identification data and other files containing information related to protein identification as exported from MaxQuant software v. 1.6.10.43.

Table S1. An overview of protein composition of the PSII supercomplex and megacomplex bands (CN–PAGE bands I and II).

Table S2. A list of all identified proteins from CN–PAGE bands I and II with corresponding characteristics and annotations.

Methods S1. Proteomic characterization of Norway spruce PSII supercomplexes and megacomplexes.

REFERENCES

Albanese, P., Nield, J., Tabares, J.A.M., Chiodoni, A., Manfredi, M., Gosetti, F., Marengo, E., Saracco, G., Barber, J. and Pagliano, C. (2016) Isolation of novel PSII-LHCII megacomplexes from pea plants characterized by a combination of proteomics and electron microscopy. *Photosynth. Res.* **130**, 19–31.

Albanese, P., Melero, R., Engel, B.D. *et al.* (2017) Pea PSII-LHCII supercomplexes form pairs by making connections across the stromal gap. *Sci. Rep.* **7**, 10067.

Ballottari, M., Dall'Osto, L., Morosinotto, T. and Bassi, R. (2007) Contrasting behavior of higher plant photosystem I and II antenna systems during acclimation. *J. Biol. Chem.* **282**, 8947–8958.

Barber, J. (2003) Photosystem II: the engine of life. *Q. Rev. Biophys.* **36**, 71–89.

Bailey, S., Walters, R.G., Jansson, S. and Horton, P. (2001) Acclimation of *Arabidopsis thaliana* to the light environment: the existence of separate low light and high light responses. *Planta*, **213**, 794–801.

Beck, S., Michalski, A., Raether, O. *et al.* (2015) The impact II, a very high-resolution Quadrupole Time-of-Flight Instrument (QTOF) for deep shotgun proteomics. *Mol. Cell. Proteomics*, **14**, 2014–2029.

Boekema, E.J., van Roon, H., Calkoen, F., Bassi, R. and Dekker, J.P. (1999a) Multiple types of association of photosystem II and its light-harvesting antenna in partially solubilized photosystem II membranes. *Biochemistry*, **38**, 2233–2239.

Boekema, E.J., van Roon, H., van Breemen, J.F.L. and Dekker, J.P. (1999b) Supramolecular organization of photosystem II and its light-harvesting antenna in partially solubilized photosystem II membranes. *Eur. J. Biochem.* **266**, 444–452.

Boekema, E.J., Folea, M. and Kouřil, R. (2009) Single particle electron microscopy. *Photosynth. Res.* **102**, 189–196.

Caffarri, S., Kouřil, R., Kereiche, S., Boekema, E.J. and Croce, R. (2009) Functional architecture of higher plant photosystem II supercomplexes. *EMBO J.* **28**, 3052–3063.

Caffarri, S., Croce, R., Cattivelli, L. and Bassi, R. (2004) A look within LHCII: Differential analysis of the Lhcbl-3 complexes building the major trimeric antenna complex of higher-plant photosynthesis. *Biochemistry*, **43**, 9467–9476.

Cox, J., Neuhauser, N., Michalski, A., Scheltema, R.A., Olsen, J.V. and Mann, M. (2011) Andromeda: a peptide search engine integrated into the MaxQuant environment. *J. Proteome Res.* **10**, 1794–1805.

Crepin, A. and Caffarri, S. (2018) Functions and evolution of Lhcb isoforms composing LHCII, the major light harvesting complex of photosystem II of green eukaryotic organisms. *Curr. Protein Pept. Sci.* **19**, 699–713.

Daum, B., Nicastro, D., Austin, J., McIntosh, J. and Kühlbrandt, W. (2010) Arrangement of photosystem II and ATP synthase in chloroplast membranes of spinach and pea. *Plant Cell*, **22**, 1299–1312.

de Bianchi, S., Dall'Osto, L., Tognon, G., Morosinotto, T. and Bassi, R. (2008) Minor antenna proteins CP24 and CP26 affect the interactions between photosystem II subunits and the electron transport rate in grana membranes of Arabidopsis. *Plant Cell*, **20**, 1012–1028.

DeLano, W.L. (2002) *The PyMOL Molecular Graphics System*. San Carlos, CA: DeLano Scientific.

de Bianchi, S., Betterle, N., Kouřil, R., Cazzaniga, S., Boekema, E., Bassi, R. and Dall'Osto, L. (2011) Arabidopsis mutants deleted in the light-harvesting protein Lhcb4 have a disrupted photosystem II macrostructure and are defective in photoprotection. *Plant Cell*, **23**, 2659–2679.

de la Rosa-Trevín, J.M., Quintana, A., Del Cano, L. *et al.* (2016) Scipion: a software framework toward integration, reproducibility and validation in 3D electron microscopy. *J. Struct. Biol.* **195**, 93–99.

Dekker, J.P. and Boekema, E.J. (2005) Supramolecular organization of thylakoid membrane proteins in green plants. *Biochim. Biophys. Acta*, **1706**, 12–39.

Drop, B., Webber-Birungi, M., Yadav, S.K., Filipowicz-Szymanska, A., Fusetti, F., Boekema, E.J. and Croce, R. (2014) Light-harvesting complex II (LHCII) and its supramolecular organization in *Chlamydomonas reinhardtii*. *Biochim. Biophys. Acta-Bioenergetics*, **1837**, 63–72.

Franc, V., Šebela, M., Řehulka, P., Končitíková, R., Lenobel, R., Madzak, C. and Kopečný, D. (2012) Analysis of N-glycosylation in maize cytokinin oxidase/dehydrogenase 1 using a manual microgradient chromatographic separation coupled offline to MALDI-TOF/TOF mass spectrometry. *J. Proteomics*, **75**, 4027–4037.

Grebe, S., Trotta, A., Bajwa, A.A., Suorsa, M., Gollan, P.J., Jansson, S., Tikkanen, M. and Aro, E.M. (2019) The unique photosynthetic apparatus of Pinaceae: analysis of photosynthetic complexes in *Picea abies*. *J. Exp. Bot.* **70**, 3211–3225.

Jansson, S. (1994) The light–harvesting chlorophyll a/b binding-proteins. *Biochim. Biophys. Acta*, **1184**, 1–19.

Kawakami, K., Tokutsu, R., Kim, E. and Minagawa, J. (2019) Four distinct trimeric forms of light-harvesting complex II isolated from the green alga *Chlamydomonas reinhardtii*. *Photosynth. Res.* **142**, 195–201.

Kirchhoff, H. (2013) Architectural switches in plant thylakoid membranes. *Photosynth. Res.* **116**, 481–487.

Kirchhoff, H., Tremmel, I., Haase, W. and Kubitscheck, U. (2004) Supramolecular photosystem II organization in grana thylakoid membranes: evidence for a structured arrangement. *Biochemistry*, **43**, 9204–9213.

Kirchhoff, H., Lenhert, S., Büchel, C., Chi, L. and Nield, J. (2008) Probing the organization of photosystem II in photosynthetic membranes by atomic force microscopy. *Biochemistry*, **47**, 431–440.

Kouřil, R., Dekker, J.P. and Boekema, E.J. (2012) Supramolecular organization of photosystem II in green plants. *Biochim. Biophys. Acta-Bioenergetics*, **1817**, 2–12.

Kouřil, R., Wientjes, E., Bultema, J.B., Croce, R. and Boekema, E.J. (2013) High-light vs. low-light: effect of light acclimation on photosystem II composition and organization in *Arabidopsis thaliana*. *Biochim. Biophys. Acta-Bioenergetics*, **1827**, 411–419.

Kouřil, R., Strouhal, O., Nosek, L., Lenobel, R., Chamrád, I., Boekema, E.J., Šebela, M. and Ilík, P. (2014) Structural characterization of a plant photosystem I and NAD(P)H dehydrogenase supercomplex. *Plant J.* **77**, 568–576.

Kouřil, R., Nosek, L., Bartoš, J., Boekema, E.J. and Ilík, P. (2016) Evolutionary loss of light-harvesting proteins Lhcb6 and Lhcb3 in major land plant groups - break-up of current dogma. *New Phytol.* **210**, 808–814.

Kouřil, R., Nosek, L., Semchonok, D., Boekema, E.J. and Ilík, P. (2018) Organization of plant photosystem II and photosystem I supercomplexes. *Subcell. Biochem.* **87**, 259–286.

Kovács, L., Damkjær, J., Kereïche, S., Ilioaia, C., Ruban, A.V., Boekema, E.J., Jansson, S. and Horton, P. (2006) Lack of the light-harvesting complex CP24 affects the structure and function of the grana membranes of higher plant chloroplasts. *Plant Cell*, **18**, 3106–3120.

Kurasová, I., Kalina, J., Urban, O., Štroch, M. and Špunda, V. (2003) Acclimation of two distinct plant species, spring barley and Norway spruce, to combined effect of various irradiance and CO_2 concentration during cultivation in controlled environment. *Photosynthetica*, **41**, 513–523.

León, I.R., Schwämmle, V., Jensen, O.N. and Sprenger, R.R. (2013) Quantitative assessment of in-solution digestion efficiency identifies optimal protocols for unbiased protein analysis. *Mol. Cell. Proteomics*, **12**, 2992–3005.

Morosinotto, T., Bassi, R., Frigerio, S., Finazzi, G., Morris, E. and Barber, J. (2006) Biochemical and structural analyses of a higher plant photosystem II supercomplex of a photosystem I-less mutant of barely. Consequences of a chronic over-reduction of the plastoquinone pool. *FEBS J.* **273**, 4616–4630.

Nosek, L., Semchonok, D., Boekema, E.J., Ilík, P. and Kouřil, R. (2017) Structural variability of plant photosystem II megacomplexes in thylakoid membranes. *Plant J.* **89**, 104–111.

Oostergetel, G.T., Keegstra, W. and Brisson, A. (1998) Automation of specimen selection and data acquisition for protein electron crystallography. *Ultramicroscopy*, **74**, 47–59.

Perez-Riverol, Y., Csordas, A., Bai, J. *et al.* (2019) The PRIDE database and related tools and resources in 2019: improving support for quantification data. *Nucleic Acids Res.* **47**, D442–D450.

Scheres, S.H. (2012) RELION: implementation of a Bayesian approach to cryo-EM structure determination. *J. Struct. Biol.* **180**, 519–530.

Schwanhäusser, B., Busse, D., Li, N., Dittmar, G., Schuchhardt, J., Wolf, J., Chen, W. and Selbach, M. (2011) Global quantification of mammalian gene expression control. *Nature*, **473**, 337–342.

Shen, L., Huang, Z., Chang, S., Wang, W., Wang, J., Kuang, T., Han, G., Shen, J.R. and Zhang, X. (2019) Structure of a $C_2S_2M_2N_2$-type PSII–LHCII supercomplex from the green alga *Chlamydomonas reinhardtii*. *Proc. Natl. Acad. Sci. USA*, **116**, 21246–21255.

Sheng, X., Watanabe, A., Li, A., Kim, E., Song, C., Murata, K., Song, D., Minagawa, J. and Liu, Z. (2019) Structural insight into light harvesting for photosystem II in green algae. *Nat. Plants*, **5**, 1320–1330.

Simerský, R., Chamrád, I., Kania, J., Strnad, M., Šebela, M. and Lenobel, R. (2017) Chemical proteomic analysis of 6-benzylaminopurine molecular partners in wheat grains. *Plant Cell Rep.* **36**, 1561–1570.

Štroch, M., Kuldová, K., Kalina, J. and Špunda, V. (2008) Dynamics of the xanthophyll cycle and non-radiative dissipation of absorbed light energy during exposure of Norway spruce to high irradiance. *J. Plant Physiol.* **165**, 612–622.

Su, X., Ma, J., Wei, X., Cao, P., Zhu, D., Chang, W., Liu, Z., Zhang, X. and Li, M. (2017) Structure and assembly mechanism of plant $C_2S_2M_2$-type PSII-LHCII supercomplex. *Science*, **357**, 815–820.

Tokutsu, R., Kato, N., Bui, K.H., Ishikawa, T. and Minagawa, J. (2012) Revisiting the supramolecular organization of photosystem II in *Chlamydomonas reinhardtii*. *J. Biol. Chem.* **287**, 31574–31581.

Tyanova, S., Temu, T. and Cox, J. (2016) The MaxQuant computational platform for mass spectrometry-based shotgun proteomics. *Nat. Protoc.* **11**, 2301–2319.

van Bezouwen, L.S., Caffarri, S., Kale, R.S., Kouřil, R., Thunnissen, A.M.W.H., Oostergetel, G.T. and Boekema, E.J. (2017) Subunit and chlorophyll organization of the plant photosystem II supercomplex. *Nat. Plants*, **3**, 17080.

van Eerden, F.J., Melo, M.N., Frederix, P.W.J.M., Periole, X. and Marrink, S.J. (2017) Exchange pathways of plastoquinone and plastoquinol in the photosystem II complex. *Nat. Commun.* **8**, 15214.

Verhoeven, A. (2014) Sustained energy dissipation in winter evergreens. *New Phytol.* **201**, 57–65.

Wei, X., Su, X., Cao, P., Liu, X., Chang, W., Li, M., Zhang, X. and Liu, Z. (2016) Structure of spinach photosystem II-LHCII supercomplex at 3.2Å resolution. *Nature*, **534**, 69–74.

Supporting information

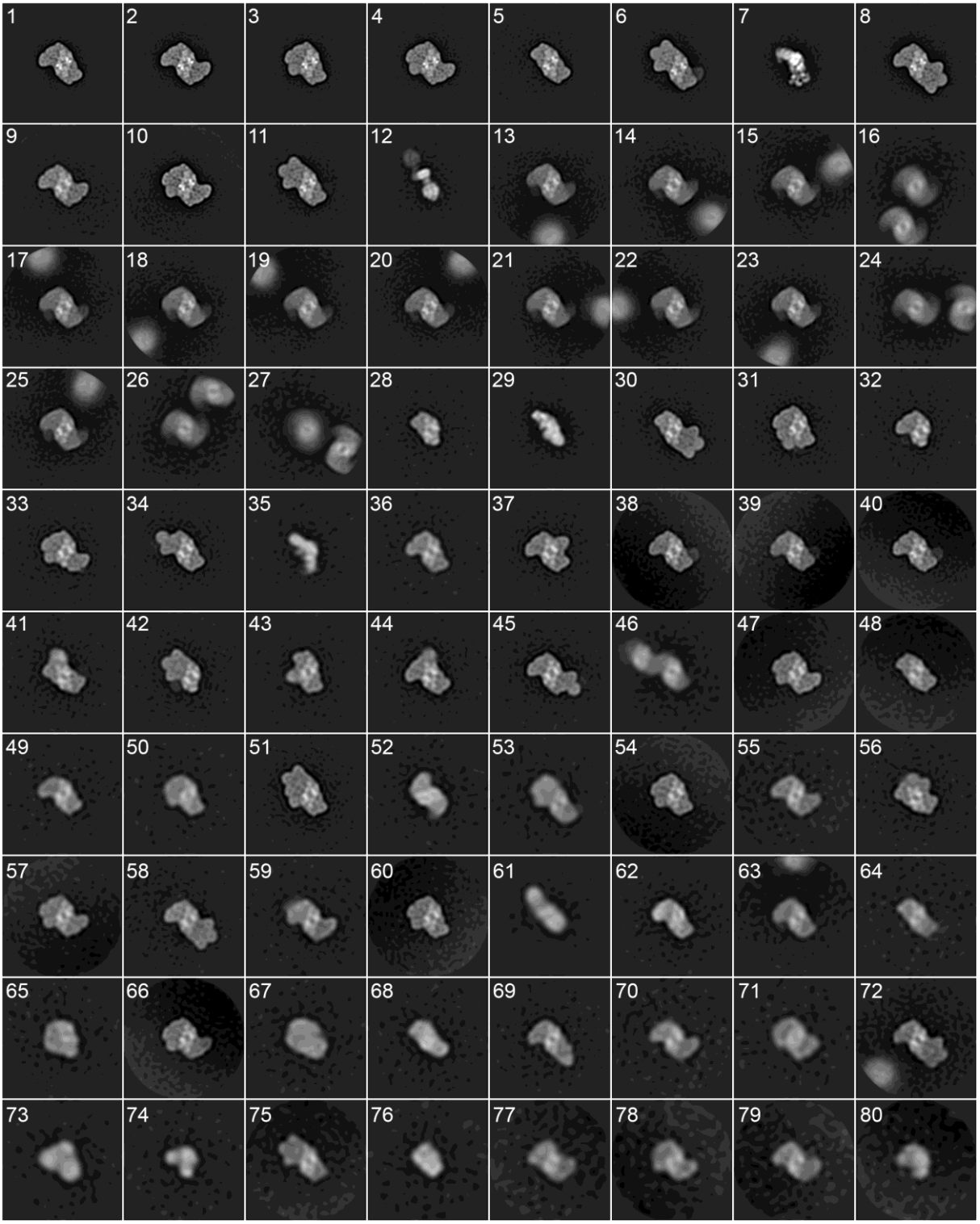

Supporting information Fig. S1 – Single-particle image analysis and classification of photosystem II supercomplexes from Norway spruce extracted from CN-PAGE band I.
Image analysis of 163447 particle projections, selected from electron micrographs of the band containing photosystem II supercomplexes, resulted in classification into 80 classes (Fig. S1).

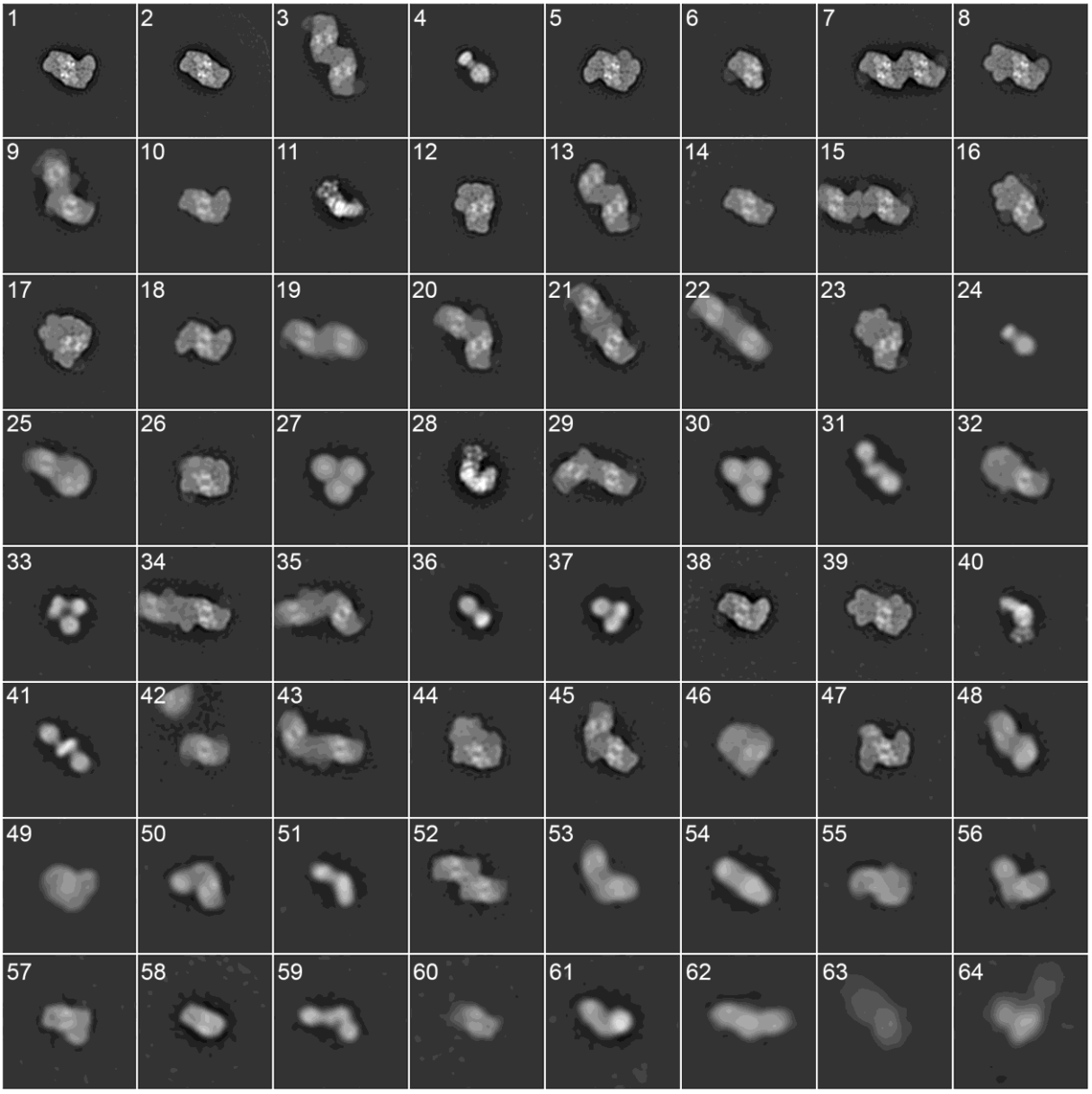

Supporting information Fig. S2 – Single-particle image analysis and classification of photosystem II supercomplexes and megacomplexes from Norway spruce extracted from CN-PAGE band II.

Image analysis of 66650 particle projections, selected from electron micrographs of the band II containing photosystem II supercomplexes and megacomplexes, resulted in classification of particles into 64 classes (Fig. S2).

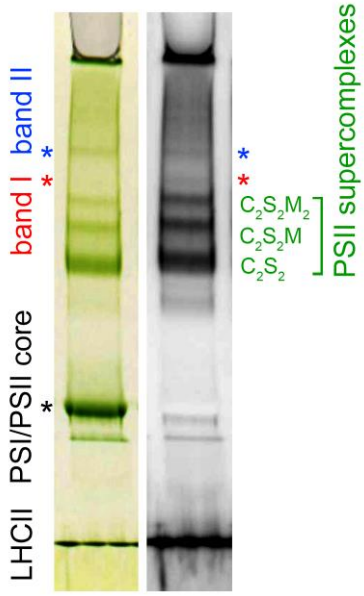

Supporting information Fig. S3 - Separation of pigment-protein complexes from Scots pine using CN-PAGE.

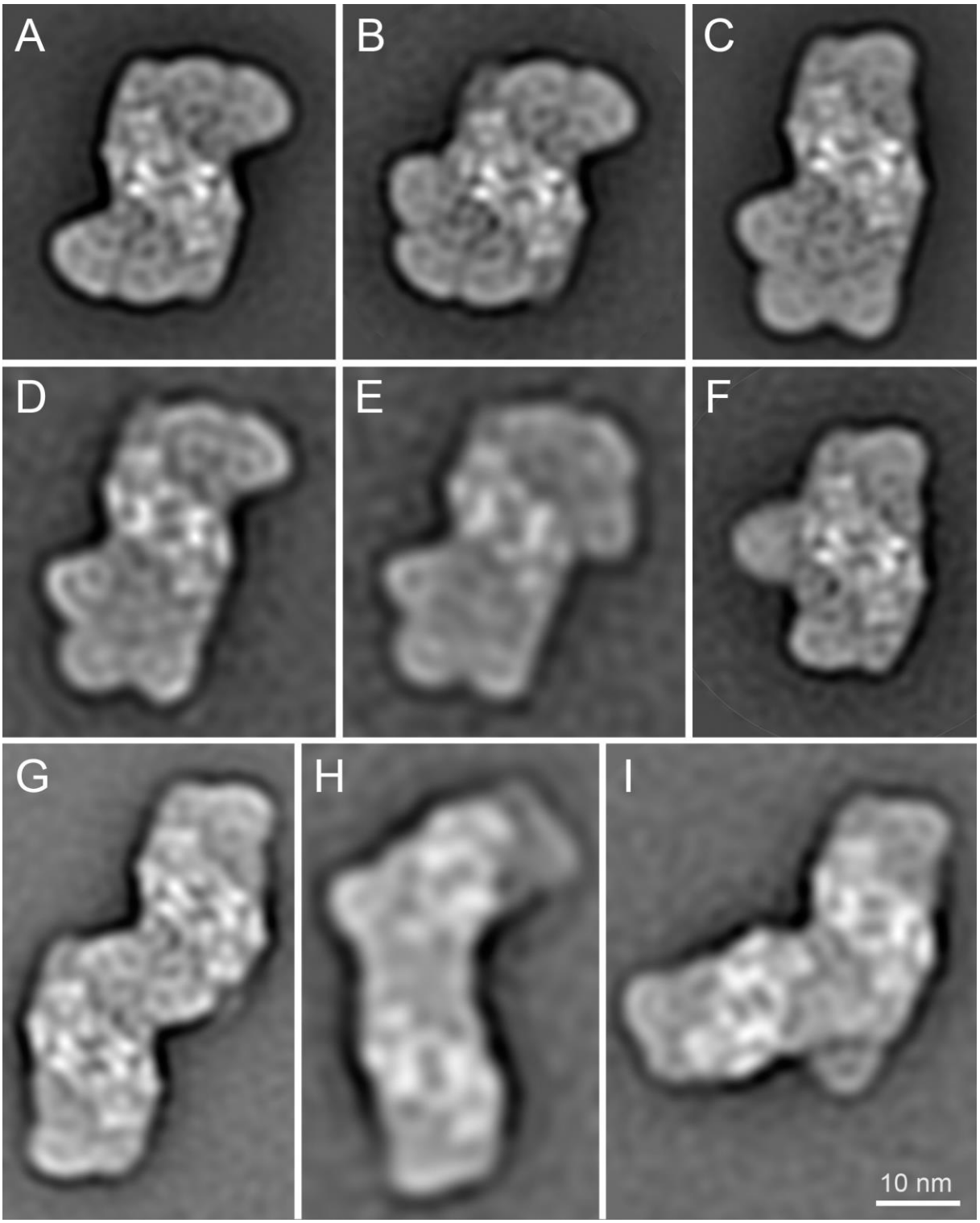

Supporting information Fig. S4 – Structural characterization of photosystem II supercomplexes and megacomplexes from Scots pine.

Supporting information Methods 1 - Proteomic characterization of Norway spruce photosystem II supercomplexes and megacomplexes.

Protein sample preparation

Electro-eluted PSII supercomplex and megacomplex samples from the band I and band II (Fig. 1) were mixed with 200 µL of 100 mM triethylammonium bicarbonate buffer pH 8.0 (TEAB) containing 6 M urea, 2 M thiourea and 0.1% (w/v) sodium deoxycholate (DOC) and concentrated by centrifugation at 14,000 g and RT for 15 min in an Amicon® Ultra-0.5 centrifugal filter device (Millipore, Germany) with 3KDa cut-off. The whole procedure was repeated two more times. Then, the concentrates (a total volume of 60 µL) were split into 20 µL aliquots.

Protein digestion and peptide desalting

To characterize the protein composition of the investigated complexes, a 20 µL sample aliquot (for both band I and band II concentrated sample) was used for in-solution protein digestion as described previously (León *et al.*, 2013). Briefly, protein complexes were reduced using 5 mM Tris(2-carboxyethyl)phosphine at RT for 30 min, alkylated using 55 mM iodoacetamide at RT in the dark for 30 min, diluted to 200 µL with 20mM TEAB containing 0.1% (w/v) DOC and digested with the use of 1 µg of Sequencing Grade Modified Trypsin (Promega, WI, USA) at 37 °C overnight. Then the digested samples were acidified with formic acid (FA; final concentration of 5% (v/v) and pH of ~2.0) and centrifuged at 20,000 g and RT for 10 min. The supernatants were recovered and the resultant peptides were desalted and fractionated employing a home-made reversed-phase micro column (PTFE capillary, id 200 µm, filled with ReproSil Gold C18, 5 µm particles; Dr. Maisch, Germany) connected to a 25-µL gas-tight micro syringe (Hamilton, NV, USA) according to Franc *et al.*, (2012). First, the whole system was wetted with 25 µL of isopropanol and 80% (v/v) acetonitrile and equilibrated twice with 25 µL of 5% (v/v) FA. The acidified digest was subsequently aspirated into the syringe and loaded on the micro column. Before sample fractionation, the micro syringe was filled consecutively with seven mobile phases consisting of 25 mM ammonium bicarbonate (pH 8) with gradually decreasing acetonitrile content (48-32-24-20-16-12-8% (v/v)). Seven fractions (4 µL each) were subsequently collected, mixed with 21 µL with 5% (v/v) FA and directly analyzed by mass spectrometry (MS).

Mass spectrometry analysis

MS analysis was performed employing a tandem mass spectrometer UHR-QTOF maXis (Bruker Daltonik, Germany) connected to a nanoflow capillary liquid chromatography system RSLCnano (Dionex, Thermo Fisher Scientific, CA, USA) via on-line nanoESI source (Bruker

Daltonik, Germany). The chromatography system and the mass analyzer were operated with the settings published by Simerský *et al.* (2017).

Data analysis

The acquired raw MS data were processed with MaxQuant software version 1.6.10.43 (Tyanova *et al.*, 2016) with an instrument parameter setting called "Bruker QTOF" (Beck *et al.*, 2015) and Andromeda search engine (Cox *et al.*, 2011) and searched against *Picea abies*-specific protein database (Grebe *et al.*, 2019) complemented with 247 sequences of common laboratory contaminant proteins (SI Table 2). All detailed parameters and settings are summarized in parameters text file included in the supplementary data SI_Data_1.zip. Search parameters for Andromeda engine were as follows: enzyme specificity was set to trypsin; 2 missed cleavages were allowed; carbamidomethylation of cysteine was included as a fixed modification and N-terminal protein acetylation, deamidation of asparagine and glutamine and methionine oxidation were selected as variable modifications. The search results were combined and filtered for protein inference and 1% FDR at both peptide and protein level. For the evaluation of abundances of the identified proteins (SI Table 1), the well-established iBAQ method (Schwanhäusser *et al.*, 2011) based on summed peak intensities of all peptides matching to a particular protein was applied. Missing annotations for the identified proteins were assigned by pBLAST homology searches against UniProtKB/Swiss-Prot database with the restriction for *Arabidopsis thaliana* as an organism of choice.

Figure legends

Fig. S1. Classification of the dataset of particles from band I (photosystem II supercomplexes). Result of image analysis and classification of 163447 single-particle projections into 80 classes. Classes were sorted according to the particle number in each class in the descending order.
Number of particles in individual classes was as follows (class number-number of particles): 1-15815; 2-12015; 3-9847; 4-9670; 5-6861; 6-6356; 7-5841; 8-4540; 9-4394; 10-4246; 11-3951; 12-3473; 13-3158; 14-2787; 15-2783; 16-2708; 17-2627; 8-2580; 19-2545; 20-2353; 21-2321; 22-2302; 23-2258; 24-2211; 25-2104; 26-2086; 27-1951; 28-770; 29-1729; 30-1579; 31-1554; 32-1469; 33-1416; 34-1373; 35-1372; 36-1237; 37-1219; 38-1057; 39-1006; 40-982; 41-899; 42-899; 43-875; 44-872; 45-860; 46-844; 47-834; 48-796; 49-786; 50-768; 51-753; 52-718; 53-669; 54-641; 55-640; 56-637; 57-618; 58-606; 59-564; 60-557; 61-545; 62-542; 63-535; 64-496; 65-476; 66-453; 67-434; 68-431; 69-412; 70-354; 71-352; 72-286; 73-285; 74-281; 75-255; 76-248; 77-195; 78-176; 79-170; 80-139.

Fig. S2. Classification of the dataset of particles from band II (photosystem II supercomplexes and megacomplexes).

Result of image analysis and classification of 66650 single-particle projections into 64 classes. Classes were sorted according to the particle number in each class in the descending order.

Number of particles in individual classes was as follows (class number-number of particles): 1-4011; 2-3635; 3-3118; 4-2535; 5-2525; 6-2467; 7-2419; 8-2067; 9-1937; 10-1936; 11-1690; 12-1570; 13-1569; 14-1564; 15-1549; 16-1299; 17-1298; 18-1297; 19-1178; 20-1103; 21-1095; 22-1036; 23-1018; 24-992; 25-965; 26-953; 27-931; 28-916; 29-915; 30-832; 31-782; 32-780; 33-775; 34-724; 35-721; 36-696; 37-667; 38-659; 39-622; 40-615; 41-601; 42-549; 43-547; 44-546; 45-525; 46-522; 47-496; 48-486; 49-453; 50-452; 51-437; 52-434; 53-429; 54-365; 55-344; 56-322; 57-301; 58-276; 59-265; 60-230; 61-218; 62-200; 63-142; 64-49.

Fig. S3. Separation of PSII supercomplexes and megacomplexes from Scots pine using CN-PAGE. Isolated thylakoid membranes were mildly solubilized by n-dodecyl α-D-maltoside. The black and white image represents the chlorophyll fluorescence emission detected from the same gel and enables the identification of PSII supercomplexes due to a higher quantum yield of PSII fluorescence at room temperature compared to the quantum yield of PSI fluorescence. The fluorescence signal was detected through a bandpass filter (690-720 nm); excitation wavelength was 460 nm. The red and blue asterisks indicate high-molecular-weight bands I and II with large PSII supercomplexes and megacomplexes, which were subjected to structural analysis by a single-particle electron microscopy. The bands of lower molecular weight represent different forms of PSII supercomplexes, PSI complex and PSII core complex, and LHCII proteins, respectively.

Fig. S4. Structural characterization of various types of larger PSII supercomplexes and megacomplexes from Scots pine.

(A-F) The largest PSII supercomplexes from Scots pine. The supercomplexes A-C and F were eluted from the band I, whereas supercomplexes D and E originate in the band II (Fig. S3). Projection maps of individual types of the PSII supercomplexes represent the best class averages of (A) 5124, (B) 2182, (C) 12250, (D) 688, (E) 141, 1574 (F) particles.

(G-I) Various PSII megacomplexes from Scots pine. The megacomplexes were eluted from the band II (Fig. S3). Projection maps of individual types of the PSII megacomplexes represent the best class averages of (G) 1876, (H) 442, (I) 1060 particles.

Supporting Table 1. An overview of protein composition of the PSII supercomplex and megacomplex bands (CN-PAGE bands I and II).

Protein category	Protein details	band I protein IDs[a]	band II protein IDs[a]	band I iBAQ[b] intensity	band II iBAQ[b] intensity	band I composition (%)	band II composition (%)
Chloroplast	PSII related	25	25	13420878	9634223	81.35	68.13
	Other	57	45	2802967	3669596	16.99	25.95
Plant contaminant	Mitochondrion	18	12	145159	81427	0.88	0.58
	Cytoplasm	6	4	73982	22095	0.45	0.16
	Nucleus	1	-	2592	-	0.02	-
	GA[c]	-	1	-	726600	-	5.13
	ER[d]	1	-	8354	-	0.05	-
	Apoplast	1	-	38657	-	0.23	-
	Peroxisome	1	-	n.a.	-	n.a.	-
	Storage protein	2	1	4571	7227	0.03	0.05
In total		112	88	16497160	14141168	100	100

[a]IDs – identifications; [b]iBAQ – intensity based absolute quantification; [c]GA – Golgi apparatus; [d]ER – endoplasmic reticulum

Palacký University Olomouc

Department of Biophysics

Faculty of Science

Czech Republic

Structural and functional analysis of the photosynthetic apparatus of Norway spruce

Summary of doctoral thesis

Monika Opatíková

Olomouc 2023

Uchádzač: Mgr. Monika Opatíková

Školiteľ: RNDr. Roman Kouřil, Ph.D.

Prírodovedecká fakulta Univerzity Palackého v Olomouci

Katedra biofyziky

Oponenti: prof. RNDr. Josef Komenda, CSc., DSc.

Mikrobiologický ústav AV ČR, CENTRUM ALGATECH, Třeboň

Laboratórium fotosyntézy

Steffen Grebe, Ph.D.

University of Helsinki

Department of Forest Sciences

Miesto a termín obhajoby

S plným textom dizertačnej práce a posudkami je možné sa oboznámiť na študijnom oddelení Prírodovedeckej fakulty Univerzity Palackého v Olomouci.

List of Publications

Opatíková M., Semchonok, D.A., Kopečný D., Ilík P., Pospíšil P., Ilíková I., Roudnický P., Zeljković S.Ć., Tarkowski P., Kyrilis F.L., Hamdi F., Kastritis P.L., Kouřil R. (2023) Cryo-EM structure of plant photosystem II supercomplex with light-harvesting protein LHCB8 and α-tocopherol. *Nat. Plants* (in press) IF(2022): 18.0 (Opatíková M *designed the experiments, prepared samples for all experiments, optimised separation on sucrose gradient to achieve a sufficiently high concentrated sample of photosystem II supercomplex for cryo-EM, partially analysed and interpreted data and prepared the article.*)

Štroch M., Karlický V., Ilík P., Ilíková I., **Opatíková M.**, Nosek L., Pospíšil P., Svrčková M., Rác M., Roudnický P., Zdráhal Z., Špunda V., Kouřil R. (2022) Spruce versus Arabidopsis: different strategies of photosynthetic acclimation to light intensity change. *Photosynth. Res.* **154**, 21–40. IF(2022): 3.7 (Opatíková M *performed a biochemical analysis of Arabidopsis thaliana and Norway spruce seedlings including isolation of thylakoid membranes and its optimisation together with preliminary biochemical experiments, which were not included in this publication.*)

Ilíková I., Ilík P., **Opatíková M.**, Arshad R., Nosek L., Karlický V., Kučerová Z., Roudnický P., Pospíšil P., Lazár D., Bartoš J., Kouřil R. (2021) Towards spruce-type photosystem II supercomplex: consequences of the loss of LHCB3 and LHCB6 in Arabidopsis. *Plant Physiol.* **187**, 2691–2715. IF(2021): 8.005 (Opatíková M *performed a biochemical analysis of Arabidopsis thaliana mutants including isolation of thylakoid membranes, optimisation of conditions for solubilisation and electrophoretic separation of protein complexes, isolation of proteins and subsequent western blot analysis, preparation of samples for transmission electron microscopy, data collection and analysis.*)

Kouřil R., Nosek L., **Opatíková M.**, Arshad R., Semchonok D.A., Chamrád I., Lenobel R., Boekema E.J., Ilík P. (2020) Unique organization of photosystem II supercomplexes and megacomplexes in Norway spruce. *Plant J.* **104**, 215–225. IF(2020): 6.486 (Opatíková M *performed a biochemical analysis of Norway spruce and Scots pine, including isolation of thylakoid membranes, optimisation of conditions for solubilisation and electrophoretic separation, preparation of samples for transmission electron microscopy, data collection and analysis.*)

Acknowledgement:

Dear reader, thank You for finding time to read my thesis…

To begin with, my deepest gratitude belongs to the people, who gave me the opportunity to realise this goal for me, specifically my supervisor Dr. Roman Kouřil and the head of the Department of Biophysics, Prof. Peter Ilík. I would also like to include here all the people from our department who supported me throughout the entire journey, whether by helping me with the experiments, making me laugh, giving me free, invaluable, and many times unasked advice or just by saying: "Everything will be OK, just give it time and another try! Now, let's go grab some coffee!" You know, who you are, as you have already heard my thanks in person.

To continue, I would like to thank Prof. Eva-Mari Aro, for accepting me for my internship and letting me "sneak peek" into her working group. The truth is that in addition to the helpful work-related advice I received, there was such a warm welcome and acceptance, for which I will always be grateful. To be precise, Stephen, Vipu, Mika, Tapio and Sana … one big "Thank You" from me. Moreover, Vipu, thank you for introducing me to a different method of gradient preparation, because you practically set my experiments on the right pathway.

And finally, I would like to express my gratitude to all the people outside the work who took their time to listen and comfort me when I was down, stressed and unpleasant, but still, they did not give up on me. To the people, who forced me out of my comfort zone just to show me that there is a world out there, and to those who deliberately decided to stay in my life, because they think I am worth it. I hope I won't let you down. My family, my friends ... Thank You.

This work was supported by the Grant Agency of the Czech Republic (GAČR) project "Role proteinu Lhcb8 v organizaci a funkci světlosběrného komplexu fotosystému II rostlin" (no. 21-05497S) and the European Regional Development Fund (ERDF) project "Plants as a tool for sustainable global development" (no. CZ.02.1.01/0.0/0.0/16_019/0000827).

Abstrakt

Táto dizertačná práca je rozdelená do štyroch hlavných sekcií. Prvá sekcia je zameraná na stručný a všeobecný prehľad fotosyntézy so zameraním na Smrek obyčajný. Cieľom tohto prehľadu je oboznámiť čitateľa s aktuálnymi poznatkami o fotosyntetickom aparáte smreku a jeho súvisiacou funkciu. Motiváciou k výskum fotosyntézy u smreku je na jednej strane jeho signifikantný príspevok ku globálnej produkcii kyslíku, na strane druhej jeho unikátnosť ako evergreenu, ktorý je schopný prežiť nepriaznivé environmentálne podmienky, konkrétne kombináciu mrznúcich teplôt a intenzívneho osvetlenia v priebehu zimy.

Druhá sekcia nadväzuje na aktuálne poznatky o smreku a pokračuje výskumom prevedeným v rámci našej skupiny súčasne zahŕňajúc môj príspevok. Táto sekcia začína odôvodnením nášho zamerania sa na špecifickú oblasť fotosyntetického výskumu u smreku, pokračuje vysvetlením dosiahnutého pokroku v danej oblasti a je ukončená krátkym zhrnutím a vyhliadkami do budúcna. Popri primárnom výskume unikátnej štruktúry fotosystému II u smreku získanej pomocou kryogénnej elektrónovej mikroskopie, je v tejto sekcii predstavený aj súvisiaci výskum, zameraný na (i) hľadanie pôvodu pozmenenej štruktúry PSII u smreku s využitím “knock-out” mutantov Arabidopsis, (ii) tvorbu superkomplexov a megakomplexov PSII u smreku a (iii) aklimačné štúdie zamerané na efekt pôsobenia dlhodobých zmien vo svetelnej intenzite.

Tretia a štvrtá sekcia sa zameriavajú na (a) všeobecný a stručný popis experimentálnych metód, ktoré boli prevedené výlučne mnou a (b) ich optimalizáciu. Z dôvodu nadväznosti na predchádzajúci výskum na našom pracovisku nebolo mojim zámerom dopodrobna vysvetliť použité metódy. Namiesto toho som sa zamerala na detailný popis optimalizácie dvoch konkrétnych metód. Prvá časť sa zameriava na optimalizáciu podmienok solubilizácie a separačných metód pre izolované tylakoidné membrány. Druhá čas optimalizácie sa zaoberá vytvorením ideálnych podmienok pre extrakciu labilných proteínových komplexov, ako je napríklad superkomplex fotosystému I s dvoma naviazanými LHCII trimermi u smreku.

Abstract

This dissertation thesis is divided into four main sections. The first focuses on a brief and general overview of photosynthesis with the main focus on the Norway spruce. The main aim of this section is to familiarise the reader with the current knowledge of spruce photosynthetic apparatus and its related functional properties. The motivation behind the detailed study is primarily the importance of spruce as a significant contributor to global oxygen production and secondary its uniqueness as an evergreen plant with the ability to withstand harsh environmental conditions, precisely the combination of freezing temperatures with simultaneous high light radiation during winter.

The second section builds on the current knowledge and continues with a description of the spruce research conducted by our group with my contribution. The primary justification for our research performed on spruce is followed by a clarification of the achieved progress in this area. It is enclosed with a summary and future perspectives. While my primary focus is on structural analysis of the unique photosystem II of spruce obtained by cryogenic electron microscopy, the related research focuses on (i) determining the origin of spruce's modified PSII shape by analysing specific Arabidopsis knock-out mutants, (ii) formation of PSII supercomplexes and megacomplexes in spruce, and (iii) its acclimation to long-term light intensity changes.

The third and fourth sections focus on (i) a general description of the experimental methods performed in our research on the spruce and (ii) their optimisation. Since I have built on previous research carried out in our group, I did not intend to explain in detail the methods used. Instead, I have concentrated on the optimisation of these methods involving two main issues. The first part focuses on the optimisation of solubilisation conditions and separation methods for isolated thylakoid membranes. The second part of the optimisation deals with setting the ideal conditions for the extraction of fragile protein complexes, such as the photosystem I supercomplex binding two LHCII trimers from spruce.

Abbreviations:

$^1O_2$	singlet oxygen
2D-SDS-PAGE	two-dimensional sodium dodecyl sulphate polyacrylamide gel electrophoresis
ACA	aminocaproic acid
AEF	alternative electron flow
At	*Arabidopsis thaliana*
ATP	adenosine triphosphate
BN-PAGE	blue-native polyacrylamide gel electrophoresis
C_2	dimeric core of photosystem II
cc	core complex
CET	cyclic electron transport
CMC	critical micelle concentration
CN-PAGE	clear-native polyacrylamide gel electrophoresis
Cr	*Chlamydomonas reinhardtii*
EM	electron microscopy
Cyt_{b6f}	cytochrome b6/f complex
ETC	electron transport chain
Fd	ferredoxin
FDP	C-class of flavodiiron protein
FNR	Fd-$NAD(P)^+$-reductase
F_V/F_M	maximum quantum efficiency of the photochemistry of photosystem II for dark-adapted state
HL	high light
Chl	chlorophyll
LET	linear electron transport
LHCI	light-harvesting complex of photosystem I
LHCII	light-harvesting complex of photosystem II
LL	low light
L-LHCII	loosely bound light-harvesting antenna of photosystem II
$NAD(P)^+$/NAD(P)H	oxidised/reduced nicotinamide adenine dinucleotide (phosphate)
NDH-like	NAD(P)H dehydrogenase-like
NPQ	non-photochemical chlorophyll fluorescence quenching parameter
mc/mcs	megacomplex/megacomplexes
M-LHCII	moderately bound light-harvesting antenna of photosystem II
OEC	oxygen evolving complex
P680	summary labelling group of chlorophylls representing primary electron donor in PSII
P700	summary labelling group of chlorophylls representing primary electron donor in PSI
PC	plastocyanin
Pp	*Physcomitrella patens*
PQ	plastoquinone (oxidised)
PQH_2	plastoquinol (reduced and protonated plastoquinone)
PGR5/PGRL1	PROTON GRADIENT REGULATION 5 PROTEIN/PROTON GRADIENT REGULATION-LIKE 1 PROTEIN
PSI	photosystem I
PSII	photosystem II

qE	regulating energy dependent non-photochemical quenching of chlorophyll fluorescence
RC	reaction centre
ROS	reactive oxygen species
sc/scs	supercomplex/supercomplexes
S-LHCII	strongly bound light-harvesting antenna of photosystem II
S-NPQ	sustained non-photochemical quenching of chlorophyll fluorescence
SPA	single particle analysis
STN7/STT7	serine/threonine-protein STATE TRANSITION 7 kinase/orthologue of serine/threonine-protein STATE TRANSITION 7 kinase in green algae
STN8	serine/threonine-protein STATE TRANSITION 8 kinase
TEM	transmission electron microscopy
X-ray	Röntgen crystallography
Y(II)	effective quantum yield of PSII photochemistry in light-adapted state
Y(NO)	quantum yield of constitutive non-regulatory energy dissipation of photosystem II in light-adapted state
Y_Z	tyrosine Z
Zm	*Zea mays*
α DDM	n-Dodecyl-α-D-Maltopyranoside
β DDM	n-Dodecyl-β-D-Maltopyranoside
α-Toc/α-TQ	α-tocopherol/α-tocopherolquinone
ΔpH	difference of pH across the thylakoid membrane
Δψ	difference of electric potential across thylakoid membrane; the membrane potential

General formatting (excluding subunits of photosystems):

PROTEIN
GENE
gene mutant

1. Norway spruce in the headlights of the photosynthesis research

Norway spruce (*Picea abies* (L.) H. Karst.) (hereafter spruce) is an evergreen conifer with global distribution, but especially a dominant plant of the boreal forests together with the Scots pine (*Pinus sylvestris* L.) (hereafter pine). Somewhat unique among land plants, conifers can simultaneously withstand harsh environmental conditions, explicitly freezing temperatures, in parallel with high irradiance (Nystedt *et al.*, 2013). Without any photoprotective mechanisms, this would undoubtedly lead to severe photodamage of the individual components of the photosynthetic apparatus and the uncoupling of the entire electron transport chain (ETC), as the excess energy would lack any safety valve for its release due to enzymes inhibition (Öquist and Huner, 2003). In order to minimise the effect of these unfavourable conditions, the evolution of spruce has led to the development of various photoprotective mechanisms. These mechanisms, specifically those observed only in evergreens such as spruce, and their regulations are subject of intensive studies (see, e.g. Grebe *et al.*, 2020; Yang *et al.*, 2020).

From an evolutionary point of view, spruce belongs to the gymnosperm genera *Picea* (family *Pinaceae*) and represents one of the intermediate stages between green algae, representatives of aquatic photosynthetic organisms, and angiosperm, the last stage of evolution of land plants. As water and land represent incomparable environmental niches, the life strategies of these photosynthetic organisms are expected to differ significantly, with implications for the functioning and efficiency of photosynthesis itself.

The main focus of my work was the structural analysis of the photosynthetic apparatus of spruce, specifically its photosystem II (PSII) and optimisation of the sample preparation for this analysis. My work included identifying the detailed composition of PSII in spruce, determining its variability compared to its counterparts in other plant species, and putting all the obtained knowledge into the context of its functional specification. Optimisation of sample preparation focused on getting high yields of homogeneous and concentrated sample for cryogenic electron microscopy (cryo-EM) and extraction of fragile protein supercomplex (sc) from thylakoid membranes. Nevertheless, I consider it appropriate to first provide the reader with a brief introduction to photosynthesis and a comprehensive picture of photosynthesis research performed on spruce, before continuing with the section about my research. Since the two specific studies on spruce are quite extensive, I have devoted an entire subsection to them so they are not omitted. Those include the evolutionary loss of LHCB3 and LHCB6 proteins (as a subsection of the structural characteristic of the light-harvesting complex of PSII (LHCII)) and sustained non-photochemical quenching of chlorophyll fluorescence (S-NPQ) (as a subsection of ETC regulation).

1.1. Brief introduction to photosynthesis

Photosynthesis is undoubtedly one of the most important processes necessary to sustain life on the planet. Across photosynthetic organisms, from the first photosynthesising cyanobacteria up to more complex vascular plants, we can study this process, which may vary in some details from organism to organism because it has evolved in parallel with the evolution of plants. This unique mechanism combines biophysical and biochemical processes, in which light energy is used to fix CO_2 into organic molecules, with oxygen produced as a by-product. It should be noted that in addition to the typical oxygenic photosynthesis mentioned above, there are several organisms, e.g. sulphur bacteria that use anoxygenic photosynthesis instead. These organisms use a broad range of either organic or inorganic electron donors for fixation CO_2 and produce sulphur compounds instead of oxygen (see e. g. Ke, 2001; Raymond and Blankenship, 2004; George *et al.*, 2020).

It is necessary to emphasise that the generally known strict division of photosynthesis into two parts, primary and secondary phases, is inaccurate, since all biophysical and biochemical processes are interconnected and interdependent at a lower or higher level. Thus, we can only speak of hypothetical division, where the function of the first part is (i) light harvesting, (ii) use of this energy to excite chlorophyll (Chl) molecules leading to primary charge separation in the PSII and photosystem I (PSI) reaction centres (RC), (iii) splitting water molecules into electrons, oxygen and protons leading to acidification of chloroplast lumen and (iv) generating proton motive force across the thylakoid membrane used in the subsequent ATP production, while (v) the transported electrons are used to reduce $NAD(P)^+$ to NAD(P)H. The second phase, the Calvin-Benson-Bassham cycle, uses the products of the first phase, i.e. NAD(P)H and ATP to incorporate atmospheric CO_2 into carbohydrates (Johnson, 2016; Stirbet *et al.*, 2020). To avoid the misinterpretation that often arises from the summary equation of photosynthesis, it must be emphasised that the released oxygen originates in water and that CO_2 is not directly incorporated into the sugar hexose, but is fixed in a stepwise process (see, e.g. Poolman and Fell, 2000; Anderson and Backlund, 2008).

With the detailed functional and structural characterisation of the main components of the electron transfer pathway involved in the first phase of photosynthesis, we can understand in depth their individual significance, specific function and contribution to the overall process. These include the four main protein complexes, namely PSI, PSII, cytochrome b6/f (Cyt_{b6f}) and ATP synthase, all embedded in the thylakoid membrane (Dekker and Van Grondelle, 2000; Nelson and Yocum, 2006).

1.2. Photosystem I and photosystem II in structural detail

In the last decades, the structures of PSI and PSII originally obtained from Röntgen crystallography (X-ray) and 2D single particle analysis (SPA) from lower resolution transmission electron microscopy (TEM) images have been gradually replaced by more detailed cryo-EM data with near-atomic resolution. These high-resolution PSI and PSII structures are currently known for several representatives of angiosperms (see, e.g. Wei *et al.*, 2016; Su *et al.*, 2017; van Bezouwen *et al.*, 2017; Graça *et al.*, 2021; Su *et al.*, 2022), green and red algae (see, e.g. Shen *et al.*, 2019; Sheng *et al.*, 2019; Suga *et al.*, 2019; Huang *et al.*, 2021; Naschberger *et al.*, 2022; You *et al.*, 2023), diatoms (see, e.g. Xu *et al.*, 2020; Nagao *et al.*, 2022) and cyanobacteria (see, e.g. Gisriel *et al.*, 2022; Semchonok *et al.*, 2022).

1.2.1. Photosystem I core complex (PSI cc)

PSI is a pigment-binding multi-protein sc embedded in the thylakoid membrane of chloroplasts with the ability to process solar energy into energy of chemical bonds with a near-maximum quantum efficiency (Nelson, 2009; Croce and van Amerongen, 2013). In higher plants, the PSI is exclusively localised at the periphery of grana stacks, in grana margins, and stromal lamellae. PSI cc of green algae, mosses and land plants is mostly conserved, consisting of 12 stably bound subunits (PsaA–PsaL) and additional four subunits with (i) either weak binding on the lumenal side (PsaN) (He and Malkin, 1992), (ii) subunit creating a docking site for LHCII after binding to PSI, PsaO (Pan *et al.*, 2018), (iii) predicted PsaP subunit with unknown position, or (iv) subunit with unclear function PsaR (Mazor *et al.*, 2015, 2017). PsaA and PsaB subunits form a heterodimer and represent the RC binding overall ~ 85 Chl *a* molecules, 2 phylloquinones and a Fe_4S_4 cluster (Pan *et al.*, 2018; Huang *et al.*, 2021; Shen *et al.*, 2022; Su *et al.*, 2022), while the function of the remaining subunits is assigned as follows: i) PsaC–PsaE – ferredoxin (Fd) binding, ii) PsaF – plastocyanin (PC) binding, iii) PsaF, PsaG, PsaJ, PsaK – LHCA proteins binding, iv)

PsaH, PsaI, PsaL, PsaO – LHCII binding (Nelson and Ben-Shem, 2004; Gorski *et al.*, 2022). The PsaG, PsaH, PsaO and PsaN subunits are not present in cyanobacteria (Caspy and Nelson, 2018) and are considered to be gained during evolution. Oppositely, PsaM represents a subunit, which was lost during evolution. This subunit was lost in green algae up to the higher plants (Nelson and Junge, 2015, Qin *et al.*, 2019), with only one known exception of its presence in the moss *Physcomitrella patens* (*Pp*) (Gorski *et al.*, 2022). For the detailed structural composition of the PSI sc, including individual subunits and contained pigments, see Tab. 1.

Table 1: Subunit compositions and identified pigments in the most complete cryo-EM structures of PSI-LHCI supercomplex from different plant species.

	Subunits	***Chlamydomonas reinhardtii*** 7D0J			***Zea mays*** 5ZJI		
PSI cc	PsaA	✓	45 Chl *a*	6 β-car	✓	45 Chl *a*	6 β-car
	PsaB	✓	40 Chl *a*	7 β-car	✓	40 Chl *a*	7 β-car
	PsaC	✓			✓		
	PsaD	✓			✓		
	PsaE	✓			✓		
	PsaF	✓	3 Chl *a*	1 β-car	✓	3 Chl *a*	1 β-car
	PsaG	✓	**2 Chl *a***	1 β-car	✓	3 Chl *a*	1 β-car
	PsaH	✓	**3 Chl *a***	**1 β-car**	✓	1 Chl *a*	
	PsaI	✓		1 β-car	✓		1 β-car
	PsaJ	✓	1 Chl *a*	1 β-car	✓	1 Chl *a*	1 β-car
	PsaK	✓	4 Chl *a*	2 β-car	✓	4 Chl *a*	2 β-car
	PsaL	✓	**4 Chl a**	3 β-car	✓	3 Chl *a*	3 β-car
	PsaN	-			✓	2 Chl *a*	
	PsaO	✓	**3 Chl *a***	**2 β-car**	✓	2 Chl *a*	
LHCI	LHCA1 (isoform a/b for *Cr*)	✓	12/12 Chl *a* 2/2 Chl *b*	3/3 Lut	✓	12 Chl *a* 2 Chl *b*	2 Lut 1 Vio 1 β-car
	LHCA2	✓	13 Chl *a*	2 Lut 1 β-car	✓	9 Chl *a* 5 Chl *b*	1 Lut 1 β-car 1 Vio
	LHCA3	✓	13 Chl *a* 1 Chl *b*	2 Lut 3 β-car	✓	12 Chl *a* 1 Chl *b*	1 Lut 1 β-car 1 Vio
	LHCA4	✓	11 Chl *a* 4 Chl *b*	2 Lut 1 β-car	✓	11 Chl *a* 4 Chl *b*	1 Lut 1 β-car 1 Vio
	LHCA5	✓	14 Chl *a* 3 Chl *b*	2 Lut 2 β-car	-		
	LHCA6	✓	13 Chl *a* 4 Chl *b*	2 Lut 2 β-car	-		
	LHCA7	✓	14 Chl *a* 1 Chl *b*	2 Lut 2 β-car	-		
	LHCA8	✓	13 Chl *a* 1 Chl *b*	2 Lut 1 β-car	-		
	LHCA9	✓	8 Chl *a* 2 Chl *b*	2 Lut	-		
SUM			248	59		160	35

Structures of PSI scs from *Chlamydomonas reinhardtii* (Huang *et al.*, 2021) and *Zea mays* (Pan *et al.*, 2018), excluding lipids and other ions or molecules. *Abbreviations: LHCI - light-harvesting complex of photosystem I, β-car - β-carotene, Chl (a/b) - chlorophyll a/b, Lut - lutein, Vio - violaxanthin, subunit presence (✓) and absence (-) in the structure. The four-letter*

code below the name of the organism represents the PDB identifier of the structure. Differences observed between structures in their PSI cc, either in the means of the presence/absence of the specific subunit or the presence/absence of different number of identified cofactors are highlighted. Differences in LHCAs were not highlighted, because their presence/absence in given PSI sc is species dependent.

1.2.2. Light-harvesting complex of photosystem I (LHCI)

Higher variability within PSI in the plant kingdom originates in the structure and organisation of the LHCI complex, which is responsible for the increase in its light-harvesting capacity due to the bound pigments (for detailed pigment composition of LHCI see Tab. 1).

In vascular plants, LHCI is represented by LHCA1–6 proteins, the latter two of which are sub-stoichiometrically abundant. With some exceptions, the *LHCA1–4* are comparably expressed in land plants and the encoded antennae bind to the PSI cc at specific positions in a "belt-like" nature as heterodimers, specifically (i) the LHCA1/4 dimer interacts with the core via PsaG, PsaB (LHCA1) and PsaF subunits (LHCA4) and (ii) the LHCA2/3 dimer binds to the core via the PsaA, PsaJ (LHCA2) and PsaA, PsaK subunits (LHCA3), respectively (see, e.g. Jansson *et al.*, 1996; Ben-Shem *et al.*, 2003; Mazor *et al.*, 2015; Pan *et al.*, 2018; Shen *et al.*, 2019; Su *et al.*, 2022). The LHCA5 and LHCA6 are present in almost all angiosperms with a few exceptions, and while LHCA5 is present in most gymnosperms, LHCA6 is specific for angiosperms only (for detailed overview, see Grebe *et al.*, 2019). The importance of these two proteins lies in the mediating of the NAD(P)H dehydrogenase-like (NDH-like) complex binding to PSI (Peng *et al.*, 2009) and their absence in spruce is thus consistent with its simultaneous loss of plastid genes encoding NDH-like (Nystedt *et al.*, 2013; Grebe *et al.*, 2019). More information about the loss of *NDH-like* in spruce is in the following sections.

In the green algae, characterised by a broader variety of LHCI isoforms (designated either as LHCA1–10 or LHCA a–j), PSI binds two LHCI semi-rings and forms a two-layered belt on the PsaF–G and Psa J–K side of PSI, plus a contingent LHCs dimer bound opposite the main semi-rings on the PsaB-H-I-M side (Qin *et al.*, 2019). See the structure from pea and green algae *Cr* in Fig. 1.

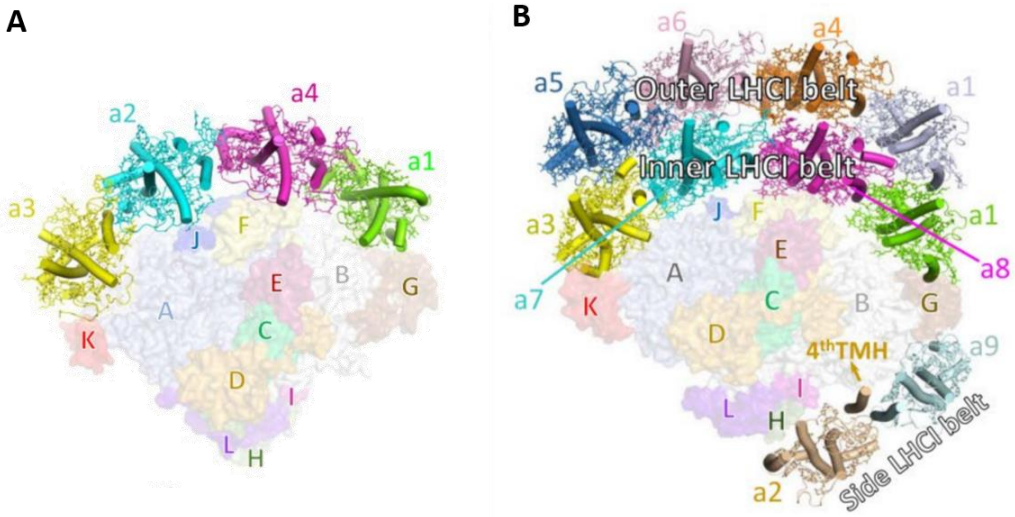

Figure 1: Structure of PSI-LHCI supercomplex from *Pisum sativum* and *Chlamydomonas reinhardtii*. Stromal view of PSI scs from pea (A) and *Cr* (B), the core subunits are represented as surface areas with single-letter designations. LHCA antennae with their assignment are visualised as cartoon with pigments and other cofactors in the form of sticks. Adapted from Shang *et al*. (2023), original structure of pea from Mazor *et al*. (2015) (PDB identifier: 4Y28) and *Cr* from Su *et al*. (2019) (PDB identifier: 6IJO).

1.2.3. Functional PSI assemblies

(I) PSI-$PSI_{(n)}$ assemblies are characteristic for (i) cyanobacteria, in which they can form oligomers, as dimers, trimers or tetramers (Malavath *et al.*, 2018; Semchonok *et al.*, 2021; Cao *et al.*, 2022) characterised by the predominant formation of trimers with typical symmetry and interaction via PsaL subunit (Jordan *et al.*, 2001), or (ii) for green algae, where their presence in dimeric form was confirmed (Naschberger *et al.*, 2022). However, the PSI oligomers observed in vascular plants appeared to be only an artificial result of the PSI scs tendency to mutually associate (Boekema *et al.*, 1987; Chitnis and Chitnis, 1993; Boekema *et al.*, 2001; Kouřil *et al.*, 2005b). Moreover, the oligomers typical for cyanobacteria cannot be formed in higher plants due to the additional PsaH subunit, which spatially blocks the access to the PsaL subunit (Ben-Shem *et al.*, 2003).

(II) PSI-NDH-like sc (PSI assembly with NAD(P)H dehydrogenase-like) is an essential component involved in one type of cyclic electron transport (CET) around PSI, which transports the electrons from reduced Fd via NDH-like back to plastoquinone (PQ) (Peng *et al.*, 2008, 2009; Kouřil *et al.*, 2014; Yadav *et al.*, 2017; Zhang *et al.*, 2020).

(III) PSI-Cyt_{b6f} assembly was observed using TEM by Yadav *et al.* (2017), with its binding on the LHCA belt of PSI. Its function has been assigned to electron transport regulation due to the distance adjustment between its individual components (Yadav *et al.*, 2017) and has been hypothesised to undergo reversible phosphorylation during state transitions (Hamel *et al.*, 2000) with the effect on the CET initiation (Iwai *et al.*, 2010).

(IV) PSI-PSII assembly has been observed in higher plants such as spinach, *Arabidopsis thaliana* (*At*) and rice, but not in the green algae. Their interactions, either via core or antennae, function as conductors of energy spillover from PSII to PSI, thus protecting the PSII (Kim *et al.*, 2023).

(V) PSI-LHCI-LHCII assembly (hereafter PSI-LHCII) is formed during the state transition (state 2) that serves as an equaliser of energy distribution between PSI and PSII in a case of their excitation imbalance caused by the variable quality and quantity of light in the natural environment (Allen, 2003). The different effect of light quality coincides with the different pigment composition of PSI and PSII and their related distinct absorption characteristics, with the absorption of PSI closer to far-red light and the absorption of PSII to red light (Rochaix, 2007; Minagawa, 2011). In general, over-reduction of the PQ pool leads to activation of the serine/threonine protein kinase STN7 (STT7: orthologue in green algae *Cr*), which is, besides the LHCB1 phosphorylation, responsible for phosphorylation of LHCB2 in LHCII trimers that subsequently bind to the PSI scs and effectively transfer the harvested energy to its cc (Depege *et al.*, 2003; Bellafiore *et al.*, 2005). Conversely, when the preferential excitation pressure on PSII dissipates, e.g. during high light (HL) or low light (LL) illumination, the STN7 kinase is inactivated due to the change in the redox state of thioredoxins, and the constitutively active serine/threonine protein phosphatase (TAP38/PPH1) dephosphorylates LHCB1 and LHCB2, leading to uncoupling of LHCII trimers from PSI and their subsequent return to their initial position (state 1) (Rintamäki *et al.*, 2000; Pribil *et al.*, 2010; Shapiguzov *et al.*, 2010; Cariti *et al.*, 2020).

The recently revealed high-resolution structures of this sc at 3.42 Å (Huang *et al.*, 2021) and at 2.84 Å (Pan *et al.*, 2021) resolution for *Cr* or at 3.3 Å resolution for *Zea mays* (*Zm*) (Pan *et al.*, 2018), provided necessary information about its structural and functional significance (see the structure of this sc in Fig. 2).

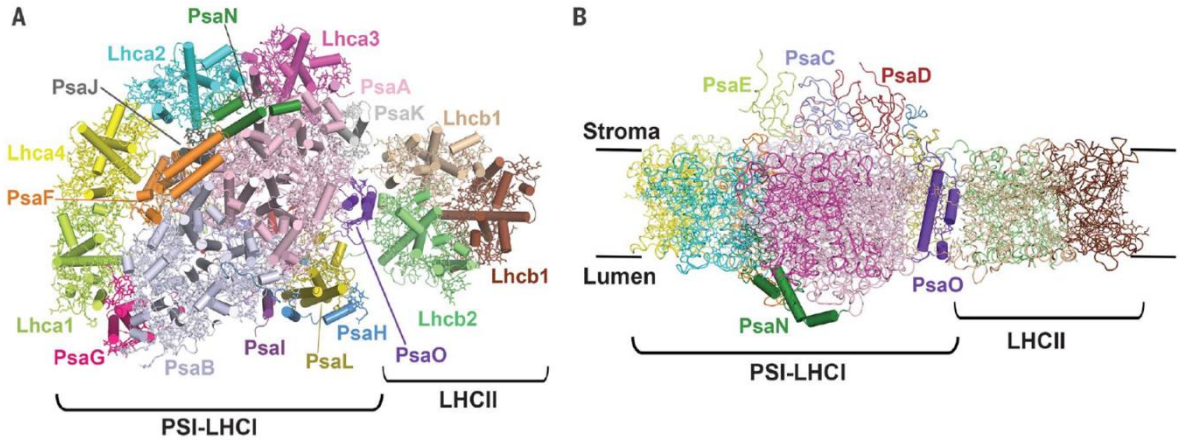

Figure 2: Structure of *Zea mays* PSI-LHCII supercomplex obtained by cryo-EM at 3.3 Å resolution. (A) View from the lumenal side with assigned PSI cc and LHCA subunits, (B) Side view along the membrane plane. Adapted from Pan *et al.* (2018) (PDB identifier: 5ZJI).

A long discussion on the origin of phosphorylated LHCII trimers led to the conclusion that they represent either loosely bound LHCII (L-LHCII) (Galka *et al.*, 2012) or, most likely, originate from a pool of free LHCIIs (Wientjes *et al.*, 2013). These free LHCIIs are located near the grana margins, the target destination of phosphorylated LHCII trimers, where they bind to PSI-LHCI (Galka *et al.*, 2012; Wientjes *et al.*, 2013; Le Quiniou *et al.*, 2015; Bos *et al.*, 2017).

Recently, based on the results of physiological and biochemical studies (e.g. Akhtar *et al.*, 2016; Bressan *et al.*, 2018; Schiphorst *et al.*, 2022) and observed structures using single particle electron microscopy (EM) (e.g. Yadav *et al.*, 2017), the possibility of binding an additional, not necessarily phosphorylated LHCII trimer in vascular plants has opened up for a discussion.

However, confirming the existence of PSI with two bound LHCII trimers (PSI-LHCII$_2$) in vascular plants, is challenging since PSI sc with one LHCII trimer is already quite fragile and difficult to obtain in sufficient quantities for structural studies. Logically, the implication of even less specific interaction of the second trimer based on the variety in its observed attachment position toward PSI would complicate its extraction. And combining all with the hard-to-refute argument that the variable structures of PSI-LHCII$_2$ observed by EM by Yadav *et al.* (2017) could have been the result of post-elution artificial binding of free LHCIIs to PSI-LHCII, analogous to the formation of the aforementioned PSI oligomers in higher plants, their verification definitely requires more thorough studies. For a detailed discussion, see Section 4.

1.2.4. Photosystem II core complex (PSII cc)

PSII is a multi-subunit pigment-protein complex embedded in the thylakoid membrane. In higher plants characterised by lateral segregation of the membrane, PSII scs are localised in the appressed grana. PSII consists of (i) a dimeric core (C_2), including the RC with 35 molecules of Chl *a* and other redox cofactors (Tab. 2, for better comparison already including spruce PSII structure, Opatíková *et al.*, 2023), (ii) LHCII, responsible for increasing the area for solar energy harvesting and its delivery to the core, and (iii) Oxygen Evolving Complex (OEC) (Minagawa and Takahashi, 2004; Dekker and Boekema, 2005; Caffarri *et al.*, 2009; Natali and Croce, 2015). In detail, the PSII cc includes a heterodimer composed of PsbA (D1) and PsbD (D2) proteins and, together with α and β subunit of cytochrome b559 (PsbE and PsbF, respectively), represents the RC of PSII, which binds other two Chl-binding inner antennae PsbB (CP47) and PsbC (CP43) (Nanba and Satoh, 1987; Webber *et al.*, 1989; Croce and van Amerongen, 2011). In addition, PSII cc binds the

extrinsic subunits of the OEC on the lumenal side composed of PsbO, PsbP, PsbQ and PsbR. The rest of the PSII cc is represented by at least 11 small subunits with low molecular weight, namely PsbH–M, with assigned functions as follows: (i) PsbH is involved in antenna association, (ii) PsbJ and PsbK in core stabilisation, (iii) PsbL and PsbM in PSII dimerisation. Rest of the subunits is represented by (iv) PsbW, PsbX and PsbZ/Ycf9 functioning in antenna association and core stabilisation, (v) PsbTc involved in PSII dimerisation, (vi) PsbTn contributing to light acclimation, and (vii) PsbS, the structurally elusive subunit involved in thermal dissipation of absorbed light energy (Shi and Schroder, 2004; Müh *et al.*, 2008). In the structure of PSII from green alga *Chlamydomonas reinhardtii* (*Cr*), the presence of additional subunits of PSII cc was confirmed, including Psb30 (Ycf12) and two unidentified subunits designated as USP (unidentified stromal protein) and SLP (small lumenal protein also designated as Psb27) (Kashino *et al.*, 2007; Sheng *et al.*, 2019). The position of the PsbTn subunit, absent in red and green algae and evolutionary older organisms, was in *Cr* occupied by the aforementioned SLP with similar binding (Sheng *et al.*, 2019).

Table 2: Subunit compositions and identified pigments per one monomer in the most complete cryo-EM structures of PSII-LHCII supercomplex from different plant species.

	Subunits	*Pisum sativum* 5XNL $C_2S_2M_2$			*Chlamydomonas reinhardtii* 6KAC/6KAD $C_2S_2/C_2S_2M_2L_2$			*Picea abies* 8C29 C_2S_2		
PSII cc	PsbA (D1)	✓	4 Chl *a* 2 Pheo	1 β-car	✓	4 Chl *a* 2 Pheo	1 β-car	✓	4 Chl *a* 2 Pheo	1 β-car
	PsbB (CP47)	✓	16 Chl *a*	3 β-car	✓	16 Chl *a*	3 β-car	✓	16 Chl *a*	3 β-car
	PsbC (CP43)	✓	13 Chl *a*	4 β-car	✓	13 Chl *a*	4 β-car	✓	13 Chl *a*	4 β-car
	PsbD (D2)	✓	2 Chl *a*	1 β-car	✓	2 Chl *a*	1 β-car	✓	2 Chl *a*	1 β-car
	PsbE (α Cyt b_{559})	✓			✓			✓		
	PsbF (β Cyt b_{559})	✓			✓			✓		
	PsbH	✓		1 β-car	✓		1 β-car	✓		1 β-car
	PsbI	✓			✓			✓		
	PsbJ	✓			✓			-		
	PsbK	✓			✓			✓		
	PsbL	✓			✓			✓		
	PsbM	✓			✓			✓		
	PsbO	✓			✓			✓		
	PsbP	✓			✓/-			-		
	PsbQ	✓			✓/-			-		
	PsbR	-			✓/-			-		
	PsbX	✓			✓			✓		
	PsbZ	✓			✓			✓		
	PsbW	✓			✓			✓		
	Psb30 (Ycf12)	-			✓			✓		
	PsbTc	✓		**1 β-car**	✓			✓		
	PsbTn	-			-			✓		
	SLP	-			✓/-			-		
	USP	-			✓/-			-		

	Subunits	*Pisum sativum* 5XNL $C_2S_2M_2$			*Chlamydomonas reinhardtii* 6KAC/6KAD $C_2S_2/C_2S_2M_2L_2$			*Picea abies* 8C29 C_2S_2		
	CP24 (LHCB6)	✓	6 Chl *a* 5 Chl *b*	1 β-car 1 Lut 1 Vio	-			-		
	CP26 (LHCB5)	✓	9 Chl *a* 4 Chl *b*	2 Lut 1 Neo	✓	**10 Chl *a*** 4 Chl *b*	2 Lut 1 Neo	✓	9 Chl *a* 4 Chl *b*	2 Lut 1 Neo
	CP29 (LHCB4/8)	✓	10 Chl *a* **4 Chl *b***	1 Lut 1 Neo 1 Vio	✓	**5**/10 Chl *a* 3 Chl *b*	**0**/1 Lut 1 Neo 1 Vio	✓	**9 Chl *a*** 3 Chl *b*	1 Lut 1 Neo 1 Vio
LHCII	S-trimer	✓	24 Chl *a* 18 Chl *b*	6 Lut 3 Neo 3 Vio	✓	24 Chl *a* 18 Chl *b*	6 Lut 3 Neo 3 Vio	✓	24 Chl *a* 18 Chl *b*	6 Lut 3 Neo 3 Vio
	M-trimer	✓	24 Chl *a* 18 Chl *b*	6 Lut 3 Neo 3 Vio	-/✓	24 Chl *a* **17 Chl *b***	6 Lut 3 Neo 3 Vio	-		
	L-trimer	-			-/✓	24 Chl *a* 16 Chl *b*	5 Lut 2 Neo 1 Vio	-		
SUM			159	44		101/187	27/48		104	28

Structures of PSII scs from pea (Su *et al.*, 2017), *Cr* (Sheng *et al.*, 2019) and spruce (Opatíková *et al.*, 2023), excluding lipids and other cofactors. *Abbreviations: Cyt b_{559} - cytochrome b559, β-car - β-carotene, Chl (a/b) - chlorophyll a/b, car - carotenoids, Pheo - pheophytin, Lut - lutein, Neo - neoxanthin, Vio - violaxanthin, subunit presence (✓) and absence (-) in the structure. For Cr, the composition of two independent structures was analysed at the same time and when the presence of a subunit or cofactor in them differs, the numbers or ✓and - symbols are separated by "/". The four-letter code below the name of the organism represents the PDB identifier of the structure. Highlighted are differences observed between structures, either in the means of the presence/absence of the specific subunit or the presence/absence of a different number of identified cofactors.*

1.2.5. Light-harvesting complex of photosystem II (LHCII)

The peripheral LHCII is mostly conserved in gene coding across the land plants and green algae and we currently distinguish between nine LHCB proteins (1–9) based on their homology. In vascular plants, LHCIIs are represented by light-harvesting pigment-binding proteins that either form trimers (sub-classes LHCB1–3) or are present as monomeric antennae (LHCB4–6, also denoted according to their molecular weight CP29, CP26 and CP24, respectively) (For detailed pigment composition of LHCII see Tab. 2). Due to the absence of sequence motives used in vascular plants to distinguish major LHCB proteins, a different designation, namely LHCBMx, is used to distinguish them in the non-vascular plants *Chlorophyta*, *Marchantiophyta*, *Bryophyta* and *Anthocerotophyta* (x represents a progressive number (1–9) defining each isoform based on sequence similarity, M (major) representing the gene orthologues of *LHCB1* and *LHCB2* of land plants in the indicated divisions) (except in bryophyte for *LHCB3*). LHCBMx in *Cr* can be further divided into four types (I–IV) based on their sequence similarity (see, e.g. Crepin and Caffarri, 2018).

In addition to the specific sequence markers used for classification, the amino acid sequences of LHCB proteins often differ at several other sites, potentially affecting the final structure and function of a particular LHCB protein. This leads to a reasonably significant diversity within the LHCB protein family, which consists of different types and isoforms, also referred to as sub-isoforms.

Of the LHCB proteins, the LHCB4 protein is the most variable in its distribution between angiosperms and gymnosperms. The LHCB4 can be present in three isoforms (4.1, 4.2 and 4.3), with the first two sharing high sequence identity and similarity and containing longer C-terminus compared to the third isoform 4.3, also referred to as LHCB8 (Klimmek *et al.*, 2006; Grebe *et al.*, 2019). While the C-terminus of LHCB4.1 and LHCB4.2 is relatively conserved in length and sequence in the plant kingdom, this is not the case for LHCB8.

Moreover, the abundance of specific isoforms of this monomeric antenna strongly depends on light conditions. The *LHCB4.1* and *LHCB4.2* isoforms, which are expressed under standard growing conditions, are substituted by the expressed *LHCB4.3* isoform under HL intensity, whose product is subsequently incorporated into the PSII structure (Klimmek *et al.*, 2006; Sawchuk *et al.*, 2008; Albanese *et al.*, 2016). In spruce, however, this position is known to be occupied exclusively by LHCB8 independently on the light conditions (Grebe *et al.*, 2019).

The LHCB1 and LHCB2 proteins also have different isoforms, when LHCB1 shows a higher variety with five isoforms, LHCB1_A1–A3 and LHCB1_B1–B2, compared to LHCB2 with four isoforms LHCB2_A1–A4, whereas LHCB3 and LHCB5 have only one isoform (Jansson, 1999). Moreover, it should be emphasised that the molar ratio of these three major isoforms seems to correlate with the copy numbers of the genes encoding each isoform, and the ratio of LHCB1:LHCB2:LHCB3 in *At* was found to be 7:3:1 (Peter and Thornber, 1991; Galka *et al.*, 2012; Crepin and Caffarri, 2018). However, this ratio can fluctuate and is highly dependent on light conditions. These major LHCII proteins differ primarily by the amino acid sequence at the N-terminus, the composition of which has a significant impact on their function because it contains a reversibly phosphorylated threonine that is involved in transitions between states (Alboresi *et al.*, 2008; Goldschmidt-Clermont and Bassi, 2015; Iwai and Yokono, 2017; Crepin and Caffarri, 2018).

As for LHCB3, its presence, together with the LHCB6 protein, is not uniform in photosynthetic organisms. Discussed in detail in the following subsection.

Within the LHCB protein family, LHCB9 and LHCB7 are among the least studied. LHCB9 has only been detected in the moss *Pp* (Alboresi *et al.*, 2008; Grebe *et al.*, 2019), where it is part of the PSI antenna (Iwai *et al.*, 2018; Pinnola *et al.*, 2018; Zhang *et al.*, 2023). The function of LHCB7, along with its rare expression, remains a mystery (Klimmek *et al.*, 2006; Peterson and Schultes, 2014).

Moreover, additional variability of LHCIIs lies in their potential to form homo- or heterotrimers. To some extent, these trimers are composed of variable triplets of major LHCB1/2/3 and attach to PSII either directly or via minor monomeric antennae (Jansson, 1999; Jackowski *et al.*, 2001; Caffarri *et al.*, 2004). The association of LHCII trimers to the PSII cc is either (i) strong (S-LHCII) via LHCB4 and LHCB5, (ii) moderate (M-LHCII) via LHCB4/(LHCB6) (Dekker and Boekema, 2005; Caffarri *et al.*, 2009; Kouřil *et al.*, 2012, 2018; Caffarri *et al.*, 2014; Pagliano *et al.*, 2014), and (iii) occasionally loose (L-LHCII) without the participation of any monomeric antenna (Boekema *et al.*, 1999a, b; Dekker and Boekema, 2005). In the majority of studied land plants, S-trimer is formed by LHCB1 and LHCB2 in different ratios, whereas M-trimer is formed by LHCB1, 2 and 3, and L-trimer mainly composed of LHCB1, LHCB2 (Dainese and Bassi, 1991; Caffarri *et al.*, 2004, 2009; Rantala *et al.*, 2017; Su *et al.*, 2017; Crepin and Caffarri, 2018). The one copy of LHCB3 in M-trimer represents the interacting partner for LHCB6 and is thus responsible for its stable binding to C_2S_2 in *At*. This arrangement of antennae provides more flexible regulation of PSII antenna size in response to fluctuating light (Caffarri *et al.*, 2004; Kovács *et al.*, 2006; Caffarri *et al.*, 2009; Kouřil *et al.*, 2013; van Bezouwen *et al.*, 2017). For a structural detail of PSII sc, see Fig. 3.

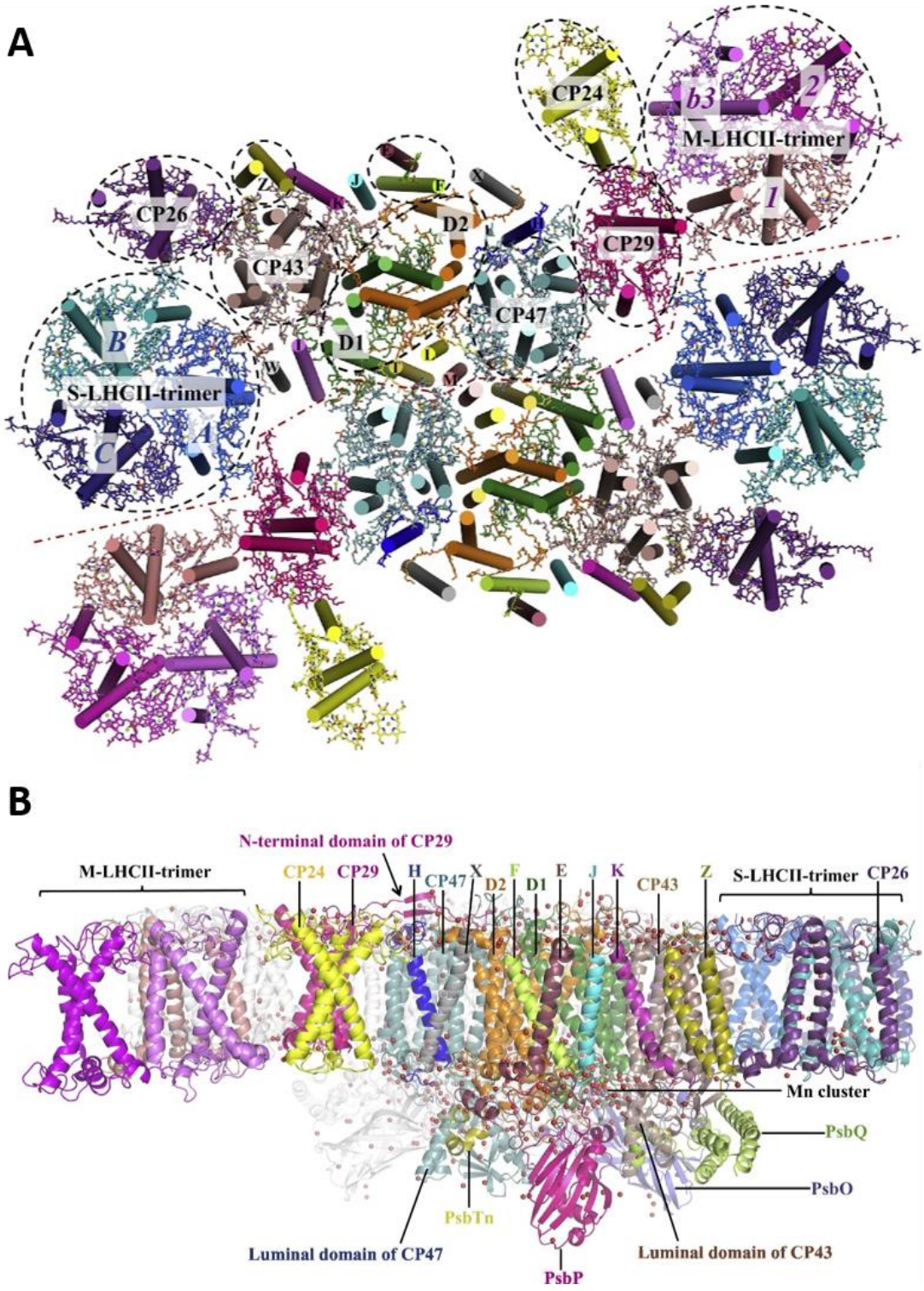

Figure 3: Structure of PSII supercomplex $C_2S_2M_2$ from *Pisum sativum* at 2.7 Å resolution. (A) View from the stromal side with exclusive visualisation of transmembrane helices (stick mode) and cofactors (cartoon). The red dashed line illustrates an imaginary division between two monomers. In one monomer, individual subunits are outlined in circles with their designations, and low-molecular-mass subunits of PSII cc are labelled with a single letter. (B) Side view along the membrane plane with coloured subunits only in one monomer. Adapted from Cao *et al.*, 2018, the original structure of pea PSII sc from Su *et al.* (2017) (5XNM) and supplemented with PsbTn subunit from spinach, Wei *et al.* (2016) (3JCU).

In greater detail, the size of the LHCII antenna, and thus its absorption cross-section, changes dynamically depending on the actual light conditions to which the photosynthetic organism is exposed. The ability to adjust the antennae size represents a highly efficient way for plants to dynamically adapt to the changes in light irradiance, either short- or long-term in their duration, and thus maintain optimal light energy utilisation while minimising potential photodamage (Bailey *et al.*, 2001; Ballottari *et al.*, 2007; Betterle *et al.*, 2009; Kouřil *et al.*, 2013; Albanese *et al.*, 2016; Bielczynski *et al.*, 2016). The aforementioned increased expression of the *LHCB4.3*, which product LHCB4.3 is characterised by a shorter C-terminus, is observed in land plants in response to HL. The LHCB4 C-terminus is involved in the LHCB6 binding to the PSII cc, thereby influencing the lateral organisation of PSII in the thylakoid membrane (Guardini *et al.*, 2022). Thus, the incorporation of LHCB4.3 to the prevalence of PSII scs leads to its weaker interaction with LHCB6 and its disconnection. In the absence of LHCB6, the M-trimer lacks an interacting partner and thus cannot bind to the PSII cc (de Bianchi *et al.*, 2011).

1.2.5.1. Loss of LHCB3 and LHCB6 antennae and its relevance

In angiosperms, the LHCB3 protein is the building stone of the M-trimer, which binds to the PSII cc specifically via its LHCB3 protein through the interaction with LHCB6 and with the contribution of LHCB4 (Kovács *et al.*, 2006; de Bianchi *et al.*, 2008, 2011; Caffarri *et al.*, 2009; Kouřil *et al.*, 2013). The evolutionary loss of *LHCB3* and *LHCB6* in *Pinaceae*, *Gnetaceae* and *Welwitschiaceae* (Kouřil *et al.*, 2016) understandably has a significant impact on the structure of PSII in spruce. The most likely candidates for replacing the LHCB3 in the spruce M-trimer are LHCB1 and LHCB2, both capable of forming trimers. However, only a detailed high-resolution analysis of this trimer structure in spruce can provide a reliable answer.

Oppositely to LHCB3, the impact of LHCB6 absence is more straightforward, as this antenna is not substituted by any protein or other molecule. Compared to *At* PSII sc, spruce has its M-trimers rotated clockwise by 52°, resulting in a tighter association of the M- and S-trimers (closing the distance by 7 Å), thus more resembling PSII structure from *Cr* (Fig. 4, adapted from Kouřil *et al.*, 2016).

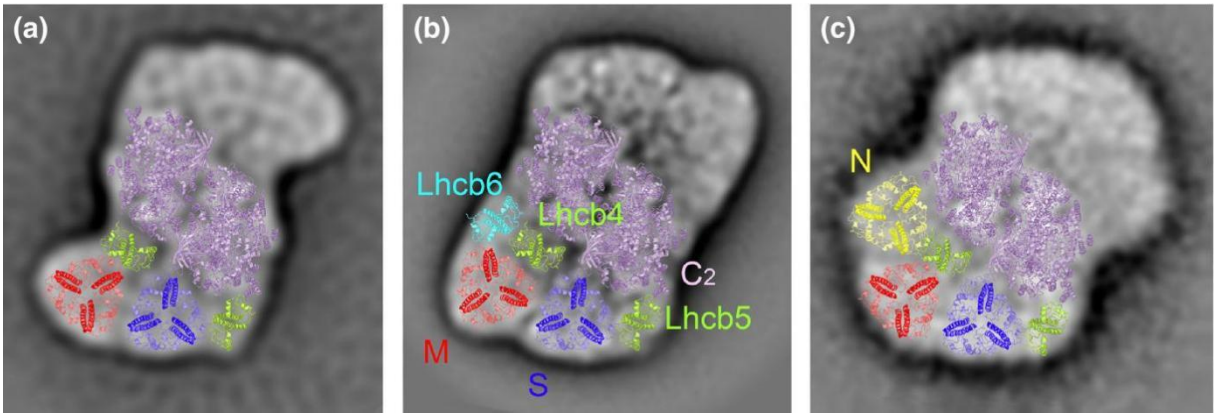

Figure 4: Electron density maps of PSII $C_2S_2M_2$ supercomplex from *spruce* (a), *Arabidopsis thaliana* (b) and $C_2S_2M_2N_2$ supercomplex from *Chlamydomonas reinhardtii* (c) with assigned subunit composition. Subunits determined based on the fitting by high-resolution structures of PSII sc, C_2 dimer (light violet), trimeric antennae S-/M-/N-trimers (blue, red and yellow, respectively) and monomeric antennae LHCB4/LHCB5/LHCB6 (green, green and cyan, respectively). Adapted from Kouřil *et al.* (2016).

From the functional point of view, the shifted position of M-trimer towards PSII cc and the absence of LHCB6 in spruce compared to angiosperms affects the regulation of the related macro-organisation of PSII scs in grana membrane and the interactions between the individual PSII scs, which reflects on the whole photochemistry of spruce PSII. Moreover, the change in Chl numbers due to the absence of LHCB6 and rotated M-trimer results in alteration in the main excitation energy transfer pathways, its rates and efficiency in PSII, compared with the land plants (Kovács *et al.*, 2006; Caffarri *et al.*, 2009, Kouřil *et al.*, 2016; Kouřil *et al.*, 2020; Croce and van Amerongen, 2020).

A partial functional resemblance between angiosperms and spruce in terms of LHCB3 and LHCB6 function can be seen in the adaptation of *At* to HL intensity. Under prolonged exposure to excessive light, angiosperms deliberately downregulate the expression of *LHCB3* and *LHCB6* (with the concurrent upregulation of *Lhcb4.3* at the expense of *Lhcb4.1* and *Lhcb4.2*, as mentioned above). However, this regulation leads explicitly to the disconnection of the M-LHCII trimers and thus to an increase in their C_2S_2:$C_2S_2M_2$ ratio, not to the formation of a PSII structure with rotated M-trimer observed in spruce (Kouřil *et al.*, 2013, 2016; Albanese *et al.*, 2016).

1.2.6. Functional PSII assemblies

PSII is capable of mutual lateral interactions in variable arrangements, either in a parallel or non-parallel way, forming PSII megacomplexes (mcs) (Dekker and Boekema, 2005; Kirchhoff, 2008). These interactions were observed at the level of thylakoid grana membranes, confirming their existence *in vivo* (Nosek *et al.*, 2017; Kouřil *et al.*, 2020). Moreover, PSII scs are able to form semi-crystalline arrays within the membrane with a functional impact on photosynthesis itself (see, e.g. Boekema *et al.*, 1999a,b, 2000; Yakushevska *et al.*, 2001; Kirchhoff *et al.*, 2007; Kouřil *et al.*, 2013; Nosek *et al.*, 2017). These two-dimensional crystals are formed by either $C_2S_2M_2$, C_2S_2M or C_2S_2 scs as building blocks. Their abundance and the composition of the individual sc forms depend on conditions such as light intensity, temperature, growing medium, or the conditions used in isolation (Garber and Steponkus, 1976; Semenova, 1995; Kouřil *et al.*, 2013). The function of arrays is still controversial and disputable, attributed to the non-photochemical quenching of chlorophyll fluorescence (NPQ) via PsbS, grana formation via interaction of adjacent membranes and, most importantly, to have an influence on PQ diffusion with a major impact on ETC (Ilíková *et al.*, 2021).

1.3. In action - the principle of the electron transport chain and its regulations

The following subsections are focused on a general explanation of the function of the photosynthetic apparatus and its regulation, again with the main focus on spruce and its specialities as an evergreen conifer. In the final subsection, the most commonly used methods for a study of the photosynthetic apparatus are shortly listed, including physiological, biochemical and structural methods.

1.3.1. Photosynthetic electron transport chain

The basic concept of light-dependent photosynthetic reactions, the first phase of photosynthesis, can be summarised as follows: the energy of photons harvested by the pigments in the PSII antennae is transferred to the PSII RC, specifically to its primary electron donor, commonly referred to as P680, and triggers the primary charge separation. The separated electron gives rise to an oxidised $P680^+$, which is immediately reduced by an electron from

tyrosine Z (Y_Z). Oxidised tyrosine Z (Y_Z^+) is reduced by an electron donated from manganese (Mn) in the Mn cluster of OEC located at the lumenal side of PSII. In the four-step Mn cluster reaction, every separated electron from P680 is donated three times in succession via Y_Z from one of the incorporated Mn ions. The fourth electron comes from split water in the OEC, while the rest of the released electrons from the water molecule reduce the Mn ions in the cluster. Besides the electrons, the split water is the source of protons and oxygen released into the lumen of thylakoid membranes. Electrons captured by the primary electron acceptor pheophytin are further transported via the ETC, where they reduce PQ to plastoquinol (PQH_2). The PQH_2 molecule moves within the PQ pool to the lumenal side of Cyt_{b6f}, where it is oxidised back to PQ with simultaneous electron transport into Cyt_{b6f} and release of two protons into the lumen. On the lumenal side, the PC molecule relocates electrons from Cyt_{b6f} to PSI, where analogous to PSII, the primary charge separation is initiated upon photon absorption in its primary electron donor, designated as P700. The separated electrons are replenished by electrons from reduced PC. Through the electron acceptors, Chl (A_0), phylloquinone (A_1) and system of Fe-S centres (F_X, F_A, F_B), electrons are finally transported from PSI to Fd, further reducing Fd-$NAD(P)^+$-reductase (FNR). The double electron reduction of $NAD(P)^+$ by two electrons from FNR with simultaneous binding of one proton from the stroma leads to the formation of a reduced NAD(P)H molecule (reviewed, e.g. in Brettel, 1997).

Proton-coupled electron transport naturally leads to the formation of proton motive force, composed of the thermodynamically equivalent electric potential $\Delta\psi$ and the ΔpH component, which powers the ATP production from ADP and inorganic phosphate by the ATP synthase protein complex (CF_0-CF_1) (Mitchell, 1966).

1.3.2. Regulation of electron transport chain - rerouting of electrons

The paragraph above describes a schematic representation of the so-called Z scheme of the linear electron transport (LET) of photosynthesis. However, an increase in absorbed light energy leading to high ΔpH across the thylakoid membrane causes inhibition of LET (Kanazawa and Kramer, 2002; Tikkanen and Aro, 2014), and therefore other mechanisms of alternative electron transport pathways (alternative electron flow - AEF) must be activated to act as protective and regulatory mechanisms. These involve CET and pseudo-CET (Alric and Johnson, 2017). CET is characterised by the return of electrons from Fd back to the Cyt_{b6f} complex, resulting in a closed cycle. It functions either as a form of photoprotection by reducing photoinhibition of both photosystems caused by over-reduction of stroma, or it is pronounced in plants when the ratio of ATP:NAD(P)H production needs to be altered in favour of ATP (Alric and Johnson, 2017).

Pseudo-CET redirects electrons either: i) from PSI to O_2 (Mehler-reaction) (Mehler, 1951), ii) from PQH_2 to O_2 by plastid terminal oxidase (PTOX) (Josse *et al.*, 2003; Yu *et al.*, 2014), or iii) in plants possessing flavodiiron (see, e.g. Ilík *et al.*, 2017; Alboresi *et al.*, 2019) from Fd (Sétif *et al.*, 2020) (originally thought to be from NAD(P)H) (Helman *et al.*, 2003; Allahverdiyeva *et al.*, 2011) to O_2. Ultimately, all reactions lead to water production, i.e. pseudo-CET, and are hypothesised to be directly involved in stress signalling, most probably via reactive oxygen species (ROS) as intermediates (see, e.g. Nawrocki *et al.*, 2015; Li and Kim, 2022). These regulatory mechanisms, among others, adjust the optimal energy use according to the plant's needs or protect the photosynthetic apparatus and are significantly controlled by the redox state of thioredoxins (Buchanan, 2016; Cejudo *et al.*, 2019; Nikkanen and Rintamäki, 2019; Yoshida *et al.*, 2019).

1.3.2.1. Cyclic electron transport and other alternative electron flows

There are two main types of CET, one involving the NDH-like complex and the other involving the PROTON GRADIENT REGULATION 5 PROTEIN/PROTON GRADIENT REGULATION-LIKE 1 PROTEIN (PGR5/PGRL1) proteins (Shikanai, 2007; Suorsa *et al.*, 2012). Since spruce and other genera from *Pinaceae*, *Welwitschiaceae*, and *Gnetaceae* lack the genes encoding *NDH-like* (Braukmann *et al.*, 2009; Nystedt *et al.*, 2013), the functional and essential type of CET for photosynthesis in conifers presumably uses PGR5/PGRL1 pathway (Munekage *et al.*, 2002, 2004). Moreover, besides PGR5/PGRL1 pathway spruce possesses a different type of AEF involving FLAVODIIRON PROTEINS (FDPs) that function as an electron safety valve and are characterised by a very fast re-oxidation of PSI upon dark-to-light transition, which is much faster than in angiosperms (Helman *et al.*, 2003; Alboresi *et al.*, 2019).

1.3.3. Regulation of electron transport chain - energy redistribution and dissipation

To continue with functional regulations of the ETC, the aforementioned AEF mechanisms represent a simple and rapid way for plants how to redirect electrons and thus prevent the potential photooxidative damage. However, the plants must be able to adequately respond to changing light conditions over a longer period of time, and therefore they have evolved additional protective mechanisms, all at the level of the ETC. These include (i) state transitions, which allow the plants to balance the accepted light energy between the two photosystems (Lemeille and Rochaix, 2010; Pesaresi *et al.*, 2010, 2011), (ii) direct dissipation of the excess of light energy triggered by the induction of NPQ (Demmig-Adams and Adams, 1996; Horton *et al.*, 1996; de Bianchi *et al.*, 2010; Niyogi and Truong, 2013; Demmig-Adams *et al.*, 2014) or, (iii) the electron transport can be regulated by direct involvement of Cyt_{b6f} complex via photosynthetic control (Rumberg and Siggel, 1969; Kramer *et al.*, 2003; Tikhonov, 2014). The long-term regulations necessary for plant acclimation to biotic and abiotic changes in the environment are accompanied by up-or down-regulation of nuclear or chloroplast gene expression of proteins involved in photosynthesis (see, e.g. Pfannschmidt *et al.*, 1999, 2001).

1.3.3.1. Sustained NPQ – a rarity of overwintering evergreens

In addition to the aforementioned NPQ, in overwintering spruce and other evergreens, a specific type of S-NPQ is induced (Öquist and Huner, 2003; Demmig-Adams and Adams, 2006; Verhoven, 2014). The S-NPQ is characterised as a state of prolonged energy dissipation emerging in plants as conifers under freezing temperatures with concurrent bright light. Compared to the relaxation kinetics of Chl fluorescence of fast-recovered energy-dependent quenching (qE) NPQ in the dark after previous illumination, S-NPQ is characterised by a significant decrease in the maximum photochemical quantum yield of PSII (F_V/F_M), which relaxes really slowly (Verhoeven, 2013; Grebe *et al.*, 2020; Walter-McNeill *et al.*, 2021). Grebe *et al.* (2020) concluded that three events interrelate with S-NPQ and are responsible for its initiation in spruce: i) freezing temperatures, which independently on light induce fast triple phosphorylation of LHCII that further initiates grana destacking due to electrostatic repulsion of adjacent membranes, ii) light- and temperature-dependent accumulation of p-PsbS and iii) limited PSII photoinhibition. The observed destacking of grana leads to concomitant linearisation of thylakoids, loss of the lateral heterogeneity of PSI and PSII distribution in the thylakoid membrane and increased PSII-PSI spillover (for a general overview, see Grebe *et al.*, 2020). Oppositely, relaxation of S-NPQ leads to 3p-LHCII dephosphorylation, re-stacking of the grana membranes, lateral segregation of PSI and PSII, and reduced spillover.

It is important to mention that the S-NPQ is manifested by an increase in the quantum yield of non-regulated energy dissipation Y(NO) and a concomitant decrease in the quantum yield of non-photochemical quenching Y(NPQ) since S-NPQ does not relax during dark adaptation (Bag *et al.*, 2020; Grebe *et al.*, 2020). Moreover, the S-NPQ in spruce could also be triggered by PSII photodamage that over-exceeded the repair capacity of regulatory NPQ.

The loss of grana stacking during S-NPQ is primarily the result of LHCII and PSII phosphorylation by STN7 and serine/threonine protein kinase 8 (STN8) (Pesaresi *et al.*, 2011; Rochaix *et al.*, 2012). The LHCII and PSII located in adjacent thylakoid membranes mediate the stacking of the membranes into grana (Trissl and Wilhelm, 1993; Anderson, 2012) and their destacking by reversible phosphorylation allows enormous quenching of excess light energy in PSI (Martin and Öquist, 1979; Öquist and Huner, 2003; Demmig-Adams *et al.*, 2015; Yang *et al.*, 2020). This phenomenon was further analysed in the analogous study by Bag *et al.* (2020), focusing on S-NPQ in pine. According to Bag *et al.* (2020), the PSII-PSI spillover represents the major component of S-NPQ, which provides significantly stronger quenching than the regulatory NPQ and thus contributes to a multiple times lower risk of oxidative photodamage. A direct energy transfer from PSII to PSI would be in agreement with the observed, significantly higher limitation of the electron transport on the donor side of PSI than on its acceptor side.

1.3.4. Photosynthesis and the experimental approach to its study

There are different approaches how to reveal the mysteries of photosynthesis. Since photochemistry and fluorescence are at significant levels competing processes in plants, biophysical methods aimed specifically at measuring fluorescence are most appropriate for determining the efficiency of photosynthesis. A wide range of fluorescence techniques, such as Chl fluorescence induction, fluorescence spectroscopy, etc., allow the study of photochemistry in real-time with the possibility of studying the effects of different biotic or abiotic stresses.

Although biochemical methods do not provide real-time data and are more destructive to the plant material, they are still irreplaceable due to the information provided about the qualitative and quantitative chemical composition of the photosynthetic apparatus with its specific modifications. These methods include optimised techniques for the isolation of DNA/RNA/proteins from biological material, separation techniques such as (non-)denaturing one- or two-dimensional electrophoresis, ultracentrifugation, high-pressure liquid chromatography (HPLC), liquid or gas chromatography combined with mass spectrometry, tandem mass spectrometry and others.

For detailed structural analysis of specific protein complexes of the photosynthetic apparatus and their final visualisation, techniques such as X-ray crystallography and cryo-EM/TEM are essential, with the latter becoming the dominant structural method in the study of large protein complexes in recent years.

In summary, it is inevitable to combine different approaches to achieve a comprehensive and complex picture of the structure and function of the photosynthetic apparatus. My research required the implementation and optimisation of biochemical methods for sample preparation (see Sections 3 and 4) and the use of EM, together with the application of computational methods for sample processing and structural analysis.

2. A deeper insight into the photosynthetic apparatus of spruce and its functional relevance

The two main objectives of my doctoral study were:

I) to study the photosynthetic apparatus of Norway spruce with a focus on a detailed structural analysis of its photosystem II using cryo-EM and,

II) to optimise the solubilisation conditions and separation methods for isolated thylakoid membranes (i) to obtain a homogeneous and highly concentrated sample of intact photosystem II supercomplex suitable for cryo-EM analysis and (ii) to isolate the transiently formed, but fragile, photosynthetic supercomplex PSI-LHCII$_{(n)}$ from Norway spruce.

Section 2 briefly summarises in four subsections the individual structural and functional studies carried out on the photosynthetic apparatus of spruce, which formed the basis of the individual publications. Section 4 summarises in detail the experimental approach used to optimise the separation of specific protein complexes from isolated thylakoid membranes that are starting points for structural or functional analysis.

2.1. Simulation of the loss of LHCB3 and LHCB6 proteins during spruce evolution in *Arabidopsis thaliana*

Spruce represents a rather unconventional model plant, and from one point of view, it is a relatively undemanding species for growing under controlled conditions and subsequent isolation and sample processing. However, on the other hand, any targeted gene manipulation in spruce represents quite an obstacle as its genome is more than 100 times bigger than that of *At* (Nystedt *et al.*, 2013). Therefore, there are strong ambitions to study its unique, photosynthesis-related traits indirectly, generally using "uncomplicated plants" with a small genome and known genome sequence, fast-growing rate and easier gene manipulation. This approach allows us to purposely mutate specific genes and to test the effect of individual modifications. The original idea of our project (Ilíková *et al.*, 2021) and our main objective was to simulate the characteristic spruce absence of LHCB3 and LHCB6 proteins in the model plant *At* by knock-outing the genes encoding both of these proteins. In this pilot study, we had a unique opportunity to observe the structural and functional effect of the loss of these proteins on the structure of *At* PSII sc. In addition, this study could shed light on the evolutionary advantage gained by spruce due to the absence of the LHCB3 and LHCB6 proteins.

The results showed that the double mutant lacking *LHCB3* and *LHCB6* genes, is able to form only smaller forms of C_2S_2 scs, mostly organised into semi-crystalline domains. The observed C_2S_2 scs arrangement in this mutant has a potential impact on the diffusion of PQ molecules and overall fitness of photosynthetic apparatus and its function (de Bianchi *et al.*, 2008). Nevertheless, the formation of C_2S_2M/M_2 with shifted M-trimer in the *lhcb3+6* mutant could be unambiguously excluded.

However, an unexpected result was the observation of the so-called "spruce-type" of PSII sc in the *At lhcb3* mutant. This "spruce-type" PSII sc was identified in the C_2S_2M fraction, with one missing M-trimer, with a minor abundance of 10 %. For the remaining 90% of the particles in this fraction, their M-trimer had a characteristic binding to the PSII cc via LHCB4 and LHCB6 antennae (Caffarri *et al.*, 2009). Importantly, mass spectrometry analysis of thylakoid membranes of *lhcb3* mutant and wild type revealed comparable small amounts of LHCB8 protein, suggesting that the formation of the "spruce-type" PSII sc is not dependent on the presence of spruce-specific LHCB8.

2.2. Cryo-EM structure of the PSII supercomplex of Norway spruce

Until recently, the highest known resolution of the PSII-LHCII sc ($C_2S_2M_2$) in spruce was 14 Å, obtained from a negative stain projection map by SPA (Kouřil *et al.*, 2016). This structure was sufficient to reveal its unique architecture described above. However, the specific composition, mostly of the peripheral LHCII antennae and their interactions, still remained undescribed. However, the nearly atomic resolution at 2.8 Å of spruce C_2S_2 PSII sc obtained in our work using cryo-EM (Opatíková *et al.*, 2023) allowed us to study this structure in much greater detail with unique insight into the composition of its specific subunits and arrangement of pigment molecules.

The PSII cc in spruce is highly conservative and its subunit composition corresponds with that observed in green algae and angiosperms (subunit and pigment composition of spruce PSII see in Tab. 2). However, the presence of one additional low molecular mass subunit, specifically Ycf12, was confirmed similarly to the green algae *Cr* (Shen *et al.*, 2019; Sheng *et al.*, 2019). Oppositely, this subunit was not observed in the known structures from angiosperms, such as spinach, *At*, or pea, as they lack the *YCF12* gene (Wei *et al.*, 2016; Su *et al.*, 2017; van Bezouwen *et al.*, 2017). It is hypothesised that the Ycf12 subunit may play a role during acclimation to the HL intensity (Kashino *et al.*, 2007).

Within the light-harvesting antennae of spruce, specifically the S-trimer, we confirmed another previously unknown speciality of spruce, and that is the homotrimeric composition of its S-trimer. In green algae *Cr*, the S-trimer represents heterotrimer, while in land plants it is generally accepted that it forms either homo- or heterotrimers. In spruce S-trimer, we were able to exclude the presence of all LHCB2 isoforms and even two LHCB1 isoforms (B1 and B2), and thus the S-trimer can be then assigned as a homotrimer of LHCB1_A (isoforms LHCB1_A1–3), oppositely to green algae and land plants. Moreover, since mass spectrometry analysis confirmed the presence of LHCB2 in the PSII sc fraction of spruce, and we ruled out its presence in the S-trimer, we assume that, unlike the composition of *At*' M-trimer from LHCB1 and LHCB3, the spruce M-trimer composition could include the LHCB2 protein. Nevertheless, whether the M-trimer in spruce represents a homotrimer or a heterotrimer would require obtaining a detailed high-resolution structure of PSII sc with bound M-trimer.

The sole presence of LHCB8 in spruce provided a unique opportunity to study this protein in detail since it is not overshadowed by other isoforms, LHCB4.1 and LHCB4.2, in the final electron density map. In this protein, we evidenced the loss of two Chls compared with the PSII structures of land plants (Chl *a*613 and Chl *b*614) and one compared with *Cr* (Chl *b*614). The loss of two Chls in the LHCB8 protein of spruce compared to LHCB4.1 and LHCB4.2 present in land plants is attributed to its shorter C-terminus and related structural properties. The ability of *Cr* to maintain one extra Chl in its LHCB4.3 protein compared to spruce, even with its shorter terminus, is probably due to a clockwise rotation of its α-helix forming C-terminus (Shen *et al.*, 2019; Sheng *et al.*, 2019).

Nevertheless, the most unexpected discovery in spruce PSII structure was the presence of α-tocopherol/α-tocopherolquinone (α-Toc/α-TQ, second one is an oxidation product of α-Toc). It is important to mention that the identification of either of the two tocopherols was somewhat complicated since multiple molecules share similar structural features and have almost indistinguishable electron density at lower resolution, such as n-Dodecyl α-D-Maltopyranoside (α DDM), n-Dodecyl-β-D-Maltopyranoside (β DDM) or plastochromanol-8. Thus the identification or exclusion of such molecules depends mainly on the final level of resolution of the electron density map in the problematic regions of the obtained structures. However, in our structure, the α DDM did not fully fit into the density map, which was confirmed by calculating the interaction energies ΔiG for the most relevant interaction interfaces.

The hypothesis explaining the function of α-Toc/α-TQ can be built on the nature of the compound itself, which is known singlet oxygen ($^1O_2$) scavenger. $^1O_2$ ranks among the ROS with a high potential to cause oxidative damage. In plants, ROS are formed in high abundance upon exposure to excessive light irradiance (Foyer and Noctor, 2003, 2005; Apel and Hirt, 2004), and while carotenoids represent a primary protective barrier capable of quenching excessive energy uptake and thus preventing the $^1O_2$ formation, α-Tocs can be considered as a secondary protection (Edge and Truscott, 1999; Krieger-Liszkay and Trebst, 2006).

2.3. Formation of PSII supercomplexes and megacomplexes and their organisation into arrays

The high structural similarity of PSII sc in spruce and *Cr* and their shared absence of LHCB3 and LHCB6 proteins led us to the conclusion that spruce may be able to potentially bind other trimers analogously to *Cr* (Drop *et al.*, 2014). Thus in our work (Kouřil *et al.*, 2020), we focused on the possible formation of larger PSII scs in spruce and its organisation and mutual associations in the thylakoid membrane. Together with a parallel analysis in pine, we determined the potential impact of their unique PSII structure on the formation of larger PSII assemblies.

We showed that spruce forms a much larger PSII scs with bound N-trimers (although they are rotated compared to those observed in *Cr*) and additional L-trimers compared to *At*. While it is hypothesised that the N-trimer in *Cr* is most probably composed of LHCBM1, 2, 3, 6 and 7 in different combinations (Drop *et al.*, 2014; Shen *et al.*, 2019), in spruce, the main components of N-trimer would be LHCB1 and LHCB2 (Kouřil *et al.*, 2016). However, the participation of LHCB5 in N-trimer formation in spruce has lately been discussed (Grebe *et al.*, 2019). Interestingly, for some of the PSII scs from both studied conifers, the binding of the N-trimer did not require the presence of the M-trimer, and the N-trimer binding was the same as for *Cr* with the M-trimer present. The origin of the different character of N-trimer binding in *Cr* and spruce is still unknown.

Furthermore, aside from the observed attachment of N-trimer in spruce PSII sc, we were able to identify PSII scs with two rows of connected LHCII trimers and experimentally confirm the existence of PSII scs with up to 7–8 LHCII trimers on one side of PSII sc. And since PSII scs have two-fold symmetry, it is logical to expect the existence of PSII sc with the ability to bind up to 18 LHCII trimers. It is important to note that according to the created hypothetical model of these large PSII scs, the LHCII binding would still allow the necessary free flow of PQ into the RC of PSII (van Eerden *et al.*, 2017).

Megacomplexes are formed as a result of lateral interactions of PSII scs in the thylakoid membrane, and this association is mediated by LHCII and C_2 (Nosek *et al.*, 2017). However, PSII scs can also interact with each other from the stromal side of two adjacent membranes (Daum *et al.*, 2010; Albanese *et al.*, 2017; Su *et al.*, 2017). The characteristic features of the observed mcs were the composition of two PSII scs with variable interaction of $C_2S_2M_2$, C_2S_2M and C_2S_2 forms, which interacted either in parallel (70 %) or non-parallel (30 %) way. The S-trimer was the most involved part in the interaction, therefore it was considered as the main mediator of the association between two PSII scs, followed by involvements of LHCB5, LHCB4, dimeric core, L- and M-trimer, respectively. The same trend was also observed in pine (Kouřil *et al.*, 2020). Compared with the 13 types of PSII mcs observed in *At* by Nosek *et al.* (2017), in spruce and pine, we observed their lower structural variability, with 7 and 3 different types, respectively. Furthermore, the stability of formed PSII mcs was noticeably weaker in spruce compared with *At*. It is hypothesised that the origin of more firm binding in *At* is in the rectangular shape of its PSII sc, which may provide more stable side-by-side interactions.

Although in spruce, we did not observe the typical arrangement of PSII scs into 2D arrays typical for land plants, we were able to identify specific interactions representing PSII mcs in the

thylakoid membrane. However, these interactions did not match those observed in the isolated PSII mcs. This phenomenon could be then explained by the disproportion between the stability of specific PSII mcs types and their abundance in membranes *in vivo* (Kouřil *et al.*, 2020).

2.4. Acclimation to long-term changes in light intensity

The motivation for a more detailed study of the mechanisms involved in adaptation to long-term light intensity changes under controlled conditions originates in the early observation of light acclimation strategies of spruce compared to *At* (Kurasová *et al.*, 2003; Štroch *et al.*, 2008). While a reduction in the size of the PSII antennae in response to intensive light is a common phenomenon in *At*, accompanied by downregulation of *LHCB1–3* and *LHCB6* and overexpression of *LHCB4.3* isoform, LHCIIs plasticity in spruce seems to be rather reduced. The reason for this phenomenon can be found in the nature of the plants, as *At* is typically a light-tolerant plant, while spruce is a shade-tolerant plant. In our work (Štroch *et al.*, 2022), we focused on characterising the different strategies of *At* and spruce with respect to their long-term acclimation to different light intensities.

In detail, while the increasing light intensity leads to an increase in PSII/LHCII ratio in *At* due to a decrease in the fraction of bound LHCII antennae to PSII cc, and to a consequential increase in its Chl *a*/*b* ratio, no such phenomenon was observed in spruce. Rather oppositely, the PSII/LHCII ratio decreases in HL, while the Chl *a*/*b* ratio in spruce remains stable, with the most likely explanation being simultaneous and proportional degradation of PSII and PSI with concomitant preservation of released Chls.

Moreover, during long-term HL, *At* is able to sustain almost maximum F_V/F_M and the effective quantum yield of PSII photochemistry, Y(II), while the F_V/F_M in spruce is significantly decreased due to the already induced "locked-in" NPQ (described in detail in the following paragraph) and the preservation of de-epoxidised photoprotective xanthophylls and PsbS in the thylakoid membrane. Moreover, the effective PSII antennae size in *At* changes in response to the light intensity, while in spruce, it remains low regardless of the light intensity. Spruce seems to operate more with loosely bound LHCIIs that are present in high abundance under HL and are characterised by their weak interactions with PSII sc. Moreover, it is hypothesised that these weak interactions may be responsible for the minimal macro-organisation of PSII scs observed in spruce grana under HL.

Unlike in *At*, the significantly low NPQ parameter in HL-acclimated spruce is not a result of rapid adaptability, and its origin lies in the pre-existing specific type of NPQ in the dark-adapted spruce, namely "locked-in" NPQ. This "static" type of NPQ is reflected by an increase of Y(NO) and thus a decrease in the NPQ parameter, slow relaxation of NPQ parameter in the dark, formation of LHCII aggregates with strong quenching capacity and decrease in the Y(II), similarly to the S-NPQ observed in spruce in winter/early spring. However, to avoid misinterpretation, it is necessary to realise that the S-NPQ and "locked-in" NPQ differ primarily in their origin. The S-NPQ is attributed to the direct energy transfer from PSII to PSI (PSII-PSI spillover due to the reduced lateral segregation in the membrane) (Bag *et al.*, 2020) and is represented by a more significant decrease in F_V/F_M close to 0.2 values and quenching of PSII (Bag *et al.*, 2020; Grebe *et al.*, 2020). In the case of "locked-in" NPQ, its origin is in the zeaxanthin-dependent formation of LHCII aggregates, although their contribution to S-NPQ is still under debate (see, e.g. Kress and Jahns, 2017).

Moreover, the existence of "locked-in" NPQ is not exclusive to spruce, as the same response to the HL was observed in the angiosperm plant Monstera (Demmig-Adams *et al.*, 2006). Thereby, induction of this type of NPQ seems to be common for shade-tolerant evergreens.

2.5. Short summary

We used two independent approaches to reveal the origin of the unique structure of spruce PSII sc and the evolutionary benefit resulting from the loss of *LHCB3* and *LHCB6*. Our project Ilíková *et al*. (2021) involved gene manipulation of the model plant *At* and was aimed at simulating the loss of LHCB3 and LHCB6 proteins and its effect on the formation of its PSII scs. The main objective of our second project (Opatíková *et al.*, 2023) was to obtain a high-resolution structure of the PSII sc of spruce using cryo-EM. The integration of the results of these two projects has deepened our understanding of the structural and functional impact of the absence of the LHCB3 and LHCB6 proteins and shed light on specific aspects leading to the formation of the "spruce-type" PSII structure, which can be summarised as follows.

Firstly, the original hypothesis that considered the absence of LHCB3 and LHCB6 as the main cause responsible for the characteristic S shape of the spruce PSII sc was refuted because *lhcb3+lhcb6* double *At* mutants were unable to form scs even larger than C_2S_2. This suggests the contribution of other unknown factors to its structure, such as the exclusive presence of LHCB8 in spruce. However, because we observed the "spruce-type" PSII sc in the *lhcb3* mutant of *At* with a comparably minor abundance of LHCB4.3 (LHCB8) protein to that confirmed in the wild type, it was necessary to reconsider the possible involvement of this specific LHCB4 isoform (Ilíková *et al.*, 2021).

To rule out a possible role of LHCB8 in the formation of the "spruce-type" PSII sc, we prepared transgenic *At* lines, specifically a PENTA mutant knock-outed in *LHCB3*, *LHCB6*, and all isoforms of *LHCB4* (4.1, 4.2 and 4.3) genes, and supplemented them with *LHCB8* gene from spruce or *LHCB4.3* gene from *At* as a part of an ongoing study. Preliminary structural analysis of the PSII scs formed in these transgenic lines confirmed that neither LHCB8 nor LHCB4.3 are essential for the formation of "spruce-type" PSII sc (unpublished data).

A new indication of a key factor required for the formation of the S-shaped PSII sc provided the high-resolution structure of this sc that we obtained for spruce (Opatíková *et al.*, 2023). Based on our designation of the spruce S-trimer as a homotrimer composed of LHCB1_A proteins (isoforms 1–3), we concluded that this specific composition is most likely one of the conditions necessary for specific binding of the M-trimer to PSII cc. However, since the structure of the M-trimer is not yet known, a role of its specific composition in the formation of the S-shaped PSII sc cannot be ruled out either. Importantly, this hypothesis could be consistent with the observed presence of the S-shaped PSII sc in the *lhcb3 At* mutant. Since the S-trimer in *At* can be present either as homo- or a heterotrimer, the specific fraction resembling the "spruce-type" PSII sc could have an S-trimer composed exclusively of LHCB1s (like spruce) and thus would be able to bind the M-trimer at a different angle.

To confirm this hypothesis, we are currently working on the preparation of CRISPR *At* mutants with the main focus on the genes *LHCB1*, *LHCB2*, *LHCB3*, *LHCB4*, *LHCB6* and all their isoforms and simultaneous creation of transgenic lines to achieve the most authentic simulation of spruce PSII formation by modifying *At* genetic makeup. In parallel, we plan to use the optimised separation conditions presented in Section 4 to obtain a highly concentrated fraction of the intact $C_2S_2M_2$ PSII sc of spruce suitable for cryo-EM analysis and obtain its complete and detailed high-resolution structure that would reveal details of the M-trimer composition (unpublished data).

To continue with structural studies of the unique spruce PSII sc with rotated M-trimer, we determined its impact on the formation of larger PSII assemblies (scs and mcs), mutual PSII interaction and overall organisation in thylakoid membrane (Kouřil *et al.*, 2020). As a

consequence, both conifers studied, spruce and pine, appeared to be able to form PSII scs with a greater LHCII trimer binding capacity and a wider range of their interactions with PSII than was observed for *At*. We hypothesise that the greater diversity in PSII scs and mcs in spruce and pine is indeed enabled by their unique S-shaped PSII structure.

The uniqueness of the photosynthetic apparatus of spruce is manifested during acclimation to changes in light conditions and, among other factors, its acclimation is closely related to the structure of its photosystems and their associated structural flexibility. Previous light acclimation studies by Kurasová *et al.* (2003) or Štroch *et al.* (2008), have already indicated that the acclimation strategies of spruce and *At* significantly differ and while *At* is characterised by a change of the size of its antennae during short-term light acclimation, spruce lacks this ability. Therefore the characteristic overabundance of the aforementioned loosely bound LHCIIs in spruce could act as quenching centres for the excess of absorbed energy. The highest demand for LHCIIs and the formation of their aggregates capable of quenching would be in the winter months, characterised by HL irradiation combined with freezing temperatures (Bailey *et al.*, 2001; Ballottari *et al.*, 2007; Kouřil *et al.*, 2013, Grebe *et al.*, 2020).

In our thorough study focused on long-term light acclimation (Štroch *et al.*, 2022) we proved that the optimisation of photosynthetic capacity in spruce is much lower than in *At* and is characterised by the induction of protective mechanisms at a relatively significant level, including "locked-in" NPQ, photosynthetic control and CET around PSI, all of which lead to a decrease in its photosynthetic efficiency. Oppositely, *At* uses its adaptive capabilities with the main objective of increasing the LET capacity and thus photosynthetic efficiency at HL intensity and maintaining this state while minimising unnecessary involvement of regulatory processes represented by photosynthetic control and NPQ induction. In a brief comparison, it seems that the angiosperms are capable of faster and more efficient acclimation with precise regulation suitable even for sub-optimal conditions, but at the same time, they are not equipped to survive under extreme stress conditions. Oppositely, evolutionary older plants such as spruce seem to lack the regulatory precision evolved in evolutionary younger plants but are able to survive even under harsh environmental conditions.

In summary, spruce is an evolutionary enigma, and we are only at the beginning of discovering its evolutionary uniqueness. While on the one hand, it behaves as a shade-tolerant plant, on the other hand, it is able to withstand weather conditions of HL intensity combined with freezing temperatures. On closer inspection, however, this apparently highly adaptable plant uses rather sub-optimal protective mechanisms during the duration of stress conditions. This involves the induction and maintenance of the massive "locked-in" or S-NPQ at the high cost of a significantly lower PSII quantum yield and a higher rate of photooxidative damage than observed in angiosperms. The significance, or rather the impact of the evolutionary loss of LHCB3 and LHCB6 antennae combined with the exclusive presence of LHCB8 on the photosynthetic apparatus in spruce is not yet fully understood and would require further studies, both structural and functional. And although the results of our studies further characterised the specific features of this unique organism, such as the detailed composition of its C_2S_2 form of PSII sc with the additional presence of α-Toc/α-TQ in the structure, the absence of LHCB3, LHCB6 and the involvement of LHCB8 in the specific binding of M-trimer to PSII cc, the impact of unique PSII structure on the formation of larger PSII assemblies or long-term light acclimation strategies of this conifer, there are even more unanswered questions that would require further research.

3. Experimental methods

3.1. Plant material and growth conditions

Arabidopsis thaliana plants (wild type (Columbia), mutants *lhcb3* (SALK_020314c), *lhcb6* (SALK_077953) and double mutant *lhcb3+lhcb6* (Ilíková *et al.*, 2021) were grown under controlled conditions in a walk-in phytoscope for 6 to 7 weeks at 22 °C, 60 % humidity, light intensity of 120 μmol photons m^{-2} s^{-1} and with the 8-h light/16-h dark cycle. In the light acclimation studies, the pre-cultivated 32-days-old *At* plants were transferred to the growth chamber HGC1014 (Weiss, Germany) for 10–14 days and grown at three different light intensities of 20 μmol photons m^{-2} s^{-1} (low light (LL)), 100 μmol photons m^{-2} s^{-1} (normal light, (NL)) or 800 μmol photons m^{-2} s^{-1} (high light, (HL)). All other cultivation conditions were kept the same as in the pre-cultivation phase.

Norway spruce (*Picea abies* (L. Karst.)) and Scots pine (*Pinus sylvestris* (L.)) seedlings were grown under the same conditions as *At* plants, but with a 16-h light/8-h dark cycle. For the light acclimation studies, the pre-cultivated 11-weeks-old spruce seedlings were exposed to the same light conditions as for *At* mentioned in the previous paragraph.

3.2. Isolation of thylakoid membranes

Prior to isolation and depending on the main focus of the study, plants were either dark-adapted (DARK) for 30 min, harvested directly in the growth chamber either after one-hour acclimation to half intensity of growing light (1/2 LIGHT) or without acclimation under the growing light (LIGHT) and immediately transferred and processed under the green light. While for spruce seedlings, only the upper part, approx. 2 cm above the soil, was used for isolation, for *At*, whole rosettes were cut off and used. Thylakoid membranes were isolated according to the protocol described by Dau *et al.* (1995). If it was necessary to maintain the phosphorylation of the proteins in the sample in a given experiment, all buffers used for isolation were supplemented with 10 mM NaF, a phosphatase inhibitor. All isolations were performed under green light and samples were kept on ice throughout the whole procedure. The Chl content of the final thylakoid membrane suspension was determined spectrophotometrically by a pigment extraction in 80% acetone according to Lichtenthaler (1987). Aliquots containing 110 μg of Chls were shock-frozen in liquid nitrogen and further stored at -80 °C.

3.3. Clear-Native (CN), Blue-Native (BN) and 2D-SDS-Polyacrylamide gel electrophoresis (PAGE)

All protein complex separations by CN-PAGE reported in the attached publications were performed according to Nosek *et al.* (2017) with minor modifications. *At* thylakoid membranes were solubilised in an amount of 10 μg of Chls with α DDM prior to gel separation, using a detergent: Chl mass ratio of 15. Similarly, thylakoid membranes from spruce were solubilised using α DDM but with a higher mass ratio of detergent to Chl of 20. To obtain the final Chl concentration of 0.33 mg/ml, the sample was supplemented with buffer (50 mM HEPES (pH 7.2/NaOH), 0.4 M sucrose, 5 mM $MgCl_2$, 15 mM NaCl, 10 % glycerol) to a final volume of 30 μl. Thus, the final detergent concentration for *At* was 0.5% and for spruce 0.67%. After short, gentle mixing for less than one minute, the samples were immediately centrifuged at 20,000 g/4 °C for 10 min to remove un-solubilised membranes. The supernatant was loaded onto a gradient polyacrylamide gel (ranging from 4% to 8%) (Wittig *et al.*, 2007) without the stacking gel. The electrophoretic separation was performed in a Bio-Rad Mini protean tetra cell

system (Bio-Rad) under the following conditions: a constant current of 3.5 mA/15 min followed by a constant current of 7 mA until the visible front representing free LHCIIs reached the bottom of the gel. The visualisation and analysis of the CN-PAGE gel were performed using an Amersham Imager 600RGB gel scanner, using both transmission mode with white light illumination for the visualisation of all bands and fluorescence mode with 460 nm excitation filter and an emission filter of Cy5 (705BP40 = 705 ± 20 nm).

Separations of protein complexes by CN-PAGE in Section 4 were performed either under the same conditions described in the previous paragraph or under the optimised conditions specified in the figure legend. The main optimisation conditions included the use of different detergents (or their combination), their concentration and solubilisation time. Standardly used non-optimised times for solubilisation were as follows: ~ 2-minute incubation for α DDM, ~ 1-minute incubation for β DDM and ~ 10–15-minute incubation for digitonin.

If used in the experiment, amphipol was added to the already solubilised sample after removal of un-solubilised membranes at a final concentration of 1% (with exceptions, see Subsection 4.2.) and incubated for 10–15 minutes on ice in the dark, while NaF was added to the solubilisation buffer with a final concentration of 10mM.

Buffer exchanges for solubilisation and separation by CN-PAGE were also tested as a part of the optimisation. HEPES buffer was replaced by MES as follows: 25mM MES (pH 6.5/NaOH), 10mM $MgCl_2$, 10mM $CaCl_2$ and 25% glycerol. Very mild solubilisation of protein scs with aminocaproic acid (ACA) in solubilisation buffer was tested using the buffer prepared according to Rantala *et al.* (2017) with the following composition: 50mM BisTris (pH 7/HCl), 375mM ACA, 1mM EDTA and 10mM NaF.

In addition to the 4–8% gradient gel, other various gradients were tested as well, either (i) self-prepared, specifically the 4–10% and 4–12% separating gel, both with 4% stacking gel, or (ii) the 4–15% pre-casted gradient gel from Bio-Rad. The specifications for the amount of Chl loaded per well and its final concentration are specified in the figure legends. The conditions for electrophoretic separation were the same as those described in the previous paragraph with the exclusion of pre-casted gel, where the conditions were as follows: 75 V/30 min => 100 V/30 min => 125 V/30 min => 150 V/1 hour => 175 V/30 min => 200 V/1.25 hours.

Conditions for protein separation using BN-PAGE were mostly identical with CN-PAGE with few changes. The gel was supplemented with critical micelle concentration (CMC) of α DDM of 0,008%, the upper buffer was composed of 0.05M Tricine, 0.015M Bis-Tris and supplemented with Coomassie Brilliant Blue-G (CBB-G) to a final concentration of 235μM. This buffer was replaced with the same buffer without CBB-G approx. one hour after separation was initiated. The loading buffer was the same as for CN-PAGE but was supplemented by CBB buffer composed of 0.75M ACA and 50mM CBB-G in a 1:9 ratio in the supernatant after solubilisation and centrifugation of the samples.

2D-SDS-PAGE was performed according to Laemmli (1970) with minor modifications. The gel was composed of 5% stacking gel and 12% separating gel (see Tab. 4 for detailed composition and gel dimensions). The cathode (upper) buffer was composed of: 25mM Tris, 0.192M glycine and 3.5mM SDS, and the anode (lower) buffer was composed of 25mM Tris (pH 8.3/HCl).

After incubation of gel strips from the first dimension in SDS buffer (25mM Tris (pH7.5/HCl), 35mM SDS) for 30 min, the strips were applied on the stacking gel and fixed in position by embedding in homogeneously dissolved 0.6% agarose in the upper buffer. The electrophoresis conditions were as follows: 10 mA/30 min => 20 mA/6.75 hours => 30 mA/0.75 hours => 40 mA/1.5 hours with continuous cooling at 4 °C.

Table 3: Composition of 2D-SDS-PAGE gel

Step	separating gel [12% acryl amid]	stacking gel [5% acryl amid]
Urea [g]	10.4	
Gel buffer 4x [ml] 2.8M Tris (pH 8.6/HCl)	5.67	2.4
Water [ml]	5.27	6.5
50% acrylamide [ml] 50% T, 2.6% C	6	1
TEMED [µl]	20	10
APS [µl]	200	50
Volume [ml]	~ 25	~ 10

Dimensions of the gel: width x height x thickness = 16.2 x 16 x 0.13 cm

3.4. Spontaneous elution and dialysis

Spontaneous elution of separated protein complexes and scs was performed from excised gel bands according to Kouřil *et al.* (2014) with two exceptions, (i) buffer was supplemented with the CMC concentration of α DDM and (ii) for less dense bands, the elution was carried out overnight rather than for 2–4 hours.

3.5. Silver staining

Silver staining was carried out according to Blum (1987) with minor modifications (see Tab. 5). After stopping the development and a short wash with Milli-Q water, the gel was scanned with an Amersham Imager 600RGB gel scanner, using the transmission mode with white light illumination.

Table 4: Protocol used for silver staining of the gel

Step	Chemical/water	Solution (500 ml)	Time of incubation
Fixing (1)	30% ethanol	150 ml	1 h
	10% acetic acid	50 ml	
Washing (2)	20% ethanol	100 ml	15 min
Washing (3)	Milli-Q H_2O		15 min
Sensitisation (4)	$Na_2S_2O_3$ x 5 H_2O	0.1 g	90 s
Washing (5)	Milli-Q H_2O		2 x 20 s
Staining (6)	$AgNO_3$	1 g	30 min
Washing (7)	Milli-Q H_2O		2 x 10 s
Developing (8)	K_2CO_3	15 g	~ 5 min
	Formaldehyde	350 µl	
	Sensitisator (step 4)	25 ml	
Stopping (9)	Tris-base	25 g	2 min
	2.5% acetic acid	12,5 ml	

3.6. Ultracentrifugation

Separation of solubilised pigment-protein complexes on a sucrose gradient by ultracentrifugation reported in the attached publications was performed according to Caffarri *et al.* (2009) with slight modifications. An aliquot of thylakoid membranes containing 200 µg of Chls was centrifuged at 4,600 g/4 °C/4 min, and the pellet was resuspended in 10 mM HEPES (pH 7.5/NaOH) to a Chl concentration of 2 mg/ml. The membranes were then solubilised by α DDM in 10 mM HEPES (pH 7.5/NaOH) with a final concentration of 1% to 0.5 mg/ml of Chls (detergent: Chl mass ratio was 20) and gently vortexed for a few seconds. The sample was subsequently centrifuged at 18,000 g/4 °C/10 min to remove un-solubilised membranes residues and then separated by ultracentrifugation on a sucrose gradient at 284,000 g/4 °C/18 hours (P40ST Swinging Bucket Rotor, ultracentrifuge Hitachi, CP90WX). Gradients were formed directly in the tube by freezing at - 80 °C and subsequent thawing at 4 °C and of 0.65M sucrose solution in 10 mM HEPES (pH 7.5/NaOH) containing CMC of α DDM. The collected PSII fractions from each tube were combined and concentrated using a Millipore Amicon filter with a 50 kDa cut-off at 14,000 g/4 °C/5 min. The sample was then washed twice in 10 mM HEPES (pH 7.5/NaOH) buffer with CMC of α DDM to remove sucrose. The concentrated sample was used directly for specimen preparation for cryo-EM analysis.

In order to further optimise the ultracentrifugation on a sucrose gradient, different buffers with added stabilisers, solubilisation conditions and gradient preparation mechanism were used in addition to the above-mentioned protocol. Two commonly used biological buffers, HEPES (10mM, pH 7.5/NaOH) and MES (25mM, pH 6.5/NaOH), were tested. According to the sucrose gradient preparation method, in addition to the freeze/thaw method mentioned above, gradients were prepared using the Gradient Master device (Model 108, BioComp Instruments, Fredericton, Canada). Sucrose gradients of the required range were prepared by mixing a given amount of light and heavy sucrose solution. The light and heavy solutions consisted of 10% and 30%/40% sucrose, respectively, as well as a buffer component (HEPES or MES) and the CMC of detergent used for solubilisation. An aliquot of the thylakoid membrane stock solution containing 200 µg of Chls was resuspended in a specific buffer (HEPES or MES) to a final Chl concentration of 1 mg/ml after a brief centrifugation at 4,600 g/4 min/4 °C. Subsequently, a buffer with a given concentration of detergent and optional additives was added to the samples, with a final Chl concentration of 0.5 mg/ml. Samples with α DDM were shortly vortexed and solubilised for a maximum of 2 minutes (1 min for β DDM); samples with digitonin were solubilised for approx. 10–15 minutes with gentle vortexing. Optional additives were used as follows: (i) 1M betaine was already included in the light and heavy solutions used to form the sucrose gradient, (ii) 10mM NaF was added into the solubilising buffer, and (iii) 1% amphipol was added into the already solubilised sample after centrifugation and incubated on ice for 10 minutes. Specifications of the loading amount of Chl and its final concentration are specified in the figure legends. The ultracentrifugation was performed at 284,000 g at 4 °C, with the total centrifugation time depending on the type of gradient (see figure legends for further specifications).

3.7. Western blot

Western blot was performed on proteins isolated from thylakoid membranes using the following procedure. A mixture with a ratio of 100 µg Chls per 1 ml of extraction buffer (14 mM DL-dithiothreitol, 28 mM Na_2CO_3, 175 mM sucrose, 5% (w/v) SDS, and 10 mM EDTA-Na_2) was properly mixed and incubated at 70 °C for 30 min followed by centrifugation at room temperature for 10 min/19,200 g. The supernatant containing the isolated proteins was supplemented with the sample buffer (Tricine Sample Buffer, Bio-Rad; 3x diluted) and dH_2O to a final volume of 20 µl with a final Chl concentration of 50 µg/ml (calculating with their hypothetical 100% extraction efficiency). After 10 minutes of incubation of this mixture at 70 °C, the entire volume was loaded onto a 10% gel (Mini-PROTEAN TGX Precast Protein Gel, Bio-Rad, Hercules, USA). The used running buffers were prepared according to Schägger (2006). The electrophoretic separation conditions were: constant voltage of 100 V/45 min. Separated proteins were transferred from the gel to the polyvinylidene fluoride membrane using Trans-Blot Turbo RTA Mini 0.2 mm PVDF Transfer Kit (Bio-Rad) and subsequently detected on the membrane by a system of two antibodies. The binding of the primary antibodies Anti-LHCB3 (AS01 002) and Anti-LHCB6 (AS01 010) (Agrisera) was detected by a secondary antibody with HRP-enzyme. All antibodies used in this study were purchased from Agrisera. After incubation with Immobilon Western Chemiluminescent HRP Substrate, the emitted chemiluminescent signal was visualised using chemiluminescence mode on the Amersham Imager 600RGB gel scanner.

3.8. Electron microscopy - sample preparation, data processing

Specific PSII scs ($C_2S_2M_2$/C_2S_2M/C_2S_2) and PSII mcs separated by gel electrophoresis were, for structural analysis by electron microscopy and SPA or for sample quality verification, obtained from excised gel bands by spontaneous elution according to Kouřil *et al.* (2014) with modifications (see Subsection 3.4.). After overnight elution, the eluted protein complexes were applied on the glow-discharged, carbon-coated copper grid and negatively stained with a 2% aqueous solution of uranyl acetate. Electron microscopy was performed on an FEI Tecnai G2 F20 microscope (FEI, Eindhoven, The Netherlands) operated at 200 kV. Images were recorded with an Eagle 4K CCD camera (FEI, Eindhoven, The Netherlands) at the final magnification of 134,028x, with the final pixel size of 2.24 Å at the specimen after binning the images to 2048 x 2048 pixels.

The recorded images were subjected to SPA using the Scipion3 image processing framework, which included a correction of the contrast transfer function (CTF) of the microscope in individual images, semi-automated particle selection and their classification into 2D classes.

The best-resolved classes representing projection maps of the most abundant types of PSII scs/mcs were fitted by a structural model of PSII scs from *At* (van Bezouwen *et al.*, 2017). The "spruce-type" PSII sc was fitted with the model of Kouřil *et al.* (2016).

Electron microscopy of isolated grana membranes from *At* and spruce, isolated according to Kouřil *et al.* (2013), was performed either on the FEI Tecnai G2 F20 microscope (FEI, Eindhoven, The Netherlands) with the Eagle 4K CCD camera ((FEI, Eindhoven, The Netherlands) or on a Jeol JEM2010 (Jeol, Tokyo, Japan) with a Quemesa CCD camera (EMSIS, Muenster, Germany).

4. Optimisation of the experimental approach to the structural analysis of spruce photosystem I and photosystem II

4.1. Optimal sample preparation - choice of solubilisation conditions and method of separation

The experimental approach of isolation procedure depends primarily on the character of the required protein complex that will be further analysed and the natural environment from which the selected protein complex is going to be extracted. Focusing on photosynthetic organisms, it is important to realise that evolutionary adaptation to a specific habitat led to the evolution of their own specific characteristics. As a result, different organisms may contain or produce different chemical substances, enzymes, etc., which may affect the efficiency of the used experimental method. Thus, for almost every organism, the solubilisation conditions need to be carefully adjusted.

Sample quality and quantity are particularly important for high-throughput methods capable of providing detailed information about the analysed organism. An example is the cryo-EM method, which can provide high-resolution structures of proteins and their complexes, however, the quality of the final electron density map is highly dependent on the quality of the original sample. The most important sample properties are high concentration of the studied protein, purity and structural homogeneity. Moreover, extraction of a specific protein complex embedded in the thylakoid membrane while maintaining its intactness is quite challenging and specific approaches have to be used. For this purpose, mild solubilisation reagents are used for their gentle extraction from the thylakoid membrane, followed by non-denaturing separation methods for retrieval of the selected protein complex from its heterogeneous environment, including CN-PAGE or ultracentrifugation.

Thereby, in the following subsections, I discuss several obstacles encountered during sample processing with standard biochemical techniques, along with adequately designed solutions or improvements.

4.1.1. Solubilisation conditions and increase of protein complexes stability

An important step in customising the solubilisation is the choice of buffer necessary to maintain a defined pH that helps to preserve the integrity of the solubilised proteins of the thylakoid membrane. Although HEPES was initially preferred due to its ability to maintain a near-neutral pH of 7.5, later, it was shown that the scs might be more stable at lower pH. Therefore, we opted for another commonly used buffer, namely MES, with pH of 6.5 (Crepin *et al.*, 2016).

Further, we optimised the conditions of solubilisation with the main objective to obtain the highest yield of specific protein sc while preserving its maximum intactness. The generally used α DDM or β DDM, mild non-ionic detergents, provide the best alternative in most cases, with high yields of solubilised protein complexes without their excessive unfavourable rate of disintegration. The other most commonly used non-ionic detergent is digitonin with more than 50 % higher molecular weight than maltosides. The amphiphilic character of the aforementioned detergents allows the extraction of membrane proteins from their constrained natural environment and, by providing them with a substitutional bilayer envelope, preserve them in a soluble form (Lichtenberg *et al.*, 2013).

The milder α DDM and the stronger detergent β DDM are commonly used to extract PSII scs from appressed grana, since their size is smaller than the size of digitonin, and they can easily fit between the grana. While the application of α DDM on *At* thylakoid membranes leads to

preferential extraction of larger PSII scs and the presence of PSI and PSII mcs, the use of stronger β DDM leads to an almost complete disintegration of these mcs and preferential extraction of smaller PSII sc forms. This phenomenon is accompanied by the higher abundance of free LHCIIs in the form of monomers or trimers (Fig. 5).

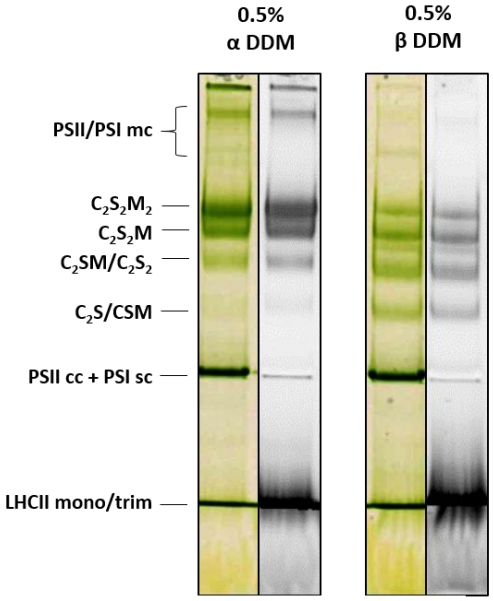

Figure 5: Different solubilisation efficiency of α and β DDM on *Arabidopsis thaliana* thylakoid membranes harvested for isolation after 30 min of dark adaptation. Electrophoretic separation using CN-PAGE of *At* thylakoid membranes solubilised with either 0.5% α DDM or 0.5% β DDM, final Chl concentration of 0.33 mg/ml. Images of selected lines from the gel were scanned at room temperature in the transmission mode (green lines) and in fluorescence mode (black and white lines). *Abbreviations: PSII - photosystem II, PSI - photosystem I, LHCII - light-harvesting complex of photosystem II, mc - megacomplex, sc - supercomplex, cc - core complex, mono - monomer, trim - trimer.*

Digitonin represents a mild detergent, milder than maltoside, and due to its size, it cannot fit into the appressed grana of the thylakoid membrane of higher plants. This fact makes the digitonin more suitable either (i) for extraction of the whole grana or (ii) for preferential extraction of PSI scs due to their localisation in the peripheral parts of grana, grana margins and stromal lamellae. For example, digitonin can be used to extract fragile scs such as PSI-LHCII sc (transition state 2) from *At*, spruce, barley, etc.

Using digitonin only, we were able to obtain the PSI-LHCII sc even from dark-adapted plants. This phenomenon was observable after the separation of solubilised thylakoid membranes either by electrophoresis or ultracentrifugation (Fig. 6, A and 7, IV). These results are consistent with the observations by Chukhutsina *et al.* (2020) and imply that plants are able to preserve the PSI-LHCII scs (state 2) even in the dark-adapted state *in vivo* for a closer unspecified period of time. We could hypothesise that their existence, even in the absence of light irradiation, is the consequence of their slower disassembly associated with slower dephosphorylation or that the stable pool of PSI-LHCII is deliberately preserved in plants and has functional relevance.

The main conditions optimised for detergents are their final concentration (or Chl to detergent ratio) and incubation time with the sample. Nevertheless, it is possible to also combine the detergents to achieve more efficient extraction. By combining detergents, lower concentrations of a stronger detergent can be used to mitigate its negative effect on the fragile bonds between the individual subunits (Galka *et al.*, 2012; Crepin *et al.*, 2020). Application of low concentrations of digitonin in *At* thylakoid membranes promotes the preferential extraction of the PSI scs and only limited extraction of PSII scs even with longer incubation times. When samples solubilised in the first round with digitonin undergo solubilisation by two times higher concentration of α DDM that is standardly used, the characteristic pattern of separated PSII scs is clearly visible, whereas the yield of the PSI scs is lower due to their previous extraction by digitonin, and PSI-LHCII is absent (Fig. 6, A). The combination of digitonin and α DDM at

low concentrations simultaneously supplemented with NaF allows for significantly more efficient extraction of PSI scs involving the fragile PSI-LHCII sc in both spruce and *At*, while application of α DDM alone, even supplemented with NaF, leads to an enormous disintegration of this sc, more pronounced in *At* than in spruce (Fig. 6, B).

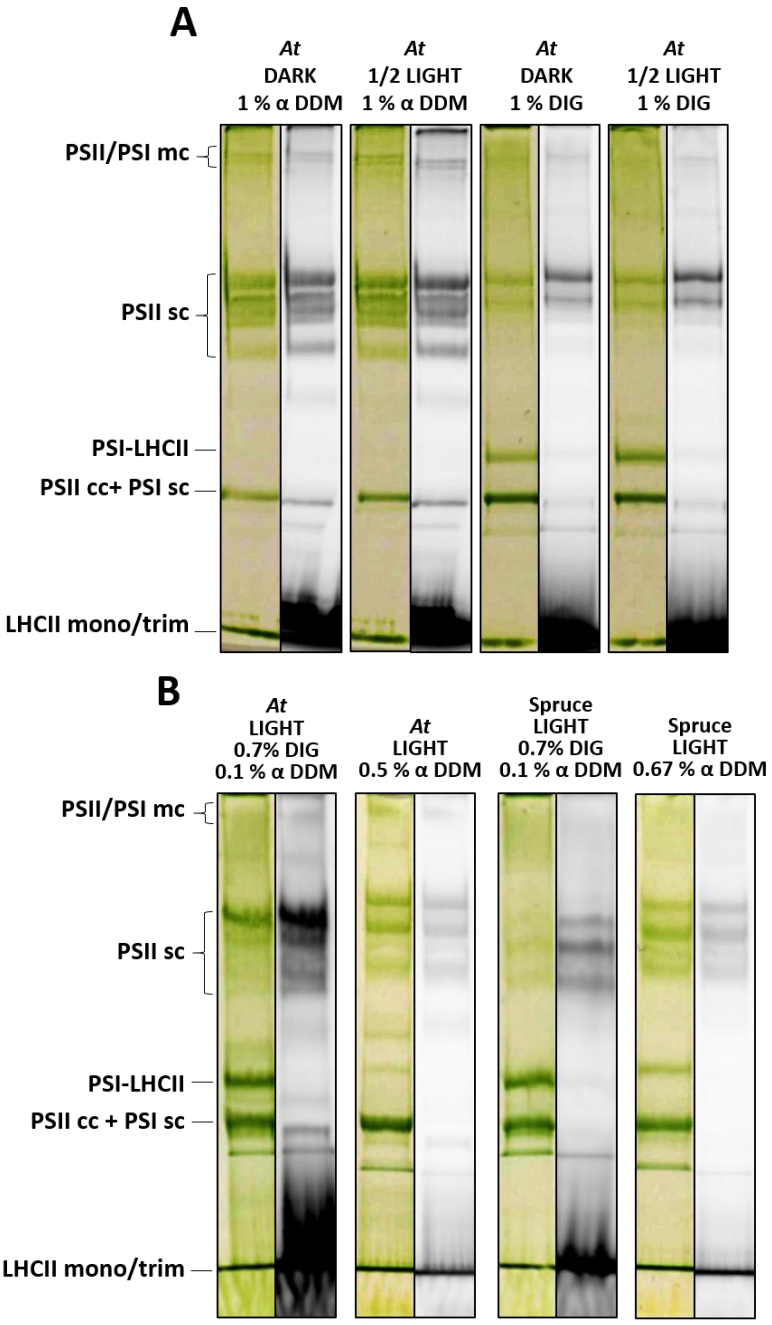

Figure 6: Different solubilisation efficiency of α DDM, digitonin and combination of α DDM and digitonin on *Arabidopsis thaliana* and spruce thylakoid membranes and stability of their PSI-LHCII supercomplex. Electrophoretic separation using CN-PAGE of *At* and spruce thylakoid membranes solubilised with A) 1% digitonin at Chl concentration of 0.33 mg/ml or 1% α DDM after previous solubilisation with 1% digitonin; B) combination of 0.7% digitonin with 0.1% α DDM at Chl concentration of 0.5 mg/ml or, solubilisation with 0.67% and 0.5% α DDM for spruce and *At*, respectively, both at Chl concentration of 0.33 mg/ml and supplemented with 10mM NaF. Membranes were harvested for isolation either after 30 min of dark adaptation (DARK), after one-hour adaptation to half intensity of growing light (1/2 LIGHT), or directly from growing light (LIGHT). Images of selected lines from the gel were scanned at room temperature in transmission mode (green lines) and in fluorescence mode (black and white lines). *Abbreviations: At - Arabidopsis thaliana, PSII - photosystem II, PSI - photosystem I, LHCII - light-harvesting complex of photosystem II, mc - megacomplex, sc - supercomplex, cc - core complex, mono - monomer, trim - trimer, DIG - digitonin.*

When working with fragile membrane protein complexes, the use of stabilisers should be considered. In optimising the extraction of the PSI or PSII scs while maintaining their intactness, we opted for three stabilisers, namely amphipol, betaine and NaF.

I) Amphipols are surfactants that substitute the detergents used for membrane protein solubilisation and replace them in the surrounding envelope of extracted protein complexes. Amphipols increase the stability of proteins and prevent their aggregation in a detergent-free environment. The most commonly used amphipol A8-35 is suitable even for sample preparation for cryo-EM (see, e.g. Flötenmeyer *et al.*, 2007).

II) Betaine is a small, highly soluble osmolyte that neutralises differences in osmotic pressure, allowing organisms to adapt to changing environment and abiotic stress caused by salinity. Betaine is also known to protect and stabilise the OEC against the dissociation of its subunits from PSII and to coordinate the included Mn cluster (Murata *et al.*, 1992; Papageorgiou and Murata, 1995).

III) NaF is an acid and serine/threonine phosphatase inhibitor, which preserves the phosphorylation state of extracted proteins. The preservation of proteins in their phosphorylated state has important implications for protein analysis, as this type of modification often determines their function and associated structural characteristics (Vener *et al.*, 1999, 2001).

4.1.2. Selection of suitable separation method and its optimisation

CN-PAGE is the ideal method for the separation of solubilised protein complexes of the photosynthetic apparatus. However, it is disadvantageous to combine CN-PAGE with methods that require high concentration of specific protein complex, such as cryo-EM. On the other hand, ultracentrifugation on a sucrose gradient currently represents the most suitable method for the separation of fragile complexes from thylakoid membranes that simultaneously reaches the cryo-EM standards.

The fractions of PSII scs from spruce in our work (Opatíková *et al.*, 2023) were obtained by ultracentrifugation, using gradient preparation by the freeze/thaw method as described by Caffarri *et al.* (2009). However, the separation was sub-optimal, as the fractions of individual scs, albeit separated, were mostly diffused. Hence, we have begun optimising this method and looking for further improvements in how to preserve intact scs and increase their stability.

The first step was to change the method of gradient preparation, for which we used Gradient Master instead of the commonly used freeze/thaw protocol. This way of preparation provided a significant breakthrough in the quality of separation of solubilised protein complexes. This device is designed to prepare the gradients with variable concentration ranges of the main gradient carrier. Its preparation is fast and precise, and the resulting gradient has smoother transitions, resulting in less diffused and less dispersed fractions with sharper edges (Fig. 7). Moreover, in combination with the optimised buffer pH and addition of aforementioned stabilisers such as NaF, betaine and amphipol, the quality and intactness of separated protein complexes has significantly increased, which can be confirmed by detailed structural analysis of extracted proteins by cryo-EM.

The necessity to optimise and improve the currently used methods is evident from the results obtained for spruce (Opatíková *et al.*, 2023). In spruce, the commonly abundant C_2S_2M and the slightly less populated $C_2S_2M_2$ forms, although present in our fraction from sucrose gradient, were underrepresented in the final data set after cryo-EM analysis, moreover, with the loss of two subunits from OEC and PsbJ subunit, all located at PSII periphery. We ascribed this loss to the suboptimal preparation conditions that increased the susceptibility of the extracted particles to the environment and made them more prone to disintegration.

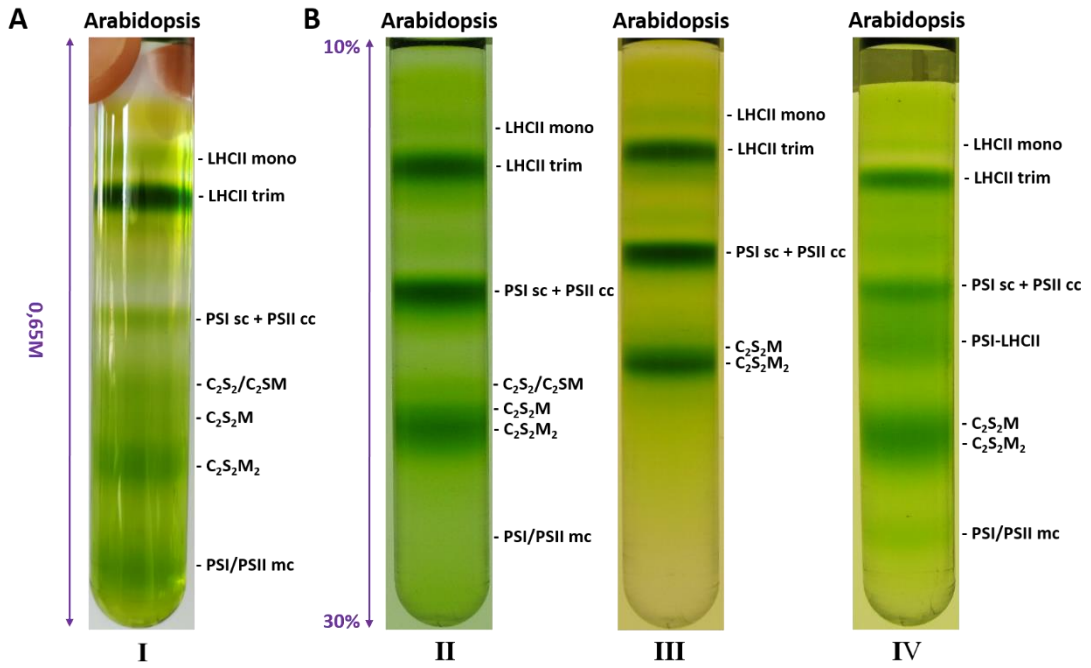

Figure 7: Optimisation of separation on sucrose gradient for solubilised thylakoid membranes from *Arabidopsis thaliana* harvested for isolation after 30 min of dark adaptation. Comparison of sucrose gradients prepared A) from 0.65M sucrose by freezing and consequential thawing at 4 °C and B) gradients prepared with Gradient Master in the range of 10 – 30% sucrose. Thylakoid membranes were solubilised and separated under different conditions as follows: I (0.75% α DDM, 10mM HEPES (pH 7.5/NaOH), Chl concentration of 0.5 mg/ml, 17 hours of separation); II (0.75% α DDM + 1% amphipol, 25mM MES (pH 6.5/NaOH), Chl concentration of 0.5 mg/ml, 13 hours of separation); III (0.75% α DDM + 1% amphipol, 25mM MES (pH 6.5/NaOH) + 1M betaine, Chl concentration of 0.5 mg/ml, 16 hours of separation); IV (1% digitonin + 1% amphipol, 25mM MES (pH 6.5/NaOH) + 1M betaine, Chl concentration of 0.33 mg/ml, 16 hours of separation). *Abbreviations: PSII - photosystem II, PSI - photosystem I, LHCII - light-harvesting complex of photosystem II, mc - megacomplex, sc - supercomplex, cc - core complex, mono - monomer, trim - trimer.*

4.2. State transitions in spruce

State transitions are characterised by the balancing of the energy absorption between the two photosystems. Upon preferential excitation of PSII, a significant reduction of PQ via thioredoxins leads to the activation of the specific kinase STN7/STT7 (in higher plants and green algae, respectively). Activated kinase phosphorylates LHCIIs (LHCB1 and LHCB2) (Bellaflore *et al.*, 2005), with the maximum phosphorylation observed under non-saturating light conditions (Rochaix *et al.*, 2014). Phosphorylated LHCII trimers bind to the PSI and effectively transfer the harvested energy to its RC.

The only high-resolution cryo-EM structure of the PSI-LHCII sc in higher plants has been solved for *Zm* at 3.3 Å resolution with one bound LHCII trimer (Pan *et al.*, 2018) and for the green alga *Cr* at 3.42 Å (Huang *et al.*, 2021) and 2.84 Å (Pan *et al.*, 2021) resolution with two bound LHCII trimers. In addition, the lower resolution of PSI-LHCII sc structures has been obtained for other land plants *At* (Kouřil *et al.*, 2005a, Yadav *et al.*, 2017), *Pisum sativum* (Qin *et al.*, 2015; Mazor *et al.*, 2015, 2017) or the moss *Pp* (Yan *et al.*, 2021; Gorski *et al.*, 2022).

Interestingly, the structural studies of this sc in land plants, combined with biochemical and fluorescence measurements data (see, e.g. Benson *et al.*, 2015; Yadav *et al.*, 2017; Schwartz

et al., 2018), strongly indicate the possibility of biding more than one LHCII trimer, as is characteristic for green algae. In *At* Yadav *et al.* (2017) observed attachment of a second LHCII trimer on the side of the LHCI belt of PSI in variable positions. However, the confirmation of PSI-LHCII$_{(n)}$ existence in higher plants remains controversial due to the absence of specific band or fraction in CN-PAGE or ultracentrifugation that would represent this supercomplex. Any structural confirmation is then biochemically unsupported.

In relation to Yadav *et al.* (2017), we observed this larger PSI-LHCII$_2$ sc also in spruce as a contaminant of the PSI-LHCII fraction obtained by CN-PAGE. Nevertheless, due to its low abundance and the relatively substantial variability in the second trimer binding position (higher than observed for *At*, Yadav *et al.*, 2017), the resulting resolution was sufficient only for the characterisation of the different binding positions of the second LHCII trimer (Fig. 8), however insufficient for a more detailed structural analysis. We hypothesise that the high variability of the second trimer position towards the PSI cc is responsible for a non-uniform migration of the specific PSI-LHCII$_2$ sc forms and thus underlies the difficulty in achieving its unique, clearly visible band/fraction by standard separation. Therefore, we aimed our efforts at obtaining a specific band/fraction where the PSI-LHCII$_2$ sc represents the major moiety.

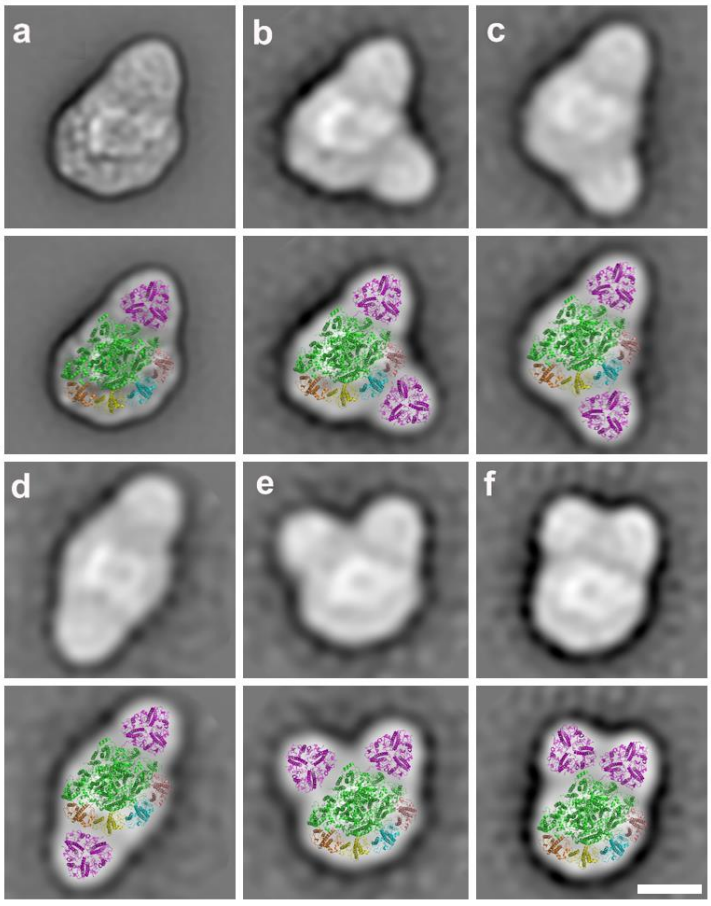

Figure 8: Projections maps of PSI-LHCII and PSI-LHCII$_{(2)}$ supercomplexes from spruce obtained by single particle electron microscopy. Projections were fitted with the known high-resolution structure of maize PSI-LHCII (Pan *et al.*, 2018, PDB identifier 5ZJI). A) Sc composed of PSI sc and one LHCII trimer attached to PSI cc subunits PsaA and PsaH, B–D) scs composed of PSI and two LHCII trimers with the second trimer attached in different positions within LHCA belt (via LHCA2/3 dimer, via both antennae LHCA2 and LHCA4 or via LHCA1/4 dimer), E–F) scs composed of one PSI and two LHCII trimers, the second trimer attached directly to the PSI cc. Structural assignment: PSI cc (green), LHCA1–4 (orange, blue, brown, yellow, respectively), LHCII trimer (magenta). The scale bar is 10 nm. Adapted from Arshad (2022).

Using our standardly optimised conditions for solubilisation (0.5% and 0.67% α DDM for *At* and spruce, respectively) and running 4–8% gradient CN-PAGE, the band with the major abundance of PSI-LHCII is clearly visible in both plants, localised above the band with co-migrating PSI sc and PSII cc (Fig. 9).

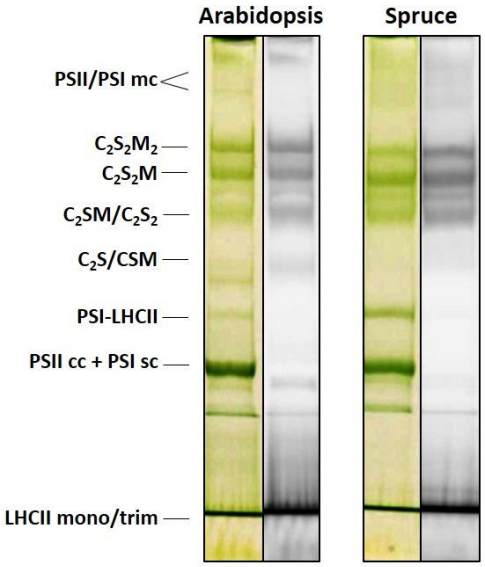

Figure 9: CN-PAGE of solubilised thylakoid membranes from spruce and *Arabidopsis thaliana* harvested for isolation directly from growing light. Electrophoretic separation of spruce and *At* thylakoid membranes solubilised with 0.67% and 0.5% α DDM, respectively, at a final Chl concentration of 0.33 mg/ml. Images of the selected lines from the gel were scanned at room temperature in transmission mode (green lines) and fluorescence mode (black and white lines). *Abbreviations: PSII - photosystem II, PSI - photosystem I, LHCII - light-harvesting complex of photosystem II, mc - megacomplex, sc - supercomplex, cc - core complex, mono - monomer, trim - trimer.*

To improve the PSI-LHCII$_2$ extraction from spruce, we tested: i) other detergents and their combination with α DDM, ii) MES buffer for the preservation of lower pH during solubilisation and separation, iii) buffer containing ACA, which loosens the appressed grana that are then more accessible to the milder detergent digitonin, iv) different gradient of acrylamide gel or pre-casted gel, and, v) different separation method, namely ultracentrifugation on a sucrose gradient. Only relevant results are described below.

Simultaneous application of α DDM and digitonin for solubilisation confirmed the previously observed phenomenon that the combination of these two detergents has a milder negative effect on weaker bonds and significantly enhances the extraction of fragile PSI-LHCII scs (Galka *et al.*, 2012). However, we did not observe the presence of the unique PSI-LHCII$_2$ band (Fig. 10), although electron microscopy confirmed the presence of this particle in small amounts as a contaminant in the PSI-LHCII band.

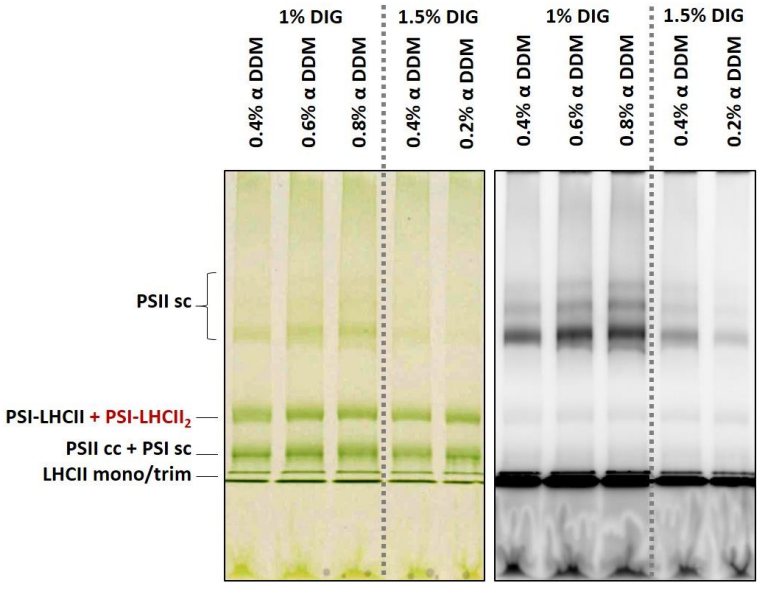

Figure 10: CN-PAGE of solubilised thylakoid membranes from spruce harvested for isolation directly from growing light. Electrophoretic separation of spruce thylakoid membranes solubilised with a combination of different concentrations of digitonin and α DDM (described in the line titles) at a final Chl concentration of 0.5 mg/ml. Images of the gel were scanned at room temperature in transmission mode (green image) and in fluorescence mode (black and white image). *Abbreviations: PSII - photosystem II, PSI - photosystem I, LHCII - light-harvesting complex of photosystem II, sc - supercomplex, cc - core complex, mono - monomer, trim - trimer, DIG - digitonin.*

The lower pH of 6.5 preserved by MES buffer, addition of amphipol a8-35 and broader acrylamide gradient of 4–10% or 4–12%, both with a 4% stacking gel, did not lead to obtaining a single specific band for PSI-LHCII$_2$.

Using only the milder detergent digitonin in combination with ACA solubilisation buffer according to Rantala *et al.* (2017) and separation on the 4–15% pre-casted gel, we were able to detect the intended PSI-LHCII$_2$ by TEM, however, only as a contaminant of other band containing mainly C_2S_2 PSII sc. Therefore even this separation cannot be considered to be a suitable method for its separation (Fig. 11).

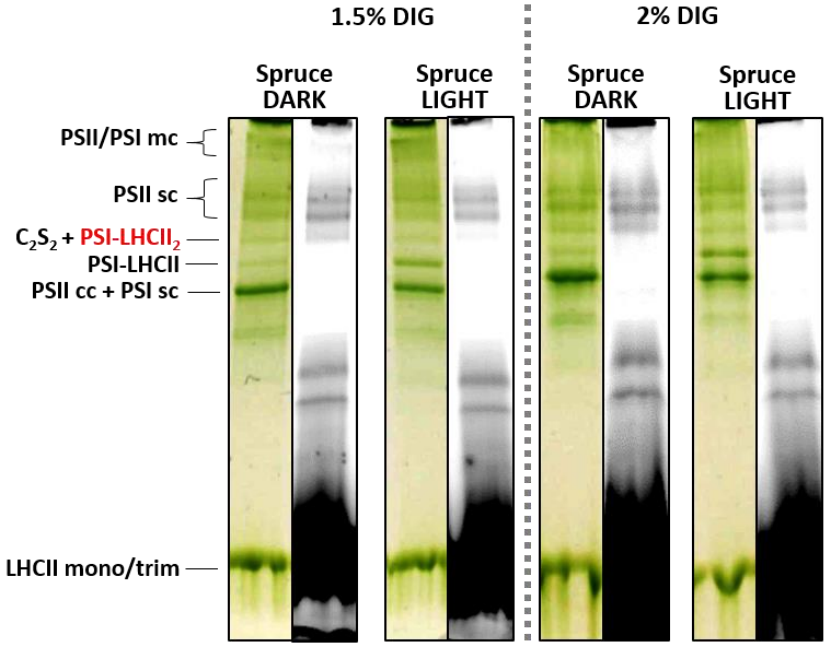

Figure 11: CN-PAGE of solubilised thylakoid membranes from spruce harvested for isolation either directly from growing light (LIGHT) or after 30 min of dark adaptation (DARK). Electrophoretic separation of spruce thylakoid membranes solubilised with 1.5 or 2% digitonin and final Chl concentration of 0.5 mg/ml with 10mM NaF in ACA buffer (loading of 25 µl per well), supplemented with 0.1% sodium deoxycholate after solubilisation, separated in 4–15% pre-casted gradient gel. Images of the selected lines from the gel were scanned at room temperature in transmission mode (green lines) and in fluorescence mode (black and white lines). *Abbreviations: PSII - photosystem II, PSI - photosystem I, LHCII - light-harvesting complex of photosystem II, mc - megacomplex, sc - supercomplex, cc - core complex, mono - monomer, trim - trimer, DIG - digitonin.*

Nevertheless, without any promising results from electrophoretic separation, we opted for separation on sucrose gradient, where we tested combinations of different (i) buffers (HEPES (pH 7.5/NaOH) or MES (pH 6.5/NaOH)), (ii) detergents (α DDM, digitonin), (iii) and different additives such as amphipol, betaine and NaF (Fig. 12). As discussed in the previous section, the gradient prepared by Gradient Master provides significantly higher resolution of the separated protein complexes, especially PSII scs and PSI/PSII mcs, under standard conditions compared to the separation on the gradient prepared by freezing at -80°C and thawing at 4°C (Fig. 12, I–II). The combination of 0.5–1% digitonin with a low concentration of α DDM (0.1–0.2%) allows the prevalent extraction of PSI scs, with the main two bands of interest further analysed and designated as the PSI sc co-migrating with PSII cc (upper one, No. 3 in Fig. 12) and the fragile PSI-LHCII sc (lower one, No. 4 in Fig. 12) (Fig. 12, III–V and VII). The highest yield of PSI-LHCII fraction was obtained with a combination of 1% digitonin and 0.2% α DDM supplemented with 0.6% amphipol separated in MES buffer at pH 6.5 with the addition of 1M betaine (Fig. 12, VII). Although the minor presence of PSI-LHCII$_2$ was confirmed in PSI-LHCII fraction, we were unable to obtain its exclusive fraction.

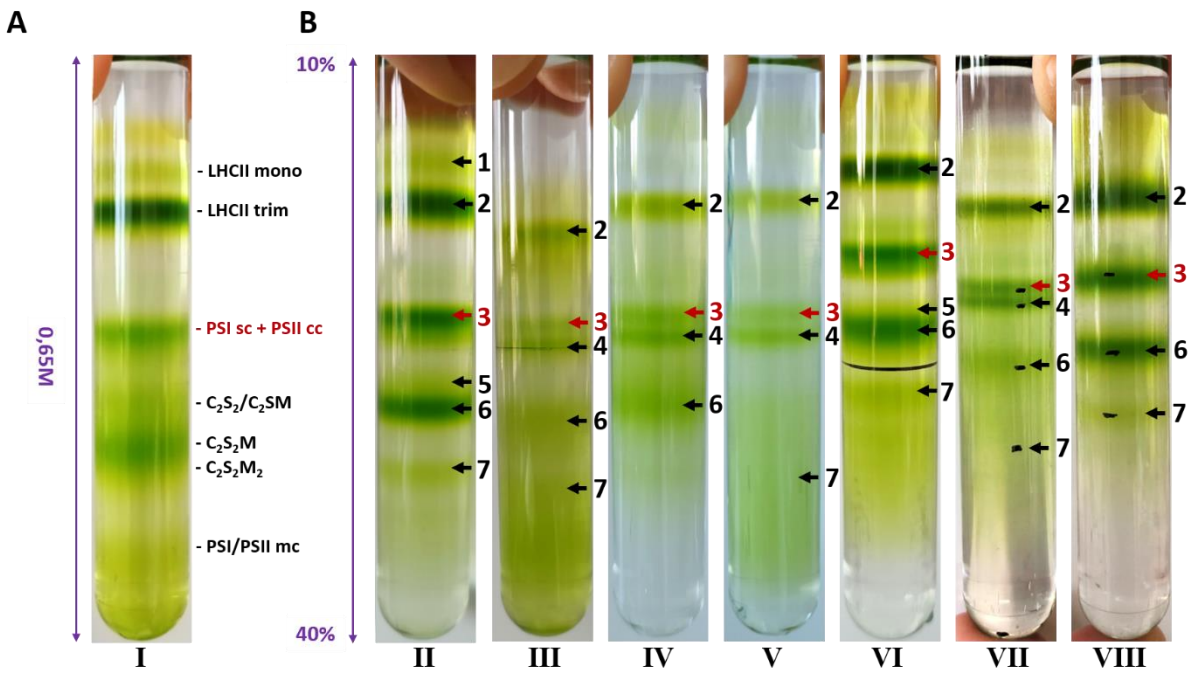

Figure 12: Optimisation of thylakoid membrane solubilisation, the preparation method of sucrose gradient, buffer composition, and addition of optional stabilisers to obtain PSI-LHCII$_2$ fraction from spruce. Thylakoid membranes were harvested for isolation directly from growing light. Images of solubilised thylakoid membranes from spruce, final Chl concentration of 0.5 mg/ml, separated by ultracentrifugation under different conditions: I and II (1% α DDM, 10mM HEPES (pH 7.5/NaOH)); III (0.1% α DDM + 0.5% digitonin, 10mM HEPES (pH 7.5/NaOH)); IV (0.2% α DDM + 1% digitonin + 10mM NaF + 1% amphipol, 10mM HEPES (pH 7.5/NaOH)); V (0.1% α DDM + 0.5% digitonin + 10mM NaF + 1% amphipol, 10mM HEPES (pH 7.5/NaOH)); VI (1% α DDM + 10mM NaF + 1% amphipol, 25mM MES (pH 6.5/NaOH) + 1M betaine); VII (0.2% α DDM + 1% digitonin + 10mM NaF + 0.6% amphipol, 25mM MES (pH 6.5/NaOH) + 1M betaine); VIII (2.5% α DDM + 1% digitonin + 10mM NaF + 0.7% amphipol, 25mM MES (pH 6.5/NaOH) + 1M betaine). Gradients I, VII and VIII: 17 hours of separation, II–V: 14 hours of separation and VI: 15 hours of separation. Protein complexes labelled with numbers as follows: 1 - LHCII monomers, 2 - LHCII trimers, 3 - PSI sc + PSII cc, 4 - PSI-LHCII, 5 - C_2S_2/ C_2SM, 6 - PSII scs ($C_2S_2M_2$ + C_2S_2M), 7 - PSI/PSII mcs. A) Gradient prepared from 0.65M sucrose by freezing and thawing and B) gradients prepared by Gradient Master in the range of 10 - 40% sucrose. Fractions representing PSI sc co-migrating with PSII cc are highlighted in red colour for easier orientation within the gradient. *Abbreviations: PSII - photosystem II, PSI - photosystem I, LHCII - light-harvesting complex of photosystem II, mc - megacomplex, sc - supercomplex, cc - core complex, mono - monomer, trim - trimer.*

To further biochemically reinforce the existence of PSI-LHCII$_2$ sc, we attempted to confirm its presence in the second dimension of electrophoresis, which is much more sensitive compared to native electrophoresis. In the first dimension of BN-PAGE, the band corresponding to PSI-LHCII was clearly visible, but no band that could represent PSI-LHCII$_2$ was observed (Fig. 13, A). Interestingly, a characteristic pattern of separated PsaA/PsaB and LHCAs proteins with a strong signal for LHCB1 and LHCB2 were observed below this apparently unoccupied region in the second dimension. The LHCAs pattern is clearly discernible in the position of the PSI mcs and in additional three lower bands from the BN-PAGE strip, two of which represent the PSI sc

co-migrating with PSII cc and PSI-LHCII (Fig. 13, B). This is further confirmation of a potentially formed PSI-LHCII$_2$ in spruce, undetectable in the first dimension, nevertheless supported in the second dimension. Admittedly, the presence of different PSI sc (with additionally attached, closely unspecified proteins) cannot be excluded without more detailed analysis, for example, by mass spectrometry. However, the position in the BN-PAGE gel derived from the characteristic pattern of PSI proteins in the 2D gel would be consistent with the expected position of PSI with two LHCII trimers based on its calculated molecular weight.

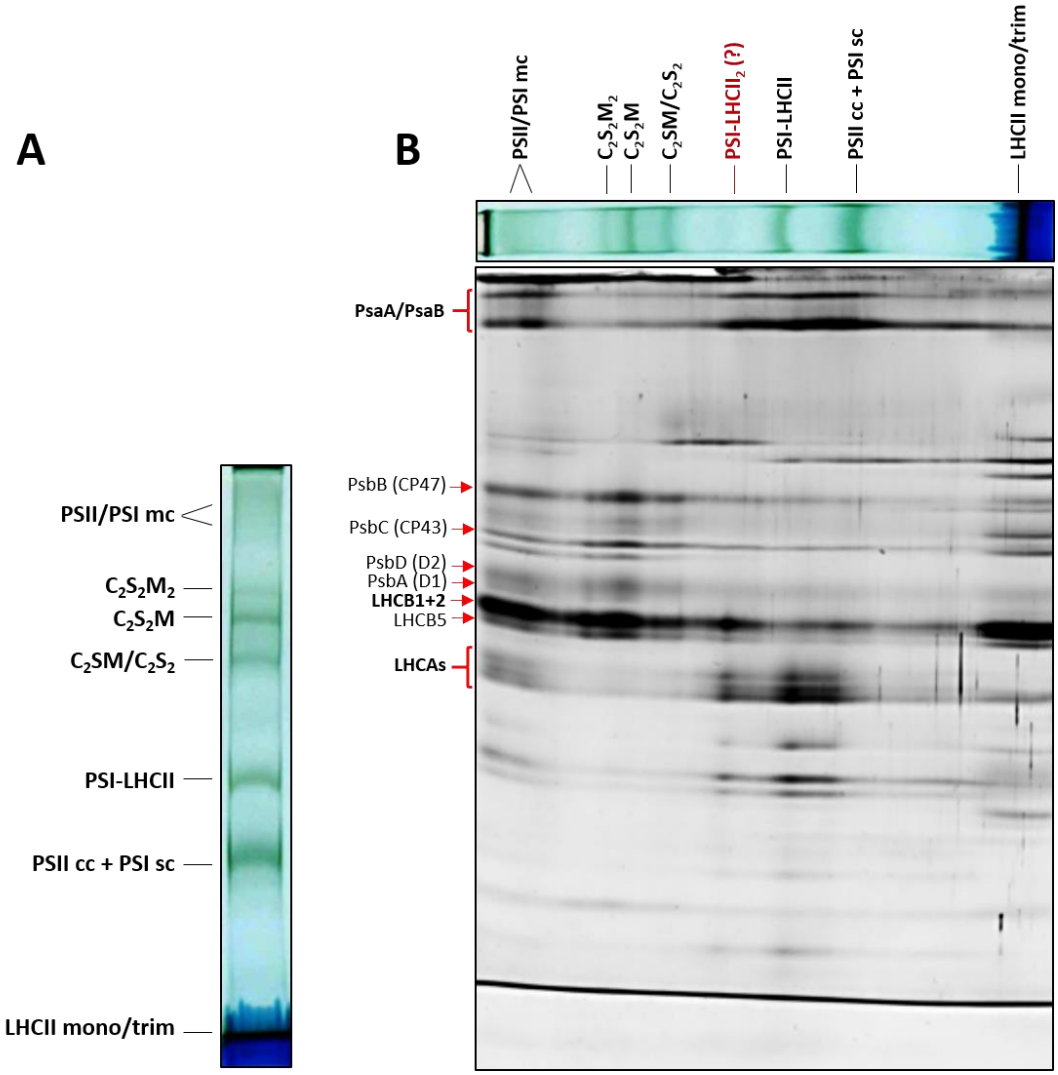

Figure 13: 2D-BN/SDS-PAGE of solubilised thylakoid membranes of spruce harvested for isolation directly from growing light. A) Electrophoretic separation of spruce thylakoid membranes solubilised with 0.7% α DDM in the gradient gel 4–8% and final Chl concentration of 0.5 mg/ml (loading of 16 µl per well). Image of the selected line from the gel scanned at room temperature in transmission mode. B) 2D-SDS-PAGE of thylakoid membrane protein complexes from spruce separated by BN-PAGE in the first dimension, applied on the gel as a gel strip, and subsequently separated in 5% stacking and 12% separating gel. A silver staining protocol was used to visualise the separated proteins, and the gel was scanned at room temperature in transmission mode. The individual protein spots are determined tentatively based on the available information from the literature and the expected molecular weight of proteins. *Abbreviations: PSII - photosystem II, PSI - photosystem I, LHCII - light-harvesting complex of photosystem II, mc - megacomplex, sc - supercomplex, cc - core complex, mono - monomer, trim - trimer, LHCAs - light-harvesting complexes of photosystem I.*

4.3. Conclusion of experimental approach - optimisation of supercomplexes extraction

In summary, the above-described biochemical experiments and their optimisations have brought a deeper insight into the plasticity of thylakoid membranes with respect to their solubilisation together with the effect of separation methods on the quality of the protein scs purification. Application of different modifications, such as (i) the use of different detergents, different concentrations or their combinations, (ii) the addition of stabilisers, or (iii) the implementation of different separation procedures, can all ensure favourable solubilisation and extraction of specific sc from the heterogeneous environment of thylakoid membranes. In addition, it can (i) improve the quality of the separation of different protein complexes through the higher resolution of individual CN-PAGE bands or sucrose gradient fractions, (ii) preserve the maximum intactness of the extracted protein complexes and keep them in the close to native state, and (iii) provide sufficient amounts of homogeneous sample for subsequent methods such as cryo-EM. The protein sample prepared in this way can be used to obtain a high-resolution structure close to its near-native state, thereby providing additional information needed to determine its function.

My primary goal in this part of my thesis was to optimise the separation protocol for the sucrose gradient ultracentrifugation to obtain homogeneous and concentrated fractions of specific protein scs suitable for analysis by cryo-EM. I was able to achieve this goal for the largest forms of the PSII sc under standard conditions, specifically (i) $C_2S_2M_2$ observed in spruce and *At* and (ii) $C_2S_2M_2N_2$ observed in *Cr*. However, even this method cannot be universally applied to obtain arbitrary scs due to the co-migration of protein scs. This is a common drawback of separation methods that are based on the molecular weight of the separated proteins. Therefore, at least in the case of the study of photosynthetic protein scs, it is recommended to prepare, e.g. specific fragments of thylakoid membranes enriched in the protein sc of our interest before the actual separation.

Protein complexes that are too fragile or their inter-subunit binding is very labile due to their regulatory function, such as in the case of state transitions, may be difficult to obtain in sufficient quantities. A low abundance of solubilised protein does not form a specific band or fraction during separation, which complicates or even prevents their structural analysis by EM. Such a protein sc, for example, is the transiently formed PSI-LHCII$_2$, where obtaining a pure, clearly visible PSI-LHCII$_2$ fraction remains elusive for now. The existence of this specific sc in higher plants is currently biochemically unprovable because the standard separation methods used in combination with different solubilisation conditions did not result in one unique fraction/band, even though this sc was observed by electron microscopy.

Focusing on induction of the state transitions in plants, obtaining a higher yield of characteristic PSI-LHCII$_2$ sc could be enhanced by fine-tuning of the light conditions in the growing chamber prior to isolation of the thylakoid membranes. The maximum level of phosphorylation of LHCB2, the conditional for the state 2 transition, does not occur under the growing light. It is known that in natural conditions, the maximal phosphorylation of LHCB2 occurs under non-saturating light (Rochaix *et al.*, 2014). It has been shown experimentally that maximum phosphorylation can be induced in plants exposed to light at half the intensity of the growing light. However, as discussed in the previous sections, a higher abundance of PSI-LHCII particles does not necessarily lead to a higher amount of PSI-LHCII$_2$, because the attachment of the second trimer in vascular plants is assumed to be independent of its phosphorylation. In conclusion, although there are numerous, more or less indirect indications for PSI-LHCII$_2$ formation in vascular plants, their structural validation and biochemical

confirmation would definitely require more creativity in the search for a non-standard optimal approach for their isolation.

As far as the experimental approach is concerned, the influence of the methods used on the results obtained must be taken into account when evaluating the structure of photosystems, especially when making hypotheses based on these results. With the increasing quality and resolution of the revealed structures of both photosystems (and a variety of their scs) or other protein complexes embedded in the membranes, we can simultaneously observe the influence of detergents and additives that were used for their extraction. On the one hand, they allow us to extract the intended protein in an "intact" state; on the other hand, the biochemical nature of these molecules may influence the final protein structure. An example could be α DDM, which was fitted in more than one electron density map of PSI sc (e.g. Pan *et al.*, 2018), even numerous molecules per one photosystem, or in the PSII sc (e.g. Sheng *et al.*, 2019), albeit with lower abundance. While the amphiphilic character of these molecules allows them to form an envelope around the extracted protein, at the same time, it allows them to expel a potentially present molecule, e.g. lipid, from the native structure and replace it with the potential effect on the final structure. However, the presence and conclusive identification of these detergent molecules in the structure is hard to achieve, as (i) the electron density map is insufficient or incomplete at some positions, most often due to the higher flexibility of the specific region in the structure, and (ii) there is a number of molecules with similar structure. Nevertheless, the presence of different molecules with physiological relevance to plants should also be considered.

A deeper insight into the effect of the used detergent on the final structure and its composition provided the study by Graca *et al.* (2021), in which they used digitonin for extraction of PSII sc from *At*. Since this detergent molecule has a relatively large molecular mass and a specific structure, its presence in the electron density map was easily detectable. And although, on the one hand, the authors emphasised its beneficial effect on the stability of PSII sc during extraction, they also highlighted the effect of its integration on the resulting structure, composition and integrity. The 22 molecules of digitonin identified in one structure of *At* PSII resulted in: i) changes in the inter-subunit distances, ii) destabilisation of the natural conformation that led to the release of molecules from the structure, for example, the loss of xanthophyll molecule from S-trimer or replacement of digalactosyldiacyl glycerol (DGD) leading to the loss of PsbJ subunit or iii) changes in flexibility within individual PSII sc due to the induced loss of several interactions between the molecules. And although this disruptive effect of digitonin, or detergents in general, on the protein structures may seem inconvenient, the achieved findings can be used to study the importance of specific subunits, molecules or interactions (protein-protein, protein-ligand, ligand-ligand) on the function and stability of a protein complex or, to evaluate the consequences of using a particular detergent and thus provide important additional information. It is, thereby, very important to be aware of such an effect and to take it into consideration when studying the structural aspects of protein complexes.

In conclusion, when researching a specific topic and performing the corresponding experiments, one has to be really careful when evaluating the obtained experimental data and, at the same time, to be aware that unknown attributes can influence the final results.

5. List of references

Akhtar, P., Lingvay, M., Kiss, T., Deák, R., Bóta, A., Ughy, B., Garab, G., Lambrev, P.H. (2016) Excitation energy transfer between Light-harvesting complex II and Photosystem I in reconstituted membranes. *Biochim. Biophys. Acta (BBA) - Bioenerg.* **1857**, 462–472.

Albanese, P., Manfredi, M., Meneghesso, A., Marengo, E., Saracco, G., Barber, J., Morosinotto, T., Pagliano, C. (2016) Dynamic reorganization of photosystem II supercomplexes in response to variations in light intensities. *Biochim Biophys Acta – Bioenerg.* **1857,** 1651–1660.

Albanese, P., Melero, R., Engel, B.D., Grinzato, A., Berto, P., Manfredi, M., Chiodoni, A., Vargas, J., Sorzano, C.Ó.S., Marengo, E., Saracco, G., Zanotti, G., Carazo, J.-M., Pagliano, C. (2017) Pea PSII-LHCII supercomplexes form pairs by making connections across the stromal gap. *Sci. Rep.* **7**, 10067.

Alboresi, A., Caffarri, S., Nogue, F., Bassi, R., Morosinotto, T. (2008) *In silico* and biochemical analysis of *Physcomitrella patens* photosynthetic antenna: identification of subunits which evolved upon land adaptation. *PLoS ONE* **3**, e2033.

Alboresi, A., Storti, M., Cendron, L., Morosinotto, T. (2019) Role and regulation of class-C flavodiiron proteins in photosynthetic organisms. *Biochem. J.* **476**, 2487–2498.

Allahverdiyeva, Y., Ermakova, M., Eisenhut, M., Zhang, P., Richaud, P., Hagemann, M., Cournac, L., Aro, E.-M. (2011) Interplay between flavodiiron proteins and photorespiration in Synechocystis sp. PCC 6803. *J. Biol. Chem.* **286**, 24007–24014.

Allen, J.F. (2003) Botany. State transitions--a question of balance. *Science*. **299**, 1530-1532.

Alric, J. and Johnson, X. (2017) Alternative electron transport pathways in photosynthesis: a confluence of regulation. *Curr. Opin. Plant Biol.* **37**, 78–86.

Anderson, J. M. (2012) Lateral heterogeneity of plant thylakoid protein complexes: Early reminiscences. *Philos. Trans. R. Soc. Lond. B: Biol. Sci.* **367**, 3384–3388.

Andersson, I. and Backlund, A. (2008) Structure and function of Rubisco. *Plant Physiol. Biochem.* **46**, 275–291.

Apel, K. and Hirt, H. (2004) Reactive oxygen species: metabolism, oxidative stress, and signal transduction. *Annu. Rev. Plant Biol.* **55**, 373–399.

Arshad, R. (2022) Supramolecular structures of thylakoid membrane protein complexes: supercomplex organization under different environmental conditions. [Thesis fully internal (DIV), University of Groningen]. *University of Groningen*. https://doi.org/10.33612/diss.199785099

Bag, P., Chukhutsina, V., Zhang, Z., Paul, S., Ivanov, A.G., Shutova, T., Croce, R., Holzwarth, A.R., Jansson, S. (2020) Direct energy transfer from photosystem II to photosystem I confers winter sustainability in Scots Pine. *Nat. Commun.* **11**, 6388.

Bailey, S., Walters, R.G., Jansson, S., Horton, P. (2001) Acclimation of Arabidopsis thaliana to the light environment: the existence of separate low light and high light responses. *Planta* **213**, 794–801.

Ballottari, M., Dall'Osto, L., Morosinotto, T., Bassi, R. (2007) Contrasting behavior of higher plant photosystem I and II antenna systems during acclimation. *J. Biol. Chem.* **282**, 8947–8958.

Bellafiore, S., Barneche, F., Peltier, G., Rochaix, J.-D. (2005) State transitions and light adaptation require chloroplast thylakoid protein kinase STN7. *Nature* **433**, 892–895.

Ben-Shem, A., Frolow, F., Nelson, N. (2003) Crystal structure of plant photosystem I. *Nature* **426**, 630–635.

Benson, S.L., Maheswaran, P., Ware, M.A., Hunter, C.N., Horton, P., Jansson, S., Ruban, A.V., Johnson, M.P. (2015) An intact light harvesting complex I antenna system is required for complete state transitions in Arabidopsis. *Nat. Plants* **1**, 15176.

Betterle, N., Ballottari, M., Zorzan, S., de Bianchi, S., Cazzaniga, S., Dall'osto, L., Morosinotto, T., Bassi, R. (2009) Light-induced dissociation of an antenna hetero-oligomer is needed for non-photochemical quenching induction. *J. Biol. Chem.* **284**, 15255–15266.

Bielczynski, L.W., Schansker, G., Croce, R. (2016) Effect of light acclimation on the organization of photosystem II super- and sub-complexes in *Arabidopsis thaliana*. *Front. Plant Sci.* **7**, 1–12.

Blum, H., Beier, H., Gross, H.J. (1987) Improved silver staining of plant proteins, RNA and DNA in polyacrylamide gels. *Electrophoresis* **8**, 93–99.

Boekema, E.J., Dekker, J.P., Vanheel, M.G., Rogner, M., Saenger, W., Witt, I., Witt, H.T. (1987) Evidence for a trimeric organization of the photosystem-i complex from the thermophilic cyanobacterium Synechococcus sp. *Febs Lett.* **217**, 283–286.

Boekema, E.J., Jensen, P.E., Schlodder, E., van Breemen, J.F.L., van Roon, H., Scheller, H.V., Dekker, J.P. (2001) Green plant photosystem I binds light-harvesting complex I on one side of the complex. Biochem. **40**, 1029–1036.

Boekema, E.J., van Breemen, J.F.L., van Roon, H., Dekker, J.P. (2000) Arrangement of photosystem II supercomplexes in crystalline macrodomains within the thylakoid membrane of green plant chloroplasts. *J. Mol. Biol*. **301**, 1123–1133.

Boekema, E.J., van Roon, H., Breemen, J. F. L., Dekker, J. P. (1999b) Supramolecular organization of photosystem II and its light-harvesting antenna in partially solubilized photosystem II membranes. *Eur. J. Biochem*. **266**, 444–452.

Boekema, E.J., van Roon, H., Calkoen, F., Bassi, R., Dekker, J.P. (1999a) Multiple types of association of photosystem II and its light-harvesting antenna in partially solubilized photosystem II membranes. *Biochem.* **38**, 2233–2239.

Bos, I., Bland, K.M., Tian, L.J., Croce, R., Frankel, L.K., van Amerongen, H., Bricker, T.M., Wientjes, E. (2017) Multiple LHCII antennae can transfer energy efficiently to a single Photosystem I. *Biochim. Biophys. Acta – Bioenerg.* **1858**, 371–378.

Braukmann, T.W.A., Kuzmina, M., Stefanovic, S. (2009) Loss of all plastid ndh genes in Gnetales and conifers: extent and evolutionary significance for the seed plant phylogeny. *Curr. Gen.* **55**, 323–337.

Bressan, M., Bassi, R., Dall'Osto, L. (2018) Loss of LHCI system affects LHCII re-distribution between thylakoid domains upon state transitions. *Photosynth. Res.* **135**, 251–261.

Brettel, K. (1997) Electron transfer and arrangement of the redox cofactors in photosystem I, *Biochim. Biophys. Acta* **1318**, 322–373.

Buchanan, B.B. (2016) The path to thioredoxin and redox regulation in chloroplasts. *Annu. Rev. Plant Biol.* **67**, 1–24.

Caffarri, S., Croce, R., Cattivelli, L., Bassi, R. (2004) A look within LHCII: differential analysis of the LHCB1−3 complexes building the major trimeric antenna complex of higher-plant photosynthesis. *Biochemistry* **43**, 9467–9476.

Caffarri, S., Kouřil, R., Kereiche, S., Boekema, E. J., Croce, R. (2009) Functional architecture of higher plant photosystem II supercomplexes. *EMBO J.* **28**, 3052–3063.

Caffarri, S., Tibiletti, T., Jennings, R.C. (2014) A comparison between plant photosystem I and photosystem II architecture and functioning. *Curr. Protein Pept. Sci.* **15**, 296–331.

Cao, P., Bracun, L., Yamagata, A., Christianson, B.M., Negami, T., Zou, B., Terada, T., Canniffe, D.P., Shirouzu, M., Li, M., Liu, L.N. (2022) Structural basis for the assembly and quinone transport mechanisms of the dimeric photosynthetic RC-LH1 supercomplex. *Nat. Commun*. **13**, 1977.

Cao, P., Su, X., Pan, X., Liu, Z., Chang, W., Li, M. (2018) Structure, assembly and energy transfer of plant photosystem II supercomplex. *Biochim. Biophys. Acta - Bioenerg*. **1859**, 633–644.

Cariti, F., Chazaux, M., Lefebvre-Legendre, L., Longoni, P., Ghysels, B., Johnson, X., Goldschmidt-Clermont, M. (2020) Regulation of light harvesting in *Chlamydomonas reinhardtii* two protein phosphatases are involved in state transitions. *Plant Physiol.* **183**, 1749–1764.

Caspy, I. and Nelson, N. (2018) Structure of the plant photosystem. *Biochem. Soc. Trans.* **46**, 285–294.

Cejudo, F.J., Ojeda, V., Delgado-Requerey, V., González, M., Pérez-Ruiz, J.M. (2019) Chloroplast redox regulatory mechanisms in plant adaptation to light and darkness. *Front. Plant Sci*. **10**, 1–11.

Chitnis, V.P., and Chitnis, P.R. (1993) PsaL subunit is required for the formation of photosystem-I trimers in the cyanobacterium Synechocystis sp pcc-6803. *Febs Lett.* **336**, 330–334.

Chukhutsina, V.U., Liu, X., Xu, P., Croce, R. (2020) Light-harvesting complex II is an antenna of photosystem I in dark-adapted plants. *Nat. Plants* **6**, 860–868.

Crepin A, Santabarbara S, Caffarri S. (2016) Biochemical and spectroscopic characterization of highly stable photosystem II supercomplexes from Arabidopsis. *J. Biol. Chem.* **291**, 19157–19171.

Crepin, A. and Caffarri, S. (2018) Functions and evolution of LHCB isoforms composing LHCII, the major light harvesting complex of photosystem II of green eukaryotic organisms. *Curr. Protein Pept. Sci.* **19**, 699–713.

Crepin, A., Kučerová, Z., Kosta, A., Durand, E., Caffarri, S. (2020) Isolation and characterization of a large photosystem I-light-harvesting complex II supercomplex with an additional Lhca1-a4 dimer in Arabidopsis. *Plant J.* **102**, 398–409.

Croce, R. and van Amerongen, H. (2011) Light-harvesting and structural organization of Photosystem II: From individual complexes to thylakoid membrane. *J. Photochem. Photobiol. B: Biol.* **104**, 142–153.

Croce, R. and van Amerongen, H. (2013) Light-harvesting in photosystem I. *Photosynth. Res.* **116**, 153–166.

Croce, R. and van Amerongen, H. (2020) Light harvesting in oxygenic photosynthesis: Structural biology meets spectroscopy. *Science* **369**, eaay2058.

Dainese, P. and Bassi, R. (1991) Subunit stoichiometry of the chloroplast photosystem-II antenna system and aggregation state of the component chlorophyll-a /b binding proteins. *J. Biol. Chem.* **266**, 8136–8142.

Damkjær, J.T., Kereiche, S., Johnson, M.P., Kovács, L., Kiss, A.Z., Boekema, E.J., Ruban, A.V., Horton, P., Jansson, S. (2009) The photosystem II light-harvesting protein LHCB3 affects the macrostructure of photosystem II and the rate state transitions in Arabidopsis. *Plant Cell* **21**, 3245–3256.

Dau, H., Andrews, J.C., Roelofs, T.A., Latimer, M.J., Liang, W.C., Yachandra, V.K., Sauer, K., Klein, M.P. (1995) Structural consequences of ammonia binding to the manganese center of the photosynthetic oxygen-evolving complex - an x-ray-absorption spectroscopy study of isotropic and oriented photosystem-II particles. *Biochem.* **34**, 5274–5287.

Daum, B., Nicastro, D., Austin, J., McIntosh, J., Kühlbrandt, W. (2010) Arrangement of photosystem II and ATP synthase in chloroplast membranes of spinach and pea. *Plant Cell* **22**, 1299–1312.

de Bianchi, S., Ballottari, M., Dall'Osto, L., Bassi, R. (2010) Regulation of plant light harvesting by thermal dissipation of excess energy. *Biochem. Soc. Trans*. **38**, 651–660.

de Bianchi, S., Betterle, N., Kouřil, R., Cazzaniga, S., Boekema, E., Bassi, R., Dall'Osto, L. (2011) Arabidopsis mutants deleted in the light-harvesting protein LHCB4 have a disrupted photosystem II macrostructure and are defective in photoprotection. *Plant Cell*. **23**, 2659–2679.

de Bianchi, S., Dall'Osto, L., Tognon, G., Morosinotto, T., Bassi, R. (2008) Minor antenna proteins CP24 and CP26 affect the interactions between photosystem II subunits and the electron transport rate in grana membranes of Arabidopsis. *Plant Cell* **20**, 1012–1028.

Dekker, J.P. and Boekema, E.J. (2005) Supramolecular organization of thylakoid membrane proteins in green plants. *Biochim. Biophys. Acta – Bioenerg.* **1706**, 12–39.

Dekker, J.P. and Van Grondelle, R. (2000) Primary charge separation in photosystem II. *Photosynth. Res*. **63**, 195–208.

Demmig-Adams, B. and Adams, W.W. (1996) The role of xanthophyll cycle carotenoids in the protection of photosynthesis. *Trends Plant Sci*. **1**, 21–26.

Demmig-Adams, B. and Adams, W.W. (2006) Photoprotection in an ecological context: the remarkable complexity of thermal energy dissipation. *New Phytol.* **172**, 11–21.

Demmig-Adams, B., Ebbert, V., Mellman, D.L., Mueh, K.E., Schaffer, L., Funk, C., Zarter, C.R., Adamska, I., Jansson, S., Adams, W.W. III (2006) Modulation of PsbS and flexible vs sustained energy dissipation by light environment in different species. *Physiol. Plant.* **127**, 670–680.

Demmig-Adams, B., Garab, G., Adams III, W., Govindjee (2014) Non-photochemical quenching and energy dissipation in plants, algae and cyanobacteria. *Advances in photosynthesis and respiration*, volume **40**, *Springer, Dordrecht.*

Demmig-Adams, B., Muller, O., Stewart, J.J., Cohu, C.M., Adams, W.W. (2015) Chloroplast thylakoid structure in evergreen leaves employing strong thermal energy dissipation. J. *Photochem. Photobiol. B*: *Biol.* **152**, 357–366.

Depege, N., Bellafiore, S., Rochaix, J.-D. (2003) Role of chloroplast protein kinase Stt7 in LHCII phosphorylation and state transition in Chlamydomonas. *Science* **299**, 1572–1575.

Drop, B., Webber-Birungi, M., Yadav, S. K. N., Filipowicz-Szymanska, A., Fusetti, F., Boekema, E. J., Croce, R. (2014) Light-harvesting complex II (LHCII) and its supramolecular organization in *Chlamydomonas reinhardtii*. *Biochim. Biophys. Acta* **1837**, 63–72.

Edge, R. and Truscott, T.G. (1999) Carotenoid radicals and the interaction of carotenoids with active oxygen species. In: Frank, H.A., Young, A.J., Britton, G., Cogdell, R.J. (eds.) The photochemistry of carotenoids. *Advances in photosynthesis and respiration*, volume **8**, 223–234, *Springer, Dordrecht.*

Flötenmeyer, M., Weiss, H., Tribet, C., Popot, J.L., Leonard, K. (2007) The use of amphipathic polymers for cryo electron microscopy of NADH:ubiquinone oxidoreductase (complex I). *J Microsc.* **227**, 229–35.

Foyer, C.H. and Noctor, G. (2003) Redox sensing and signaling associated with reactive oxygen in chloroplasts, peroxisomes and mitochondria. *Physiol. Plant.* **119**, 355–364.

Foyer, C.H. and Noctor, G. (2005) Redox homeostasis and antioxidant signaling: a metabolic interface between stress perception and physiological responses. *Plant Cell* **17**, 1866–75.

Galka, P., Santabarbara, S., Thi, T.H.K., Degand, H., Morsomme, P., Jennings, R.C., Boekema, E.J., Caffarri, S. (2012) Functional analyses of the plant photosystem I-light-harvesting complex II supercomplex reveal that light-harvesting complex II loosely bound to photosystem II is a very efficient antenna for photosystem I in state II. *Plant Cell* **24**, 2963–2978.

Garber, M.P., and Steponkus, P.L. (1976). Alterations in chloroplast thylakoids during cold-acclimation. *Plant Physiol.* **57**, 681–686.

George, D.M., Vincent, A.S., Mackey, H.R. (2020) An overview of anoxygenic phototrophic bacteria and their applications in environmental biotechnology for sustainable Resource recovery. *Biotech. Rep.* **28**, e00563.

Gisriel, C.J., Wang, J., Liu, J., Flesher, D.A., Reiss, K.M., Huang, H.L., Yang, K.R., Armstrong, W.H., Gunner, M.R., Batista, V.S., Debus, R.J., Brudvig, G.W. (2022) High-

resolution cryo-electron microscopy structure of photosystem II from the mesophilic cyanobacterium, Synechocystis sp. PCC 6803. *Proc. Natl. Acad. Sci. U. S. A.* **119**, e2116765118.

Goldschmidt-Clermont, M. and Bassi, R. (2015) Sharing light between two photosystems: mechanism of state transitions. *Curr. Opin. Plant Biol.* **25**, 71–78.

Gorski, C., Riddle, R., Toporik, H., Da, Z., Dobson, Z., Williams, D., Mazor, Y. (2022) The structure of the *Physcomitrium patens* photosystem I reveals a unique Lhca2 paralogue replacing Lhca4. *Nat. Plants* **8**, 307–316.

Graça, A.T., Hall, M., Persson, K., Schröder, W.P. (2021) High-resolution model of Arabidopsis Photosystem II reveals the structural consequences of digitonin-extraction. *Sci. Rep.* **11**, 15534.

Grebe, S., Trotta, A., Bajwa, A., Mancini, I., Bag, P., Jansson, S., Tikkanen, M., Aro, E.-M. (2020) Specific thylakoid protein phosphorylations are prerequisites for overwintering of Norway spruce (*Picea abies*) photosynthesis. *Proc. Natl. Acad. Sci. U. S. A.* **117**, 17499–17509.

Grebe, S., Trotta, A., Bajwa, A.A., Suorsa, M., Gollan, P.J., Jansson, S., Tikkanen, M., Aro, E.-M. (2019) The unique photosynthetic apparatus of *Pinaceae*: analysis of photosynthetic complexes in *Picea abies*. *J. Exp. Bot.* **70**, 3211–3225.

Guardini, Z., Gomez, R.L., Caferri, R., Dall'Osto, L., Bassi, R. (2022) Loss of a single chlorophyll in CP29 triggers re-organization of the Photosystem II supramolecular assembly. *Biochim. Biophys. Acta – Bioenerg.* **1863**, 148555.

Hamel, P., Olive, J., Pierre, Y., Wollman, F.-A., de Vitry, C. (2000) A new subunit of cytochrome b6f complex undergoes reversible phosphorylation upon state transition. *J. Biol. Chem.* **275**, 17072–17079.

He, W.Z. and Malkin, R. (1992) Specific release of a 9-kDa extrinsic polypeptide of photosystem I from spinach chloroplasts by salt washing. *FEBS Lett.* **308**, 298–300.

Helman, Y., Tchernov, D., Reinhold, L., Shibata, M., Ogawa, T., Schwarz, R., Ohad, I., Kaplan, A. (2003) Genes encoding A-type flavoproteins are essential for photoreduction of O_2 in cyanobacteria. *Curr. Biol.* **13**, 230–235.

Hodges, M., Cornic, G., Briantais, J.-M. (1989) Chlorophyll fluorescence from spinach leaves: resolution of non-photochemical quenching. *Biochim. Biophys. Acta* **974**, 289–293.

Horton, P., Ruban, A. V., Walters, R.G. (1996) Regulation of light harvesting in green plants. *Annu. Rev. Plant Physiol. Plant Mol. Biol.* **47**, 655–684.

Huang, Z., Shen, L., Wang, W., Mao, Z., Yi, X., Kuang, T., Shen, J.R., Zhang, X., Han, G. (2021) Structure of photosystem I-LHCI-LHCII from the green alga *Chlamydomonas reinhardtii* in state 2. *Nat. Commun.* **12**, 1100.

Ilík, P., Pavlovič, A., Kouřil, R., Alboresi, A., Morosinotto, T., Allahverdiyeva, Y., Aro, E.-M., Yamamoto, H., Shikanai, T. (2017) Alternative electron transport mediated by flavodiiron proteins is operational in organisms from cyanobacteria up to gymnosperms. *New Phytol.* **214**, 967–972.

Ilíková I., Ilík P., Opatíková M., Arshad R., Nosek L., Karlický V., Kučerová Z., Roudnický P., Pospíšil P., Lazár D., Bartoš J., Kouřil R. (2021) Towards spruce-type photosystem II supercomplex: consequences of the loss of LHCB3 and LHCB6 in Arabidopsis. *Plant Physiol.* **187**, 2691–2715.

Iwai, M. and Yokono, M. (2017) Light-harvesting antenna complexes in the moss *Physcomitrella patens*: implications for the evolutionary transition from green algae to land plants. *Curr. Opin. Plant Biol.* **37**, 94–101.

Iwai, M., Grob, P., Iavarone, A.T., Nogales, E., Niyogi, K.K. (2018) A unique supramolecular organization of photosystem I in the moss *Physcomitrella patens. Nat. Plants* **4**, 904–909.

Iwai, M., Takizawa, K., Tokutsu, R., Okamuro, A., Takahashi, Y., Minagawa, J. (2010) Isolation of the elusive supercomplex that drives cyclic electron flow in photosynthesis. *Nature* **464**, 1210–1213.

Jackowski, G., Kacprzak, K., Jansson, S. (2001) Identification of LHCB1/LHCB2/LHCB3 heterotrimers of the main light-harvesting chlorophyll a/b-protein complex of Photosystem II (LHC II). *Biochim. Biophys. Acta* **1504**, 340–345.

Jansson, S. (1999) A guide to the Lhc genes and their relatives in Arabidopsis. *Trends Plant Sci.* **4**, 236–240.

Jansson, S., Andersen, B., Scheller, H.V. (1996). Nearest-neighbor analysis of higher plant photosystem I holocomplex. *Plant Physiol.* **112**, 409–420.

Johnson M.P. (2016) Photosynthesis. *Essays in Biochem*. **60**, 255–273.

Jordan, P., Fromme, P., Witt, H.T., Klukas, O., Saenger, W., Krauss, N. (2001) Three dimensional structure of cyanobacterial photosystem I at 2.5 angstrom resolution. *Nature* **411**, 909–917.

Josse, E.-M., Alcaraz, J.-P., Laboure, A.-M., Kuntz, M. (2003) In vitro characterization of a plastid terminal oxidase (PTOX). *Eur. J. Biochem.* **270**, 3787–3794.

Kanazawa, A. and Kramer, D.M. (2002) In vivo modulation of nonphotochemical exciton quenching (NPQ) by regulation of the chloroplast ATP synthase. *Proc. Natl. Acad. Sci. U. S. A.* **99**, 12789–12794.

Kashino, Y., Takahashi, T., Inoue-Kashino, N., Ban, A., Ikeda, Y., Satoh, K., Sugiura, M. (2007) Ycf12 is a core subunit in the photosystem II complex. *Biochim. Biophys. Acta* **1767**, 1269–1275.

Ke, B. (2001) Photosynthesis – photobiochemistry and photobiophysics. *Advances in photosynthesis and respiration*, volume **10**, *Kluwer, Dordrecht.*

Kim, E., Yokono, M., Tsugane, K., Ishii, A., Noda, C., Minagawa, J. (2023) Formation of a stable PSI-PSII megacomplex in rice that conducts energy spillover. *Plant Cell Physiol.* pcad037.

Kirchhoff, H. (2008) Significance of protein crowding, order and mobility for photosynthetic membrane functions. *Biochem. Soc. Trans*. **36**, 967–970.

Kirchhoff, H., Haase, W., Wegner, S., Danielsson, R., Ackermann, R., Albertsson, P.-A. (2007) Low-light-induced formation of semicrystalline photosystem II arrays in higher plant chloroplast. *Biochem.* **46**, 11169-11176.

Klimmek, F., Sjödin, A., Noutsos, C., Leister, D., Jansson, S. (2006) Abundantly and rarely expressed Lhc protein genes exhibit distinct regulation patterns in plants. *Plant Physiol.* **140**, 793–804.

Kouřil, R., Dekker, J.P., Boekema, E.J. (2012) Supramolecular organization of photosystem II in green plants. *Biochim. Biophys. Acta-Bioenerg.* **1817**, 2–12.

Kouřil, R., Nosek, L., Bartoš, J., Boekema, E.J., Ilík, P. (2016) Evolutionary loss of light-harvesting proteins LHCB6 and LHCB3 in major land plant groups - break-up of current dogma. *New Phytol*. **210**, 808–814.

Kouřil, R., Nosek, L., Opatíková, M., Arshad, R., Semchonok, D.A., Chamrád, I., Lenobel, R., Boekema, E.J., and Ilík, P. (2020). Unique organization of photosystem II supercomplexes and megacomplexes in Norway spruce. *Plant J.* **104**, 215–225.

Kouřil, R., Nosek, L., Semchonok, D., Boekema, E.J., Ilík, P. (2018) Organization of plant photosystem II and photosystem I supercomplexes. In Harris, J.R., Boekema, E.J. (eds.) Membrane proteincomplexes: structure and function. *Subcellular Biochemistry*, volume **87**, 259–286, *Springer, Singapore*.

Kouřil, R., Strouhal, O., Nosek, L., Lenobel, R., Chamrád, I., Boekema, E.J., Šebela, M., Ilík, P. (2014) Structural characterization of a plant photosystem I and NAD(P)H dehydrogenase supercomplex. *Plant J.* **77**, 568–576.

Kouřil, R., van Oosterwijk, N., Yakushevska, A.E., Boekema, E.J. (2005b) Photosystem I: a search for green plant trimers. *PPS* **4**, 1091–1094.

Kouřil, R., Wientjes, E., Bultema, J. B., Croce, R., Boekema, E. J. (2013) High-light vs. low-light: Effect of light acclimation on photosystem II composition and organization in *Arabidopsis thaliana*. *Biochim. Biophys. Acta – Bioenerg*. **1827**, 411–419.

Kouřil, R., Zygadlo, A., Arteni, A.A., de Wit, C.D., Dekker, J.P., Jensen, P.E., Scheller, H.V., Boekema, E.J. (2005a) Structural characterization of a complex of photosystem I and light-harvesting complex II of *Arabidopsis thaliana*. *Biochem.* **44**, 10935–10940.

Kovács, L., Damkjær, J., Kereïche, S., Ilioaia, C., Ruban, A.V., Boekema, E.J., Jansson, S., Horton, P. (2006) Lack of the light-harvesting complex CP24 affects the structure and function of the grana membranes of higher plant chloroplasts. *Plant Cell* **18**, 3106–3120.

Kramer, D.M., Cruz, J.A., Kanazawa, A. (2003) Balancing the central roles of the thylakoid proton gradient. *Trends Plant Sci.* **8**, 27–32.

Kress, E. and Jahns, P. (2017) The dynamics of energy dissipation and xanthophyll conversion in Arabidopsis indicate an indirect photoprotective role of zeaxanthin in slowly inducible and relaxing components of non-photochemical quenching of excitation energy. *Front. Plant Sci.* **8**, 2094.

Krieger-Liszkay, A. and Trebst, A. (2006) Tocopherol is the scavenger of singlet oxygen produced by the triplet states of chlorophyll in the PSII reaction centre. *J. Exp. Bot.* **57**, 1677–1684.

Kurasová, I., Kalina, J., Urban, O., Štroch, M., Špunda, V. (2003) Acclimation of two distinct plant species, spring barley and Norway spruce, to combined effect of various irradiance and CO2 concentration during cultivation in controlled environment. *Photosynthetica* **41,** 513–523.

Laemmli, U. K. (1970). Cleavage of structural proteins during the assembly of the head of bacteriophage T4. *Nature* **227**, 680–685.

Le Quiniou, C., van Oort, B., Drop, B., van Stokkum, I.H.M., Croce, R. (2015) The high efficiency of Photosystem I in the green alga *Chlamydomonas reinhardtii* is maintained after the antenna size is substantially increased by the association of light-harvesting complexes II. *J. Biol. Chem.* **290**, 30587–30595.

Lemeille, S. and Rochaix, J.D. (2010) State transitions at the crossroad of thylakoid signalling pathways. *Photosynth. Res.* **106**, 33–46.

Li, M. and Kim, C. (2022) Chloroplast ROS and stress signaling. *Plant Communications*. **3**, 100264.

Lichtenberg, D., Ahyayauch, H., Goñi, F.M. (2013) The mechanism of detergent solubilization of lipid bilayers. *Biophys. J.* **105**, 289–299.

Lichtenthaler, H.K. (1987) Chlorophylls and carotenoids - pigments of photosynthetic biomembranes. *Meth. Enzymol*. **148**, 350–382.

Malavath, T., Caspy, I., Netzer-El, S.Y., Klaiman, D., Nelson, N. (2018) Structure and function of wild-type and subunit-depleted photosystem I in *Synechocystis. Biochim. Biophys. Acta - Bioenerg*. **1859**, 645–654.

Martin, B. and Öquist, G. (1979) Seasonal and experimentally induced changes in the ultrastructure of chloroplasts of *Pinus silvestris*. *Physiol. Plant*. **46**, 42–49.

Mazor, Y., Borovikova, A., Caspy, I., Nelson, N. (2017) Structure of the plant photosystem I supercomplex at 2.6 Å resolution. *Nat. Plants* **3**, 17014.

Mazor, Y., Borovikova, A., Nelson, N. (2015) The structure of plant photosystem I super-complex at 2.8 Å resolution. *Elife* **4**, e07433.

Mehler, A.H. (1951) Studies on reactions of illuminated chloroplasts. *Arch. Biochem. Biophys.* **33**, 65–77.

Minagawa, J. (2011) State transitions - The molecular remodeling of photosynthetic supercomplexes that controls energy flow in the chloroplast. *Biochim. Biophys. Acta − Bioenerg.* **1807**, 897–905.

Minagawa, J. and Takahashi, Y. (2004) Structure, function and assembly of photosystem II and its light-harvesting proteins. *Photosyn. Res.* **82**, 241–263.

Mitchell, P. (1966) Chemiosmotic coupling in oxidative and photosynthetic phosphorylation. *Biol. Rev.* **41**, 445–502.

Müh, F., Renger, T., Zouni, A. (2008) Crystal structure of cyanobacterial photosystem II at 3.0 A resolution: a closer look at the antenna system and the small membrane-intrinsic subunits. *Plant Physiol. Biochem.* **46**, 238–64.

Munekage, Y., Hashimoto, M., Miyake, C., Tomizawa, K.I., Endo, T., Tasaka, M., Shikanai, T. (2004) Cyclic electron flow around photosystem I is essential for photosynthesis. *Nature* **429**, 579–582.

Munekage, Y., Hojo, M., Meurer, J., Endo, T., Tasaka, M., Shikanai, T. (2002) PGR5 is involved in cyclic electron flow around photosystem I and is essential for photoprotection in Arabidopsis. *Cell* **110**, 361–371.

Murata, N., Mohanty, P.S., Hayashi, H., Papageorgiou, G.C. (1992) Glycinebetaine stabilizes the association of extrinsic proteins with the photosynthetic oxygen-evolving complex. *FEBS Lett.* **296** , 187–189.

Nagao, R., Kato, K., Kumazawa, M., Ifuku, K., Yokono, M., Suzuki, T., Dohmae, N., Akita, F., Akimoto, S., Miyazaki, N., Shen, J.R. (2022) Structural basis for different types of hetero-tetrameric light-harvesting complexes in a diatom PSII-FCPII supercomplex. *Nat. Commun.* **13**, 1764.

Nanba, O. and Satoh, K. (1987) Isolation of a photosystem II reaction center consisting of D-1 and D-2 polypeptides and cytochrome b-559, *Proc. Natl. Acad. Sci. U. S. A.* **84**, 109–112.

Naschberger, A., Mosebach, L., Tobiasson, V., Kuhlgert, S., Scholz, M., Perez-Boerema, A., Ho, T.T.H., Vidal-Meireles, A., Takahashi, Y., Hippler, M., Amunts, A. (2022) Algal photosystem I dimer and high-resolution model of PSI-plastocyanin complex. *Nat. Plants* **8**, 1191–1201.

Natali, A. and Croce, R. (2015) Characterization of the major light-harvesting complexes (LHCBM) of the green alga *Chlamydomonas reinhardtii*. *PLoS ONE* **10**, e0119211.

Nawrocki, W.J., Tourasse, N.J., Taly, A., Rappaport, F., Wollman, F.-A. (2015) The plastid terminal oxidase: its elusive function points to multiple contributions to plastid physiology. *Annu. Rev. Plant Biol.* **66**, 49–74.

Nelson, N. (2009) Plant photosystem I - the most efficient nano-photochemical machine. *J. Nanosci. Nanotech.* **9**, 1709–1713.

Nelson, N. and Ben-Shem, A. (2004) The complex architecture of oxygenic photosynthesis. *Nature Rev. Mol. Cell Biol.* **5**, 971–982.

Nelson, N. and Junge, W. (2015) Structure and energy transfer in photosystems of oxygenic photosynthesis. *Annu. Rev. Biochem.* **84**, 659–683.

Nelson, N. and Yocum, C.F. (2006) Structure and function of photosystems I and II. *Annu. Rev. Plant Biol.* **57**, 521–565.

Nikkanen, L. and Rintamäki, E. (2019) Chloroplast thioredoxin systems dynamically regulate photosynthesis in plants. *Biochem. J.* **476**, 1159–1172.

Niyogi, K. K. and Truong, T. B. (2013) Evolution of flexible non-photochemical quenching mechanisms that regulate light harvesting in oxygenic photosynthesis. *Curr. Opin. Plant Biol.* **16**, 307–314.

Nosek, L., Semchonok, D., Boekema, E.J., Ilík, P., Kouřil, R. (2017) Structural variability of plant photosystem II megacomplexes in thylakoid membranes. *Plant J.* **89**, 104–111.

Nystedt, B., Street, N.R., Wetterbom, A., Zuccolo, A., Lin, Y.C., Scofield, D.G., Vezzi, F., Delhomme, N., Giacomello, S., Alexeyenko, A., Vicedomini, R., Sahlin, K., Sherwood, E., Elfstrand, M., Gramzow, L., Holmberg, K., Hällman, J., Keech, O., Klasson, L., Koriabine, M., Kucukoglu, M., Käller, M., Luthman, J., Lysholm, F., Niittylä, T., Olson, A., Rilakovic, N., Ritland, C., Rosselló, J.A., Sena, J., Svensson, T., Talavera-López, C., Theißen, G., Tuominen, H., Vanneste, K., Wu, Z.Q., Zhang, B., Zerbe, P., Arvestad, L., Bhalerao, R., Bohlmann, J., Bousquet, J., Garcia Gil, R., Hvidsten, T.R., de Jong, P., MacKay, J., Morgante, M., Ritland, K., Sundberg, B., Thompson, S.L., Van de Peer, Y., Andersson, B., Nilsson, O., Ingvarsson, P.K., Lundeberg, J., Jansson, S. (2013) The Norway spruce genome sequence and conifer genome evolution. *Nature* **497**, 579–584.

Opatíková M., Semchonok, D.A., Kopečný D., Ilík P., Pospíšil P., Ilíková I., Roudnický P., Zeljković S.Ć., Tarkowski P., Kyrilis F.L., Hamdi F., Kastritis P.L., Kouřil R. (2023) Cryo-EM structure of plant photosystem II supercomplex with light-harvesting protein LHCB8 and α-tocopherol. *Nat. Plants* (in press).

Öquist, G. and Huner, N. P. (2003) Photosynthesis of overwintering evergreen plants. *Annu. Rev. Plant Biol.* **54**, 329–355.

Ozawa, S., Onishi, T., Takahashi, Y. (2010) Identification and characterization of an assembly intermediate subcomplex of photosystem I in the green alga *Chlamydomonas reinhardtii. J. Biol. Chem.* **285**, 20072–20079.

Pagliano, C., Nield, J., Marsano, F., Pape, T., Barera, S., Saracco, G., Barber, J. (2014) Proteomic characterization and three-dimensional electron microscopy study of PSII-LHCII supercomplexes from higher plants. *Biochim. Biophys. Acta.* **1837**, 1454-1462.

Pan, X., Ma, J., Su, X., Cao, P., Chang, W., Liu, Z., Zhang, X., Li, M. (2018) Structure of the maize photosystem I supercomplex with light-harvesting complexes I and II. *Science.* **360**, 1109–1113.

Pan, X., Tokutsu, R., Li, A., Takizawa, K., Song, C., Murata, K., Yamasaki, T., Liu, Z., Minagawa, J., Li, M. (2021) Structural basis of LHCBM5-mediated state transitions in green algae. *Nat. Plants* **7**, 1119–1131.

Papageorgiou, G.C, and Murata, N. (1995) The unusually strong stabilizing effects of glycine betaine on the structure and function of the oxygen-evolving Photosystem II complex. *Photosynth Res.* **44**, 243–52.

Peng, L., Shimizu, H., Shikanai, T. (2008) The chloroplast NAD(P)H dehydrogenase complex interacts with photosystem I in Arabidopsis. *J. Biol. Chem.* **283**, 34873–34879.

Peng, L.W., Fukao, Y., Fujiwara, M., Takami, T., Shikanai, T. (2009) Efficient operation of NAD(P)H dehydrogenase requires supercomplex formation with photosystem I via minor LHCI in Arabidopsis. *Plant Cell* **21**, 3623–3640.

Pesaresi, P., Hertle, A., Pribil, M., Schneider, A., Kleine, T., Leister, D. (2010) Optimizing photosynthesis under fluctuating light: the role of the Arabidopsis STN7 kinase. *Plant Signal. Behav.* **5**, 21–25.

Pesaresi, P., Pribil, M., Wunder, T. and Leister, D. (2011) Dynamics of reversible protein phosphorylation in thylakoids of flowering plants: The roles of STN7, STN8 and TAP38. *Biochim. Biophys. Acta – Bioenerg.* **1807**, 887–896.

Peter, G.F. and Thornber, J.P. (1991) Biochemical composition and organization of higher plant photosystem II light-harvesting pigment - proteins. *J. Biol. Chem.* **266**, 16745–16754.

Peterson, R.B. and Schultes, N.P. (2014) Light-harvesting complex B7 shifts the irradiance response of photosynthetic light-harvesting regulation in leaves of *Arabidopsis thaliana. J. Plant Physiol.* **171**, 311–318.

Pfannschmidt, T., Nilsson, A., Allen, J.F. (1999) Photosynthetic control of chloroplast gene expression. *Nature* **397**, 625–628.

Pfannschmidt, T., Schutze, K., Brost, M., Oelmuller, R. (2001) A novel mechanism of nuclear photosynthesis gene regulation by redox signals from the chloroplast during photosystem stoichiometry adjustment. *J. Biol. Chem.* **276**, 36125–36130.

Pinnola, A., Alboresi, A., Nosek, L., Semchonok, D., Rameez, A., Trotta, A., Barozzi, F., Kouřil, R., Dall'Osto, L., Aro, E.-M., Boekema, E.J., Bassi, R. (2018) A LHCB9-dependent photosystem I megacomplex induced under low light in *Physcomitrella patens. Nat. Plants* **4**, 910–919.

Poolman, M.G. and Fell, D.A. (2000) Modelling photosynthesis and its control. *J. Exp. Bot.* **51**, 319–328.

Pribil, M., Pesaresi, P., Hertle, A., Barbato, R., Leister, D. (2010) Role of plastid protein phosphatase TAP38 in LHCII dephosphorylation and thylakoid electron flow. *PLoS Biol.* **8**, e1000288.

Qin, X., Pi, X., Wang, W., Han, G., Zhu, L., Liu, M., Cheng, L., Shen, J.-R., Kuang, T., Sui, S.-F. (2019) Structure of a green algal photosystem I in complex with a large number of light-harvesting complex I subunits. *Nat. Plants* **5**, 263–272.

Qin, X., Suga, M., Kuang, T., Shen, J.R. (2015) Photosynthesis. Structural basis for energy transfer pathways in the plant PSI-LHCI supercomplex. *Science* **348**, 989–995.

Rantala, M., Rantala, S., Aro, E-M. (2020) Composition, phosphorylation and dynamic organisation of photosynthetic protein complexes in plant thylakoid membrane. *Photochem. Photobiol. Sci.* **19**, 604-619.

Rantala, M., Tikkanen, M. Aro, E.-M. (2017) Proteomic characterization of hierarchical megacomplex formation in Arabidopsis thylakoid membrane. *Plant J.* **92**, 951–962.

Raymond, J. and Blankenship, R.E. (2004) Biosynthetic pathways, gene replacement and the antiquity of life. *Geobiol.* **2**, 199–203.

Rintamäki, E., Martinsuo, P., Pursiheimo, S. and Aro, E.-M. (2000) Cooperative regulation of lightharvesting complex II phosphorylation via the plastoquinol and ferredoxin-thioredoxin system in chloroplasts. *Proc. Natl. Acad. Sci. U. S. A.* **97**, 11644–11649.

Rochaix, J.-D. (2007) Role of thylakoid protein kinases in photosynthetic acclimation. *FEBS Lett.* **581**, 2768–2775.

Rochaix, J.-D. (2014) Regulation and dynamics of the light-harvesting system. *Annu. Rev. Plant Biol.* **65**, 287–309.

Rochaix, J.-D., Lemeille, S., Shapiguzov, A., Samol, I., Fucile, G., Willig, A., Goldschmidt-Clermont, M. (2012) Protein kinases and phosphatases involved in the acclimation of the photosynthetic apparatus to a changing light environment. *Philos. Trans. R. Soc. Lond. B Biol. Sci.* **367**, 3466–3474.

Rumberg, B. and Siggel, U. (1969) pH changes in the inner phase of the thylakoids during photosynthesis. *Naturwissenschaften* **56**, 130–132.

Sawchuk, M.G., Donner, T.J., Head, P., Scarpella, E. (2008) Unique and overlapping expression patterns among members of photosynthesis associated nuclear gene families in Arabidopsis. *Plant Physiol.* **148**, 1908–1924.

Schägger, H. (2006) Tricine-SDS-PAGE. *Nat Protoc.* **1**, 16-22.

Schiphorst, C., Achterberg, L., Gómez, R., Koehorst, R., Bassi, R., van Amerongen, H., Dall'Osto, L. Wientjes, E. (2022) The role of light-harvesting complex I in excitation energy transfer from LHCII to photosystem I in Arabidopsis. *Plant Physiol.* **188**, 2241–2252.

Schwarz, E.M., Tietz, S., Froehlich, J.E. (2018) Photosystem I-LHCII megacomplexes respond to high light and aging in plants. *Photosynth. Res.* **136**, 107–124.

Semchonok, D.A., Mondal, J., Cooper, C.J., Schlum, K., Li, M., Amin, M., Sorzano, C.O.S., Ramírez-Aportela, E., Kastritis, P.L., Boekema, E.J., Guskov, A., Bruce, B.D. (2021) Cryo-EM structure of a tetrameric photosystem I from Chroococcidiopsis TS-821, a

thermophilic, unicellular, non-heterocyst-forming cyanobacterium. *Plant Commun.* **3**, 100248.

Semenova, G.A. (1995). Particle regularity on thylakoid fracture faces is influenced by storage-conditions. *Canad. J. Bot.* **73**, 1676–1682.

Sétif, P., Shimakawa, G., Krieger-Liszkay, A., Miyake, C. (2020) Identification of the electron donor to flavodiiron proteins in Synechocystis sp. PCC 6803 by in vivo spectroscopy. *Biochim. Biophys. Acta – Bioenerg.* **1861**, 148256.

Shang, H., Li, M., Pan, X. (2023) Dynamic Regulation of the Light-Harvesting System through State Transitions in Land Plants and Green Algae. *Plants (Basel)* **12**, 1173.

Shapiguzov, A., Ingelsson, B., Samol, I., Andres, C., Kessler, F., Rochaix, J.-D., Vener, A.V., Goldschmidt-Clermont, M. (2010) The PPH1 phosphatase is specifically involved in LHCII dephosphorylation and state transitions in Arabidopsis. *Proc. Natl. Acad. Sci. U. S. A.* **107**, 4782–4787.

Shen, L., Huang, Z., Chang, S., Wang, W., Wang, J., Kuang, T., Han, G., Shen, J.R., Zhang, X. (2019) Structure of a $C_2S_2M_2N_2$-type PSII–LHCII supercomplex from the green alga *Chlamydomonas reinhardtii*. *Proc. Natl. Acad. Sci. U. S. A.*, **116**, 21246−21255.

Shen, L., Tang, K., Wang, W., Wang, C., Wu, H., Mao, Z., An, S., Chang, S., Kuang, T., Shen, J.R., Han, G., Zhang, X. (2022) Architecture of the chloroplast PSI-NDH supercomplex in *Hordeum vulgare*. *Nature* **601**, 649–654.

Sheng, X., Watanabe, A., Li, A., Kim, E., Song, Ch., Murata, K., Song, D., Minagawa, J., Liu, Z. (2019) Structural insight into light harvesting for photosystem II in green algae. *Nat. Plants* **5**, 1320–1330.

Shi, L.X. and Schroder, W.P. (2004) The low molecular mass subunits of the photosynthetic supracomplex, photosystem II. *Biochim. Biophys. Acta – Bioenerg.* **1608**, 75–96.

Shikanai, T. (2007) Cyclic electron transport around photosystem I: genetic approaches. *Annu. Rev. Plant Biol.* **58**, 199–217.

Stirbet, A., Lazár, D., Guo, Y., Govindjee, G. (2020) Photosynhesis: basics, history, and modeling. *Ann. Bot.* **126**, 511-537.

Štroch, M., Karlický, V., Ilík, P., Ilíková, I., Opatíková, M., Nosek, L., Pospíšil, P., Svrčková, M., Rác, M., Roudnický, P., Zdráhal, Z., Špunda, V., Kouřil, R. (2022) Spruce versus Arabidopsis: different strategies of photosynthetic acclimation to long-term light intensity changes. *Photosynth. Res.* **154**, 21–40.

Štroch, M., Kuldová, K., Kalina, J., Špunda, V. (2008) Dynamics of the xanthophyll cycle and non-radiative dissipation of absorbed light energy during exposure of Norway spruce to high irradiance. *J. Plant Physiol.* **165,** 612–622.

Su, X., Cao, D., Pan, X., Shi, L., Liu, Z., Dall'Osto, L., Bassi, R., Zhang, X., Li, M. (2022) Supramolecular assembly of chloroplast NADH dehydrogenase-like complex with photosystem I from *Arabidopsis thaliana*. *Mol. Plant* **15**, 454–467.

Su, X., Ma, J., Pan, X., Zhao, X., Chang, W., Liu, Z., Zhang, X., Li, M. (2019) Antenna arrangement and energy transfer pathways of a green algal photosystem-I–LHCI supercomplex. *Nat. Plants* **5**, 273–281.

Su, X., Ma, J., Wei, X., Cao, P., Zhu, D., Chang, W., Liu, Z., Zhang, X., Li, M. (2017) Structure and assembly mechanism of plant C2S2M2-type PSII-LHCII supercomplex. *Science* **357**, 815–820.

Suga, M., Ozawa, S.I., Yoshida-Motomura, K., Akita, F., Miyazaki, N., Takahashi, Y. (2019) Structure of the green algal photosystem I supercomplex with a decameric light-harvesting complex I. *Nat. Plants* **5**, 626–636.

Sun, H., Shang, H., Pan, X., Li, M. (2023) Light-harvesting complex Lhcb9 confers a green alga-type photosystem I supercomplex to the moss Physcomitrella patens

Suorsa, M., Järvi, S., Grieco, M., Nurmi, M., Pietrzykowska, M., Rantala, M., Kangasjärvi, S., Paakkarinen, V., Tikkanen, M., Jansson, S., Aro, E.-M. (2012) PROTON GRADIENT REGULATION5 is essential for proper acclimation of Arabidopsis photosystem I to naturally and artificially fluctuating light conditions. *Plant Cell* **24**, 2934–2948.

Tikhonov, A.N. (2014) The cytochrome b6f complex at the crossroad of photosynthetic electron transport pathways. *Plant Physiol. Biochem.* **81**, 163–83.

Tikkanen, M. and Aro, E.-M. (2014). Integrative regulatory network of plant thylakoid energy transduction. *Trends Plant Sci.* **19**, 10–17.

Trissl, H.-W. and Wilhelm, C. (1993) Why do thylakoid membranes from higher plants form grana stacks? *Trends Biochem. Sci.* **18**, 415–419.

van Bezouwen, L.S., Caffarri, S., Kale, R.S., Kouřil, R., Thunnissen, A.-M.W.H., Oostergetel, G.T., Boekema, E.J. (2017) Subunit and chlorophyll organization of the plant photosystem II supercomplex. *Nat. Plants* **3**, 17080.

van Eerden, F.J., Melo, M.N., Frederix, P.W.J.M., Periole, X., Marrink, S.J. (2017) Exchange pathways of plastoquinone and plastoquinol in the photosystem II complex. *Nat. Commun.* **8**, 15214.

Vener, A.V., Harms, A., Sussman, M.R., Vierstra, R.D. (2001) Mass spectrometric resolution of reversible protein phosphorylation in photosynthetic membranes of *Arabidopsis thaliana*. *J. Biol. Chem.* **276**, 6959–6966.

Vener, A.V., Rokka, A., Fulgosi, H., Andersson, B., Herrmann, R.G. (1999) A cyclophilin-regulated PP2A-like protein phosphatase in thylakoid membranes of plant chloroplasts. *Biochem.* **38**, 14955–14965.

Verhoeven, A. (2014) Sustained energy dissipation in winter evergreens. *New Phytol.* **201**, 57–65.

Verhoeven, A.S. (2013) Recovery kinetics of photochemical efficiency in winter stressed conifers: the effects of growth light environment, extent of the season and species. *Physiol. Plant.* **147**, 147–158.

Walter-McNeill, A., Garcia, M.A., Logan, B.A., Bombard, D.M., Reblin, J.S., Lopez, S., Southwick, C.D., Sparrow, E.L. and Bowling, D.R. (2021) Wide variation of winter-induced sustained thermal energy dissipation in conifers: a common-garden study. *Oecologia* **197**, 589–598.

Webber, A.N., Packman, L., Chapman, D.J., Barber, J., Gray, J.C. (1989) A fifth chloroplast-encoded polypeptide is present in the photosystem II reaction centre complex, *FEBS Lett.* **242**, 259–262.

Wei, X., Su, X., Cao, P., Liu, X., Chang, W., Li, M., Zhang, X., Liu, Z. (2016) Structure of spinach photosystem II–LHCII supercomplex at 3.2 Å resolution. *Nat. Cell Biol.* **534**, 69–74.

Wientjes, E., Drop, B., Kouril, R., Boekema, E.J., Croce, R. (2013) During state 1 to state 2 transition in *Arabidopsis thaliana*, the photosystem II supercomplex gets phosphorylated but does not disassemble. *J. Biol. Chem.* **288**, 32821–32826.

Wittig, I., Karas, M., Schägger, H. (2007) High resolution clear native electrophoresis for in-gel functional assays and fluorescence studies of membrane protein complexes. *Mol. Cell. Proteomics.* **6**, 1215–1225.

Xu, C., Pi, X., Huang, Y., Han, G., Chen, X., Qin, X., Huang, G., Zhao, S., Yang, Y., Kuang, T., Wang, W., Sui, S.F., Shen, J.R. (2020) Structural basis for energy transfer in a huge diatom PSI-FCPI supercomplex. *Nat. Commun.* **11**, 5081.

Yadav, K.N., Semchonok, D.A., Nosek, L., Kouřil, R., Fucile, G., Boekema, E.J., Eichacker, L.A. (2017) Supercomplexes of plant photosystem I with cytochrome b6f, light-harvesting complex II and NDH. *Biochim. Biophys. Acta – Bioenerg.* **1858**, 12-20.

Yakushevska, A.E., Jensen, P.E., Keegstra, W., van Roon, H., Scheller, H.S., Boekema, E.J., Dekker, J.P. (2001) Supermolecular organization of photosystem II and its associated light-harvesting antenna in *Arabidopsis thaliana*. *Eur. J. Biochem.* **268**, 6020–6028.

Yan, Q., Zhao, L., Wang, W., Pi, X., Han, G., Wang, J., Cheng, L., He, Y.K., Kuang, T., Qin, X., Sui, S.-F., Shen, J.-R. (2021) Antenna arrangement and energy-transfer pathways of PSI-LHCI from the moss *Physcomitrella patens*. *Cell Discov.* **7**, 10.

Yang, Q., Blanco, N. E., Hermida-Carrera, C., Lehotai, N., Hurry, V., Strand, Å. (2020) Two dominant boreal conifers use contrasting mechanisms to reactivate photosynthesis in the spring. *Nat. Commun.* **11**, 128.

Yoshida, K., Yokochi, Y., Hisabori, T. (2019) New light on chloroplast redox regulation: molecular mechanism of protein thiol oxidation. *Front. Plant Sci.* **10**, 1–6.

You, X., Zhang, X., Cheng, J., Xiao, Y., Ma, J., Sun, S., Zhang, X., Wang, H.W., Sui, S.F. (2023) In situ structure of the red algal phycobilisome-PSII-PSI-LHC megacomplex. *Nature* **616**, 199–206.

Yu, Q., Feilke, K., Krieger-Liszkay, A., Beyer, P. (2014) Functional and molecular characterization of plastid terminal oxidase from rice (Oryza sativa). *Biochim. Biophys. Acta – Bioenerg.* **1837**, 1284–1292.

Zhang, C., Shuai, J., Ran, Z., Zhao, J., Wu, Z., Liao, R., Wu, J., Ma, W., Lei, M. (2020) Structural insights into NDH-1 mediated cyclic electron transfer. *Nat. Commun.* **11**, 888.

Zhang, S., Tang, K., Yan, Q., Li, X., Shen, L., Wang, W., He, Y.K., Kuang, T., Han, G., Shen, J.R., Zhang, X. (2023) Structural insights into a unique PSI-LHCI-LHCII-Lhcb9 supercomplex from moss *Physcomitrium patens*. *Nat. Plants* **9**, 832–846.